DOCTOR OF PHILOSOPHY

Pterosins and Pterosides in Bracken (Pteridium aquilinum (L.) Kuhn)

Mohammad, Rizgar

Award date:
2016

Awarding institution:
Bangor University

Pterosins and Pterosides in Bracken (*Pteridium aquilinum* (L.) Kuhn)

by

Rizgar Hassan Mohammad

A Thesis Submitted in Partial Fulfilment of the

Requirements for the Degree of

Doctor of Philosophy

in the

School of Chemistry

College of Physical and Applied Sciences

Bangor University

Bangor University

2016

Declaration and Consent

Details of the Work

I hereby agree to deposit the following item in the digital repository maintained by Bangor University and/or in any other repository authorized for use by Bangor University.

Author Name: ……..

Title: ……..……

Supervisor/Department: .....

Funding body (if any): .....

Qualification/Degree obtained: …… …….

This item is a product of my own research endeavours and is covered by the agreement below in which the item is referred to as "the Work". It is identical in content to that deposited in the Library, subject to point 4 below.

Non-exclusive Rights

Rights granted to the digital repository through this agreement are entirely non-exclusive. I am free to publish the Work in its present version or future versions elsewhere.

I agree that Bangor University may electronically store, copy or translate the Work to any approved medium or format for the purpose of future preservation and accessibility. Bangor University is not under any obligation to reproduce or display the Work in the same formats or resolutions in which it was originally deposited.

Bangor University Digital Repository

I understand that work deposited in the digital repository will be accessible to a wide variety of people and institutions, including automated agents and search engines via the World Wide Web.

I understand that once the Work is deposited, the item and its metadata may be incorporated into public access catalogues or services, national databases of electronic theses and dissertations such as the British Library's EThOS or any service provided by the National Library of Wales.

I understand that the Work may be made available via the National Library of Wales Online Electronic Theses Service under the declared terms and conditions of use (http://www.llgc.org.uk/index.php?id=4676). I agree that as part of this service the National Library of Wales may electronically store, copy or convert the Work to any approved medium or format for the purpose of future preservation and accessibility. The National Library of Wales is not under any obligation to reproduce or display the Work in the same formats or resolutions in which it was originally deposited.

Statement 1:

This work has not previously been accepted in substance for any degree and is not being concurrently submitted in candidature for any degree unless as agreed by the University for approved dual awards.

Signed …….. (candidate)

Date ……..

Statement 2:

This thesis is the result of my own investigations, except where otherwise stated. Where correction services have been used, the extent and nature of the correction is clearly marked in a footnote(s).

Other sources are acknowledged by footnotes giving explicit references. A bibliography is appended.

Signed ……. (candidate)

Date …….

Statement 3:

I hereby give consent for my thesis, if accepted, to be available for photocopying, for inter-library loan and for electronic repositories, and for the title and summary to be made available to outside organisations.

Signed ……. (candidate)

Date …….

NB: Candidates on whose behalf a bar on access has been approved by the Academic Registry should use the following version of **Statement 3:**

Statement 3 (bar):

I hereby give consent for my thesis, if accepted, to be available for photocopying, for inter-library loans and for electronic repositories after expiry of a bar on access.

Signed …… (candidate)

Date ……

Statement 4:

Choose **one** of the following options

a) I agree to deposit an electronic copy of my thesis (the Work) in the Bangor University (BU) Institutional Digital Repository, the British Library ETHOS system, and/or in any other repository authorized for use by Bangor University and where necessary have gained the required permissions for the use of third party material.	✓
b) I agree to deposit an electronic copy of my thesis (the Work) in the Bangor University (BU) Institutional Digital Repository, the British Library ETHOS system, and/or in any other repository authorized for use by Bangor University when the approved **bar on access** has been lifted.	
c) I agree to submit my thesis (the Work) electronically via Bangor University's e-submission system, however I **opt-out** of the electronic deposit to the Bangor University (BU) Institutional Digital Repository, the British Library ETHOS system, and/or in any other repository authorized for use by Bangor University, due to lack of permissions for use of third party material.	

Options B should only be used if a bar on access has been approved by the University.

In addition to the above I also agree to the following:

1. That I am the author or have the authority of the author(s) to make this agreement and do hereby give Bangor University the right to make available the Work in the way described above.
2. That the electronic copy of the Work deposited in the digital repository and covered by this agreement, is identical in content to the paper copy of the Work deposited in the Bangor University Library, subject to point 4 below.
3. That I have exercised reasonable care to ensure that the Work is original and, to the best of my knowledge, does not breach any laws – including those relating to defamation, libel and copyright.
4. That I have, in instances where the intellectual property of other authors or copyright holders is included in the Work, and where appropriate, gained explicit permission for the inclusion of that material in the Work, and in the electronic form of the Work as accessed through the open access digital repository, *or* that I have identified and removed that material for which adequate and appropriate permission has not been obtained and which will be inaccessible via the digital repository.
5. That Bangor University does not hold any obligation to take legal action on behalf of the Depositor, or other rights holders, in the event of a breach of intellectual property rights, or any other right, in the material deposited.
6. That I will indemnify and keep indemnified Bangor University and the National Library of Wales from and against any loss, liability, claim or damage, including without limitation any related legal fees and court costs (on a full indemnity bases), related to any breach by myself of any term of this agreement.

Signature: ……..…… Date ……...……

Dedication

To my wife **Payam** for her endurance, prayers and unwavering support

and

my children **Ronya** (5.5 years) and **Raman** (2.5 years).

May this inspire them to continue learning.

Acknowledgments

I would like to express my special appreciation and deepest gratitude to my supervisor Dr Vera Thoss for her endless support and productive criticism during my PhD study, you have been a tremendous mentor for me. I would also like to thank you for encouraging my research and for allowing me to grow as a research scientist. Your advice on both research as well as on my career have been priceless.

I would also like to extend my sincerest gratitude and acknowledge the following people and groups who assisted me in different ways in the completion of these studies:

- ✓ Dr Mohammad Nur-e-Alam for his guidance and observations during working in the laboratory, for teaching me the basic principles of natural products chemistry and for his help in structural elucidation of the isolated compounds.
- ✓ All Plant Chemistry Group members, including Dr Anna Santoro, for their suggestions, helpful ideas and discussions during our weekly group meeting in which somehow supported progression of this research.
- ✓ My research committee members, Professor Mark Baird and Dr Hongyun Tai, for their support and valuable suggestions throughout the study.
- ✓ The technical staff at School of Chemistry, especially Dr David Davenport Hughes and Shon Glyn Jones for their help with technical NMR and chromatographic (HPLC) problems. I would also like to thank Kathleen Tailliart, Gwynfor Davies and Toby Vye for providing technical assistance.
- ✓ The administrative and clerical ladies staff in the general office at School of Chemistry, Mrs Caroline Randall, Mrs Tracey Roberts, Miss Siobhan Jones and Miss Bryony Jones.
- ✓ Dr Dotsha Raheem, Victor Ebuele and Jason Fitzsimmons for their support and contribution with the seasonal plant sampling.
- ✓ Dr Martina Lahmann for her help in the determination of the absolute configuration of sugar moieties in pteroside compounds.
- ✓ Mr Nigel Brown from Treborth Botanical Garden, Bangor, for identification of the bracken plant as *Pteridium aquilinum* (L.) Kuhn and depositing a voucher specimen of bracken at the Treborth Botanical Garden.
- ✓ Muhammad Yousaf, King Saudi University, Saudi Arabia, for confirming previously undescribed compounds.

- ✓ Ifat Parveen from Institute of Biological, Environmental and Rural Sciences (IBERS), Aberystwyth University, Aberystwyth, UK, for measuring the high resolution mass (FT-ICR-MS) of the isolated novel compounds.
- ✓ Dr Ahmed Tawfike from Strathclyde Institute of Pharmacy and Biomedical Sciences (SIPBS), University of Strathclyde, Glasgow, for measuring the high resolution mass (HR-ESI-MS) for the previously reported pterosins and pterosides.
- ✓ Dr Graham J. Tizzard and Simon J. Coles, UK National Crystallography Service, School of Chemistry, University of Southampton, Southampton, UK, for determining the absolute stereochemistry of six compounds through single x-ray crystallography.
- ✓ Dr Derren Heyes from Manchester Institute of Biotechnology (MIB), Faculty of Life Sciences, University of Manchester, Manchester, UK, for his assistance to measure the CD spectra for all the isolated compounds.
- ✓ Dr Alex F. Drake from Biomolecular Spectroscopy Centre, Pharmaceutical Optical & Chiroptical Spectroscopy Facility, King's College London, London, UK, for his outstanding interpretation of the Circular Dichroism results.
- ✓ Dr Stephania Christou from MBI, School of Chemistry, University of Manchester, UK, for measuring the specific optical rotations for the previously unreported compounds.
- ✓ Mark Fowler and Mark Berry from Strategic Science Group, Unilever R & D Colworth, Bedford, UK, for assisting with anti-diabetic activity (Glucose Transport Assay) for six selected pterosins and pterosides.
- ✓ Dr Diane Irvin, Syngenta, UK for assessing pesticidal activity.
- ✓ Dr Carol Clements from SIPBS, University of Strathclyde, Glasgow, for biological screening including antibacterial activity (MRSA, *Klebsiella pneumonia*, and *Mycobacterium marinum*) and antitrypanosomal assay (*Trypanosoma brucei brucei*).
- ✓ Professor Steve Kelly's Group from Centre for P450 Biodiversity, College of Medicine, University of Swansea, for assisting with antifungal assays using *Candida albicans strains*.
- ✓ Professor Karl Hoffman and Dr Helen Whiteland from IBERS, Aberystwyth University for assessing the antihelminthic activity of 20 pterosins and pterosides funded through the National Research Network.
- ✓ Dr Ana Winters from IBERS, University of Aberystwyth, for conducting the HPLC-ESI-MS^n analysis of methanol extract of bracken rhizomes.

- ✓ The Kurdish Ministry of Higher Education and Scientific Research - Kurdistan Regional Government (MHESR-KRG) for awarding me the scholarship to accomplish PhD Degree in Chemistry. Without this, the study would not have been possible.
- ✓ My relatives, acquaintances, colleagues and friends.
- ✓ My parents for their endless love and continuous prayers for me which gave me the strength and patience to complete my study.
- ✓ My brothers, Umed Hassan and Rasul Hassan, for their continued assistance in my home country.
- ✓ Last, but not least, I would like to express appreciation and special thanks to my beloved wife **Payam** who spent sleepless nights with me and was always my support in the moments when there was no one to answer my queries. Words cannot express how grateful I am to her for all of the sacrifices that she has made on my behalf throughout this study.

Table of Contents

List of Tables

List of Figures

List of Figures in Appendices

Abbreviations and Acronyms

ACN	Acetonitrile
amu	Atomic mass unit
CC	Column chromatography
CD	Circular dichroism
COSY	Correlation spectroscopy
d	doublet
dd	doublet of doublet
Da	Dalton
DAD	Diode array detector
DEPTQ	Distortionless enhancement by polarisation transfer
DW	Dry weight
ELSD	Evaporative light scattering detector
EtOAc	Ethyl acetate
Et_2O	Diethyl ether
FA	Formic acid
FC	Flash chromatography
FT-ICR-MS	Fourier transform ion cyclotron resonance mass spectroscopy
FT-IR	Fourier transform infrared
FW	Fresh weight
GLUT	Glucose transporter
h	hours
HR-ESI-MS	High resolution electrospray ionisation mass spectroscopy
IR	Infrared
J	Coupling constant
EC_{50}	Half maximal effective concentration
HPLC	High performance liquid chromatography
HMBC	Heteronuclear multiple-bond correlation
HSQC	Heteronuclear single quantum correlation
HSQC-TOCSY	Heteronuclear single quantum coherence - Total correlation spectroscopy
Hz	Hertz

LOD	Limit of detection
LOQ	Limit of quantification
Me	Methyl
MHz	MegaHertz
min	minutes
mL	millilitres
MIC	Minimum inhibitory concentration
MeOH	Methanol
MRSA	Methicillin-resistant staphylococcus aureus
MWt	Molecular weight
MS	Mass spectroscopy
NOESY	Nuclear overhauser effect spectroscopy
NMR	Nuclear magnetic resonance
ºC	Degrees Celsius
P. aquilinum	*Pteridium aquilinum*
ppm	part per million
q	quartet
r	Correlation coefficient
R_f	Retention factor
RP	Reverse phase
RRt	Relative retention time
rpm	Revolutions per minute
RSD	Relative standard deviation
s	singlet
Subsp.	Subspecies
SEM	Standard error of the mean
SGLT	Sodium-dependent glucose transporter
SPE	Solid phase extraction
t	triplet
TIC	Total ion current
TLC	Thin layer chromatography
TMS	Tetramethylsilane
UV	Ultraviolet

Abstract

An intensive study was undertaken in order to isolate and identify bioactive compounds in bracken, *Pteridium aquilinum* (L.) Kuhn (Dennstaedtiaceae). A systematic phytochemical investigations of the underground rhizomes of this plant afforded thirty-five pterosins and pterosides along with the main carcinogen in bracken, ptaquiloside, 5-hydroxyisocalamene and 5-(*β*-hydroxy)ethyl-2, 2, 4, 6-tetramethyl-1, 3-indandione. By detailed analysis of one- and two-dimensional nuclear magnetic resonance spectroscopy, circular dichroism and high-resolution mass spectrometric data, thirteen previously undescribed pterosins and pterosides have been identified. Interestingly, for the first time 12-*O*-*β*-D-glucopyranoside substituted pterosins, rhedynosides C and D, and the sulfate-containing pterosin, rhedynosin H, alongside the two known compounds, *trans*-histiopterosin A and (2*S*)-pteroside A2, were isolated from the rhizomes of subsp. *aquilinum* of bracken. In addition, the six-membered cyclic ether pterosins and pterosides rhedynosin A and rhedynoside A are the first examples of this type of pterosin-sesquiterpenoids. Additionally, the three previously reported compounds [(2*S*)-rhedynosin I, (2*S*)-2-hydroxymethylpterosin E and (2*S*)-12-hydroxypterosin A] were obtained for the first time from plant source as opposed to mammalian metabolic products. Single crystal X-ray diffraction analysis was applied to the previously undescribed compounds (2*R*)-rhedynoside B, (2*R*)-pteroside B and (2*S*)-pteroside K, yielding the first crystal structures for pterosides, and three known pterosins, (2*S*)-pterosin A, *trans*-pterosin C and *cis*-pterosin C. Rhedynosin C is the only example of the cyclic lactone pterosin with a keto group at position C-14. Six selected pterosins ((2*S*)-pterosin A, (2*R*)-pterosin B and *trans*-pterosin C) and associated glycosides ((2*S*)-pteroside A, (2*R*)-pteroside B and pteroside Z) were assessed for their anti-diabetic activity using an intestinal glucose uptake assay; all were found to be inactive at 300 µM.

A simple, reproducible and rapid reverse phase high performance liquid chromatography (RP-HPLC) method was developed which was linked to the UV detection source. The method validated for quantification of pterosin B and pteroside B in different plant matrices, soil and water samples. A new solid phase extraction (SPE) method was developed and established for sample preparation based on using 500 mg Supelco-SPE cartridges. The RP-HPLC was performed with mobile phase containing 0.1% formic acid (FA) in water and 0.1% FA in acetonitrile with an appropriate gradient and a flow rate of 1 mL/min. Detection of the analyte peaks was performed at 254 nm. The method showed

good linearity (correlation coefficient (r) > 0.99), and appropriate limit of detection (LOD) and limit of quantification (LOQ). The proposed RP-HPLC-UV method has a retention time of 20 min (3 samples/h).

Overall, this work focuses on the application of SPE–HPLC-UV analysis to quantify pterosin B and pteroside B in different matrices including soil, water and bracken samples. The method involves pre-concentration and clean-up by SPE cartridges. Final analysis of the selected compounds was carried out by the developed HPLC-UV method.

The extraction efficiency was checked by recovery experiment while the accuracy of the method was tested by relative standard deviation (% RSD). Recoveries were ranged from 90.29 to 96.23 % (pterosin B) and 93.64 to 101.03 % (pteroside B). The RSD (%) for both target analytes (pterosin B and pteroside B) was less than 2.5 % for all the analysed bracken stem samples. Preliminary results demonstrated that the present method was suitable for determination of pterosin B and pteroside B in bracken tissues, soil and water samples.

The simplicity, accuracy and sensitivity of the developed SPE-HPLC-UV method, recommending that the method is also convenient and useful for quick check and detection of trace amounts of pterosin B and pteroside B in water, soil and plant samples. The quantification of pterosin B and pteroside B was applied to bracken, divided into rhizomes, stems and fronds, the top soil of the sample cores and a set of water samples. The rhizome contained the largest concentration of pteroside B through the completed bracken growth period (750-2950 mg/kg). Its concentration was approximately one order of magnitude above pterosin B (10-245 mg/kg). The above ground stems and fronds showed distinct increases in concentrations of pterosin B (*ca.* 500 mg/kg) and pteroside B (*ca.* 250 mg/kg) at the time of crosier emergence, that were about one order of magnitude higher than the other samples collected during the growth periods. The soil sampled reflected the increased mobilisation of pterosin B during the onset of above ground growth (May to June) while no pteroside B was detected. The absolute pterosin B concentrations determined were about three orders of magnitudes lower (0.02-0.3 mg/kg). Water samples that drain bracken covered areas were found to contain pterosin B between 9-47 ng/L and pteroside B in range of 16-85 ng/L. Overall, the seasonal variation of pterosin B and pteroside B showed that the compounds are stored in the rhizome, preferably as the glycoside, and are mobilised to protect the early tissue as a means of chemical defence. The stability of pterosin B was exemplified by its environmental presence in plant, soil and water.

CHAPTER ONE

BRACKEN

1. INTRODUCTION

1.1. BRACKEN (*PTERIDIUM AQUILINUM*)

The term 'bracken' is used as a common name for the four *Pteridium* species (*P. aquilinum*, *P. caudatum*, *P. esculentum* and *P. semihastatum*) belonging to the Dennstaedtiaceae family (Marrs and Watt, 2006; Rasmussen et al., 2015). This is in agreement with Thomson's revision which classifies bracken into four species: a) the most dominant northern hemisphere *P. aquilinum* comprising eleven subspecies (*latiusculum*, *lanuginosum*, *pseudocaudatum*, *feei*, *japonicum*, *decompositum*, *wightianum*, *aquilinum*, *pinetorum*, *capense*, *centrali-africanum*); b) *P. esculentum*, predominates mostly in the Southern hemisphere, consisting of two subspecies (*arachnoideum* and *esculentum*); c) *P. caudatum* of Central and South America and d) *P. semihastatum* of South-East Asia and Australia (Marrs and Watt, 2006; Thomson and Alonso-Amelot, 2002; Thomson, 2008). However, Tryon's review concluded that bracken fern is a single species *Pteridium aquilinum* including two main subspecies, subsp. *aquilinum* and subsp. *caudatum*, with twelve varieties between the two subspecies (Marrs and Watt, 2006; Tryon, 1941). In Britain two species of bracken, *P. aquilinum* subsp. *aquilinum* and *P. aquilinum* subsp. *pinetorum*, are recorded. The vast majority of bracken in Britain is made up by the former while the latter (the second subspecies) has only been found in a local area near Aviemore, Scotland's Highland region (Marrs and Watt, 2006). *P. aquilinum* is usually represented by *P. aquilinum* (L.) Kuhn with three different subspecies: *aquilinum*, *atlanticum* and *fulvum* (Page and Mill, 1995). Throughout the thesis the word bracken is used for *P. aquilinum*. The general life cycle of bracken fern (*Pteridium*) is illustrated in Figure 1 (Marrs and Watt, 2006).

In Britain, bracken fronds start to emerge in late spring (mid-May) and they become mature in late summer (late August to early September). Bracken fronds are usually getting premature senescence in autumn (October to November). Sporulation might be initiated by the end of July. Sporulation is a complicated process as in all parts of Britain bracken is not producing spores every year (Marrs and Watt, 2006; Rasmussen et al., 2013). The only factors that inhibit bracken growth and its distribution are severe conditions, such as extremely high temperature

and lack of moisture or waterlogging (Smith and Seawright, 1995). Bracken is mostly found on moderately acidic soils in Britain (Marrs and Watt, 2006; Rasmussen et al., 2015).

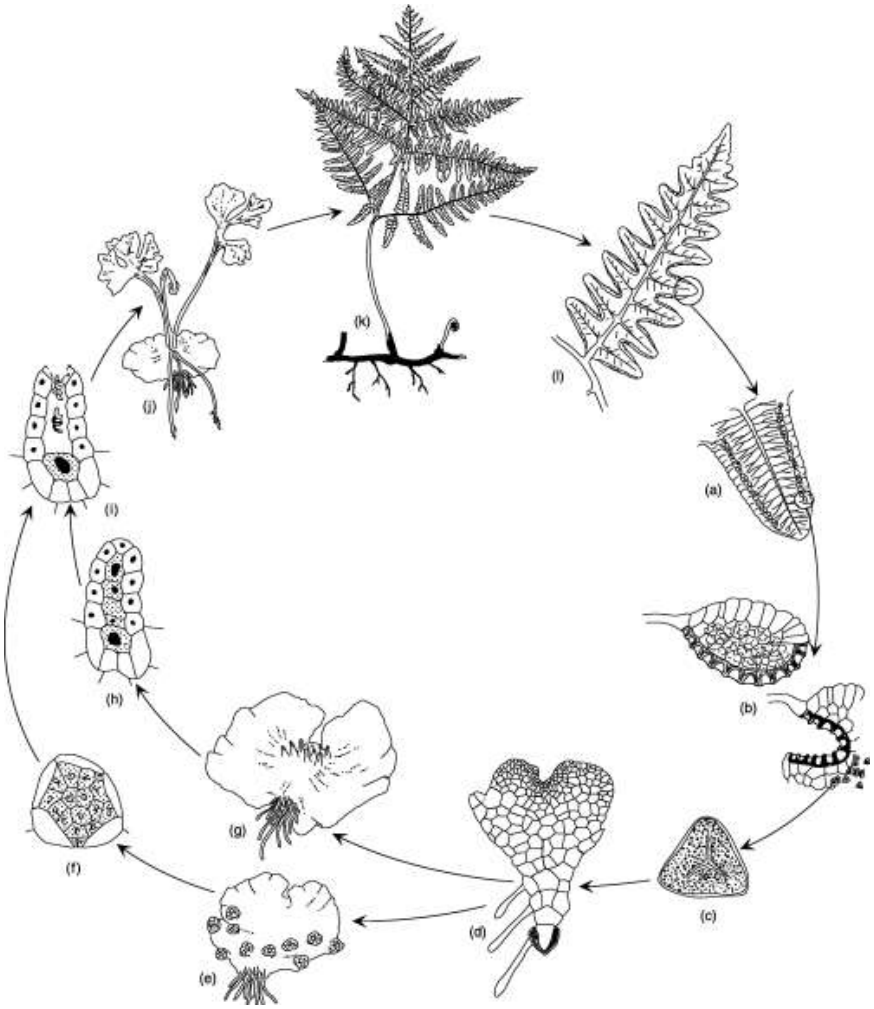

Figure 1: Generalized life cycle of bracken fern, *Pteridium*.

(a) Lower surface of a fertile leaf (pinnulet[1]); (b) Mature sporangium[2] before and after release of spores; (c) Spore; (d) Germinated spore; (e, f) Smaller young prothallus[3] with antheridia[4]; (g, h) Larger, older prothallus bearing archegonia[5]; (i) Spermatozoids[6] released from the antheridia move towards the mature egg cell; (j) Developing sporeling[7]; (k) The adult sporophyte[8] does not become fertile (l) before 3-4 years of age (Marrs and Watt, 2006).

[1] A secondary division of a pinnate leaf, especially of a fern.
[2] A receptacle in which asexual spores are formed.
[3] The gametophyte of ferns and other primitive plants.
[4] The male sex organ of ferns and other nonflowering plants.
[5] The female sex organ in bracken ferns.
[6] A motile male gamete produced by ferns.
[7] A young plant produced by a germinated spore.
[8] The asexual phase of the frond of a fern, producing spores from which the gametophyte arises

Globally, bracken (*Pteridium aquilinum* (L.) Kuhn) is one of the most widely distributed vascular plant species to date. In the United Kingdom, *P. aquilinum* subsp. *aquilinum* comprises the majority of bracken with a dense coverage estimated at 1.5-1.7 million hectares, which is equivalent to approximately 7% of the land surface in the UK, including sparse bracken (Pakeman et al., 1996; Robinson, 2009). This corresponds to 1.1 - 5 Gigatonne of plant material above ground and 5 - 20 Gigatonne of rhizome biomass [dry weight, calculated from data in (Marrs and Watt, 2006)].

In addition, bracken coverage is increasing annually by 1-3% in the UK (Rasmussen et al., 2003b). A higher frond biomass (> 1000 g/m^2) of subsp. *aquilinum* has been recorded in Britain in comparison with the Northern European countries, e.g. in Denmark the annual frond biomass reaches up to 460 g/m^2 (Marrs and Watt, 2006; Rasmussen et al., 2015, 2003b). Bracken fern is a ubiquitous plant and has the ability to start growing in forests and pastures all over the world (Fletcher et al., 2011). A change in methods of land management caused the apparent spread of bracken over the last 200 years in Great Britain. For instance, as a result of less demand in the use of bracken fern for a variety of purposes within the rural economy, bracken has spread (Marrs and Watt, 2006). Bracken rhizomes are located about 10 to 20 cm deep under the earth so they are protected against fire and frost. Bracken is an invasive species that can produce leaves even on burnt areas quickly. Because of its high canopy, it shadows out the surrounding areas and consequently reduces access to light for the other competitors or adjacent vegetation. Additionally, it is capable of suppressing the growth of other plants in the nearby vicinity by releasing allelopathic phytotoxins or secondary metabolites (Madeja et al., 2009).

1.2. ALTITUDINAL AND GEOGRAPHICAL DISTRIBUTION

Bracken, as described by Page in 1976, is the most widely distributed of the Pteridophytes. Bracken is a cosmopolitan genus (Madeja et al., 2009) and considered as one of the five most abundant plants on the earth (Shahin et al., 1999). It is described as a carcinogenic species (Gil da Costa et al., 2012). It has a global range as it occurs on all continents except at high altitudes, in desert regions and in Antarctica (Marrs and Watt, 2006; Page, 1976). Figure 2 mapped by H.R. Arnold shows the wide distribution of bracken in the British Isles. Bracken also has a widespread distribution in Europe which is illustrated in Figure 3 (Jermy et al., 1978; Marrs and Watt, 2006).

Bracken essentially remains in a temperate environment and occurs from sea level to over 3000 m, and at increasing altitude at lower latitudes. In the UK, the reported altitudinal limit for bracken is about 600 m (Marrs and Watt, 2006; Pearman and Corner, 2004).

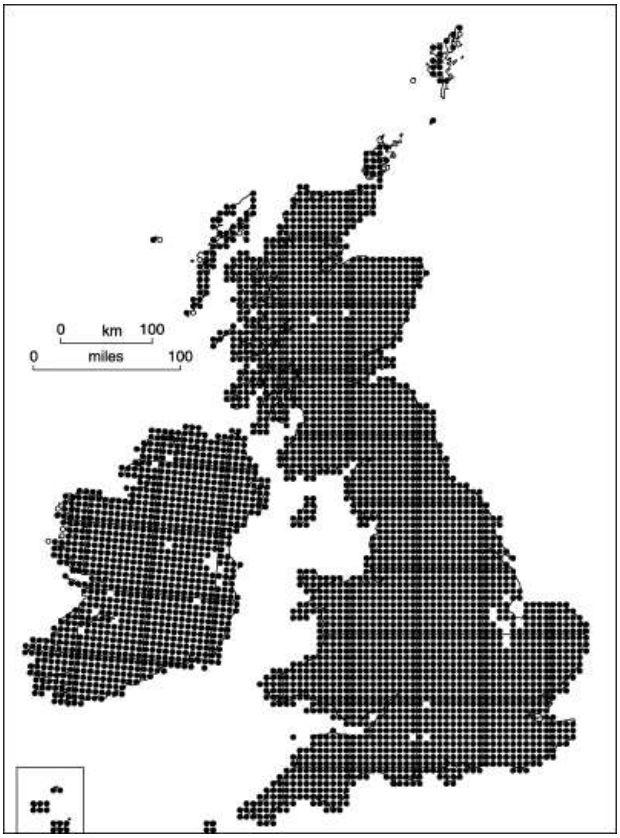

Figure 2: The distribution of bracken (*P. aquilinum*) in the British Isles. Each dot represents at least one record in a 10 km^2 of the British National Grid: (○) pre-1950, (•) 1950 onwards (Marrs and Watt, 2006).

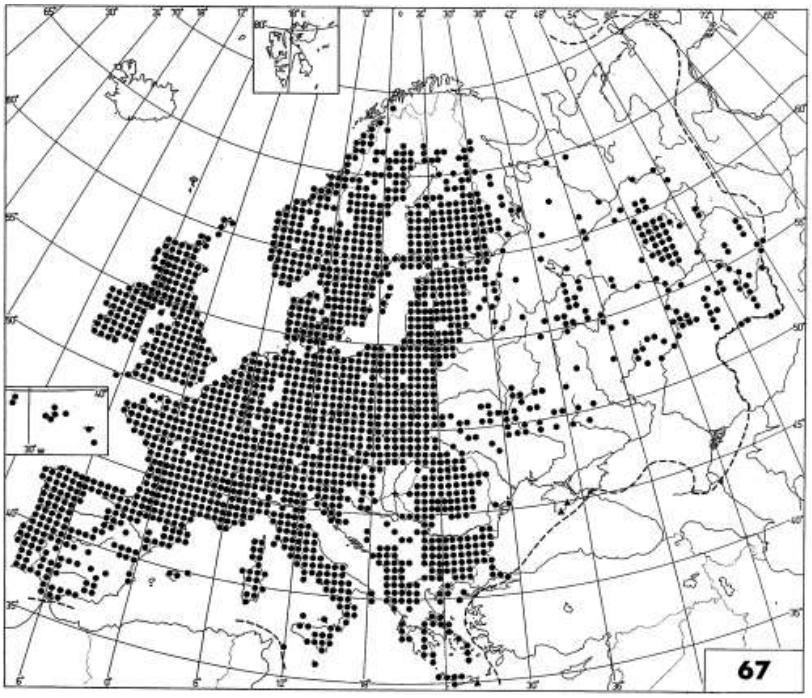

Figure 3: The European distribution of bracken (*P. aquilinum*) (•) on a 50 km^2 basis (Marrs and Watt, 2006).

1.3. HISTORICAL USES

Historically, bracken has been used for many purposes by mankind, including thatch roofing, animal bedding and soap production. Bracken ash was mixed with oil to make soaps and washing detergents. Potash was obtained by lixiviating bracken ashes after evaporating the solvent (water). It is a very rich source of potassium carbonate, hence, it was used in the manufacturing of soap, glass and bleaching. Moreover, people used bracken rhizomes for culinary purposes as an alternative food during shortages, because bracken rhizomes contain about 60% starch and were also used as a source of starch (Madeja et al., 2009; Rymer, 1976). Bracken has long been recognised for its potential pharmaceutical uses and its toxicity. Furthermore, bracken has been used medicinally as an anthelminthic agent (Marrs and Watt, 2006).

In many parts of the world, bracken rhizomes were dried and milled in the past and then mixed with flour to bake bread (Pieroni, 2005), particularly during famines, for example, in France during periods of war. In Great Britain, poor people used fern roots as a source of food to make bread. In Wales, the chopped dried fronds and rhizomes of bracken were mixed with hay and then given to animals pulling trams (horses and mules) as fodder in winter (Madeja et al., 2009; Rymer, 1976). Bracken was used as a human food in Scotland during the First World War (Fenwick, 1988). Up to the 1930s, a kind of porridge (called *gofio*) was prepared in the Canary Isles by mixing ground rhizomes with barley meal (Pieroni, 2005).

In Asia, mainly Japan and Korea, where bracken is part of the diet, an archaic method is used to get rid of the toxic compounds present in bracken crosiers. In this method, young shoots of bracken, with addition of ash, are soaked in water for a day, then boiled and afterwards served and consumed as a vegetable or as a soup (Madeja et al., 2009; Pieroni, 2005). A kind of beer has been produced from bracken fern shoots by native peoples in North America and Siberia. Shepherds in the Mediterranean frequently use bracken leaves to filter sheep's milk and to store freshly made ricotta cheese (unsalted Italian cheese) (Pieroni, 2005).

In Brazil, Canada and Japan, bracken crosiers are known as *broto de samambaia*, as "fiddleheads", and as *warabi*, respectively, where populations use crosiers as a delicacy (Gil da Costa et al., 2012). People used bracken fern commercially in Canada, China, Siberia, parts of the USA and Japan as a food or herbal remedy. During the 1970s, the annual consumption of bracken in Tokyo was 300 tonnes, also Hirono (1986) stated that 13000 tonnes / year of bracken fern in salted form is imported into Japan (Fenwick, 1988).

In the middle of the 15th century, dried and powdered bracken rhizomes were used in folk medicine due to their chemical properties. The drug was prepared and administered by dissolving the powder in wine or honeyed water. It was known for its anti-parasitic and anti-ascaris properties because of its ability to kill small intestinal ascaris roundworms in the body (Madeja et al., 2009). Another use of bracken was that a mixture was made of residue of burnt bracken leaves (cinder) and a small quantity of olive oil which was used as a treatment for livestock by applying it to bite wounds caused by wolves (Guarrera et al., 2005).

Composted bracken can provide an extremely useful peat alternative for horticultural uses (Pitman and Webber, 2013) and is still used nowadays in the United Kingdom for this purpose (Gil da Costa et al., 2012; Sanderson and Prendergast, 2002). It has been reported that composting is effective in destroying toxins in bracken, especially ptaquiloside (Gil da Costa et al., 2012). For example, during 1992-1993 about 1500 cubic meters of bracken were composted and the quantity doubled in the following year (Gil da Costa et al., 2012; Potter and R.M. Pitman, 1994). The maximum bracken biomass reported was 11.12 tonnes wet weight per hectare. The global increase of land covered with bracken potentially raises the contact of bracken with both human society and domestic animals (Smith et al., 1994). As a consequence, it is thought that bracken toxicity passing into ruminants may affect human populations as well (Gil da Costa et al., 2012).

1.4. HUMAN AND PUBLIC HEALTH RISKS

Bracken fern (*Pteridium*) is a well-recognized vascular plant that can cause a variety of severe health issues in animals (Alonso-Amelot and Avendaño, 2001; Fenwick, 1988). There are only a few other higher plants as well-known as bracken to cause cancer naturally in vertebrates (Shahin et al., 1999). Studies on the carcinogenic nature of bracken fern have recently been undertaken (Galpin et al., 1990; Wilson et al., 1998). The lethal properties of bracken for cattle were reported for the first time at the end of 19th century and its carcinogenicity was discovered in 1960 (Kigoshi et al., 1989). Poisoning of animals such as caprine, bovine and equine livestock by bracken has long been recorded and is known as “bracken poisoning” (Alonso-Amelot and Avendano, 2002). A water soluble norsesquiterpene glycoside ptaquiloside, is the major carcinogen in bracken (Smith and Seawright, 1995). Phytochemical studies of bracken are most often concerned with ptaquiloside, because of its established carcinogenicity (Fenwick, 1988; Hirono, 1986). Significant health concerns have been raised for both human populations and grazing domestic animals and have been linked with bracken fern (*Pteridium* genus) due to the presence of ptaquiloside (Fletcher et al., 2011).

In the absence of alternative nutritious feed, young bracken fern will readily be consumed by domestic herbivores and pigs as the juvenile parts are soft and easy to cut effortlessly. Depending on the age and species of the animals, bracken availability (quantity and quality) and the duration and rate of consumption, a number of disease syndromes might occur in animals. Acute bracken poisoning happens frequently in livestock, particularly in cattle, and to a smaller extent in sheep as a result of the toxic substances in bracken which usually target the faster dividing animal cells (Shahin et al., 1999). It has been researched and demonstrated that direct consumption of bracken fern by cattle causes diseases such as bovine enzootic haematuria (Rasmussen et al., 2015; Somvanshi et al., 2006).

Most toxic compounds are accumulated in fronds and crosiers which are preferred by grazing animals (McGlone et al., 2005; Rasmussen et al., 2003b). There is a probability that both animals and people may be affected and suffer from diseases caused by direct or indirect exposure to bracken (Alonso-Amelot and Avendaño, 2001). This fact was confirmed by Agnew and Lauren (1991) and Fletcher et al. (2011) who stated that considerable health problems for both humans and grazing domestic livestock are associated with bracken fern around the globe. Consequently, numerous governmental reports have been published concerning the protection of the public health against bracken toxins. For example, the British Committee[9] on Toxicity of Chemicals in Food, Consumer Products and the Environment (COT), has recently addressed the risks of contaminated food products with ptaquiloside, in particular the milk of farm animals (Attya et al., 2012; Gil da Costa et al., 2012). Ptaquiloside was identified in both the milk and the meat of domestic animals which fed on a substantial portion of bracken (D'Mello, 1997; Francesco et al., 2011). Alonso-Amelot et al. reported that approximately 8.6 ± 1.16 % of the total amount of ptaquiloside ingested by cows is effectively excreted into milk (Alonso-Amelot et al., 1998; Rasmussen et al., 2003b). It is important and necessary to recognise bracken as a carcinogenic plant at all stages of ingestion (Gil da Costa et al., 2012). As bracken contains high amounts of ptaquiloside, care should be taken to avoid farm animals accessing territories covered by bracken and consequently protecting them from grazing on emerging toxic crosiers (Rasmussen et al., 2015).

Epidemiological studies showed a positive correlation between the occurrence of stomach cancer and exposure to bracken in rural areas of North Wales (Galpin et al., 1990; Rasmussen

[9] It is an independent scientific committee that provides advice to the Food Standards Agency, the Department of Health and other Government Departments and Agencies on matters concerning the toxicity of chemicals.

et al., 2003b) and Costa Rica (Smith and Seawright, 1995), especially between people who spent their childhood in bracken-infested areas.

It has been evaluated that the rate of gastric cancer is directly increased in areas where bracken is consumed (relative risk or risk ratio of 2.34). In other regions, where bracken is not eaten directly by people, a lower figure of gastric cancer rate was recorded (relative risk of 2.09) (Alonso-Amelot and Avendaño, 2001; Galpin et al., 1990; Hirono et al., 1972). Because of this observation, milk has been suggested as the carrier (Bonadies et al., 2004) as it has been reported that ptaquiloside is not destroyed completely after heating or cooking or by pasteurisation (Attya et al., 2012) and remains as a chemical residue in agricultural products. It has also been noticed that ptaquiloside withstands eighty degree centigrade for three hours (Smith and Seawright, 1995). However, concentrations of ptaquiloside in milk have been shown to decrease by pasteurisation (50%) and by boiling (75%). Based on these findings, rural populations, who are suspected of being exposed to considerable amounts of ptaquiloside, are advised to boil milk before drinking it (Gil da Costa et al., 2012; Oliveira, 2012; Tourchi-Roudsari, 2014).

Human populations in the world are exposed to bracken carcinogenicity via multiple sources (Gil da Costa et al., 2012): Either eating bracken as a traditional dish (directly), or indirectly through water, animal products (meat and milk derived from bracken fed cows), inhalation and ingestion of bracken spores, and insect vectors (Wilson et al., 1998).

As a connection between human health and ptaquiloside, ptaquiloside has long been suspected to lead to neoplasia in humans (i.e. formation of new abnormal growth tissues), either directly via bracken consumption or indirectly from secondary sources through environmental contamination. For instance, ptaquiloside was detected in the surface-water, groundwater and soils in areas where bracken is dominant (Fletcher et al., 2011; Yamada et al., 2007). In high bracken coverage countries, in particular Venezuela, a considerable increase (high percentage) of human gastric cancer has been identified in bracken-rich areas (Alonso-Amelot and Avendaño, 2001), and it is thought that the reason behind this is ptaquiloside which comes from spores during sporulation every year. The assumption being that the spores might be inhaled and also lead to contamination of soil and surface water (Wynn et al., 2000). Moreover, Evans and Galpin (1990) investigated that there is a link between spores and occurrence of leukaemia as they stated that ‘‘the sporulation of bracken is regional and influenced by several factors, but one good sized frond can yield 1.0 g of the brown powder, enough to produce leukaemias in 5 susceptible mice’’.

The potential risks of bracken to public health have been recognised since Evans and Mason's experiment in 1965 indicated the carcinogenicity of bracken as it showed the development of cancer (adenocarcinoma of the mucosa) in rats which had been fed bracken (Hirono et al., 1984a, 1983). Also, Pamukcu and coworkers demonstrated that the bracken carcinogen is excreted in the milk and urine of cows had been fed bracken and not present in the milk of cows which did not have access to bracken in their diet (Pamukcu et al., 1978).

Ptaquiloside readily alkylates the DNA in animals (Ojika et al., 1987) and this causes the carcinogenic behaviour of ptaquiloside (Prakash et al., 1996). According to recent findings, ptaquiloside was detected indirectly by using HPLC-UV method in liver (up to 0.75 µg/g), kidney (up to 1.16 µg/g) and skeletal and cardiac muscles (<0.2 µg/gm) of livestock, in particular calves, 15 days after bracken consumption ended (Fletcher et al., 2011; Gil da Costa et al., 2012).

As stated by the International Agency for Research on Cancer (IARC), bracken is categorized as a cancer-causing plant to animals and probably carcinogenic to people. The Dutch government believed that ptaquiloside should be deemed as a carcinogenic compound to human society (Gil da Costa et al., 2012).

Due to its carcinogenic influences on mammals, such as humans, ptaquiloside caused environmental concerns (D'Mello, 1997). The carcinogenic function of ptaquiloside and its responsibility for tumours in the urinary bladder in cows has been shown in laboratory experiments (Attya et al., 2012). Hence, a significant concern has been raised for humans due to the existence of ptaquiloside in secondary products such as milk and honey (Ferguson and Philpott, 2008). Figure 4 shows the possible pathways of the human and environmental exposure to ptaquiloside (Oliveira, 2012).

There is a theoretical risk that bracken spores cause carcinogenicity in humans after inhalation and subsequent ingestion by people as spores have already been demonstrated to be carcinogenic in mice. The aerial spreading of the bracken spores and their inhalation is considered as another potential route for transfer of bracken carcinogen to human populations (Shahin et al., 1999). But apart from direct ingestion of spores, there have been no studies on the exposure of animals to air-borne spores (Wilson et al., 1998). A spatial relationship between bracken and cancer has also been studied in England and Wales (Shahin et al., 1999).

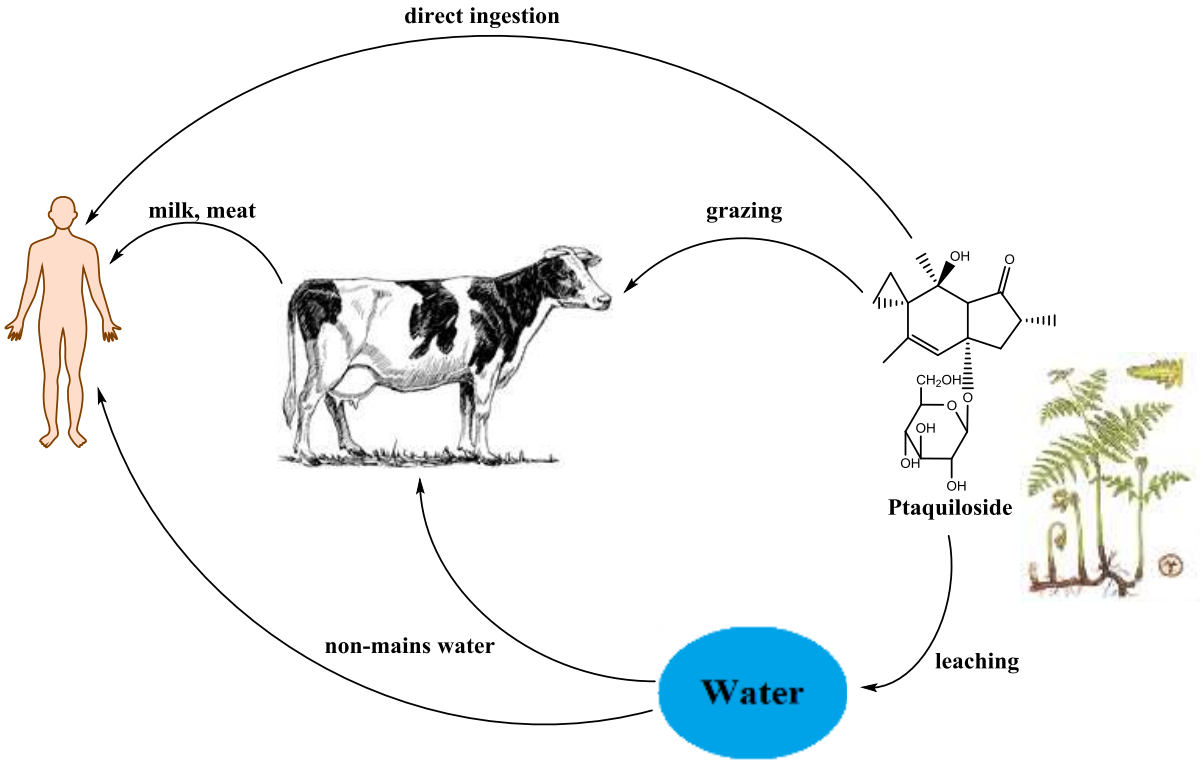

Figure 4: How ptaquiloside is exposed to the environment and human.

1.5. THE CHEMISTRY OF BRACKEN

Studies on the chemistry of bracken have commonly been concentrated on the concern of 'bracken poisoning' to livestock, bracken control and management as an unfavourable weed or its use as food and subsequent poisonous impacts on humans and animals. However, there have been studies on its distribution, its chemical composition and its taxonomy and the reasons behind is its ecological success (Cooper-Driver, 1976).

Bracken biosynthesis has a wide variety of heterogeneous secondary metabolites (Cooper-Driver, 1990). The compounds involve sesquiterpene indanones (pterosins and pterosides) (Hayashi et al., 1972; Hikino et al., 1970; Saito et al., 1989), ptaquiloside (Niwa et al., 1983; Ojika et al., 1985), quercetin (Hirono, 1986; Hirono et al., 1984b), phytoecdysteroids (Jones and Firn, 1978) [such as 20-hydroxyecdysone (Kaplanis et al., 1967; Wright et al., 1971)], and cyanogenic glycosides which release cyanide (Cooper-Driver et al., 1977). Some of these compounds are toxic and play an important role in protecting bracken against potential pathogens. This suggests that the chemistry of bracken should have played a vital role in the ecological success of bracken (Cooper-Driver, 1990).

1.5.1. PTAQUILOSIDE

The carcinogenic effects of bracken on domestic animals have been studied since the end of the nineteenth century. As a result of wide and intensive investigations of toxins in bracken, ptaquiloside was isolated and characterized by the Yamada group in 1983 in Japan as the major toxin in bracken. Meanwhile, ptaquiloside was also discovered and separated in 1983 by van der Hoeven et al. in the Netherlands and named it aquilide A. Ptaquiloside was obtained as a colourless and non-crystalline hygroscopic compound. Structural elucidation and stereochemistry of ptaquiloside were successfully achieved by Yamada and coworkers (Niwa et al., 1983; van der Hoeven et al., 1983; Yamada et al., 2007). Ptaquiloside is soluble in both water and ethyl acetate, and its partition ratio between these two solvents (aqueous and organic) is about 6:1 (H_2O-EtOAc) by weight (Ojika et al., 1987; Yamada et al., 2007).

Ptaquiloside has been isolated from different bracken ferns such as *P. aquilinum* and var. *latiusculum.* Its chemical structure has been fully elucidated in 1987 (Ojika et al., 1987). Ptaquiloside has also been found in some other fern genera such as *Pteris cretica, Prunus nipponica, Cheilanthes myriophylla, Dennstaedtia scabra, Histiopteris incisa, Cibotium harometz, Pityrogramma calomelanos, Pinus wallichiana, Prionospio oshimensis* and *Populus tremula* (Saito et al., 1989; Somvanshi et al., 2006). Toxicologically, ptaquiloside is the most interesting compound in bracken. The major carcinogenic properties of bracken fern is associated with ptaquiloside (Niwa et al., 1983; Smith and Seawright, 1995). Several methods have been developed for the determination and quantification of ptaquiloside in bracken samples (Rasmussen et al., 2003a). Ptaquiloside has also been quantified in biological samples (milk) (Francesco et al., 2011), soil and groundwater samples (Jensen et al., 2008).

Rasmussen et al. (2003b, 2015) stated that the ptaquiloside content in fronds from Denmark is related to the frond height and its exposure to light in the ecosystem, while different parameters determined the content of ptaquiloside in soil materials, e.g. the carbon content, the amount of bracken litter, precipitation and the size of bracken stands (Alonso-Amelot et al., 1992b; Rasmussen et al., 2003b). The amount of ptaquiloside in bracken fronds is highly changeable. It is known that ptaquiloside reaches the highest concentration in young crosiers when they emerge at the beginning of the growing season in spring. Afterwards, once the crosier stage is over, the concentration quickly diminishes to 10-20% of the maximum level (Rasmussen et al., 2015, 2003b). It is reported that the two main factors, rainfall wash-off and bracken die off, are most likely have the effect on decreasing of ptaquiloside concentrations in fronds (O'Driscoll et al., 2016).

All analysed parts of bracken, including fronds, roots and rhizomes, have shown to contain ptaquiloside. It has been reported that the contents of ptaquiloside in fronds ranged from 0.02 to 0.16% and higher than those in rhizomes, which ranged from 0.03 to 0.12% (calculated based on dry matter) (Saito et al., 1989). In general, the ptaquiloside content in rhizomes peaks after fronds reaches maturity. It was shown that rhizome content had a negative correlation with frond content at different locations if the ptaquiloside content was less than 400 µg/g in rhizomes. This outcome confirms the hypothesis that ptaquiloside transfers to the rhizomes at the end of the growth period (Rasmussen et al., 2015). It is found that the concentration of ptaquiloside in fronds of common bracken ferns globally was in the range of 60-10000 µg/g and up to 1200 µg/g in rhizomes (Rasmussen et al., 2003a; Smith et al., 1994). Rasmussen et al. (2013, 2015) found that the ptaquiloside content of bracken fronds in Britain ranged from 50 to 5790 µg/g and it is six-fold lower than the ptaquiloside content of fronds in other parts of the globe. Also they demonstrated that the concentration of ptaquiloside decreased as the fronds matured, and the maximum concentration was recorded in May. The underground rhizomes in Britain have also been analysed and found that the concentration range of ptaquiloside is 11-657 µg/g (Rasmussen et al., 2015). Rasmussen and coworkers (2003a) in Denmark have also shown that the highest content of ptaquiloside in Danish bracken fronds ranged between 213 and 2145 µg/g at the beginning of growth stage while rhizomes contained ptaquiloside concentrations in range of 11-902 µg/g at the end of the growth season. Ptaquiloside has been detected in soil materials in Denmark with the concentration range of 0.22–8.49 µg/g which was not in correlation with the content of ptaquiloside of fronds or rhizomes (Rasmussen et al., 2003a).

Kinetics of ptaquiloside hydrolysis in acidic and alkaline aqueous solutions (pH 2.88–8.93) at constant temperature (22 °C) has been studied by Ayala-Luis et al. (2006) and the following is an outline of their study. The hydrolysis of several natural toxins, including ptaquiloside, in aqueous solutions involves acid-catalysed, base-catalysed and neutral pathways. So, the rate law (rate equation) for the vanishing of ptaquiloside with time can be expressed as below:

$$\frac{d[PTQ]}{dt} = -k_A[H^+][PTQ] - k_N[PTQ] - k_B[OH^-][PTQ] \qquad (1)$$

Where d = the differentiation function, t = the reaction time, [PTQ] = ptaquiloside concentration, [H^+] = hydronium ion concentration, [OH^-] = hydroxide ion concentration, k_A = rate constant for acid catalysis, k_B = rate constant for base catalysis and k_N = rate constant for

neutral reaction. At constant pH, Equation 1 can be simplified to a pseudo-first order reaction as below:

$$\frac{d[PTQ]}{dt} = -k_{obs}\,[PTQ] \qquad (2)$$

$$k_{obs} = k_A[H^+] + k_N + k_B[OH^-] \qquad (3)$$

Where k_{obs} = the observed rate constant. A nonlinear relationship between k_{obs} and $[H^+]$ can be obtained from the rearrangement of Equation 3 into Equation 4:

$$k_{obs} = k_A[H^+] + k_N + k_B k_w[H^+]^{-1} \qquad (4)$$

where k_w = $10^{-14.1}$ at 22 °C.

Ayala-Luis and coworkers have also been carried out the experiment at different temperatures using a constant aqueous buffered solution of pH 4.46 (Table 1). They found that the rate constant of ptaquiloside (k_{obs}) is mainly dependent on pH of the reaction medium (see Table 1 and Figure 5). Also, they investigated that ptaquiloside is highly sensitive to the temperature, i.e. the temperature has a great impact on ptaquiloside hydrolysis. Based on that, it can be stated that the high rate constant of ptaquiloside will be available at high temperature, and therefore the possibility of ptaquiloside hydrolysis will be increased. They have been noticed that ptaquiloside hydrolysis follows first-order kinetics at all pH and temperature conditions.

Table 1: Apparent rate constants (k_{obs}) for ptaquiloside hydrolysis a) in different aqueous buffer solutions at 22 °C and b) in an aqueous solution of pH 4.46 at different temperatures.

a)	**pH**	**rate constant** (k_{obs}) h^{-1}
	2.88	4.34×10^{-2}
	4.03	2.61×10^{-3}
	4.46	1.53×10^{-3}
	5.07	1.01×10^{-3}
	5.47	3.71×10^{-4}
	6.07	1.26×10^{-3}
	6.77	5.57×10^{-3}
	8.93	2.46×10^{-1}
b)	**Temperature**	
	5 °C	1.80×10^{-4}
	13 °C	4.80×10^{-4}
	35 °C	4.15×10^{-3}

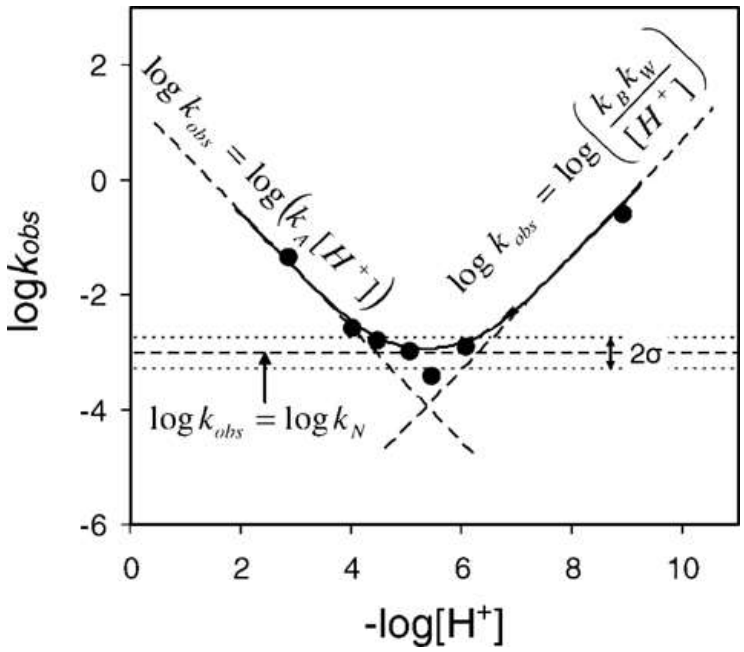

Figure 5: Hydrolysis of ptaquiloside as a function of pH (k_{obs}; h^{-1}). Solid line is extrapolated from nonlinear regression fit of Equation 3. σ represents standard error of log k_N (Ayala-Luis et al., 2006).

As shown in Table 1, ptaquiloside is the most stable and has a lowest reaction rate in aqueous solution of pH 5.47 at 22 °C. Based on Equation 4, the researchers also shown the experimental data and the corresponding nonlinear-regression curve by plotting $\log k_{obs}$ versus $-\log[H^+]$ as illustrated in Figure 5. Ultimately, Ayala-Luis's group concluded that ptaquiloside hydrolysis is dominated by the acid-catalysed reaction at pH < 4.43, while at pH > 6.93 the overall reaction is dominated by base-catalysed reaction. In addition, in the pH range of 4-7, the hydrolysis of ptaquiloside is slow as it is mostly controlled by the neutral reaction. It can be summarized that ptaquiloside hydrolysis is readily occurred at certain circumstances such as low pH, high pH and higher temperatures with an activation energy (E_a) of 74.4 kJ mol^{-1}, while at slightly acidic solutions and low temperatures, the rate of ptaquiloside hydrolysis is the lowest. Rasmussen et al. (2005) has previously been mentioned this behaviour who investigated ptaquiloside degradation in Danish soils at 25 °C.

It is possible to transfer ptaquiloside to human populations via drinking water. It was reported that ptaquiloside has a very low octanol-water partitioning coefficient ($\log K_{ow} = -0.63 \pm 0.01$) and consequently it is highly soluble in water, and this shows the very poor affinity of ptaquiloside to be sorbed onto humic matters in soils (Rasmussen et al., 2005). As ptaquiloside is not sorbed in soil, leaching of ptaquiloside to deep soil layers and aquifers is most predominant especially in slightly acidic sandy soils and cold climates. Because of the high

solubility of ptaquiloside in aqueous solutions, it has been proposed that ptaquiloside may leach through the topsoil into drinking-water reservoirs, thus representing a concern for the public sector (Ayala-Luis et al., 2006). Based on this finding, ptaquiloside transferred from living or dead plant material to the soil environment by rain water will therefore be leached and contaminate the soil and groundwater (Rasmussen et al., 2005, 2003a, 2003b). Ptaquiloside is found to be stable in the soil environment for a few months in low temperatures (5 ºC) at pH range 4.0-6.5, while it was found that ptaquiloside degrades rapidly at pH below 4 and pH above 6.5. It is stated that ptaquiloside concentration in soils can be decreased significantly due to both microbial degradation and abiotic hydrolysis process (Ovesen et al., 2008). Furthermore, in the upper layers of soil, microorganisms cause degradation of ptaquiloside (Rasmussen et al., 2015). In addition, there are also other factors that have an influence on ptaquiloside degradation in soils, for example reactive humic substances, the existence of metal cations, or enzymatic processes (Ayala-Luis et al., 2006). Very recently, in order to assess the risk of ptaquiloside to drinking water, ptaquiloside has been quantified by using LC-MS method in receiving water at 3 drinking water abstraction sites in Ireland (1 surface water stream and 2 private spring wells). Ptaquiloside has been observed in all three receiving waters. The lowest and maximum ptaquiloside concentrations in water samples were detected, 0.01 µg/L in private spring well and 0.67 µg/L in surface water (O'Driscoll et al., 2016). Similarly, Clauson-Kaas and coworkers (2014) confirmed the presence of ptaquiloside in Danish groundwater in concentration up to 0.23 nmol/L (0.092 µg/L).

At room temperature, ptaquiloside is unstable in both acidic and basic solutions which ultimately convert ptaquiloside to 1-indanone compounds such as pterosin O or pterosin B with the release of D-glucose (depending on the type of solvent used) (Niwa et al., 1983; Ojika et al., 1987). Ptaquiloside gradually undergoes aromatization process in weakly acidic aqueous solutions to afford the main product, pterosin B, after releasing of glucose molecule (Figure 6) (Kigoshi et al., 1989; Niwa et al., 1983; Yamada et al., 2007). The mechanism of acid hydrolysis of ptaquiloside is illustrated in Figure 6 (Ayala-Luis et al., 2006).

In weakly alkaline aqueous solutions (pH 8-11), ptaquiloside is readily converted into ptaquilosin with liberation of D-glucose and subsequently an unstable and very high reactive intermediate product, called bracken dienone, is yielded quickly (Figure 7). The active form of ptaquiloside, bracken dienone, was found to be stable in basic solution at least for 60 minutes at 25 ºC while it is exceptionally unstable under weakly acidic aqueous solutions at room temperature and immediately transferred to pterosin B, a stable compound under all conditions

(Figure 7). The degradation of ptaquiloside in different buffer solutions has also been reported by Saito et al. in 1989, and found that the ptaquiloside half-life was around 7 days at pH 4.0 while at pH 5.5 and 7.0 (at 37 ºC) about 40% and 10% of the original concentration was degraded after one week, respectively (Rasmussen et al., 2003b; Saito et al., 1989). The half-lives of ptaquiloside in various conditions are shown in Table 2 (Ojika et al., 1987; Yamada et al., 2007). Saito et al. (1989) also studied the effect of sunlight on the stability of ptaquiloside in fronds, and found that less than 75% of the initial concentration of ptaquiloside was degraded after 6 weeks (Saito et al., 1989).

Table 2: Half-lives of ptaquiloside

Conditions	pH	Half-life
Solid state in dry atmosphere at low temperature (-20-0 ºC)	-	> 6 months
Solid state in dry atmosphere at room temperature	-	> 7 days
Aqueous solution of H_2SO_4 (5 mM) at 25 ºC	2.0	174 min
Aqueous solution of Na_2CO_3 (10 mM) buffer at 25 ºC	9.0	40 min
	10.0	6.3 min
	11.0	1.2 min

The reactions of biomolecules with ptaquiloside and its derivatives were discussed. Bracken dienone, through its highly reactive electrophile (cyclopropylidene ring), has been shown to react with nucleophiles such as water, alcohols, and aminoacids (methionine, cysteine) to produce a number of different adducts, e.g. DNA-adduct (Freitas et al., 2001; Ojika et al., 1987).

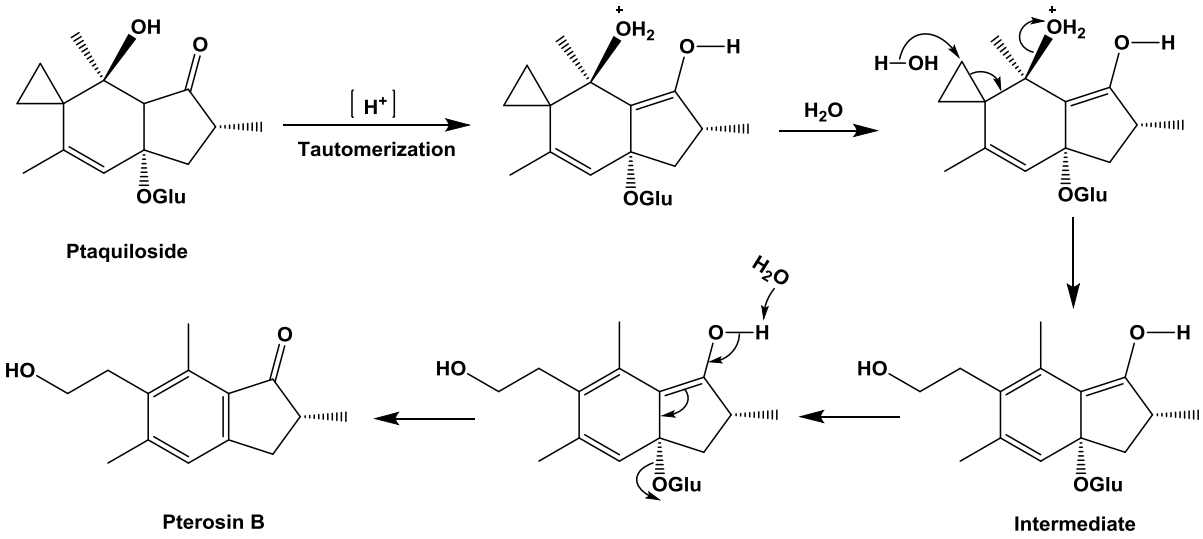

Figure 6: Proposed mechanism for the acid hydrolysis of ptaquiloside (Ayala-Luis et al., 2006).

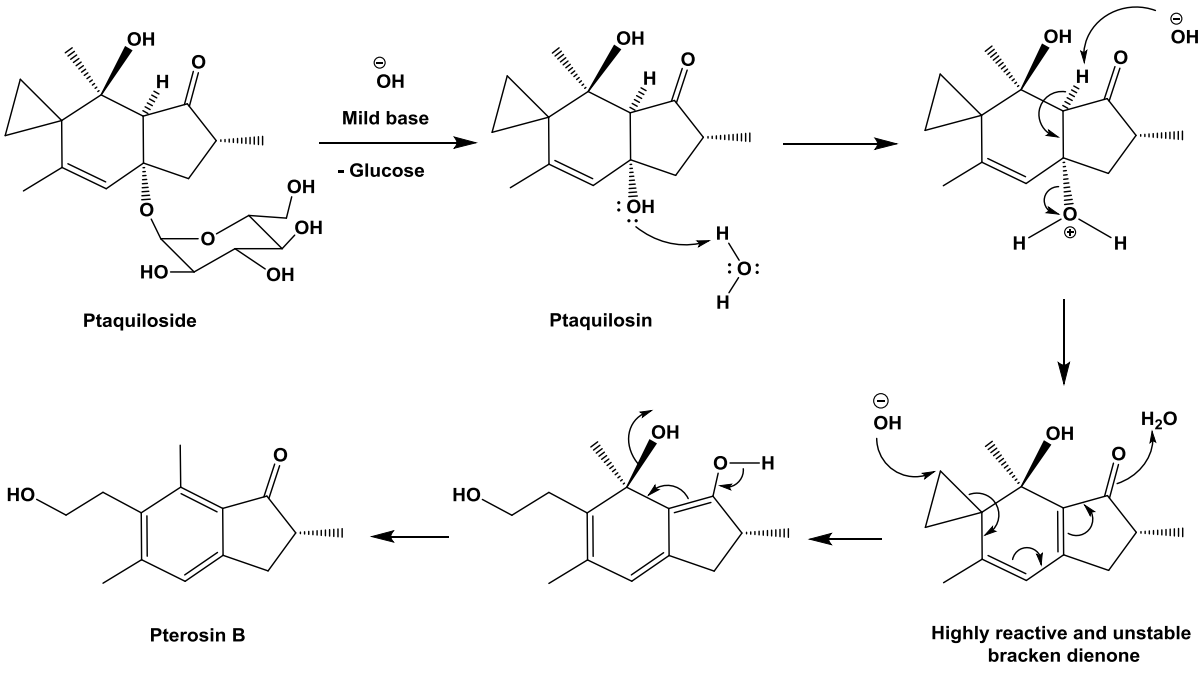

Figure 7: Schematic diagram of ptaquiloside degradation in alkaline medium.

1.5.2. PTEROSINS AND PTEROSIDES

Pterosins are a large group of compounds which are naturally occurring in different plant ferns including bracken (Sheridan et al., 1999). Pterosins are sesquiterpenoids and their structures are derivatives of 1-indanone skeletons (Figure 8). These compounds were first isolated from the bracken fern *Pteridium aquilinum* var. *latiusculum* (Pteridaceae) in Japan (Chen et al., 2015; Hikino et al., 1970). They have also been obtained from different subsp. of *Pteridium aquilinum* (Fukuoka et al., 1978; Kuraishi et al., 1985; Murakami et al., 1980; Sengupta et al., 1976; Tanaka et al., 1982; Yoshihira et al., 1971). Pterosins have been found to occur widely in various fern species (Hayashi et al., 1972; Kobayashi et al., 1975; Kuroyanagi et al., 1974a; Murakami et al., 1974; Sengupta et al., 1976), and apart from ferns, pterosins are also occurred in certain fungi of the class Basidiomycetes including *Cyathus bulleri* and *Fomes annosus* (Potter, D.M., Baird, 2000). During 1970-1975, more than 30 pterosins have been separated from different varieties of ferns. Some pterosins have been isolated as glucosides, named pterosides, while the others have been separated in the free state (Sengupta et al., 1976).

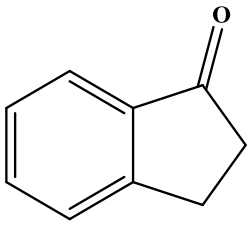

Figure 8: Chemical structure of 1-indanone.

Pterosins have been isolated from the extract of all parts of the bracken, for instance, they are found in bracken fronds (Fukuoka et al., 1978; Yoshihira et al., 1971) and rhizomes (Hikino et al., 1976; Kuroyanagi et al., 1979a). More than one type of pterosin will be available after hydrolysis of unstable precursor ptaquiloside. For example, as a result of acid-base treatment of the cleaned-up extracts of *P. aquilinum* Var. *caudatum*, pterosins A, B, K and Z along with ptaquiloside have been isolated using preparative high performance liquid chromatography (HPLC) and have been identified based on NMR data (Castillo et al., 1997). Pterosin A and B have been isolated in bracken fronds by Kovganko et al. in Belarus and they structurally elucidated using IR, UV and NMR data (Kovganko et al., 2004).

In the structural elucidation of the natural products, a challenging aspect is frequently related to the determination of the absolute configuration (Nugroho and Morita, 2014). In order to confirm the absolute stereochemistry of the isolated compounds described and

discussed in chapter three, two powerful techniques were utilized which are single crystal X-ray crystallography and Circular Dichroism (CD) spectroscopy. X-ray crystallography remains the definitive tool to determine the absolute configuration but requires crystals of the target compound. The application of X-ray crystallography is extensively utilized for the determination of molecular structure of the compound, when the molecules are organised in a regular crystalline array. No optics are required for this technique and it does not need strict resolution of the detector (Miao et al., 1999). X-ray diffraction analysis is necessary but has only been used twice for determining the absolute configuration of pterosin compounds. X-ray crystal analysis has first been reported for the natural product, pterosin H (Sheridan et al., 1990). Afterwards, the absolute configuration of (2*R*)-pterosin P has been determined by X-ray data (Ouyang et al., 2010). In this thesis, the structure of six isolated pterosins and pterosides including a novel compound (**RH10**) was determined by single crystal X-ray diffraction.

CD spectroscopy may offer an alternative approach to determine the absolute configuration of chiral compounds containing appropriate chromophores (Nugroho and Morita, 2014). CD spectroscopy is a technique that can be used to assign the configuration in solution with less than 1 mg of compound (Warnke and Furche, 2012). The UV and CD spectra in the 380 nm to 260 nm region associated with the keto group $n \rightarrow \pi^*$ transition can be complex. The presence of vibronic[10] effects (coincidental change of vibrational and electronic energy levels) may add further complexity to the signal, e.g., in form of additional shoulders in the UV spectra (see appendix IV). The corresponding CD spectra obey different selection rules. The CD associated with the $n \rightarrow \pi^*$ transition may mimic the absorption spectrum and be relatively plain or may be fine structured indicating the importance of particular vibronic progressions.

There are mainly two types of the electronic transitions in pterosin compounds, $n \rightarrow \pi^*$ and $\pi \rightarrow \pi^*$ transitions which are related to the carbonyl group (C=O) and phenyl ring, respectively. However, the absorption may relate to the Phenyl-carbonyl conjugated part ($\pi \rightarrow \pi^*$ or charge transfer) marked as an arrow in Figure 9.

[10] The Franck–Condon principle is a rule in spectroscopy and quantum chemistry that explains the intensity of vibronic transitions. Vibronic transitions are the simultaneous changes in vibrational and electronic energy levels of a molecule due to the absorption or emission of a photon of the appropriate energy. Electronic transitions are typically observed in the visible and ultraviolet regions, in the wavelength range approximately 200–700 nm (50,000–14,000 cm^{-1}), whereas fundamental vibrations are observed below about 4000 cm^{-1}.
Reference: https://en.wikipedia.org/wiki/Franck%E2%80%93Condon_principle

Pterosins and pterosides have been studied previously by Kuroyanagi and coworkers using CD spectroscopy. These compounds have shown CD Cotton effects associated with transition of electrons of conjugated ketones in the range of 260-380 nm. The stereochemistry of pterosin type compounds have then determined based on the electronic transitions present in the molecule (Kuroyanagi et al., 1979b).

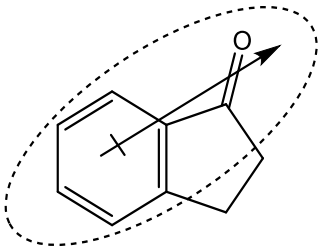

Figure 9: Electronic transition between phenyl ring and keto group in conjugated pterosin type compounds.

1.6. BIOLOGICAL ACTIVITY ASSESSMENT

Bracken has historically been associated with incidents of livestock poisoning (Hopkins, 1990; Vetter, 2009) resulting in many mechanistic studies on distinct pterosins and their biological targets. Many reports regarding the biological activities of pterosins and pterosides have been published during the last decades. For example, pterosins have shown the resistance against insects and pests (Cooper-Driver, 1990). In the middle of seventies, isolation of the active constituents, pterosins B and O, have been achieved from the fern *Pteris inaequalis*, and they tested for their antimicrobial activities, in which both pterosins B and O were found to inhibit the Gram-positive bacterium *Bacillus subtilis* at minimum inhibitory concentration (MIC) of 30 µg ml^{-1} (Kobayashi et al., 1975).

The carcinogenicity and cytotoxicity tests have been performed by Yoshihira and coworkers on some pterosins and pterosides, and the results showed that none of them were found to be carcinogenic, especially the major indanones pterosin B and pteroside B, as they did not induce tumour under the employed experimental conditions although some pterosins were cytotoxic to HeLa cells (Yoshihira et al., 1978). Pterosins B, F, H, I, O, Z, and V have been identified to show cytotoxic effects on a ciliate, *Paramecium caudatum*, and also caused abnormal development of the sea urchin embryos, however, in feeding experiments it was shown that these pterosins did not inhibit DNA synthesis of the sea urchin embryos (Kobayashi and Koshimizu, 1980). Wallichoside (3-*β*-D-glucoside of (2*S*, 3*S*)-pterosin C) has been isolated from *Pteris wallichiana* which grows in the Himalayan region, and it has been reported that

the *n*-butanol extract of the plant rhizomes exhibited appreciable activity against *Staphylococcus aureus* (Sengupta et al., 1976). The effect of pterosin B on chromosomes has been examined by incubation of pterosin B with HeLa cells at concentrations 100 and 32 µg/ml. While some effect on mitosis was evident, no morphological breakages have been observed. Pterosin B has also been found to inhibit the cellular uptake of DNA, RNA and protein precursors (Saito et al., 1976).

In general, pterosins are cytotoxic to cancer cell lines, but are inactive to antioxidant assays (Chen et al., 2008). Pterosins have shown bioactivities such as cytotoxic activities (Ouyang et al., 2010), antibacterial (Kobayashi et al., 1975), and antispasmodic (Sheridan et al., 1999). Furthermore, recently two pterosin dimers named bimutipterosins A and B, and dehydropterosin Q (Figure 10) were separated from *Pteris multifida* Poir and they exhibited moderate cytotoxic activities versus HL 60 cancer cells (human leukemia) with the half maximal inhibitory concentration (IC_{50}) values of 12.8, 26.6 and 58.7 µM, respectively (Liu et al., 2011). Pterosin B and (2*R*, 3*R*)-pterosin L 3-*O*-*β*-D-glucopyranoside have also been shown to have selective activity against HL 60 human leukemia cancer cells with the IC_{50} values of 8.7 and 3.7 µg/mL, respectively (Chen et al., 2008). Pterosin Z and calomelanolactone have been isolated from the aerial parts of the silver fern called ‘‘*Pityrogramma calomelanos* L.’’ in which the aqueous extract of this plant has been used as a treatment for venereal diseases in Guyana (Bardouille et al., 1978; Ng and McMorris, 1984). Pterosin Z has been shown a potent relaxant to smooth muscle with the half maximal effective concentration (EC_{50}) value of 1.3 ± 0.1 µM (Sheridan et al., 1999).

In addition, the interaction of bracken extract with vitamin C in human submandibular gland cells and oral epithelial cell lines has been assessed. The results demonstrated that the bracken extract was cytotoxic to both types of cells even in the presence of vitamin C, i.e. vitamin C did not have the ability to reduce DNA damage of the cells caused by bracken, and hence it was not capable to revert the toxicity effects (Campos-da-Paz et al., 2008).

The dependency of the biological effect of bracken extract in different cell assays has been evaluated. The cytogenetic effects of different bracken-fern extracts (hot water, cold water, hexane and ethanol extracts) have been investigated on chromosomes of bone-marrow and peritoneal cells of Swiss mice. The results showed that these extracts able to induce structural chromosome aberrations in both peritoneal and bone-marrow cells. Thus, it has been suggested that cytogenetic damage is induced by bracken fern through breaking DNA strands and consequently have an influence on chromosome segregation (Almeida Santos et al., 2006).

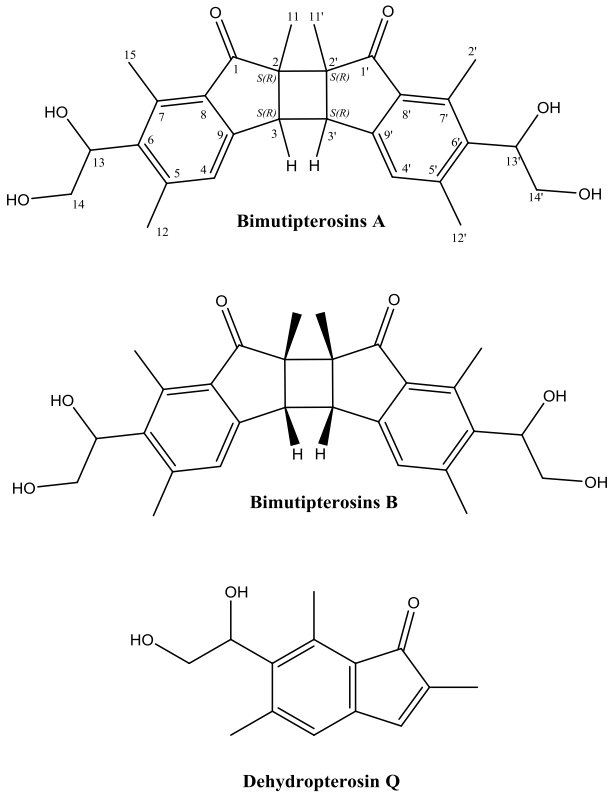

Figure 10: Chemical structures bimutipterosins A and B, and dehydropterosin Q from *Pteris multifida* Poir.

In addition, three other compounds from the aerial parts of *Pteris multifida* Poir have been isolated. They were named dehydropterosin B, (2*R*, 3*R*)-pterosin L 3-*O*-*β*-D-glucopyranoside and (2*S*, 3*S*)-pterosin C 3-*O*-*β*-D-glucopyranoside (Figure 11). These compounds were evaluated for their cytotoxicities against different human cancer cells including PANC-1, NCI-H446, LOVO and A549. They displayed significant inhibitory against NCI-H446 (small-cell lung cancer of human) cells with IC_{50} values of 5.19, 4.27, and 4.95 μM, respectively. They also demonstrated moderate cytotoxic effects on PANC-1 (pancreatic cancer of human) tumour cells with IC_{50} values of 14.63, 12.07, and 5.45 μM, respectively (Table 3). These outcomes support that pterosins might be played a vital role in development of cytotoxic actions toward cancer cell lines (Ouyang et al., 2010).

Table 3: Cytotoxic activities of the compounds against 4 different tumour cell lines

Compounds	IC_{50} (μM)			
	PANC-1	**NCI-H446**	**LOVO**	**A549**
dehydropterosin B	14.63	5.19	37.64	58.80
(2*R*, 3*R*)-pterosin L 3-*O*-*β*-D-glucopyranoside	12.07	4.27	29.11	37.61
(2*S*, 3*S*)-pterosin C 3-*O*-*β*-D-glucopyranoside	5.45	4.95	35.58	47.98

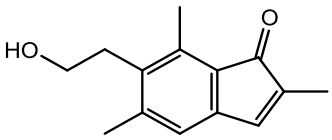

Dehydropterosin B

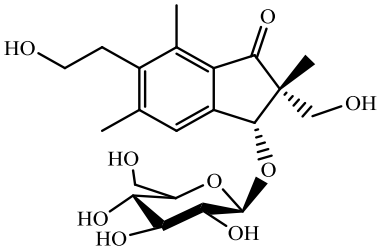

(2*R*,3*R*)-pterosin L 3-*O*-*β*-D- glucopyranoside

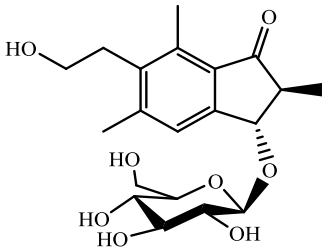

(2*S*,3*S*)-pterosin C 3-*O*-*β*-D- glucopyranoside

Figure 11: Chemical structures of dehydropterosin B, (2*R*, 3*R*)-pterosin L 3-*O*-*β*-D-glucopyranoside and (2*S*, 3*S*)-pterosin C 3-*O*-*β*-D-glucopyranoside from *Pteris multifida* Poir.

Pterosins are recently observed to possess anti-diabetic and anti-obesity activities. Several biochemical protocols have so far been patented utilising pterosin compounds to treat people living with diabetes and obesity, especially pterosin A. In the patent, a total of eighty four different pterosin compounds have been examined for their anti-diabetic and anti-obesity properties both *in vivo* and in *vitro*. The pterosin compounds used have been extracted and isolated from the natural plant sources, e.g. bracken, or prepared by a synthetic method. It has been stated that specifically 15 compounds including pterosins A, C, D, G, I, L, N, X and pteroside Z showed effectively biological activities against diabetes, type I (insulin-dependent diabetes) and type II (non-insulin-dependent diabetes). Among these 15 pterosin compounds, pterosins A, C, D, N, X, and pteroside Z are naturally occurring in different plant sources. The compounds have also been indicated to significantly enhance glucose consumption/uptake and the insulin sensitivity. It has also been suggested that pterosin compounds may activate GLUT4 (Glucose Transporter-4, the insulin-regulated glucose transporter) and in turn minimise the levels of blood glucose in diabetic mice (Hsu et al., 2014). Ultimately, Hsu et al. concluded that "Taken together, the preliminary results suggest that these compounds may activate AMPK, which in turn regulate insulin regulation of carbohydrate and fatty acid metabolism, and can be considered as a potential antidiabetic and antiobesity agent".

1.7. GLUCOSE UPTAKE IN THE BODY

The glucose transport cell model (detailed in section 4.2.1. and appendix V), is a novel *in vitro* cell system designed to mimic the localised changes in glucose concentration in the small intestine during the consumption of a carbohydrate rich meal (Figure 12) (Kellett and Brot-Laroche, 2005). Before the meal, the concentration of free glucose in the lumen of the intestine is low (< 5mM) and the apically expressed SGLT1 transporter actively transports any available glucose into the enterocyte. GLUT2 transporters are also active on the basolateral membrane of the enterocyte, transporting glucose from the blood into the cell to maintain cellular metabolism if required. During a meal, the local concentration of glucose begins to increase (5-10 mM) and is transported from the intestinal lumen by SGLT1 and subsequently into the systemic circulation via GLUT2. As a consequence of this initial glucose transport across the enterocyte, intracellular stores of GLUT2 are mobilised and targeted to the apical membrane. Shortly after the meal, very high local concentrations of glucose occur (25-100 mM) as the carbohydrate content of the meal is broken down into monosaccharides by alpha-glucosidase enzymes located on the apical enterocyte membrane. At these high levels of glucose, the high affinity, low capacity transporter SGLT1 becomes saturated and the majority of glucose transport across the enterocyte is due to the low affinity, high capacity GLUT2 transporters now present in the apical membrane. These localised changes in luminal glucose concentrations are mimicked *in vitro* through an initial short incubation of differentiated Caco-2 cells with a low level of D-glucose (5 mM for 15 mins) immediately followed by a sustained incubation with a high level of D-glucose (final concentration of 25 mM for 45 mins).

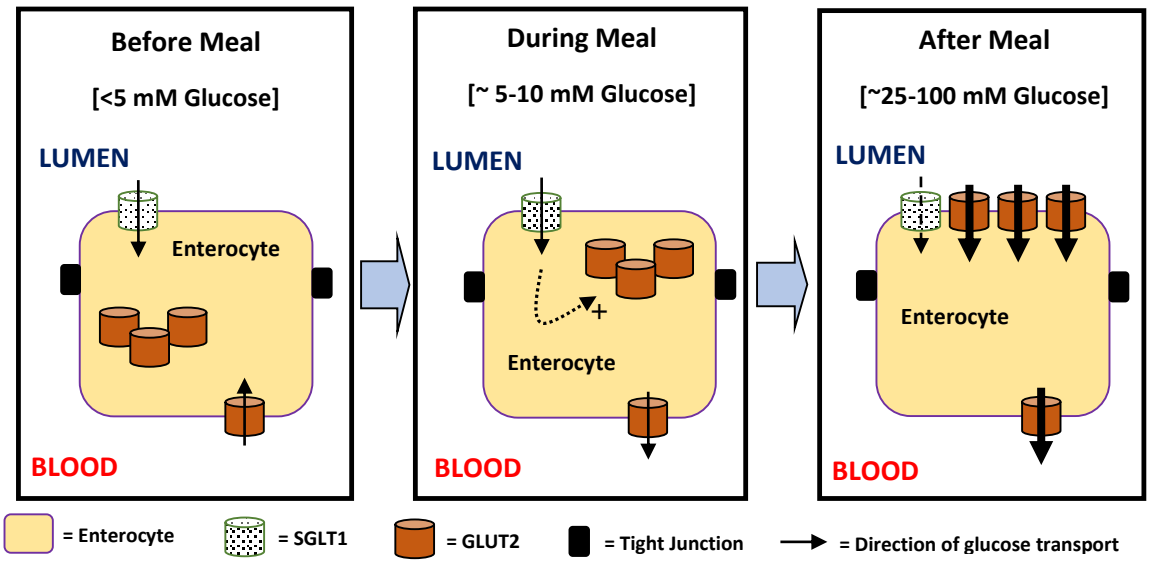

Figure 12: Glucose concentration timeline during a meal.

1.8. AIMS OF THE STUDY:

This PhD project ‘‘Pterosins and pterosides in bracken (*Pteridium aquilinum* (L.) Kuhn)’’ was aimed at the following:

1. Isolation of pterosins and pterosides from bracken rhizome.
2. Structural elucidation of isolated pterosins and pterosides, including the determination of their absolute stereochemistry.
3. Biological activity screening of isolated pterosins and pterosides.
4. Seasonal sampling of bracken (rhizomes, fronds and stems) and associated soil.
5. Development of a new method for sample preparation using SPE cartridges.
6. Development of a new HPLC-UV method for quantification of pterosin B and pteroside B in bracken rhizomes, fronds and stems alongside soil and water samples.
7. Seasonal variations of pterosin B and pteroside B in bracken and soil samples using the developed new SPE- HPLC-UV method.
8. Calculation of dry matter content and water percentage in the rhizomes, fronds and stems of bracken.

CHAPTER TWO

2. MATERIALS AND METHODS

2.1. SOLUTIONS AND REAGENTS

2.1.1. GENERAL LABORATORY CHEMICALS

All Chemicals used during isolation and structural elucidation of the compounds were purchased from Sigma Aldrich, UK.

Formic acid	Sigma Aldrich, UK
Acetic anhydride	Sigma Aldrich, UK
Phosphomolybdic acid (PMA)	Sigma Aldrich, UK
Dry pyridine	Sigma Aldrich, UK

2.1.2. HPLC GRADE SOLVENTS

HPLC grade solvents were used for all purposes in this study including extraction and chromatographic isolation of compounds in bracken rhizomes. All the solvents (2.5 L) were supplied by Fisher Scientific, UK.

Acetone	Fisher Scientific, UK
Acetonitrile (ACN)	Fisher Scientific, UK
Chloroform	Fisher Scientific, UK
Diethyl ether	Fisher Scientific, UK
Ethyl acetate	Fisher Scientific, UK
n-Hexane	Fisher Scientific, UK
Methanol	Fisher Scientific, UK
Water	Fisher Scientific, UK

2.1.3. DEUTERATED SOLVENTS FOR NMR ANALYSIS

All deuterated solvents, acetone-d_6 ($(CD_3)_2CO$, 99.9%), chloroform-d_1 ($CDCl_3$, 99.8%) and methanol-d_4 (CD_3OD, 99.8%), were purchased from Cambridge Isotope Laboratories, Inc., UK, and then they were used for NMR analysis as shown in Table 4. Norell® NMR capillary tubes [5 mm × 4.2 mm (O.D. × I.D.); 178 mm (L.)], were purchased from Sigma-Aldrich, UK.

Table 4: Deuterated solvents used in NMR experiments

Deuterated solvents	^{1}H shift (s) (ppm) (*multiplicity*)	^{13}C shift (s) (ppm) (*multiplicity*)	Trace water peak (ppm)
Chloroform-*d* ($CDCl_3$)	7.26 (*1*)	77.16 (*3*)	1.56
Methanol-d_4 (CD_3OD)	3.31 (*5*)	49.00 (*7*)	4.87
Acetone-d_6 $(CD_3)_2CO$	2.05 (*5*)	29.84 (*7*) 206.26 (*1*)	2.84

2.2. EQUIPMENT AND INSTRUMENTATION

2.2.1. GENERAL APPARATUS AND INSTRUMENTS

Three rotary evaporators (Type: R-210 and Stuart® RE300) were used and they purchased from BÜCHI, Switzerland and Bibby Scientific, UK. The two UV lamps, UVS-14 EL Series UV Lamp and UVGL-55 Handheld UV Lamp, and C-10 Mini Cabinet (for handheld lamps) were purchased from UVP, Cambridge, UK. Infrared (IR) spectra for the samples were recorded on a PerkinElmer Spectrum 100 FT-IR Spectrometer using sodium chloride (NaCl) plate, and the samples were prepared as a solution. Optical rotation measurements of the novel compounds were performed in methanol and chloroform solutions on an ADP 440+ Polarimeter from Bellingham Stanley Ltd, USA. Column chromatography (CC) was performed using silica gel (LC60A 40-63 MICRON, Germany). Techne Dri-Block DB-3 Sample Concentrator, UK with the help of stream of nitrogen (N_2) was used for accomplishing concentration and dehydration of the samples in screw vials [1.8 mL (31 × 7 mm) and 28 mL (72 × 21 mm)]. UV spectra for the novel compounds were recorded on PerkinElmer (Singapore) Lambda 35 UV/Vis Spectrophotometer. The Stuart® SBH 200D/3 Block Heater was purchased from Bibby Scientific Ltd., Staffordshire, UK. The heat gun (DURATOOL 2000W, ADJ) was the product of Premier Farnell plc, UK.

2.2.2. NUCLEAR MAGNETIC RESONANCE

One and two dimensional Nuclear Magnetic Resonance (NMR) spectra were recorded on a Bruker Avance-III UltraShield™ Plus 400 MHz (9.4 Tesla magnet) and 500 MHz (11.75 Tesla magnet) Spectrometers (Bruker BioSpin Group, Germany) in deuterated solvents. A set of experiments were run for the isolated compounds including ^{1}H, ^{13}C, COSY, DEPTQ, HSQC and HMBC NMR. NOESY NMR was also run for some of the compounds. All ^{1}H and ^{13}C NMR chemical shifts were reported in ppm relative to trace resonance of internal references, acetone-d_6 at δ_H 2.05 and δ_C 206.26, chloroform-d_1 at δ_H 7.26 and δ_C 77.16, methanol-d_4 at δ_H

3.31 and δ_C 49.00. Spectral analyses were done using MestReNova Version 6.0 software. Proton NMR data were reported as follows: chemical shift, integration, multiplicity (s, singlet; d, doublet; dd, doublet of doublet; t, triplet; m, multiple), coupling constant.

2.2.3. HIGH PERFORMANCE LIQUID CHROMATOGRAPHY

The High Performance Liquid Chromatography (HPLC) was carried out using Dionex UltiMate 3000 system instrument from Thermo Scientific, Germany. The HPLC machine was equipped with binary gradient pump, autosampler, diode array detector (DAD) monitoring wavelength ranged 190-400 nm (UV-Vis detector) and reverse phase analytical column, Spherisil ODS-2 (RP-C18) (250 × 4.6 mm, id, 5µm). The HPLC was used to achieve method development, chromatographic profiling and assessment of purity of isolated pterosins and pterosides from each fraction of bracken rhizome chloroform extract. High resolution chromatograms were recorded based on using different ratios of two mobile phase systems, MeOH-H_2O and ACN-H_2O. The solvents were acidified with 0.1% formic acid and run at a flow rate of 1.0 mL/min at 40 °C. Ultraviolet detection was set at 254 nm. The Chromeleon 7 Software was used to control gradient setting, data acquisition, auto-sampler, and ultimately all chromatograms were recorded.

2.2.4. HIGH RESOLUTION MASS SPECTROMETRY

Ultra-high mass accuracy analysis for the novel compounds was performed on a Nano-Flow (Triversa Nanomate; Advion biosciences limited, Norfolk, UK) linear trap quadrupole Fourier Transformation Ion Cyclotron Resonance Mass Spectrometry Ultra (FT-ICR-MS), where ultra refers to the high sensitivity ICR cell. The samples were reconstituted in 100 µL of HPLC grade MeOH / ultra-pure water (7:3). The samples were vortexed and then centrifuged for 4 min at 13,000 rpm at a temperature of 0 ºC. 20 µL of supernatant was transferred to a clean well on a 128-well plate, and then the sample was injected (13 µL) by the nano-flow injection system, with a 5 µL aliquot being delivered to the ICR cell. Gas pressure was maintained at 0.5 psi with an applied voltage of 1.5 kV to maintain a consistent current of 60-120 nA. When operating in narrow SIM mode, the resolution was 100,000 and the scan window was 30 *m/z*. Each scan window was acquired in 60 sec.

High resolution mass spectra for the reported compounds were recorded on a Thermo Finnigan LTQ HR-ESI-MS spectrometer equipped with Dionex Ultimate 3000-ThermoScientific Exactive HPLC system instrument, Germany.

2.2.5. HPLC-ELECTROSPRAY IONISATION-ION TRAP MASS SPECTROMETRY (HPLC-ESI-MS^n)[11]

In order to confirm the presence of chlorinated isolated compounds, 10 g of air-dried ground bracken rhizomes was extracted with 100 ml of non-chlorinated organic solvent, methanol, and the extract was analysed by reverse-phase HPLC with on-line photodiode array detection and electrospray ionisation-ion trap mass spectrometry (ESI-MS^n). HPLC/ESI-MS^n analysis was performed on a Thermo Finnigan LC-MS system (Thermo Electron Corporation, USA) comprising a Finnigan Surveyor PDA Plus detector, a Finnigan LTQ linear ion trap with ESI source and a Waters C_{18} Nova-Pak column (4 µm, 3.9 mm x 100 mm). The autosampler tray temperature was maintained at 5 °C and the column temperature at 30 °C. Sample injection volume was typically 10µL, the detection wavelength was set to 210-400 nm and the flow rate was 1 ml min^{-1}, with 100 µL min^{-1} going to the mass spectrometer. The mobile phase consisted of water:formic acid (A; 100:0.1, v/v) and MeOH:formic acid (B; 100:0.1, v/v). The column was equilibrated with 95% solvent A, and the percentage of B increased linearly to 100% over 25 min. Ionisation parameters were optimised by infusion of chlorogenic acid standard at a constant rate into the LC flow. Mass spectra were acquired in negative ionisation mode with the following interface and MS parameters: nitrogen sheath gas 30 arbitrary units, nitrogen auxiliary gas 15 units, spray voltage 4 KV, capillary temperature 320 °C, capillary voltage −1 V and tube lens offset −68 V. MS/MS fragmentation was carried out at normalised collision energy of 35% and isolation width 2.0 (*m/z*).

2.2.6. REVERSE PHASE FLASH CHROMATOGRAPHY (RP-FC)

The Reveleris® automated Flash Chromatography system (FC) was used for separation and purification of pterosins and pterosides. The RP-FC system has four main independent channels with up to four different solvents. It was used in a binary gradient during a single run. The samples were pre-adsorbed onto silica gel and subsequently run on the Reveleris® C_{18} (40 µm, 12 g) column (GRACE) for 64 min. Two different solvent systems, MeOH-H_2O and ACN-H_2O (acidified with 0.1% (v/v) formic acid), were used to elute the targeted compounds at a flow rate of 18 mL/min. Evaporative Light Scattering Detector (ELSD) and UV detector were used in this system to monitor, visualise and record the chromatographic peaks. In the UV detector, two selected wavelengths, 254 nm and 280 nm, were used to detect the UV-active compounds. The default fraction volume of 25 mL was applied for separation of the

[11] HPLC-ESI-MS^n analysis of methanol extract of bracken rhizomes has been conducted by Dr Ana Winters from IBERS, University of Aberystwyth.

components using Reveleris flash system. Fractions were collected in test tubes which were put into two automated trays controlled by the Reveleris® X2 Navigator™ software.

2.2.7. CIRCULAR DICHROISM SPECTROSCOPY

Circular Dichroism (CD) spectra for the compounds were recorded at 25 °C using a Chirascan CD spectrometer (Applied Photophysics Ltd). Samples (~1 mg/ml) were measured in methanol using a 1 mm pathlength quartz cuvette. Data were recorded every 0.5 nm between 280 nm and 400 nm with a 1 nm spectral bandwidth and an integration time of 2 seconds per data point.

2.2.8. X-RAY CRYSTALLOGRAPHY PROCEDURE:

Single crystal X-ray diffraction data were collected either on a Rigaku AFC11 quarter chi goniometer equipped with an enhanced sensitivity (HG) Saturn944+ detector mounted at the window of 007 HF copper rotating anode generator with Varimax optics (*cis*-pterosin C, *trans*-pterosin C and (2*S*)-pterosin A), or on a Rigaku AFC12 goniometer equipped with an enhanced sensitivity (HG) Saturn724+ detector mounted at the window of an FR-E+ SuperBright molybdenum rotating anode generator with VHF Varimax optics (70µm focus) ((2*R*)-pteroside B, (2*S*)-pteroside K and (2*R*)-rhedynoside B). Rigaku CrystalClear (Rigaku Corporations, The Woodlands, Texas, USA) was used to record images. Data integration was carried out using Agilent CrysAlisPro (Agilent- Technologies UK Ltd) (*cis*-pterosin C, *trans*-pterosin C, (2*S*)-pterosin A and rhedynoside B) or Rigaku CrystalClear ((2*R*)-pteroside B, (2*S*)-pteroside K). The structures were solved by charge-flipping methods using SUPERFLIP (Palatinus and Chapuis, 2007) and refined on F_o^2 by full-matrix least squares refinement using SHELXL-2014 (Sheldrick, 2008). All non-hydrogen atoms were refined with anisotropic displacement parameters. Hydrogen atoms were added at calculated positions and refined using a riding model with isotropic displacement parameters based on the equivalent isotropic displacement parameter (Ueq) of the parent atom. The structures were deposited on the Cambridge Structural Database with the deposition numbers CCDC 1050917, 1050918, 1050920, 1406891, 1418452 and 1418453.

2.3. THIN LAYER CHROMATOGRAPHY (TLC)

Thin layer chromatography (TLC) and preparative TLC were conducted using pre-coated E. Merck TLC silica gel glass plates (TLC Silica gel 60 F_{254}, Germany, 1.0 mm thickness, 20 × 20 cm). The plates were visualised with the UV lamp if the components were UV-active or using PMA (20% in ethanol) when the compounds were UV-inactive.

2.4. BRACKEN PLANT MATERIAL AND EXTRACTION

2.4.1. PLANT COLLECTION AND DRYING

The bracken rhizomes (11.8 kg) were collected from Llanberis in Wales, UK, N 53° 07′ and W 04° 08′, on 21 February 2013. The bracken plant was identified and confirmed by Nigel Brown (Bangor University) as *Pteridium aquilinum* (L.) Kuhn. A voucher specimen was deposited at Treborth Botanical Garden, Bangor. The fresh rhizomes were cleaned of soil by manual brushing to avoid matter loss and then cut into small pieces. They were left in the laboratory to be air-dried at room temperature for a week. Finally, the total dry weight of *ca*. 3.5 kg rhizomes was obtained.

2.4.2. EXTRACTION AND ISOLATION

The air-dried chopped (0.5-1.0 cm length) bracken rhizomes (*ca*. 3.5 kg) were macerated and extracted with chloroform (14.0 L) at room temperature for 3 × 24 h. The sample mixture was filtered under gravity using filter paper (Wattman No. 1), and the filtrate (organic solvent) was reduced and concentrated to dryness under pressure at 40 ºC using rotary evaporator to give 7.1 g of the crude extract. The TLC characteristics of this extract showed major spots under the UV light. The extract was then examined preliminarily for the presence of aromatic proton signals of pterosins and pterosides by ^{1}H-NMR. The spectrum was showed the main characteristic peaks of pterosins and pterosides. The extract was pre-adsorbed onto silica gel (14.0 g) and subjected to CC (5 cm, *d*; 50 cm, *l*) to separate these main spots. The column was then eluted with gradient mixture of chloroform-methanol (100:0 → 0:100). A total of seventy six fractions (F1-F76) were collected (250 ml each). All the eluted fractions were concentrated in vacuum and transferred to screwed glass containers (25 ml). In order to identify and combine similar fractions:

a) ^{1}H NMR spectrum in chloroform-*d* was taken for each fraction.
b) All fractions were applied to HPLC.
c) The fractions were monitored with TLC as described below:

Dilute solution of each fraction was spotted onto TLC plate. The plate was then inserted into a jar contained the solvent system. Various solvent systems with different ratios were studied such as hexane:chloroform (1:1), hexane:EtOAc (3:7), methanol:chloroform (1:9). The main spots were detected and visualised with PMA reagent and/or UV light.

Similar fractions were pooled together based on their proton NMR spectra, TLC and HPLC profiles to give thirteen major fractions, designated BR1, BR2, BR3, BR4, BR5, BR6, BR7, BR8, BR9, BR10, BR11, BR12 and BR13, as shown in Table 5.

Table 5: Main fractions obtained from column chromatography of chloroform extract.

Resultant fractions[⌂]	Weight (mg)	Physical appearance
BR1	25	Pale yellow liquid
BR2	350	Pale yellow liquid
BR3	128.9	Pale yellow liquid
BR4	37	Pale yellow liquid
BR5	109	Pale yellow liquid
BR6	375	Pale yellow liquid
BR7	600	Pale yellow liquid
BR8	119.7	Pale yellow liquid
BR9	110	Pale yellow liquid
BR10	50	Pale yellow liquid
BR11	261.7	Pale yellow liquid
BR12	161.8	Pale yellow liquid
BR13	200	Pale yellow liquid

[⌂] These fractions were further investigated based on their TLC and ^{1}H NMR signals.

From these fractions, thirteen new compounds (**RH1**, 6.0 mg; **RH2**, 11.0 mg; **RH3**, 5.8 mg; **RH4**, 2.6 mg; **RH5**, 4.5 mg; **RH6**, 6.0 mg; **RH7**, 4.1 mg; **RH8**, 13.0 mg; **RH9**, 3.0 mg; **RH10**, 11.6 mg; **RH11**, 3.2 mg; **RH12**, 9.1 mg; and **RH13**, 3.8 mg) and twenty five known compounds (**RH14**, 6.0 mg; **RH15**, 160.0 mg; **RH16**, 110.0 mg; **RH17**, 18.0 mg; **RH18**, 20.0 mg; **RH19**, 60.0 mg; **RH20**, 17.0 mg; **RH21**, 10.0 mg; **RH22**, 5.0 mg; **RH23**, 3.0 mg; **RH24**, 15.4 mg; **RH25**, 4.0 mg; **RH26**, 14.0 mg; **RH27**, 14.7 mg; **RH28**, 3.0 mg; **RH29**, 4.0 mg; **RH30**, 10.2 mg; **RH31**, 203.0 mg; **RH32**, 4.9 mg; **RH33**, 47.0 mg; **RH34**, 4.2 mg; **RH35**, 30.0 mg; **RH36**, 4.0 mg; **RH37**, 21.0 mg and **RH38**, 4.0 mg were isolated as the following:

Preparative TLC was applied to purify fraction BR1 (25.0 mg) using *n*-hexane-acetone (9:1) to give **RH21** (10.0 mg). Fraction BR2 (350 mg) was further chromatographed on a silica gel column eluting with gradient of *n*-hexane-EtOAc (100:0 → 45:55) to obtain five sub-fractions (BR2A-BR2E). Sub-fraction BR2A (170.0 mg) was subjected to RP-FC using a gradient elution of ACN-H_2O (35-45%, 1 h) to give **RH20** (17.0 mg); **RH22** (5.0 mg); **RH23** (3.0 mg) and **RH26** (14.0 mg). Sub-fractions BR2B (130.0 mg), BR2D (20.0 mg) and BR2E (10 mg) were subjected individually to preparative TLC using *n*-hexane-EtOAc (4:6), EtOAc (%100) and MeOH-Et_2O (1:49) to give **RH16** (110.0 mg), **RH14** (6.0 mg) and **RH4** (2.6 mg), respectively. Sub-fraction BR2C (22 mg) was purified using preparative TLC (diethyl ether) to afford compounds **RH1** (6.0 mg) and **RH3** (5.8 mg). Fractions BR3 (128.9 mg) and BR4 (37 mg) were purified separately by preparative TLC using *n*-hexane-acetone (1:1 and 6:4) to afford **RH8** (13.0 mg) and **RH7** (4.1 mg), respectively. Preparative TLC (diethyl ether) was

applied to fraction BR5 (109 mg) to afford **RH5** (4.5 mg) and **RH24** (15.4 mg). Fraction BR6 (375 mg) was fractionated by applying it on RP-FC with an isocratic gradient elution (20-20%, ACN-H_2O, 1 h) to give **RH15** (160.0 mg) and **RH19** (60.0 mg). Fraction BR7 (600 mg) was resolved by a silica gel CC eluted with gradients of *n*-hexane-EtOAc and EtOAc-MeOH with increasing polarity, respectively, to yield four sub-fractions (BR7A-BR7D). Sub-fraction BR7A (51.5 mg) was chromatographed on RP-FC using a gradient elution of ACN-H_2O (20-23%, 1 h) to afford **RH6** (6.0 mg) and **RH27** (14.7 mg). RP-FC was applied on sub-fraction BR7B (33.0 mg) using ACN-H_2O (20-23%, 1 h) as a gradient elution to obtain **RH28** (3.0 mg). Sub-fraction BR7C (242.0 mg) was subjected to RP-FC using a gradient elution of ACN-H_2O (20-23%, 1 h) to obtain four main fractions (BR7C1-BR7C4), and then the second peak (BR7C2) (38 mg) was further chromatographed on RP-FC using a gradient elution of ACN-H_2O (06-06-10-11%, 2 h) to afford **RH17** (16.5 mg) and **RH18** (19.5 mg). Sub-fraction BR7D (97.0 mg) was resolved on RP-FC using a gradient elution of ACN-H_2O (15-20%, 1 h) to give **RH25** (4.0 mg). Fraction BR8 (119.7 mg) was subjected to RP-FC using a gradient elution of MeOH-H_2O (40-50%, 1 h) to give **RH10** (11.6 mg) and **RH29** (4.0 mg). Fraction BR9 (110 mg) was separated with RP-FC using a gradient elution of MeOH-H_2O (40-50%, 1 h) to obtain four sub-fractions (BR9A-BR9D). Sub-fractions BR9A, BR9B and BR9D gave **RH11** (3.2 mg), **RH12** (9.1 mg) and **RH35** (30.0 mg), respectively. The purification of sub-fraction BR9C (15.0 mg) on RP-FC using gradient elution (25-30% ACN-H_2O, 1 h) yielded **RH13** (3.8 mg). Fraction BR11 (261.7 mg) was resolved on RP-FC using MeOH-H_2O (40-50%, 1 h) as a mobile phase to obtain **RH2** (11.0 mg), **RH31** (203.0 mg) and **RH33** (47.0 mg). Fraction BR13 (200 mg) was further fractionated by applying it to RP-FC with a gradient elution (10-25% ACN-H_2O, 1 h) to obtain four sub-fractions (BR13A-BR13D). Compounds **RH32** (4.9 mg), **RH30** (10.2 mg) and **RH34** (4.2 mg) were obtained from sub-fractions BR13A, BR13B and BR13C, respectively, while sub-fraction BR13D (30 mg) was re-subjected to RP-FC using a gradient elution (40-50% ACN-H_2O, 1 h) to afford **RH9** (3.0 mg).

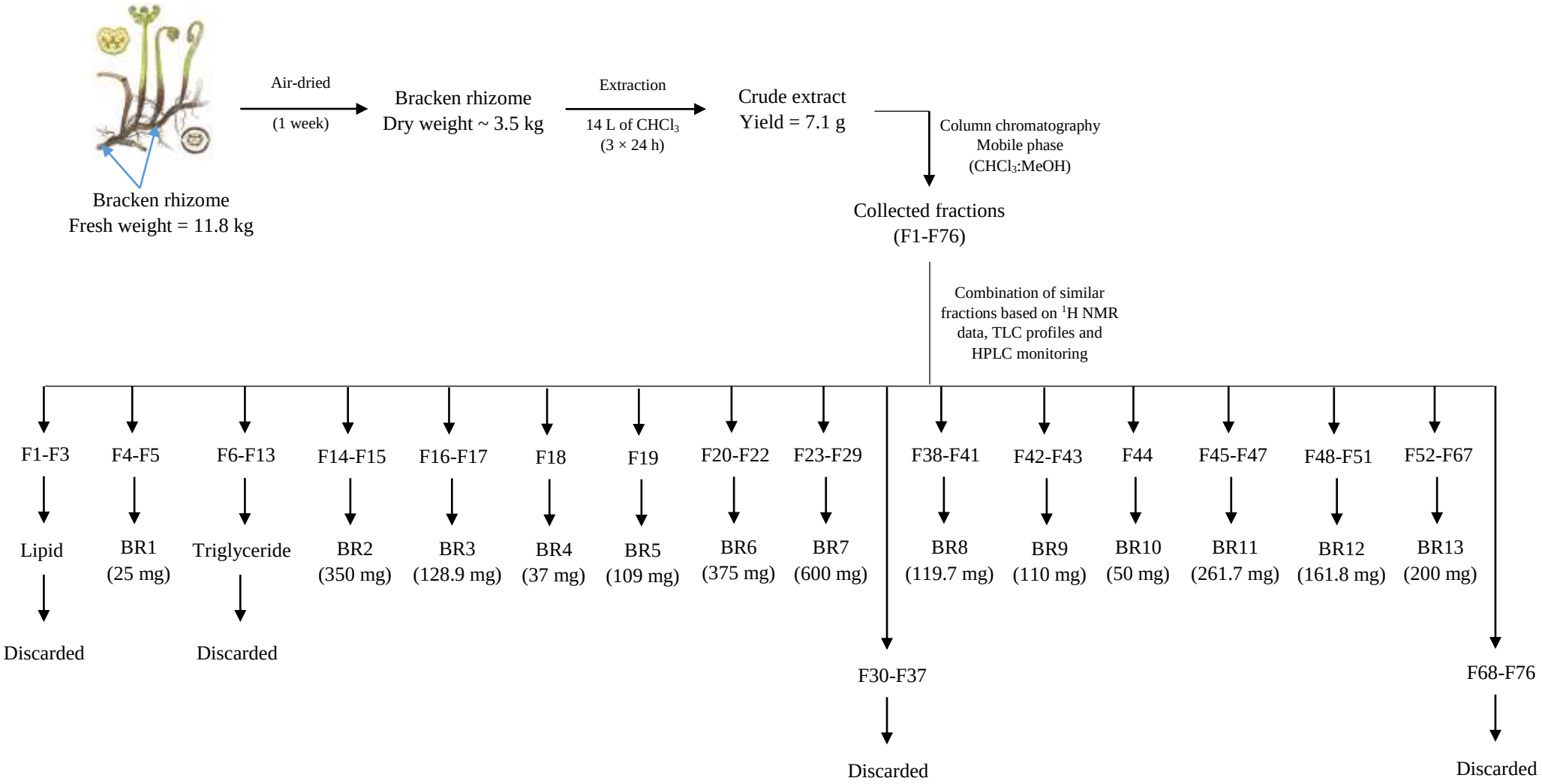

Figure 13: Extraction and fractionation scheme from the rhizome of bracken (*Pteridium aquilinum* (L.) Kuhn).

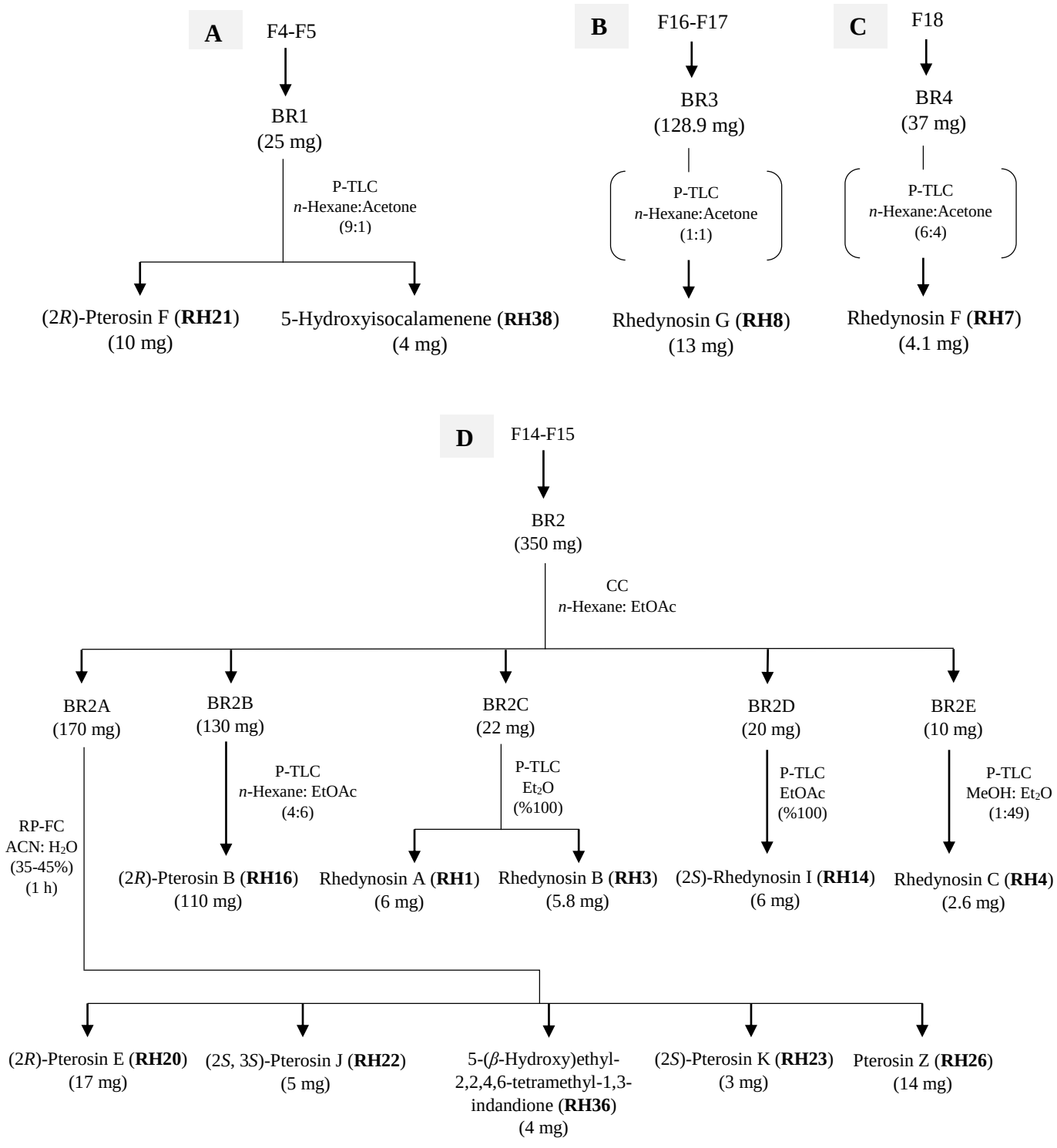

Figure 14: Schematic flow diagrams of isolation of pterosins and pterosides from fractions A) F4-F5, B) F16-F17, C) F18 and D) F14-F15.

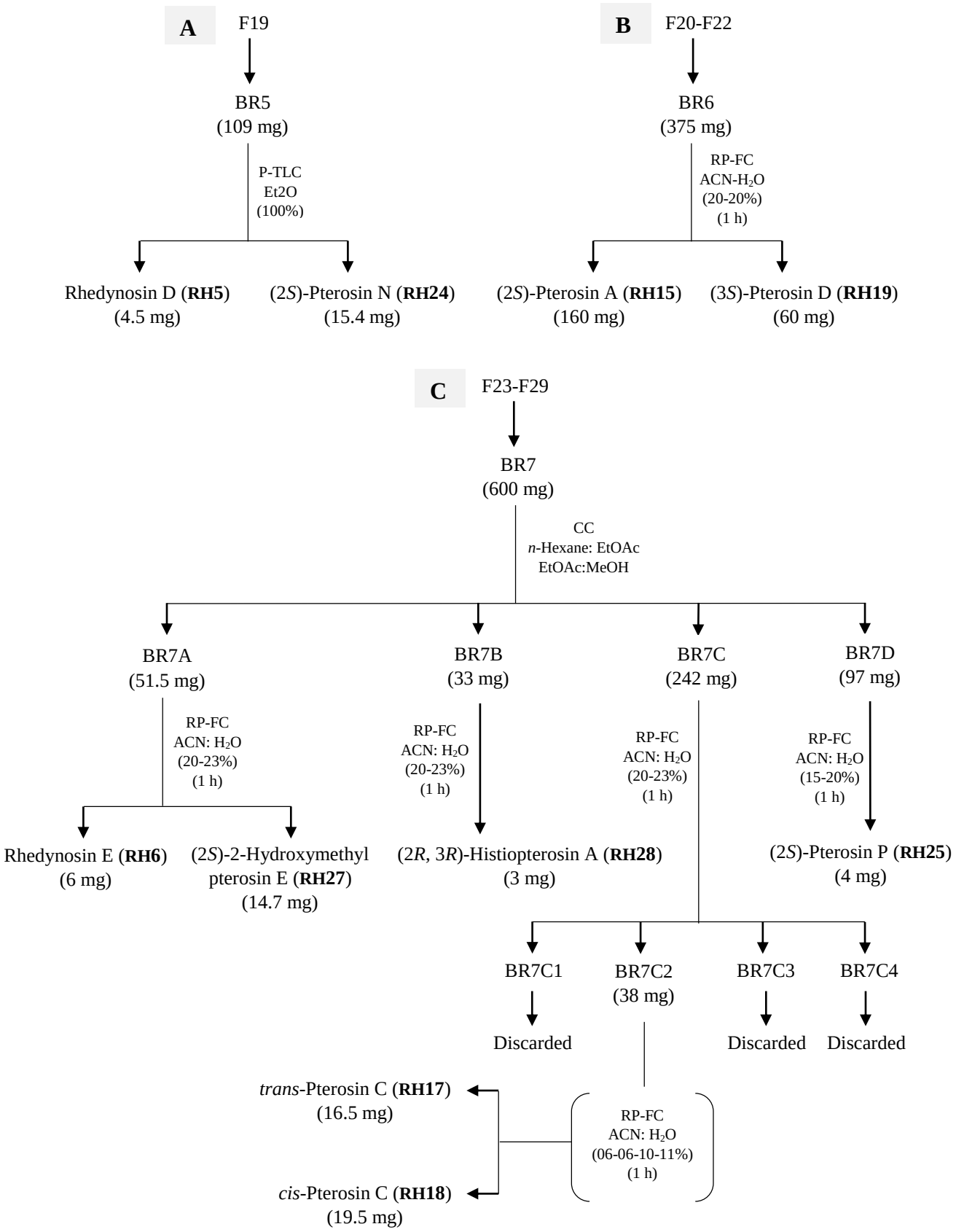

Figure 15: Flow chart diagrams of isolation of pterosins and pterosides from fractions A) F19, B) F20-F22 and C) F23-F29.

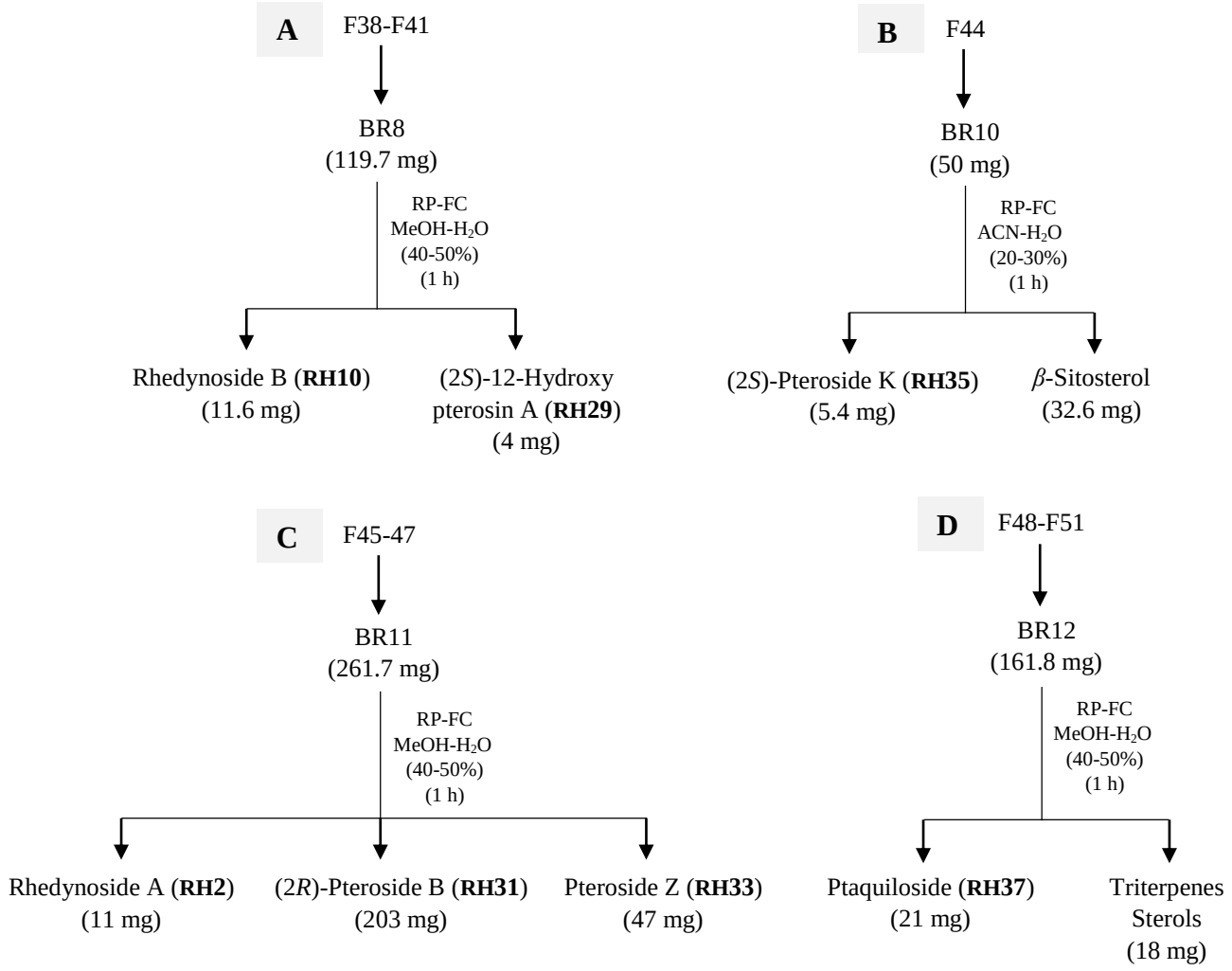

Figure 16: Flow diagrams of isolation of pterosins and pterosides from fractions A) F38-F41, B) F44, C) F45-F47 and D) F48-F51.

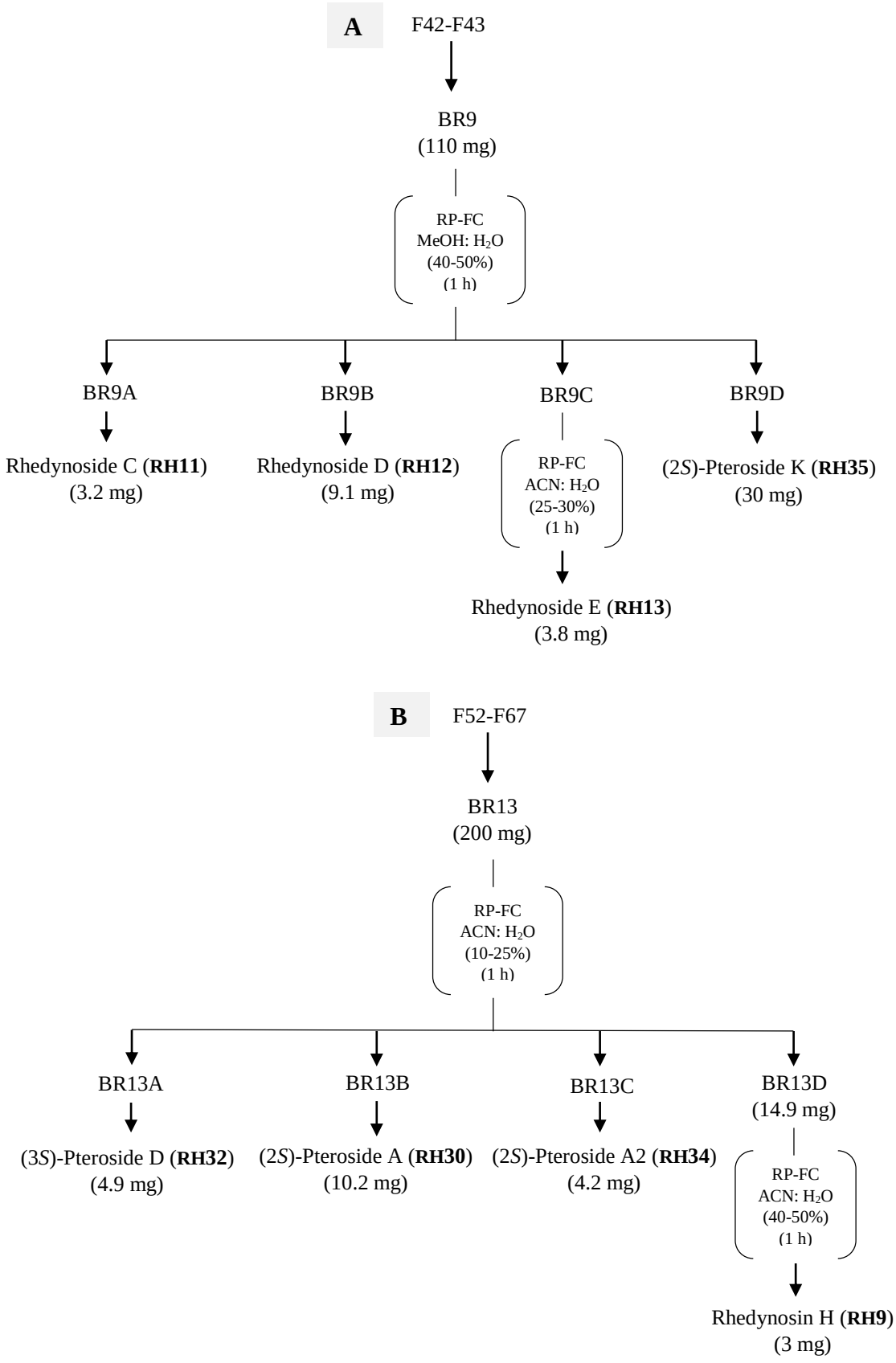

Figure 17: Schematic diagrams of isolation of pterosins and pterosides from fractions A) F42-F43 and B) F52-F67.

2.5. ACETYLATION METHOD

Accurately 1 mg of each compound, **RH2** and **RH10**- **RH13**, was dissolved with 100 µL of dry pyridine in a HPLC vial and then 50 µL of acetic anhydride was added. The vial was immersed and sonicated for 1 hour and left overnight. The reaction mixture was diluted with 400 µL of $CDCl_3$ containing tetramethylsilane (TMS) as an internal standard. ^1H NMR and COSY were recorded in the range of 3.0-6.0 ppm. DEPTQ was recorded from -50 to 250 ppm.

CHAPTER THREE

STRUCTURAL ELUCIDATION OF ISOLATED PTEROSINS AND PTEROSIDES

3. RESULTS AND DISCUSSION

3.1. INTRODUCTION:

The underground parts (rhizomes) of bracken fern (*Pteridium aquilinum* (L.) Kuhn) were air-dried, chopped and then extracted with chloroform. The extract was subjected repeatedly to column, thin-layer and automated reverse phase flash chromatography. The collected fractions were further analysed and chromatographed on silica-gel to afford 38 compounds.

The toxicity of North Wales bracken, 'Rhedyn' in the Welsh language, to cattle has been studied previously (Potter, D.M., Baird, 2000; Wells, A.J. and McNally, 1989). In the present study, a traditional phytochemical investigation of bracken rhizomes using various analytical techniques such as one- and two-dimensional NMR spectroscopy combined with mass spectrometry led to isolate and identify thirteen novel natural products (**RH1**-**RH13**) belonging to the sesquiterpenoid family, together with twenty five previously reported compounds: (2*S*)-rhedynosin I (**RH14**) (Lee et al., 2012), (2*S*)-pterosin A (**RH15**) (Kuroyanagi et al., 1979a), (2*R*)-pterosin B (**RH16**) (Fukuoka et al., 1983, 1978), (2*R*, 3*R*)-pterosin C (*trans*-pterosin C) (**RH17**) (Ayer and McCaskill, 1981; Kuroyanagi et al., 1979a), (2*S*, 3*R*)-pterosin C (*cis*-pterosin C) (**RH18**) (Kuroyanagi et al., 1979a), (3*S*)-pterosin D (**RH19**) (Ng and McMorris, 1984), (2*R*)-pterosin E (**RH20**) (Fukuoka et al., 1978; Nambudiry and Rao, 1974), (2*R*)-pterosin F (**RH21**) (Fukuoka et al., 1983, 1978), (2*S*, 3*S*)-pterosin J (**RH22**) (Ng and McMorris, 1984), (2*S*)-pterosin K (**RH23**) (Castillo et al., 2003, 1997), (2*S*)-pterosin N (**RH24**) (Kuroyanagi et al., 1974a; Wu et al., 2014), (2*S*)-pterosin P (**RH25**) (Fukuoka et al., 1978), pterosin Z (**RH26**) (Kuraishi et al., 1985; Tanaka et al., 1982), (2*S*)-2-hydroxymethylpterosin E (**RH27**) (Lee et al., 2012), (2*R*, 3*R*)-histiopterosin A (*trans*-histiopterosin A) (**RH28**) (Murakami et al., 1980), (2*S*)-12-hydroxypterosin A (**RH29**) (Lee et al., 2012), (2*S*)-pteroside A (**RH30**) (Fukuoka et al., 1983), (2*R*)-pteroside B (**RH31**) (Fukuoka et al., 1983, 1978), (3*S*)-pteroside D (**RH32**) (Kuroyanagi et al., 1979a), pteroside Z (**RH33**) (Hikino et al., 1971), (2*S*)-pteroside A2 (**RH34**) (Castillo et al., 2003), (2*S*)-pteroside K (**RH35**) (Kuroyanagi et al., 1979a), 5-(*β*-hydroxy)ethyl-2, 2, 4, 6-tetramethyl-1, 3-indandione (**RH36**) (Ng and McMorris, 1984), ptaquiloside (**RH37**) (Castillo et al., 1997;

Ojika et al., 1987) and 5-hydroxycalamenene (**RH38**) (Tanaka and Adachi, 1990), of which compounds **RH14** and **RH27- RH29** are identified for the first time from the genus *Pteridium* which belongs to Dennstaedtiaceae family. Herein described are the isolation and structural elucidation of these compounds.

3.2. STRUCTURAL ELUCIDATION OF NOVEL COMPOUNDS

Compound **RH1** was obtained as a yellow powder (Figure 18). Its molecular formula was established as $C_{15}H_{18}O_3$ based on the positive mode quasi-molecular ion peak at *m/z* 247.1330 $[M + H]^+$ (Calcd for $C_{15}H_{19}O_3$: 247.1334) showing seven degrees of unsaturation (Figure 27). Its UV absorbance maxima at 211, 258 and 306 nm (Figure 28) were consistent with 1-indanone derivatives. The IR absorption bands at 3014, 1605, 3418 and 1704 cm^{-1} (Figure 29) indicated the presence of aromatic C-H, C=C, hydroxy and carbonyl groups, respectively, which concur with the presence of a 1-indanone skeleton (Fukuoka et al., 1978; Kuroyanagi et al., 1979a). ^1H and ^{13}C NMR data used for the structural identification of compound **RH1** is listed in Table 6. The spectra yielded by compound **RH1** are presented in Figure 21-Figure **26**.

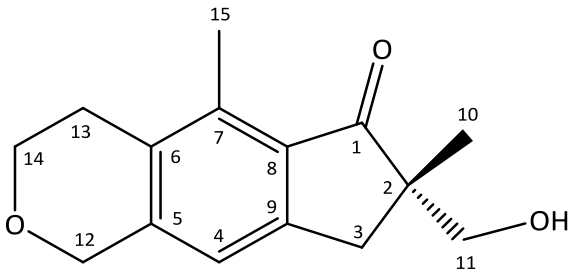

Figure 18: Chemical Structure of (2*S*)-Rhedynosin A (**RH1**).

The full assignment of ^1H and ^{13}C NMR resonances was deduced from ^1H-^1H COSY, DEPTQ, HSQC and HMBC analyses (Table 6, Figure 23-Figure **26** and appendix I). In addition, the signals for all protonated carbons were assigned by analysis of the DEPTQ and HSQC spectra to establish the connectivities. The ^1H NMR spectrum of **RH1** (Figure 21) shows signals of one secondary methyl [δ_H 2.56 (3H, s, H-15)], one tertiary methyl [δ_H 1.23 (3H, s, H-10)], two methylenes [δ_H 3.06 (1H, d, J = 17.5 Hz, H_a-3), 2.77 (1H, d, J = 17.5 Hz, H_b-3) and 2.76 (2H, t, J = 5.9 Hz, H-13)], three oxygenated methylenes [δ_H 3.78 (1H, d, J = 10.8 Hz, H_a-11), 3.62 (1H, d, J = 10.8 Hz, H_b-11), 4.80 (2H, s, H-12) and 4.01 (2H, td, J = 1.3, 5.9, 11.8 Hz, H-14)] and one methine [δ_H 6.93 (1H, s, H-4)] signal in the aromatic region. The DEPTQ spectrum (Figure 23), in combination with HSQC and HMBC experiments, displays 15 carbon

resonances, including two quaternary methyls at δ_C 21.1 (C-10) and δ_C 13.1 (C-15), five methylenes (including three oxygenated carbons), one methine at δ_C 120.0 (C-4) and seven quaternary carbons. As three of the seven degrees of unsaturation are accounted for by a tricyclic system of **RH1**, the remaining four degrees of unsaturation require four double bonds.

Table 6: ^{1}H (400 MHz) and ^{13}C (100 MHz) NMR spectral data of compound **RH1** in $CDCl_3$ (δ in ppm, multiplicity, *J* in Hz).

Position	δ_H	δ_C	HMBC[±]
1	-	210.5, C	-
2	-	50.9, C	-
3a 3b	3.06 (d, *J* = 17.5) 2.77 (d, *J* = 17.5)	37.1, CH_2	C: 2, 7, 8, 9, 10, 11
4	6.93 (s)	120.0, CH	C: 3, 6, 12
5	-	142.1, C	-
6	-	131.8, C	-
7	-	138.2, C	-
8	-	131.3, C	-
9	-	151.0, C	-
10	1.23 (s)	21.1, CH_3	C: 1, 2, 3, 11
11a 11b	3.78 (d, *J* =10.8) 3.62 (d, *J* =10.8)	68.3, CH_2	C: 1, 3, 10
12	4.80 (s)	68.8, CH_2	C: 4, 5, 6, 14
13	2.76 (t, *J* = 5.9)	25.8, CH_2	C: 5, 6, 7
14	4.01 (td, *J* = 1.3, 5.9, 11.8)	65.6, CH_2	C: 6, 12, 13
15	2.56 (s)	13.1, CH_3	C: 6, 7, 8

[±] HMBC correlations are from proton(s) stated to the indicated carbon(s)

The key HMBC correlations are shown in Figure 20. In the HMBC spectrum (Figure 26), the signals at δ_H 3.06 (1H, d, *J* = 17.5 Hz, H_a-3) and 2.77 (1H, d, *J* = 17.5 Hz, H_b-3) show correlations with δ_C 50.9 (C-2), δ_C 138.2 (C-7), δ_C 131.3 (C-8), δ_C 151.0 (C-9), δ_C 21.1 (C-10) and δ_C 68.3 (C-11). δ_H 4.80 (2H, s, H-12) displays correlations with δ_C 120.0 (C-4), δ_C 142.1 (C-5), δ_C 131.8 (C-6) and δ_C 65.6 (C-14). δ_H 2.76 (2H, t, *J* = 5.9 Hz, H-13) exhibits correlations with δ_C 142.1 (C-5), δ_C 131.8 (C-6) and δ_C 138.2 (C-7). δ_H 4.01 (2H, td, *J* = 1.3, 5.9, 11.8 Hz, H-14) reveals correlations with δ_C 131.8 (C-6), 68.8 (C-12) and δ_C 25.8 (C-13). δ_H 3.78 (1H, d, *J* = 10.8 Hz, H_a-11) and 3.62 (1H, d, *J* = 10.8 Hz, H_b-11) were correlated with δ_C 210.5 (C-1), δ_C 50.9 (C-2), δ_C 37.1 (C-3) and δ_C 21.1 (C-10). The latter correlations confirmed the position of the hydroxymethylene (CH_2OH) group at C-2. Other connectivities shown in this spectrum are: δ_H 6.93 (1H, s, H-4) with C-3, C-6 & C-12, δ_H 1.23 (3H, s, H-10) with C-1, C-2, C-3 & C-11 and δ_H 2.56 (3H, s, H-15) with C-6, C-7 & C-8. Additionally, the presence of an ether link

was assigned to be between positions C-12 and C-14 as their proton and carbon chemical shifts appeared at low field region due to the deshielding influence of the oxygen atom. This was further confirmed with the HMBC spectrum that showed the correlations from H-12 (δ_H 4.80) to C-14 (δ_C 65.6) and from H-14 (δ_H 4.01) to C-12 (δ_C 68.8). The *J*-coupling systems were confirmed by the COSY spectrum (Figure 24) that displays coupling between signals: δ_H 2.76 & δ_H 4.01, δ_H 2.77 & δ_H 3.06, and δ_H 3.62 & δ_H 3.78, respectively (Figure 20).

The CD spectrum of **RH1** (Figure 19) shows a vibronic n → π* transition which concurs with C-2 having 2*S* configuration. The observed transitions for the assignment of the absolute stereochemistry were based on the comparison of CD spectrum of **RH1** with X-ray crystallography data of **RH15** (Figure 58) and the CD interpretation provided for **RH15** by Kuroyanagi et al., 1979. They measured the CD spectra of substituted pterosins and pterosides after their absolute configurations were unequivocally determined by degradation and correlation reactions. Based on the above analysis, the structure of this compound was determined as a new natural product and named rhedynosin A (**RH1**). Its physical and spectroscopic features were consistent with the proposed structure in Figure 18.

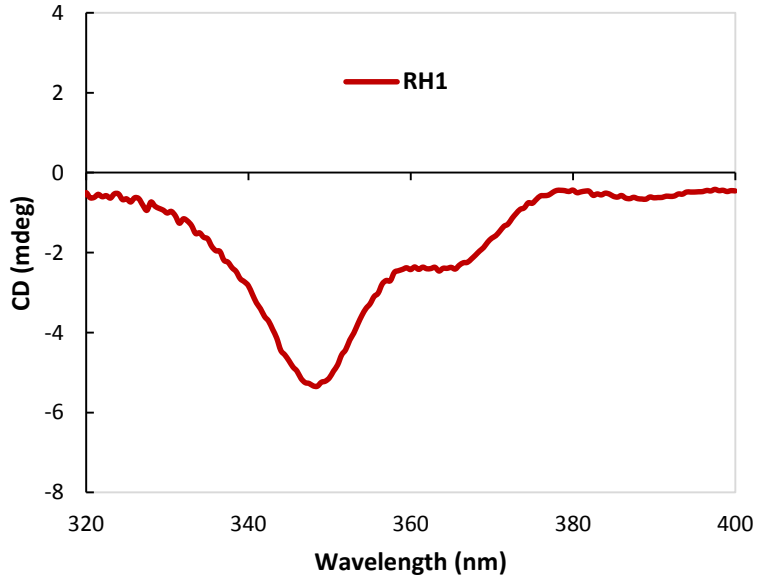

Figure 19: The CD spectra of the tricyclic compound **RH1** recorded in methanol.

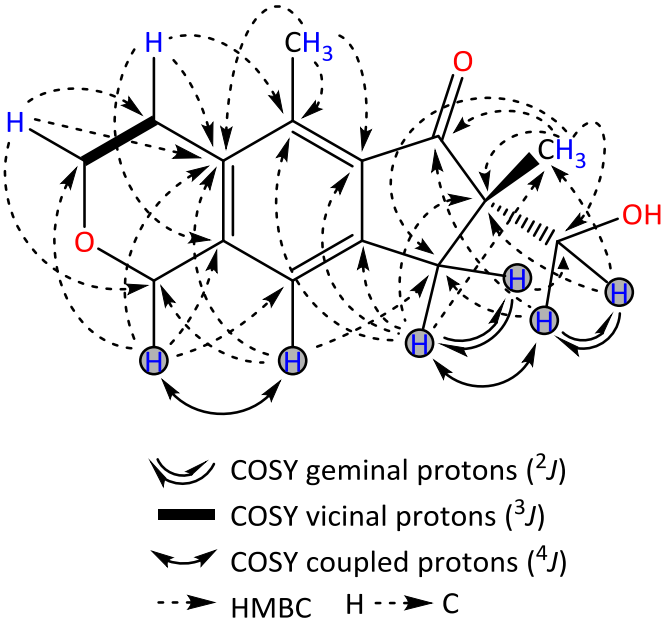

Figure 20: 2D NMR key correlations including COSY and HMBC used in the structural identification of the compound **RH1**.

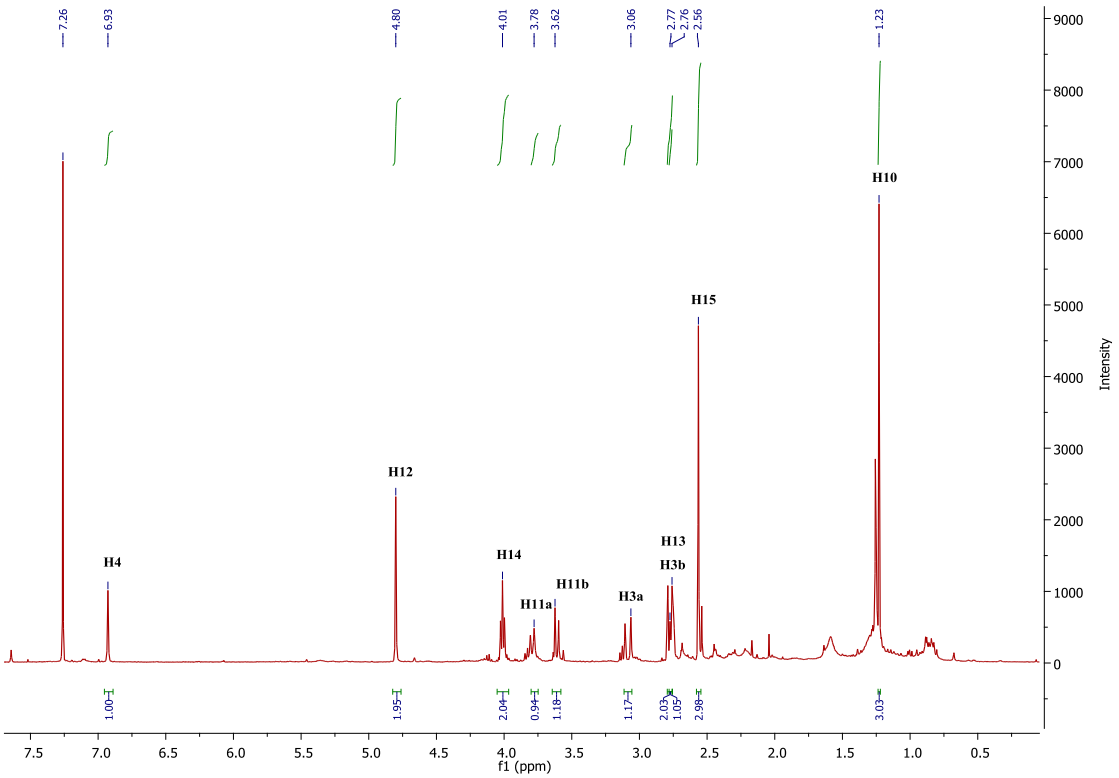

Figure 21: ^{1}H NMR ($CDCl_3$, 400 MHz) spectrum of compound **RH1**.

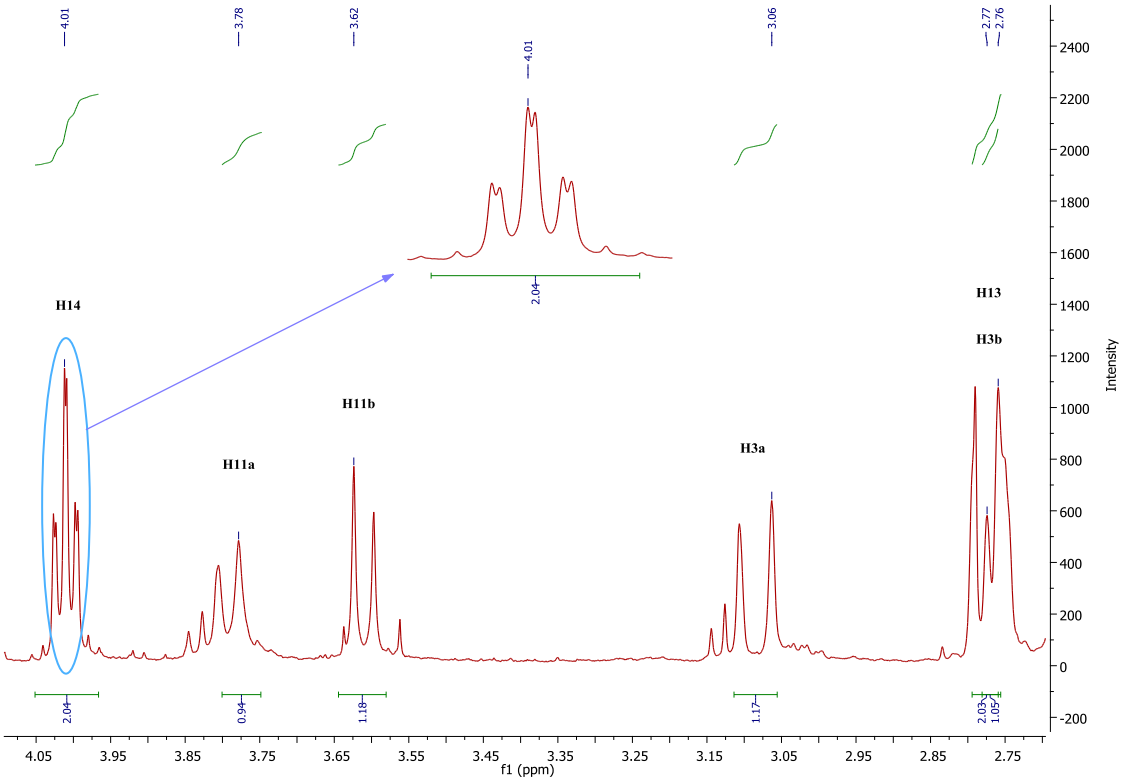

Figure 22: Expanded ^{1}H NMR ($CDCl_3$, 400 MHz) spectrum of compound **RH1** (2.70-4.05).

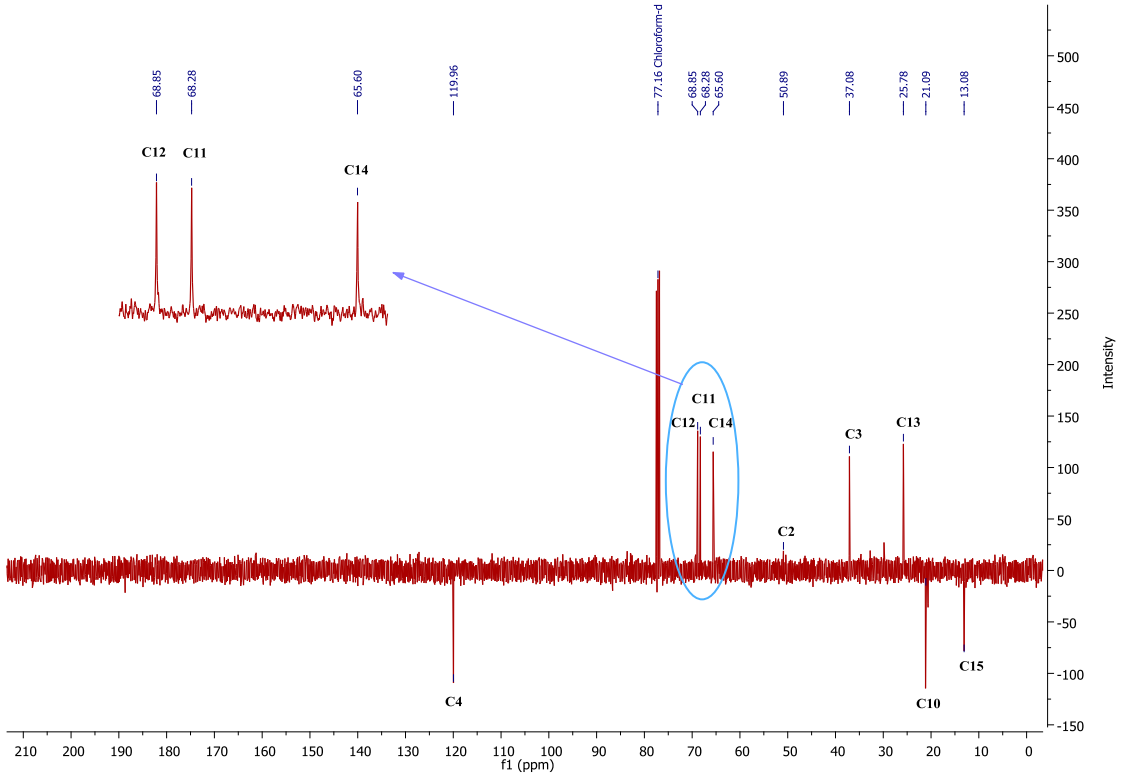

Figure 23: DEPTQ NMR ($CDCl_3$, 100 MHz) spectrum of compound **RH1**.

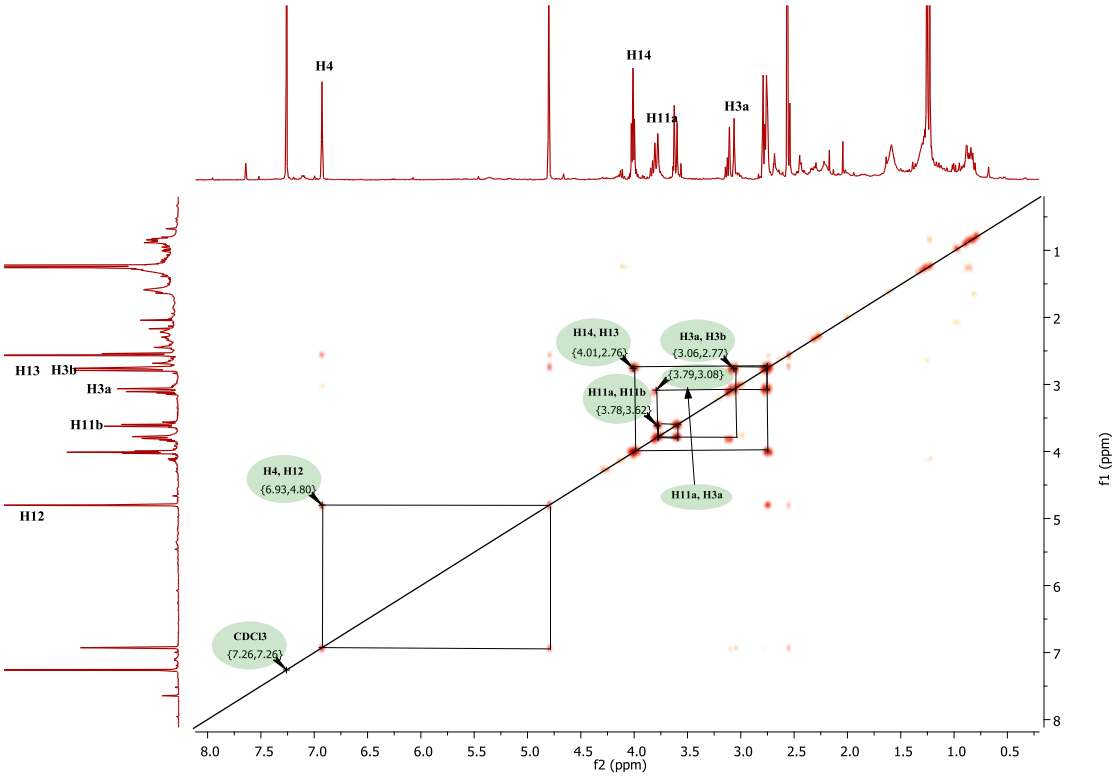

Figure 24: ^{1}H-^{1}H COSY NMR ($CDCl_3$, 400 MHz) spectrum of compound **RH1**.

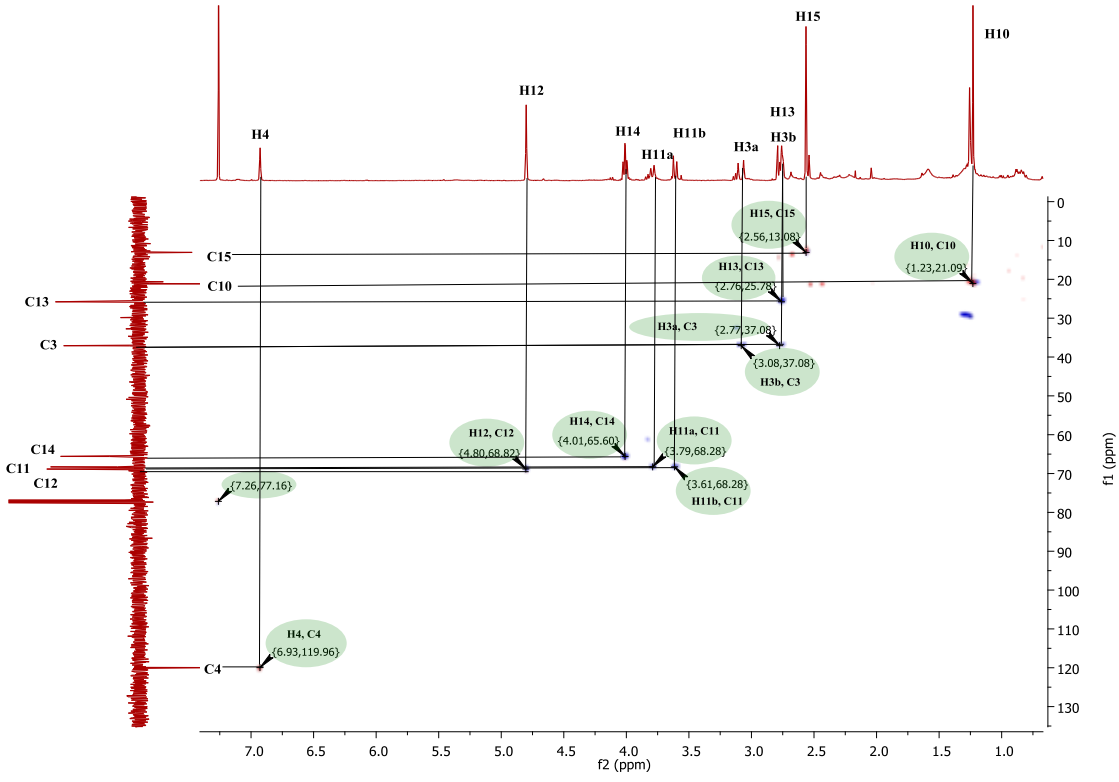

Figure 25: ^{1}H-^{13}C HSQC NMR spectrum of compound **RH1** in $CDCl_3$.

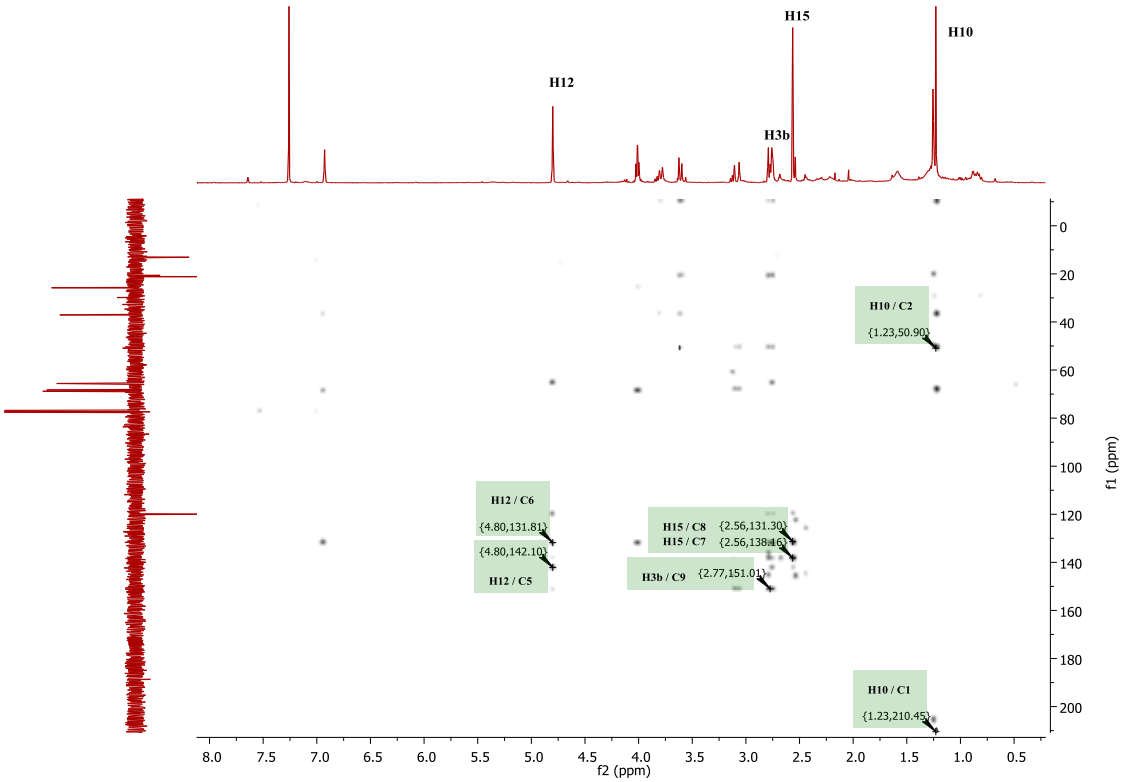

Figure 26: ^{1}H-^{13}C HMBC NMR spectrum of compound **RH1** in $CDCl_3$.

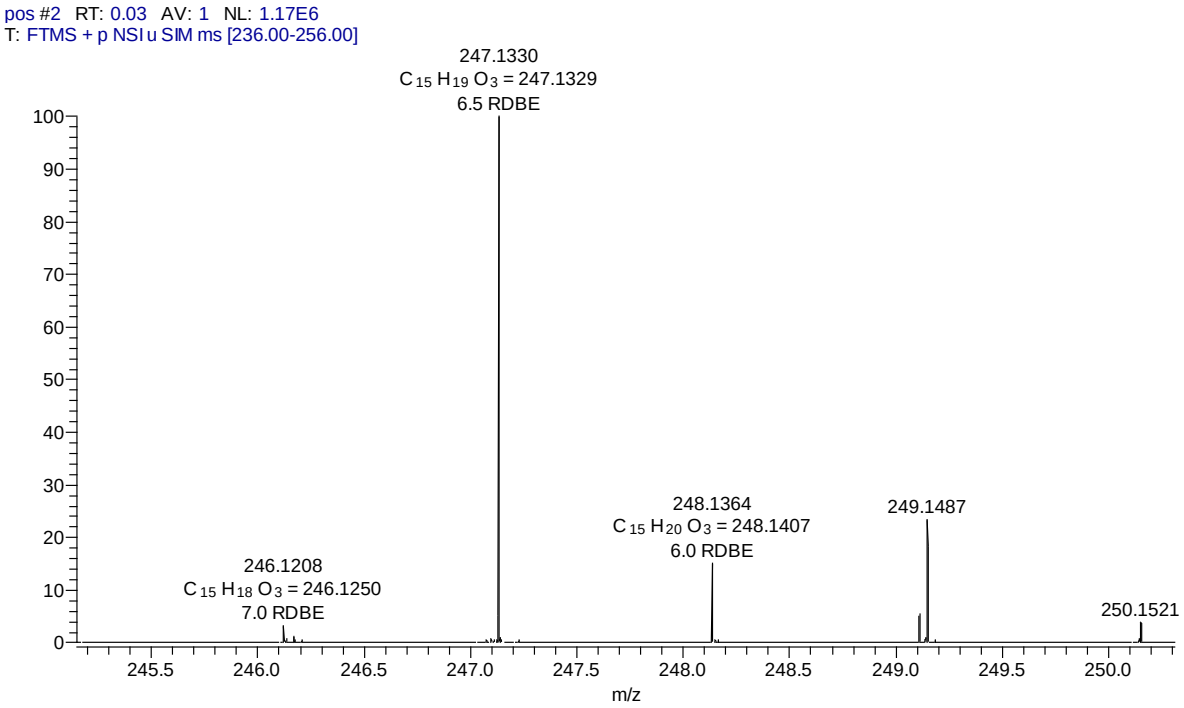

Figure 27: FT-ICR-MS spectrum of compound **RH1** in $[M+H]^+$ positive ion mode.

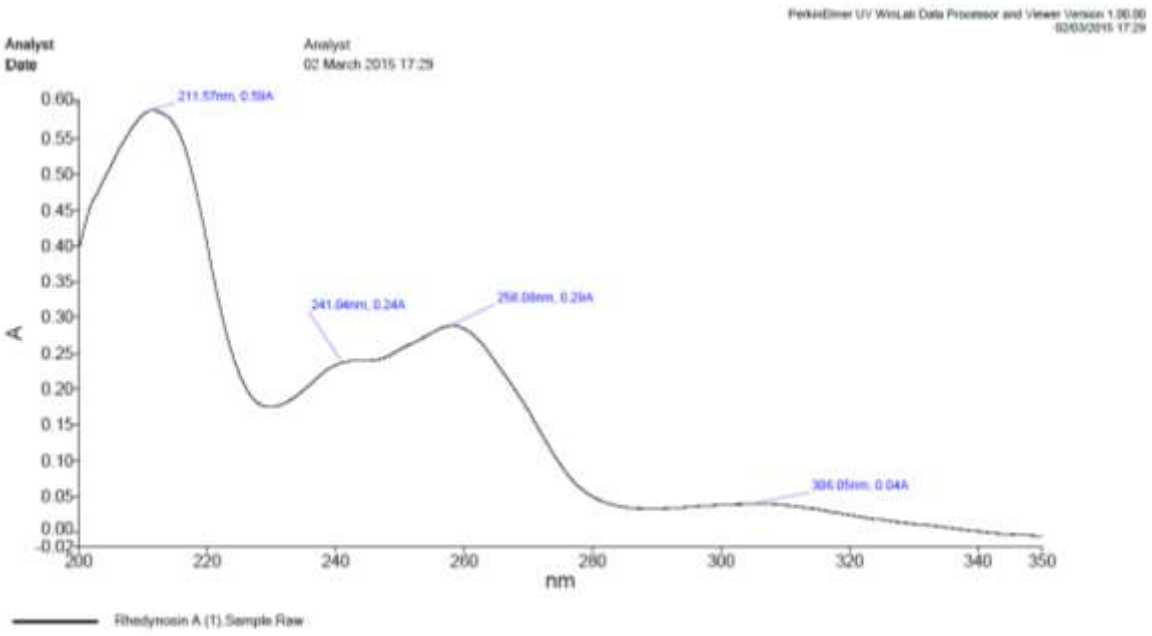

Figure 28: UV spectrum of compound **RH1** in MeOH.

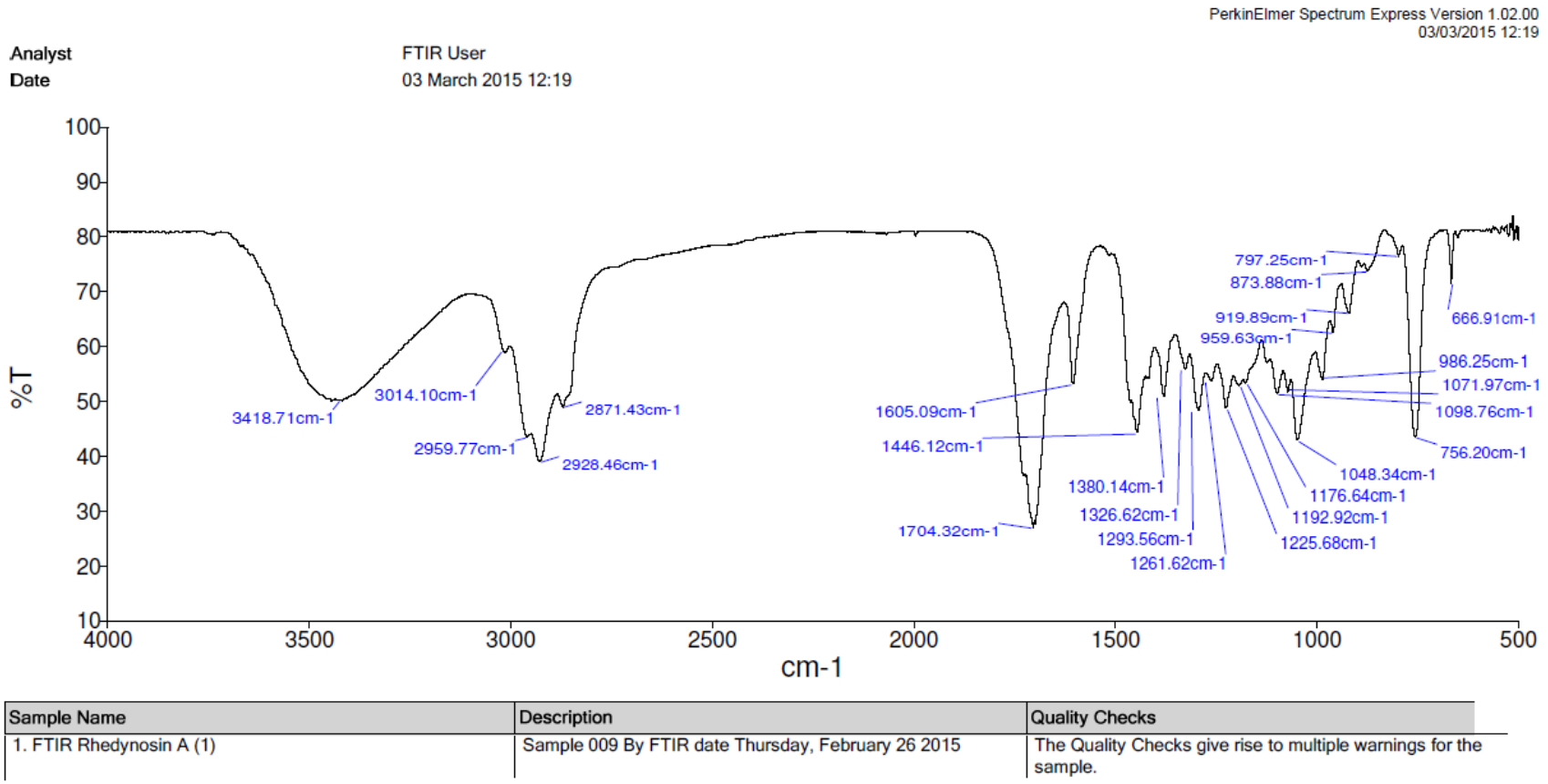

Sample Name	Description	Quality Checks
1. FTIR Rhedynosin A (1)	Sample 009 By FTIR date Thursday, February 26 2015	The Quality Checks give rise to multiple warnings for the sample.

Figure 29: FT-IR spectrum of compound **RH1** in $CHCl_3$.

Compound **RH2** was isolated as a white powder (Figure 30) exhibiting negative optical rotation ($[\alpha]_D^{24}$ -26.1° (*c* 0.33, MeOH)). Its IR spectrum showed absorption bands in the regions 1602, 1692 and 3369 cm^{-1} (see appendix III) attributable to the aromatic ring, carbonyl and hydroxyl groups, respectively. In its UV spectrum, absorption maxima were observed at 304 (log ε 2.99), 259 (log ε 3.92) and 216 (log ε 4.27) nm (see appendix IV).

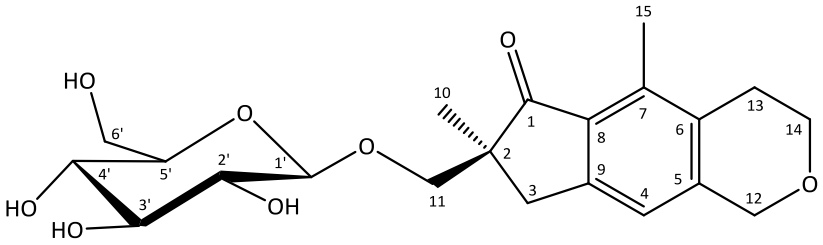

Figure 30: Chemical Structure of (2*S*)-Rhedynoside A (**RH2**).

Table 7: ^{1}H (400 MHz) and ^{13}C (100 MHz) NMR spectral data of compound **RH2** in CD_3OD (δ in ppm, multiplicity, *J* in Hz).

Position	δ_H	δ_C	HMBC[¤]
1	-	212.4, C	-
2	-	51.5, C	-
3a 3b	3.45 (d, *J* = 17.4) 2.75 (d, *J* = 17.4)	37.7, CH_2	C: 2, 9, 10
4	7.01 (s)	121.2, CH	C: 6
5	-	143.6, C	-
6	-	132.9, C	-
7	-	139.0, C	-
8	-	127.3, C	-
9	-	153.1, C	-
10	1.14 (s)	22.0, CH_3	C: 1, 2, 3, 11
11a 11b	4.13 (d, *J* = 9.4) 3.48 (d, *J* = 9.4)	75.0, CH_2	C: 1´, 2, 3, 10
12	4.79 (s)	69.6, CH_2	C: 4, 5, 6, 12
13	2.77 (t, *J* = 5.9)	26.6, CH_2	C: 6
14	4.00 (t, *J* = 5.9)	66.5, CH_2	C: 6, 12
15	2.54 (s)	13.0, CH_3	C: 6, 7, 8
1′	4.21 (d, $J_{1',2'}$ = 7.8)	104.7, CH	C: 2´, 11
2′	3.03 (dd, $J_{2',3'}$ = 8.9)	74.9, CH	-
3′	3.29 (m)	78.1, CH	C: 4´
4′	3.24 (m)	71.5, CH	-
5′	3.20 (m)	77.9, CH	-
6′a 6′b	3.78 (dd, $J_{5',6'a}$ = 1.5, $J_{6'a,6'b}$ = 12.0) 3.61 (dd, $J_{5',6'b}$ = 4.6)	62.7, CH_2	-

[¤] HMBC correlations are from proton(s) stated to the indicated carbon(s)

The positive mode FT-ICR-MS spectrum of **RH2** (Figure 39) demonstrates a quasi-molecular ion peak at *m/z* 409.1866 $[M+H]^+$ suggesting the molecular formula $C_{21}H_{28}O_8$ (Calcd for $C_{21}H_{29}O_8$: 409.1862). Compound **RH2** exhibited ^1H and ^{13}C NMR data closely resembling those of **RH1**. Comparison of the UV, IR and NMR spectroscopic data of **RH2** (Table 7) with those of rhedynosin A (**RH1**) showed the following differences, the main one being the presence of an additional hexose sugar moiety having a signal for an anomeric-H at δ_H 4.21 (d, J = 7.8 Hz) and remaining sugar proton signals at δ_H 3.03-3.78. The ^{13}C NMR spectrum of **RH2** contained an anomeric carbon signal of a hexose moiety at δ_C 104.7 and signals for the remaining five sugar carbons at δ_C 62.7 - 78.1, which were in good agreement with those reported for glycoside compounds (Fukuoka et al., 1983). This indicated that compound **RH2** was a glycoside of compound **RH1**. The coupling constant (J = 7.8 Hz) is consistent with *trans* $^3J_{H\text{-}H}$, showing that it is a β-hexoside and that the adjacent proton on the sugar is axial in the chair conformation of the pyranose ring. The 8.9 Hz coupling between H-2′ and H-3′ is also only consistent with a *trans*-diaxial coupling, showing that the OH at C-3′ is equatorial. Thus, the sugar must be glucose or galactose. Since the ^1H NMR signals for H-3′ and H-4′ overlap in the spectrum of **RH2**, a sample was peracetylated, on an analytical scale, forming the tetraacetate. The introduction of the electron withdrawing groups shifts the signals for the ring protons H-2′, H-3′, H-4′ and H-6′ downfield and resolves them clearly (Figure 34, see method in section 2.5). The $J_{H3',H4'}$ coupling was determined by examination of the H-3′ and H-4′ signals and was found to be *ca*. 8 Hz. This value is only consistent with a *trans*-diaxial relationship between these protons in the chair conformation of the hexopyranose. Three *trans*-diaxial relationships derived from the ring protons of a pyranose are indicating a glycosyl residue. To our knowledge, no L-glucose has been reported being isolated from a plant source yet. Thus, it is most likely that this glycosyl residue belongs to the D- series. Carbon resonances at δ_C 104.7, 78.1, 77.9, 74.9, 71.5 and 62.7 in the ^{13}C NMR spectrum (Table 7 and Figure 35) provided further evidence for the presence of the glucopyranyl residue. The key HMBC and COSY correlations are shown in Figure 31. The linkage position of the sugar moiety to C-11 of the aglycone was confirmed by an HMBC experiment, which shows correlations between the anomeric resonance H-1′ (δ 4.21) and C-11 (δ 75.0), and between H-11 (δ 4.13 and 3.48) and the anomeric carbon C-1′ (δ 104.7). The CD spectrum shows a plain positive n → π* component at ~330 nm that can be correlated with the configuration at C-2 being 2*S*

(Kuroyanagi et al., 1979a). Based upon the above evidence, the structure of **RH2** was identified as rhedynosin A 11-*O*-*β*-D-glycoside and named rhedynoside A (Figure 30).

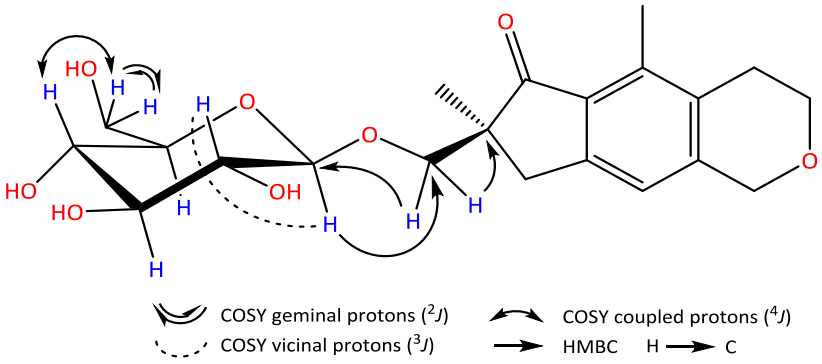

Figure 31: Some of HMBC and COSY key correlations used in the structural identification of the compound **RH2**.

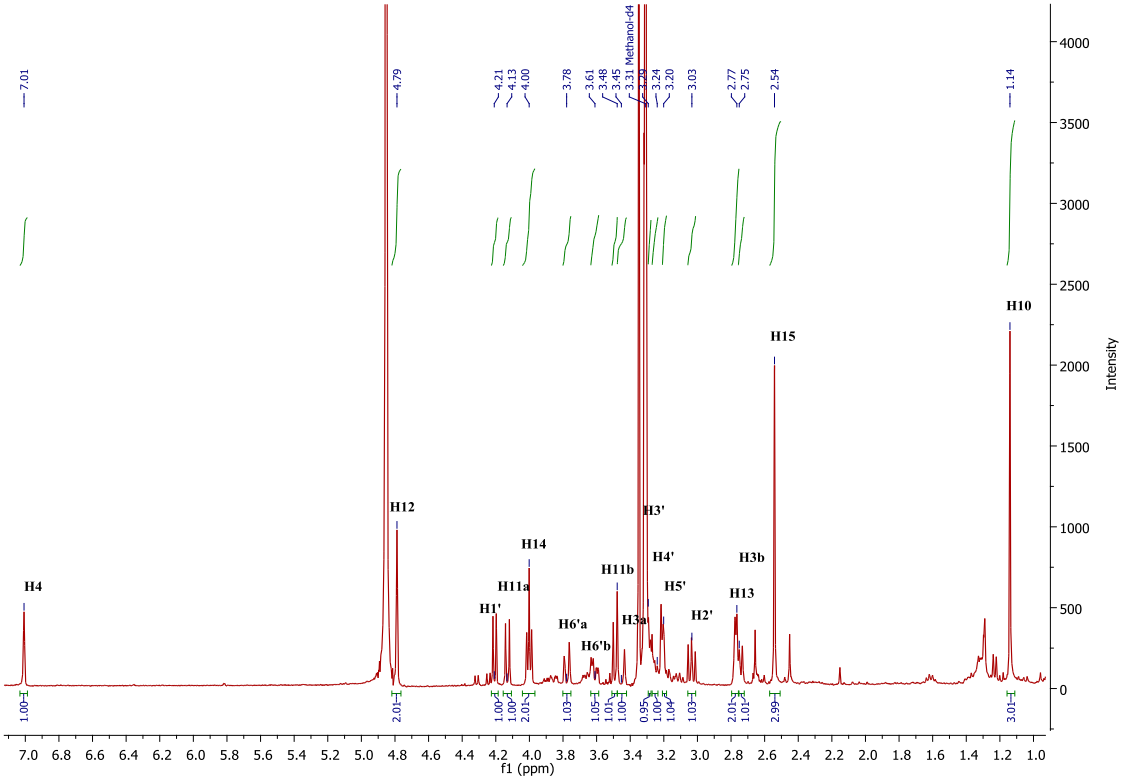

Figure 32: ^{1}H NMR (CD_3OD, 400 MHz) spectrum of compound **RH2**.

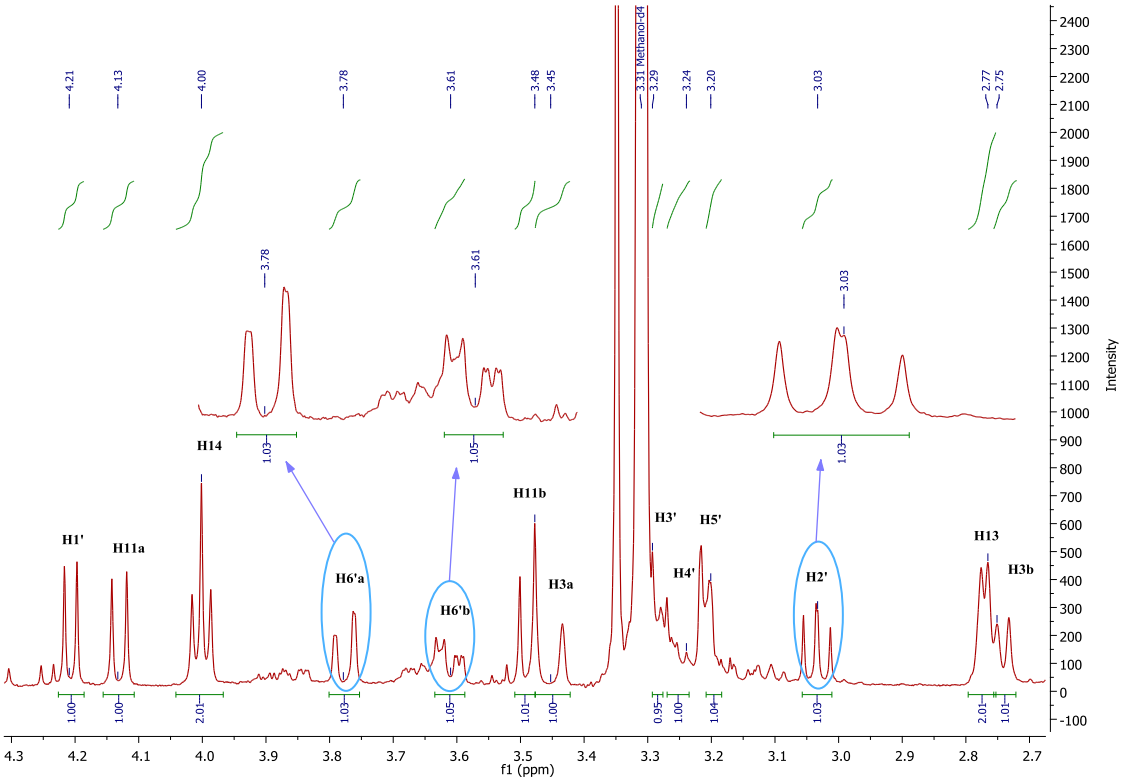

Figure 33: Expanded ^{1}H NMR (CD_3OD, 400 MHz) spectrum of **RH2** (2.7 – 4.3 ppm).

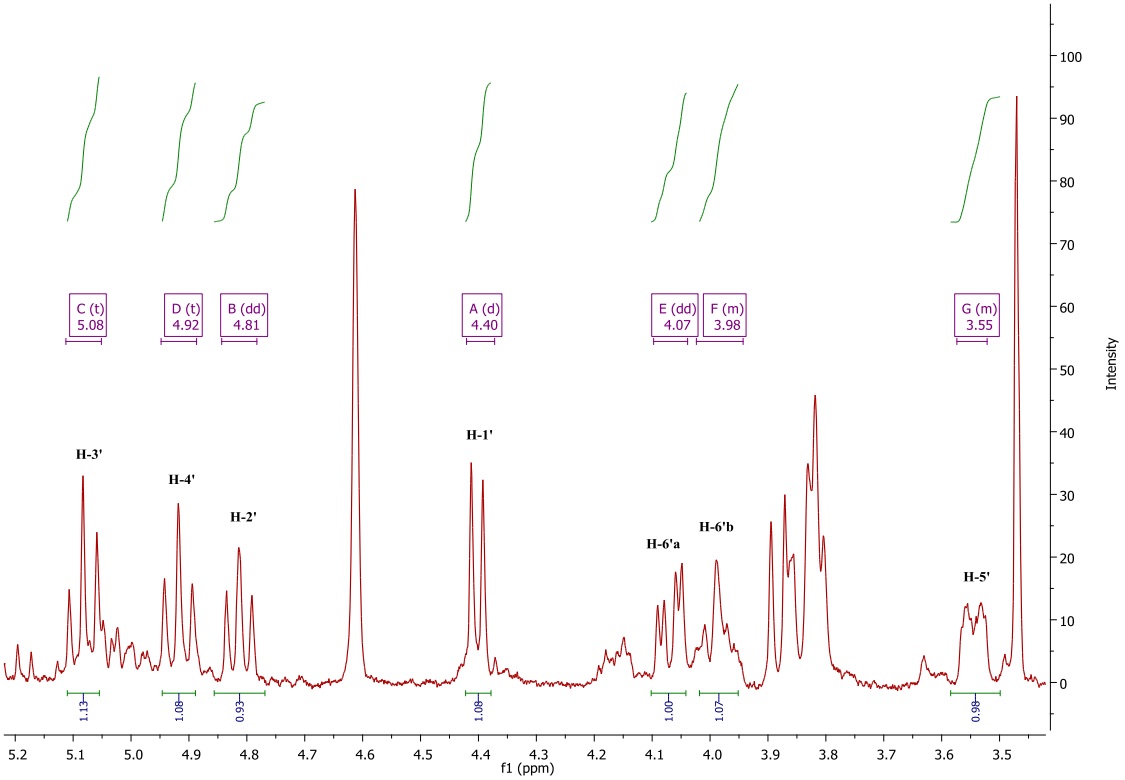

Figure 34: ^{1}H NMR ($CDCl_3$, 400 MHz) spectrum of compound **RH2** after acetylation.

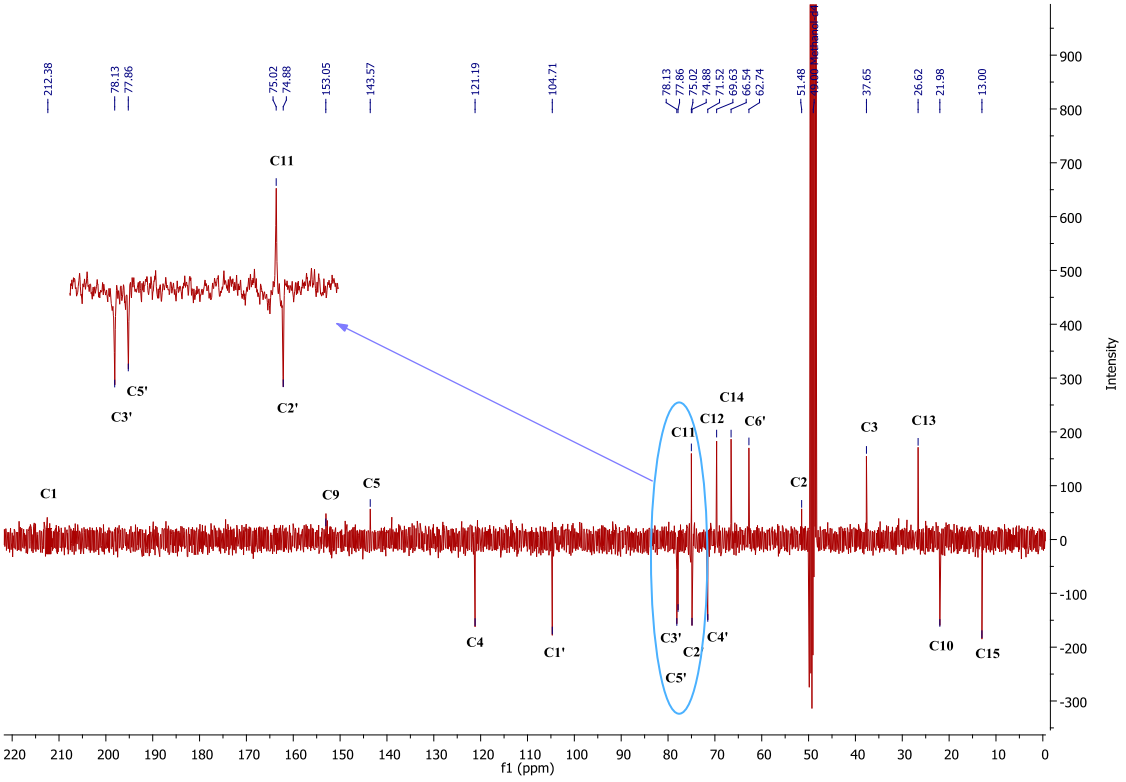

Figure 35: DEPTQ NMR (CD_3OD, 100 MHz) spectrum of compound **RH2**.

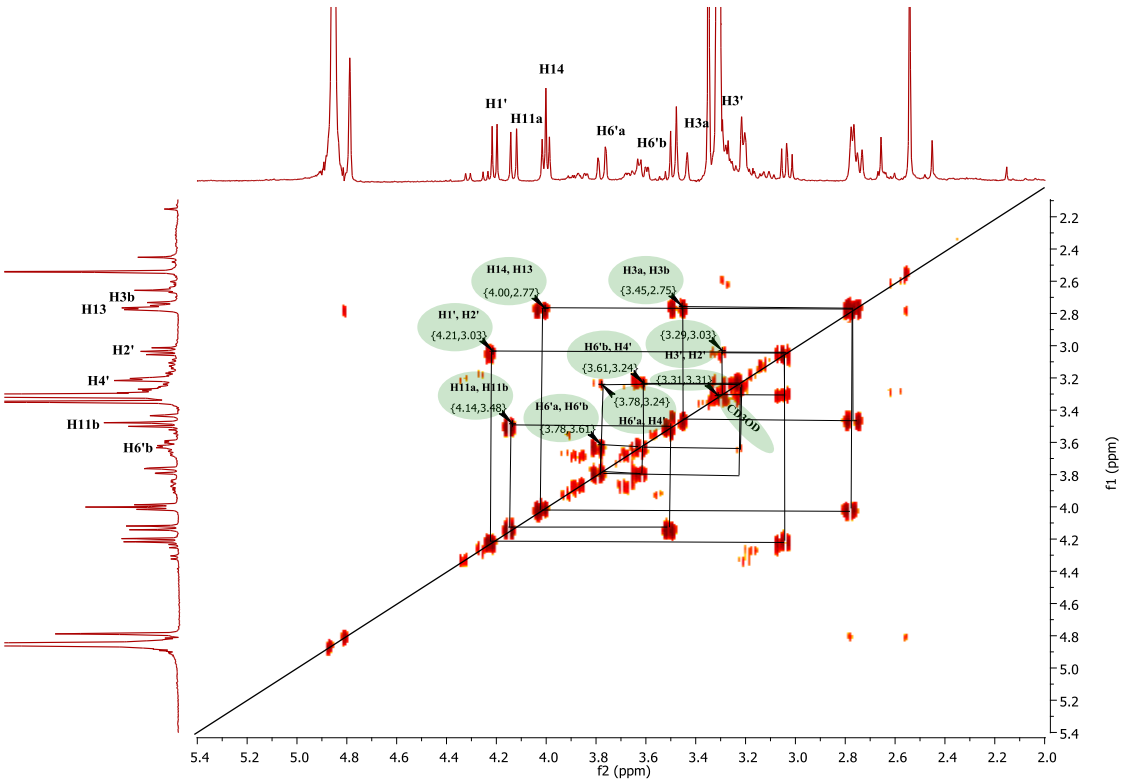

Figure 36: ^1H-^1H COSY NMR (CD_3OD, 400 MHz) spectrum of compound **RH2**.

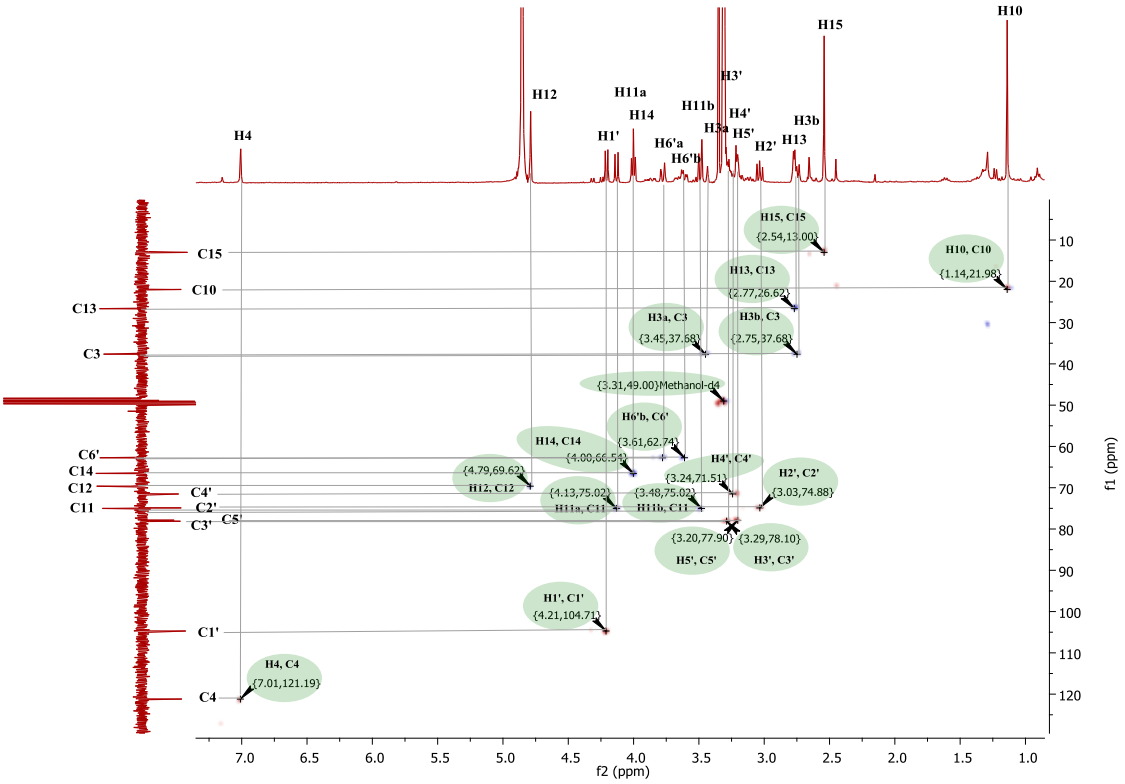

Figure 37: ^{1}H-^{13}C HSQC NMR spectrum of compound **RH2** in CD_3OD.

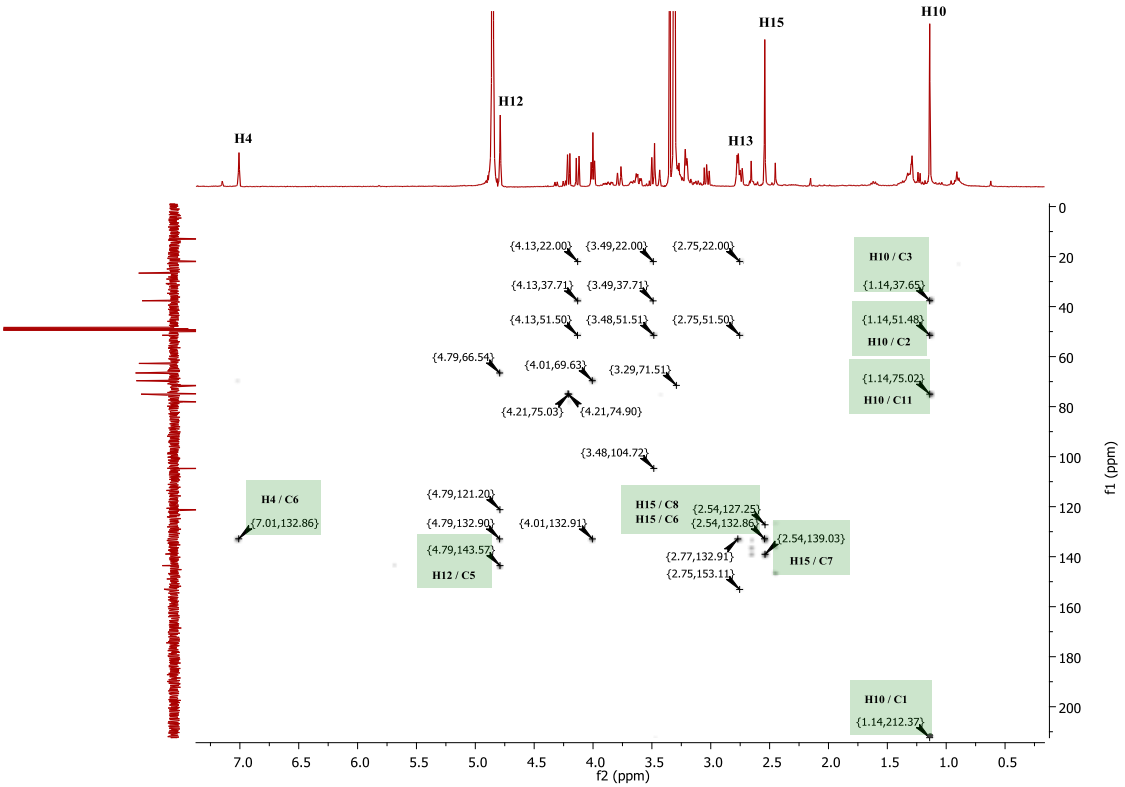

Figure 38: ^{1}H-^{13}C HMBC NMR spectrum of compound **RH2** in CD_3OD.

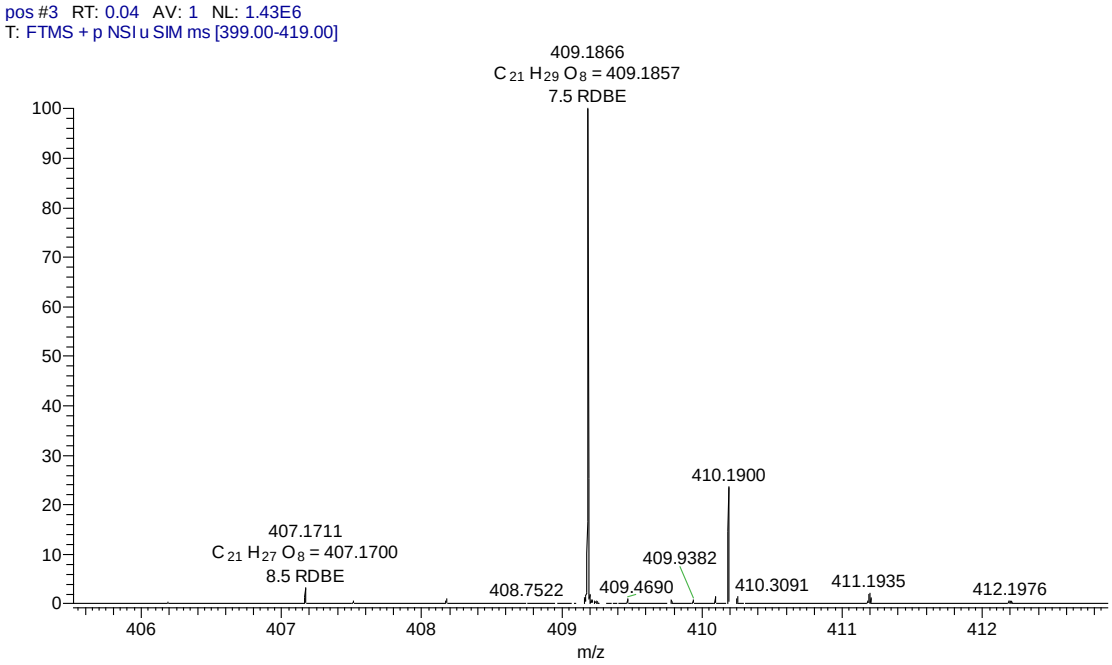

Figure 39: FT-ICR-MS spectrum of compound **RH2** in $[M+H]^+$ positive ion mode.

A new natural product, compound **RH3**, was isolated as a yellow powder (Figure 40). In the accurate mass spectrum measured by positive mode FT-ICR-MS, a molecular ion peak similar to **RH1** at *m/z* 247.0967 $[M+H]^+$ (Calcd for $C_{14}H_{15}O_4$: 247.0970) was obtained, indicating a molecular formula of $C_{14}H_{14}O_4$ along with eight degrees of unsaturation (see appendix II). The IR bands were due to a hydroxyl, carbonyl and aromatic carbon-carbon double bond observed at 3419, 1715 and 1603 cm^{-1}, respectively (see appendix III).

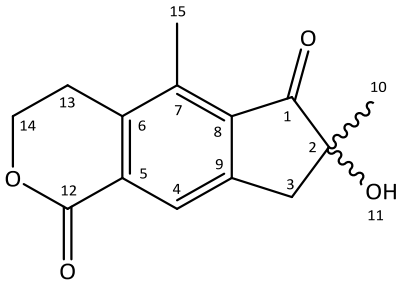

Figure 40: Chemical Structure of Rhedynosin B (**RH3**).

The ^1H NMR spectrum (Table 8 and see appendix I) of **RH3** closely resembles that of **RH1** but the ^{13}C NMR spectrum, in combination with HMBC experiment, displays 14 carbon resonances instead of the 15 signals that appear in the spectrum of **RH1**. These signals were ascribed to two methyls, three methylenes, one methine, six quaternary carbons and two carbonyl functional groups (Table 8). The major differences in the NMR data for compound **RH3** are: ***i***) the absence of a methylene signal at δ_H 4.80 (CH_2-12, ^1H NMR) and ***ii***) the

appearance of a quaternary carbon in the downfield region at δ_C 165.0[12] (^{13}C NMR) corresponding to an ester (see appendix I), thus indicating that the methylene group (CH_2-12) of **RH1** is oxidised and present as a carbonyl in **RH3**. This interpretation explains the downfield shift (δ_H 8.05) of the methine signal (H-4) due to the influence of the carbonyl at position C-12. However, the HMBC and COSY experiments of compound **RH3** were shown similar C-H correlations as for **RH1**, they displayed extra correlations used in structurally elucidation of **RH3**.

Table 8: ^{1}H (400 MHz) and ^{13}C (100 MHz) NMR spectral data of compound **RH3** in $CDCl_3$ (δ in ppm, multiplicity, J in Hz).

Position	δ_H	δ_C	HMBC*
1	-	209.2, C	-
2	-	78.0, C	-
3	3.22 (s)	41.4, CH_2	C: 1, 2, 6, 9, 10
4	8.05 (s)	126.3, CH	C: 5, 6, 12
5	-	138.2, C	-
6	-	134.6, C	-
7	-	137.3, C	-
8	-	130.7, C	-
9	-	149.7, C	-
10	1.42 (s)	26.0, CH_3	C: 1, 2, 3
11	-	-	-
12	-	165.0, C	-
13	3.05 (t, J = 6.0)	24.6, CH_2	C: 5, 8, 14
14	4.55 (t, J = 6.0)	66.9, CH_2	C: 5, 12, 13
15	2.64 (s)	13.7, CH_3	C: 4, 6, 7, 8

* HMBC correlations are from proton(s) stated to the indicated carbon(s)

The main HMBC and COSY correlations are outlined in Figure 41. The HMBC spectrum confirmed the location of the carbonyl group. Furthermore, in the HMBC experiment (see appendix I) strong correlations were observed from both proton signals at δ_H 8.05 (H-4) & 4.55 (H-14) to the carbon signal at δ_C 165.0 (C-12). The other significant difference was the absence of CH_2 signals at δ_H 3.78 and δ_H 3.62 (CH_2-11) in the ^{1}H NMR spectrum. The ^{13}C NMR spectrum showed that the methylene signal from C-11 was absent and that the signal for C-2 had moved downfield to δ_C 78.0, showing the presence of an oxygen. While CD spectra were obtained for **RH3**, the absolute stereochemistry was not assignable as there was neither an X-ray reference with hydroxyl substitution on C-2 nor a previous literature report of a CD

[12] This carbon signal was assigned with HMBC experiment.

spectrum of a compound with a suitable chromophore core. Using this data, compound **RH3** was identified as a previously unreported natural product (new compound) and named rhedynosin B (Figure 40).

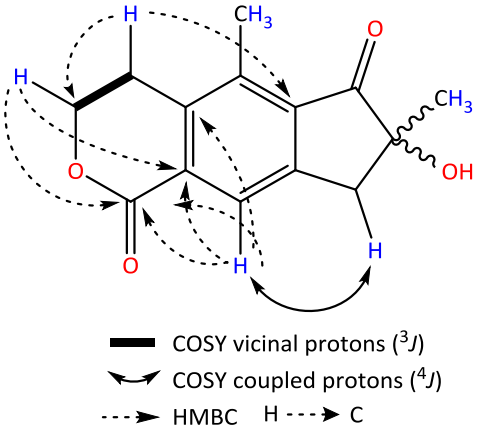

Figure 41: 2D NMR key correlations including COSY and HMBC used in the structural identification of the compound **RH3**.

Compound RH4 was obtained as a white powder with an optical rotation $[\alpha]_D^{24}$ +3.8º (Figure 42). The negative mode mass spectrum showed a molecular ion peak at *m/z* 245.0821 $[M-H]^-$ (see appendix II), compatible with $C_{14}H_{13}O_4$ (Calcd as 245.0814) and consequently indicated $C_{14}H_{14}O_4$ as a molecular formula of **RH4**. In the IR spectrum, strong bands at ν_{max} 1703 and 3428 cm^{-1} were indicative of carbonyl and hydroxyl groups, respectively (see appendix III).

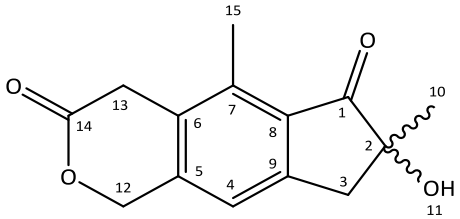

Figure 42: Chemical Structure of Rhedynosin C (**RH4**).

The maximum UV absorbances of **RH4** appeared at 214, 258 and 306 nm (see appendix IV), and in agreement with 1-indanone compounds (Tanaka et al., 1982; Yoshihira et al., 1971). The ^1H and ^{13}C NMR spectroscopic data of **RH4** are listed in Table 9. Analysis of the NMR and mass spectral data showed that **RH4** is structurally similar to **RH3**. The major differences were detected by NMR spectroscopic data, for example the presence of two isolated methylene signals at δ_H 5.40 (2H, s, H-12) and δ_H 3.83 (2H, s, H-13) which appear as singlets and thus

indicated that the carbonyl group was at position C-14 in **RH4**. The chemical shift for CH_2-12 (δ_H 5.40) also indicated a very electron-deficient environment, consistent with $ArCH_2OC{=}O$.

Table 9: ^1H (400 MHz) and ^{13}C (100 MHz) NMR spectral data of compound **RH4** in CD_3OD (δ in ppm, multiplicity, J in Hz).

Position	δ_H	δ_C	HMBC‡
1	-	209.7, C	-
2	-	78.1, C	-
3a 3b	3.10 (d, J = 17.0) 3.10 (d, J = 17.0)	42.9, CH_2	C: 1, 2, 9
4	7.29 (s)	121.9, CH	C: 8, 12
5	-	140.5, C	-
6	-	136.9, C	-
7	-	137.8, C	-
8	-	131.3, C	-
9	-	152.1, C	-
10	1.36 (s)	25.2, CH_3	C: 1, 2, 3
11	-	-	-
12	5.40 (s)	71.1, CH_2	C: 4, 5, 8, 14
13	3.83 (s)	32.8, CH_2	-
14	-	173.5, C	-
15	2.62 (s)	13.0, CH_3	C: 7, 8

‡ HMBC correlations are from proton(s) stated to the indicated carbon(s)

The main HMBC correlations of **RH4** which were not observed in compound **RH3** are illustrated in Figure 43. The HMBC spectrum confirmed the assignments and connectivities, and also showed a cross peak between H-12 (δ_H 5.40) and C-14 (δ_C 173.5) (Figure 43 & see appendix I). The data provided further evidence for the carbonyl being present at the position C-14. Thus, the structure of **RH4** was identified as a new compound and named rhedynosin C (Figure 42). However, the absolute configuration at position C-2 was not assignable with the CD spectroscopy and hence it remains undetermined.

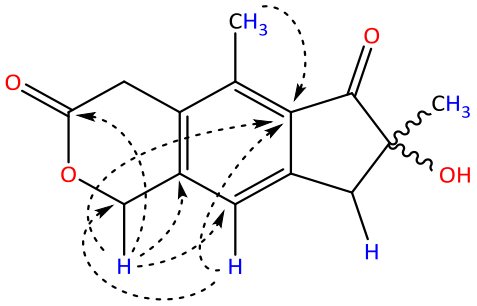

Figure 43: HMBC key correlations used in the structural identification of **RH4**.

Compound **RH5** was obtained as a yellow solid (Figure 44). In the positive mode spectrum, *pseudo*-molecular ion peaks at *m/z* 269.0941 and *m/z* 271.0912 $[M + H]^+$ in the pattern ratio 3:1 are observed, indicate the presence of one chlorine atom and suggested a molecular formula of $C_{14}H_{18}ClO_3$ (Calcd as 269.0944) (see appendix II). Proton and carbon NMR data of **RH5** are shown in Table 10.

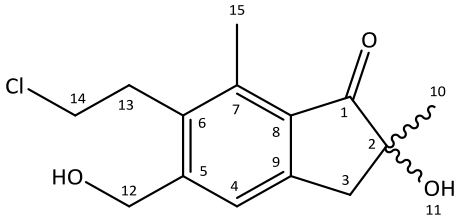

Figure 44: Chemical Structure of Rhedynosin D (**RH5**).

Table 10: ^1H (400 MHz) and ^{13}C (100 MHz) NMR spectral data of compound **RH5** in $CDCl_3$ (δ in ppm, multiplicity, *J* in Hz).

Position	δ_H	δ_C	HMBC[±]
1	-	208.9, C	-
2	-	77.8, C	-
3	3.15 (d, *J* = 2.8)	41.4, CH_2	C: 2, 4, 9, 10
4	7.39 (s)	124.0, CH	C: 3, 6, 8, 12
5	-	146.9, C	-
6	-	134.7, C	-
7	-	139.3, C	-
8	-	131.0, C	-
9	-	151.0, C	-
10	1.40 (s)	26.2, CH_3	C: 1, 2, 3
11	-	-	-
12	4.84 (s)	63.8, CH_2	C: 4, 5, 6
13	3.21 (t, *J* = 8.0)	31.7, CH_2	C: 5, 6, 7, 14
14	3.62 (t, *J* = 8.0)	42.8, CH_2	C: 6, 13
15	2.67 (s)	14.0, CH_3	C: 4, 5, 6, 7, 8

[±] HMBC correlations are from proton(s) stated to the indicated carbon(s)

The IR spectrum shows major absorption bands at 3418 cm^{-1} (OH), 1714 cm^{-1} (C=O) and 1602 and 1447 cm^{-1} (aromatic C=C) (see appendix III). The UV spectrum exhibits UV signals at 212, 215 and 303 nm (see appendix IV). The ^1H NMR data (Table 10) of **RH5** indicates a pentasubstituted benzene ring with a single aromatic proton signal at δ_H 7.39 (1 H, s). Two coupled methylene groups at δ_H 3.21 (2H, t, *J* = 8.0 Hz) and δ_H 3.62 (2H, t, *J* = 8.0 Hz) indicate

an $ArCH_2CH_2X$ system, with the chemical shift of the latter triplet suggesting that X = Cl. The remaining ^1H NMR signals were in agreement with a pterosin-type structure (Fukuoka et al., 1978; Kovganko et al., 2004; Kuraishi et al., 1985; Tanaka et al., 1982). The ^{13}C NMR data of **RH5** (see appendix I and Table 10) shows fourteen distinct carbon environments, confirming the presence of a pentasubstituted aromatic ring, including a low-field signal at δ_C 208.9 ppm (C=O) assigned as the C-1 of a pterosin-type sesquiterpene skeleton. The distinctive COSY and HMBC correlations distinguishing **RH5** from **RH4** are displayed in Figure 45. The HMBC proton-carbon correlations confirmed a pterosin K side chain, a 2-chloroethyl group (CH_2CH_2Cl) attached to C-6 of benzene ring. A singlet methylene signal at δ_H 4.84 was assigned as the hydroxymethylene (CH_2OH) group attached to C-5 of the benzene ring. All assignments were confirmed by HMBC correlations and **RH5** was thus identified as rhedynosin D (Figure 44). However, the absolute configuration in C-2 was not assigned by the CD spectroscopy and therefore it remains undetermined.

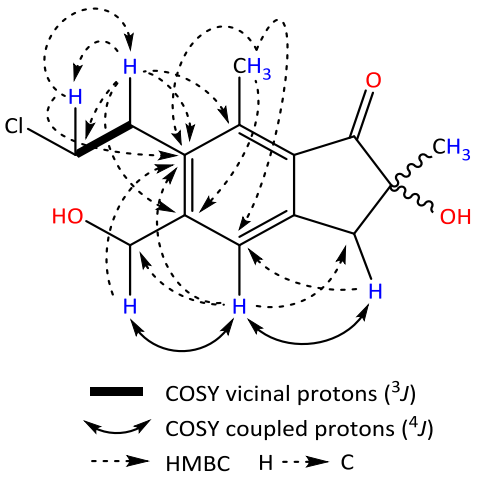

Figure 45: COSY and HMBC key correlations used in the structural identification of **RH5**.

Compound **RH8** was obtained as a yellow gum (Figure 46), whose molecular formula, $C_{14}H_{17}ClO_3$, was determined by a combination of a positive mode HR-ESI-MS at *m/z* 269.0941 $[M+H]^+$ (Calcd for $C_{14}H_{18}ClO_3$: 269.0944) and NMR spectroscopic analysis. This molecular formula was exactly identical to that of **RH5**, designating **RH8** as an isomer of **RH5**. The UV spectrum showed absorption bands at 218, 260 and 299 nm (see appendix IV). Table 11 shows the ^1H and ^{13}C NMR data of compound **RH8**.

The IR, NMR and MS data of **RH8** (see appendices I-III) were similar to those of **RH5**, with detailed exceptions which allowed identification of **RH8**. Differences were found in the NMR

signals for the positions C-12 and C-13 for these two compounds. The differences were concluded based on the following observations. First, in comparison with **RH5**, ^{1}H NMR of compound **RH8** displayed signal of protons in 12-position at up-field region while the chemical shifts of 13-position protons were shifted down-field indicating the presence of the electron withdrawing hydroxyl group (Figure 47).

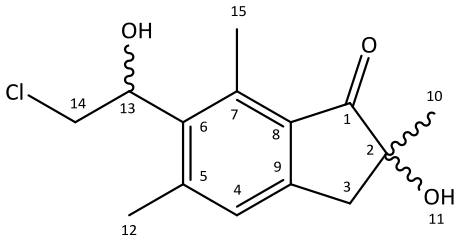

Figure 46: Chemical Structure of Rhedynosin G (**RH8**).

Second, the ^{1}H NMR spectrum of **RH8** showed a methyl group resonating at δ_H 2.55 that gave a proton-carbon correlation to the carbon resonating at δ_C 22.0 in the HSQC spectrum and by HMBC experiment this was assigned as C-12. A methine group, resonating at δ_H 5.45 (1 H, dd, J = 5.2, 8.7 Hz), that gave proton-carbon correlation to the carbon resonating at δ_C 71.4 in the HSQC spectrum, was assigned as the C-13. This confirmed that the hydroxyl group, which had been at C-12 in **RH5**, was in position C-13 in **RH8**.

Table 11: ^{1}H (400 MHz) and ^{13}C (100 MHz) NMR spectral data of compound **RH8** in $(CD_3)_2CO$ (δ in ppm, multiplicity, J in Hz).

Position	δ_H	δ_C	HMBC$^{\Delta}$
1	-	208.5, C	-
2	-	77.4, C	-
3	3.05 (d, J = 9.5)	42.2, CH_2	C: 2, 4, 5, 7, 8, 9, 10
4	7.13 (s)	128.0, CH	C: 3, 7, 8, 12
5	-	145.7, C	-
6	-	134.6, C	-
7	-	138.5, C	-
8	-	131.1, C	-
9	-	151.9, C	-
10	1.32 (s)	25.5, CH_3	C: 1, 2, 3
11	-	-	-
12	2.55	22.0, CH_3	C: 4, 5, 7, 8
13	5.45 (dd, J = 5.2, 8.7)	71.4, CH	C: 5, 7, 14
14a 14b	3.98 (dd, $J_{13, 14a}$ = 8.7, $J_{14a, 14b}$ = 11.2) 3.81 (dd, $J_{13, 14b}$ = 5.2)	48.1, CH_2	C: 7, 13
15	2.75 (s)	14.6, CH_3	C: 4, 5, 6, 7, 8

Δ HMBC correlations are from proton(s) stated to the indicated carbon(s)

Compound **RH8** revealed more proton-carbon correlations in the HMBC experiment which were not shown by **RH5**. However, CD spectroscopy was applied, the stereochemistry of **RH8** in position C-2 was not assignable and thus it remains undetermined. Compound **RH8** was thus identified as rhedynosin G (Figure 46).

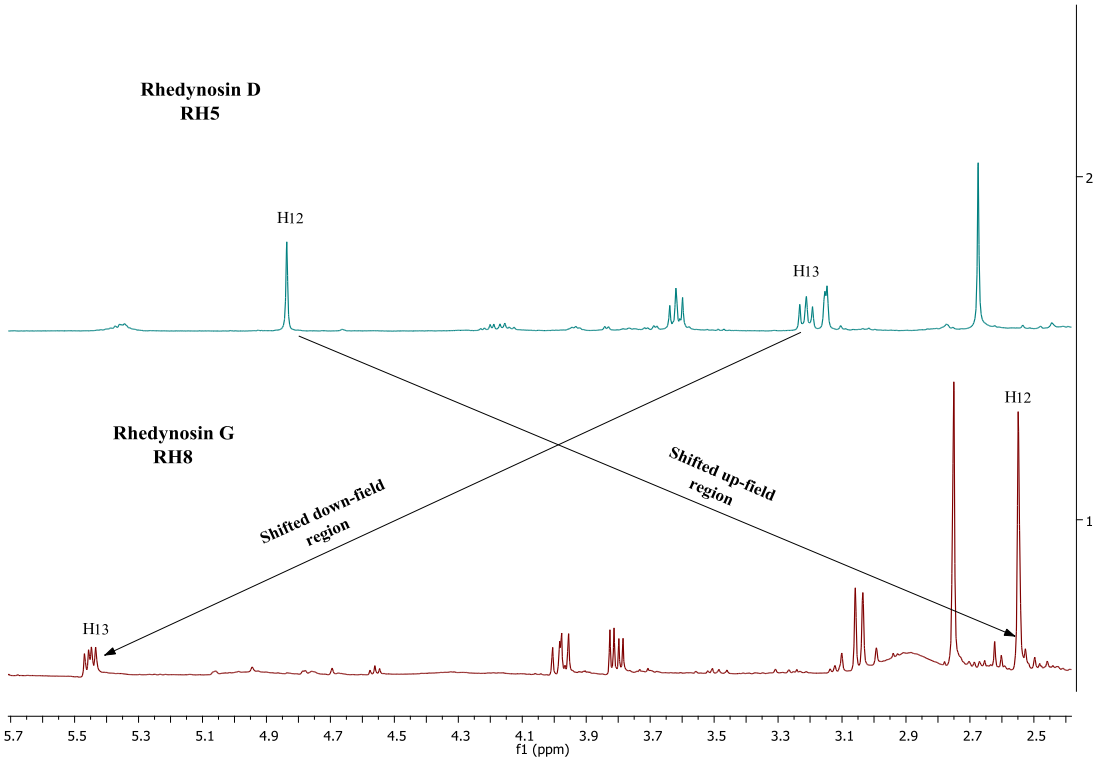

Figure 47: Up and down-field shifting of selected signals in ^{1}H NMR of compounds **RH5** and **RH8**.

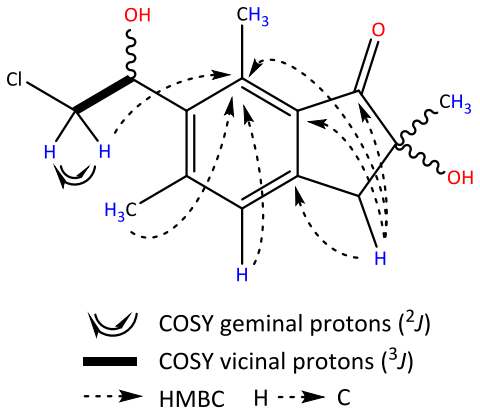

Figure 48: COSY and HMBC key correlations used in the structural identification of **RH8**.

Compound **RH7** was obtained as a pale yellow crystalline powder (Figure 49). From the molecular ion peak shown by a positive mode FT-ICR-MS at *m/z* 283.1098 $[M+H]^+$ (Calcd for $C_{15}H_{20}ClO_3$: 282.1023), the molecular formula of **RH7** was concluded to be $C_{15}H_{19}ClO_3$, suggesting an additional CH_2 when compared to **RH8**. The UV, IR and NMR data were similar to those of **RH8** (see appendices I, III and IV). However, an additional CH_2 was evident from the NMR data of **RH7**, with two geminally coupled doublets δ_H 3.79 (1 H, d, J = 10.7 Hz) and δ_H 3.59 (1 H, d, J = 10.7 Hz), correlating through one-bond with a new carbon signal at δ_C 68.1.

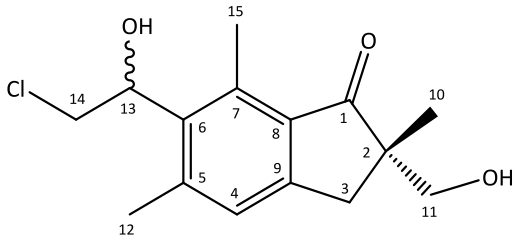

Figure 49: Chemical Structure of Rhedynosin F (**RH7**).

Table 12: ^1H (400 MHz) and ^{13}C (100 MHz) NMR spectral data of compound **RH7** in $CDCl_3$ (δ in ppm, multiplicity, J in Hz).

Position	δ_H	δ_C	HMBC$^\Phi$
1	-	211.7, C	-
2	-	51.0, C	-
3a 3b	3.08 (d, J = 17.3) 2.74 (d, J = 17.3)	36.8, CH_2	C: 2, 9, 10, 11
4	7.11 (s)	127.5, CH	C: 3, 6, 8, 12
5	-	144.8, C	-
6	-	135.4, C	-
7	-	139.0, C	-
8	-	132.4, C	-
9	-	154.0, C	-
10	1.20 (s)	21.2, CH_3	C: 2, 3, 11
11a 11b	3.79 (d, J = 10.7) 3.59 (d, J = 10.7)	68.1, CH_2	C: 2, 3, 10
12	2.53 (s)	22.2, CH_3	C: 4, 5, 6
13	5.41 (dd, J = 3.5, 10.0)	71.5, CH	C: 5, 6, 7, 14
14a 14b	3.98 (dd, $J_{13, 14a}$ = 10.2, $J_{14a, 14b}$ =11.4) 3.65 (dd, $J_{13, 14b}$ = 3.7)	47.8, CH_2	C: 13
15	2.77 (s)	14.8, CH_3	C: 4, 6, 7, 8, 10

$^\Phi$ HMBC correlations are from proton(s) stated to the indicated carbon(s)

The chemical shifts indicated that this new methylene was attached to the oxygen and thus the hydroxymethylene group was in position C-2. On the basis of the above mentioned evidence, the structure of **RH7** was confirmed as rhedynosin F (Figure 49). The CD spectroscopy allowed

a *S* assignment of configuration at position C-2. Table 12 demonstrates the proton and carbon NMR data of compound **RH7**.

Compound **RH9** was isolated as an off-white powder and its mass spectrum in the negative ion mode FT-ICR-MS showed a molecular ion peak at *m/z* 297.0802 $[M-H]^-$ corresponding to a molecular formula of $C_{14}H_{17}O_5S$ (Calcd as 297.0797). The UV, IR, and NMR data of **RH9** were very similar to those of pterosin B (**RH16**) (Table 20 and see appendices I, III and IV).

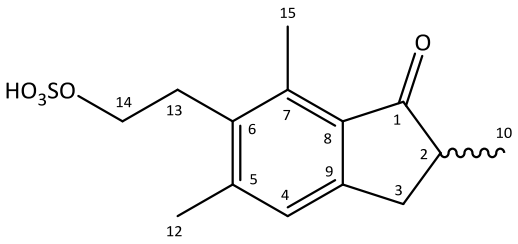

Figure 50: Chemical Structure of Rhedynosin H (**RH9**).

Table 13: ^1H (125 MHz) and ^{13}C (500 MHz) NMR spectral data of compound **RH9** in CD_3OD (δ in ppm, multiplicity, *J* in Hz).

Position	δ_H	δ_C	HMBC[π]
1	-	208.8, C	-
2	2.63 (m)	43.7, CH	C: 4, 5, 6, 7, 8, 10
3a 3b	3.27 (m) 2.59 (m)	34.6, CH_2	C: 2, 4, 8, 9
4	7.16 (s)	126.9, CH	C: 3, 6, 8, 12
5	-	146.8, C	-
6	-	135.3, C	-
7	-	139.0, C	-
8	-	132.5, C	-
9	-	155.0, C	-
10	1.23 (d, *J* = 7.5)	16.9, CH_3	C: 1, 2, 3
11	-	-	-
12	2.46 (s)	21.4, CH_3	C: 4, 5, 6, 7, 8
13	3.15 (t, *J* = 8.0)	29.3, CH_2	C: 5, 6, 9, 14
14	4.05 (t, *J* = 8.0)	67.4, CH_2	C: 6, 13
15	2.67 (s)	13.9, CH_3	-

[π] HMBC correlations are from proton(s) stated to the indicated carbon(s)

The ^1H and ^{13}C NMR data of **RH9** is shown in Table 13. This molecular formula and an 80 amu difference in mass between **RH9** (298 amu) and **RH16** (218 amu) strongly suggested that the primary alcohol of **RH16** had been sulfated in **RH9**, i.e. the OH group was replaced with the hydrogen sulfate substituent (HSO_4^-). This was confirmed by a downfield shift of the proton

and carbon resonances for the adjacent methylene (CH_2-14) to δ_H 4.05 and δ_C 67.4, respectively. Moreover, the HMBC cross peaks from H-14 (δ_H 4.05) to each of C-6 (δ_C 135.3) and C-13 (δ_C 29.3), and from H-13 (δ_H 3.15) to C-14 (δ_C 67.4) verified the location of C-13 and C-14. Sulfated monoesters are common in marine natural products (McKee et al., 1994; Uddin et al., 2011). Compound **RH9** was subjected to CD spectroscopy, however no significant spectrum was observed. It is hypothesised that compound **RH9** is racemised due to the presence of an acidic proton in the α-position to the carbonyl group. Therefore, the structure of **RH9** was confirmed by full analysis of the data as rhedynosin H (Figure 50).

Compound **RH6** was obtained as an off-white powder (Figure 51). Its molecular formula ($C_{15}H_{18}O_4$) was determined from the positive mode FT-ICR-MS which exhibited a molecular ion peak at *m*/*z* 263.1280 $[M+H]^+$ (Calcd for $C_{15}H_{19}O_4$: 263.1283). Table 14 exhibits the ^1H and ^{13}C NMR data of **RH6**. The UV, IR and NMR data of **RH6** were very similar to *trans*-histiopterosin A (**RH28**) (Murakami et al., 1980) (see appendices I, III and IV). Two carbonyl resonances were evident in the ^{13}C NMR spectrum, with the ketone signal at δ_C 211.6 and a carboxylic acid signal at δ_C 175.3. In the ^1H NMR spectrum of **RH6,** an additional methyl signal is present, which was shown to be connected to C-2 by HMBC. Thus, two magnetically inequivalent methyl groups are attached to C-2, which resonate as singlets at δ_H 1.05 and δ_H 1.19.

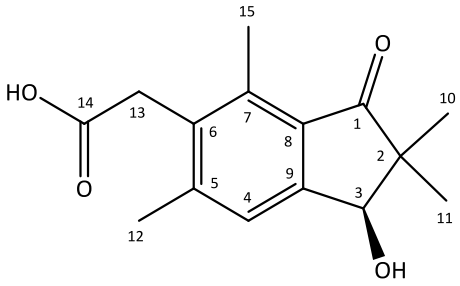

Figure 51: Chemical Structure of (3*S*)-Rhedynosin E (**RH6**).

The application of CD spectroscopy to compound **RH6** showed a non-vibronic n → π* transition which was compared to the CD spectrum for **RH19** reported by Kuroyanagi et al. (1979b) and assigned the configuration as *S* on C-3. Therefore, the structure of **RH6** was confirmed as rhedynosin E (Figure 51).

Table 14: ^{1}H (100 MHz) and ^{13}C (400 MHz) NMR spectral data of compound **RH6** in CD_3OD (δ in ppm, multiplicity, J in Hz).

Position	δ_H	δ_C	HMBC[#]
1	-	211.6, C	-
2	-	52.5, C	-
3	4.76 (s)	77.6, CH	C: 4, 8, 9, 10
4	7.39 (s)	126.0, CH	C: 3, 6, 8, 12
5	-	146.6, C	-
6	-	136.0, C	-
7	-	138.9, C	-
8	-	131.1, C	-
9	-	154.3, C	-
10	1.19 (s)	23.5, CH_3	C: 1, 2, 3, 11
11	1.05 (s)	20.7, CH_3	C: 1, 2, 3, 10
12	2,44 (s)	21.6, CH_3	C: 4, 5, 6
13	3.78 (s)	35.1, CH_2	C: 5, 6, 7, 14
14	-	175.3, C	-
15	2.61 (s)	14.2, CH_3	C: 4, 5, 6, 7, 8

[#] HMBC correlations are from proton(s) stated to the indicated carbon(s)

Compound **RH10** was obtained as a white crystalline product (Figure 52). An accurate mass spectrum of **RH10** was recorded by a positive mode FT-ICR-MS, exhibited a molecular ion peak at *m/z* 415.1528 $[M+H]^+$ and correlated to the molecular formula $C_{20}H_{28}ClO_7$ (Calcd as 415.1524). The ^{1}H and ^{13}C NMR data of **RH10** is illustrated in Table 15. The UV, IR, and NMR data for **RH10** were very similar to those reported for pterosin F (**RH21**) (Fukuoka et al., 1978; Kuroyanagi et al., 1979a) (see appendices I, III and IV), except for the presence of a sugar moiety in **RH10** which was connected to the aglycone through C-2, as determined by the HMBC experiment. Careful study of the coupling constants around the hexopyranose in the ^{1}H NMR spectrum suggested that the sugar was a glucose; $J_{1',2'}$ = 7.8 Hz, $J_{2',3'}$ = 8.0 Hz and $J_{3',4'}$ = 8.9 Hz, consistent only with *trans*-diaxial arrangements of these protons. X-ray crystallography confirmed **RH10** as rhedynoside B and assigned the configuration at C-2 as *R* (Figure 52-Figure **53**). The single crystal X-ray data is submitted to Cambridge X-ray data centre. The CD spectroscopy was applied to further confirm the stereochemistry of compound **RH10** at position C-2, however no absorption bands were obtained in range of 300-360 nm.

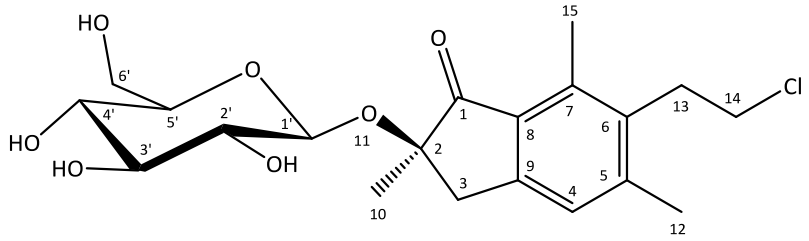

Figure 52: Chemical Structure of (2*R*)-Rhedynoside B (**RH10**).

Table 15: ^{1}H (100 MHz) and ^{13}C (400 MHz) NMR spectral data of compound **RH10** in CD_3OD (δ in ppm, multiplicity, *J* in Hz).

Position	δ_H	δ_C	HMBC$^{\Psi}$
1	-	207.3, C	-
2	-	84.1, C	-
3a 3b	3.45 (d, *J* = 17.4) 3.08 (d, *J* = 17.4)	40.9, CH_2	C: 2, 8, 9, 10
4	7.17 (s)	127.3, CH	C: 3, 6, 8, 12
5	-	147.2, C	-
6	-	136.7, C	-
7	-	139.6, C	-
8	-	131.5, C	-
9	-	152.3, C	-
10	1.44 (s)	23.7, CH_3	C: 1, 2, 3
11	-	-	-
12	2.45 (s)	21.3, CH_3	C: 4, 5, 6, 7, 8
13	3.22 (t, *J* = 8.0)	33.0, CH_2	C: 5, 6, 7, 14
14	3.63 (t, *J* = 8.0)	43.1, CH_2	C: 6, 13
15	2.65 (s)	14.1, CH_3	C: 4, 5, 6, 7, 8
1′	4.42 (d, $J_{1',2'}$ = 7.8)	100.5, CH	C: 2, 5′
2′	3.16 (dd, $J_{2',3'}$ = 8.0)	75.1, CH	C: 3′
3′	3.32^{++}	78.0, CH	C: 4′
4′	3.28 (dd ~ t, $J_{3',4'}$ = 8.9)	71.3, CH	C: 5′
5′	3.12 (m)	77.7, CH	-
6′a 6′b	3.70 (dd, $J_{5',6'a}$ = 2.5, $J_{6'a,6'b}$ = 12.0) 3.60 (dd, $J_{5',6'b}$ = 5.0)	62.5, CH_2	-

$^{++}$ Signal under solvent, confirmed by HSQC experiment.

$^{\Psi}$ HMBC correlations are from proton(s) stated to the indicated carbon(s)

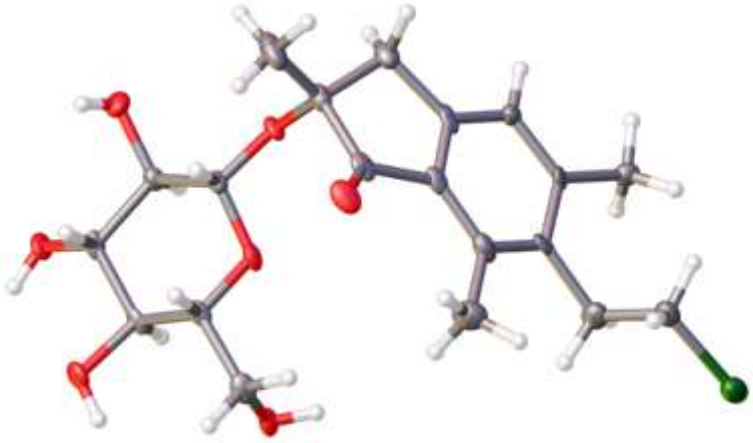

Figure 53: Thermal ellipsoid plot of compound Rhedynoside B (**RH10**) with ellipsoids shown at 50% probability. N.B. Rhedynoside B crystallises as a hemihydrate with four molecules of Rhedynoside B and two molecules of water in the asymmetric unit. Only one molecule of the Rhedynoside B structure is shown here for clarity.

Compound **RH11** was obtained as an off-white crystalline powder (Figure 54). The mass spectrum showed a strong ion signal of $[M-H]^-$ at *m/z* 427.1531 (Calcd for $C_{21}H_{28}ClO_7$: 427.1524) in the negative mode FT-ICR-MS, indicating the molecular formula of $C_{21}H_{29}ClO_7$ with a molecular mass 14 Da higher than **RH10**. The ^1H and ^{13}C NMR data of **RH11** are shown in Table 16. The UV, IR and NMR data of **RH11** were similar to those of pterosin H (Hayashi et al., 1972; Padwa et al., 1996; Tanaka et al., 1982) with the exception that **RH11** contained a sugar moiety (see appendices I, III and IV). Of particular interest was a pair of geminally coupled doublets in the ^1H NMR spectrum at δ_H 5.11 (1 H, d, J = 12.4 Hz) and δ_H 4.78 (1 H, d, J = 12.4 Hz). These signals gave a one-bond H-C correlation with the ^{13}C NMR signal at δ_C 70.2. The chemical shifts corresponded to an $ArCH_2O$ system. An HMBC experiment assigned this carbon signal being connected to C-12. Moreover, the HMBC also linked the sugar to this methylene. The ^1H NMR spectrum of **RH11** confirmed the sugar as a hexopyranoside and identified the configuration of the glycosidic bond as β, with $J_{1',2'}$ = 7.7 Hz (also suggesting that the sugar was glucose or galactose). Peracetylation of the sugar separated the ^1H NMR signals of the sugar sufficiently to provide a full diastereomeric assignment of the sugar as glucose (see the discussion for **RH2** above). On the basis of this evidence, compound **RH11** was identified as rhedynoside C (Figure 54).

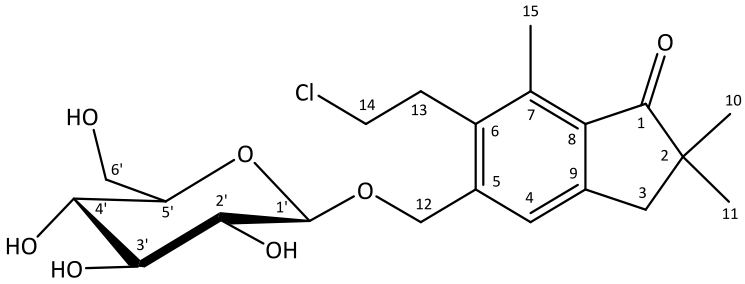

Figure 54: Chemical Structure of Rhedynoside C (**RH11**).

Table 16: ^{1}H (400 MHz) and ^{13}C (100 MHz) spectral data of compound **RH11** in CD_3OD (δ in ppm, multiplicity, *J* in Hz).

Position	δ_H	δ_C	HMBC†
1	-	211.2, C	-
2	-	46.9, C	-
3	2.93 (s)	42.7, CH_2	C: 2, 4, 8, 9, 10
4	7.50 (s)	126.5, CH	C: 6, 8
5	-	144.9, C	-
6	-	136.5, C	-
7	-	139.6, C	-
8	-	133.4, C	-
9	-	153.4, C	-
10	1.17 (s)	25.8, CH_3	C: 1, 2, 3, 11
11	1.17 (s)	25.8, CH_3	C: 1, 2, 3, 10
12a 12b	5.11 (d, *J* = 12.4) 4.78 (d, *J* = 12.4)	70.2, CH_2	C: 4, 5, 6, 1′
13	3.26 (m)	32.5, CH_2	C: 5, 6, 7, 14
14	3.63 (m)	43.8, CH_2	-
15	2.66 (s)	13.7, CH_3	C: 6, 7, 8
1′	4.40 (d, *J* = 7.7)	103.5, CH	C: 12
2′	3.29 (m)	75.2, CH	-
3′	3.31 (m)	78.2, CH	-
4′	3.31 (m)	71.8, CH	-
5′	3.36 (m)	78.2, CH	-
6′a 6′b	3.92 (dd, $J_{5',6'a}$ = 2.0, $J_{6'a,6'b}$ = 12.0) 3.70 (dd, $J_{5',6'b}$ = 4.0)	62.9, CH_2	-

† HMBC correlations are from proton(s) stated to the indicated carbon(s)

Compound **RH12** (Figure 55), a novel natural product, was obtained as yellow powder with the negative optical rotation $[\alpha]_D^{25}$ -0.6 (*c* 0.33, MeOH). In the negative mode FT-ICR-MS, **RH12** gave a quasi-molecular ion peak at *m/z* 413.1374 $[M-H]^-$, appropriate for a molecular formula $C_{20}H_{26}ClO_7$ (Calcd as 413.1367), and indicating that it was an isomer of **RH10**. Table 17 demonstrates the proton and carbon NMR data of compound **RH12**. The UV, IR and NMR

data of **RH12** were broadly similar to those of **RH10** except that the point of attachment of the sugar was clearly different (see appendices I, III and IV). As for **RH11**, a diastereotopic methylene group was observed in the NMR spectra at δ_H 5.10 (1 H, d, J = 12.3 Hz) & 4.78 (1 H, d, J = 12.3 Hz) and δ_C 70.2.

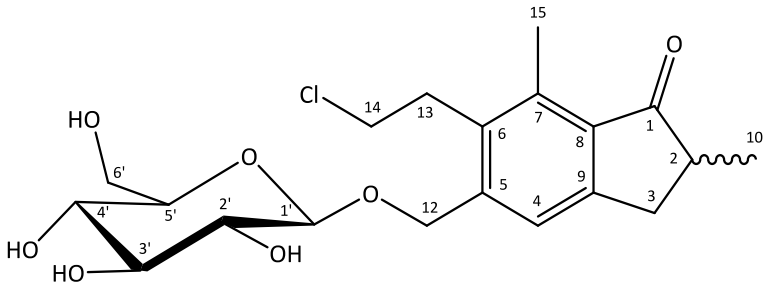

Figure 55: Chemical Structure of Rhedynoside D (**RH12**).

Table 17: ^{1}H (400 MHz) and ^{13}C (100 MHz) spectral data of compound **RH12** in CD_3OD (δ in ppm, multiplicity, J in Hz).

Position	δ_H	δ_C	HMBC[¤]
1	-	212.5, C	-
2	2.66 (m)	43.9, CH	-
3a 3b	3.33 (m) 2.64 (m)	34.9, CH_2	C: 2, 9
4	7.51 (s)	126.4, CH	C: 3, 6, 8, 12
5	-	144.7, C	-
6	-	136.4, C	-
7	-	139.1, C	-
8	-	134.4, C	-
9	-	154.7, C	-
10	1.25 (d, J = 7.2)	16.7, CH_3	C: 1, 2, 3
11	-	-	-
12a 12b	5.10 (d, J = 12.3) 4.78 (d, J = 12.3)	70.2, CH_2	C: 4, 5, 6, 1′
13	3.26 (t, J = 8.0)	32.5, CH_2	C: 5, 6, 7, 14
14	3.70 (t, J = 8.0)	43.8, CH_2	-
15	2.66 (s)	13.7, CH_3	C: 4, 5, 6, 7, 8
1′	4.39 (d, J = 7.7)	103.5, CH	C: 12, 3′, 5′
2′	3.26 (m)	75.2, CH	C: 1′, 3′, 5′
3′	3.31 (m)	78.2, CH	-
4′	3.31 (m)	71.8, CH	-
5′	3.36 (m)	78.2, CH	C: 4′
6′a 6′b	3.92 (dd, $J_{5',6'a}$ = 1.5, $J_{6'a,6'b}$ = 11.5) 3.69 (dd, $J_{5',6'b}$ = 3.0)	62.9, CH_2	-

[¤] HMBC correlations are from proton(s) stated to the indicated carbon(s)

Using the same rationale as for determination of the location of the sugar as for **RH11**, HMBC data confirmed that the sugar was attached through a glycosidic linkage to C-12. Examination of the ^{1}H NMR coupling constants for protons around the hexopyranose in native and peracetylated forms demonstrated that it was β-linked glucose. Also notable was the presence of only one methyl group at C-2, δ_H 1.25 (3 H, d, J = 7.2 Hz), with the ^{13}C NMR signal for C-2 now reported as a methine. Compound **RH12** was subjected to CD spectroscopy, but the absolute configuration in C-2 was not determined. It is assumed that **RH12** is racemised due to the presence of an acidic proton in the α-position to the carbonyl group. The structure of **RH12** was thus established as rhedynoside D (Figure 55).

A novel compound **RH13** was isolated as an off-white crystalline powder (Figure 56). Its molecular formula, $C_{21}H_{29}ClO_7$, was deduced from the negative ion mode FT-ICR-MS at *m*/*z* 427.1531 (Calcd for $C_{21}H_{28}ClO_7$: 427.1524), indicating that it was another isomer of **RH11**. The spectroscopic NMR data (^{1}H and ^{13}C) of **RH13** is displayed in Table 18. The UV, IR and NMR data for the aglycone of **RH13** were very similar to those of (3*R*)-hydroxypterosin H (Tanaka et al., 1982) indicating that it has the same structure in the aglycone part (see appendices I, III and IV). A NOESY study of compound **RH13** showed through-space correlations between H-1′ and H-3′ and between H-1′ and H-5′, confirming that these three protons are all axial and that the sugar is glucose. Singlet signals for three methyl groups were evident in the ^{1}H NMR spectrum, with HMBC confirming that two methyl signals (δ_H 1.28 and δ_H 1.09) formed a geminal pair. The third (δ_H 2.49) was in an ArMe environment and was confirmed by HMBC data to correspond to C-12. The signal for H-3 was identified as being at δ_H 4.85, appropriate to ArCHO; thus, the glycoside was tentatively located at C-3. The HMBC correlations from H-3 (δ_H 4.85, s) to C-1′ (δ_C 105.9), and from H-1′ (δ_H 4.58, d, J = 7.7 Hz) to C-3 (δ_C 86.1) evidence that the glycosyl residue is connected through C-3 to the aglycone part (see appendix I). The application of CD spectroscopy to compound **RH13** showed a non-vibronic n → π* transition which is opposite to the transition observed for **RH6**. Based on the comparison of CD data of **RH13** to that for **RH19** reported by Kuroyanagi et al., 1979b, the absolute configuration of compound **RH13** was assigned as *R* in position C-3. The reported compounds, 13-chloro-spelosin 3-*O*-β-D-glucopyranoside (Chen et al., 2015) and (2*R*,3*R*)-pterosin L 3-*O*-β-D-glucopyranoside (Chen et al., 2008), whose ^{1}H and ^{13}C NMR data are very similar to compound **RH13**, also show *R* configuration in position C-3. As a result of these observations, **RH13** was identified as rhedynoside E (Figure 56).

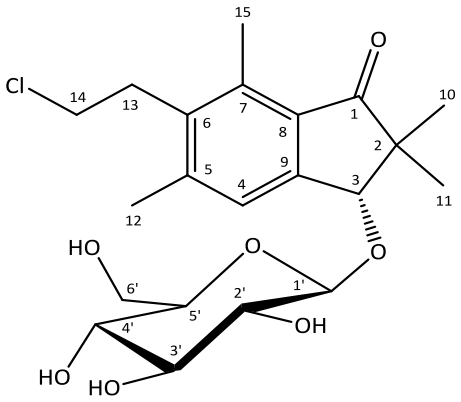

Figure 56: Chemical Structure of (3*R*)-Rhedynoside E (**RH13**).

Table 18: ^{1}H (400 MHz) and ^{13}C (100 MHz) spectral data of compound **RH13** in CD_3OD (δ in ppm, multiplicity, *J* in Hz).

Position	δ_H	δ_C	HMBC[±]
1	-	211.2, C	-
2	-	52.6, C	-
3	4.85 (s)	86.1, CH	C: 8, 9, 10, 1´
4	7.56 (s)	127.0, CH	C: 7, 8, 12
5	-	146.0, C	-
6	-	136.8, C	-
7	-	138.2, C	-
8	-	131.0, C	-
9	-	152.5, C	-
10	1.28 (s)	22.8, CH_3	C: 1, 2, 3, 11
11	1.09 (s)	22.0, CH_3	C: 1, 2, 3, 10
12	2.49 (s)	21.3, CH_3	C: 4, 5, 7, 8
13	3.24 (t, *J* = 8.0)	33.1, CH_2	C: 5, 7, 14
14	3.63 (t, *J* = 8.0)	43.0, CH_2	C: 7
15	2.65 (s)	14.1, CH_3	C: 4, 7, 8
1′	4.58 (d, *J* = 7.7)	105.9, CH	C: 3
2′	3.30 (m)	75.3, CH	-
3′	3.36 (m)	78.0, CH	-
4′	3.36 (m)	71.7, CH	-
5′	3.42 (m)	78.3, CH	C: 4´
6′a 6′b	3.93 (dd, $J_{5',6'a}$ = 1.5, $J_{6'a,6'b}$ = 11.8) 3.75 (dd, $J_{5',6'b}$ = 4.0)	62.9, CH_2	-

[±] HMBC correlations are from proton(s) stated to the indicated carbon(s)

3.4. PHYSICO-CHEMICAL PARAMETERS OF NOVEL COMPOUNDS (RH1-RH13):

*(2S)-Rhedynosin A (**RH1**)*; Yellow powder; $[\alpha]_D^{24}$ -4.3º (*c* 0.33, $CHCl_3$); UV (MeOH) λ_{max} nm (log ε): 211 (4.16), 241 (3.77), 258 (3.85), 306 (2.99); IR (film) ν_{max} 3418, 3014, 2928, 1704, 1605, 1446, 1380, 1048, 755, 666 cm^{-1}; for ^1H and ^{13}C NMR spectroscopic data, see Table 6; FT-ICR-MS *m/z* 247.1330 $[M+H]^+$ (Calcd for $C_{15}H_{19}O_3$: 247.1334).

*(2S)-Rhedynoside A (**RH2**)*: White powder; $[\alpha]_D^{24}$ -26.1º (*c* 0.33, MeOH); UV (MeOH) λ_{max} nm (log ε): 216 (4.27), 259 (3.92), 304 (2.99); IR (film) ν_{max} 3369, 2927, 1692, 1602, 1444, 1378, 1075, 918 cm^{-1}; for ^1H and ^{13}C NMR spectroscopic data, see Table 7; FT-ICR-MS *m/z* 409.1866 $[M+H]^+$ (Calcd for $C_{21}H_{29}O_8$: 409.1862).

*Rhedynosin B (**RH3**)*: Yellow powder; $[\alpha]_D^{24}$ -12.8º (*c* 0.33, $CHCl_3$); UV (MeOH) λ_{max} nm (log ε): 209 (4.31), 260 (3.96), 313 (3.09); IR (film) ν_{max} 3419, 3018, 2926, 1715, 1603, 1446, 1379, 1290, 1196, 1096, 985, 856, 754, 666 cm^{-1}; for ^1H and ^{13}C NMR spectroscopic data, see Table 8; FT-ICR-MS *m/z* 247.0967 $[M+H]^+$ (Calcd for $C_{14}H_{15}O_4$: 247.0970).

*Rhedynosin C (**RH4**)*: White powder; $[\alpha]_D^{24}$ +3.8º (*c* 0.33, MeOH); UV (MeOH) λ_{max} nm (log ε): 214 (3.24), 242 (2.97), 258 (2.94), 306 (2.51); IR (film) ν_{max} 3428, 2924, 1703, 1608 1458, 1379, 1260, 1034, 800 cm^{-1}; for ^1H and ^{13}C NMR spectroscopic data, see Table 9; FT-ICR-MS *m/z* 245.0821 $[M-H]^-$ (Calcd for $C_{14}H_{13}O_4$: 245.0814).

*Rhedynosin D (**RH5**)*: Yellow solid; $[\alpha]_D^{24}$ -19.1º (*c* 0.33, $CHCl_3$); UV (MeOH) λ_{max} nm (log ε): 215 (4.13), 259 (3.75), 303 (2.76); IR (film) ν_{max} 3418, 2925, 1714, 1602, 1447, 1379, 1093, 855, 756, 666 cm^{-1}; for ^1H and ^{13}C NMR spectroscopic data, see Table 10; FT-ICR-MS *m/z* 269.0941 $[M+H]^+$ (Calcd for $C_{14}H_{18}{}^{35}ClO_3$: 269.0944).

*(3S)-Rhedynosin E (**RH6**)*: Off-white powder; $[\alpha]_D^{24}$ -15.0º (*c* 0.33, MeOH); UV (MeOH) λ_{max} nm (log ε): 217 (4.35), 258 (4.02), 295 (3.13); IR (film) ν_{max} 3419, 2932, 1699, 1600, 1465, 1382, 1203, 1099, 995, 884 cm^{-1}; for ^1H and ^{13}C NMR spectroscopic data, see Table 14; FT-ICR-MS *m/z* 263.1280 $[M+H]^+$ (Calcd for $C_{15}H_{19}O_4$: 263.1283).

*(2S)-Rhedynosin F (**RH7**)*: Light yellow crystalline powder; $[\alpha]_D^{24}$ +15.4º (*c* 0.33, $CHCl_3$); UV (MeOH) λ_{max} nm (log ε): 219 (4.27), 259 (3.87), 298 (2.92); IR (film) ν_{max} 3417, 2929, 1698, 1598, 1455, 1379, 1223, 1042, 923, 859, 755 cm^{-1}; for ^1H and ^{13}C NMR spectroscopic data, see Table 12; FT-ICR-MS *m/z* 283.1098 $[M+H]^+$ (Calcd for $C_{15}H_{20}{}^{35}ClO_3$: 283.1101).

*Rhedynosin G (**RH8**)*: Yellow gum; $[\alpha]_D^{24}$ +4.0º (*c* 0.33, MeOH); UV (MeOH) λ_{max} nm (log ε): 218 (4.34), 260 (3.97), 299 (3.03); IR (film) ν_{max} 3405, 2929, 1705, 1599, 1447, 1378, 1217, 1094, 983, 887, 751 cm^{-1}; for ^{1}H and ^{13}C NMR spectroscopic data, see Table 11; FT-ICR-MS *m*/*z* 269. 0941 $[M+H]^+$ (Calcd for $C_{14}H_{18}{}^{35}ClO_3$: 269.0944).

*Rhedynosin H (**RH9**)*: Off-white powder; $[\alpha]_D^{24}$ -28.0º (*c* 0.33, $CHCl_3$); UV (MeOH) λ_{max} nm (log ε): 217 (4.71), 258 (4.37), 303 (3.55); IR (film) ν_{max} 2919, 1704, 1601, 1456, 1377, 1325, 1221, 1129, 1020, 970, 885, 756, 702 cm^{-1}; for ^{1}H and ^{13}C NMR spectroscopic data, see Table 13; FT-ICR-MS *m*/*z* 297. 0802 $[M-H]^-$ (Calcd for $C_{14}H_{17}O_5S$: 297.0797).

*(2R)-Rhedynoside B (**RH10**)*: White crystalline compound; $[\alpha]_D^{24}$ -10.8º (*c* 0.33, MeOH); UV (MeOH) λ_{max} nm (log ε): 219 (4.48), 263 (4.12), 304 (3.11), nm; IR (film) ν_{max} 3391, 2926, 1703, 1601 1451, 1376, 1327, 1227, 1074, 918, 872 cm^{-1}; for ^{1}H and ^{13}C NMR spectroscopic data, see Table 15; FT-ICR-MS *m*/*z* 415.1527 $[M+H]^+$ (Calcd for $C_{20}H_{28}{}^{35}ClO_7$: 415.1523).

*Rhedynoside C (**RH11**)*: Off-white crystalline powder; $[\alpha]_D^{25}$ -0.5º (*c* 0.33, MeOH); UV (MeOH) λ_{max} nm (log ε): 216 (4.43), 257 (3.98), 303 (2.93); IR (film) ν_{max} 3391, 2927, 1699, 1601, 1440, 1379, 1326, 1077, 918, 888 cm^{-1}; for ^{1}H and ^{13}C NMR spectroscopic data, see Table 16; FT-ICR-MS *m*/*z* 427.1530 $[M-H]^-$ (Calcd for $C_{21}H_{28}{}^{35}ClO_7$: 427.1524).

*Rhedynoside D (**RH12**)*: Yellow powder; $[\alpha]_D^{25}$ -0.6º (*c* 0.33, MeOH); UV (MeOH) λ_{max} nm (log ε): 216 (4.43), 256 (4.01), 303 (2.98); IR (film) ν_{max} 3374, 2928, 1700, 1600, 1440, 1376, 1312, 1163, 1075, 921, 890 cm^{-1}; for ^{1}H and ^{13}C NMR spectroscopic data, see Table 17; FT-ICR-MS *m*/*z* 413.1374 $[M-H]^-$ (Calcd for $C_{20}H_{26}{}^{35}ClO_7$: 413.1367).

*(3R)-Rhedynoside E (**RH13**)*: Off-white crystalline powder; $[\alpha]_D^{25}$ +0.4º (*c* 0.33, MeOH); UV (MeOH) λ_{max} nm (log ε): 218 (4.40), 258 (3.92), 300 (2.63); IR (film) ν_{max} 3390, 3018, 2928, 1703, 1599, 1462, 1380, 1325, 1162, 1076, 898, 757 cm^{-1}; for ^{1}H and ^{13}C NMR spectroscopic data, see Table 18; FT-ICR-MS *m*/*z* 427.1530 $[M-H]^-$ (Calcd for $C_{21}H_{28}{}^{35}ClO_7$: 427.1524).

3.5. STRUCTURAL ELUCIDATION OF PREVIOUSLY REPORTED COMPOUNDS

Table 19: Compound **RH14** [(2*S*)-Rhedynosin I]

IUPAC name	(*S*)-7-(hydroxymethyl)-5,7-dimethyl-3,4,7,8-tetrahydrocyclopenta [*g*]isochromene-1,6-dione
Sample ID	**RH14**
Sample quantity	6 mg
Physical appearance	Yellow gum
Molecular formula	$C_{15}H_{16}O_4$
Molecular Weight	260.2890 g/mol

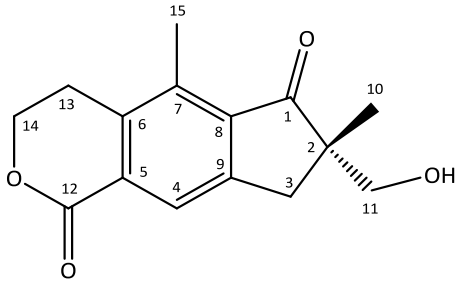

NMR data

^{1}H NMR (400 MHz, MeOD): δ_H ppm 8.02 (1H, s, H-4), 4.55 (2H, t, *J* = 6.0 Hz, H_2-14), 3.77 (1H, d, *J* = 10.6 Hz, H_a-11), 3.50 (1H, d, *J* = 10.6 Hz, H_b-11), 3.37 (1H, d, *J* = 17.3 Hz, H_a-3), 3.09 (2H, t, *J* = 6.0 Hz, H_2-13), 2.89 (1H, d, *J* = 17.3 Hz, H_b-3), 2.64 (3H, s, H_3-15), 1.12 (3H, s, H_3-10).

^{13}C NMR (101 MHz, MeOD): δ_C ppm 210.6 (C-1), 167.4 (C-12), 153.4 (C-9), 139.8 (C-5), 138.2 (C-7), 137.7 (C-6), 126.7 (C-4), 130.9 (C-8), 68.4 (C-14), 68.3 (C-11), 53.1 (C-2), 37.7 (C-3), 25.2 (C-13), 21.0 (C-10), 13.2 (C-15).

Compound **RH14**, obtained as a yellow gum, gave the molecular formula of $C_{15}H_{17}O_4$ by HR-ESI-MS at *m/z* 261.1123 $[M+H]^+$ (Calcd for $C_{15}H_{17}O_4$: 261.1127), with eight degrees of unsaturation. The ^{1}H NMR spectrum of **RH14** closely resembled that of **RH1**. The major difference was the absence of a methylene signal at δ_H 4.80 (CH_2-12) in **RH14**. The presence of a downfield chemical shift at δ_C 167.4, as a quaternary C-12, in the ^{13}C NMR spectrum of **RH14** indicated that the methylene group (CH_2-12) of **RH1** was oxidised to a carbonyl group in **RH14**. The HMBC of **RH14** supported the presence of carbonyl at position C-12. Also, the appearance of carbonyl group at C-12 verified further with the accurate mass spectrum of **RH14** which showed 14 Da more than of **RH1**. Thus, compound **RH14** was confirmed as (*S*)-7-hydroxymethyl-5, 7-dimethyl-3, 4, 7, 8-tetrahydrocyclopenta-[g]isochromene-1, 6-dione. CD spectroscopy allowed to assign the configuration of **RH14** at position C-2 as 2*S*. This compound has previously been isolated and identified along with 18 other compounds as a metabolism product of (2*S*)-pterosin A (**RH15**) in rat urine (Lee et al., 2012). This compound

isolated for the first time from plant material as opposed to mammalian metabolic products. In this thesis, hence rhedynosin I was suggested as a common name for compound **RH14**.

Table 20: Compound **RH16** [(2*R*)-Pterosin B]

IUPAC name	(*R*)-6-(2-hydroxyethyl)-2,5,7-trimethyl-2,3-dihydro-1*H*-inden-1-one
Sample ID	**RH16**
Sample quantity	110 mg
Physical appearance	Yellow needles solid
Molecular formula	$C_{14}H_{18}O_2$
Molecular Weight	218.2960 g/mol

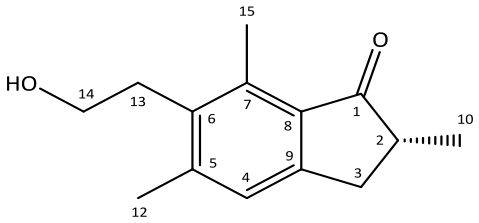

NMR data

^{1}H NMR (400 MHz, $CDCl_3$): δ_H ppm 7.09 (1H, s, H-4), 3.75* (1H, t, *J* = 7.5 Hz, H_a-13), 3.75* (1H, t, *J* = 7.5 Hz, H_a-14), 3.23 (1H, dd, *J* = 16.6, 7.7 Hz, H_a-3), 3.02* (1H, t, *J* = 7.5 Hz, H_b-13), 3.02* (1H, t, *J* = 7.5 Hz, H_b-14), 2.68 (3H, s, H_3-15), 2.64 (1H, m, H-2), 2.58 (1H, dd, *J* = 17.4, 3.4 Hz, H_b-3), 2.43 (3H, s, H_3-12), 1.27 (3H, d, *J* = 7.3 Hz, H_3-10).

^{13}C NMR (101 MHz, $CDCl_3$): δ_C ppm 210.6 (C-1), 152.6 (C-9), 144.5 (C-5), 137.9 (C-7), 135.0 (C-6), 132.1 (C-8), 125.7 (C-4), 61.5 (C-14), 42.6 (C-2), 33.8 (C-3), 31.9 (C-13), 21.7 (C-12), 16.6 (C-10), 13.7 (C-15).

* These data were confirmed from the HSQC experiment.

Compound **RH16** was obtained as a yellow needles solid substance. It has a molecular formula of $C_{14}H_{18}O_2$ which was determined on the basis of HR-ESI-MS (positive ion mode) at *m*/*z* 219.1384 $[M + H]^+$ (Calcd for $C_{14}H_{19}O_2$: 219.1385). The ^{1}H NMR data of **RH16** indicated a pentasubstituted benzene ring with a single aromatic proton signal at δ_H 7.09 (1H, s). Two coupled methylene groups at δ_H 3.02 (2H, t, *J* = 7.5 Hz) and δ_H 3.75 (2H, t, *J* = 7.5 Hz) suggested the attachment of an ethylene chain to the aromatic ring.

The ^{1}H NMR spectrum shows two singlets at δ_H 2.43 (s) and 2.68 (s) which are referred to the two methyl groups at positions C-5 and C-7, respectively. The only doublet signal at δ_H 1.27 (d, *J* = 7.3 Hz) is due to the methyl group at C-2, while the multiplet signal at δ_H 2.64 (m) is assigned to H-2. The two signals appeared as doublet of doublet at δ_H 2.58 (dd, *J* = 17.4, 3.4 Hz) and δ_H 3.23 (dd, *J* = 16.6, 7.7 Hz) are indicated the presence of two protons at position C-3. The ^{1}H NMR signals were all consistent with a C_{14} pterosin sesquiterpene structure (Fukuoka

et al., 1983; Kuraishi et al., 1985). The ^{13}C NMR data of **RH16** showed 14 distinct carbon signals, which were assigned by HSQC experiment to three methyls, three methylenes, two methines and six quaternary carbons including one benzene ring and one ketone group. The carbon signals also supported the presence of a pentasubstituted aromatic ring, including a low-field signal at 210.61 ppm (C=O), as assigned to C-1 of a pterosin-type sesquiterpene skeleton (Fukuoka et al., 1983).

The HMBC spectrum utilized to support the structure elucidation of compound **RH16** which showed the proton-carbon correlations of H-3/C-1, H-3/C-2, H-3/C-4, H-3/C-5, H-3/C-9, H-3/C-10, H-4/C-3, H-4/C-5, H-4/C-6, H-4/C-12, H-13/C-6, H-13/C-7, H-13/C-8, H-13/C-14, H-14/C-6 and H-14/C-13, H-10/C-1, H-10/C-2, H-10/C-3, H-12/C-4, H-12/C-5, H-12/C-6, H-12/C-7, H-12/C-8, H-12/C-9, H-12/C-14, H-15/C-4, H-15/C-5, H-15/C-6, H-15/C-7, H-15/C-8, H-15/C-9 and H-15/C-14, and confirmed that the compound **RH16** is a pterosin-type sesquiterpenoid. Moreover, the HMBC spectrum (see appendix I) exhibited cross peaks from H-15 to C-6, and H-12 to C-7, establishing the location of hydroxyethyl group at position C-6. The NMR data of **RH16** thus showed signals typical of (2*R*)-pterosin B, and this was confirmed by comparison of its ^{1}H and ^{13}C NMR data with those reported in the literature (Fukuoka et al., 1983, 1978; Kuroyanagi et al., 1979a). While CD spectroscopy has been applied to compound **RH16** in order to determine and confirm its absolute configuration at position C-2, the resulting spectrum did not show chirality which is thought to be caused by formation of the racemic mixture (Kuroyanagi et al., 1979b).

(2*R*)-pterosin B is abundant in plant ferns and has been isolated from the young fronds of bracken, *P. aquilinum* var. *latiusculum* (Yoshihira et al., 1978) and *P. aquilinum* var. *caudatum* (Castillo et al., 1997), the whole plants of *Pteris ensiformis* (Chen et al., 2013, 2008), *Pteris setuloso-costulata* and *Histiopteris incisa* (Murakami et al., 1980) and fronds of *Pteris bella* TAGAWA (Tanaka et al., 1982). This compound has been evaluated for its cytotoxicity toward human lung carcinoma, A549; breast carcinoma, MCF-7; human breast carcinoma, MDA-MB-231; human liver cancer, Hep G2; human oral squamous carcinoma, Ca9-22; and human leukemia HL 60 cell lines. As a result, it showed selective activity against HL 60 (human leukemia) cell lines with the IC_{50} value of 8.7 µg/mL while it displayed no effect (pharmacological activity) against the other cell lines (Chen et al., 2008). (2*R*)-pterosin B along with pterosins F, I, O, Z and V have showed activities that induce abnormal development of urchin embryos, and they have also been found to have cytotoxic effect on ciliate, *Paramecium caudatum* (Kobayashi and Koshimizu, 1980). Recently, it has been identified that intra-

articular injection of mice with pterosin B can effectively protect cartilage from osteoarthritis development and inhibit chondrocyte hypertrophy. Based on the histological study of the pellets, it has also been found that the addition of pterosin B in the medium had effect on the protection of chondrocytes from hypertrophy and mineralization (Yahara et al., 2016). Eventually, Yahara et al. state that "Collectively, our results suggest Sik3 (salt-inducible kinase) regulates the homeostasis of articular cartilage and is a target for the treatment of osteoarthritis, with pterosin B as a candidate therapeutic". Furthermore, it is also patented that pterosin B enables to increase cartilage matrices production and prevent hypertrophy of human chondrocytes. Thus, pterosin B has been showed to be active in promoting the growth of hyaline cartilage in humans as it has been tested *in vivo* by administration of pterosin B into the knee articular cavity (Tsumaki et al., 2015).

Table 21: Compound **RH31** [(2*R*)-Pteroside B]

IUPAC name	(*R*)-2,5,7-trimethyl-6-(2-(((2*R*,3*R*,4*S*,5*S*,6*R*)-3,4,5-trihydroxy-6-(hydroxymethyl)tetrahydro-2*H*-pyran-2-yl)oxy)ethyl)-2,3-dihydro-1*H*-inden-1-one
Sample ID	**RH31**
Sample quantity	203 mg
Physical appearance	Pale-yellow crystalline solid
Molecular formula	$C_{20}H_{28}O_7$
Molecular Weight	380.4370 g/mol

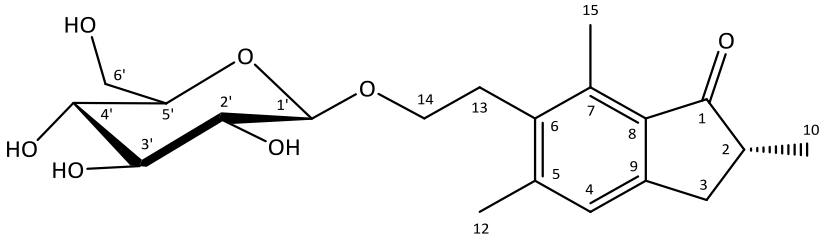

NMR data

[1]H NMR (400 MHz, MeOD): δ_H ppm 7.13 (1H, s, H-4), 4.31 (1H, d, *J* = 7.8 Hz, H-1′), 3.89 (1H, dd, *J* = 17.1, 8.3 Hz, H_a-14), 3.85 (1H, dd, *J* = 11.8, 1.9 Hz, H_a-6′), 3.66 (1H, dd, *J* = 11.7, 5.0 Hz, H_b-6′), 3.64 (1H, dd, *J* = 17.7, 9.1 Hz, H_b-14), 3.36 (1H, t, *J* = 8.3 Hz, H-3′), 3.30 (1H, m, H-4′), 3.27 (1H, m, H-5′), 3.24 (1H, dd, *J* = 16.9, 7.4 Hz, H_a-3), 3.19 (1H, dd, *J* = 7.2, 6.4 Hz, H-2′), 3.09 (2H, t, *J* = 8.0 Hz, H_2-13), 2.64 (3H, s, H_3-15), 2.61 (1H, m, H-2), 2.56 (1H, dd, *J* = 16.9, 4.5 Hz, H_b-3), 2.44 (3H, s, H_3-12), 1.22 (3H, d, *J* = 7.2 Hz, H_3-10).

[13]C NMR (101 MHz, MeOD): δ_C ppm 212.6 (C-1), 154.4 (C-9), 146.3 (C-5), 138.8 (C-7), 136.2 (C-6), 132.8 (C-8), 126.8 (C-4), 104.4 (C-1′), 78.2 (C-3′), 78.0 (C-5′), 75.1 (C-2′), 71.6 (C-4′), 69.2 (C-14), 62.7 (C-6′), 43.8 (C-2), 34.7 (C-3), 30.1 (C-13), 21.4 (C-12), 16.8 (C-10), 13.8 (C-15).

Compound **RH31** was obtained as a pale-yellow crystalline powder. The positive mode HR-ESI-MS showed a quasimolecular ion peak at *m/z* 381.1907 $[M+H]^+$, suggesting a molecular formula of $C_{20}H_{29}O_7$ (Calcd for 381.1913). The ^{1}H and ^{13}C NMR spectra of this compound (see appendix I and Table 21) showed signals that are similar to those of **RH16** with the exception of signals for the glucose moiety and the downfield shift of the resonance at C-14 (δc 69.16), suggesting it to be the site of glycosylation. The ^{1}H NMR spectrum also exhibited the chemical shift of an anomeric proton at δ_H 4.31 (d, *J* = 7.8 Hz) and the other proton signals of the sugar moiety at δ_H 3.19-3.85. Based on the coupling constant of the anomeric proton, the configuration of the sugar moiety was determined to be β-oriented indicating a β-glycosyl moiety.

The ^{13}C NMR spectrum of **RH31** displayed twenty carbon signals, and the DEPTQ spectrum (see appendix I) showed that these comprised of three methyls, four methylenes, seven methines and six quaternary carbons. The anomeric carbon appeared at δc 104.42. In addition,

other signals for the glucose occurred at δc 75.12 (C-2′), 78.15 (C-3′), 71.56 (C-4′), 77.96 (C-5′) and 62.67 (C-6′) which are typical signals for the glucose molecule (Fukuoka et al., 1983). This indicated that the compound **RH31** was a glycoside of the compound **RH16**. The X-ray crystallography applied for the first time to compound **RH31** (Figure 57) which confirmed the sugar moiety as D-glucose and also indicated that the absolute configuration of the compound at a chiral centre C-2 is *R*.

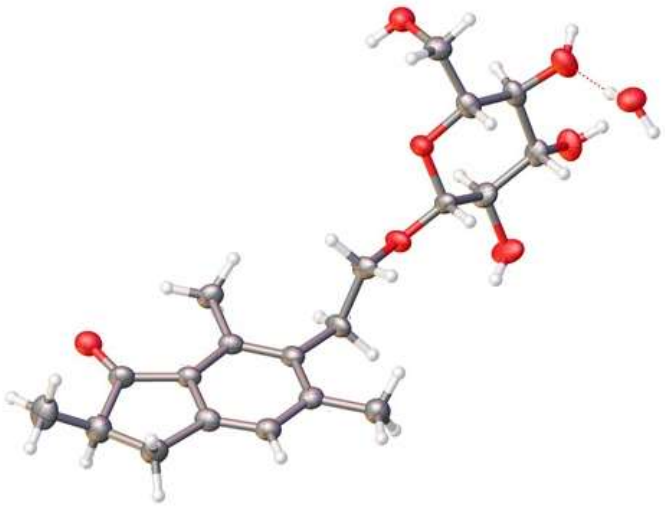

Figure 57: X-ray crystallographic structure of the compound **RH31**.

Even though the CD spectrum measured in methanol for this compound, unpredictably no Cotton effect (n → π* transition at 300-360 nm) was observed. The absolute configuration of **RH31** (Figure 57) was established based on X-ray diffraction analysis for its single crystals, in which the result is in agreement with the CD curve reported by Kuroyanagi et al. (1979b) for this compound. The single crystal X-ray data is deposited with Cambridge Crystallographic Data Centre.

In the analysis of HMBC spectrum (see appendix I), it is noticed that the H-1′ (δ_H 4.31) was linked to C-14 (δ_C 69.16) and H_2-14 (δ_H 3.64 and 3.89) was connected to C-1′ (δ_C 104.42), signifying that the β-D-glucose moiety was located at position C-14 of the pterosin skeleton. Thus, the absolute chemical structure of **RH31** confirmed to be (2*R*)-pteroside B (synonym: pterosin B glycoside). The ^{1}H and ^{13}C NMR data (Table 21) of this compound are consistent with the reported literature values (Fukuoka et al., 1983, 1978). Compound **RH31** has been isolated from *P. aquilinum* Kuhn var. *latiusculum* (Hikino et al., 1970) and the whole plant of *Pteris multifida* Poir. (Pteridaceae) (Ge et al., 2008).

Table 22: Compound **RH15** [(2*S*)-Pterosin A]

IUPAC name	(*S*)-6-(2-hydroxyethyl)-2-(hydroxymethyl)-2,5,7-trimethyl-2,3-dihydro-1*H*-inden-1-one
Sample ID	**RH15**
Sample quantity	160 mg
Physical appearance	Yellow crystalline solid
Molecular formula	$C_{15}H_{20}O_3$
Molecular Weight	248.3220 g/mol

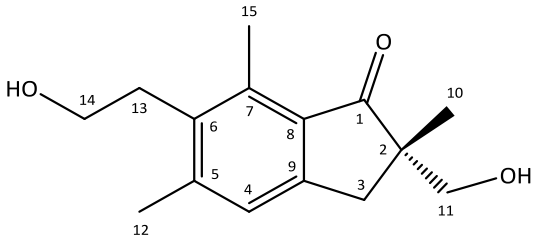

NMR data

^{1}H NMR (400 MHz, MeOD): δ_H ppm 7.16 (1H, s, H-4), 3.71 (1H, d, *J* = 10.6 Hz, H_a-11), 3.61* (1H, t, *J* = 7.6 Hz, H_a-13), 3.61* (1H, t, *J* = 7.6 Hz, H_a-14), 3.46 (1H, d, *J* = 10.6 Hz, H_b-11), 3.23 (1H, d, *J* = 17.1 Hz, H_a-3), 2.99* (1H, t, *J* = 7.6 Hz, H_b-13), 2.99* (1H, t, *J* = 7.6 Hz, H_b-14), 2.72 (1H, d, *J* = 17.1 Hz, H_b-3), 2.65 (3H, s, H_3-15), 2.44 (3H, s, H_3-12), 1.09 (3H, s, H_3-10).

^{13}C NMR (101 MHz, MeOD): δ_C ppm 212.9 (C-1), 154.1 (C-9), 146.2 (C-5), 138.8 (C-7), 136.4 (C-6), 133.1 (C-8), 126.9 (C-4), 68.3 (C-11), 61.7 (C-14), 52.6 (C-2), 37.5 (C-3), 32.9 (C-13), 21.3 (C-10), 21.3 (C-12), 13.9 (C-15).

* These data were confirmed from the HSQC experiment.

Compound **RH15**, isolated as a yellow crystalline solid, exhibited the molecular formula $C_{15}H_{21}O_3$ by positive mode HR-ESI-MS (*m/z* 249.1489; Calcd for 249.1491), indicating six degrees of unsaturation in its structure. Comparison of the NMR spectral data of **RH15** with those of **RH16** revealed that they were quite similar to each other with some exceptions. The ^{1}H NMR spectrum exhibited that the tertiary proton at position C-2 in **RH16** was replaced by a hydroxymethylene group in **RH15**. This fact was established based on the absence of a multiplet peak of H-2 (δ_H 2.64) and the appearance of H_3-10 as a singlet (δ_H 1.09) in **RH15**.

The DEPTQ spectrum also showed an extra methylene in addition of detecting C-2 as quaternary carbon. On the other hand, their mass values gave a difference of 30 amu which corresponds to the replacement observed. The correlations of H-11 (δ_H 3.46 and 3.71) with C-2 (δ_C 52.16), C-3 (δ_C 37.50), and C-10 (δ_C 21.33) in HMBC spectrum of **RH15** confirmed the above deduction. The CD spectrum of **RH15** exhibited negative and positive vibronic components associated with the n → π* transition in the range of 320-360 nm (Figure 59).

Thus, compound **RH15** was assigned to be 2*S* configuration (Kuroyanagi et al., 1979b) and confirmed by X-ray diffraction (Figure 58). The single crystal X-ray data is submitted to Cambridge Crystallographic Data Centre. Based on the above analysis and comparison of the NMR data (Table 22) with those reported in the literature (Hsu et al., 2013; Kovganko et al., 2004; Lee et al., 2012), the structure of this compound was determined as (2*S*)-pterosin A (**RH15**).

This compound has been isolated from the aerial part (frond) of the bracken-fern *P. aquilinum* L. (Hypolepidaceae) (Kovganko et al., 2004), fresh fronds of *P. aquilinum* var. *caudatum* (Castillo et al., 1997), the air-dried fronds of *Microlepia substrigosa* TAGAWA (Kuraishi et al., 1985) and the rhizomes of *P. aquilinum* var. *latiusculum* (Kuroyanagi et al., 1979a; Yoshihira et al., 1978), and it is reported to show no inhibition effect on sea urchin embryonic development and no cytotoxic effect against a ciliate, *Paramecium caudatum* (Kobayashi and Koshimizu, 1980).

Interestingly, the therapeutic effect of pterosin A on diabetes has recently been investigated using several diabetic mouse models, and found that the oral administration of pterosin A can alleviate hyperglycemia and glucose intolerance in streptozotocin (STZ) and high-fat diet-fed (HFD) diabetic mice (Hsu et al., 2013). It has been concluded that pterosin A can significantly reverse the increased serum insulin and insulin resistance in diabetic mice. It has also been observed that pterosin A is capable of reducing the high serum levels of total cholesterol and LDL-cholesterol in STZ- and HFD-induced diabetic mice. Furthermore, it has also been noticed that pterosin A has the ability to improve glucose homeostasis and insulin resistance, i.e. it can recover the decreased body weight in STZ-diabetic mice and reduce the increased body weight in HFD-fed mice. Based on these findings, Hsu et al. (2013) have indicated that pterosin A may possibly be an alternative therapeutic for diabetes.

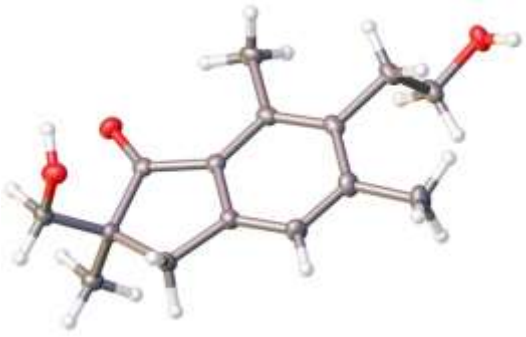

Figure 58: X-ray crystallographic structure of the compound **RH15**.

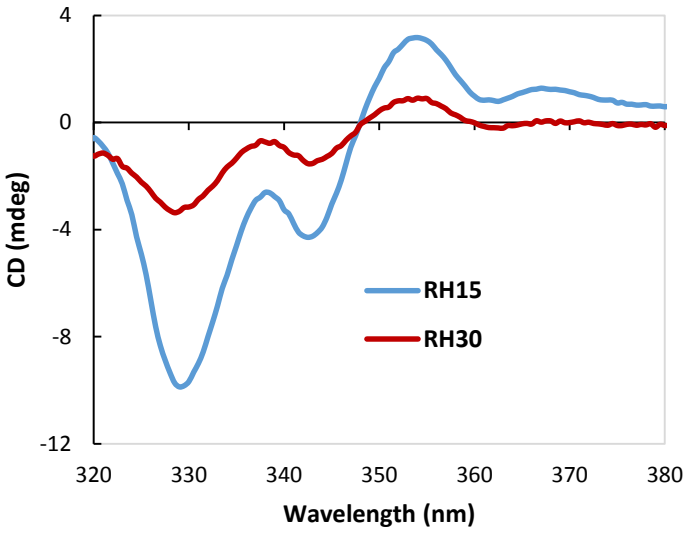

Figure 59: The CD spectra of **RH15** and **RH30** in methanol illustrating the superposition of a longer wavelength positively signed vibronic progression and a shorter wavelength negatively signed vibronic progression.

Table 23: Compound **RH30** [(2*S*)-Pteroside A]

IUPAC name	(*S*)-2-(hydroxymethyl)-2,5,7-trimethyl-6-(2-(((2*R*,3*R*,4*S*,5*S*,6*R*)-3,4,5-trihydroxy-6-(hydroxymethyl)tetrahydro-2*H*-pyran-2-yl) oxy)ethyl)-2,3-dihydro-1*H*-inden-1-one
Sample ID	**RH30**
Sample quantity	10.2 mg
Physical appearance	Yellow-orange gum
Molecular formula	$C_{21}H_{30}O_8$
Molecular Weight	410.4630 g/mol

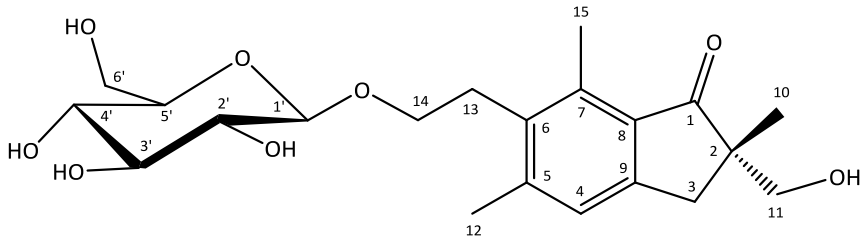

NMR data

[1]H NMR (400 MHz, MeOD): δ_H ppm 7.16 (1H, s, H-4), 4.32 (1H, d, *J* = 7.8 Hz, H-1′), 3.90 (1H, m, H_a-14), 3.85 (1H, dd, *J* = 11.9, 1.5 Hz, H_a-6′), 3.71 (1H, d, *J* = 10.6 Hz, H_a-11), 3.66 (1H, dd, *J* = 11.7, 5.3 Hz, H_b-6′), 3.64 (1H, m, H_b-14), 3.46 (1H, d, *J* = 10.6 Hz, H_b-11), 3.34 (1H, m, H-3′), 3.30 (1H, m, H-4′), 3.27 (1H, m, H-5′), 3.23 (1H, d, *J* = 17.2 Hz, H_a-3), 3.18 (1H, t, *J* = 8.7 Hz, H-2′), 3.10 (2H, t, *J* = 8.0 Hz, H_2-13), 2.72 (1H, d, *J* = 17.2 Hz, H_b-3), 2.66 (3H, s, H_3-15), 2.45 (3H, s, H_3-12), 1.09 (3H, s, H_3-10).

[13]C NMR (101 MHz, MeOD): δ_C ppm 212.88 (C-1), 154.2 (C-9), 146.4 (C-5), 138.9 (C-7), 136.1 (C-6), 133.1 (C-8), 126.9 (C-4), 104.4 (C-1′), 78.2 (C-3′), 78.0 (C-5′), 75.1 (C-2′), 71.6 (C-4′), 69.2 (C-14), 68.3 (C-11), 62.7 (C-6′), 52.6 (C-2), 37.5 (C-3), 30.1 (C-13), 21.4 (C-10), 21.3 (C-12), 13.9 (C-15).

Compound **RH30** (10.2 mg) was obtained as a pale-yellow gum substance. It has a molecular formula of $C_{21}H_{30}O_8$ which was established on the basis of positive mode HR-ESI-MS at *m/z* 411.2019 $[M + H]^+$ (Calcd for $C_{21}H_{31}O_8$: 411.2019). The DEPTQ spectrum (see appendix I) showed 21 carbon signals, which consisted of three methyls, five methylenes, six methines and seven quaternary carbons. The comparison of the ^{1}H and ^{13}C NMR data (Table 23) with that of **RH15** revealed close similarity except for the presence of signals for glucose moiety. Hence, the aglycone is suggested to be a pterosin A.

The ^{1}H NMR spectrum showed one anomeric proton at δ_H 4.32 (H-1′, d, *J* = 7.8 Hz), indicating a *β*-glycosyl moiety based on the coupling constant. Moreover, in the COSY spectrum (see appendix I), the correlation between the anomeric proton signal δ_H 4.32 (d, 7.8 Hz, H-1′) with δ_H 3.18 (t, 8.7 Hz, H-2′) assigned to position C-2′ was observed. The anomeric carbon appeared

at δc 104.44 and the remaining ^{13}C NMR data for the glucose moiety occurred at δc 75.14 (C-2′), 78.17 (C-3′), 71.58 (C-4′), 77.99 (C-5′) and 62.68 (C-6′) which are consistent with those of glucose.

The attachment of the glucose unit at C-14 was apparent from the downfield shift of the resonance at C-14 (δc 69.20) and the H-1′ to C-14 HMBC connectivity (see appendix I). Comparison of the NMR values (Table 23) with those published (Fukuoka et al., 1983), identified pteroside A as the compound isolated. The absolute configuration of **RH30** was determined from the CD spectrum (Figure 59), which showed a negative Cotton effect at 329 nm in methanol, indicating the (2*S*)-configuration. This is in agreement with the reported CD curve for this compound (Kuroyanagi et al., 1979b). Accordingly, compound **RH30** was confirmed to be (2*S*)-pteroside A.

Table 24: Compound **RH34** [(2*S*)-Pteroside A2]

IUPAC name	(*S*)-6-(2-hydroxyethyl)-2,5,7-trimethyl-2-((((2*R*,3*R*,4*S*,5*S*,6*R*)-3,4,5-trihydroxy-6-(hydroxymethyl)tetrahydro-2*H*-pyran-2-yl)oxy)methyl)-2,3-dihydro-1*H*-inden-1-one
Sample ID	**RH34**
Sample quantity	4.2 mg
Physical appearance	Pale-yellow gum
Molecular formula	$C_{21}H_{30}O_8$
Molecular Weight	410.4630 g/mol

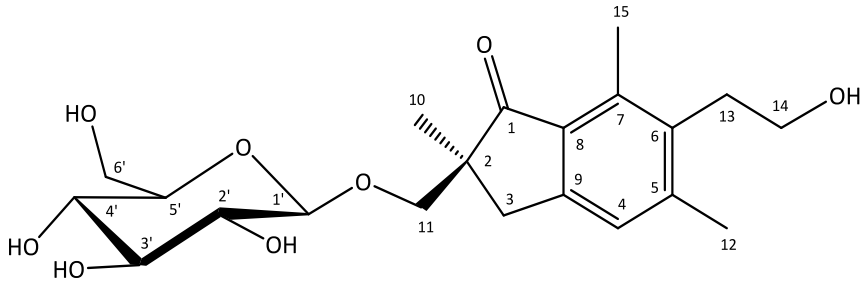

NMR data

^{1}H NMR (400 MHz, MeOD): δ_H ppm 7.16 (1H, s, H-4), 4.20 (1H, d, *J* = 7.8 Hz, H-1′), 4.12 (1H, d, *J* = 9.4 Hz, H_a-11), 3.77 (1H, dd, *J* = 12.0, 1.1 Hz, H_a-6′), 3.61 (1H, m, H_b-6′), 3.61 (2H, t, *J* = 7.8 Hz, H_2-14), 3.48 (1H, d, *J* = 9.4 Hz, H_b-11), 3.43 (1H, d, *J* = 17.0 Hz, H_a-3), 3.29 (1H, m, H-3′), 3.21 (1H, m, H-4′), 3.21 (1H, m, H-5′), 3.04 (1H, dd, *J* = 8.8, 8.1 Hz, H-2′), 2.99 (2H, t, *J* = 7.8 Hz, H_2-13), 2.72 (1H, d, *J* = 17.0 Hz, H_b-3), 2.64 (3H, s, H_3-15), 2.44 (3H, s, H_3-12), 1.13 (3H, s, H_3-10).

^{13}C NMR (101 MHz, MeOD): δ_C ppm 212.4 (C-1), 154.1 (C-9), 146.4 (C-5), 138.9 (C-7), 136.4 (C-6), 132.6 (C-8), 127.1 (C-4), 104.7 (C-1′), 78.1 (C-3′), 77.9 (C-5′), 75.0 (C-11), 74.9 (C-2′), 71.5 (C-4′), 62.7 (C-6′), 61.7 (C-14), 51.4 (C-2), 37.5 (C-3), 32.9 (C-13), 22.1 (C-10), 21.3 (C-12), 13.9 (C-15).

Compound **RH34** (4.2 mg), obtained as a pale-yellow sticky compound, has a molecular formula of $C_{21}H_{30}O_8$ as shown by high resolution mass spectrum HR-ESI-MS at *m/z* 411.2014 $[M + H]^+$ (Calcd for $C_{21}H_{30}O_8$: 411.2019), and this indicating seven degrees of unsaturation in its structure. Similarly, when comparing the ^{1}H NMR spectra of this compound with that of **RH15**, the presence of all the proton signals of **RH15** can be observed with the exception of the signals for a glucose moiety. Hence, this observation suggests that the aglycone is a pterosin A. Based on the coupling constant of the anomeric proton showed by the ^{1}H NMR spectrum at δ_H 4.20 (d, *J* = 7.8 Hz, H-1′), the sugar moiety configuration is assigned to be *β*-oriented indicating a *β*-glycosyl moiety. The COSY spectrum (see appendix I), also shows the coupling of H-1′ with H-2′ (δ_H 3.04), H-2′ with H-3′ (δ_H 3.29), H-4′ and H-5′ (δ_H 3.21) with H_b-6′ (δ_H 3.61), H_a-3 (δ_H 3.43) with H_b-3 (δ_H 2.72), H-13 (δ_H 2.99) with H-14 (δ_H 3.61) and H_a-11 (δ_H 4.12) with H_b-11 (δ_H 3.48).

The DEPTQ spectrum (see appendix I) revealed 21 signals equivalent to three methyls, five methylenes, six methines and seven quaternary carbons. The spectrum also showed an anomeric carbon at 104.72 (C-1′) and other signals for glucose (C-2′ to C-6′) were observed at range of δ_H 62.74-78.13 which are compatible with those of glucose. Moreover, the C-11 site of glycoside resonated at higher field δ_C 75.03, thus showing a shielding effect and this indicated that the attachment of the sugar moiety was at C-11 through a C-O-C linkage. Likewise, the HMBC experiment (see appendix I), exhibited the correlation from the anomeric proton signal at δ_H 4.20 (H-1′) to δ_C 76.1 (C-3) confirming the site of linkage mentioned above. Accordingly, the structure of **RH34** was confirmed as (2*S*)-pteroside A2 which is a positional isomer of compound **RH30**. The application of CD spectroscopy allowed to determine the absolute stereochemistry of **RH34** as 2*S* at position C-2.

This compound isolated for the first time from the rhizomes of *P. aquilinum* (L.) Kuhn subsp. *aquilinum*. Compound **RH34** has been previously isolated by Castillo et al. (2003) from the young fronds of *Pteridium caudatum* (L.) Maxon (Synonym: *P. aquilinum* (L.) Kuhn var. *caudatum*). The ^{1}H and ^{13}C NMR data (Table 24) of this compound are consistent with the reported values published in the literature (Castillo et al., 2003).

Table 25: Compound **RH17** [(2*R*, 3*R*)-Pterosin C or *trans*-Pterosin C]

IUPAC name	(2*R*,3*R*)-3-hydroxy-6-(2-hydroxyethyl)-2,5,7-trimethyl-2,3-dihydro-1*H*-inden-1-one
Sample ID	**RH17**
Sample quantity	18 mg
Physical appearance	Pale-yellow crystalline powder
Molecular formula	$C_{14}H_{18}O_3$
Molecular Weight	234.2950 g/mol

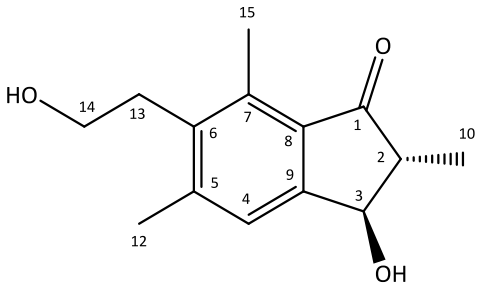

NMR data

^{1}H NMR (400 MHz, MeOD): δ_H ppm 7.36 (1H, s, H-4), 4.69 (1H, d, *J* = 4.0 Hz, H-3), 3.61* (1H, t, *J* = 7.8 Hz, H_a-13), 3.61* (1H, t, *J* = 7.8 Hz, H_a-14), 3.01* (1H, t, *J* = 7.8 Hz, H_b-13), 3.01* (1H, t, *J* = 7.8 Hz, H_b-14), 2.65 (3H, s, H_3-15), 2.48 (3H, s, H_3-12), 2.43 (1H, m, H-2), 1.30 (3H, d, *J* = 7.3 Hz, H_3-10).

^{13}C NMR (101 MHz, MeOD): δ_C ppm 206.2 (C-1), 153.1 (C-9), 144.8 (C-5), 136.7 (C-7), 136.5 (C-6), 130.9 (C-8), 124.2 (C-4), 74.4 (C-3), 60.1 (C-14), 53.1 (C-2), 31.5 (C-13), 19.9 (C-12), 12.5 (C-15), 11.7 (C-10).

* These data were confirmed from the HSQC experiment.

Compound **RH17** was isolated as a pale-yellow crystalline powder, and its molecular formula was established as $C_{14}H_{18}O_3$ by HR-ESI-MS as *m/z* 235.1329 $[M + H]^+$ (Calcd for $C_{14}H_{19}O_3$: 235.1334). The comparison of the ^{1}H and ^{13}C NMR data of **RH17** (Table 25) with those of **RH16** revealed close similarity except for the downfield shifts of the signals at H-3 (δ_H 4.69, d, *J* = 4.0 Hz) and position C-3 (δc 74.42), suggesting the presence of one hydroxyl group (OH) at position C-3, i.e. one of the protons at position C-3 replaced with an OH group. The HSQC spectrum (see appendix I), showed direct correlation between C-3 and H-3.

The ^{1}H NMR disclosed the existence of one carbinyl proton (δ_H 4.69, H-3), one methine proton (δ_H 2.43, H-2), one deshielded aromatic proton (δ_H 7.36, H-4), three methyl groups including two aromatic methyls appeared as singlet signals and one hydroxylethyl group. The structure was therefore deduced to be the 3-hydroxy derivative of pterosin B (**RH16**). The ^{1}H and ^{13}C NMR data of this compound are consistent with those reported in the literature (Ayer and McCaskill, 1981; Kuroyanagi et al., 1979a; Ng and McMorris, 1984). Ng and McMorris have

reported that can be distinguished between the *cis* and *trans* isomers from their NMR data. Thus, the *trans*-configuration of the methyl at C-2 and the hydroxyl (OH) at C-3 in **RH17** was assigned by the vicinal coupling constant value ($J_{2,3}$ = 4.0 Hz) and the appearance of C2-metheyl and C3-proton as doublets at δ_H 1.30 and δ_H 4.69, respectively (Ge et al., 2008; Murakami et al., 1985; Ng and McMorris, 1984).

The absolute configuration of compound **RH17** was established from its CD spectrum (Figure 61), which revealed a strong negative Cotton effect at 330 nm in methanol, indicating the (2*R*, 3*R*)-configuration, i.e. the OH group at C-3 is present in pseudo-axial conformation irrespective of the configuration at C-2 and the solvent (Kuroyanagi et al., 1979b, 1974b). Consequently, compound **RH17** was assigned as (2*R*, 3*R*)-pterosin C. To further confirm the structure and the absolute stereochemistry of **RH17**, X-ray crystallographic study was conducted and ultimately the structure of **RH17** confirmed as shown in Table 25. The single crystal X-ray data is submitted to Cambridge Crystallographic Data Centre. This compound has been isolated from the rhizomes of *P. aquilinum* var. *latiusculum* (Kuroyanagi et al., 1979a).

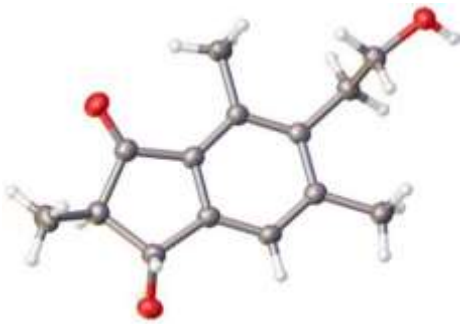

Figure 60: X-ray crystallographic structure of the compound **RH17**.

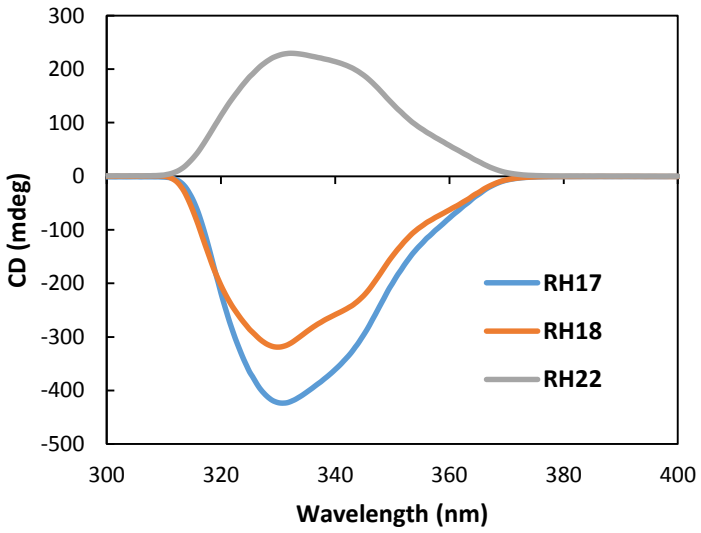

Figure 61: The CD spectra of **RH17**, **RH18**, and **RH22** recorded in methanol.

Table 26: Compound **RH18** [(2*S*, 3*R*)-Pterosin C or *cis*-Pterosin C]

IUPAC name	(2*S*,3*R*)-3-hydroxy-6-(2-hydroxyethyl)-2,5,7-trimethyl-2,3-dihydro-1H-inden-1-one
Sample ID	**RH18**
Sample quantity	20 mg
Physical appearance	White - pale yellow crystalline solid
Molecular formula	$C_{14}H_{18}O_3$
Molecular Weight	234.2950 g/mol

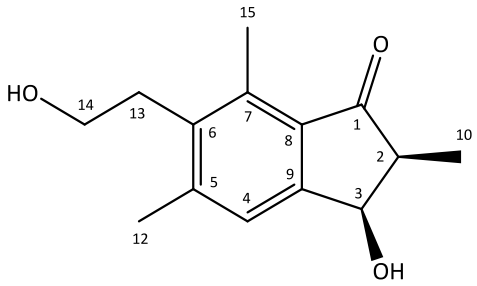

NMR data

^{1}H NMR (400 MHz, MeOD): δ_H ppm 7.37 (1H, s, H-4), 5.15 (1H, d, *J* = 6.6 Hz, H-3), 3.61* (1H, t, *J* = 7.8 Hz, H_a-13), 3.61* (1H, t, *J* = 7.8 Hz, H_a-14), 3.01* (1H, t, *J* = 7.8 Hz, H_b-13), 3.01* (1H, t, *J* = 7.8 Hz, H_b-14), 2.76 (1H, m, H-2), 2.65 (3H, s, H_3-15), 2.48 (3H, s, H_3-12), 1.17 (3H, d, *J* = 7.5 Hz, H_3-10).

^{13}C NMR (101 MHz, MeOD): δ_C ppm 210.4 (C-1), 155.2 (C-9), 146.3 (C-5), 138.5 (C-7), 138.1 (C-6), 132.2 (C-8), 126.7 (C-4), 70.2 (C-3), 61.6 (C-14), 49.7 (C-2), 33.1 (C-13), 21.4 (C-12), 14.0 (C-15), 10.7 (C-10).

* These data were confirmed from the HSQC experiment.

Compound **RH18** was obtained as a whit-pale yellow crystalline solid. The molecular formula of $C_{14}H_{18}O_3$ established from the positive mode HR-ESI-MS at *m/z* 235.1327 $[M + H]^+$ (Calcd for $C_{14}H_{19}O_3$: 235.1334), which is exactly identical to that of **RH17** discussed above. The NMR spectral data of this compound were quite similar to those of **RH17**, except for the chemical shifts and coupling constant values due to H-2, H-3, and methyl-2 of the 1-indanone skeleton. The observed vicinal coupling constant value, $J_{2,3}$ = 6.6 Hz, indicated **RH18** to be a *cis*-isomer, i.e. the larger coupling constant refers to the *cis*-isomer 1-indanone derivatives (Ge et al., 2008; Ng and McMorris, 1984).

The CD spectrum exhibited a negative Cotton effect at 330 nm in methanol (Figure 61), indicating that **RH18** has *R*-configuration at C-3, regardless of the configuration at C-2 (Kuroyanagi et al., 1979b, 1974b). In addition, for the first time the X-ray crystallography (Figure 62) was carried out which further confirmed the structure and the absolute stereochemistry of **RH18** as shown in Table 26. The single crystal X-ray data is submitted to

Cambridge Crystallographic Data Centre. The structure of compound **RH18** was therefore determined to be (2*S*, 3*R*)-pterosin C. The NMR data of **RH18** are in a good agreement with those published in the literature (Kuroyanagi et al., 1979a; Ng and McMorris, 1984). The compound has been isolated from the fronds of *P. aquilinum* var. *latiusculum* (Fukuoka et al., 1978; Kuroyanagi et al., 1979a).

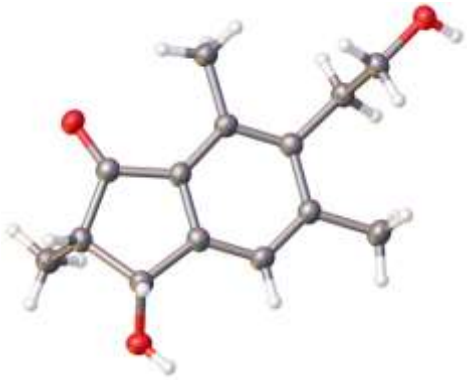

Figure 62: X-ray crystallographic structure of the compound **RH18**.

Table 27: Compound **RH28** [(2*R*, 3*R*)-Histiopterosin A = *trans*-Histiopterosin A]

IUPAC name	2-(1-hydroxy-2,4,6-trimethyl-3-oxo-2,3-dihydro-1*H*-inden-5-yl)acetic acid
Sample ID	**RH28**
Sample quantity	3 mg
Physical appearance	Yellow sticky
Molecular formula	$C_{14}H_{16}O_4$
Molecular Weight	248.2780 g/mol

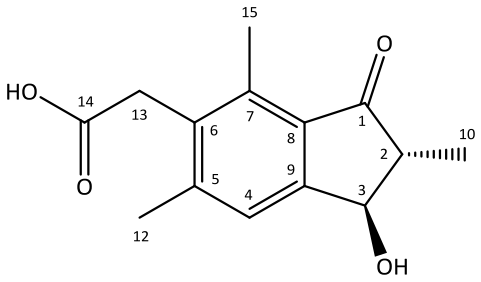

NMR data

^{1}H NMR (400 MHz, MeOD): δ_H ppm 7.39 (1H, s, H-4), 4.71 (1H, d, *J* = 4.1 Hz, H-3), 3.78 (2H, s, H_2-13), 2.62 (3H, s, H_3-15), 2.47 (1H, m, H-2), 2.44 (3H, s, H_3-12), 1.31 (3H, d, *J* = 7.3 Hz, H_3-10).

^{13}C NMR (101 MHz, MeOD): δ_C ppm 207.5 (C-1), 175.3 (C-14), 155.1 (C-9), 146.6 (C-5), 138.4 (C-7), 135.9 (C-6), 132.3 (C-8), 125.5 (C-4), 75.9 (C-3), 54.8 (C-2), 35.3 (C-13), 21.6 (C-12), 14.2 (C-15), 13.3 (C-10).

Compound **RH28** was isolated as a yellow sticky substance. The HR-ESI-MS data indicated a molecular formula of $C_{14}H_{16}O_4$ based on the $[M-H]^-$ ion signal at *m*/*z* 247.0968 (Calcd for $C_{14}H_{15}O_4$: 247.0970). In Table 27, the full NMR signal assignments of compound **RH28** are reported, as the ^{13}C-NMR data have not been published previously. The NMR data showed seven quaternary carbons; three methines; one methylene and three methyls, indicating that **RH28** is an indanone-type sesquiterpenoid compound (Fukuoka et al., 1978; Ng and McMorris, 1984; Yoshihira et al., 1971). The ^{1}H and ^{13}C NMR (Table 27) of **RH28** were extremely similar with **RH17** regarding 1-indanone skeleton part and also resembled closely those of **RH20** in respect to the site chain located on position C-6. The molecular formula of **RH28** and a 14 Da and 16 Da differences in mass between **RH28** (248 amu) and **RH17** (234 amu), and **RH28** and **RH20** (232 amu), respectively, suggested the oxidising of CH_2-14 in **RH17** to carbonyl group in **RH28** and hence verified the above analysis. This was proved by the deshielded signals at δ_H 3.78, δ_C 35.3 and δ_C 175.3 assigned to H-13, C-13 and C-14, respectively. Moreover, the

H-C cross peaks shown by HSQC, HMBS and COSY experiments (see appendix I) were also analogous to those of **RH17** and **RH20**.

Similar to the compound **RH17**, the small vicinal coupling constant value, J = 4.1 Hz, of H-3 was observed and hence determined the *trans*-configuration of **RH28** at positions C-2 and C-3, this was confirmed by the signals resonated at δ_H 1.31 (CH_3-2) and δ_H 4.71 (H-3) (Ge et al., 2008; Murakami et al., 1985; Ng and McMorris, 1984). The compound **RH28** exhibited a strong negative CD-curve in methanol at 337 nm (Figure 63), establishing the absolute configuration of **RH28** at C-3 as 3*R*, regardless of the stereochemistry at position C-2 (Kuroyanagi et al., 1979b, 1974b). These observations all together therefore confirmed the structure of the compound **RH28** as (2*R*, 3*R*)-histiopterosin A (Table 27). *trans*-Histiopterosin A isolated for the first time from *P. aquilinum* (L.) Kuhn as it has been first obtained as a natural product from the fern, *Histiopteris incisa* (Murakami et al., 1980).

The ^{1}H NMR data of **RH28** are in a good agreement with those published by Murakami et.al (1980) except for the chemical shift and coupling constant of H-3 which have not been mentioned in this publication. However, the positive CD value in methanol has been reported for histiopterosin A by Murakami et.al (1980), the absolute configuration has been left unambiguously as neither the stereochemistry of the compound was shown structurally nor was it written in text. In addition, the most important data of H-3 has not been recorded to decide on the absolute configuration at positions C-2 and C-3. Based on the CD results of the pterosin C type compounds reported by Kuroyanagi et al. (1979b), the positive value of the CD indicates (3*S*)-configuration for the reported histiopterosin A. Therefore, it is concluded that histiopterosin A reported by Murakami et al. (1980) may have either *trans*-configuration [(2*S*, 3*S*) or (2*R*, 3*R*)] or *cis*-configuration [(2*S*, 3*R*) or (2*R*, 3*S*)] depending on the coupling constant of H-3 and the positive sign of its CD.

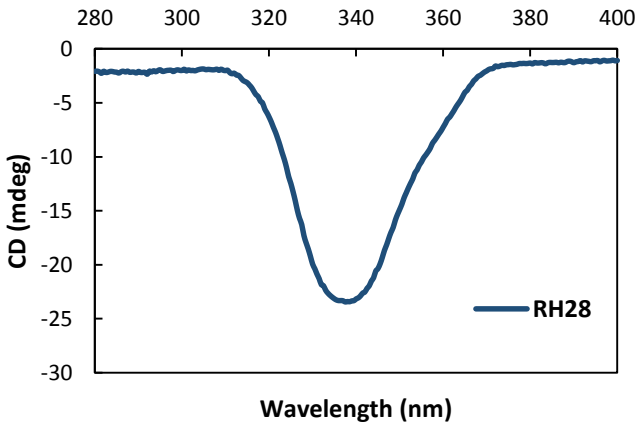

Figure 63: The CD spectra of the compound **RH28** recorded in methanol.

Table 28: Compound **RH21** [(2*R*)-Pterosin F]

IUPAC name	(*R*)-6-(2-chloroethyl)-2,5,7-trimethyl-2,3-dihydro-1*H*-inden-1-one
Sample ID	**RH21**
Sample quantity	10 mg
Physical appearance	White needles
Molecular formula	$C_{14}H_{17}ClO$
Molecular Weight	236.7390 g/mol

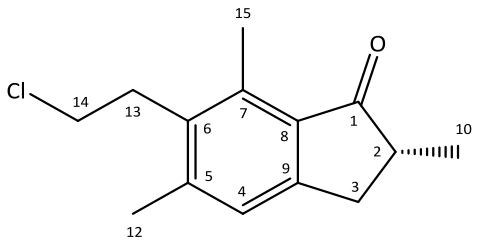

NMR data

^{1}H NMR (400 MHz, $CDCl_3$): δ_H ppm 7.11 (1H, s, H-4), 3.54* (1H, t, *J* = 8.3 Hz, H_a-14), 3.54* (1H, t, *J* = 8.3 Hz, H_a-13), 3.25 (1H, dd, *J* = 16.8, 7.8 Hz, H_a-3), 3.02* (1H, t, *J* = 8.3 Hz, H_b-13), 3.02* (1H, t, *J* = 8.3 Hz, H_b-14), 2.68 (3H, s, H_3-15), 2.65 (1H, m, H-2), 2.58 (1H, dd, *J* = 16.8, 4.1 Hz, H_b-3), 2.43 (3H, s, H_3-12), 1.28 (3H, d, *J* = 7.3 Hz, H_3-10).

^{13}C NMR (101 MHz, $CDCl_3$): δ_C ppm 210.2 (C-1), 153.2 (C-9), 144.05 (C-5), 137.9 (C-7), 134.7 (C-6), 132.5 (C-8), 126.1 (C-4), 42.7 (C-2), 42.2 (C-14), 34.0 (C-3), 32.4 (C-13), 21.3 (C-12), 16.6 (C-10), 13.8 (C-15).

* These data were confirmed from the HSQC experiment.

Compound **RH21**, a white needles, was obtained as a chlorine containing substance as the positive mode HR-ESI-MS showed the molecular formula of $C_{14}H_{17}ClO$ at 237.1047 $[M + H]^+$ (Calcd for $C_{14}H_{18}ClO$: 237.1046). The ^{1}H and ^{13}C NMR data of **RH21** (Table 28) were closely resembling those of **RH16** (pterosin B) (Table 20) in respect to the chemical shifts that appeared due to one aromatic-H at δ_H 7.11, one methine-H at δ_H 2.65, methylene protons on each positions C-3 and C-13 at δ_H 2.58 & 3.25 and δ_H 3.02, one secondary methyl at δ_H 1.28 and two aromatic-methyls at δ_H 2.43 and 2.65 (Table 28 and see appendix I). The direct correlation between H-14 and C-14 is exhibited in the HSQC spectrum (see appendix I). The downfield shift of proton and carbon signals at position C-14 (δ_H 3.54 and δ_C 42.24) along with the molecular formula of **RH21** suggested that the hydroxyl group of the hydroxyethyl group in **RH16** was replaced with a chlorine atom. Additionally, the high resolution mass spectrum of **RH21** showed quasi-molecular ion peaks at *m/z* 237.1047 and *m/z* 239.1014 $[M+H]^+$ defining the pattern isotope ratio (3:1, ^{35}Cl and ^{37}Cl), which is consistent with a monochlorinated compound.

Comparison of the ^{1}H and ^{13}C NMR data of **RH21** with those reported in literature (Fukuoka et al., 1983, 1978; Ng and McMorris, 1984) verified the structure of this compound as (2*R*)-pterosin F (Table 28). CD spectroscopy was applied to confirm the absolute configuration of **RH21**, however, the spectrum showed no absorption peaks in the range of 300-360 nm.

The compound has been isolated as a natural product from young leaves of *P. aquilinum* var. *latiusculum* (Yoshihira et al., 1978, 1971), young shoots of *P. aquilinum* (L.) Kuhn (Kobayashi and Koshimizu, 1980), *Histiopteris incisa* (Murakami et al., 1980), fronds of *P. aquilinum* subsp. *wightiaunm* (Tanaka et al., 1982) and fronds of *Microlepia substrigosa* TAGAWA (Kuraishi et al., 1985). (2*R*)-pterosin F has been reported to show toxicity as it totally inhibited the early embryonic development in sea urchin at a concentration of 12.5 µg/mL (Kobayashi and Koshimizu, 1980).

Table 29: Compound **RH22** [(2*S*, 3*S*)-Pterosin J or *trans*--Pterosin J]

IUPAC name	(2*S*,3*S*)-6-(2-chloroethyl)-3-hydroxy-2,5,7-trimethyl-2,3-dihydro-1*H*-inden-1-one
Sample ID	**RH22**
Sample quantity	5 mg
Physical appearance	White needles
Molecular formula	$C_{14}H_{17}ClO_2$
Molecular Weight	252.7380 g/mol

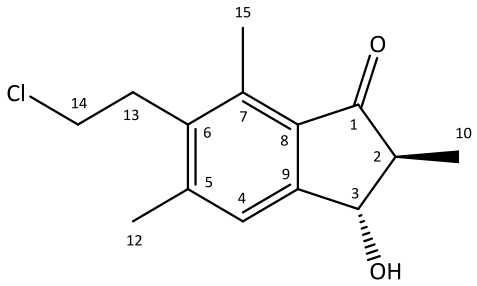

NMR data

^{1}H NMR (400 MHz, $CDCl_3$): δ_H ppm 7.36 (1H, s, H-4), 4.80 (1H, d, *J* = 2.2 Hz, H-3), 3.55 (2H, t, *J* = 8.2 Hz, H_2-14), 3.21 (2H, t, *J* = 8.2 Hz, H_2-13), 2.68 (3H, s, H_3-15), 2.54 (1H, m, H-2), 2.47 (3H, s, H_3-12), 1.36 (3H, d, *J* = 7.3 Hz, H_3-10).

^{13}C NMR (101 MHz, $CDCl_3$): δ_C ppm 205.1 (C-1), 152.8 (C-9), 144.7 (C-5), 137.2 (C-7), 136.9 (C-6), 131.9 (C-8), 124.7 (C-4), 75.7 (C-3), 54.0 (C-2), 42.1 (C-14), 32.5 (C-13), 21.4 (C-12), 14.1 (C-15), 13.2 (C-10).

Compound **RH22**, obtained as a white needles solid, was isolated as a monochlorinated compound and gave the molecular formula of $C_{14}H_{17}ClO_2$ by a positive mode HR-ESI-MS *m/z* 253.0992 (Calcd for $C_{14}H_{18}ClO_2$: 253.0995 $[M + H]^+$), with six degrees of unsaturation.

The NMR spectroscopic data of **RH22** were very similar to those of **RH17** regarding the chemical shifts and coupling constant values due to the three methyl groups, one ethylene, one aromatic-H and one methine-H of the 1-indanone skeleton as shown in Table 29, meanwhile the characteristic chemical shifts and coupling patterns were showed by the signals of the two methylene groups at δ_H 3.21 (2H, t, *J* = 8.2 Hz) and δ_H 3.55 (2H, t, *J* = 8.2 Hz) as those of **RH21**, establishing the presence of a chloroethyl group at position C-6. Similar to **RH21**, the high resolution mass spectrum of **RH22** also demonstrated the isotope pattern (3:1) at *m/z* 253.0992 and 255.0960 confirming the presence of one chlorine atom in the molecule (see appendix II). Thus, this compound was identified as pterosin J.

The *trans*-configuration of pterosin J at positions C-2 and C-3 was ascertained on the basis of the small value of the vicinal coupling constant of H-3 (*J* = 2.2 Hz) and chemical shifts of the

secondary methyl (δ_H 1.36) and the carbinyl proton (δ_H 4.80) (Ge et al., 2008; Murakami et al., 1985; Ng and McMorris, 1984). Finally, the absolute stereochemistry of **RH22** was established as (2*S*, 3*S*)-configuration by its CD spectrum (Figure 61) which exhibited a strong positive Cotton effect at 332 nm in methanol (Kuroyanagi et al., 1979b, 1974b). Compound **RH22** was therefore confirmed as (2*S*, 3*S*)-pterosin J as shown in Table 29. The NMR spectroscopic data of the compound are in consistent with those reported in the literature (Fukuoka et al., 1978; Ng and McMorris, 1984). It has been obtained from the young fronds of *P. aquilinum* var. *latiusculum* (Fukuoka et al., 1972; Yoshihira et al., 1978) and *Histiopteris incisa* (Murakami et al., 1980).

Table 30: Compound **RH19** [(3*S*)-Pterosin D]

IUPAC name	(*S*)-3-hydroxy-6-(2-hydroxyethyl)-2,2,5,7-tetramethyl-2,3-dihydro-1*H*-inden-1-one
Sample ID	**RH19**
Sample quantity	60 mg
Physical appearance	White amorphous solid
Molecular formula	$C_{15}H_{20}O_3$
Molecular Weight	248.3220 g/mol

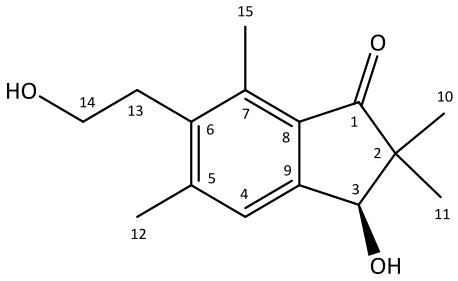

NMR data

^{1}H NMR (400 MHz, MeOD): δ_H ppm 7.36 (1H, s, H-4), 4.74 (1H, s, H-3), 3.62* (1H, t, *J* = 7.5 Hz, H_a-13), 3.62* (1H, t, *J* = 7.5 Hz, H_a-14), 3.01* (1H, t, *J* = 7.5 Hz, H_b-13), 3.01* (1H, t, *J* = 7.5 Hz, H_b-14), 2.64 (3H, s, H_3-15), 2.48 (3H, s, H_3-12), 1.18 (3H, s, H_3-11), 1.04 (3H, s, H_3-10).

^{13}C NMR (101 MHz, MeOD): δ_C ppm 211.7 (C-1), 153.7 (C-9), 146.3 (C-5), 138.4 (C-7), 138.4 (C-6), 131.2 (C-8), 126.1 (C-4), 77.5 (C-3), 61.6 (C-14), 52.4 (C-2), 33.1 (C-13), 23.5 (C-11), 21.4 (C-12), 20.7 (C-10), 14.1 (C-15).

* These data were confirmed from the HSQC experiment.

Compound **RH19** was obtained as a white amorphous solid (Table 30). The HR-ESI-MS data indicated a molecular formula of $C_{15}H_{20}O_3$ based on the $[M + H]^+$ ion signal at *m*/*z* 249.1482 (Calcd for $C_{15}H_{21}O_3$: 249.1491). The NMR spectroscopic data of **RH19** were similar to those of **RH17** in respect to the chemical shifts of the carbinyl proton, aromatic-H, the two aromatic

methyl groups and hydroxylethyl group, with some exceptions. The ^{1}H NMR spectrum of **RH19** revealed the existence of two singlets of a geminal dimethyl group resonated at δ_H 1.04 and 1.18 instead of a doublet signal of the secondary methyl group (δ_H 1.30, d, J = 7.3 Hz) and a multiplet peak of the methine proton (δ_H 2.43, m) in **RH17** (Figure 64). Moreover, the mass difference (14 Da) between **RH17** (*m/z* 235.1329) and **RH19** (*m/z* 249.1482) firmly suggested the replacement of H-2 in **RH17** with a methyl group in **RH19**. The H-C correlations of H-10/C-2, H-10/C-3, H-10/C-11, H-11/C-2, H-11/C-3 and H-11/C-10 showed by the HMBC experiment are also evident to exist two methyl groups on position C-2. In addition, the HSQC spectrum confirmed the direct proton-carbon link between δ_H 1.04 (H-10) and δ_C 20.73 (C-10), and between δ_H 1.18 (H-11) and δ_C 23.48 (C-11).

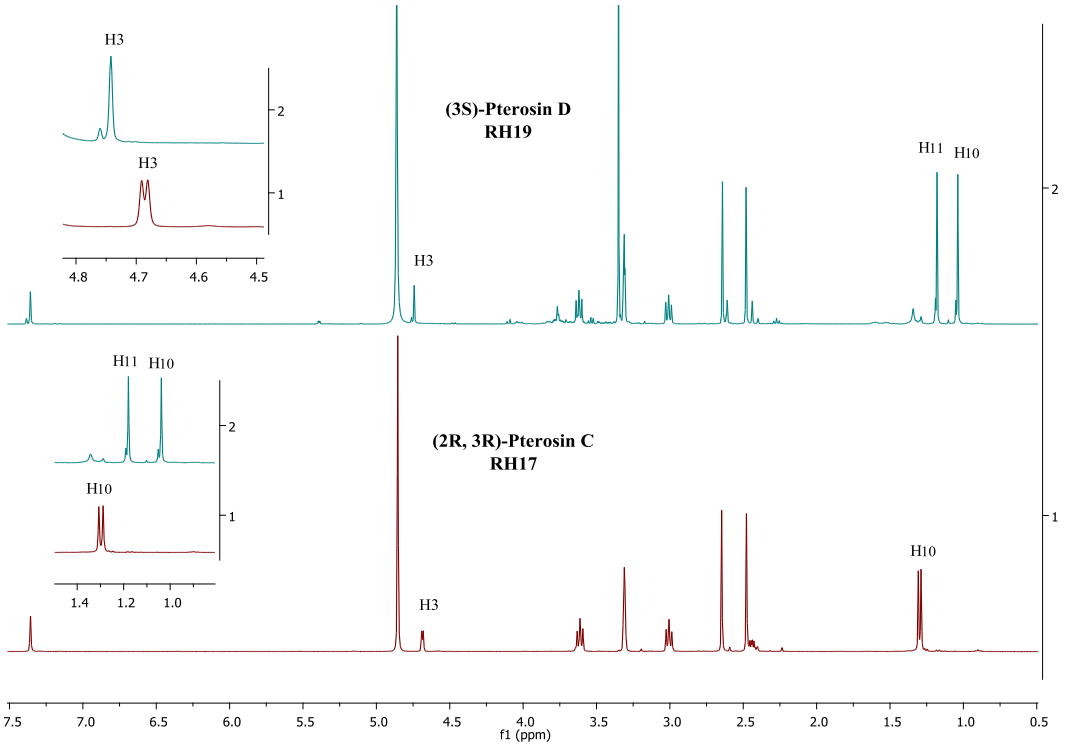

Figure 64: ^{1}H NMR spectra of compounds **RH17** and **RH19** showing the main differences occurred to the selected signals.

The CD spectrum of **RH19** showed a strong negative Cotton effect at 333 nm in methanol (Figure 65) confirming the configuration of the hydroxyl group at the position C-3 as 3*S* as it is stated that the OH group at position C-3 of pterosin D type compounds exists mainly in the pseudo-axial conformation regardless of the configuration at position C-2 whether it is opposite or the same (Kuroyanagi et al., 1979b). Comparison of the NMR data of **RH19** are also consistent with those published (Kuroyanagi et al., 1979a; Ng and McMorris, 1984). From the

above evidence, the structure of **RH19** was therefore confirmed as (3*S*)-pterosin D. It has been obtained from *Hypolepis punctata* (THUNB.) METT. (Murakami et al., 1976) and the rhizomes of *P. aquilinum* var. *latiusculum* (Kuroyanagi et al., 1979a).

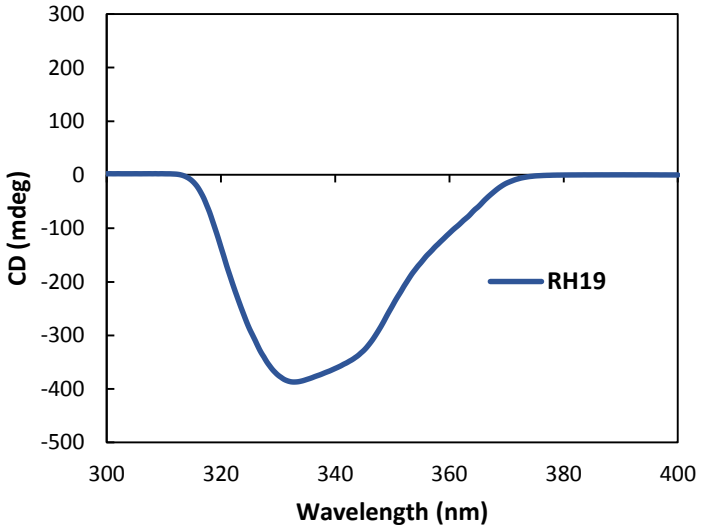

Figure 65: The CD spectrum of **RH19** recorded in methanol.

Table 31: Compound **RH32** [(3*S*)-Pteroside D]

IUPAC name	(*S*)-3-hydroxy-2,2,5,7-tetramethyl-6-(2-(((2*R*,3*R*,4*S*,5*S*,6*R*)-3,4,5-trihydroxy-6-(hydroxymethyl)tetrahydro-2*H*-pyran-2-yl)oxy)ethyl)-2,3-dihydro-1*H*-inden-1-one
Sample ID	**RH32**
Sample quantity	4.9 mg
Physical appearance	Yellow amorphous solid
Molecular formula	$C_{21}H_{30}O_8$
Molecular Weight	410.4630 g/mol

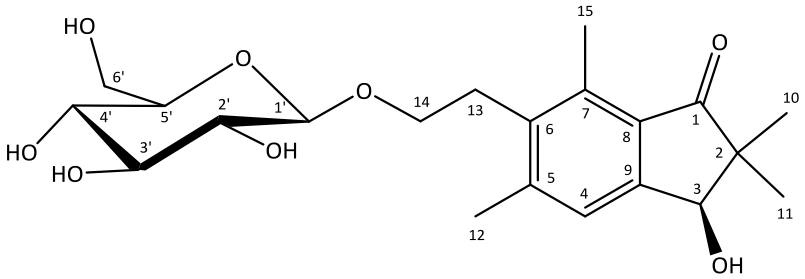

NMR data

^{1}H NMR (400 MHz, MeOD): δ_H ppm 7.36 (1H, s, H-4), 4.74 (1H, s, H-3), 4.32 (1H, d, *J* = 7.8 Hz, H-1′), 4.02 (2H, t, *J* = 7.8 Hz, H_2-14), 3.81 (1H, dd, *J* = 11.9, 2.1 Hz, H_a-6′), 3.68 (1H, dd, *J* = 11.9, 5.2 Hz, H_b-6′), 3.34 (1H, m, H-3′), 3.30 (1H, m, H-4′), 3.28 (1H, m, H-5′), 3.19 (1H, dd, *J* = 8.8, 8.0 Hz, H-2′), 3.13 (2H, t, *J* = 8.0 Hz, H_2-13), 2.65 (3H, s, H_3-15), 2.49 (3H, s, H_3-12), 1.18 (3H, s, H_3-10), 1.04 (3H, s, H_3-11).

^{13}C NMR (101 MHz, MeOD): δ_C ppm 211.7 (C-1), 153.8 (C-9), 146.5 (C-5), 138.6 (C-7), 138.1 (C-6), 131.1 (C-8), 126.1 (C-4), 104.4 (C-1′), 78.1 (C-3′), 78.0 (C-5′), 77.5 (C-3), 75.1 (C-2′), 71.3 (C-4′), 69.1 (C-14), 62.7 (C-6′), 52.4 (C-2), 30.3 (C-13), 23.5 (C-10), 21.5 (C-12), 20.8 (C-11), 14.1 (C-15).

Compound **RH32 (**Table 31**)**, isolated as a yellow amorphous solid, was determined to have the molecular formula $C_{21}H_{30}O_8$ (7 degrees of unsaturation) on the basis of positive mode HR-ESI-MS analysis at *m/z* 411.2008 $[M + H]^+$ (Calcd for $C_{21}H_{31}O_8$: 411.2019). Twenty one carbon signals are shown by the DEPTQ spectrum (see appendix I), referring to the presence of four methyls, three methylenes, seven methines and seven quaternary carbons. The ^{1}H and ^{13}C NMR data of **RH32** closely resemble those of **RH19**, except that **RH32** has one more sugar unit. On the basis of this observation, pterosin D was therefore indicated to be the aglycone portion. The sugar moiety was assigned as a β-glycosyl based on the coupling constant value, *J* = 7.8 Hz, of the anomeric proton that resonated at δ_H 4.32 (H-1′). In addition, the chemical shifts and coupling constants of the sugar part were very similar to those of **RH31**. The strong correlation between the H-1′ (δ_H 4.32) and H-2′ (δ_H 3.18) was also shown by the COSY experiment (see appendix I). The characteristic carbon signals of the glucose moiety including the anomeric carbon (δc 104.41) were revealed by the ^{13}C NMR spectrum in the range of δc 62.65 – 78.14.

The HMBC experiment shows apparent correlation from the anomeric-H (H-1′) to C-14, suggesting the attachment of the glucose moiety at position C-14. The $C_{1'}$-O-C_{14} linkage is also evident from the chemical shifts of H-14 and C-14 appeared in the downfield region at δ_H 4.02 and δc 69.07, respectively (see appendix I).

The CD spectrum of the **RH32** is similar to that of **RH19**, exhibiting the negative band at 333 nm in methanol (Figure 66) and was consistent with the reported CD spectra of pterosin D type compounds (Kuroyanagi et al., 1979b). This result confirms the (3*S*)-configuration of **RH32** for the same reason as discussed above for **RH19**. The NMR spectroscopic data of **RH32** (Table 31) are very similar to those reported previously (Kuroyanagi et al., 1979a). Based on the above evidence, the structure of compound **RH32** was thus elucidated and established as (3*S*)-pteroside D (Table 31). The compound was first isolated in 1971 and 1979 from the rhizomes of Japanese bracken, *P. aquilinum* KUHN var. *latiusculum* UNDERWOOD (Pteridaceae) (Hikino et al., 1971; Kuroyanagi et al., 1979a).

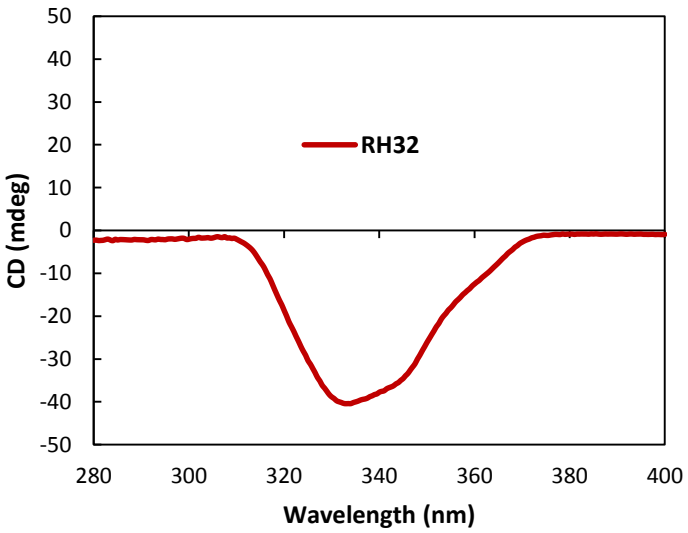

Figure 66: The CD spectrum of **RH32** recorded in methanol.

Table 32: Compound **RH20** [(2*R*)-Pterosin E]

IUPAC name	(*R*)-2-(2,4,6-trimethyl-3-oxo-2,3-dihydro-1*H*-inden-5-yl)acetic acid
Sample ID	**RH20**
Sample quantity	17 mg
Physical appearance	Yellow-orange needles
Molecular formula	$C_{14}H_{16}O_3$
Molecular Weight	232.2790 g/mol

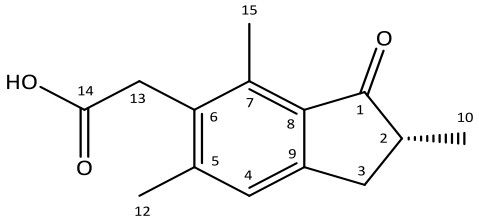

NMR data

^{1}H NMR (400 MHz, $CDCl_3$): δ_H ppm 7.13 (1H, s, H-4), 3.78 (2H, s, H_2-13), 3.25 (1H, dd, *J* = 16.6, 7.6 Hz, H_a-3), 2.66 (3H, s, H_3-15), 2.63 (1H, m, H-2), 2.59 (1H, dd, *J* = 17.3, 4.6 Hz, H_b-3), 2.39 (3H, s, H_3-12), 1.27 (3H, d, *J* = 7.3 Hz, H_3-10).

^{13}C NMR (101 MHz, $CDCl_3$): δ_C ppm 210.2 (C-1), 175.8 (C-14), 153.6 (C-9), 144.2 (C-5), 138.4 (C-7), 132.1 (C-6), 131.1 (C-8), 125.7 (C-4), 42.4 (C-2), 33.7 (C-13), 33.7 (C-3), 21.3 (C-12), 16.4 (C-10), 13.6 (C-15).

Compound **RH20** was obtained as a yellow-orange needles (Table 32). Its HR-ESI-MS spectrum gave a pseudo-molecular ion peak at *m*/*z* 231.1015 $[M-H]^-$ (Calcd for $C_{14}H_{15}O_3$: 231.1021) compatible with the molecular formula $C_{14}H_{16}O_3$, requiring seven degrees of unsaturation. The ^{13}C and HSQC NMR spectra of **RH20** displayed resonances for 14 carbon signals: 3 methyls, 2 methylenes, 2 methines, and 7 quaternary carbons including 2 carbonyl carbons. The NMR spectral data of **RH20** were similar to those of **RH16** regarding the 1-indanone skeleton, except the appearance of a singlet peak at δ_H 3.78 instead of the 2 doublet signals of the hydroxyethyl group.

Furthermore, compound **RH20** was 14 mass units and one degree of unsaturation more than **RH16**, indicating that one of the methylene group (H_2-C14) of the side chain positioned on C-6 in **RH16** was oxidised to the carbonyl group in **RH20**. Hence, the singlet signal appeared at δ_H 3.78 was assigned to the methylene group located between the benzene ring and the carbonyl group. Moreover, the HMBC spectrum (see appendix I) showed cross peaks from H-13 (δ_H 3.78) to each of C-5 (δ_C 144.20), C-7 (δ_C 138.37) and C-14 (δ_C 175.75), supporting the assignment of the singlet peak as a methylene group at 13-position. Thus, the deshielded

resonance peak assignable to position C-14 is observed at δ_C 175.75. From the above analyses, the structure of **RH20** was confirmed to be pterosin E (Table 32). Despite that the CD spectroscopy was carried out in methanol to **RH20** in order to determine the absolute stereochemistry, no Cotton effect was observed in the spectrum in range of 300-360 nm. Similarity and consistency were showed by the NMR data of **RH20** when compared with those reported previously in the literature (Fukuoka et al., 1978; Nambudiry and Rao, 1974; Ng and McMorris, 1984), verifying the structure of this compound as (2*R*)-pterosin E (Table 32). It has been separated as a natural compound from young leaves of *P. aquilinum* var. *latiusculum* (Pteridaceae) (Yoshihira et al., 1978, 1971) and *Histiopteris incisa* (Murakami et al., 1980).

Table 33: Compound **RH23** [(2*S*)-Pterosin K]

IUPAC name	(*S*)-6-(2-chloroethyl)-2-(hydroxymethyl)-2,5,7-trimethyl-2,3-dihydro-1*H*-inden-1-one
Sample ID	**RH23**
Sample quantity	3 mg
Physical appearance	White sticky
Molecular formula	$C_{15}H_{19}ClO_2$
Molecular Weight	266.7650 g/mol

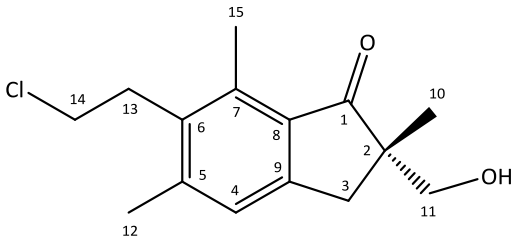

NMR data

^{1}H NMR (400 MHz, $CDCl_3$): δ_H ppm 7.12 (1H, s, H-4), 3.78 (1H, d, *J* = 10.7 Hz, H_a-11), 3.60 (1H, d, *J* = 10.7 Hz, H_b-11), 3.54* (1H, t, *J* = 8.7 Hz, H_a-13), 3.54* (1H, t, *J* = 8.7 Hz, H_a-14), 3.19* (1H, t, *J* = 8.7 Hz, H_b-13), 3.19* (1H, t, *J* = 8.7 Hz, H_b-14), 3.06 (1H, d, *J* = 17.1 Hz, H_a-3), 2.75 (1H, d, *J* = 17.1 Hz, H_b-3), 2.67 (3H, s, H_3-15), 2.43 (3H, s, H_3-12), 1.22 (3H, s, H_3-10).

^{13}C NMR (101 MHz, $CDCl_3$): δ_C ppm 211.9 (C-1), 153.0 (C-9), 144.8 (C-5), 138.3 (C-7), 135.0 (C-6), 131.9 (C-8), 126.3 (C-4), 68.3 (C-11), 50.8 (C-2), 42.2 (C-14), 37.0 (C-3), 32.4 (C-13), 21.4 (C-12), 21.2 (C-10), 13.9 (C-15).

* These data were confirmed from the HSQC experiment.

Compound **RH23** (Table 33), obtained as a white sticky substance, was identified as a chlorine-containing compound and possessed the molecular formula of $C_{15}H_{19}ClO_2$ which was deduced from the HR-ESI-MS *m*/*z* 267.1151 (Calcd. for $C_{15}H_{20}ClO_2$: 267.1152 $[M+H]^+$, indicating six degrees of unsaturation. Analysis of the ^{1}H and ^{13}C NMR data suggested a molecular skeleton

of pterosin compounds. The close similarity was clearly observed in the 1D and 2D NMR spectra of **RH29** and **RH15** (see appendix I) except for the presence of a chlorine group at position C-14 in **RH23** instead of a hydroxyl group as in **RH15**. This was supported by its mass spectrum which showed a ratio of (3:1) typical for chlorine isotopes (^{35}Cl: ^{37}Cl) of natural products. Furthermore, the coupling constant values and the chemical shifts of the ethylene protons (-CH_2-CH_2-) in **RH23** were very similar to those of chloroethyl group as in pterosins F (**RH21**) and J (**RH22**), confirming the existence of the chlorine atom in the molecule at position C-14. From the above conclusion, the structure of **RH23** was established to be pterosin K as shown in Table 33.

This compound was determined to have 2*S* configuration, as its CD curve exhibited a negative Cotton effect at 329 nm for the n → π* absorption band (Figure 67). This result is in a good agreement with the CD data provided previously for pterosin K (Kuroyanagi et al., 1979b). Thus, the absolute configuration of **RH23** was deduced as (2*S*)-pterosin K (Table 33).

The NMR data of **RH23** were identical to those published in the literature (Castillo et al., 2003, 1997; Fukuoka et al., 1978; Ng and McMorris, 1984). (2*S*)-pterosin K has been achieved as a natural product from methanol extract of young leaves of *P. aquilinum* KUHN var. *latiusculum* UNDERWOOD (Pteridaceae) (Fukuoka et al., 1972; Kuroyanagi et al., 1979a; Yoshihira et al., 1978) and fresh fronds of *P. aquilinum* var. *caudatum* (Castillo et al., 1997).

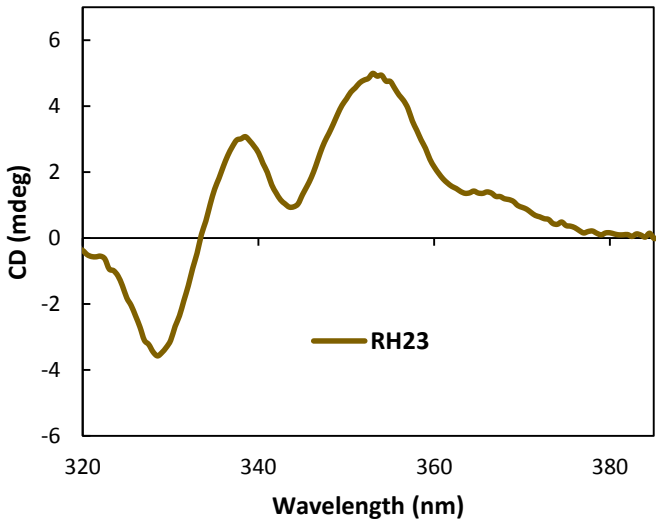

Figure 67: The CD spectrum of **RH23** in methanol showing positive (longer wavelength) and negative (shorter wavelength) signed vibronic progressions.

Table 34: Compound **RH35** [(2*S*)-Pteroside K]

IUPAC name	(*S*)-6-(2-chloroethyl)-2,5,7-trimethyl-2-((((2*R*,3*R*,4*S*,5*S*,6*R*)-3,4,5-trihydroxy-6-(hydroxymethyl)tetrahydro-2*H*-pyran-2-yl)oxy)methyl)-2,3-dihydro-1*H*-inden-1-one
Sample ID	**RH35**
Sample quantity	30 mg
Physical appearance	White crystalline solid
Molecular formula	$C_{21}H_{29}ClO_7$
Molecular Weight	428.9060 g/mol

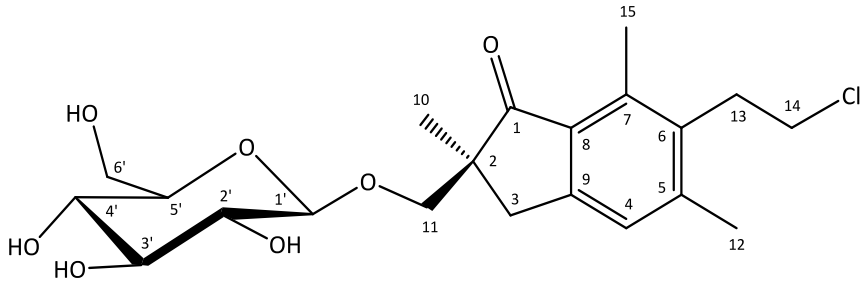

NMR data

^{1}H NMR (400 MHz, MeOD): δ_H ppm 7.19 (1H, s, H-4), 4.20 (1H, d, *J* = 7.8 Hz, H-1′), 4.12 (1H, d, *J* = 9.4 Hz, H_a-11), 3.77 (1H, dd, *J* = 11.8, 1.6 Hz, H_a-6′), 3.61* (1H, t, *J* = 8.0 Hz, H_a-14), 3.61* (1H, m, H_a-13), 3.61 (1H, m, H_b-6′), 3.48 (1H, d, *J* = 9.4 Hz, H_b-11), 3.44 (1H, d, *J* = 17.2 Hz, H_a-3), 3.29 (1H, m, H-3′), 3.21* (1H, t, *J* = 8.0 Hz, H_b-13), 3.21* (1H, m, H_b-14), 3.21 (1H, m, H-5′), 3.21 (1H, m, H-4′), 3.04 (1H, dd, *J* = 8.9, 7.8 Hz, H-2′), 2.73 (1H, d, *J* = 17.2 Hz, H_b-3), 2.65 (3H, s, H_3-15), 2.45 (3H, s, H_3-12), 1.13 (3H, s, H_3-10).

^{13}C NMR (101 MHz, MeOD): δ_C ppm 212.2 (C-1), 154.7 (C-9), 146.2 (C-5), 139.0 (C-7), 136.1 (C-6), 132.8 (C-8), 127.4 (C-4), 104.7 (C-1′), 78.1 (C-3′), 77.9 (C-5′), 75.0 (C-11), 74.9 (C-2′), 71.5 (C-4′), 62.7 (C-6′), 51.4 (C-2), 43.1 (C-14), 37.7 (C-3), 33.0 (C-13), 22.0 (C-10), 21.2 (C-12), 13.9 (C-15).

* These data were confirmed from the HSQC experiment.

Compound **RH35** (Table 34), achieved as a white crystalline solid, showed the molecular formula $C_{21}H_{29}ClO_7$, as determined by the positive ion mode HR-ESI-MS at m/z 429.1671 $[M+H]^+$ (Calcd for $C_{21}H_{30}ClO_7$: 429.1680). This molecular formula revealed 7 equivalents of unsaturation, one more than **RH23**. The ^{1}H and ^{13}C NMR data of **RH35** were closely related to those of (2*S*)-pterosin K (**RH23**) regarding the aglycone part except the presence of signals of an additional sugar unit.

The DEPTQ experiment showed resonances for exactly 21 carbons including characteristic signals of sugar moiety. The 14 protonated carbons were assigned by HSQC spectrum (see appendix I). From the coupling constant value, *J* = 7.8 Hz, of the anomeric proton (δ_H 4.20), the sugar moiety was considered to be a β-glycosyl. Further, the ^{1}H NMR spectrum showed signals and coupling constants of the sugar moiety that were consistent with those of **RH30**

and **RH31**. This is evident from the ^{1}H-^{1}H COSY cross peaks of H-1′ (δ_H 4.20)/H-2′ (δ_H 3.04), H-3′ (δ_H 3.29)/H-2′ (δ_H 3.04), H-6′ (δ_H 3.77 and 3.60)/H-4′ and H-5′ (δ_H 3.21) and H_a-6′ (δ_H 3.77)/H_b-6′ (δ_H 3.60). The significant downfield shift of H_a-11 (δ_H 4.11) and C-11 (δ_C 74.99) of the aglycone suggested the linkage site of sugar moiety at position C-11, which was further supported by the key HMBC correlations from the anomeric proton (δ_H 4.20) to C-11 (δ_C 74.99) and from H_a-11 (δ_H 4.11) and H_b-11 (δ_H 3.48) to the anomeric carbon (δ_C 104.70).

The CD spectrum of **RH35** was measured in methanol as shown in Figure 68. The spectrum illustrates a positive Cotton effect sign at 325 nm similar to that obtained by Kuroyanagi et al. (1979b) for the same compound, confirming the absolute configuration at the chiral center of C-2 as 2*S*. An X-ray diffraction analysis of a single crystal was performed for the first time, which confirmed the stereochemistry of compound **RH35** and also indicated the sugar unit as D-glucose. The X-ray structure (Figure 69) supports the CD result as it indicates the absolute configuration of **RH35** as 2*S*. The single crystal X-ray data is submitted to Cambridge Crystallographic Data Center. Based on the above information, the structure of **RH35** was established as (2*S*)-pterosin K *β*-D-glucopyranoside, called (2*S*)-pteroside K (Table 34). By comparison, the NMR data of **RH35** showed similarity with those published before in the literature (Kuroyanagi et al., 1979a). It was first isolated from the underground parts of *P. aquilinum* var. *latiusculum* by Kuroyanagi et al. (1979a).

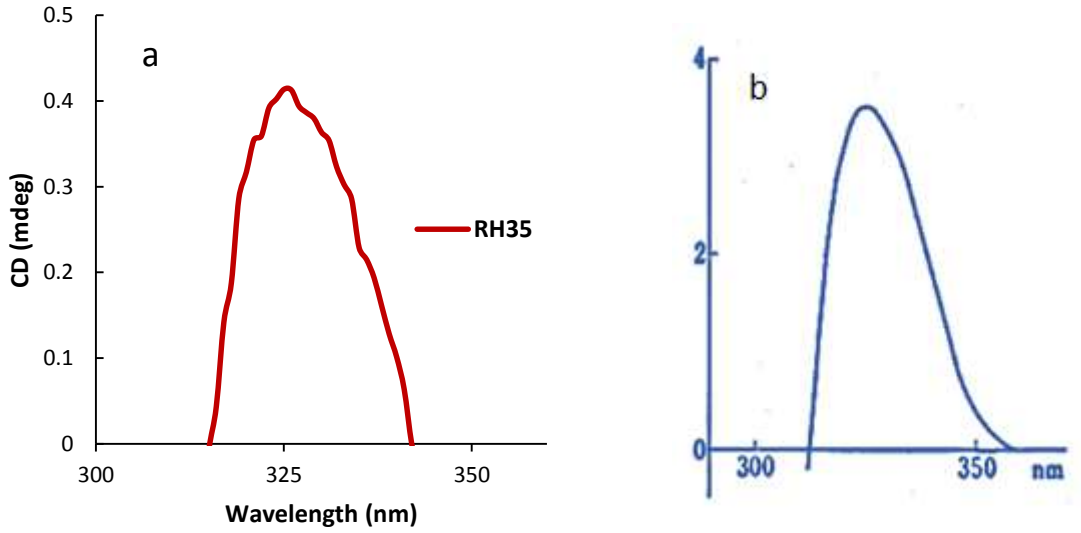

Figure 68: CD spectra recorded in methanol of the: a) isolated compound **RH35** and b) (2*S*)-pteroside K achieved by Kuroyanagi et al (1979b).

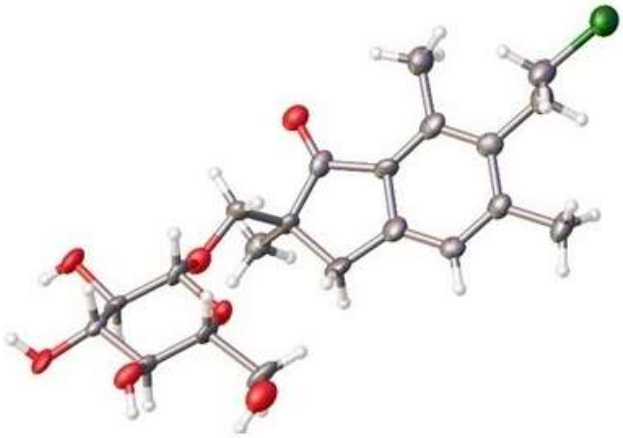

Figure 69: X-ray crystallographic structure of the compound **RH35**.

Table 35: Compound **RH24** [(2*S*)-Pterosin N]

IUPAC name	(*S*)-2-hydroxy-6-(2-hydroxyethyl)-2,5,7-trimethyl-2,3-dihydro-1*H*-inden-1-one
Sample ID	**RH24**
Sample quantity	15.4 mg
Physical appearance	White crystalline solid
Molecular formula	$C_{14}H_{18}O_3$
Molecular Weight	234.2950 g/mol

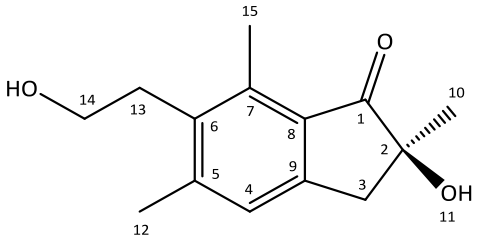

NMR data

^{1}H NMR (400 MHz, MeOD): δ_H ppm 7.13 (1H, s, H-4), 3.62* (1H, t, *J* = 7.8 Hz, H_a-13), 3.62* (1H, t, *J* = 7.8 Hz, H_a-14), 3.09 (1H, d, *J* = 16.8 Hz, H_a-3), 3.01 (1H, d, *J* = 16.8 Hz, H_b-3), 2.99* (1H, t, *J* = 7.8 Hz, H_b-13), 2.99* (1H, t, *J* = 7.8 Hz, H_b-14), 2.64 (3H, s, H_3-15), 2.44 (3H, s, H_3-12), 1.33 (3H, s, H_3-10).

^{13}C NMR (101 MHz, MeOD): δ_C ppm 209.9 (C-1), 151.2 (C-9), 146.9 (C-5), 139.4 (C-7), 137.0 (C-6), 130.8 (C-8), 127.0 (C-4), 78.1 (C-2), 61.7 (C-14), 42.8 (C-3), 32.9 (C-13), 25.4 (C-10), 21.3 (C-12), 14.0 (C-15).

* These data were confirmed from the HSQC experiment.

Compound **RH24** was isolated as a white crystalline solid, whose molecular formula was established as $C_{14}H_{18}O_3$ based on a quasimolecular ion peak at *m*/*z* 235.1328 $[M+H]^+$ (Calcd for $C_{14}H_{19}O_3$: 235.1334) in the positive HR-ESI-MS measurements. Analysis of the NMR spectroscopic data of **RH24** (Table 35) suggested high structural similarity with pterosin B (**RH16**) regarding the signals that appeared at δ_H 7.13 (H-4, s), δ_H 3.62 (H-14, t, J = 7.8 Hz), δ_H 2.99 (H-13, t, J = 7.8 Hz), δ_H 2.64 (H-15, s) and δ_H 2.44 (H-12, s), except that the proton at position C-2 in pterosin B was replaced by a hydroxyl group in **RH24**. This variation was deduced from some facts: first, the carbon signals of C-2 and C-10 were strongly shifted downfield to δ_C 78.13 and δ_C 25.43, respectively, due to the strong influence of hydroxyl group at position C-2; second, the secondary methyl at position C-2 appeared as a singlet peak instead of a doublet signal at δ_H 1.33 (CH_3-2), and the multiplet peak of H-2 in **RH16** was absent in compound **RH24**; third, the signals of the methylene group at C-3 appeared as two doublets at a slightly lower field (δ_H 3.01 , d, J = 16.8 Hz and 3.09, d, J = 16.8 Hz). These observations were evident for the above analysis. Therefore, compound **RH24** was deduced as pterosin N.

The CD spectrum of this compound did not show any absorption bands around 300-360 nm typical for pterosin B type compounds (Kuroyanagi et al., 1979b). The ^1H and ^{13}C NMR spectral data of **RH24** are consistent with those reported previously (Fukuoka et al., 1983, 1978; Kuroyanagi et al., 1974a; Wu et al., 2014). On the basis of the above detailed spectral analysis, the compound **RH24** was elucidated as (2*S*)-pterosin N (Table 35). It has been isolated from *Histiopteris incisa* and *Pteris oshimensis* (Murakami et al., 1974), young leaves of *P. aquilinum* van. *Latiusculum* (Kuroyanagi et al., 1974a) and *Pteris setuloso-costulata* (Murakami et al., 1980).

Table 36: Compound **RH25** [(2*S*)-Pterosin P]

IUPAC name	(*S*)-6-(2-hydroxyethyl)-5-(hydroxymethyl)-2,7-dimethyl-2,3-dihydro-1*H*-inden-1-one
Sample ID	**RH25**
Sample quantity	4 mg
Physical appearance	Colourless needles
Molecular formula	$C_{14}H_{18}O_3$
Molecular Weight	234.2950 g/mol

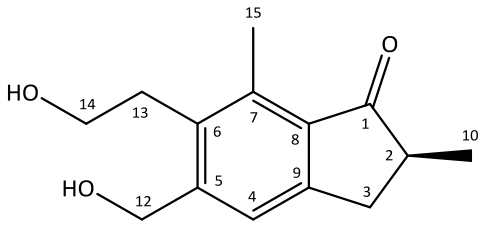

NMR data

^{1}H NMR (400 MHz, $CDCl_3$): δ_H ppm 7.32 (1H, s, H-4), 4.73 (2H, s, H_2-12), 3.91 (2H, t, *J* = 6.0 Hz, H_2-14), 3.29 (1H, dd, *J* = 17.4, 8.5 Hz, H_a-3), 3.09 (2H, t, *J* = 6.0 Hz, H_2-13), 2.67 (3H, s, H_3-15), 2.64 (1H, m, H-2), 2.63 (1H, dd, *J* = 17.4, 3.5 Hz, H_b-3), 1.28 (3H, d, *J* = 7.2 Hz, H_3-10).

^{13}C NMR (101 MHz, $CDCl_3$): δ_C ppm 210.7 (C-1), 152.6 (C-9), 145.7 (C-5), 138.5 (C-7), 135.8 (C-6), 133.7 (C-8), 125.2 (C-4), 64.1 (C-12), 61.7 (C-14), 42.8 (C-2), 34.1 (C-3), 30.7 (C-13), 16.6 (C-10), 14.0 (C-15).

Compound **RH25** (4 mg) was isolated as colourless needles (Table 36). Its HR-ESI-MS exhibited a $[M+H]^+$ peak at *m/z* 235.1330, suggesting a molecular formula of $C_{14}H_{18}O_3$ (Calcd for $C_{14}H_{19}O_3$: 235.1334). This molecular formula highlighted a difference of one oxygen atom as compared to that of **RH16**. The DEPTQ spectrum of **RH25** (see appendix I) showed 14 carbon signals including one carbonyl carbon. Study of the NMR spectroscopic data of **RH25** indicated a structural resemblance with pterosin B (**RH16**), except that the methyl group at position C-12 in **RH16** was substituted by hydroxymethyl (CH_2OH) group in **RH25**. The downfield shift noticed for the signals of methylene-12 (δ_H 4.73) and C-12 (δ_C 64.1), and this firmly confirmed the attachment of the CH_2-12 to the hydroxyl group. The resonance of H-4 at a lower field (δ_H 7.32) and the 16 Da difference in mass between **RH16** (218 amu) and **RH25** (234 amu) were also evident for the above variation. Based on the above observations and by comparison of the NMR data with those reported in the literature (Kuraishi et al., 1985; Kuroyanagi et al., 1979a; Ouyang et al., 2010), the structure of **RH25** (Table 36) was assigned to (2*S*)-pterosin P.

In order to confirm the configuration at the chiral center of C-2, a CD spectroscopy was undertaken. Unluckily, the CD spectrum of **RH25** showed no Cotton effect for n → π* transition at 300-360 nm. (2*S*)-pterosin P has been isolated from various plant ferns, for instance, the rhizomes of *P. aquilinum* var. *latiusculum* (Kuroyanagi et al., 1979a), the fronds of *Microlepia strigosa* (THUNB.) PRESL ((Kuraishi et al., 1985) and the aerial parts of *Pteris multifida* Poir (Ouyang et al., 2010). The compound has been assessed by Ouyang et al. (2010) for its cytotoxicity against four human cancer cell lines (A549, LOVO, PANC-1, and NCI-H446), and the results showed no significant inhibitory activity of pterosin P against all the cancer cell lines.

Table 37: Compound **RH26** [Pterosin Z]

IUPAC name	6-(2-hydroxyethyl)-2,2,5,7-tetramethyl-2,3-dihydro-1*H*-inden-1-one
Sample ID	**RH26**
Sample quantity	14 mg
Physical appearance	White amorphous solid
Molecular formula	$C_{15}H_{20}O_2$
Molecular Weight	232.3230 g/mol

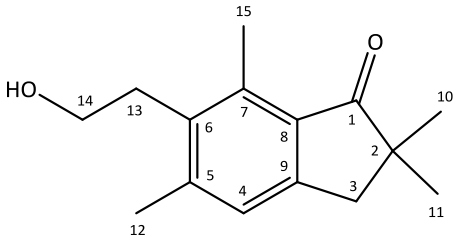

NMR data

^{1}H NMR (400 MHz, $CDCl_3$): δ_H ppm 7.08 (1H, s, H-4), 3.76* (1H, t, *J* = 7.5 Hz, H_a-13), 3.76* (1H, t, *J* = 7.5 Hz, H_a-14), 3.02* (1H, t, *J* = 7.5 Hz, H_b-13), 3.02* (1H, t, *J* = 7.5 Hz, H_b-14), 2.85 (2H, s, H_2-3), 2.69 (3H, s, H_3-15), 2.44 (3H, s, H_3-12), 1.19 (3H, s, H_3-10), 1.19 (3H, s, H_3-11).

^{13}C NMR (101 MHz, $CDCl_3$): δ_C ppm 212.4 (C-1), 151.5 (C-9), 144.6 (C-5), 138.5 (C-7), 134.9 (C-6), 131.3 (C-8), 126.0 (C-4), 61.8 (C-14), 45.7 (C-2), 41.9 (C-3), 32.0 (C-13), 25.7 (C-10), 25.7 (C-11), 21.5 (C-12), 13.9 (C-15).

* These data were confirmed from the HSQC experiment.

Compound **RH26**, isolated as a white amorphous solid, was determined to have the molecular formula $C_{15}H_{20}O_2$ (6 degrees of unsaturation) on the basis of HR-ESI-MS analysis which showed a quasi-molecular ion peak at *m*/*z* 233.1537 $[M+H]^+$ (Calcd. For $C_{15}H_{21}O_2$: 233.1542). The molecular formula of **RH26** indicated one carbon atom and two protons more than **RH16**. The DEPTQ and ^{13}C NMR spectra (see appendix I) of compound **RH26** showed 14 signal

peaks, representing 15 carbon atoms and including 4 methyl signals. Both C-10 and C-11 resonated at δ_C 25.73 and appeared as one big signal. Comparison of the ^{13}C NMR data of **RH26** with those of **RH16** revealed that they were quite similar. The ^{1}H NMR spectrum of **RH26** disclosed a chemical shift of an equivalent geminal-dimethyl group instead of the secondary methyl group at position C-2, i.e. one proton at position C-2 in **RH16** was replaced by an additional methyl group in **RH26**. The ^{1}H NMR data (Table 37) of **RH26** showed two singlet signals at δ_H 1.19 and δ_H 2.85 assignable to the two tertiary methyls and methylene at C-3, respectively, contrary to the multiplet (H-2), doublet of doublet (H-3) and doublet (CH_3-2) signals revealed by the ^{1}H NMR spectrum of **RH16** (Figure 70). The direct HSQC correlations from H-10 to C-10 and H-11 to C-11 were evident for the presence of the two geminal methyls at position C-2. In addition, the HMBC cross peaks of H-10 and H-11(δ_H 1.19, s) with C-2 (δ_C 45.72) and C-3 (δ_C 41.88), H-10 with C-11 and H-11 with C-10, further confirmed the above argument. By comparison of the NMR data of **RH26** with the literature values (Fukuoka et al., 1983, 1978; Neeson and Stevenson, 1988; Padwa et al., 1996) and based on the above evidence, the compound **RH26** was established as pterosin Z.

It has been previously reported from fronds of *P. aquilinum* var. *caudatum* (Castillo et al., 1997), *Microlepia substrigosa* TAGAWA, *Microlepia speluncae* (L.) MOORE and *Microlepia trapeziformis* (ROXB.) KUHN (Kuraishi et al., 1985), fronds of *P. aquilinum* subsp. *wightiaunm* (Tanaka et al., 1982), young shoots of *P. aquilinum* (L.) Kuhn (Kobayashi and Koshimizu, 1980), aerial parts of *Pityrogramma calomelanos* (Bardouille et al., 1978), leaves of a fern Hypolepis punctata Mett. (Hayashi et al., 1972) and fronds of *P. aquilinum* var. *latiusculum* (Saito et al., 1975; Yoshihira et al., 1978, 1971). Pterosin Z has been shown to have smooth muscle relaxant activity against calcium contractions, with an EC_{50} value of 1.3×10^{-6} M (Sheridan et al., 2009, 1999). It has been reported that pterosin Z showed cytotoxic effect on a ciliate, *Paramecium caudatum*, along with inhibitory effect on sea urchin embryo at the early development stages (Kobayashi and Koshimizu, 1980). Moreover, pterosin Z has been found to have the effect of promoting cartilage growth in humans and showed to be effective in inhibiting chondrocyte hypertrophy as well (Tsumaki et al., 2015).

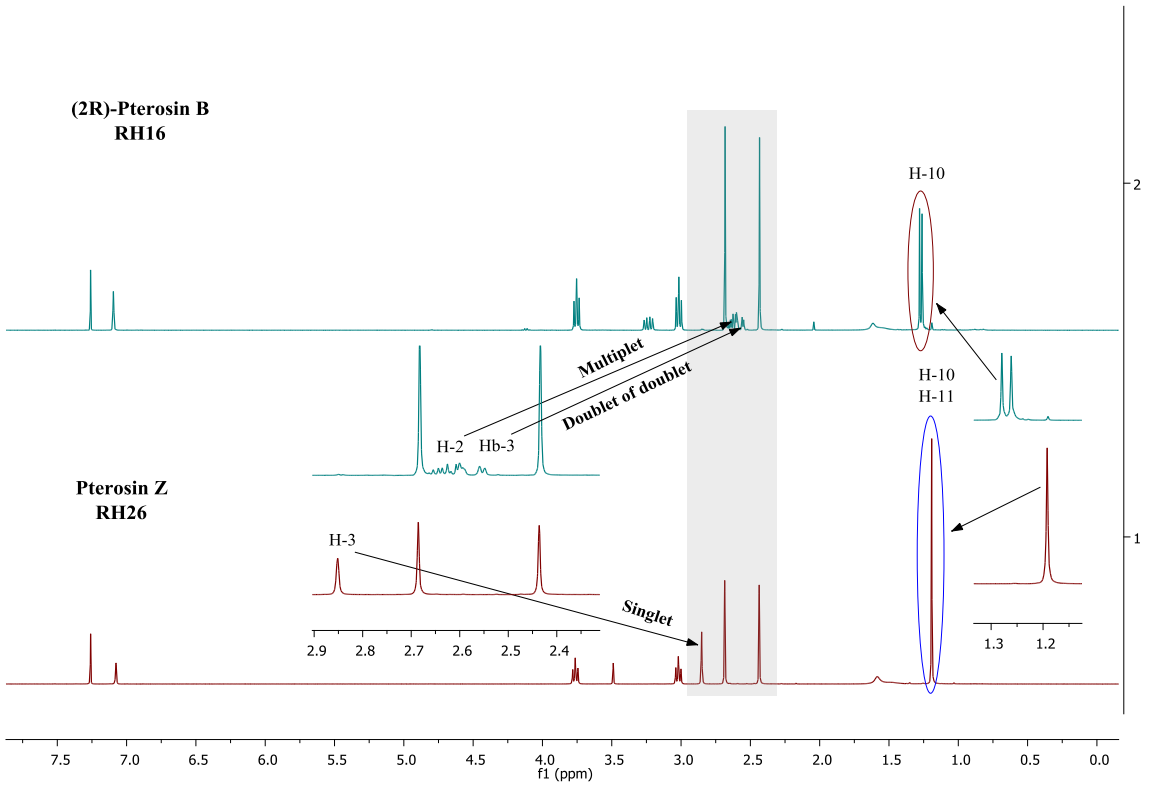

Figure 70: Combined ^{1}H NMR spectra showing the main variation between **RH16** and **RH26**.

Table 38: Compound **RH33** [Pteroside Z]

IUPAC name	2,2,5,7-tetramethyl-6-(2-(((2*R*,3*R*,4*S*,5*S*,6*R*)-3,4,5-trihydroxy-6-(hydroxymethyl)tetrahydro-2*H*-pyran-2-yl)oxy)ethyl)-2,3-dihydro-1*H*-inden-1-one
Sample ID	**RH33**
Sample quantity	47 mg
Physical appearance	Yellow-orange gum
Molecular formula	$C_{21}H_{30}O_7$
Molecular Weight	394.4640 g/mol

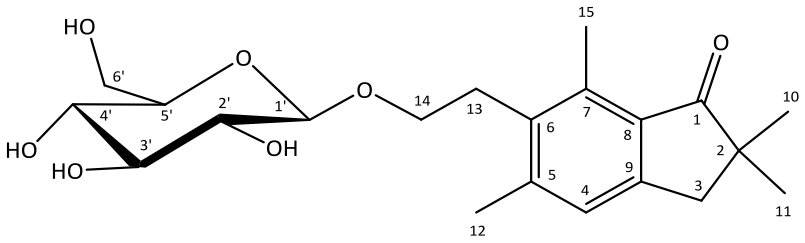

NMR data

^{1}H NMR (400 MHz, MeOD): δ_H ppm 7.13 (1H, s, H-4), 4.32 (1H, d, *J* = 7.8 Hz, H-1′), 3.91 (1H, dd, *J* = 17.1, 8.5 Hz, H_a-14), 3.85 (1H, dd, *J* = 11.8, 1.6 Hz, H_a-6′), 3.66 (1H, dd, *J* = 11.8, 5.3 Hz, H_b-6′), 3.65 (1H, dd, *J* = 17.1, 7.8 Hz, H_b-14), 3.35 (1H, t, *J* = 8.4 Hz, H-3′), 3.29 (1H, m, H-4′), 3.27 (1H, m, H-5′), 3.19 (1H, t, *J* = 8.3 Hz, H-2′), 3.11 (2H, t, *J* = 8.0 Hz, H_2-13), 2.87 (2H, s, H_2-3), 2.65 (3H, s, H_3-15), 2.45 (3H, s, H_3-12), 1.16 (3H, s, H_3-10), 1.16 (3H, s, H_3-11).

^{13}C NMR (101 MHz, MeOD): δ_C ppm 214.5 (C-1), 153.1 (C-9), 146.5 (C-5), 139.3 (C-7), 136.4 (C-6), 131.8 (C-8), 127.0 (C-4), 104.5 (C-1′), 78.2 (C-3′), 78.0 (C-5′), 75.2 (C-2′), 71.6 (C-4′), 69.2 (C-14), 62.7 (C-6′), 46.7 (C-2), 42.6 (C-3), 30.1 (C-13), 25.8 (C-10), 25.8 (C-11), 21.4 (C-12), 13.9 (C-15).

Compound **RH33** (47 mg) was isolated as a yellow-orange gum material (Table 38). It was characterized by NMR spectroscopic studies and HR-ESI-MS. Its positive HR-ESI-MS spectrum indicated a pseudo-molecular ion peak at *m*/*z* 395.2060 $[M+H]^+$ suggesting a molecular formula of $C_{21}H_{30}O_7$ (Calcd for $C_{21}H_{31}O_7$: 395.2070), and indicating the presence of 7 degrees of unsaturation in the molecule.

The ^{1}H and ^{13}C NMR spectroscopic data of **RH33** (Table 38) were found to be similar to those of **RH26** except for the presence of identical and characteristic signals for a sugar moiety. The aglycone part was therefore determined as a pterosin Z. The coupling constant, *J* = 7.8 Hz, of the anomeric proton resonated at δ_H 4.32 (d, H-1′) confirmed the *β*-configuration for the sugar residue, indicating *β*-glycosyl moiety. Further, the presence of glucose as a *β*-D-glucopyranoside was confirmed based on data similarity between glucose signals and those for (2*S*)-pteroside A (**RH30**) and (2*R*)-pteroside B (**RH31**). The COSY spectrum showed the ^{1}H-^{1}H cross peaks between H-1′ (δ_H 4.32)/H-2′ (δ_H 3.19), H-2′ (δ_H 3.19)/H-3′ (δ_H 3.35), H-5′ (δ_H

3.27)/H_a-6′ (δ_H 3.85), H-5′ (δ_H 3.27)/H_b-6′ (δ_H 3.66) and H_a-6′ (δ_H 3.85)/H_b-6′ (δ_H 3.66) assignable for the glucose moiety. The ^{13}C NMR data (Table 38) and DEPTQ spectrum (see appendix I) revealed carbon resonances for the glucose including the anomeric carbon (δc 104.45), which are in good agreement with those of glucose.

The location of the attachment of the glucose to the aglycone at C-14 was evident from the downfield chemical shifts resonated at δ_H 3.91 (H_a-14) and δ_C 69.21 (C-14). This attachment was confirmed by HMBC spectrum (see appendix I), by which HMBC cross peaks from the anomeric proton H-1′ (δ_H 4.32) of the sugar moiety to the C-14 (δ_C 69.21) and from H_b-14 (δ_H 3.91) to the anomeric carbon C-1′ (δ_C 104.45) were observed confirming the above mentioned link. On the basis of these evidence and by comparison of the NMR data with those reported before (Hikino et al., 1971; Kuroyanagi et al., 1979a), the structure of **RH33** was concluded to be pteroside Z as shown in Table 38. The NMR spectral data of **RH33** are consistent with those previously published by Hikino et al. (1971) and Kuroyanagi et al (1979a). This glycoside has been obtained for the first time from the rhizomes of *P. aquilinum* KUHN var. *latiusculum* UNDERWOOD (Pteridaceae) (Hikino et al., 1971; Kuroyanagi et al., 1979a).

Table 39: Compound **RH27** [(2*S*)-2-Hydroxymethylpterosin E]

IUPAC name	(*S*)-2-(2-(hydroxymethyl)-2,4,6-trimethyl-3-oxo-2,3-dihydro-1*H*-inden-5-yl)acetic acid
Sample ID	**RH27**
Sample quantity	14.7 mg
Physical appearance	Yellow sticky
Molecular formula	$C_{15}H_{18}O_4$
Molecular Weight	262.3050 g/mol

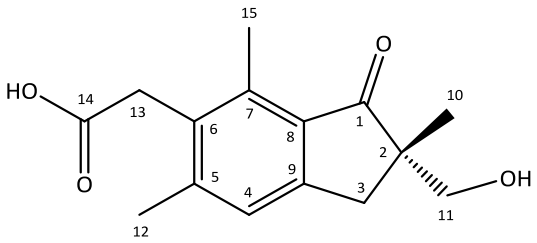

NMR data

^{1}H NMR (400 MHz, MeOD): δ_H ppm 7.19 (1H, s, H-4), 3.76 (2H, s, H_2-13), 3.72 (1H, d, *J* = 10.7 Hz, H_a-11), 3.46 (1H, d, *J* = 10.7 Hz, H_b-11), 3.26 (1H, d, *J* = 17.2 Hz, H_a-3), 2.74 (1H, d, *J* = 17.2 Hz, H_b-3), 2.61 (3H, s, H_3-15), 2.40 (3H, s, H_3-12), 1.10 (3H, s, H_3-10).

^{13}C NMR (101 MHz, MeOD): δ_C ppm 212.8 (C-1), 174.9 (C-14), 154.8 (C-9), 146.5 (C-5), 139.3 (C-7), 133.8 (C-6), 133.0 (C-8), 126.8 (C-4), 68.2 (C-11), 52.7 (C-2), 37.5 (C-3), 35.0 (C-13), 21.5 (C-12), 21.3 (C-10), 14.0 (C-15).

Compound **RH27** was obtained as a yellow sticky material (Table 39). The negative mode HR-ESI-MS data showed a quasimolecular ion peak at *m*/*z* 261.1126 $[M-H]^-$, suggesting a molecular formula of $C_{15}H_{18}O_4$ (Calcd for $C_{15}H_{17}O_4$: 261.1127), hence it required one more degree of unsaturation than **RH15**. This molecular formula also indicated that **RH27** has one oxygen more and two hydrogens less than **RH15**. The DEPTQ spectrum of **RH27** revealed resonances for 15 carbons including 2 carbonyl carbons. It is found that the NMR spectral data of this compound closely resembled those of compound **RH15** in relation to signals belonging to the skeleton of 1-indanone, and were very similar to those of **RH20** regarding the signals of the side chain linked at position C-6. Based on this information, the compound is suggested to have an analogous structure as pterosin A.

The ^{1}H NMR spectrum showed the major difference between **RH27** and **RH15** due to the downfield shift of signals δ_H 3.76 (H-13, s) and δ_C 174.85 (C-14) attributed to the methylene and carboxylic group of the side chain, respectively, indicating that the CH_2-14 in **RH15** was oxidised to carbonyl group in **RH27**. This was evident from the 14 Da difference in mass

between these two compounds, the absence of CH_2-14 signal and the appearance of a singlet peak of CH_2-13 in **RH27** in comparison with those of **RH15**. Further analysis of its HMBC spectrum (see appendix I) revealed key correlations from H-13 (δ_H 3.76) to each of C-14 (δ_C 174.85), C-5 (δ_C 146.45), C-6 (δ_C 133.84) and C-7 (δ_C 139.25) confirming the above variation and hence the presence of the -CH_2COOH group as a side chain at position C-6. Thus, compound **RH27** was established as 2-hydroxymethylpterosin E.

In order to establish the stereochemistry of **RH27** at position C-2, the CD spectrum of **RH27** was studied (Figure 71). Similar to compound **RH15**, the spectrum of **RH27** in methanol exhibited Cotton effects around 320-360 nm ascribed to the n → π* transition, confirming the absolute configuration of **RH27** as 2*S* (Kuroyanagi et al., 1979b). The NMR spectral data of **RH27** were in a good agreement when compared with those stated in the literature (Lee et al., 2012). The compound was therefore structurally confirmed to be (2*S*)-2-hydroxymethyl pterosin E as shown in Table 39. The isolation of this compound was reported as a natural product from *P. aquilinum* (L.) Kuhn for the first time, as the compound has been previously obtained by Lee et al. (2012) as a major metabolite product from the metabolism of (2S)-pterosin A in rats.

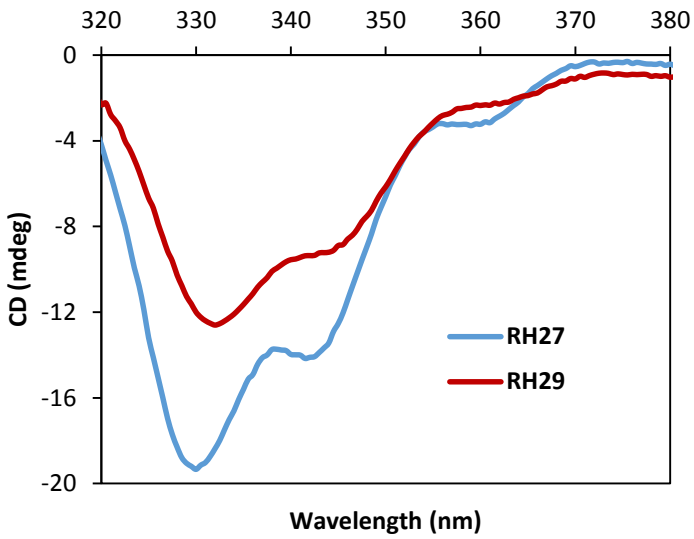

Figure 71: The CD spectra of the compounds **RH27** and **RH29** recorded in methanol.

Table 40: Compound **RH29** [(2*S*)-12-Hydroxypterosin A]	
IUPAC name	(*S*)-6-(2-hydroxyethyl)-2,5-bis(hydroxymethyl)-2,7-dimethyl-2,3-dihydro-1*H*-inden-1-one
Sample ID	**RH29**
Sample quantity	4 mg
Physical appearance	Pale-yellow solid
Molecular formula	$C_{15}H_{20}O_4$
Molecular Weight	264. 3210 g/mol

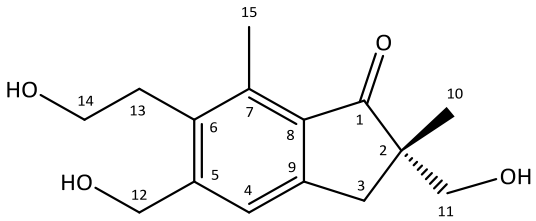

NMR data

^{1}H NMR (400 MHz, MeOD): δ_H ppm 7.44 (1H, s, H-4), 4.75 (2H, s, H_2-12), 3.72 (1H, d, *J* = 10.6 Hz, H_a-11), 3.66 (2H, t, *J* = 7.4 Hz, H_2-14), 3.47 (1H, d, *J* = 10.6 Hz, H_b-11), 3.29 (1H, d, *J* = 17.2 Hz, H_a-3), 3.00 (2H, t, *J* = 7.4 Hz, H_2-13), 2.77 (1H, d, *J* = 17.2 Hz, H_b-3), 2.66 (3H, s, H_3-15), 1.10 (3H, s, H_3-10).

^{13}C NMR (101 MHz, MeOD): δ_C ppm 213.0 (C-1), 154.2 (C-9), 148.5 (C-5), 139.0 (C-7), 135.7 (C-6), 134.1 (C-8), 124.4 (C-4), 68.3 (C-11), 63.6 (C-12), 62.1 (C-14), 52.7 (C-2), 37.7 (C-3), 31.9 (C-13), 21.3 (C-10), 13.8 (C-15).

Compound **RH29** was isolated as a pale-yellow amorphous solid. The positive mode HR-ESI-MS exhibited a pseudo-molecular ion peak at *m*/*z* 265.1435 $[M+H]^+$ (Calcd for $C_{15}H_{21}O_4$: 265.1440), indicating the molecular formula $C_{15}H_{20}O_4$, possessing one oxygen atom more than **RH15** whilst having the same equivalent of unsaturation as **RH15**. The NMR spectroscopic data of **RH29** (Table 40) were quite similar to those of **RH15**. Comparing the NMR data between **RH29** and **RH15** (Table 40 & Table 22) assigned the replacement of the methyl group at position C-5 in **RH15** by a hydroxymethylene group in **RH29**. This variation was apparent from the mass spectrum of **RH29** (264 amu) which demonstrated a 16 Da difference in mass with that of **RH15** (248 amu).

The HSQC spectrum exhibited the direct cross peak between H-12 and C-12. In the ^{1}H and ^{13}C NMR data of **RH29** (Table 40), the significant low field chemical shifts of H-12 (δ_H 4.75) and C-12 (δ_C 63.57) were observed confirming the above mentioned replacement at position C-5. This was verified by detailed analysis of 2D NMR data of compound **RH29**. The HMBC experiment demonstrated correlations from H-12 (δ_H 4.75) to each of C-4 (δ_C 124.41), C-5 (δ_C

148.53), C-6 (δ_C 135.69); indicated that the hydroxymethylene group (CH_2OH) was linked to the position C-5. On the basis of these observations, compound **RH29** was elucidated as 12-hydroxypterosin A (Table 40).

The absolute configuration of **RH29** at position C-2 was determined by an intensive study of its CD spectrum (Figure 71). The spectrum was obtained in methanol which showed close similarity with that of **RH27** and **RH15** in relation to display the Cotton effects (n → π* transition) around 320-360 nm, thus the stereochemistry of **RH29** was confirmed to be 2*S* (Kuroyanagi et al., 1979b). The NMR data of **RH29** showed resemblance when compared with the literature values (Lee et al., 2012). Consequently, the chemical structure of compound **RH29** was confirmed as (2*S*)-12-hydroxypterosin A (Table 40). This compound isolated and characterised here for the first time as a natural product from *P. aquilinum* (L.) Kuhn. It has been first obtained as a metabolite product from an *in vivo* study on the metabolism of (2*S*)-pterosin A in rats (Lee et al., 2012).

Table 41: Compound **RH36** [(5-(*β*-hydroxy)ethyl-2, 2, 4, 6-tetramethyl-1, 3-indandione]

IUPAC name	5-(2-hydroxyethyl)-2,2,4,6-tetramethyl-1*H*-indene-1,3(2*H*)-dione
Sample ID	**RH36**
Sample quantity	4 mg
Physical appearance	Pale-yellow solid
Molecular formula	$C_{15}H_{18}O_3$
Molecular Weight	246.3060 g/mol

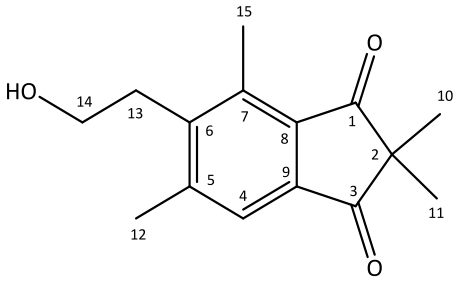

NMR data

^{1}H NMR (400 MHz, MeOD): δ_H ppm 7.64 (1H, s, H-4), 3.70 (2H, t, *J* = 7.4 Hz, H_2-14), 3.12 (2H, t, *J* = 7.4 Hz, H_2-13), 2.78 (3H, s, H_3-12), 2.56 (3H, s, H_3-15), 1.20 (3H, s, H_3-10), 1.20 (3H, s, H_3-11).

^{13}C NMR (101 MHz, MeOD): δ_C ppm 203.2 (C-1), 202.7 (C-3), 147.7 (C-9), 147.2 (C-5), 140.3 (C-7), 136.0 (C-6), 135.4 (C-8), 123.3 (C-4), 61.3 (C-14), 51.0 (C-2), 33.7 (C-13), 21.5 (C-12), 20.8 (C-10), 20.8 (C-11), 14.6 (C-15).

Compound **RH36** was obtained as a pale-yellow solid (Table 41). The molecular formula of **RH36** was found to be $C_{15}H_{18}O_3$ from its positive mode HR-ESI-MS at *m/z* 247.1329 $[M+H]^+$ (Calcd for $C_{15}H_{19}O_3$: 247.1334), indicating 7 degrees of unsaturation, one more than compound **RH26**. The ^{1}H and ^{13}C NMR spectral data of **RH36** (Table 41) are very similar to those of **RH26** except for the large downfield shift of the C-3 signal (δ_C 202.71) and deshielding of the aromatic proton (H-4) resonated at δ_H 7.64, suggesting the replacement of the methylene (2H-3) in **RH26** with a carbonyl group in **RH36**. This variation was evident from the absence of the methylene singlet signal (δ_H 2.85, s, H-3) in **RH36**, and was verified with the 14 Da difference in mass between **RH26** (232 amu) and **RH36** (246 amu). Depended upon the NMR data comparison of **RH36** with those reported in the past (Fukuoka et al., 1978; Ng and McMorris, 1984) and from the above information, compound **RH36** was thus concluded to be 5-(*β*-hydroxy)ethyl-2, 2, 4, 6-tetramethyl-1, 3-indandione.

Here, the isolation of this compound as a natural product from the rhizomes of *P. aquilinum* (L.) Kuhn has been reported for the first time. The compound has been prepared previously based on oxidation reaction of pterosin D with chromic anhydride and pyridine in order to

confirm the location of hydroxyl group at position C-3 in pterosin D (Fukuoka et al., 1978). It has also been achieved by Ng and McMorris in 1984 by treatment of 5-(*β*-methoxy)ethyl-2, 2, 4, 6-trimethyl-1, 3-indandione with 48% hydrobromic acid in glacial acetic acid.

Table 42: Compound **RH37** [Ptaquiloside]

IUPAC name	(2'*R*,3a'*R*,4'*S*,7a'*R*)-4'-hydroxy-2',4',6'-trimethyl-7a'-(((2*S*,3*R*,4*S*,5*S*,6*R*)-3,4,5-trihydroxy-6-(hydroxymethyl)tetrahydro-2*H*-pyran-2-yl)oxy)-1',3a',4',7a'-tetrahydrospiro[cyclopropane-1,5'-inden]-3'(2'*H*)-one
Sample ID	**RH37**
Sample quantity	21 mg
Physical appearance	Colourless amorphous material
Molecular formula	$C_{20}H_{30}O_8$
Molecular Weight	398.4520 g/mol

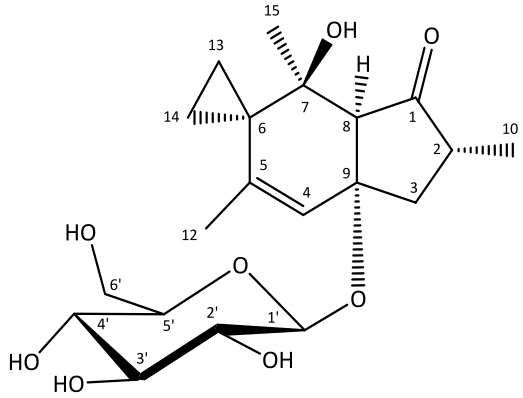

NMR data

^{1}H NMR (400 MHz, MeOD): δ_H ppm 5.77 (1H, s, H-4), 4.60 (1H, d, *J* = 7.7 Hz, H-1′), 3.90 (1H, dd, *J* = 11.9, 1.4 Hz, H_a-6′), 3.66 (1H, dd, *J* = 11.9, 5.4 Hz, H_b-6′), 3.37 (1H, m, H-3′), 3.29 (1H, m, H-5′), 3.29 (1H, m, H-4′), 3.20 (1H, dd, *J* = 9.0, 7.8 Hz, H-2′), 2.65 (1H, d, *J* = 1.3 Hz, H-8), 2.50 (1H, dd, *J* = 12.3, 8.1 Hz, H_a-3), 2.23 (1H, m, H-2), 1.93 (1H, t, *J* = 12.7 Hz, H_b-3), 1.53 (3H, d, *J* = 0.7 Hz, H_3-12), 1.29 (3H, s, H_3-15), 1.07 (3H, d, *J* = 6.9 Hz, H_3-10), 0.88 (1H, m, H_a-14), 0.84 (1H, m, H_a-13), 0.69 (1H, ddd, *J* = 9.3, 5.2, 4.1 Hz, H_b-14), 0.48 (1H, ddd, *J* = 9.3, 5.4, 4.1 Hz, H_b-13).

^{13}C NMR (101 MHz, MeOD): δ_C ppm 212.6 (C-1), 144.5 (C-5), 123.2 (C-4), 99.3 (C-1′), 82.1 (C-9), 78.2 (C-3′), 77.8 (C-5′), 75.2 (C-2′), 71.9 (C-7), 71.9 (C-4′), 62.8 (C-6′), 62.5 (C-8), 45.2 (C-2), 45.2 (C-3), 30.1 (C-6), 27.0 (C-15), 19.5 (C-12), 13.6 (C-10), 10.6 (C-13), 5.9 (C-14).

Compound **RH37** (Table 42), a colourless amorphous powder, was obtained as an unstable compound. It gave a quasimolecular ion peak in the negative mode HR-ESI-MS at *m*/*z* 397.1879 $[M-H]^-$, consistent with the molecular formula $C_{20}H_{30}O_8$ (Calcd for $C_{20}H_{29}O_8$: 397.1862). From the ^{1}H NMR spectrum of **RH37**, a doublet peak at δ_H 1.07 alongside two singlet signals at δ_H 1.29 and δ_H 1.53 were observed corresponding to three methyls at positions C-10, C-15 and C-12, respectively, for which the latter (δ_H 1.53) showed a long

range coupling to the aromatic proton (δ_H 5.77) at position C-4. Surprisingly, a doublet signal (J = 1.3 Hz) was observed for an isolated hydrogen at position C-8.

A total of twenty carbon signals were exhibited by its DEPTQ spectrum including characteristic resonances for sugar moiety. The spectrum showed the presence of an anomeric carbon signal at δ_C 99.31 and a ketone at δ_C 212.62. The DEPTQ spectrum also indicated the presence of three methyls, four methylenes and eight methine groups along with carbon signals corresponding to five quaternary carbon atoms. The connectivity of the quaternary carbons was determined by HMBC spectrum.

The assignment of all the protonated carbon signals were performed by HSQC experiment. The HSQC spectrum signified that the chemical shifts resonated at δ_H 0.48 and 0.84 were attached to the carbon at δ_C 10.57 (C-13), and also showed the direct correlations from δ_H 0.69 and 0.88 to δ_C 5.88 (C-14). This supported the presence of one cyclopropane ring in the molecule.

The hydrogen connectivities were established by COSY experiment. The cross-peaks H-2/H-10, H-2/H_a-3, H-2/H_b-3, H_a-3/H_b-3 and H-2/H-10 were observed in the spectrum. The spectrum also exhibited correlations H-1′/H-2′, H-4′/H_a-6′, H-4′/H_b-6′, H-5′/H_a-6′, H-5′/H_b-6′ and H_a-6′/H_b-6′ associated with glucose moiety and cross-peaks related to the cyclopropane ring [H_a-13 (δ_H 0.84)/H_b-14 (δ_H 0.69), H_b-13 (δ_H 0.48)/H_a-14 (δ_H 0.88) and H_b-13 (δ_H 0.48)/H_b-14 (δ_H 0.69)] which proved that no proton was attached to position C-6 except the cyclopropane ring. This fact was confirmed by HMBC experiment (see appendix I) which demonstrated key correlations from H_a-13 (δ_H 0.84) and H_a-14 (δ_H 0.88) to each of C-5 (δ_C 144.49), C-6 (δ_C 30.09) and C-7 (δ_C 71.93). The position of the double bond between C-4 and C-5 was derived from the cross-peak between H-4 (δ_H 5.77) and H-12 (δ_H 1.53).

The ^{1}H NMR data (Table 42) showed a doublet signal for an anomeric proton resonated at δ_H 4.60, indicating the presence of a sugar moiety in the molecule. Based on the H-l′/H-2′ coupling constant of 7.7 Hz and comparison with that of **RH30**-**RH35**, the configuration of sugar unit was suggested to be β-oriented indicating a β-glycosyl moiety. The location of the glycosidic linkage (C-O-C) at position C-9 was confirmed by the HMBC experiment which revealed a strong correlation from the anomeric proton signal (δ_H 4.60, 1H, d, J = 7.7 Hz) to the carbon signal resonated at δ_C 82.05 (C-9). In the COSY spectrum, the existence of spatial cross peaks H-4/H-8, H-8/H-15, H-8/H-4′ along with

H-4/H-12 indicates that the glucose moiety, H-8 and methyl-15 are all face to same direction, i.e. they all have β-orientation. Based on the spectral data discussed above, the structure of **RH37** was fully established to be ptaquiloside as shown in Table 42.

The NMR spectroscopic data of **RH37** were identical with those given in the literature for the norsesquiterpene glycoside, called ptaquiloside (Castillo et al., 1997; Fletcher et al., 2010; Niwa et al., 1983; Oelrichs et al., 1995; Ojika et al., 1987). Ptaquiloside has been isolated previously from variety of fern, for example, *P. aquilinum* var. *latiusculum* (Niwa et al., 1983; Ojika et al., 1987), *Pteris cretica* and *Histiopteris incisa* (Saito et al., 1990), *P. aquilinum* var. *revolutum* (Oelrichs et al., 1995), fresh fronds of *P. aquilinum* var. *caudatum* (Castillo et al., 1998, 1997), *P. aquilinum* (L.) Kuhn (Rasmussen et al., 2005) and Australian bracken *P. esculentum* (Fletcher et al., 2010).

Table 43: Compound **RH38** [5-Hydroxyisocalamenene]

IUPAC name	8-isopropyl-3,5-dimethyl-5,6,7,8-tetrahydronaphthalen-1-ol
Sample ID	**RH38**
Sample quantity	4 mg
Physical appearance	Yellow sticky
Molecular formula	$C_{15}H_{22}O$
Molecular Weight	218.3400 g/mol

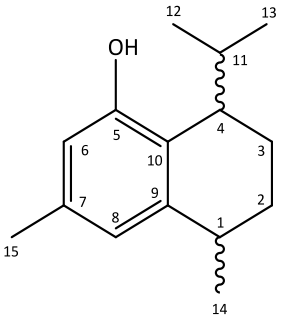

NMR data

^{1}H NMR (500 MHz, $CDCl_3$): δ_H ppm 6.58 (1H, s, H-8), 6.43 (1H, s, H-6), 4.57 (1H, s, OH-5), 3.06 (1H, m, H-1), 2.45 (1H, m, H-4), 2.24 (3H, s, H_3-15), 2.01 (1H, m, H-11), 1.78 (2H, m, H_2-3), 1.50 (2H, m, H_2-2), 1.20 (3H, d, J = 7.0 Hz, H_3-14), 0.98 (3H, d, J = 6.8 Hz, H_3-13), 0.82 (3H, d, J = 6.8 Hz, H_3-12).

^{13}C NMR (125 MHz, $CDCl_3$): δ_C ppm 153.1 (C-5), 141.3 (C-9), 135.2 (C-7), 126.1 (C-10), 123.1 (C-8), 113.5 (C-6), 43.2 (C-4), 33.3 (C-11), 27.3 (C-2), 26.7 (C-1), 22.3 (C-13), 21.3 (C-14), 21.2 (C-15), 19.8 (C-12), 19.2 (C-3).

Compound **RH38** was obtained as a yellow sticky material, and its molecular formula was confirmed as $C_{15}H_{22}O$ by a negative ion mode HR-ESI-MS $[M-H]^-$ at 217.1590 (Calcd for $C_{15}H_{21}O$: 217.1592), implying 5 degrees of unsaturation. The ^{1}H and ^{13}C NMR data (Table 43) along with coupling constant values were verified and confirmed with COSY, HSQC, HMBC, and HSQC-TOCSY experiments. The signals of NMR spectra of **RH38** (see appendix I) suggest that it does not possess features of 1-indanone compounds. From ^{1}H NMR data, molecular formula and equivalents of unsaturation, it was clear that the compound **RH38** contained an aromatic ring and a cyclohexane ring.

By comparison with the literature values, the NMR data of **RH38** showed close similarity with those reported for 5-hydroxycalamenene (Figure 73) (Tanaka and Adachi, 1990) with some exceptions. The main difference was apparent from the multiplicity of the two aromatic proton signals, resonated at 6.43 ppm and 6.58 ppm, in which they both appeared as singlets in **RH38** (Figure 72) instead of doublets in 5-hydroxycalamenene. This indicated that the aromatic hydrogens were in *meta*-position, i.e. the aromatic protons in **RH38** were separated by a

quaternary carbon atom (C-7) holding a methyl group, while they are adjacent protons in 5-hydroxycalamenene.

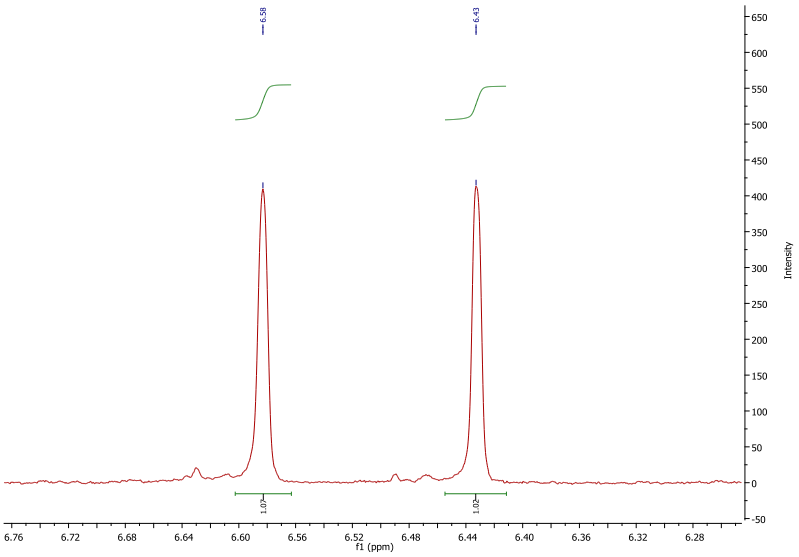

Figure 72: The expanded ^{1}H NMR (500 MHz) spectrum of **RH38** in $CDCl_3$.

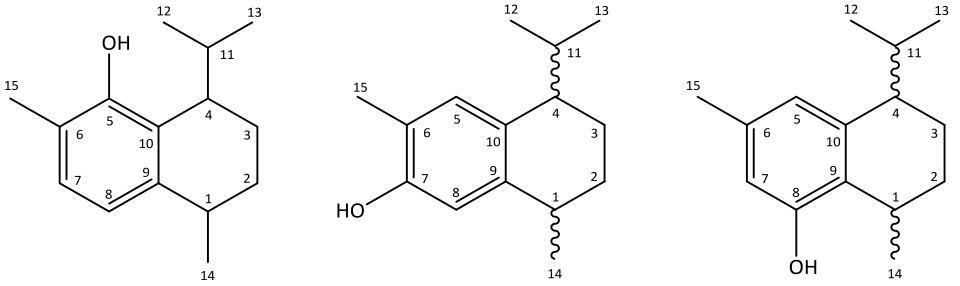

(±)-*cis*-5-Hydroxycalamenene 7-Hydroxycalamenene 8-Hydroxycalamenene

Figure 73: Chemical structures of 5, 7 and 8-hydroxycalamenes.

The ^{1}H NMR spectrum showed the characteristic chemical shifts at 0.82 ppm (d, J = 6.8 Hz), 0.98 ppm (d, J = 6.8 Hz) and 2.01 ppm (m) compatible with those of an isopropyl group. The key HMBC cross peaks from H-11 to C-4 and C-13, H-12 to C-4, C-11 and C-13, H-13 to C-4, C-11 and C-12, H-14 to C-2 and C-10, and H-15 to C-6, C-7 and C-8 were evidence of the connection (presence) of the isopropyl group at position C-4, secondary methyl at position C-1 and aromatic methyl group at position C-7. The above analysis was further confirmed from the key ^{1}H-^{1}H COSY correlations H-1/H-14, H-2/H-3, H-3/H-4, H-4/H-11, H-11/H-12, H-11/H-13, H-6/H-15 and H-8/H-15 which verified the presence of the $(CH_3)_2CH$-, secondary-methyl and aromatic-methyl groups at positions C-4, C-1 and C-7, respectively. The stereochemistry of **RH38** at positions C-1 and C-4 remains unknown as no CD spectrum was

recorded of **RH38**. From the above evidence, the chemical structure of compound **RH38** was established to be 5-hydroxyisocalamenene as illustrated in Table 43.

5-Hydroxyisocalamenene (**RH38**), a phenolic sesquiterpenoid, has been synthesised from *m*-cresol (Tanaka and Adachi, 1989). In this thesis, the isolation of this compound along with its NMR spectroscopic data have been reported for the first time as no NMR data have been documented previously. Several isomers of compound **RH38** have been described previously, for instance, 5, 7 and 8-hydroxycalamenenes have been naturally isolated from the essential oil of liverwort *Bazzania tricrenata* (Konečný et al., 1985; Tanaka and Adachi, 1990), and 7-hydroxycalamenene has also been synthesised by Krause and Bohlmann in 1987.

3.6. Structural Relationships between New and Known Pterosins and Pterosides

Rhedynoside B (**RH10**) is the first example of a pteroside bearing the glucose moiety at the position C-2 and hence being directly attached to the five membered ring in *α*-position to the keto group. In addition, this is also the first report of glycosylation at C-12 with the 12-*O*-*β*-D-glucopyranoside substituted pterosins: rhedynosides C (**RH11**) and D (**RH12**).

Most previously reported pterosides have had the sugar moiety at the following positions: C-11, for example, pterosides A2 and K (Castillo et al., 2003; Kuroyanagi et al., 1979a); C-14, such as pterosides A, B, C, D, P and Z (Hikino et al., 1972, 1971; Kuroyanagi et al., 1979a) or C-3, e.g. 13-chloro-spelosin 3-*O*-*β*-D-glucopyranoside (Chen et al., 2015), (2*R*, 3*R*)-pterosin L 3-*O*-*β*-D-glucopyranoside (separated from *Ceratopteris thalictroides*) (Chen et al., 2008) and (2*S*, 3*S*)-pterosin C 3-*O*-*β*-D-glucoside (wallichoside) (isolated from *Pteris ensiformis*) (Sengupta et al., 1976) (see Figure 74). Furthermore, rhedynosin A (**RH1**) and rhedynoside A (**RH2**) are novel compounds, being the first examples of a six-membered cyclic ether containing pterosin and pteroside.

For the first time rhedynosin C (**RH4**) was isolated from the rhizomes of *P. aquilinum* (L.) Kuhn as a new cyclic lactone pterosin with a keto group at position C-14. However, another cyclic lactone pterosin, (*S*)-12-hydroxy-2-hydroxymethylpterosin E 14, 12-lactone, with one extra methylene has been reported as a metabolic product of (2*S*)-pterosin A in rat urine via oral administration (100 mg/kg) (Lee et al., 2012).

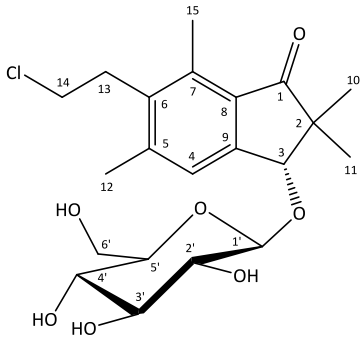

Rhedynoside E (**RH13**)

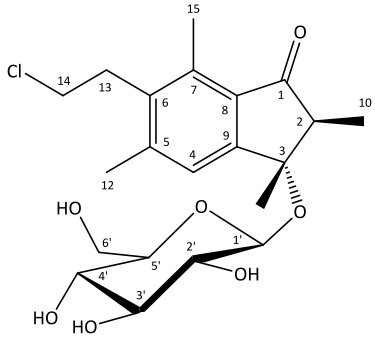

(2*S*, 3*S*)-pterosin C 3-*O*-*β*-D-glucoside (Wallichoside)

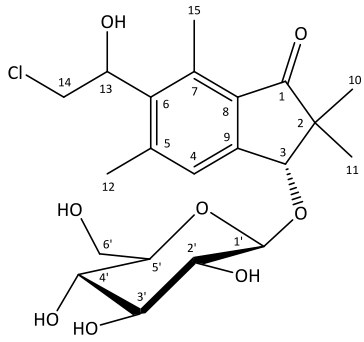

13-chloro-spelosin 3-*O*-*β*-D-glucopyranoside

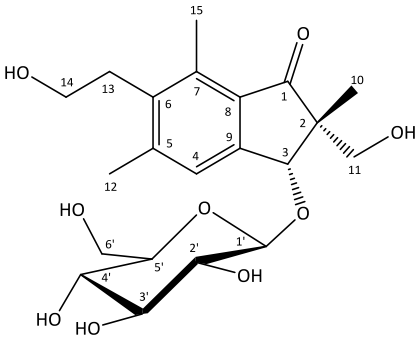

(2*R*, 3*R*)-pterosin L 3-*O*-*β*-D-glucopyranoside

Figure 74: Structural similarity between the novel compound **RH13** and the reported glycosides from the literature.

Other metabolites of (2*S*)-pterosin A were compounds **RH14**, **RH27** and **RH29**, which have been isolated for the first time from plant material. Compound **RH14** was suggested to be named as "rhedynosin I". Moreover, (2*S*)-pteroside A2 and *trans*-histiopterosin A are being reported for the first time from the rhizomes of subsp. *aquilinum* of bracken, as they have previously been isolated from the young fronds of *P. aquilinum* (L.) Kuhn var. *caudatum* (synonym: *Pteridium caudatum L.* Maxon) (Castillo et al., 2003) and *Histiopteris incisa* (Murakami et al., 1980), respectively.

More interestingly, for the first time a novel sulfated-pterosin, rhedynosin H (**RH9**), was isolated from belowground rhizomes of *P. aquilinum* (L.) Kuhn. Previously, (2*R*, 3*S*)-sulfated pterosin C and (2*S*, 3*S*)-sulfated pterosin C have been reported from the methanolic extract of the aerial parts of *Acrostichum aureum* (Uddin et al., 2011). These sulfated pterosins have one extra hydroxyl group at position C-3 (Figure 75).

In addition, rhedynosins B (**RH3**) and I (**RH14**) exhibit close similarity with Deoxypterolactone A (Figure 76) which has been obtained as an oxidation product from

the reaction of calamelanolactone with Jones reagent[13] (Bardouille et al., 1978). Echinolactone D, an illudalane sesquiterpenoid, is also structurally similar to compounds **RH3** and **RH14** (Figure 76). This compound has been isolated from the cultured mycelia of the basidiomycetous fungus *Echinodontium japonicum* (Suzuki et al., 2006).

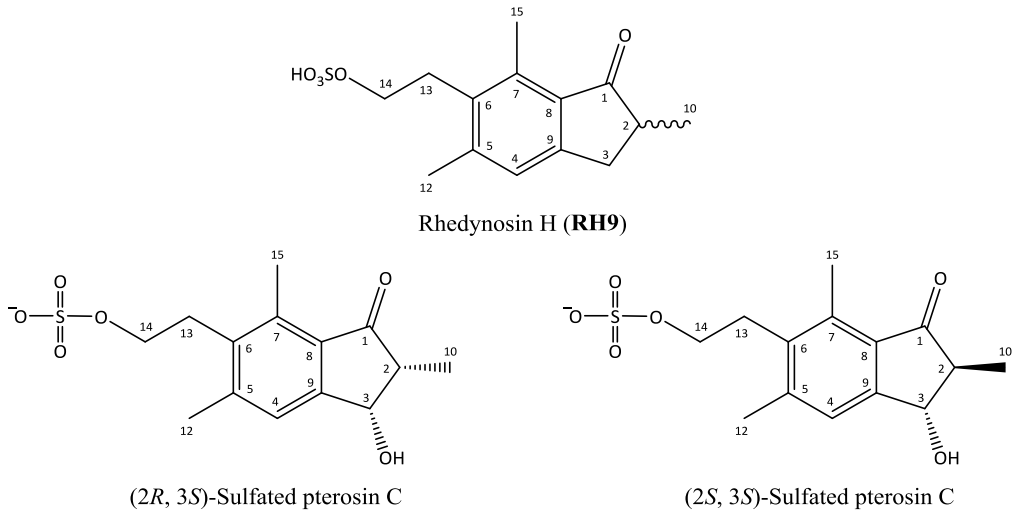

Figure 75: Chemical structural similarity between a new compound **RH7** and reported sulfated pterosins in the literature.

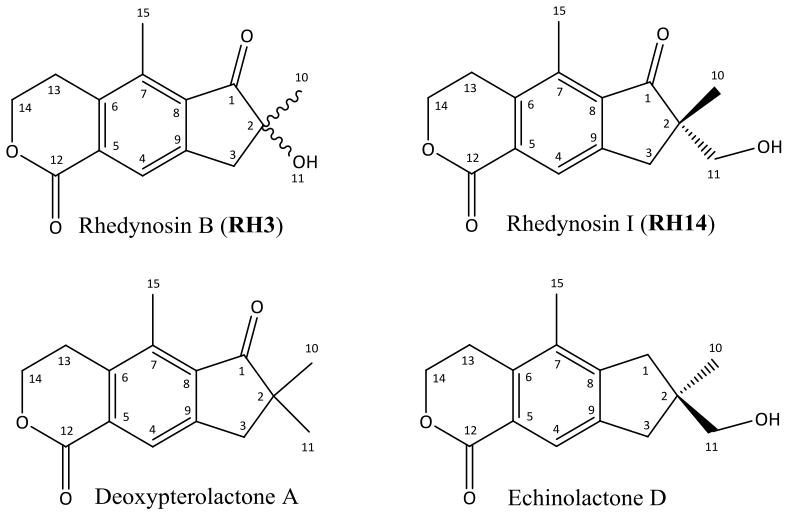

Figure 76: Structural similarity of rhedynosins B and I with reported compounds in the literature.

[13] The Jones Reagent is a solution of chromium trioxide (CrO_3) in diluted sulfuric acid that can be used safely for oxidations of organic substrates in acetone.

Reference: http://www.organic-chemistry.org/chemicals/oxidations/jones-reagent.shtm.

There is also similarity between the new compound, rhedynosin D, and setulosopterosin which has previously reported by Murakami et al in 1980 (Figure 77).

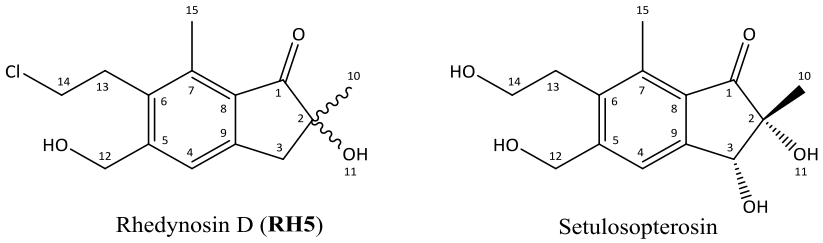

Figure 77: Structural similarity between the new compound, rhedynosin D, and setulosopterosin from the literature.

Additionally, the two new compounds, rhedynosins F (**RH7**) and G (**RH8**), are very similar to (2*S*)-13-hydroxypterosin A which has been isolated from the whole plants of *Pteris ensiformis* (Chen et al., 2013). The hydroxyl group of (2*S*)-13-hydroxypterosin A at position C-14 has been replaced with a chlorine atom in both rhedynosins F and G (Figure 78).

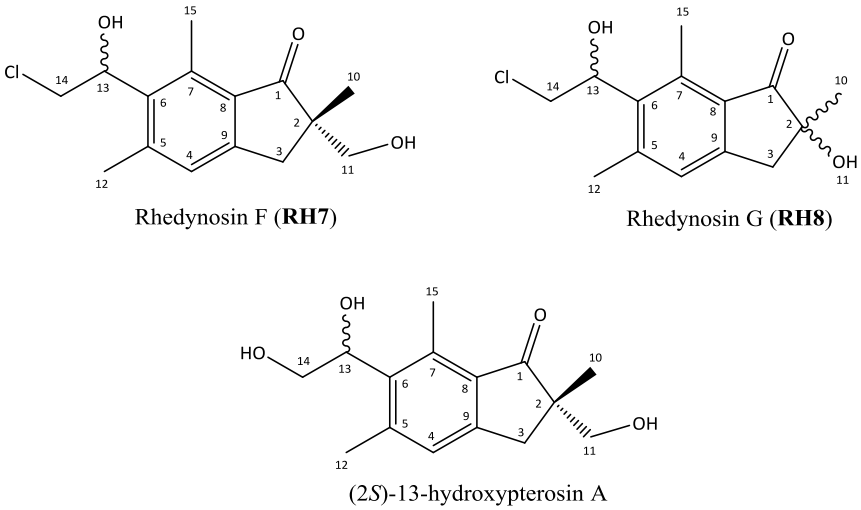

Figure 78: Similarity between chemical structures of two novel compounds, **RH7** and **RH8**, and a published pterosin in the literature.

The absolute stereochemistry of the novel compound rhedynoside B (**RH10**) was determined by single crystal X-ray diffraction analysis (Figure 52-Figure **53**). The 2*S* configurations of compounds **RH15** and **RH35** were assigned by their CD spectra (Figure 59 & Figure 68) which coincide with those reported in the literature (Kuroyanagi et al., 1979b), and consequently confirmed by X-ray crystallography (Figure 58 & Figure 69). The n → π* CD components of compounds **RH17** and **RH18** exhibit a strong negative Cotton effect around 330 nm (Figure

61) which is in agreement with the reported CD data. Thus the configurations of **RH17** and **RH18** were determined to be 2*R*, 3*R* and 2*S*, 3*R*, respectively (Kuroyanagi et al., 1979b), and again this was confirmed with X-ray diffraction (Figure 60-Figure **62**). X-ray data for the known compound (2*R*)-pteroside B (**RH31**) confirmed the absolute configuration determined previously by CD spectroscopy (Figure 57) (Hikino et al., 1970; Kuroyanagi et al., 1979b)

Both *cis* and *trans* motifs at C2-C3 were identified in compounds **RH17**, **RH18**, **RH22** and **RH28** (Table 25-Table **27Table 26** & Table 29). The position C-2 adjacent to the keto group readily epimerises if there is simply a methyl substituent. As a result, at this stage it was not possible to assign and/or confirm the absolute configurations for compounds **RH9**, **RH12**, **RH16**, **RH20**, **RH21** and **RH25** using the CD spectroscopy. A hydroxymethyl group at C-2 is apparently optically stable as in compounds **RH1**, **RH2**, **RH7**, **RH14**, **RH15**, **RH23**, **RH27**, **RH29**, **RH30**, **RH34** and **RH35**. Epimerisation may well be inhibited through intermolecular hydrogen bonding in these compounds (Kuroyanagi et al., 1979b).

Finally, the yield and concentrations of all isolated compounds (mg/kg dry weight) are shown in Table 44. Also, details of previously reported pterosins and pterosides including source of their isolation and related references from 1970 up to date are summarised and given in Table 45.

Table 44: Yield and concentration of minor and major isolated compounds.

Compound's name (sample ID)	Weight (mg)	Concentration (mg/kg dry weight)	Minor components	Major components
(2*S*)-Rhedynosin A (**RH1**)	6.0	1.7	✓	
(2*S*)-Rhedynoside A (**RH2**)	11.0	3.1	✓	
Rhedynosin B (**RH3**)	5.8	1.7	✓	
Rhedynosin C (**RH4**)	2.6	0.7	✓	
Rhedynosin D (**RH5**)	4.5	1.3	✓	
(3*S*)-Rhedynosin E (**RH6**)	6.0	1.7	✓	
(2*S*)-Rhedynosin F (**RH7**)	4.1	1.2	✓	
Rhedynosin G (**RH8**)	13.0	3.7	✓	
Rhedynosin H (**RH9**)	3.0	0.9	✓	
(2*R*)-Rhedynoside B (**RH10**)	11.6	3.3	✓	
Rhedynoside C (**RH11**)	3.2	0.9	✓	
Rhedynoside D (**RH12**)	9.1	2.6	✓	
(3*R*)-Rhedynoside F (**RH13**)	3.8	1.1	✓	
(2*S*)-Rhedynosin I (**RH14**)	6.0	1.7	✓	
(2*S*)-Pterosin A (**RH15**)	160.0	45.7		✓
(2*R*)-Pterosin B (**RH16**)	110.0	31.4		✓
trans-Pterosin C (**RH17**)	18.0	5.1		✓
cis-Pterosin C (**RH18**)	20.0	5.7		✓
(3*S*)-Pterosin D (**RH19**)	60.0	17.1		✓
(2*R*)-Pterosin E (**RH20**)	17.0	4.9		✓
(2*R*)-Pterosin F (**RH21**)	10.0	2.9	✓	
trans-Pterosin J (**RH22**)	5.0	1.4	✓	
(2*S*)-Pterosin K (**RH23**)	3.0	0.9	✓	
(2*S*)-Pterosin N (**RH24**)	15.4	4.4		✓
(2*S*)-Pterosin P (**RH25**)	4.0	1.1	✓	
Pterosin Z (**RH26**)	14.0	4.0		✓
(2*S*)-2-Hydroxymethylpterosin E (**RH27**)	14.7	4.2		✓
trans-Histiopterosin A (**RH28**)	3.0	0.9	✓	
(2*S*)-12-Hydroxypterosin A (**RH29**)	4.0	1.1	✓	
(2*S*)-Pteroside A (**RH30**)	10.2	2.9	✓	
(2*R*)-Pteroside B (**RH31**)	203.0	58.0		✓
(3*S*)-Pteroside D (**RH32**)	4.9	1.4	✓	
Pteroside Z (**RH33**)	47.0	13.4		✓
(2*S*)-Pteroside A2 (**RH34**)	4.2	1.2	✓	
(2*S*)-Pteroside K (**RH35**)	30.0	8.6		✓
5-(*β*-hydroxy)ethyl-2, 2, 4, 6-tetramethyl-1, 3-indandione (**RH36**)	4.0	1.1	✓	
Ptaquiloside (**RH37**)	21.0	6.0		✓
5-hydroxycalamenene (**RH38**)	4.0	1.1	✓	

Table 45: Previous description and source details for previously reported pterosins and pterosides.

Compounds	Derived from	References
(2*S*)-Rhedynosin I (**RH14**)	Isolated as a metabolite of (2*S*)-pterosin A from rat urine	(Lee et al., 2012)
(2*S*)-pterosin A (**RH15**)	Aerial part of bracken-fern *P. aquilinum*	(Kovganko et al., 2004)
	P. aquilinum var. *caudatum* (Pteridaceae)	(Castillo et al., 1997)
	Microlepia substrigosa TAGAWA	(Kuraishi et al., 1985)
	Rhizomes of bracken fern, *P. aquilinum* var. *latiusculum* (Pteridaceae)	(Kuroyanagi et al., 1979a)
	Young fronds of bracken fern, *P. aquilinum* var. *latiusculum* (Pteridaceae)	(Fukuoka et al., 1978; Yoshihira et al., 1978)
(2*R*)-pterosin B (**RH16**)	The whole plant of *Pteris ensiformis*	(Chen et al., 2013, 2008)
	Aerial parts of *Pteris semipinnata* L. (Pteridaceae)	(Zhan et al., 2010)
	The whole plant of *Pteris multifidi* Poir (Pteridaceae)	(Ge et al., 2008)
	P. aquilinum var. *caudatum* (Pteridaceae)	(Castillo et al., 1997)
	Microlepia strigosa (THUNB.) PRESL	(Kuraishi et al., 1985)
	Pteris bella TAGAWA	(Tanaka et al., 1982)
	Pteris setulosocostulata and *Histiopteris incisa*	(Murakami et al., 1980)
	Rhizomes of bracken fern, *P. aquilinum* var. *latiusculum* (Pteridaceae)	(Kuroyanagi et al., 1979a)
	Young fronds of bracken fern, *P. aquilinum* var. *latiusculum* (Pteridaceae)	(Fukuoka et al., 1978; Yoshihira et al., 1978)
	Methanol extract of air-dried young leaves of bracken, *P. aquilinum* KUHN var. *latiusculum* UNDERWOOD (Pteridaceae)	(Yoshihira et al., 1971)
(2*R*, 3*R*)-pterosin C (**RH17**)	Rhizomes of bracken fern, *P. aquilinum* var. *latiusculum* (Pteridaceae)	(Kuroyanagi et al., 1979a)
	P. aquilinum var. *latiusculum*	(Kuroyanagi et al., 1979b)
	Methanol extract of air-dried young leaves of bracken, *P. aquilinum* KUHN var. *latiusculum* UNDERWOOD (Pteridaceae)	(Yoshihira et al., 1971)
(2*S*, 3*R*)-pterosin C (**RH18**)	*P. aquilinum* var. *latiusculum*	(Fukuoka et al., 1978; Kuroyanagi et al., 1979a, 1979b; Yoshihira et al., 1978)
	It was obtained from enzymatic hydrolysis of pteroside C	(Hikino et al., 1972)
	Methanol extract of air-dried young leaves of bracken, *P. aquilinum* KUHN var. *latiusculum* UNDERWOOD (Pteridaceae)	(Yoshihira et al., 1971)
(3*S*)-pterosin D (**RH19**)	*Microlepia speluncae* (L.) MOORE *Microlepia strigosa* (THUNB.) PRESL	(Kuraishi et al., 1985)
	Dicksonia gigantea KARST. (1984, p.4620)	(Satake et al., 1984)
	P. aquilinum subsp. *wightianum*	(Tanaka et al., 1982)
	Coniogramme japonica	(Murakami et al., 1980)
	Young fronds of bracken fern, *P. aquilinum* var. *latiusculum* (Pteridaceae)	(Fukuoka et al., 1978; Yoshihira et al., 1978)
	Hypolepis punctate (Thunb.)	(Murakami et al., 1976)
	Methanol extract of air-dried young leaves of bracken, *P. aquilinum* KUHN var. *latiusculum* UNDERWOOD (Pteridaceae)	(Yoshihira et al., 1971)
(2*R*)-pterosin E (**RH20**)	*Histiopteris incisa*	(Murakami et al., 1980)
	Young fronds of bracken fern, *P. aquilinum* var. *latiusculum* (Pteridaceae)	(Fukuoka et al., 1978; Yoshihira et al., 1978)
	Methanol extract of air-dried young leaves of bracken, *P. aquilinum* KUHN var. *latiusculum* UNDERWOOD (Pteridaceae)	(Yoshihira et al., 1971)
(2*R*)-pterosin F (**RH21**)	*Microlepia substrigosa* TAGAWA *Microlepia strigosa* (THUNB.) PRESL	(Kuraishi et al., 1985)
	P. aquilinum subsp. *wightianum*	(Tanaka et al., 1982)
	Histiopteris incisa	(Murakami et al., 1980)
	Rhizomes of bracken fern, *P. aquilinum* var. *latiusculum* (Pteridaceae)	(Kuroyanagi et al., 1979a)
	Young fronds of bracken fern, *P. aquilinum* var. *latiusculum* (Pteridaceae)	(Fukuoka et al., 1978; Yoshihira et al., 1978)
	Methanol extract of air-dried young leaves of bracken, *P. aquilinum* KUHN var. *latiusculum* UNDERWOOD (Pteridaceae)	(Yoshihira et al., 1971)
(2*S*, 3*S*)-pterosin J (**RH22**)	*Histiopteris incisa*	(Murakami et al., 1980)
	P. aquilinum var. *latiusculum* (Pteridaceae)	(Kuroyanagi et al., 1979b)
	Young fronds of bracken fern, *P. aquilinum* var. *latiusculum* (Pteridaceae)	(Fukuoka et al., 1978; Yoshihira et al., 1978)
	Methanol extract of air-dried young leaves of bracken fern, *P. aquilinum* var. *latiusculum*	(Kuroyanagi et al., 1974b)
(2*S*)-pterosin K (**RH23**)	*P. aquilinum* var. *caudatum* (Pteridaceae)	(Castillo et al., 1997)
	P. aquilinum var. *latiusculum*	(Fukuoka et al., 1983)
	Rhizomes of bracken fern, *P. aquilinum* var. *latiusculum* (Pteridaceae)	(Kuroyanagi et al., 1979a)
	P. aquilinum var. *latiusculum* (Pteridaceae)	(Kuroyanagi et al., 1979b)
	Young fronds of bracken fern, *P. aquilinum* var. *latiusculum* (Pteridaceae)	(Fukuoka et al., 1978; Yoshihira et al., 1978)
	Methanol extract of air-dried young leaves of bracken fern, *P. aquilinum* var. *latiusculum*	(Kuroyanagi et al., 1974b)
(2*S*)-pterosin N (**RH24**)	*P. aquilinum* var. *latiusculum*	(Fukuoka et al., 1983)
	Young fronds of bracken fern, *P. aquilinum* var. *latiusculum* (Pteridaceae)	(Fukuoka et al., 1978; Yoshihira et al., 1978)
	Methanol extract of air-dried young leaves of bracken fern, *P. aquilinum* var. *latiusculum*	(Kuroyanagi et al., 1974a)
(2*S*)-pterosin P (**RH25**)	The aerial parts of *Pteris multifida* Poir. (Pteridaceae)	(Ouyang et al., 2010)
	Microlepia strigosa (THUNB.) PRESL	(Kuraishi et al., 1985)
	Rhizomes of bracken fern, *P. aquilinum* var. *latiusculum* (Pteridaceae)	(Kuroyanagi et al., 1979a)
	P. aquilinum var. *latiusculum* (Pteridaceae)	(Kuroyanagi et al., 1979b)

Continuation of Table 45.

Compounds	Derived from	References
Pterosin Z (**RH26**)	*Pteridium aquilinum* var. *caudatum* (Pteridaceae)	(Castillo et al., 1997)
	Microlepia speluncae (L.) MOORE *Microlepia trapeziformis* (ROXB.) Kuhn *Microlepia substrigosa* TAGAWA	(Kuraishi et al., 1985)
	Pteridium aquilinum var. *latiusculum*	(Fukuoka et al., 1983)
	Fronds of *Pteridium aquilinum* subsp. *wightianum*	(Tanaka et al., 1982)
	Methanol extract of the young shoots of bracken fern, *Pteridium aquilinum* (L.) Kuhn	(Kobayashi and Koshimizu, 1980)
	Pityrogramma cabmelanos	(Bardouille et al., 1978)
	Young fronds of bracken fern, *Pteridium aquilinum* var. *latiusculum* (Pteridaceae)	(Fukuoka et al., 1978; Yoshihira et al., 1978)
	Hypolepis punctata Mett.	(Hayashi et al., 1972)
	Methanol extract of air-dried young leaves of bracken, *Pteridium aquilinum* KUHN var. *latiusculum* UNDERWOOD (Pteridaceae)	(Yoshihira et al., 1971)
(2*S*)-2-Hydroxymethyl pterosin E (**RH27**)	*Isolated* as a major metabolite of (2*S*)-pterosin A from rat urine	(Lee et al., 2012)
(2*R*, 3*R*)Histopterosin A (**RH28**)	*Histiopteris incisa*	(Murakami et al., 1980)
(2*S*)-12-Hydroxypterosin A (**RH29**)	*Isolated* as a metabolite of (2*S*)-pterosin A from rat urine	(Lee et al., 2012)
(2*S*)-pteroside A (**RH30**)	*Pteridium aquilinum* var. *latiusculum*	(Fukuoka et al., 1983)
	Rhizomes of bracken fern, *Pteridium aquilinum* var. *latiusculum* (Pteridaceae)	(Kuroyanagi et al., 1979a)
	Young fronds of bracken fern, *Pteridium aquilinum* var. *latiusculum* (Pteridaceae)	(Fukuoka et al., 1978; Yoshihira et al., 1978)
	Japanese bracken, *Pteridium aquilinum* KUHN var. *latiusculum* UNDERWOOD (Pteridaceae)	(Hikino et al., 1972)
	Japanese bracken, *Pteridium aquilinum* KUHN var. *latiusculum* UNDERWOOD (Pteridaceae)	(Hikino et al., 1970)
(2*R*)-pteroside B (**RH31**)	The whole plant of *Pteris multifidi* Poir (Pteridaceae)	(Ge et al., 2008)
	Pteridium aquilinum var. *latiusculum*	(Fukuoka et al., 1983)
	Methanol extract of the young shoots of bracken fern, *Pteridium aquilinum* (L.) Kuhn	(Kobayashi and Koshimizu, 1980)
	Rhizomes of bracken fern, *Pteridium aquilinum* var. *latiusculum* (Pteridaceae)	(Kuroyanagi et al., 1979a)
	Young fronds of bracken fern, *Pteridium aquilinum* var. *latiusculum* (Pteridaceae)	(Fukuoka et al., 1978; Yoshihira et al., 1978)
	Japanese bracken, *Pteridium aquilinum* KUHN var. *latiusculum* UNDERWOOD (Pteridaceae)	(Hikino et al., 1970)
(3*S*)-pteroside D (**RH32**)	Rhizomes of bracken fern, *Pteridium aquilinum* var. *latiusculum* (Pteridaceae)	(Kuroyanagi et al., 1979a)
	young fronds of bracken fern, *Pteridium aquilinum* var. *latiusculum* (Pteridaceae)	(Fukuoka et al., 1978; Yoshihira et al., 1978)
	Japanese bracken, *Pteridium aquilinum* KUHN var. *latiusculum* UNDERWOOD (Pteridaceae)	(Hikino et al., 1971)
Pteroside Z (**RH33**)	Rhizomes of bracken fern, *Pteridium aquilinum* var. *latiusculum* (Pteridaceae)	(Kuroyanagi et al., 1979a)
	Pteris wallichiana AGARDH	(Aoyama et al., 1977)
	Japanese bracken, *Pteridium aquilinum* KUHN var. *latiusculum* UNDERWOOD (Pteridaceae)	(Hikino et al., 1971)
(2*S*)-pteroside A2 (**RH34**)	Young fronds of *Pteridium caudatum L.* Maxon (Syn. *P. aquilinum* var. *caudatum*)	(Castillo et al., 2003)
(2*S*)-pteroside K (**RH35**)	Rhizomes of bracken fern, *Pteridium aquilinum* var. *latiusculum* (Pteridaceae)	(Kuroyanagi et al., 1979a)

3.8. PROOF AND CONFIRMATION OF SULFATE AND CHLORINE-CONTAINING COMPOUNDS USING HPLC-ESI-MS^N METHOD

In this research, a moderately polar organic solvent "chloroform" was selected to start the extraction of the bracken rhizomes. This resulted in the isolation of a number of pterosins and pterosides along with ptaquiloside. These isolated pterosins and pterosides from bracken rhizomes showed surprising structural diversity, which even encompassed chloride and sulfate substituents. The biosynthesis of pterosin B is thought to be derived from the sesquiterpenoid biosynthetic pathway established by using the incorporation of radiolabelled mevalonate. Specifically, Hikino et al. (1976) suggested pterosin B (**RH16**) to be derived from mevalonic acid via farnesyl pyrophosphate and humulene. It is hypothesised that at least compounds **RH9** and **RH12** derive from ptaquiloside degradation *in planta* as the major ptaquiloside degradation product, pterosin B (**RH16**), originates from a nucleophilic addition of present nucleophiles for example hydroxide ion (OH^-) and hydroxide ion (Cl^-). The less abundant nucleophiles *in planta* Cl^- and SO_4^{2-} can also act by a similar mechanism to yield the chlorinated rhedynosins D (**RH5**), F (**RH7**) & G, rhedynosides B (**RH10**), C (**RH11**), D (**RH12**) & E (**RH13**), pterosins F (**RH21**), J (**RH22**) & K (**RH23**) and pteroside K (**RH35**).

It seems more likely that chlorinated compounds may produce from the reactions involve chlorinated solvents such as chloroform. This may take place, for instance, during organic synthesis of biologically active compounds. From this perspective, it is necessary and important to confirm the existence of compounds which possess chlorine and sulfate groups in the plant extract. In order to investigate this purpose, a non-chlorinated organic solvent "methanol" was used to prepare a crude extract from ground bracken rhizomes. The methanolic extract was then analysed by HPLC-ESI-MS^n. This analysis was used to indicate and confirm that the isolated pterosins and pterosides containing chlorine or sulfate group were present in the extract itself rather than synthesis of these compounds as a result of their reactions with chloroform during extraction and chromatographic isolation process.

The results of HPLC/ESI-MS^n analysis of the methanolic crude rhizome extract confirmed the presence of the above mentioned chlorinated and sulfated compounds. Both negative molecular ions (427 and 429 Da) of compounds **RH11**, **RH13** and **RH35** showed a constant neutral loss of 162 Da to give ions at *m/z* 265 and 267, respectively, which corresponded to the loss of an *O*-linked hexose moiety (glucose) (Felipe et al., 2014; Levandi et al., 2014; Qu et al., 2004; Scholz et al., 2005) (Figure 79-Figure **83**). The presence of only one sulfated metabolite amongst the group of reported pterosins suggests that it is rather a degradation product than a

compound of biosynthetic origin. The other reported sulfated pterosins (Uddin et al., 2011) occurred as both *trans* and *cis* isomers at C2-C3. The origin of these sulfated compounds is also suggested to be from degradation of ptaquiloside rather than through direct biosynthesis (Yamada et al., 2007).

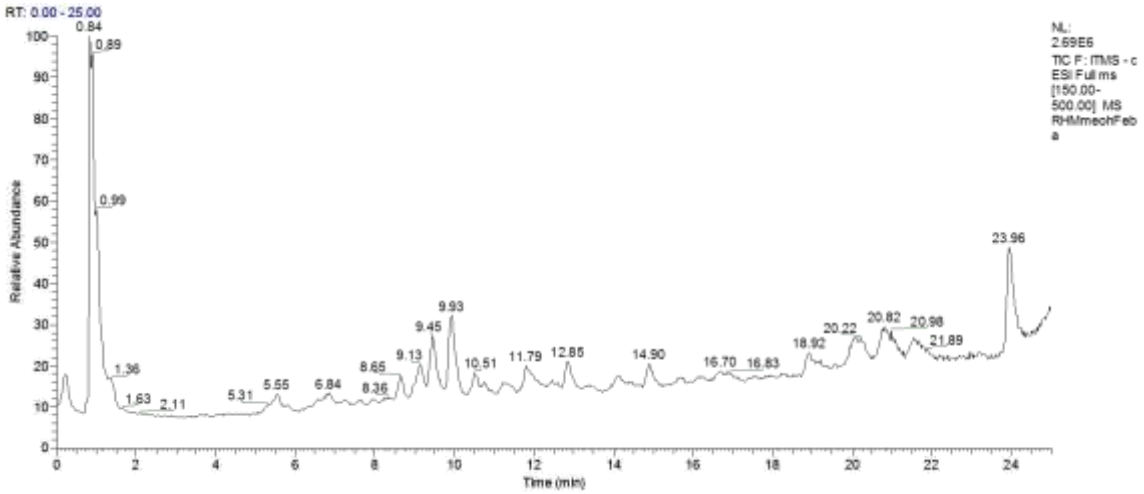

Figure 79: Reverse phase HPLC-ESI-MS total ion current (TIC) chromatogram of methanolic crude extract of bracken rhizomes in the negative ion mode.

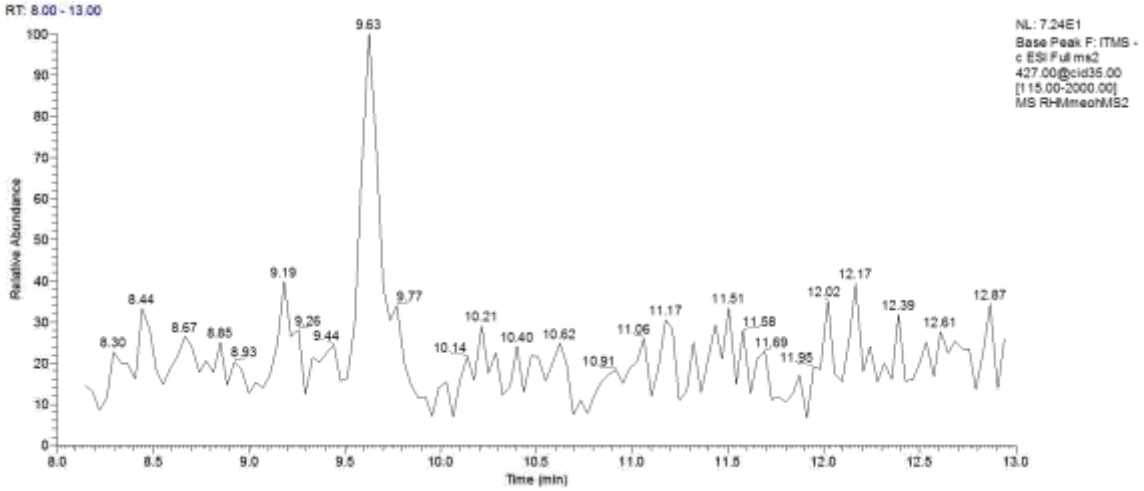

Figure 80: HPLC-ESI–MS/MS base peak chromatogram of methanolic crude extract of bracken rhizomes in the negative ion mode.

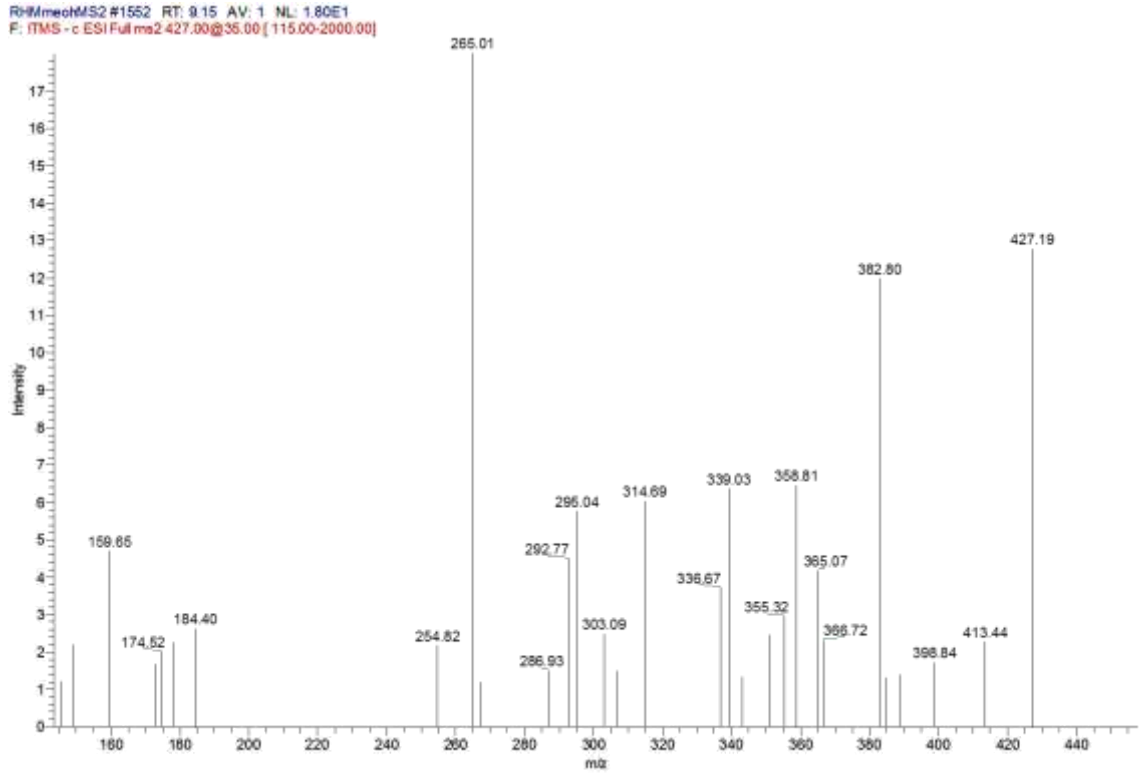

Figure 81: HPLC/ESI–MS/MS total ion current chromatogram of a selected peak (relative retention time (*RRt*) = 9.15 min) of methanolic crude extract of bracken rhizomes in the negative ion mode.

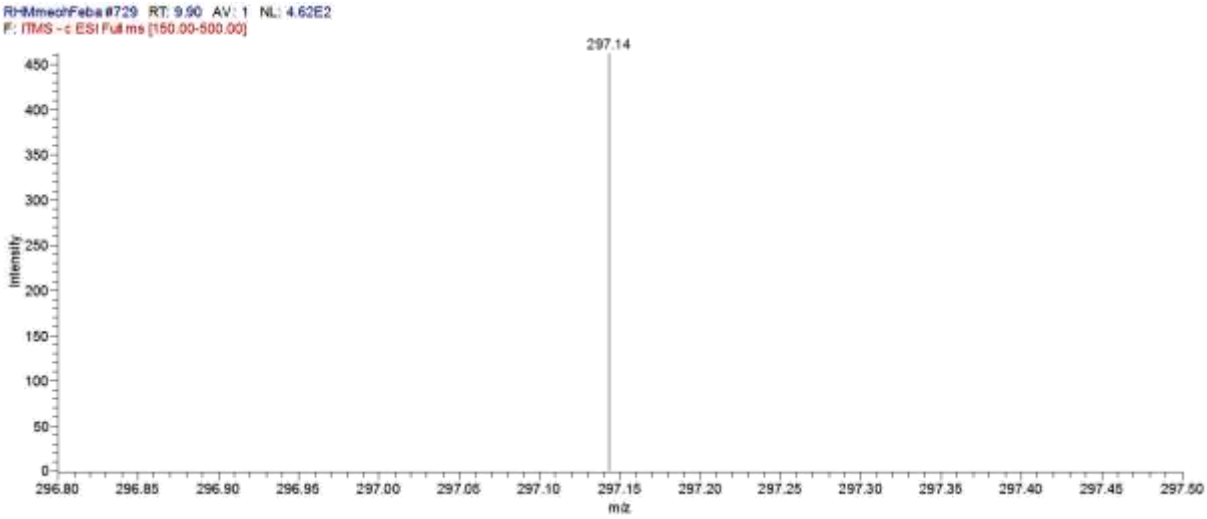

Figure 82: HPLC/MS identification of the sulfated-pterosin (**RH9**) in methanolic crude extract of bracken rhizomes. HPLC/MS spectrum showing $[M-H]^-$ (297.14 amu) in the negative ion mode at *RRt* of 9.90 min for compound (**RH9**).

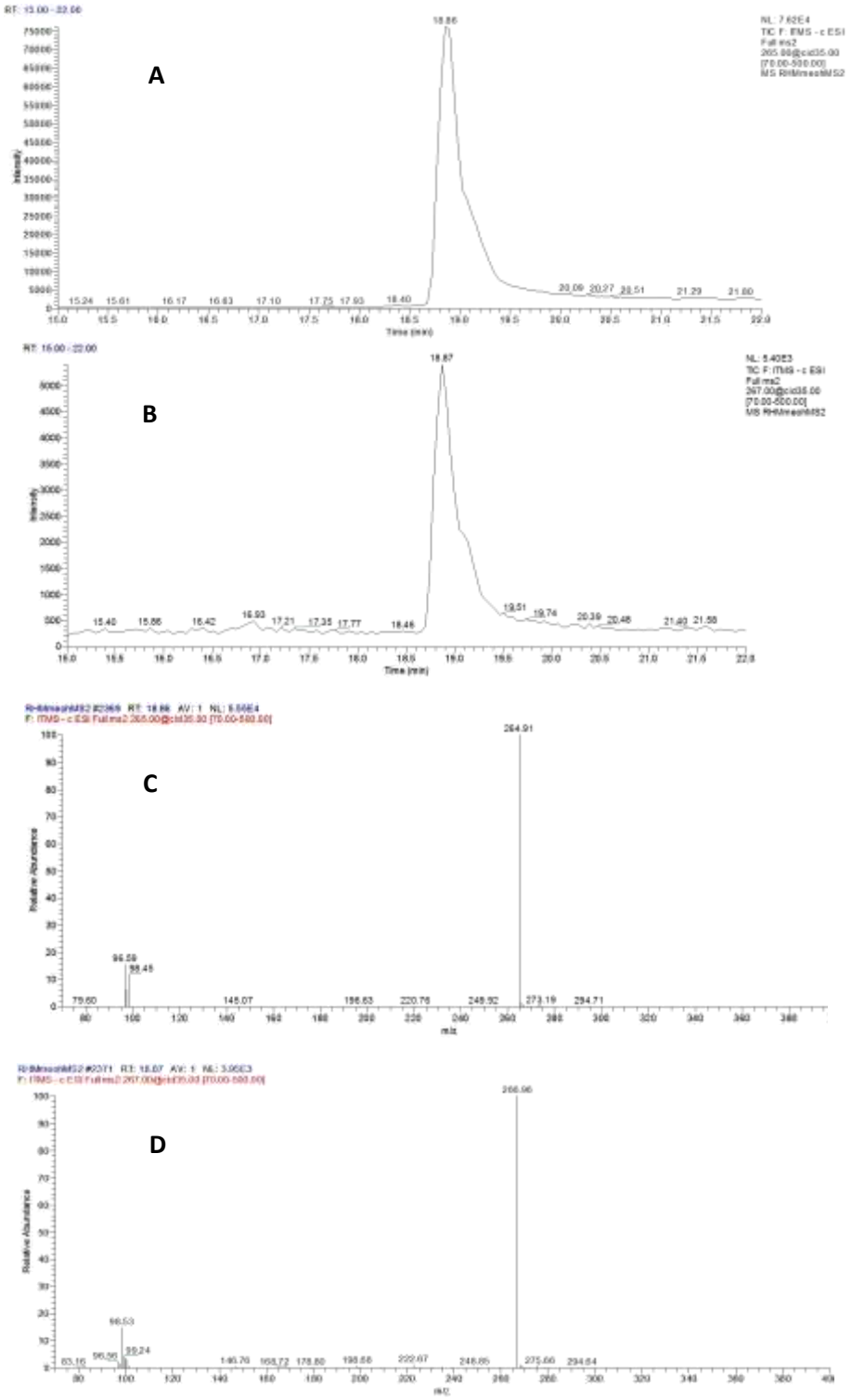

Figure 83: Further HPLC/MS/MS identification of the chlorinated compounds (**RH11**, **RH13** and **RH35**) (loss of 162 amu) in methanol extract of bracken rhizomes. TIC of compounds at *RRt* of 18.8 min: (**A**) with ^{35}Cl isotope; (**B**) with ^{37}Cl isotope. HPLC/MS/MS spectrum showing $[M\text{-}H\text{-}Glc]^-$ (265 amu) in the negative mode at *RRt* of 18.8 min for (**C**) ^{35}Cl-compounds and (**D**) ^{37}Cl-compounds.

CHAPTER FOUR

4. BIOLOGICAL ACTIVITY ASSESSMENT OF PTEROSINS AND PTEROSIDES IN BRACKEN

The aim of this chapter is to investigate whether the isolated pterosins and pterosides show any significant biological activity towards different test species. The traditional use of bracken suggests that pterosins or pterosides maybe biologically active on their own as this has been documented in the scientific literature (details chapter 1 and chapter 3).

4.1. EXPERIMENTAL PART OF BIOASSAYS

4.1.1. ALAMAR BLUE ASSAY TO DETERMINE DRUG SENSITIVITY OF AFRICAN TRYPANOSOMES *IN VITRO*[14]

A modification of the microplate Alamar blue assay was used to test the antitrypanosomal activity of 21 pterosins and pterosides (**RH2**, **RH8**, **RH10**, **RH12**, **RH14**-**RH21**, **RH24**, **RH26** –**RH27** and **RH30** –**RH35**) against the blood stream form of the *Trypanosoma brucei brucei* S427. The solutions of these compounds were prepared as 10 mg/mL stock solutions in DMSO (100%). The test solutions (200 µg/ml) were prepared by pipetting 4 µl of 10 mg/ml test stock solution and adding 196 µl HMI-9 medium (%10 fetal calf serum (FCS)) (Invitrogen) into each well. 100 µl of the test solution (HMI-9 medium) was pipetted in duplicate into the first column of a 96-well microplates (polyethylene storage plate) and the serial 1:1 dilutions were carried out using a multi-channel pipette from columns 2 to 11 (Table 46). DMSO at a concentration range of 0.001–1% and suramin[15] over a concentration range of 0.008–1 µM were included as negative and positive controls. A sterility check was conducted by using 90µl of the diluted bacterial inoculum to all the assay plates with the exception of well A1. The microplates were incubated at 37 ºC in a humidified 5% CO_2 atmosphere for 48 hours. Thereafter, 10% alamar blue™ was added to each well and the microplates were incubated for a further 24 hours. Fluorescence was determined using a microplate fluorometer at an excitation wavelength of 560 nm and an emission wavelength of 590 nm. Percentages of control values were calculated and the MIC was determined as the lowest compound concentration with <5 % of the control values.

[14] Biological activity tests against *T. brucei* and *M. marinum* were undertaken by Carol Clements. Strathclyde Institute of Pharmacy and Biomedical Sciences in collaboration.
[15] Suramin is an antiparasitic drug developed by Oskar Dressel and Richard Kothe of Bayer, Germany in 1916. It has been shown to have potent antineoplastic properties.

Table 46: Final assay concentrations µg/ml. +ve control

	1	2	3	4	5	6	7	8	9	10	11	12
A	control	100	50	25	12.5	6.25	3.1	1.55	0.78	0.34	0.17	1.0µM suramin
B	control	100	50	25	12.5	6.25	3.1	1.55	0.78	0.34	0.17	0.5µM suramin
C	control	100	50	25	12.5	6.25	3.1	1.55	0.78	0.34	0.17	0.25µM suramin
D	control	100	50	25	12.5	6.25	3.1	1.55	0.78	0.34	0.17	0.125µM suramin
E	control	100	50	25	12.5	6.25	3.1	1.55	0.78	0.34	0.17	0.062µM suramin
F	control	100	50	25	12.5	6.25	3.1	1.55	0.78	0.34	0.17	0.031µM suramin
G	control	100	50	25	12.5	6.25	3.1	1.55	0.78	0.34	0.17	0.015µM suramin
H	control	equivalent solvent control e.g. DMSO										0.008µM suramin

4.1.2. ANTIMICROBIAL ASSAY - *M. MARINUM* ATCC.BAA535

A modification of the microplate Alamar blue method for susceptibility testing of fast growing species of *Mycobacterium* was used. *Mycobacterium marinum* ATCC.BAA535 from the thawed stock cryoculture was streaked onto Columbia (5% horse blood) agar slopes and incubated at 31 ^{o}C for 5 days. A loopful of the culture was then transferred to a sterile universal container containing 10 mL of sterile 0.9% NaCl and glass beads. The bacterial suspension was mixed vigorously and allowed to settle. One millilitre of the supernatant was added to a fresh tube containing 10 mL sterile MHB (Mueller Hinton broth) saline that had previously been used to Zero the turbidity meter. The turbidity of the solution was adjusted to be the same as a 0.5 McFarland standard. A few drops of Tween 80 0.02% were filter sterilized and added to homogenise the suspension. This was then shaken and the inoculum diluted 1 in 1000 with MHB for use in the assay. Samples were dissolved in a sufficient quantity of DMSO to reach a concentration of 10 mg/mL or 1 mg/100 µL. For the initial screen, the 10 mg/mL stock solutions of the samples were diluted to 1000 µg/mL using MHB. Then 20 µL of each extract was placed in each well and 80 µL of MHB was added. DMSO was added as the negative control at a concentration range of 1 to 0.002% and gentamycin as positive control at a range of 100 to 0.78 µg/mL. Then one hundred microlitres of the bacterial suspension were added to the wells. The plates were sealed and incubated at 31 ^{o}C for 5 days before the addition of 10 µl of Alamar blue. The plates were again sealed and incubated at the same temperature for 24 hours after which fluorescence was determined using the Wallac Victor microplate reader in fluorescence mode (Excitation 530 nm; Emission 590 nm). The results were calculated as percentages. The conditions used in *M. marinum* ATCC.BAA535 assay can be summarised as shown in Table 47.

Table 47: Conditions of *M. marinum* ATCC.BAA535 assay.

Bacterium	*M.marinum* ATCC.BAA535
Incubation temperature (°C)	31
Incubation time (CA slope)	5 days
Inoculum suspension density	0.5 McFarland standard then 1 in 10 dilution
Positive control	Gentamycin 50 mg/ml stock then 1 in 50 dil. 1:1 serial dilution, then 20µl in 200µl in assay plate
Positive control range/ usual MIC	100 to 0.78µg/ml MIC 6.25µg/ml
Assay Incubation time	5 days
Incubation time until Fluorescence determined	24 hours

The same method was used for *Klebsiella pneumonia* (strains ATCC 13883 and BAA 2146 NDM-1) and *Methicillin resistant staphylococcus aureus* (MRSA) (strains 16 and 106) except that a loopful of each bacterial strain was streaked on to individual Columbia 5% horse blood agar slopes and were incubated at 37 ºC for 20 hours.

4.1.3. ANTIFUNGAL ASSAY[16]

Five strains of *C. albicans* harbouring a range of *ERG3* and *ERG11* mutations (Table 48), and representing different anti-fungal resistance spectra were selected to analyse the potential toxic properties of 21 pterosins and pterosides (**RH2**, **RH8**, **RH10**, **RH12**, **RH14-RH21**, **RH24**, **RH26** –**RH27** and **RH30** –**RH35**). The 5 strains were SC514 (wild type), CA12, CA488, CA490 and CA1008. A description of the mutations present in each strain is detailed in Table 48. All *C. albicans* strains were cultured on YPD (1% yeast extract, 2% peptone, and 1% dextrose) agar plates at 30 °C. For routine growth, yeast strains were grown with rotary shaking at 37 °C in RPMI-1640 + 2% glucose media. The plated cultures of *C. albicans* were grown for 24 hours at 30 °C. Isolated colonies were then selected from this plated culture, transferred to 0.85% Saline and cell density determined by haemocytometer counts. Cell suspensions at a density of 1.5 x 10^3 cells/mL were prepared in RPMI-1640 media, and 100 µL of inoculate transferred to each well of 96 well flat-bottomed plate. Working stocks of the 21 pterosins and pterosides were prepared in RPMI-1640 media at concentrations of 40 µg/mL and 80 µg/mL and 100 µL added to each of triplicate wells to give final concentrations of 20 µg/mL and 40 µg/ml, respectively. Thus, each plate consisted of a specific yeast strain with each compound assessed in triplicate. Plates were incubated with shaking at 37 °C for 24 hours and then the

[16] Undertaken by Prof Steve Kelly's Group, University of Swansea in collaboration.

cell growth assessed by microscopy with a 10x objective. The experiments were performed in duplicate.

Table 48: *Candida albicans* strains.

Strain	ERG3 Mutation	ERG11 Mutation
SC514	-	-
CA12	W332R	-
CA488	H243N; T330A; A351V	D225G; E266D; E391G; V488I
CA490	D147G; T330A; A351V	F72S; T229A; E266D; N440S; V488I; R523G
CA1008	K97E; L193P; V237A; A351V; A353T	E266D

4.1.4. AGROCHEMICAL RELEVANT ASSAYS[17]

4.1.4.1. FUNGICIDE ASSAYS

Eighteen selected pterosins and pterosides (**RH2**, **RH8**, **RH10**, **RH12**, **RH15** – **RH21**, **RH24**, **RH26** – **RH27**, **RH30** – **RH31**, **RH33** and **RH35**) were evaluated in mycelial growth tests in artificial media against *Pythium dissimile*, *Alternaria solani*, *Botryotinia fuckeliana* and *Gibberella zeae*, at rates of 20 ppm.

Test species	Media	Rate (ppm)
Pythium dissimile	Semi-solid	20
Alternaria solani	Semi-solid	20
Botryotinia fuckeliana (*Botrytis cinerea*)	Semi-solid	20
Gibberella zeae (*Fuscarium graminearum*)	Semi-solid	20

The compounds were also evaluated against several pathogens on leaf-piece assays at the rate of 100 ppm for *Uromyces viciae-fabae* on bean and *Zymoseptoria tritici* on wheat, and at the rate of 200 ppm for *Phytophthora infestans* on tomato. The compounds were applied prior to inoculation with the pathogens. Mycelial growth or disease inhibition was assessed visually and scored using a 3 band system (0, 55 and 99 where 99 = total inhibition of hyphal growth / disease development, 55 = partial inhibition, 0 = no inhibition), 4-14 days after inoculation depending on the assay.

[17] Undertaken at Syngenta, UK.

Test species	Host	Rate (ppm)
Zymoseptoria tritici	Wheat	100
Phytophthora infestans	Tomato	200
Uromyces viciae-fabae	Bean	100

4.1.4.2. HERBICIDE ASSAYS

The pterosins and pterosides (18 compounds) were tested for herbicidal activity against *Arabidopsis thaliana* at 10 ppm and *Poa annua* at 32 ppm. Test plates were stored for seven days in a controlled environment cabinet. They were scored as 0 or 99, where 99 = significant herbicidal effect, and 0 = no effect.

Test species	Treatment timing	Rate (ppm)
Arabidopsis thaliana	Pre-emergence	10
Poa annua	Pre-emergence	32

4.1.4.3. INSECTICIDE ASSAYS

The 18 pterosins and pterosides were tested for activity against an aphid species at 1000 ppm on a leaf-piece based assay, and against *Plutella xylostella* and *Diabrotica balteata* at 500 ppm in artificial diet assays. Chemicals were applied to feeding aphids, or prior to infestation with *P. xylostella* and *D. balteata* larvae. Mortality was assessed relative to control wells using a 2 band system (0 or 99 where 99 = significant mortality, 0 = no effect), 3-6 days after the treatments depending on the assay.

Test species	Treatment type	Media	Rate (ppm)
Aphid species	Feeding / contact	Leaf disc	1000
Plutella xylostella	Feeding / contact	Artificial diet	500
Diabrotica balteata	Feeding / contact	Artificial diet	500

Positive controls: In addition to the test compounds, positive control compounds were included in each test: azoxystrobin and prochloraz for fungicide assays, thiamethoxam and indoxacarb for insecticide assays and norflurazon for herbicide assays. For all screens, data were recorded for replicates and averaged.

4.1.5. ANTI-SCHISTOSOMAL SCREENING[18]

Cercaria from *Schistosoma mansoni* were shed from *Biomphalaria* snails upon exposure to light and were subsequently mechanically transformed to obtain schistosomula. Solutions of the test compounds were dissolved in DMSO to obtain a working concentration of 1.6 mM and added to a stock plate. Basch culture media (80 µL) and approximately 120 schistosomula were pipetted into a 384 well plate (known as the master plate), and compounds were transferred from the stock plate to the master plate using the Biomek platform (Beckman Coulter) to give a final concentration of 10 µM within each well. On each plate two controls were used- Auranofin which completely kills the parasite (positive control) and DMSO (negative control). Each plate also contained the currently used drug for treating the disease- Praziquantel. All control compounds were run at a concentration of 10 µM. The plates were then incubated at 37 ºC for 72 hours in an incubator containing 5% CO_2 after which the Biomek platform was used to re-suspend the schistosomula mixture. The 384 well plate was then imaged for both phenotype and motility using the Molecular Devices ImageXpress XL microscope. Phenotype was imaged at 10x objective in four well locations and combined into one image tile. Motility was imaged at 10x objective over six seconds, five times and displayed as a video.

The data generated from the images were analysed using Pipeline pilot to quantify the effect of the test compounds in comparison to the control compounds. Any compound that falls within the 'hit' area has had an effect on both motility and phenotype of the parasites within the Schistosomula life cycle stage of the parasite.

4.1.6. ASSESSMENT OF EFFECT OF COMPOUNDS ON GLUCOSE TRANSPORT ACROSS CELL MEMBRANES[19]

4.1.6.1. GLUCOSE TRANSPORT INHIBITOR CELL SCREENING ASSAY

Differentiated cell monolayers were washed gently in Dulbecco's Phosphate Buffered Saline containing $CaCl_2$ & $MgCl_2$ (PBS(+) (Invitrogen) and the inserts transferred to a new Corning® HTS Transwell®-96 well receiver plate (Sigma). The cells were incubated with fresh PBS(+) (75 µl per insert & 225 µl per well) for 60 mins at 37 ºC, 5% CO_2. The PBS(+) was gently aspirated and replaced with 75 µl per insert of either 5mM D-Glucose (Sigma) ± test active or

[18] Undertaken by Prof Karl Hoffman and Dr Helen Whiteland, IBERS, Aberystwyth University. Funded by National Research Network.
[19] Undertaken by Mark Fowler and Mark Berry from Strategic Science Group, Unilever R & D Colworth, Bedford, UK.

25 mM D-Glucose ± test active in triplicate and 225 µl per well of PBS(+) quickly added to each well. The 5 mM glucose wells and the 45 mM glucose wells were incubated at 37 °C, 5% CO_2 for 15 mins and 30 mins, respectively. Details of all the actives tested can be found in Table 49. The cell inserts were transferred to a new receiver plate, the supernatant gently aspirated from the cells and replaced with 100 µl of 100 µM of Lucifer Yellow (Sigma) solution to confirm the integrity of the monolayers. 225 µl of PBS(+) was added to each well and incubated at 37 °C, 5% CO_2 for 1 hr. The cell inserts were then discarded and the permeability of the membranes to Lucifer Yellow checked by measuring the fluorescence of the samples at 485 nm (excitation) & 530 nm (emission) on a Spectramax Gemini EM fluorescence microplate reader.

4.1.6.2. GLUCOSE TRANSPORT ASSAY

The amount of glucose transported across the cell monolayers was measured using a glucose assay based on Invitrogen's Amplex Red Glucose/Glucose oxidase Assay Kit. Briefly, 50 µl of each sample was transferred to a black sided / clear bottom 96-well plate (Greiner Bio-One) to which 100 µl of reaction buffer [0.5 µl 10 mM Ampliflu Red, 1 µl 10U/ml HRP, 1 µl 100U/ml Glucose Oxidase and 97.5 µl Phosphate Buffered Saline (PBS) (all Sigma)] was added. After incubation for 10 minutes at room temperature, the fluorescence of the samples was measured at 530 nm (excitation) & 590 nm (emission) on a Spectramax Gemini EM fluorescence microplate reader and the glucose concentration extrapolated from a standard curve.

4.2. RESULTS AND DISCUSSION

The compounds tested for biological screening were isolated from bracken rhizomes. These compounds are thought to be produced either from biochemical pathways or more likely they are derived from the degradation of ptaquiloside *in planta*. They have been found to have, for instance, antibacterial, antimicrobial (Kobayashi et al., 1975) and antispasmodic activity (Sheridan et al., 1999). Cellular uptake of ^{3}H-labelled DNA, RNA and protein precursors were inhibited by pterosin B (Saito et al., 1976). In this project, some biological activity screens were performed for a group of compounds as discussed and listed below. Hereafter, depending on the inhibition percentages of the tested compounds against bacterial and pesticidal growth, the activity of each compound in all the biological tests (except for glucose transport assay) is considered as the following: moderate-high for 55-85% inhibition, moderate for 45-55%, mild-moderate for 40-45% and mild (low) for less than 40%.

4.2.1. GLUCOSE TRANSPORT ASSAY:

Hsu *et al*. (2014) patented the use of pterosins and pterosides, including 84 distinct compounds of natural and synthetic origin. Their biological activity for treating diabetes and obesity was investigated predominantly with (2*S*)-pterosin A, but claimed for all described compounds. On this basis, it was decided to evaluate whether pterosins or pterosides were more active. Hence a selection of pterosins (**RH15** - **RH17**) and their associated glycosides (**RH30**, **RH31** and **RH33**) were assessed for their anti-diabetic activity specifically against two types of glucose transporters, SGLT1 and GLUT2, using an intestinal glucose uptake assay *in vitro*, however, they were found to be inactive at 300 µM. This finding does not support the patented observation of Hsu *et al*. (2014) who claimed anti-diabetic activity for extracts of bracken against STZ-induced disease in mice at 100 mg/Kg/d for 14 days by activating GLUT4. This discrepancy could have multiple origins, including the dosing schedule and activity in the latter assay through a mechanism other than through SGLT1 and GLUT2 transporters.

Table 49 shows the percentage of inhibition of each compound (test active) against the transport of glucose across a differentiated Caco-2 cell monolayer, i.e. it represents the preliminary results of glucose transport assay of (2*S*)-pterosin A, (2*R*)-pterosin B and (2*R*, 3*R*)-pterosin C, and (2*S*)-pteroside A, (2*R*)-pteroside B and pteroside Z, along with positive controls, phloridzin and phloretin. At the lower concentration of D-glucose (5 mM), the early

transport of glucose across the cell monolayer is predominantly performed through the high affinity, low capacity SGLT1 glucose transporter. At higher D-glucose concentrations, the SGLT1 transporter becomes saturated and consequently the majority of glucose transport across the monolayer is driven by the low affinity, high capacity GLUT2 glucose transporter (Kellett and Brot-Laroche, 2005). Each compound (active) was tested at low and high concentrations of glucose (5 mM D-glucose for 15 minutes and 25 mM D-glucose for 30 minutes). The compounds were classed as SGLT1 inhibitors if they exhibited a greater than 20% inhibition of glucose transport at 5 mM D-glucose and a corresponding less than 20% inhibition at 25 mM D-glucose. Actives that were able to inhibit glucose transport by greater than 20% in both conditions were classed as GLUT2 inhibitors. This approach was qualified through the use of the widely recognised specific inhibitors of both SGLT1 and GLUT2, namely phloridzin and phloretin respectively. In general, (2*S*)-pterosin A, (2*R*)-pterosin B, (2*R*, 3*R*)-pterosin C and pteroside Z showed some slight inhibition against both glucose transporters. The patterns of inhibition at low and high concentrations of glucose suggests that these pterosins and pterosides are very weak GLUT2 inhibitors. Neither glycosides A and B demonstrated significant SGLT1 inhibition. Overall, it is concluded that pterosins have negligible inhibitory effect on the main glucose transporters found in the intestine.

Table 49: Results of pterosins and pterosides tested for SGLT1 and GLUT2 inhibition activity in Caco-2 cells using 5 mM D-glucose (15 min) and 25 mM D-glucose (30 min), respectively.

Test Active [a]	Solvent	% Inhibition of glucose transport				Class [b]
		5 mM Glucose		25 mM Glucose		
		Ave.	S.D.	Ave.	S.D.	
Phloridzin [c]	DMSO	35.50	1.71	16.03	2.32	SGLT1
Phloretin [c]	DMSO	85.89	0.95	81.33	2.71	GLUT2
(2*S*)-pterosin A	DMSO	12.93	5.14	4.97	1.98	None
(2*R*)-pterosin B	DMSO	22.10	3.19	8.49	3.21	SGLT1
(2*R*, 3*R*)-pterosin C	DMSO	14.41	5.10	3.03	3.00	None
(2*S*)-pteroside A	DMSO	6.69	5.16	-1.89	3.19	None
(2*R*)-pteroside B	DMSO	3.50	3.91	-4.63	3.53	None
Pteroside Z	DMSO	14.27	4.93	4.35	4.82	None

[a] – All actives tested at 300 µM

[b] – Based on SGLT1 inhibitors having ≥ 20 inhibition of glucose transport at 5 mM D-glucose and ≤ 20 inhibition at 25 mM D-glucose, and GLUT2 inhibitors having ≥ 20 inhibition at both 5 mM and 25 mM glucose levels

[c] – Positive control

4.2.3. ALAMAR BLUE ASSAY (ANTITRYPANOSOMAL ACTIVITY)

The antitrypanosomal activity of 12 pterosins and 9 pterosides were tested against *Trypanosoma brucei brucei* which was conducted by Dr Carol Clements. The results are presented in Table 50. This assay was applied for the first time for pterosins and pterosides as no pterosins have been examined for antitrypanosomal activities and documented in the literature. It was noticed that the novel compound, rhedynosin G (**RH8**), showed highest activity when tested against blood stream *Trypanosoma brucei brucei* at a rate of 20 µM resulting in 79% inhibition, while all other tested compounds (except for **RH12** and **RH32** which showed negative value) were found to be almost inactive as they displayed mild inhibition ranged between 4.5% – 37.5% at a rate of 20 µM against this type of bacterium. It is proposed that the activity of **RH8** might be related to the feature of its structure due to the presence of keto group at C-1 and active functional groups, chlorine and two free hydroxyl groups at positions C-14, C-13 and C-2, respectively.

4.2.4. ANTIBACTERIAL ACTIVITY

This biological test was conducted by Dr Carol Clements. In general, 21 pterosins and pterosides were screened for antibacterial activity against five different bacterial strains. The compound **RH35** ((2*S*)-pteroside K) was found to have a mild – moderate inhibition of 44.1% against *M. marinum* (an indicator species for activity against tuberculosis) at a rate of 100 µM, while the rest of the tested compounds showed low inhibition at the same rate against *M. marinum*. According to preliminary antibacterial screening, compounds **RH2**, **RH8**, **RH20**, **RH30** and **RH34** were found to be moderately active at a rate of 100 µM against *Klebsiella pneumonia* BAA 2146 compared to **RH27** and **RH33** (mild – moderate inhibition, 41.1-43.8%) and the other tested compounds which displayed low inhibition (< 40%) against this bacterium. Moreover, these compounds all showed low activity at the same rate against *Klebsiella pneumonia* ATCC 13883 except (2*S*)-pterosin D (**RH19**) (moderate inhibition, 46.6%) and rhedynosins B and D (**RH10** and **RH12**) (moderate inhibition, 40.1% and 40.5%, respectively). Also the tested pterosins and pterosides exhibited very low antibacterial activity when they tested against methicillin-resistant *staphylococcus aureus* (MRSA) strains 16 and 106 at a rate of 100 µM.

4.2.6. AGROCHEMICAL RELEVANT ASSAYS

A number of selected pterosins and pterosides (18 compounds) were screened to evaluate their fungicidal and insecticidal activity on both artificial media and leaf-piece based assays in order to determine their potential activity as agrochemicals. Table 51 lists a summary of the agrochemical relevant assays tested on pterosins and pterosides. According to the initial results, only the 2 compounds, *trans*-pterosin C (**RH17**) and pterosin N (**RH24**), displayed moderate activity at the concentration of 10 µg/mL against *Arabidopsis thaliana* on the herbicide assay, meanwhile all the tested compounds were found to be inactive when tested against *Poa annua* at the concentration of 32 µg/mL. Additionally, none of the compounds produced any significant activity in the fungicide assay against 4 kinds of pathogens (*Phytophthora infestans*, *Alternaria solani*, *Botryotinia fuckeliana* and *Gibberella zeae*) nor in the insecticide assay against aphid species, *Plutella xylostella* and *Diabrotica balteata*. At the same time, the fungicidal results showed that the compounds **RH15** and **RH35** showed low (49%, 100 µg/mL) and very low (27%, 100 µg/mL) fungicidal activity against *Uromyces viciae-fabae*. Moreover, moderate inhibition was recorded for the pterosins **RH16** (51%, 100 µg/mL) and **RH20** (55%, 20 µg/mL) against *Zymoseptoria tritici* and *Pythium dissimile*, respectively. Three other pterosins (**RH17**, **RH24** and **RH33**) also showed very low potential activity (18-33%, 100 µg/mL) against *Zymoseptoria tritici* with all of the eighteen compounds failing to pass the selection criteria for progression of higher tier screens and therefore these were not selected as potential fungicides.

4.2.7. ANTIFUNGAL ACTIVITY

The aim of this biological test was to study the anti-fungal activity of 21 pterosins and pterosides by testing them for toxicity in the clinically important yeast species *Candida albicans*. This was conducted by Professor Steve Kelly's group. All the compounds were tested in triplicate against five strains of the yeast species *Candida albicans*. The results showed that the compounds were ineffective against the five *C. albicans* strains as no growth inhibition was observed in any of the five *C. albicans* strains analysed after treatment with all of the 21 compounds at 20µg/mL or at the higher concentration of 40µg/mL. These negative results illustrate that *C. albicans* has no susceptibility to any of the 21 pterosins and pterosides tested (Table 50).

Table 50: Summary of biological assay results for the selected pterosins and pterosides.

Compound ID	Species tested											
	Antitrypanosomal activity	Anti-bacterial activity					Anti-fungal activity					
	Blood stream *Trypanosoma brucei brucei* (S427)	*Mycobacterium marinum* ATCC.BAA535	*Klebsiella pneumonia* ATCC 13883	*Klebsiella pneumonia* BAA 2146	MRSA 16	MRSA 106	*Candida albicans* SC514	*Candida albicans* CA12	*Candida albicans* CA488	*Candida albicans* CA490	*Candida albicans* CA1008	
RH2	7.0	31.0	35.0	54.8	5.2	10.0	–	–	–	–	–	Results (as % inhibition)
RH8	79.0	-6.0	37.3	45.1	4.4	4.3	–	–	–	–	–	
RH10	9.0	9.4	40.1	33.7	5.2	8.5	–	–	–	–	–	
RH12	-0.7	37.5	40.5	39.9	2.4	4.8	–	–	–	–	–	
RH14	37.5	9.1	29.0	15.7	2.2	1.1	–	–	–	–	–	
RH15	9.6	33.3	27.4	18.0	2.5	5.5	–	–	–	–	–	
RH16	14.9	2.5	28.4	30.0	6.2	6.6	–	–	–	–	–	
RH17	10.2	-3.7	32.4	30.6	7.5	7.0	–	–	–	–	–	
RH18	4.5	-9.7	41.3	25.3	8.3	7.6	–	–	–	–	–	
RH19	10.6	-12.1	46.6	27.9	5.0	8.3	–	–	–	–	–	
RH20	5.2	12.9	42.5	52.7	3.9	4.1	–	–	–	–	–	
RH21	16.6	-8.0	22.6	19.8	-1.4	-0.1	–	–	–	–	–	
RH24	33.6	14.3	22.9	11.6	0.1	1.4	–	–	–	–	–	
RH26	18.0	3.9	30.7	31.4	2.2	6.1	–	–	–	–	–	
RH27	11.5	-6.0	44.3	41.1	6.2	6.1	–	–	–	–	–	
RH30	20.6	11.9	37.8	48.2	3.8	6.5	–	–	–	–	–	
RH31	12.2	13.5	41.0	29.8	2.6	1.9	–	–	–	–	–	
RH32	-2.7	11.4	38.6	23.8	3.0	16.0	–	–	–	–	–	
RH33	30.7	6.2	40.2	43.8	6.7	5.8	–	–	–	–	–	
RH34	5.4	-11.4	44.4	51.9	2.1	8.2	–	–	–	–	–	
RH35	4.7	44.1	34.3	30.6	5.0	3.6	–	–	–	–	–	
Rate	20 µM	100 µM					20 mg/mL and 40 mg/mL					

Note: = Moderate-high activity; = Moderate activity; = Mild-moderate activity; – = No activity; MRSA = Methicillin resistant *staphylococcus aureus.*

Table 51: Summary of biological assay results for the selected pterosins and pterosides.

Compound ID	Species tested												Results (as % inhibition)
	Pesticidal activity												
	Fungicidal activity							Herbicidal activity		Insecticidal activity			
	Phytophthora infestans (tomato)	*Zymoseptoria tritici* (wheat)	*Uromyces viciae-fabae* (bean)	*Pythium dissimile*	*Alternaria solani*	*Botryotinia fuckeliana* (*Botrytis cinerea*)	*Gibberella zeae* (*Fuscarium graminearum*)	*Arabidopsis thaliana*	*Poa annua*	Aphid species	*Plutella xylostella*	*Diabrotica balteata*	
RH2	–	–	–	–	–	–	–	–	–	–	–	–	
RH8	–	–	–	–	–	–	–	–	–	–	–	–	
RH10	–	–	–	–	–	–	–	–	–	–	–	–	
RH12	–	–	–	–	–	–	–	–	–	–	–	–	
RH15	–	–	49	–	–	–	–	–	–	–	–	–	
RH16	–	51	–	–	–	–	–	–	–	–	–	–	
RH17	–	18	–	–	–	–	–	49	–	–	–	–	
RH18	–	–	–	–	–	–	–	–	–	–	–	–	
RH19	–	–	–	–	–	–	–	–	–	–	–	–	
RH20	–	–	–	55	–	–	–	–	–	–	–	–	
RH21	–	–	–	–	–	–	–	–	–	–	–	–	
RH24	–	18	–	–	–	–	–	49	–	–	–	–	
RH26	–	-	–	–	–	–	–	–	–	–	–	–	
RH27	–	33	–	–	–	–	–	–	–	–	–	–	
RH30	–	–	–	–	–	–	–	–	–	–	–	–	
RH31	–	–	–	–	–	–	–	–	–	–	–	–	
RH33	–	–	–	–	–	–	–	–	–	–	–	–	
RH35	–	–	27	–	–	–	–	–	–	–	–	–	
Rate	200 ppm	100 ppm		20 ppm				10 ppm	32 ppm	1000 ppm	500 ppm		

Note: = Low activity; = Very low activity; – = No activity.

4.2.8. ANTI-SCHISTOSOMAL SCREENING

Bracken has traditionally been used as an antihelminthic (Marrs and Watt, 2006), hence the pterosins and pterosides were used in a motility assay for the intestinal flatworm *Schistosoma mansoni* a vector transferring schistosomiasis. No studies have been conducted so far to examine the anti-schistosomal properties of pterosins and pterosides both *in vivo* and *in vitro*. Thus, in order to investigate the bioactivity of pterosins and pterosides, 20 compounds (**RH2**, **RH8**, **RH10**, **RH12**, **RH14-RH21**, **RH24**, **RH26** –**RH27** and **RH30** –**RH34**) along with the current anti-schistosomal drug praziquantel (PZQ) were tested for their schistosomicidal activity against *Schistosoma mansoni* at early stage of its life cycle, known as the *schistosomula* stage, at which a parasitic schistosome enters the blood vessels of its host. The preliminary results of the test (Figure 84) showed that none of the tested compounds were active against the parasite used as they displayed lower negative scores on both the phenotype and motility axes.

Compound ID	Phenotype score	Motility score
RH2	-0.1055	0.1705
RH8	0.0151	0.16
RH10	-0.0681	-0.1285
RH12	-0.1178	-0.0337
RH14	-0.0986	-0.0248
RH15	-0.137	0.0343
RH16	-0.0148	0.0728
RH17	-0.1112	-0.0154
RH18	-0.1363	-0.0387
RH19	-0.0773	0.1586
RH20	-0.1128	-0.0087
RH21	-0.0798	0.1206
RH24	-0.0592	0.0495
RH26	-0.0581	-0.0306
RH27	-0.0696	0.1074
RH30	-0.1161	-0.0709
RH31	-0.0721	0.2319
RH32	-0.0781	0.0513
RH33	-0.0859	0.0181
RH34	-0.1249	0.1992
DMSO	-0.0908	-0.0346
AUR	-0.6426	-0.9184
PZQ	-0.394	-0.7506

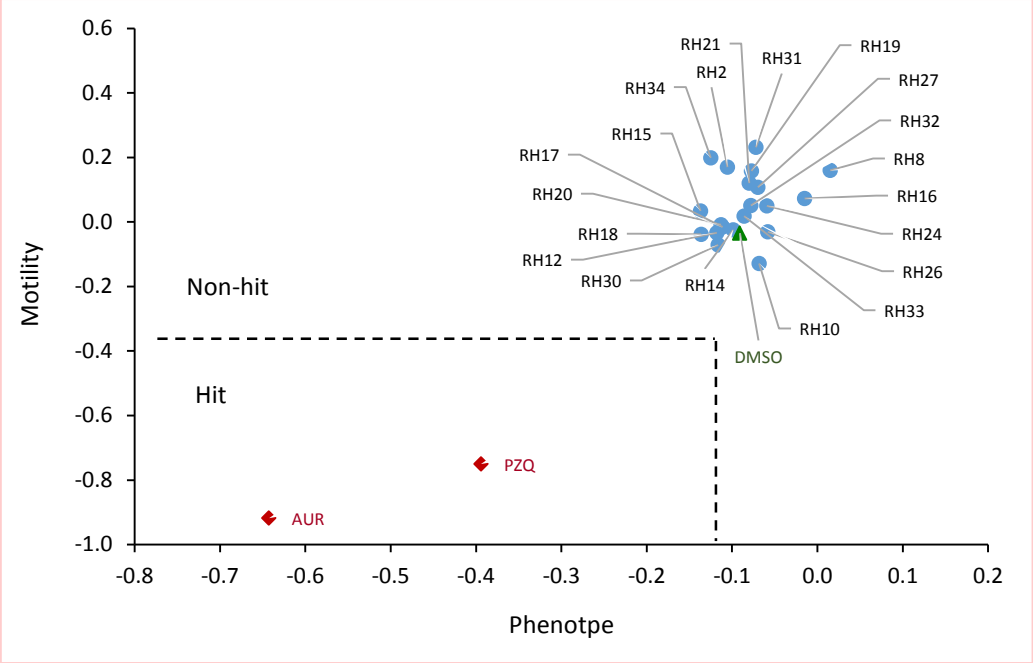

Figure 84: Tabular and graphical representation of the anti-schistosomal activity score of a selection of pterosins and pterosides in comparison to the current anti-schistosomal drug and controls.

Overall, while the biological activity of the different pterosins and pterosides was investigated, only compound **RH8** showed relatively high activity against *Trypanosoma brucei brucei* and moderate effects were recorded for only a few pterosins against *Klebsiella pneumonia* ATCC 13883, *Uromyces viciae-fabae*, *Zymoseptoria tritici*, *Pythium dissimile* and *Arabidopsis thaliana*, while no biological effects were recorded for the 5 strains of *C. albicans*. This was unexpected because of reported traditional use and patented applications of pterosins. There are a number of contributing factors for the observations. Concentration always needs to be considered for biological activity, as mostly the concentrations utilised reflect the best available treatment at the moment. It seems that none of the individual pterosins or pterosides would be sufficiently biologically active to justify further investigations in the areas studied. On the other hand, traditional use, for example, is not based on isolated compounds, rather it employs whole plant material or crude extracts. The same can be applied to bracken as a food or fodder crop. Because of the structural similarities of pterosins and pterosides with ptaquiloside, all are most likely present is crude extracts. Hence the biological activities traditionally associated with bracken and recently with pterosins, may in fact derive from ptaquiloside.

CHAPTER FIVE

5. SEASONAL VARIATION AND QUANTIFICATION OF PTEROSIN B AND PTEROSIDE B IN BRACKEN SAMPLES

5.1. INTRODUCTION

Because ptaquiloside is an unstable compound, so analysis, identification and determination has taken a long time to be developed. Some attempts have so far been made in order to develop a successful separation of ptaquiloside and then its quantification methods (Burkhalter et al., 1996; Niwa et al., 1983; Oelrichs et al., 1995; Ojika et al., 1985). Eventually, this problem has been tackled during sample preparation by transforming ptaquiloside into the stable compound, pterosin B. Consequently the concentration of pterosin B was quantified which is equivalent to the ptaquiloside concentration (Rasmussen et al., 2003b). In 1991, a simple high-performance liquid chromatography (HPLC-UV) method was described by Agnew and Lauren for the quantification of ptaquiloside in bracken. In this method, aqueous extraction has used to prepare the samples and polyamide resin column utilized to clean-up the sample solutions. An alternative method has also been mentioned to analyse ptaquiloside based on the base-acid conversion of ptaquiloside to pterosin B, followed by HPLC-UV analysis (Agnew and Lauren, 1991).

The most common method for carrying out quantification is by using HPLC with external standards. Generally, the indirect method is used to quantify the concentration of ptaquiloside. Before the analysis, ptaquiloside is converted to pterosin B in acidic or alkaline medium or by heat treatment. It is more preferable to use indirect method for determination of ptaquiloside which has the following advantages: a) pterosin B is a stable compound while ptaquiloside is quite unstable, b) the UV response of pterosin B is much higher than ptaquiloside (5-6 times greater). Subsequently, the limit of detection will be decreased during sample analysis with a UV detection source, and this may overcome the difficulties linked with the handling of ptaquiloside (Agnew and Lauren, 1991; Aranha et al., 2014).

Various analytical techniques have so far been developed in order to determine the amount of pterosin B and ptaquiloside in different sample matrices, but HPLC-UV method being the most popular. These analytical methods have been used to analyse and quantify the concentrations of pterosin B and/or ptaquiloside in bracken extract (Alonso-Amelot et al., 1992a), soil (Rasmussen et al., 2005), groundwater (Jensen et al., 2008),

biological samples (Fletcher et al., 2011) and milk (Alonso-Amelot et al., 1998; Francesco et al., 2011).

Table 52 shows the summary of different analytical methods which have so far been used for determination of pterosin B and ptaquiloside in the literature.

A developed HPLC-UV method has been used to estimate the contents of pterosins B and ptaquiloside quantitatively, for example, in the extracts of fronds and rhizomes of bracken, *P. aquilinum* var. *caudatum*, from Northern South America (Alonso-Amelot et al., 1992a) and in milk from cows fed bracken in Venezuela (Alonso-Amelot et al., 1998; Rasmussen et al., 2003b).

Using the mass spectrometry method offers the advantage of confirming the structure of the compound. It has been found that the most suitable analogues for the detection of ptaquiloside derivatives by mass spectrometry are pterosin B and bromopterosin. Recently, the mass spectrometric system has been effectively applied. This approach is depended on the ptaquiloside conversion to bromopterosin or methoxypterosin subsequent with gas chromatography-mass spectrometry (GC-MS) and stable isotope dilution tests utilizing deuterated bromopterosin as internal standard (Attya et al., 2012). A sensitive liquid chromatography-tandem mass spectrometry (LC-MS/MS) method has recently been published for the quantification of pterosin B and ptaquiloside in groundwater and soil samples, based on the transformation of ptaquiloside to pterosin B (Bonadies et al., 2004; Francesco et al., 2011; Jensen et al., 2008).

Table 52: Various analytical methods for determination of pterosin B and ptaquiloside in different sample matrices.

Analytical instrument	UV detection (nm)	Matrix	Compound	Concentration range (ng/mL)	Recovery (%)	LOD [a] (ng/mL)	LOQ [a] (ng/mL)	References
HPLC-UV	260	Bracken fronds	Pterosin B	0.54-0.79 [b]	-	-	-	(Alonso-Amelot et al., 1992a; Aranha et al., 2014)
			Ptaquiloside	1.78-1.96 [b]	-	-	-	
		Bracken rhizome	Pterosin B	$3.1\text{-}4.4 \times 10^{-3}$ [b]	-	-	-	
			Ptaquiloside	$2.0\text{-}7.5 \times 10^{-3}$ [b]	-	-	-	
		Bracken crosiers	Pterosin B	0.69-0.80 [b]	-	-	-	
			Ptaquiloside	1.88-2.34 [b]	-	-	-	
HPLC-UV	220	Bracken extract	Pterosin B [c]	-	89	5 [d]	-	(Agnew and Lauren, 1991)
			Ptaquiloside	-	95	30 [d]	-	
LC-MS	-	Plasma	Pterosin B	5.5-250	75	1.1	3.7	(Aranha et al., 2014)
			Ptaquiloside	5-500	71	0.35	1.2	
		Urine	Pterosin B	5.5-250	82	1.0	3.3	
			Ptaquiloside	10-500	88	1.6	5.2	
		Milk	Pterosin B	6.85-137	63	1.6	5.3	
			Ptaquiloside	10-250	77	1.7	5.8	
LC-MS/MS	-	Soil	Pterosin B	0.3-60	84-91	0.15 (0.60 [e])	-	(Jensen et al., 2008)
			Ptaquiloside	0.5-100	48-71	0.19 (0.76 [e])	-	
		Groundwater	Pterosin B	-	84-89	8×10^{-3}	-	
			Ptaquiloside	-	52-66	14×10^{-3}	-	
HPLC-UV	220	Blood plasma	Ptaquiloside	-	81	40	100	(Fletcher et al., 2011)
		Tissue	Ptaquiloside	-	-	20	40	
HPLC-UV	260	Milk	Pterosin B [c]	-	91	500	-	(Alonso-Amelot et al., 1998)
GC-MS	-	Milk	Bromo-pterosin [c]	3-20	79	0.3	0.4	(Francesco et al., 2011)

[a] LODs and LOQs have been measured for the analytical instrument methods used in the experiment.
[b] mg/g dry weight.
[c] Ptaquiloside converted.
[d] µg/g dry weight.
[e] ng/g fresh weight.

5.2. MATERIALS AND METHODS

5.2.1. GENERAL EQUIPMENT

The analytical miller (Type: Retsch cyclone mill) was purchased from Retsch GmbH, Germany. A Jenway Model 3510 pH meter (Bibby Scientific, UK) was used to measure the pH of water samples. Heraeus™ Megafuge™ 16R refrigerated centrifuge from Thermo Fisher Scientific was used for the purpose of centrifugation of the water extract samples. A tabletop shaker (model: MaxQ 2000 Shaker-Analog) was purchased from Thermo Scientific and utilized to shake the samples at speed of 350 rpm. The Stuart® SBH 200D/3 Block Heater was purchased from Bibby Scientific Ltd., Staffordshire, UK.

5.2.2. SAMPLE COLLECTIONS

5.2.2.1. PLANT AND SOIL SAMPLES

Bracken plants and soil samples used in this study were collected from the location N 53° 07′ and W 04° 08′ at a height of 250 m above sea level in the Snowdonia National Park (Llanberis, Wales-United Kingdom). The site area belongs to the upland vegetation type U20a (*Pteridium aquilinum-Gallium saxatile* community U20, *Anthoxanthum odoratum* sub-community U20a) (Thoss et al., 2012). This community is widespread in the British uplands. It is one of the common vegetation types in many parts of England, Wales and the south and west of Scotland. The most dominant vegetation exist in this community is bracken with a height of up to 1.5 m. Also a short and very common grassy sward is present underneath the fronds of bracken including *Agrostis capillaris*, *Festuca ovina*, *Galium saxatile*, *Holcus lanatus*, *Potentilla erecta*, *Rumex* acetosa, *Viola riviniana*, and small flowerless green plants such as *Hypnum jutlandicum*, *Rhytidiadelphus squarrosus* and *Scleropodium purum*. The site is categorised as rough grazing for agricultural purposes. It is typical of the zone where the farmed lowlands adjoin the unenclosed highlands with infertile and well-drained soils (Averis et al., 2004; Thoss et al., 2012) (Figure 85). The site encompasses approximately 1000 m^2 (*ca.* 25m × 40m) with mostly bracken (*P. aquilinum* (L.) Kuhn) and bluebell (*Hyacinthoides non-scripta (L.) Chouard ex Rothm)* coverage. The site zone was gridded and divided into 144 quadrants. Bracken (rhizomes, fronds and stems) and soil samples were collected between March 2014 and August 2015. A stainless steel (5 mm thickness) square hollow section (20 × 20 × 30 cm, $W \times L \times H$) was used for sampling.

In 2014, two quadrants were sampled in duplicate on each sampling occasion during the main growing stages of Bluebell plants, while samples collected in 2015 comprised of one core per

sampling occasion. Thus, the lifecycle of Bluebell plant (growth pattern) was used as a base for collection of bracken and soil samples as follow:

a) Weekly: from leaf emergence to end of flowering (March 2014 to mid-June 2014).
b) After seed ripening until dormancy i.e. until bracken senescence:
    i. Fortnightly (June 2014 to August 2014).
    ii. Monthly (September 2014 to November 2014).
c) Once every six weeks throughout the winter (December 2014 to end of January 2015).
d) Once every three weeks until bluebell shoot emergence in March 2015.
e) Fortnightly (March 2015 to August 2015).

To diminish the effect of daytime variation, samples were collected always at the same time from 9:00 am to 11:00 am.

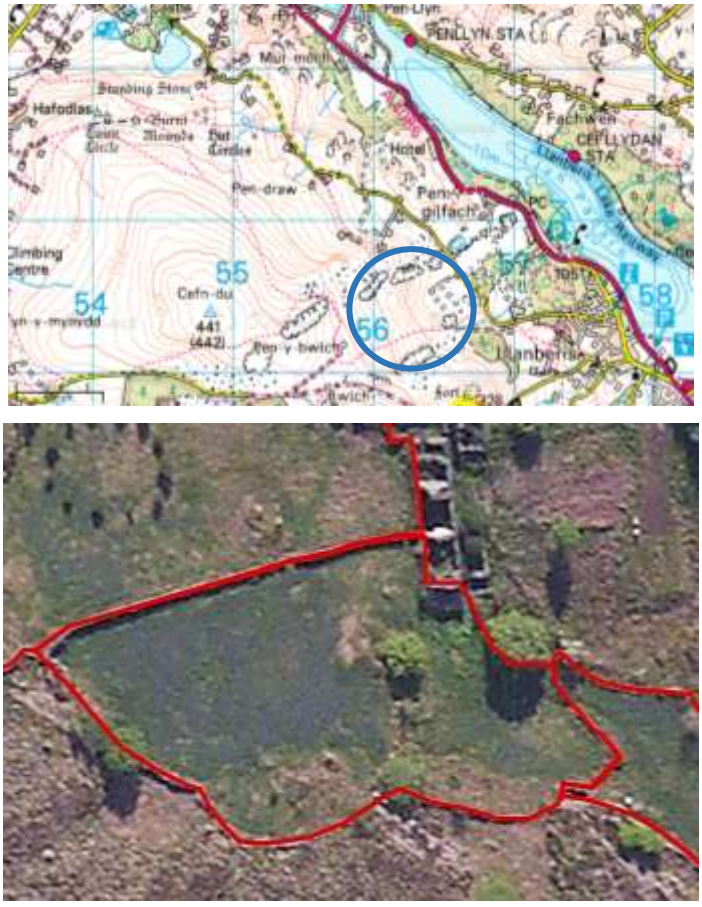

Figure 85: A, Sampling site location and **B**, aerial view of the sampling site with bracken vegetation and bluebell flowers.

5.2.2.2. WATER SAMPLES

In this experiment, in order to identify and quantify trace amounts of pterosin B and pteroside B in water, three types of water samples were chosen for validating the developed SPE-HPLC-UV method. The samples were tap water, groundwater (Well water) and surface water. All the samples were collected from the local regions surrounded by bracken in North of Wales - UK. Tap water sample was obtained in Bangor from the laboratory in chemistry building. The surface waters were collected in three different areas in Llanberis 1) at the bracken field site, 2) somewhere down the bracken field site and 3) the same hillside and elevation but different watershed. The groundwater sample was taken from a private water supply (Well water) with bracken on watershed and geological chalk areas in Anglesey. Table 53 shows the acidity degree (pH) of water samples measured by using a pH meter. All environmental water samples were stored at room temperature in the lab for two weeks and then analysed.

Table 53: The pH value of water samples

Water samples	Location	pH measurement
Private water supply (Well water)	Anglesey	7.50
Surface water (unfiltered)	Llanberis[a]	7.10
Surface water (filtered)	Llanberis[a]	7.50
Surface water (below field side)	Llanberis[b]	7.38
Surface water (pale-yellow colour)	Llanberis[c]	6.0
Tap water	Chemistry building in Bangor	7.50

[a] The samples were taken from a private water supply that abstracts surface water above the bracken field side.
[b] The sample was taken somewhere below the bracken field side.
[c] The sample was taken at similar elevation and vegetation as the field side but used a different watershed.

5.2.3. PRE-TREATMENT OF PLANT AND SOIL SAMPLES:

5.2.3.1. BRACKEN PLANT SAMPLES

Bracken samples were manually processed in the laboratory and separated from the rest of the core. The rhizomes were separated and thoroughly cleaned from the soil with a spatula, meanwhile the fronds were divided into stems and leaves (called pinna) (Figure 86), in which they were used for SPE-HPLC-UV quantification of pterosin B and pteroside B.

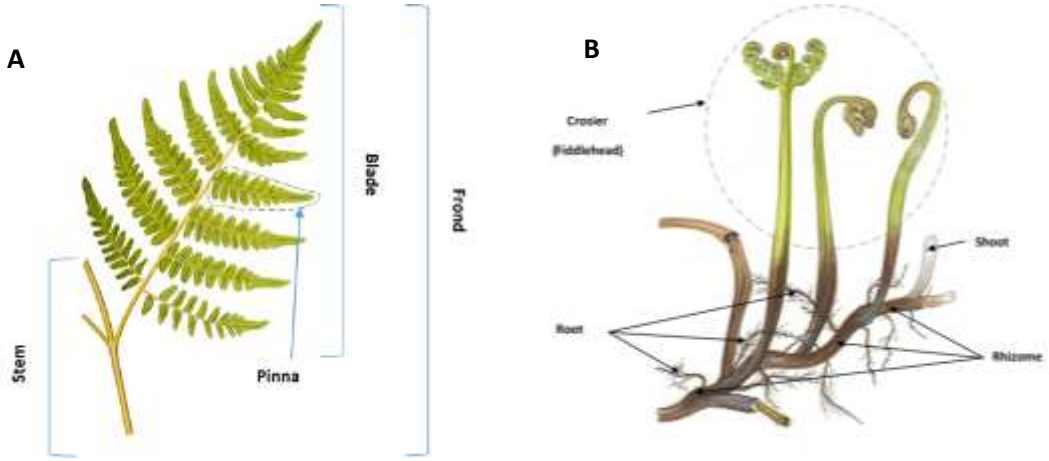

Figure 86: Main parts of bracken fern (*Pteridium aquilinum* (L.) Kukn), **A**: fronds; **B**: rhizomes and crosiers.

The samples were then air-dried at room temperature in the laboratory for a week. On each sampling occasion, fresh and dry weights were also recorded. The percentage of dry matter content ($D_w\%$) and water ($W\%$) were calculated from the fresh weight (F_w) and dry weight (D_w) using Equations 1 and 2, respectively.

$$D_w\% = \frac{D_w}{F_w} \times 100 \qquad (1)$$

$$W\% = \frac{F_w - D_w}{F_w} \times 100 \qquad (2)$$

The air-dried plant samples were ultimately ground and milled into a homogeneous particles using a Retsch cyclone mill and passed through a 1 mm sieve in order to obtain a representative sample for analysis. The milled samples were placed in tightly sealed plastic bags and stored at 4 °C in the refrigerator until the day of analysis.

5.2.3.2. SOIL SAMPLES[20]

The soil core samples were processed in the laboratory and thoroughly separated from the plants by hand. Soil samples were air dried, ground in a porcelain mortar, passed through a 2 mm sieve and combined to form a composite sample for each sampling occasion. The samples were kept at room temperature in the laboratory until analysis. The top soil of the samples was used for the purpose of quantification and seasonal variation of pterosin B and pteroside B.

[20] Soil samples were prepared by Victor Ebuele, PhD student, who has also been supervised by Dr Vera Thoss.

5.2.3.3. WATER SAMPLES

The pH of the water samples was measured in the lab (see Table 53). The samples were prepared for SPE-RP-HPLC analysis by filtering them utilizing Wattman No. 1 filter paper.

5.2.4. PREPARATION OF SOLID PHASE EXTRACTION (SPE) CARTRIDGES[21]

SPE cartridges (500 mg Discovery® DSC-18Lt, 52615-U Supelco, Volume 6 mL) were supplied by Sigma Aldrich and contained silica gel based material (C_{18}-trimethyl(octadecyl)silane). The cartridges were preconditioned with 3 ml of methanol and washed with 3 ml of water in order to activate and prepare them for loading the plant and soil supernatants or water samples.

5.2.5. REAGENTS AND STANDARDS

All solvents used in this experiment including water, methanol and acetonitrile were HPLC grade and purchased from Fisher Scientific, UK, while formic acid (HPLC-grade) was supplied by Sigma Aldrich, UK. Standard compounds, pterosin B and pteroside B, were isolated from the chloroform extract of bracken rhizomes in the lab (see chapter two and three), and they were used for monitoring seasonal changes of pterosin B and pteroside B and/or quantification purpose in bracken, soil and water samples. Methanol was selected as the most suitable solvent for preparation of the solutions of standard compounds.

5.2.6. PREPARATION OF STANDARD SOLUTIONS

A stock standard solution of 100 mg/L of each compounds (pterosin B and pteroside B) was freshly prepared by dissolving an accurate weight of 1 mg of each compound with methanol. The solution was transferred into a 10-mL volumetric flask and then filled with methanol up to the etched line. All the standard solutions were kept at 5 °C in the refrigerator and protected from light. The methanolic solutions of a series of working standards, for example 0.2-1, 1-5 and 10-60 µg/mL (see Table 55), were prepared daily by diluting each stock standard solution with methanol and then they were injected into the HPLC instrument to make a calibration curve. All the glassware employed in this experiment was cleaned well with water and then rinsed three times with methanol.

[21] The SPE cartridges have only been used twice.

5.2.7. SAMPLE PREPARATION AND EXTRACTION PROCEDURE BY SPE METHOD:

5.2.7.1. PLANT AND SOIL SAMPLES

A 4-digit balance was used for weighing 100 mg of milled bracken samples [rhizomes, fronds (pinna) and stems] and 5.00 g of soil samples into a 50 mL disposable centrifuge tube, and then 10 mL (plant samples) or 25 mL (soil samples) of water was added. Samples were shaken for 2 hr on a tabletop shaker at a speed of 350 rpm. The extract solutions were filtrated using qualitative filter paper (150 mm, Fisher Scientific) and then centrifuged with tabletop centrifuge machine at room temperature for 30 minutes at a speed of 5000 rpm.

The sample supernatants were passed through the activated cartridges at a flow-rate of 1-2 ml min^{-1}. To remove undesired polar compounds, the loaded SPE cartridges were washed with 15% (5 mL) and 50% methanol-water (1 mL, method A; 4 mL method B, see below), respectively. Subsequently, the less polar fraction which contained the target analytes (third fraction) was eluted with an optimal volume 4 mL of methanol:water (v/v, 80:20). In order to pre-concentrate this fraction, the eluent was evaporated to dryness under a stream of nitrogen at 40 °C using the block-heater, and the temperature was constantly set at 40 °C to avoid any deterioration may occur to the pterosin compounds. It was then redissolved with 1 ml of MeOH and transferred to a HPLC vial. Afterward, the prepared sample along with standard solutions were submitted to the HPLC system for analysis.

5.2.7.2. METHOD A:

In method A, 15% aqueous solution of methanol (5 mL) was passed through the cartridges followed by 1 mL of 50% methanol:water to remove of undesired analytes. The third fraction which contained pterosin B and pteroside B was then collected with 4 mL of 80% methanol:water. This method was applied for quantification of:

a) Pterosin B in soil, water and all plant samples except rhizomes.
b) Pteroside B in all bracken (rhizomes, fronds and stems), soil and water samples.

5.2.7.3. METHOD B:

The concentration of pteroside B was higher than pterosin B in bracken rhizome samples while frond and stem samples contained almost equivalent amounts of pterosin B and pteroside B, as a result the peak height of pterosin B nearly disappeared in the chromatograms of rhizome samples. In order to obtain a better peak shape of pterosin B in rhizome samples, the volume of the second eluent (%50 methanol:water) was re-optimized. The maximum concentration of pterosin B with an obvious peak was obtained from the third fraction when 4 ml of %50

methanol:water used in the second eluent. Therefore, in method B, 15% (5 mL) and 50% (4 mL) of methanol-water were used as first and second wash steps to remove unwanted polar compounds, respectively. Pterosin B was then eluted with 4 mL of 80% methanol: water. This method was only used for quantification of pterosin B in bracken rhizome samples.

5.2.7.4. WATER SAMPLES

After treatment of the samples as described above, they were considered as a supernatant and directly loaded on the SPE cartridges. The fractions were collected based on using method A.

5.2.8. RP-HPLC-UV INSTRUMENTATION AND CONDITIONS

5.2.8.1. RP-HPLC-UV INSTRUMENT

The samples and standard compounds were injected automatically into a DIONEX UltiMate 3000 HPLC system from Thermo Scientific equipped with a binary gradient pump, autosampler and diode array detector (DAD) monitoring 190-400 nm (UV-Vis range). The HPLC system was equipped with a Waters Spherisorb® ODS2 (C_{18}) reverse phase analytical column (4.6 mm ID × 250 mm L) with a spherical particle size of 5 µm (purchased from Waters, UK).

5.2.8.2. RP-HPLC-UV CONDITIONS

The reverse phase C_{18} HPLC column was used and kept at 25 °C during sample analysis. The mobile phase consisted of a binary solvent system using water (solvent A) and acetonitrile (solvent B). The solvents were acidified with 0.1% formic acid. The elution gradient program started with 80% eluent A and 20% eluent B at a flow rate of 1.0 mL/min, and these percentages were maintained for 2 min, and then eluent B was ramped linearly to 100% in 14 min. This percentage (100% eluent B) was continued for 1 min, and then was declined to 20% eluent B within 1 min and then again maintained for 2 min to flush the column. A sample volume of 20 µL was injected with the total run time of 20 min. Absorption spectral data of the main peaks were monitored concurrently and recorded with DAD at 254 nm. The Chromeleon 7 Software was used to control and process chromatographic data and analysis in terms of gradient setting, data acquisition and auto-sampler. Table 54 shows summary of the optimum conditions of the developed HPLC method.

Table 54: The optimised conditions of RP-HPLV-UV method

Column	Waters Spherisorb® ODS-2 C18 (250mm × 4.6mm, 5µm)
Mobile phase	Acetonitrile and water (acidified with 0.1% Formic acid)
Gradient	20% ACN (2 min), 20-100% ACN (14 min), 100% ACN (1 min), 100-20% ACN (1 min), 20% ACN (2 min).
Flow rate	1 mL/min
UV detection	254 nm
Column temperature	25 °C
Injection volume	20 µL

5.2.8.3. LINEAR RANGE AND SENSITIVITY OF THE RP-HPLC-UV METHOD

The standard calibration curves in bracken tissues, soil and water samples were linear over the pterosin B concentration ranges from 0.2 to 70 µg/mL (stems and fronds), from 0.2 to 30 µg/mL (rhizomes), from 0.2 to 2 µg/mL (soil) and from 0.2 to 1 µg/mL (water), while the samples showed linearity for pteroside B in the range of concentrations from 0.5 to 30 µg/mL (stems and fronds), from 0.5 to 300 µg/mL (rhizomes), from 0.2 to 1 µg/mL (soil and water) (Table 55). The detection and quantification limits (LOD & LOQ), linear regression equations and correlation coefficients (r) for bracken (rhizomes, stems and fronds), soil and water samples are given in Table 55. All the linear equations were obtained over a wide concentration range in accordance with the levels of pterosin B and pteroside B found in the bracken, soil and water samples. The RP-HPLC method was linear in all cases ($r > 0.99$).

5.2.9. PRECISION, ACCURACY AND RECOVERY

For bracken stem samples, precision, accuracy and recovery experiments for pterosin B and pteroside B were performed. A 100 µL (V_1) of three different concentrations of each standard solution (pterosin B and pteroside B) (C_1 = 10, 50 and 100 mg/L) were spiked separately to 10 mL of HPLC-grade water containing 100 mg of powdered bracken stem sample. The extract solution of unspiked and spiked bracken stem samples were then processed following the developed SPE-HPLC-UV method. Triplicate analysis were performed for spiked and unspiked bracken stem samples. A final volume of 1000 µL (V_2) of each samples were subjected to HPLC-UV for analysis.

$$C_1 \times V_1 = C_2 \times V_2 \qquad (3)$$

Where: C_1 = concentration of spiked standard solution; V_1 = spiked volume of standard solution = 100 µL; C_2 = concentration of analytes in final volume (V_2) of 1000 µL.

Therefore:

$$C_1 \times 100 = C_2 \times 1000 \qquad (4)$$

The spiked amount of each compound (pterosin B and pteroside B) was calculated based on using Equation 5 (see data below).

Spiked volume V_1 (µL)	Spiked concentration C_1 (mg/L)	Final volume V_2 (µL)	Analytes concentration in final volume C_1 (mg/L)
100	10	1000	1
100	50	1000	5
100	100	1000	10

The inter-day precision and accuracy were calculated by determining three replicates for bracken stem sample. Percent recovery was determined by comparison of the recovered amount to the spiked amount and using Equation 5 (see Table 56).

$$\% \text{ Recovery} = \frac{\text{Amount recovered } \left(\frac{\text{mg}}{\text{L}}\right)}{\text{Amount spiked } \left(\frac{\text{mg}}{\text{L}}\right)} \times 100 \qquad (5)$$

In addition, in order to perform the recovery study of both analytes in the unspiked and spiked bracken stem samples, a series of standard solutions (0.5, 1, 5, 10, 15, 20 and 25 mg/L) of each compound (pterosin B and pteroside B) were freshly prepared and subjected to HPLC-UV instrument along with the sample solutions.

5.3. RESULTS

A simple, accurate and reproducible RP-HPLC-UV method was developed and carried out to quantify and identify pterosin B and pteroside B in bracken rhizomes, fronds, stems, soil and water samples. Sample preparation for HPLC analysis were processed in duplicate through the methods A and B.

5.3.1. WATER EXTRACTION PROCEDURE

5.3.1.1. PRELIMINARY METHOD:

During method optimisation, a 100 mg of plant material (stem) was accurately weighed and extracted with HPLC-grade water (15 mL), and then shaken for half an hour. It was then filtrated and the solution was centrifuged for 30 minutes. The supernatant was passed through a preconditioned SPE-cartridge. Three fractions were collected into 25-mL glass vials by passing 3 mL of 25%, 60% and 80% MeOH/ H_2O through the cartridges, respectively. These fractions were dried on the block-heater at 40 °C under the stream of nitrogen. The dried fractions were redissolved in MeOH (1 ml) and transferred to labelled HPLC-vials. The solution of samples and standard compounds were then analysed with HPLC. The results displayed that the first fraction did not contain the target compounds, at the same time the peaks of desired components were observed in the chromatograms of fractions 2 and 3. Therefore, at this early stage the first fraction was used as a wash step and discarded as it only contained unwanted polar compounds.

5.3.1.2. OPTIMIZATION OF THE METHOD

To develop and improve the preliminary method, the following parameters were taken into account for optimization:

a) Extraction time.
b) Extraction volume of water.
c) Percentage and volume of first and second fractions.
d) Volume of third fraction.

To figure out the effect of extraction time and obtain the highest concentration of the analyte (peak area), seven bracken stem samples (n_1-n_7) (100 mg each) were studied using the preliminary procedure in which the samples were shaken for 0.5, 1, 2, 3, 4, 5 and 15 hrs (overnight), respectively. Figure 87 shows that up to an hour the extraction of the analytes was obviously not completed, while shaking for 2 hr is sufficient to extract the entire amount of pterosin B and pteroside B present in the samples. Figure 87 illustrates

that the extraction times of 2, 3, 4 and 5 hours give approximately the same peak areas for both analytes, while their peak areas decline dramatically when the solutions shake overnight for 15 hr. This might have been due to microbial degradation which changed the chemical composition of the extract. Therefore, 2 hr was used as an optimum value in the improvement of the subsequent parameter.

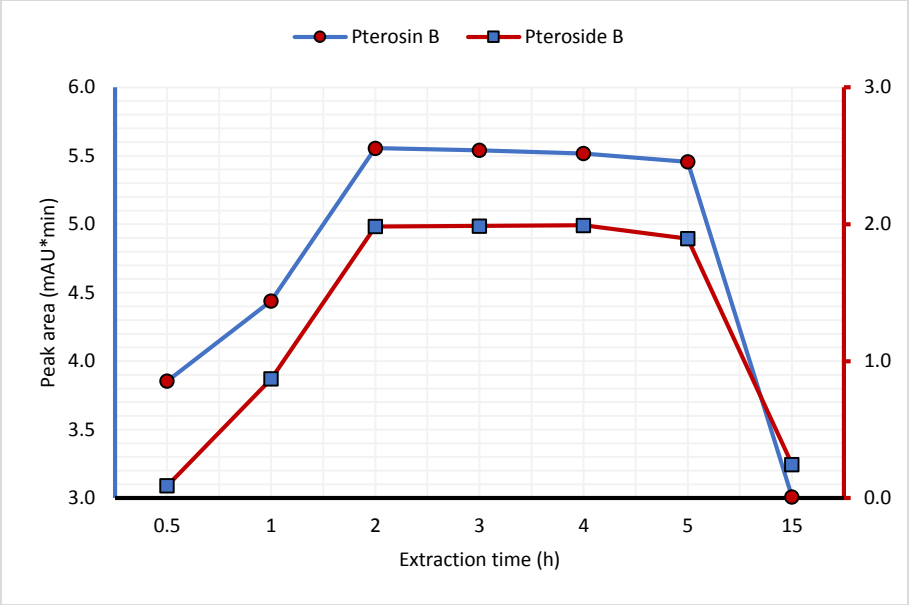

Figure 87: Effect of extraction time on the peak areas of pterosin B and pteroside B.

Under above experimental conditions, various volumes of water (5, 10, 15, 20 and 25 mL) were examined in order to obtain the optimal value of the extraction volume. As shown in Figure 88, the peak areas of the target components increase with increasing the extraction volume of water from 5-10 mL, and then the effect of the volume of water (from 10-25 mL) remains nearly constant. Based on this result, the volume of 10-mL was chosen to be the optimum for the extraction process, and this volume was fixed and used in the optimisation of the next variable.

Degree of polarity of solvent system may play a great role in development of analytical methods. From this point of view and using the above conditions, different percentages of methanol (5, 10, 15, 20 and 25%) in the first fraction were studied. Figure 89 illustrates that the sensitivity of the method reaches the maximum at %15 methanol, and afterward the trend continues as a straight line from 15% to 25% methanol. Therefore, 15% of methanol was selected as an optimal percentage of the 1st fraction in this study.

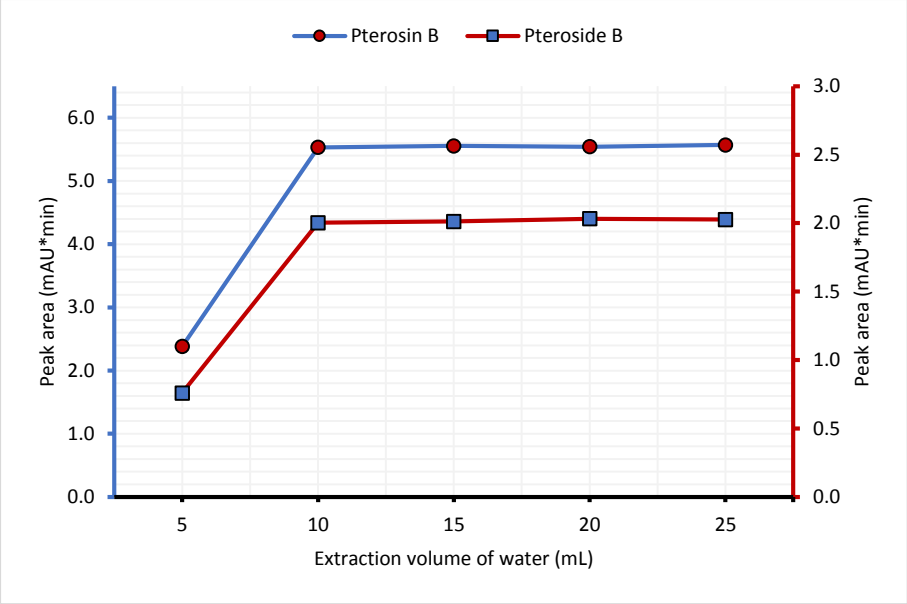

Figure 88: Effect of extraction volume of water on the peak areas of pterosin B and pteroside B.

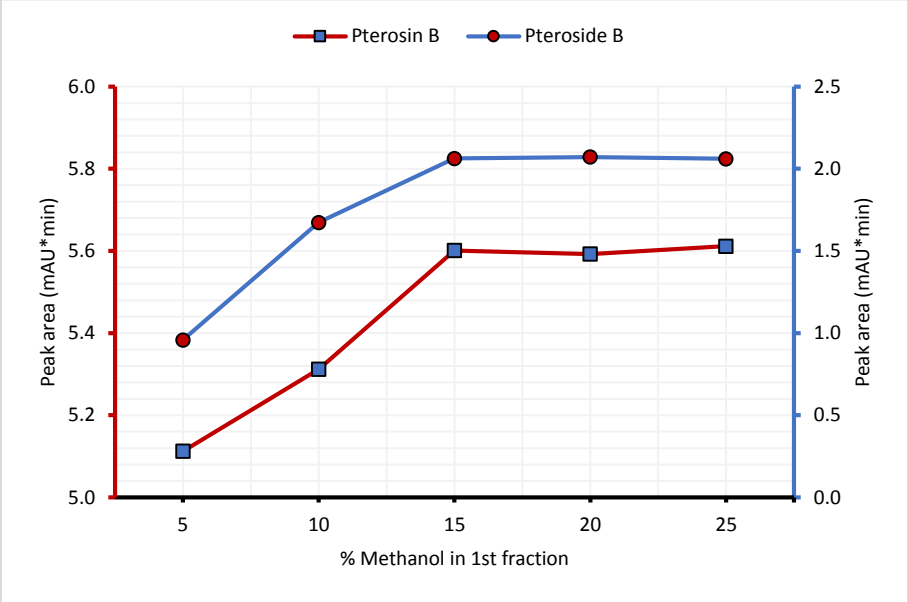

Figure 89: Effect of percentage of methanol (1st fraction) on the peak areas of pterosin B and pteroside B.

Further improvement of the method was performed based on the conditions mentioned above. The influence of different volumes of %15 methanol (1, 2, 3, 4, 5 and 6 mL) in collection of the 1st fraction was examined. As it is clear from Figure 90, the peak areas of both components rise gradually with increasing the volume of methanol and reach a peak at 5 mL, and afterward with using 6 mL of methanol the trend keeps steady. Therefore, 5 mL of methanol was denoted as an optimum volume and used in development of the method in a subsequent stage of the experiment.

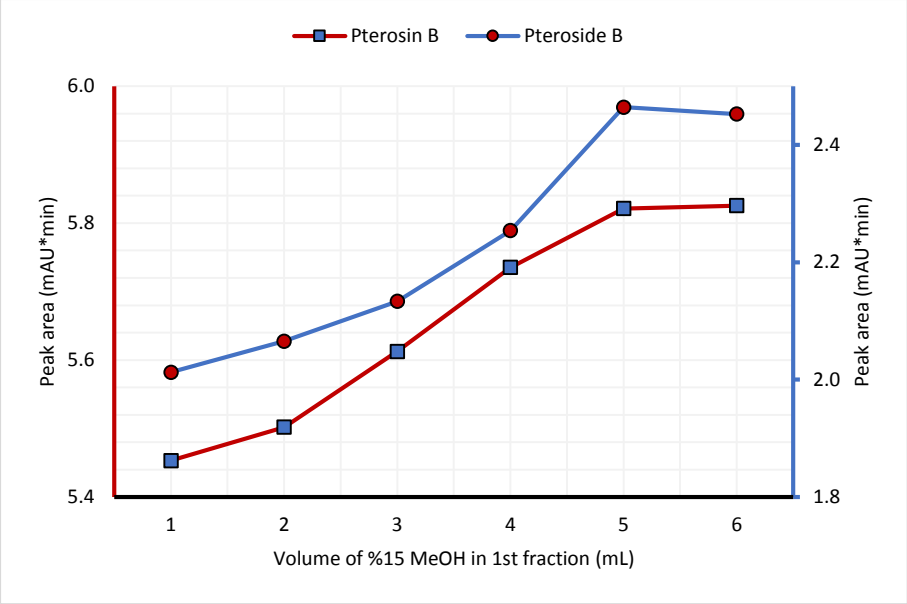

Figure 90: Effect of volume of methanol (15%, 1st fraction) on the peak areas of pterosin B and pteroside B.

Following the preliminary method and using the optimum value of the above variables, different volumes of 50% methanol in second fraction (1, 2, 3, 4, 5 and 6 mL) were tested in order to further develop the method. It was realised that this variable has a great impact in improving the method. Figure 92 exhibits that there is an inverse proportional between the peak areas of the analytes and the volume of 50% methanol (2nd fraction), in which the graph shows a gradual drop down of the peak areas with increasing the volume from 1 mL to 6 mL. Thus, volume of 1 mL 50% methanol (2nd fraction) was indicated as an optimal volume which gave the maximum peak areas. This volume was then fixed in the method and used in next optimization step.

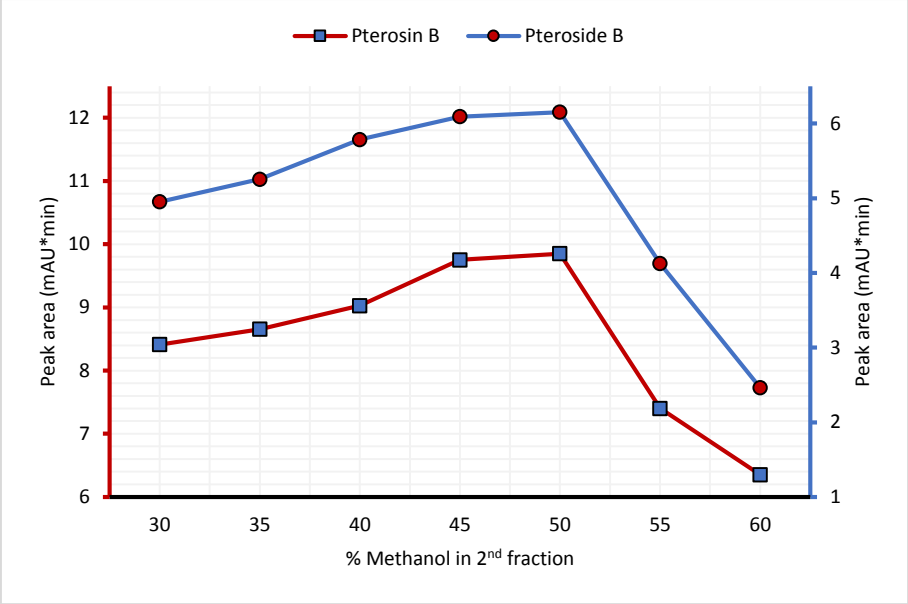

Figure 91: Effect of percentage of methanol (2nd fraction) on the peak areas of pterosin B and pteroside B.

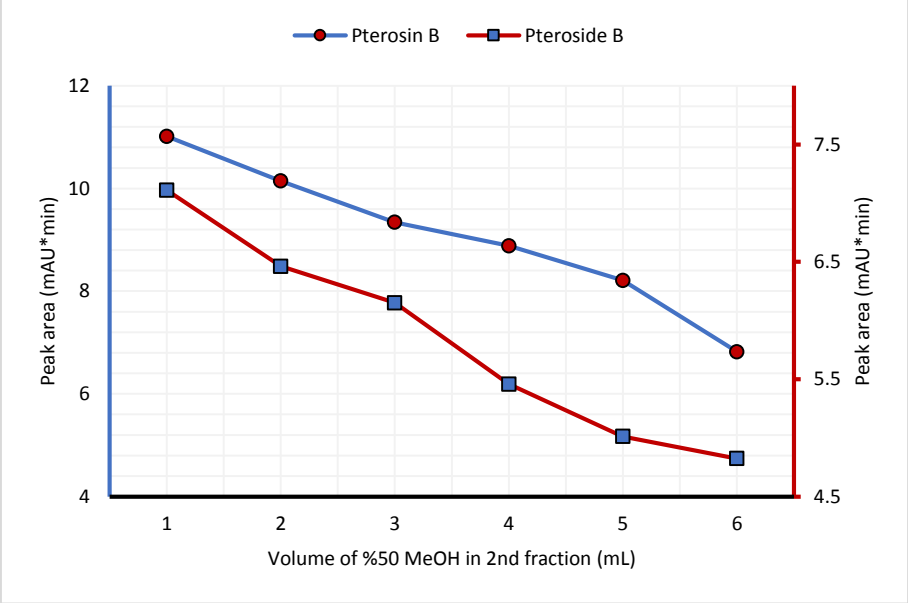

Figure 92: Effect of volume of methanol (50%, 2nd fraction) on the peak areas of pterosin B and pteroside B.

Figure 93 demonstrates how the peak areas affect by the volume of methanol (80%) in the third fraction. This was performed by examining different volumes (1, 2, 3, 4, 5 and 6 mL) of methanol (80%) in the preliminary method based on using values of other parameters optimised above. A proportional relationship between the peak areas and the volumes is apparent as it can be noticed in Figure 93, in which the peak areas of both compounds climb rapidly with increasing volume of methanol from 1 mL to 4 mL. Later on, the trend of the peak areas levels

off (reaches a plateau) with using of 5 mL and 6 mL of methanol. Based on these observations, the volume 4 mL of 80% methanol (3rd fraction) was chosen as a maximum value of the method and fixed in the experiment.

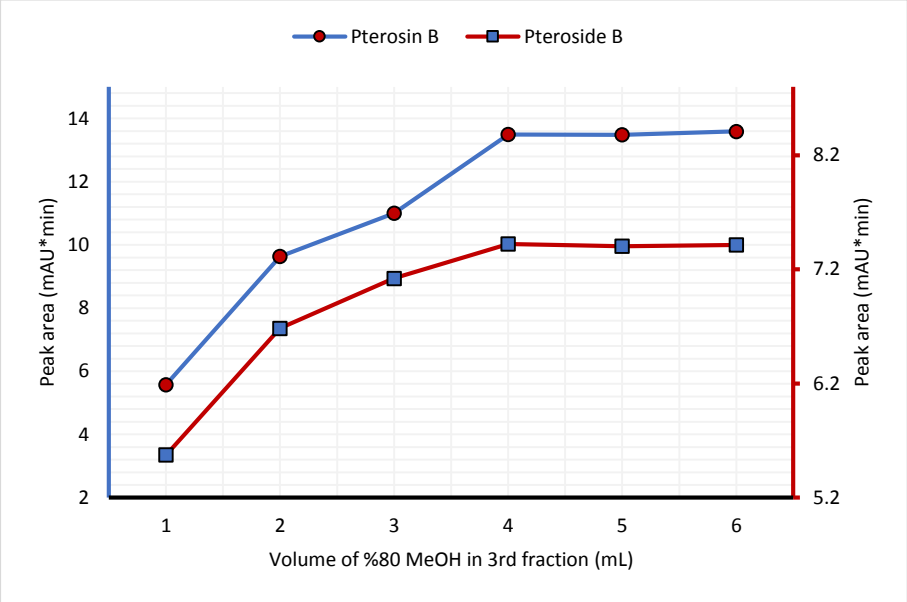

Figure 93: Effect of volume of methanol (80%, 3rd fraction) on the peak areas of pterosin B and pteroside B.

5.3.2. Optimization of RP-HPLC-UV Parameters

The composition of the RP-HPLC solvent system was optimized in order to attain a good resolution between the chromatographic peaks. Different gradients of water:methanol mixture acidified with 0.1% formic acid and a mixture of water:acetonitrile (0.1% formic acid) were assayed separately. Water was denoted as solvent A. When methanol used as solvent B, the resultant chromatogram showed that the peaks were co-eluted, meanwhile the best resolution and peak shapes were achieved in the case of using acetonitrile as solvent B, and in addition the chromatogram was appeared better. The effect of flow rate was investigated by carrying out the experiment at various flow rates of 0.5, 1.0 and 1.5 ml/min. The flow rate of 1.0 ml/min was selected to be the optimal value as it gave a better resolution chromatogram than the others. Detection of the peaks were performed at different wavelengths of 220, 254, 280 and 320 nm. It was found that the peaks absorb the maximum energy at 254 nm as they exhibited higher absorbance unit. Furthermore, the influence of column temperature in range of 20-30 °C were examined, and 25 °C was chosen as the optimum temperature in which the chromatogram displayed a straight baseline of the peaks. The experiment also tested with different injection

volumes ranged 10-30 µL, the resulted chromatograms were all measurable and they were differing from each other in terms of their peak heights only, and hence 20 µL was selected as the optimum injection volume. Figure 94 shows the HPLC-UV chromatograms of pterosin B and pteroside B in standards solutions, bracken tissues (rhizomes, fronds & stems) and soil sample.

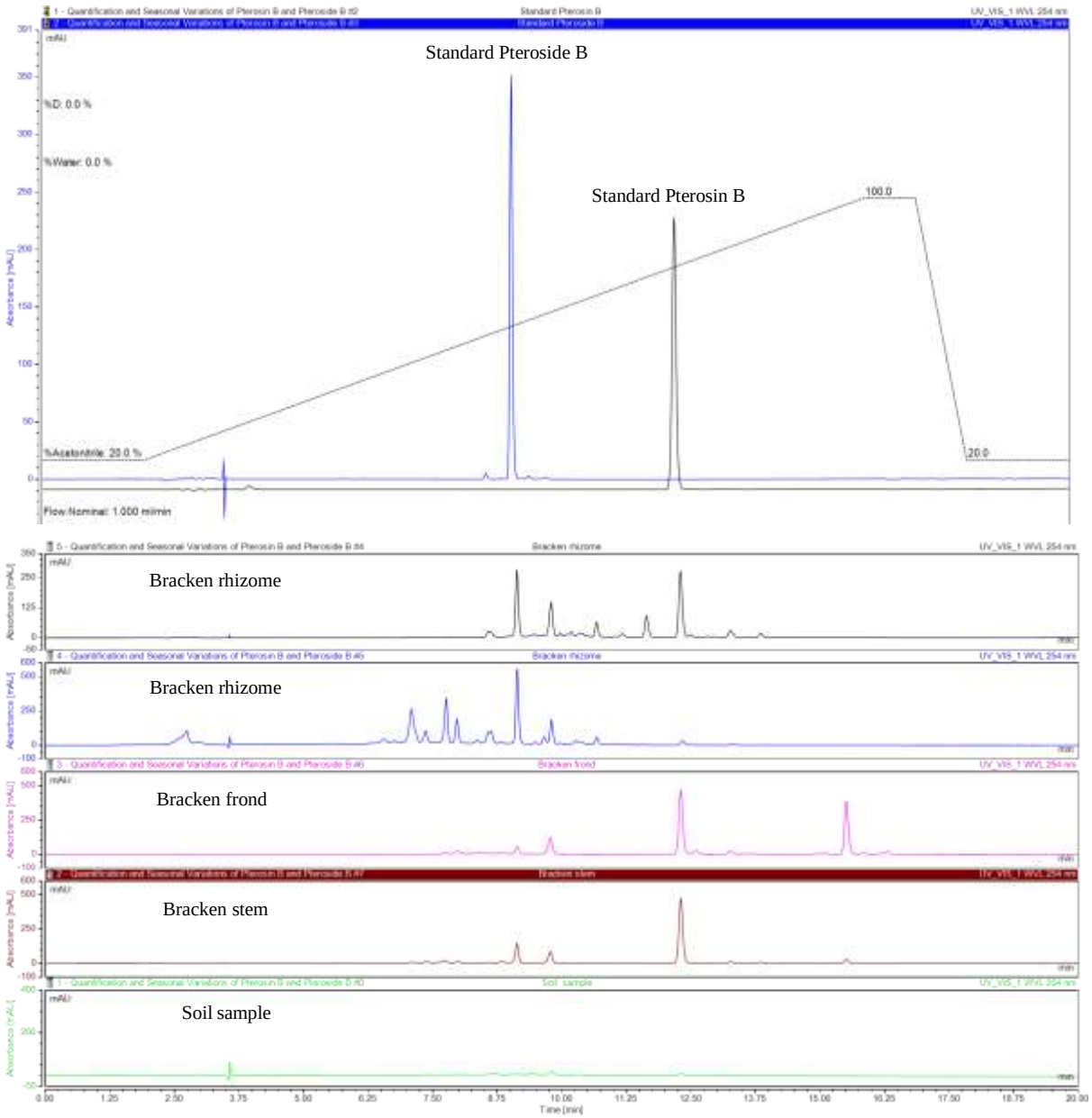

Figure 94: HPLC-UV chromatograms of pterosin B and pteroside B in bracken (rhizome, frond and stem), soil and standard solutions.

Table 55: Linearity of pterosin B and pteroside B standards and sensitivity of the RP-HPLC-UV method.

Compounds	ID Samples	Concentration range (µg/mL)	Linear regression equation	r	n	LOD (µg/mL)	LOQ (µg/mL)
Pterosin B	BR [a], BS [b] and BF [c] 2014	0.2-10 [d]	Y = 0.8458x – 0.0141	0.9999	5	0.14	0.48
	BR 2014	10-30 [e]	Y = 0.8477x + 0.0537	0.9991	5	1.13	3.77
	BS and BF 2014	10-60 [e]	Y = 0.8149x + 0.4594	0.9998	7	1.13	4.04
	Water samples 2015 BR 2015	0.2-1 [d]	Y = 0.6639x – 0.0068	0.9998	5	0.02	0.07
	BR 2015	1-25 [e]	Y = 1.0452x + 0.0862	0.9999	9	0.42	1.42
	BS and BF 2015	1-5 [d] 5-70 [e]	Y = 1.0680x – 0.0291 Y = 1.0360x + 0.0979	0.9999 0.9997	8 5	0.86 0.12	2.87 0.40
	Soil samples 2014 & 2015	0.2-2	Y = 0.6844x – 0.018	0.9998	6	0.04	0.12
Pteroside B	BR 2014 & 2015	0.5-30 [d] 20-300 [e]	Y = 0.5817x + 0.0167 Y = 0.4176x + 0.1307	0.9999 0.9999	8 8	0.44 2.91	1.46 9.69
	BS and BF 2014	1-100	Y = 0.4155x + 0.1554	0.9999	7	0.85	2.83
	BS and BF 2015	1-10 [d] 0.5-30 [e]	Y = 0.7413x + 0.0397 Y = 0.5817x + 0.0167	0.9999 0.9999	6 8	0.16 0.44	0.54 1.46
	Soil samples 2014 & 2015 Water samples 2015	0.2-1	Y = 0.7603x + 0.0006	0.9999	5	0.01	0.04

[a] BR: Bracken rhizome; [b] BS: Bracken stem; [c] BF: Bracken frond; [d] First linear range; [e] Second linear range

5.3.3. RECOVERY OF PTEROSIN B AND PTEROSIDE B WITH SPE-HPLC-UV METHOD IN BRACKEN STEM SAMPLES

The recoveries and relative standard deviation (RSD) of the target analytes in unspiked (used as a control) and spiked bracken stem samples were calculated in order to assess the efficiency of the extraction procedure and determine the accuracy of the developed SPE-HPLC-UV method for quantification of pterosin B and pteroside B. The recovery experiment was carried out by spiking known amount of the standard pterosin B and pteroside B to the bracken stem samples. Three different levels (1, 5 and 10 mg/L) covering the naturally observed range of each target compound were directly spiked to the aqueous extracts of bracken stem samples and analysed in triplicate (n=3), i.e. the recovery studies were carried out in triplicate. Recovery of both target analytes were calculated from a) the amount recovered and b) the spiked amount of each compound, by using Equation 5 (see section 5.2.9).

Recoveries and associated RSDs are listed in Table 56. The recoveries ranged between 90.29 – 96.23 % and 93.64 – 101.03 % in bracken stem samples for pterosin B and pteroside B, respectively, and this indicates the accuracy of the method. The inter-day precision of the method was ranged from 0.19 to 2.45 % for pterosin B and 0.43 to 2.25 % for pteroside B. Moreover, a reasonable linearity from the calibration curves of the standard compounds (prepared in particular for recovery experiment) was obtained for pterosin B (Y=1.4439x + 0.0443) and pteroside B (Y=0.6603x + 0.0715) with the determination coefficients (R^2) of 0.9998 and 0.9997, respectively.

Table 56: Recoveries (%) of pterosin B and pteroside B in bracken stem samples and the associated relative standard deviations (% RSD).

Name of matrices	Amount added (spiked) (mg/L)		Amount recovered (mg/L)		% RSD (n=3)		% Recovery (n=3)	
	Pterosin B	Pteroside B	Pterosin B	Pteroside B	Pterosin B	Pteroside B	Pterosin B	Pteroside B
Unspiked bracken stem	0	0	0	0	0.27	0.57	0	0
Spiked bracken stem 1	1	1	0.96	0.95	2.45	2.25	96.23	94.53
Spiked bracken stem 2	5	5	4.51	5.05	0.19	2.03	90.29	101.03
Spiked bracken stem 3	10	10	9.46	9.36	1.24	0.43	94.56	93.64

5.3.4. BIOMASS AND WATER CONTENT MEASUREMENT OF BRACKEN ORGANS

The variations percentage of dry matter and water content have been determined in bracken stems, fronds and rhizomes over a period of 18 months. Shoots emerge from rhizome. Croziers start to emerge above ground at a certain time (May to June) by uncurling. Stems are formed and fronds are elongated and grow from July to September. The tissue of crosiers is light green and soft, because of its high water content and growth is more apparent with little differentiation. Adult stems and fronds are much harder to the touch and have lower water content. Overall, from the biomass being solely rhizome during dormancy, above ground growth is equal in biomass (zero percentage) between stems and fronds from December to May (Figure 95).

Figure 96 illustrates that the water content in fronds and stems has a similar trend and decreases gradually from May to October. The highest percentage of water (*ca*. 90%) accumulates in stems and fronds of young crosiers in May and June (Figure 96). On the other hand, even though rhizomes show a slight fluctuation in water content, it can be concluded that rhizomes contain almost the similar percentage of water (70-75%) during the whole season. This result is consistent with that reported previously in the literature (Alonso-Amelot et al., 1992b).

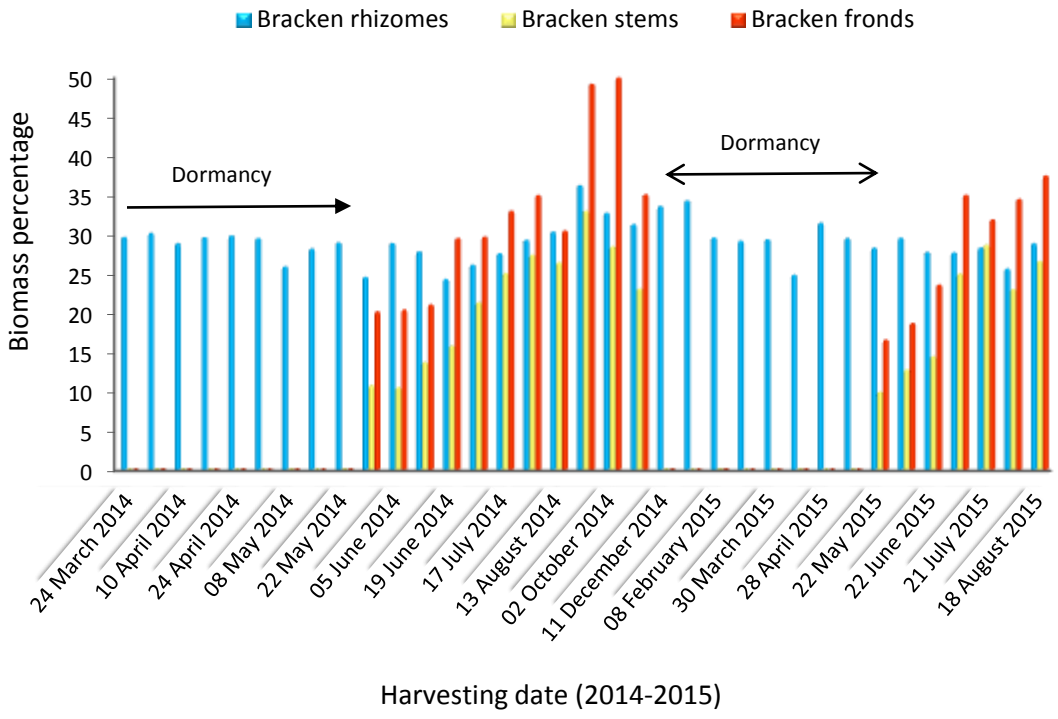

Figure 95: Biomass percentage of bracken rhizomes, fronds and stems (calculated based on dry weight separately).

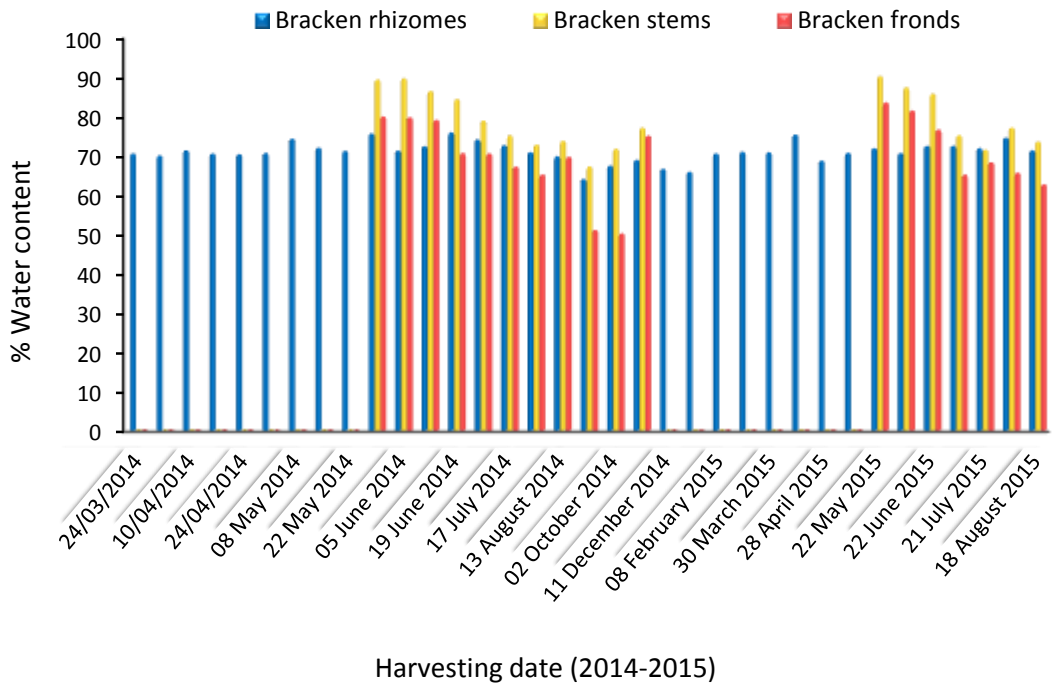

Figure 96: Water content percentage in bracken rhizomes, fronds and stems.

5.3.5. SEASONAL VARIATIONS AD QUANTIFICATION OF PTEROSIN B AND PTEROSIDE B USING SOLID PHASE EXTRACTION AND RP-HPLC-UV METHOD

Bracken is well-recognised to contain the main carcinogenic compound, ptaquiloside. Ptaquiloside is unstable due to the presence of a spirocyclopropane moiety. It is supposed that pterosin B is derived from the same biochemical pathway as ptaquiloside (Rasmussen et al., 2013), i.e. the main degradation product of ptaquiloside is pterosin B (Hirono, 1986). Due to instability of ptaquiloside, it is difficult and challenge to establish an appropriate method to determine its quantity directly. Therefore, researchers were thought about development indirect methods in order to quantify it.

Development of a method to quantify a stable compound, pterosin B, is found to be fundamental and important for assessment of the carcinogenic property of bracken fern, by which its concentration is equivalent to the amount of ptaquiloside present in the sample. Pterosin B may therefore serve as a memory to detect the presence of ptaquiloside (Clauson-Kaas et al., 2014). From this perspective, scientific researchers were attempted keenly to establish various analytical methods to quantify the amount of this carcinogenic compound (Agnew and Lauren, 1991; Burkhalter et al., 1996; O'Driscoll et al., 2016; Smith et al., 1994). Research has been concentrated on the quantification of ptaquiloside in the plant (Alonso-Amelot et al., 1992b; Rasmussen et al., 2003b), in biological samples, such as urine, milk and plasma (Aranha et al., 2014) and in soil and groundwater samples (Jensen et al., 2008). The

main goal here was the development of a new HPLC method for quantification of pterosin B and pteroside B, which can use as an indirect and reliable method for determination and detection of ptaquiloside in plant, soil and water samples.

5.3.5.1. SEASONAL VARIATIONS AND QUANTIFICATION OF PTEROSIN B AND PTEROSIDE B IN BRACKEN RHIZOMES, STEMS AND FRONDS

Pterosin B and pteroside B were quantified in the different bracken tissues for 2 active growth periods 2014 and 2015. Variations in concentrations of both compounds occurred in bracken rhizomes during the growing period (Figure 97). The two compounds were used because pterosin B is the main degradation product of ptaquiloside and the associated pteroside B was hypothesised to give a good estimation of glycosylation and possible translocation potential. It was found that the pteroside B was about one order of magnitude[22] more concentrated in the tissues when compared to pterosin B (Figure 97). This could also be a reflection on the high starch and glucose content of bracken in the rhizome with 60% (Madeja et al., 2009; Rymer, 1976). There was a distinct spike in the pterosin B concentration early in the growth period, coinciding with shoot and crosier emergence (Figure 97-Figure **98**). In stage of dormancy, extending from December to May, there is a fluctuate pattern in concentrations of pterosin B and pteroside B in bracken rhizomes. The lowest amount of each compounds recorded in January and April (Figure 97).

It is expected to vary the emergence of bracken fronds between years and different locations with changing the atmospheric conditions, specifically with temperature (Ader, 1988; O'Driscoll et al., 2016). Figure 98 shows the variations of pterosin B content in both stems and fronds through the period starting from April 2014 to August 2015 with the exception of dormancy period (early May to December). Pterosin B levels in bracken fronds and stems were closely linked and showed similar trends i.e. there was no discernible difference in the pterosin B concentration between stems and fronds. The minimum concentration of pterosin B in fronds and stems was recorded in July to September (5-15 mg/kg fronds, 15-40 mg/kg stems). By May, the accumulation of pterosin B and pteroside B in both tissue types reached peak as they showed high initial concentration (Figure 98), and this refers to the growing of bracken crosiers. Surprisingly, the pteroside B concentration in stems and fronds was half that of pterosin B and when compared to the rhizome was almost one order of magnitude less.

[22] The expression "orders of magnitude" sometimes appears in comparisons. One order of magnitude means one power of ten. So, the numbers 100 and 10,000 differ by two orders of magnitude; or we can say that 10,000 is two orders of magnitude greater than 100. Similarly, a meter and a micrometre differ by six orders of magnitude.
Reference: http://pirate.shu.edu/~rawncarr/metric/change.htm.

While for pterosin B the concentrations in fronds and stems nearly overlapped (Figure 98), there was a different pattern observed for pteroside B with a lower concentration in fronds early in the growth period in 2014 and higher concentration in the stems (Figure 99). This could be attributed to the fronds growing and differentiating later compared to the stems.

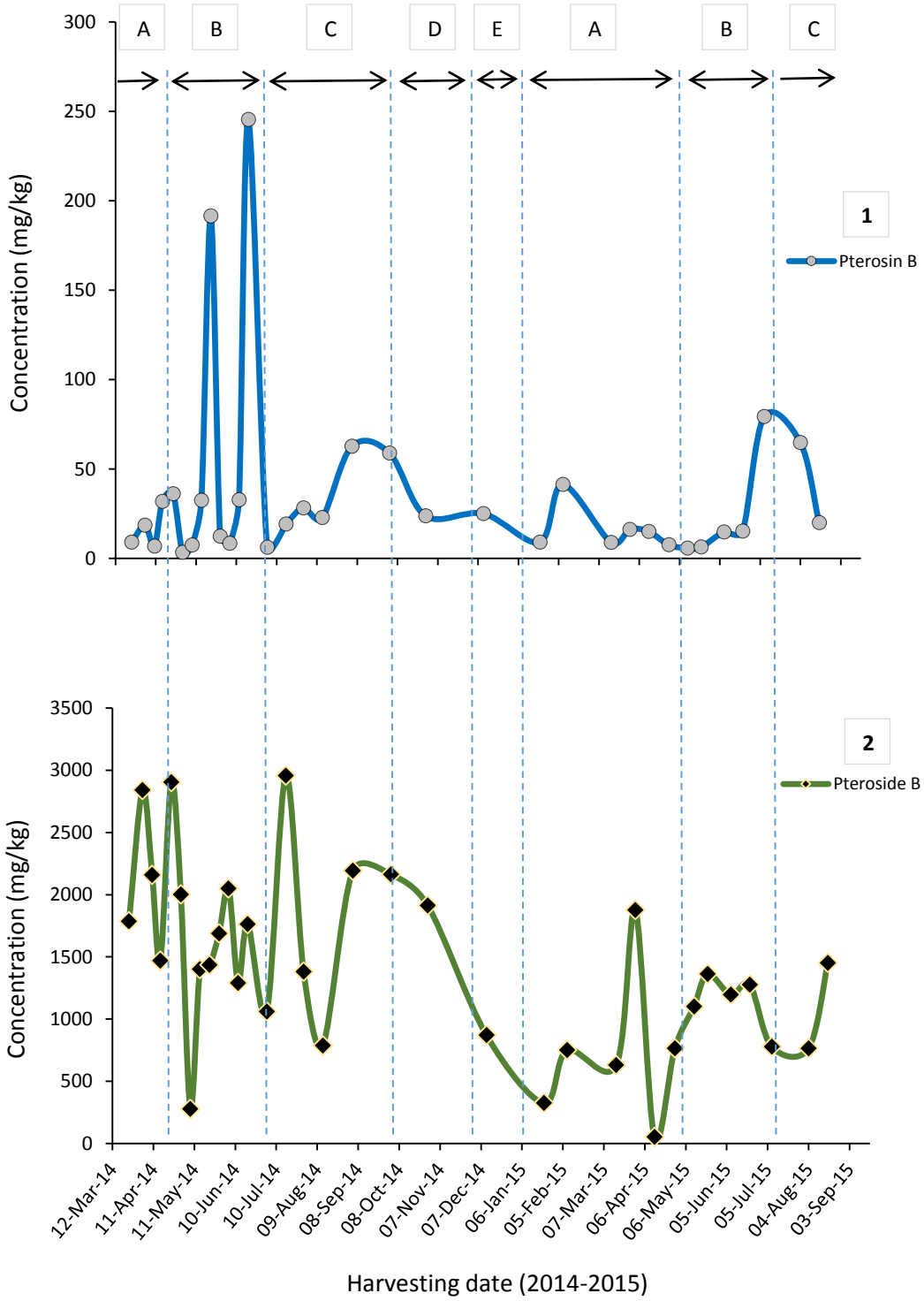

Figure 97: Seasonal variations of pterosin B (**1**) and pteroside B (**2**) in bracken rhizomes. The areas between the dashed lines represent A: solely dormant rhizomes; B: shoot

growing; C: stem extension and mature fronds; D: premature senescence fronds and E: dead fronds and stems.

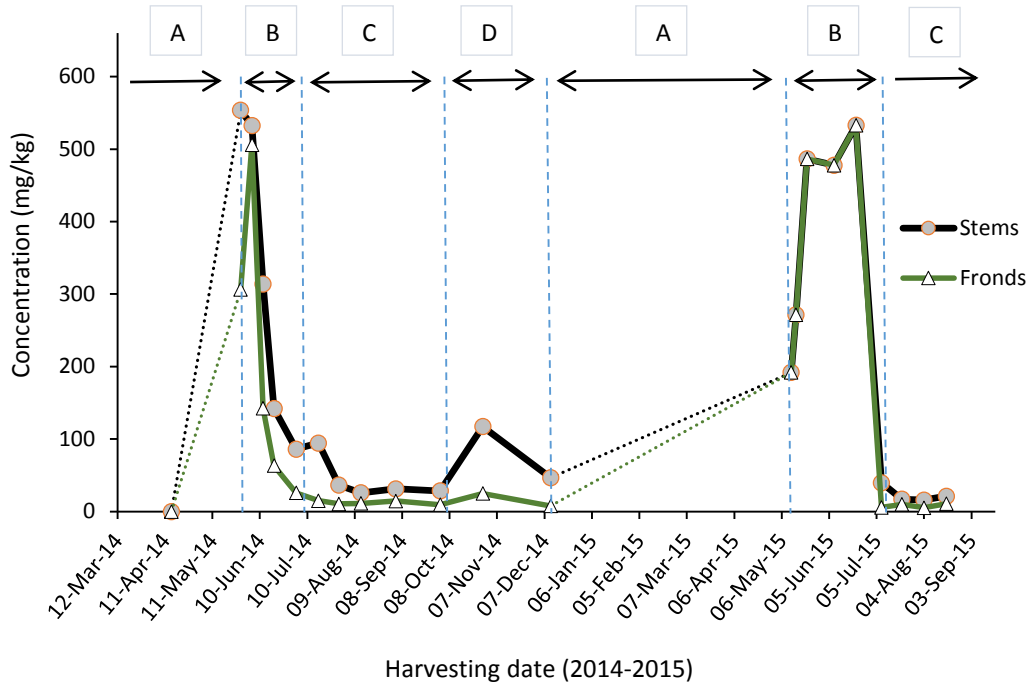

Figure 98: Seasonal variation of pterosin B in bracken stems and fronds. The areas between the dashed lines represent A: dead bracken and dormancy period; B: crosiers emergence; C: stem extension and mature fronds; D: premature senescence fronds.

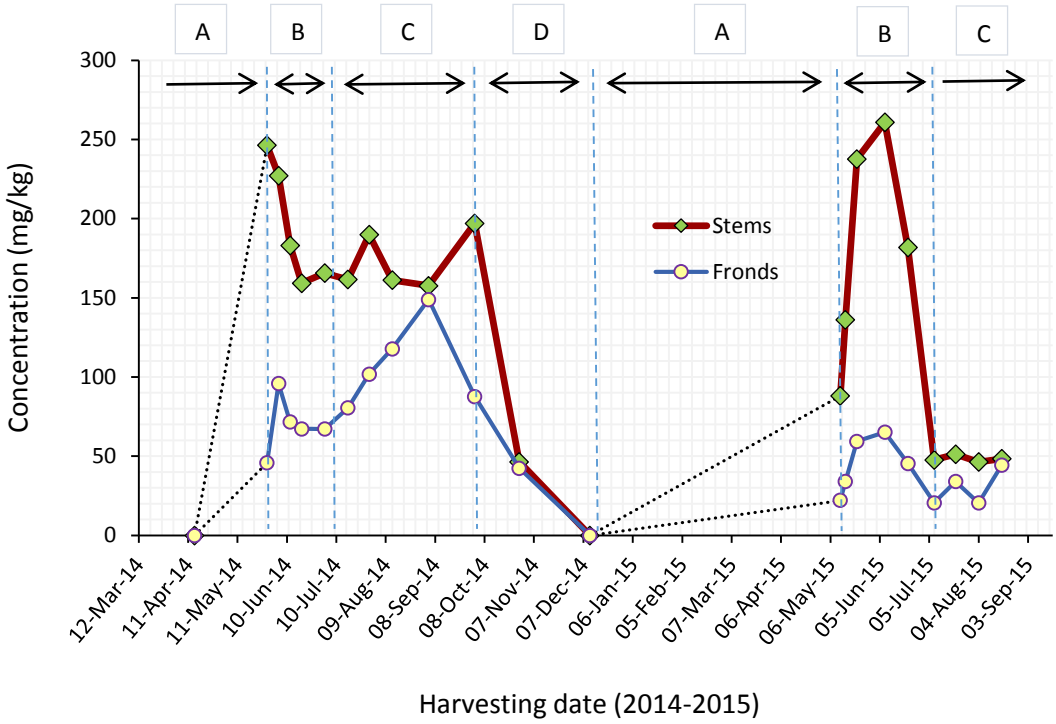

Figure 99: Seasonal variation of pteroside B in bracken stems and fronds. The areas between the dashed lines represent A: dead bracken and dormancy period; B: crosiers emergence; C: stem extension and mature fronds; D: premature senescence fronds.

5.3.5.2. SEASONAL VARIATIONS OF PTEROSIN B AND PTEROSIDE B IN SOIL SAMPLES

The fate of ptaquiloside from plant to soil and then to groundwater has been researched in detail (Clauson-Kaas et al., 2014; Jensen et al., 2008; Rasmussen et al., 2003a). There are few reports for pterosin B and none for pteroside B. In this study could not detect any pteroside B in soil samples which might be a reflection on glycosides serving as a source of glucose for soil microorganisms. Pterosin B in soil ranged from below detection limit to 0.3 mg / kg soil. For both growth periods (2014-2015), increases in concentration were observed post bluebell flowering (April to early June) and after crosier emergence (early in active growth period). This coincides well with the concentrations observed above ground, in fact it concurs with roots described as being leaky. In addition, bracken has been shown to add ptaquiloside to rainwater, another potential route of pterosin B into soil.

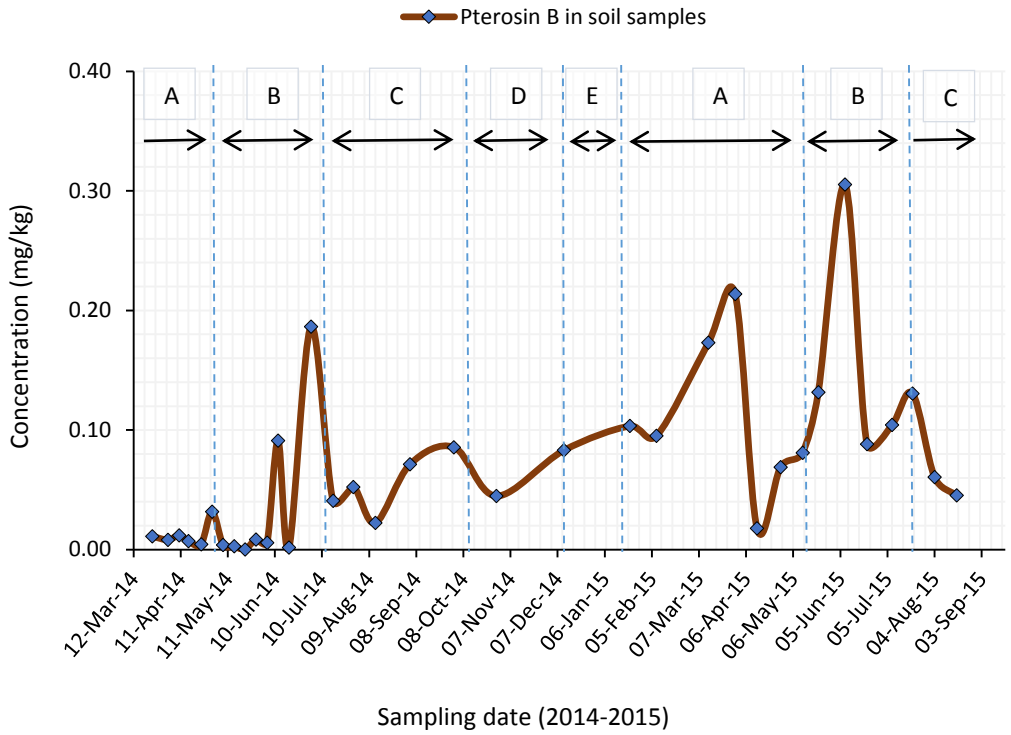

Figure 100: Seasonal variation of pterosin B in soil samples. The areas between the dashed lines represent A: solely dormant rhizomes; B: shoot growing; C: stem extension and mature fronds; D: premature senescence fronds and E: dead fronds and stems.

5.3.5.3. SEASONAL VARIATIONS OF PTEROSIN B AND PTEROSIDE B IN WATER SAMPLES

Water samples were taken near from bracken covered areas using groundwater and surface water (filtered and unfiltered). In addition, pre-treated tap water was also analysed and found to not contain pterosin B or pteroside B. The concentrations measured for pterosin B ranged from 0.009 to 0.085 µg/L (Figure 101), which agrees well with water samples that have been analysed for pterosin B produced from ptaquiloside (Jensen et al., 2008).

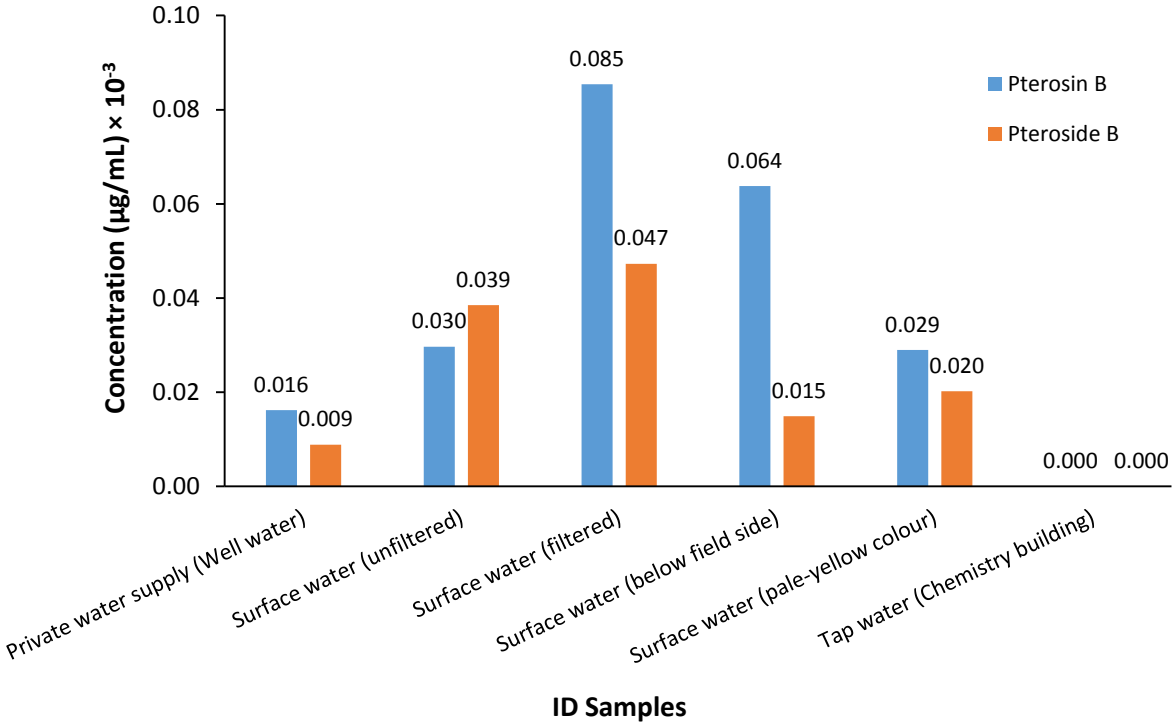

Figure 101: Concentrations of pterosin B and pteroside B in water samples.

5.4. Discussion

In this study, it was observed that the aboveground bracken fronds in North Wales emerged in early-May and dieback occurred in November-December, and this is in agreement with the results observed by Rasmussen et al. (2015) who have studied bracken in Scotland, as opposed to Ireland where bracken frond growth began in late-May to early-June and die off happened in late October to November (O'Driscoll et al., 2016).

Ptaquiloside has been quantified in different samples in the last two decades. These analyses were based on the conversion of ptaquiloside to pterosin B. Shown here are the concentrations of pterosin B and pteroside B in different tissues and soil samples for a UK population through two growth periods. There were no previous determinations of pteroside B in bracken tissues. The high concentration of pteroside B in rhizome through most of the observed period is thought to reflect the transformation of pterosin B to pteroside B in order to improve storage and increase mobility for translocation in bracken. This is also supported with the observation that stems and fronds contain only half the concentration of pteroside B compared to pterosin B (Figure 98-Figure **99**). The translocation of ptaquiloside to roots and rhizomes has been anticipated (Rasmussen, 2003). Thus, the low pterosin B and pteroside B concentrations in

stems and fronds may suggest translocation into the rhizome, especially pteroside B where it was present in a magnitude higher concentration when compared with stems and fronds.

The lowest concentrations of pteroside B in rhizome were determined around shoot emergence (May to June) (Figure 97) when the concentration is diluted due to increased biomass (Figure 95). The translocation of pteroside B into the shoot gives protection for the growing tissue according to classical chemical defence theory (Wink, 2003). This may also contribute to the pterosin B spike observed in the above ground tissue during crosier emergence and early for stems and fronds.

It is unclear whether pterosin B is solely a degradation product of ptaquiloside or is also biosynthesised. The only study that used radiolabelled substrate (Hikino et al., 1976) did not consider both possible routes. When spiking soil with ptaquiloside, an increased pterosin B concentration was noticed during analysis and hypothesised to derive from ptaquiloside degradation (Jensen et al., 2008). The results of this study show that while the concentration of pterosin B is very similar for stem and fronds, the concentrations differ for pteroside B with an initially lower concentration in the fronds which gradually increases until it equals the stems during senescence in 2014. This may suggest the formation of pteroside B due to glycosylation of pterosin B and is only indirectly related to ptaquiloside.

The concentrations of pterosin B in the adjacent soil were three magnitudes lower compared to the rhizome concentration. However, the pattern of high pterosin B concentration during shoot and crosier emergence is reflected in the spikes in pterosin B concentration observed for the soil samples. Surprisingly, pteroside B was not detected in any soil sample. The abundance of glycosidases in soil may be responsible as glucose serves as a carbon source for soil microorganisms and extracellular glycosidases are common (Blagodatskaya and Kuzyakov, 2008; German et al., 2011; Skujiņš and Burns, 1976).

The concentrations of pterosin B found in this study compare well with the results of Alonso-Amelot et al (1992a) who have reported pterosin B concentrations in bracken fronds and crosiers (Table 52). The results also showed a good agreement with the pterosin B concentrations in soil samples reported by Rasmussen et al. (2005). Jensen et al. (2008) quantified pterosin B in different types of soil and determined 0.0668 ± 0.0049 and 3.8 ± 0.88 mg/kg (dry weight) of pterosin B in a sandy and an organic-rich forest soils, respectively.

Contrary to the soil samples, pteroside B was detected in water samples, as was pterosin B. The locations followed a stream, that drained the field site where the concentration of pteroside B and pterosin B were 0.015 µg/L and 0.064 µg/L, respectively. In the same area, but from a higher elevation, the filtered and unfiltered surface water samples originated, whose

concentrations were slightly higher. Surprisingly, the filtered surface water sample had a higher pterosin B (0.085 µg/L) and pteroside B (0.047 µg/L) concentration compared to the unfiltered surface water sample, this may be due to the removal of microorganisms in the filtered surface water samples. As this was only a one-off sampling occasion, no causes for this could be attributed. The "surface water sample" originated at the same bracken covered hillside, but used a different watershed, and it was found that the concentrations of pterosin B (0.029 µg/L) and pteroside B (0.020 µg/L) were also similar. The Anglesey private well water (groundwater) sample originated from a limestone area with bracken presence on the watershed. The concentrations of pterosin B (0.016 µg/L) and pteroside B (0.009 µg/L) were slightly lower compared to the other water samples, but still detectable. Finally, the Welsh Water supplied tap water was also examined, but it did not show a detectable trace of either pterosin B or pteroside B.

CHAPTER SIX

6. CONCLUSIONS

6.1. STRUCTURAL ELUCIDATION OF THE ISOLATED COMPOUNDS

This study describes the successful isolation and identification of 38 natural products from the rhizome of *Pteridium aquilinum* (L.) Kuhn. These compounds comprise 35 pterosin-type sesquiterpenoids including eight new pterosins (**RH1** & **RH3**-**RH9**) and five new pterosides (**RH2** & **RH10**-**RH13**), alongside 5-(*β*-hydroxy)ethyl-2, 2, 4, 6-tetramethyl-1, 3-indandione (**RH36**), a potent bracken carcinogen "ptaquiloside" (**RH37**) and 5-hydroxyisocalamenene (**RH38**). Their chemical structures were elucidated mainly by 1D and 2D NMR spectroscopic analysis along with using high resolution mass spectroscopy. A guideline in order to find the chemical structures of the isolated compounds in this thesis is shown in Table 57.

The absolute configurations were also determined for six novel compounds by using either single crystal X-ray diffraction (**RH10**) or CD spectroscopy (**RH1**, **RH2**, **RH6**, **RH7**, and **RH13**). The X-ray structure of (2*R*)-pteroside B (**RH31**) was also established from its crystallographic data. Moreover, both techniques X-ray crystallography and CD spectroscopy were successfully used to determine the absolute configuration of pterosins **RH15**, **RH17** and **RH18** and (2*S*)-pteroside K (**RH35**). In addition, CD spectroscopy yielded the absolute configuration for the previously reported pterosins (**RH19**, **RH22**, **RH23**, **RH27** and **RH28**) and pterosides (**RH30** and **RH32**), whilst the stereochemistry of the rest known compounds were established based on comparison of their NMR spectroscopic and accurate MS data with those published in the literature. Because of the large perturbing influence of a glycosyl-residue in the structures of **RH31** and **RH34**, comparison of their CD spectra with those of the corresponding aglycones is inconclusive.

In this series of compounds outlined herein, compounds **RH1**, **RH15**, **RH17**, **RH18**, **RH19**, **RH22**, **RH23**, **RH27**, **RH28**, **RH29**, **RH30**, **RH32** and **RH35** present CD spectra with vibronic fine structure, while compounds **RH2**, **RH6**, **RH7**, **RH13**, **RH14** and **RH34** render relatively featureless CD spectra. The rest of the compounds (except **RH11**, **RH26**, **RH33**, **RH36**, **RH37** and **RH38**) which are of the pterosin B type failed to show CD spectra as a result of epimerisation.

Table 57: A guideline to find the chemical structures of **RH** compounds throughout the thesis

RH compounds	Name of compounds	Location	Page number
RH1	(2*S*)-Rhedynosin A [a]	Figure 18	41
RH2	(2*S*)-Rhedynoside A	Figure 30	50
RH3	Rhedynosin B	Figure 40	56
RH4	Rhedynosin C	Figure 42	58
RH5	Rhedynosin D	Figure 44	60
RH6	(3*S*)-Rhedynosin E	Figure 51	66
RH7	(2*S*)-Rhedynosin F	Figure 49	64
RH8	Rhedynosin G	Figure 46	62
RH9	Rhedynosin H	Figure 50	65
RH10	(2*R*)-Rhedynoside B	Figure 52	68
RH11	Rhedynoside C	Figure 54	70
RH12	Rhedynoside D	Figure 55	71
RH13	(3*R*)-Rhedynoside F	Figure 56	73
RH14	(2*S*)-Rhedynosin I [b]	Table 19	76
RH15	(2*S*)-Pterosin A	Table 22	82
RH16	(2*R*)-Pterosin B	Table 20	77
RH17	*trans*-Pterosin C	Table 25	89
RH18	*cis*-Pterosin C	Table 26	91
RH19	(3*S*)-Pterosin D	Table 30	98
RH20	(2*R*)-Pterosin E	Table 32	103
RH21	(2*R*)-Pterosin F	Table 28	95
RH22	*trans*-Pterosin J	Table 29	97
RH23	(2*S*)-Pterosin K	Table 33	104
RH24	(2*S*)-Pterosin N	Table 35	108
RH25	(2*S*)-Pterosin P	Table 36	110
RH26	Pterosin Z	Table 37	111
RH27	(2*S*)-2-Hydroxymethylpterosin E	Table 39	116
RH28	*trans*-Histiopterosin A	Table 27	93
RH29	(2*S*)-12-Hydroxypterosin A	Table 40	118
RH30	(2*S*)-Pteroside A	Table 23	85
RH31	(2*R*)-Pteroside B	Table 21	80
RH32	(3*S*)-Pteroside D	Table 31	101
RH33	Pteroside Z	Table 38	114
RH34	(2*S*)-Pteroside A2	Table 24	87
RH35	(2*S*)-Pteroside K	Table 34	106
RH36	5-(*β*-hydroxy)ethyl-2, 2, 4, 6-tetra methyl-1, 3-indandione	Table 41	120
RH37	Ptaquiloside	Table 42	121
RH38	5-hydroxycalamenene	Table 43	124

[a] The blue colours are representing the novel compounds.
[b] The red colours are representing the known isolated compounds.

Careful pair-wise comparison of the CD spectra of the isolated compounds with identical chromophore cores (Figure 102) and similar dissymmetric environments enabled correlation. Comparison of the CD spectra with X-ray data or published CD data (Kuroyanagi et al., 1979a) revealed that the stereogenic centre in the core aglycone (Figure 102) of the compounds **RH1**, **RH2**, **RH7**, **RH14**, **RH15**, **RH23**, **RH27**, **RH29**, **RH30**, **RH34** and **RH35** can be assigned as 2*S*.

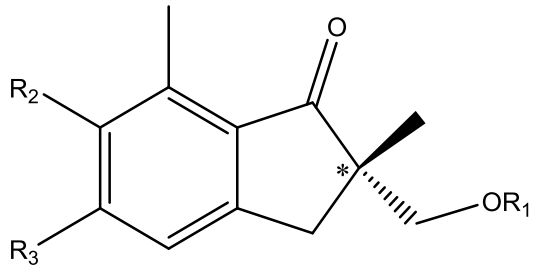

Figure 102: Chromophore core in compounds **RH1, RH2**, **RH7**, **RH14**, **RH15**, **RH23**, **RH27**, **RH29**, **RH30**, **RH34** and **RH35**.

Pterosin glycoside compounds so far reported possess the glucose residue at different positions, for example, (2*R*, 3*R*)-pterosin L 3-*O*-*β*-D-glucopyranoside (Chen et al., 2008) and (2*S*, 3*S*)-pterosin C 3-*O*-*β*-D-glucoside (Sengupta et al., 1976) at position C-3; pterosides A2 and K (Castillo et al., 2003; Kuroyanagi et al., 1979a) at position C-11 and pterosides A, B, C, D, P and Z (Hikino et al., 1972, 1971; Kuroyanagi et al., 1979a) at position C-14. Thus, rhedynoside B (**RH10**) is first example for pterosides bearing glucose portion at the position C-2. To the best of our knowledge, rhedynosides C (**RH11)** and D (**RH12)** are the first reported glucosides with the glucose moiety on the position C-12 of the aglycone. In addition, one previously unreported sulfate-containing pterosin, rhedynosin H (**RH9**), together with two other reported compounds, (2*R*, 3*R*)-histiopterosin A (**RH28**) and (2*S*)-pteroside A2 (**RH34**), were isolated for the first time from the rhizomes of bracken. For the first time compounds (2*S*)-rhedynosin I (**RH14**), (2*S*)-2-Hydroxymethylpterosin E (**RH27**) and (2*S*)-12-hydroxypterosin A (**RH29**) were isolated from the plant source (bracken rhizomes). Previously, they were isolated as metabolite products of (2*S*)-pterosin A from rat urine 24 hrs after oral administration (100 mg/kg) (Lee et al., 2012). Furthermore, the two novel compounds, rhedynosin A (**RH1**) and rhedynoside A (**RH2**), have a relatively rare aglycone, containing a six-membered cyclic ether.

The origin of the pterosins and pterosides reported could be either by direct biosynthesis *in planta* or are products of ptaquiloside degradation. Also further chemical modification through environmental conditions *in planta* or during plant processing could have occurred. The

methodology employed was not able to address this questions, however, a grouping of the compounds identified (Figure 103-Figure 106) allows to develop hypotheses that further research may target. Ptaquiloside degradation results in pterosin B being the major product (Figure 6-Figure **7**). Pterosin B arises due to the final ring opening step of the cyclopropane moiety that captures the nearest and most abundant nucleophile: hydroxyl group (OH^-). Of the reported compounds (**RH1 - RH35**) nine equally contain the resulting hydroxyl substitution on position C-14 (Figure 103). The structural variation observed in this grouping relates mostly to the variation in the five-membered ring. Ptaquiloside contained a methyl substitution on position C-2 with *R* configuration, as was found for **RH16**. The α-position to the carbonyl functionality leads to easy racemisation on position C-2 resulting in **RH25**. Hydroxylation at position C-2 for **RH24** and position C-3 for **RH17** and **RH18** was observed, possibly caused by additional environmental hydroxylation. Compounds **RH19** and **RH26** have two methyl substituents on position C-2, which are unlikely to have derived from environmental conditions during ptaquiloside degradation. **RH15** and **RH29** have an additional hydroxymethyl substituent on position C-2. A biosynthetic origin for this substitution is thought more likely.

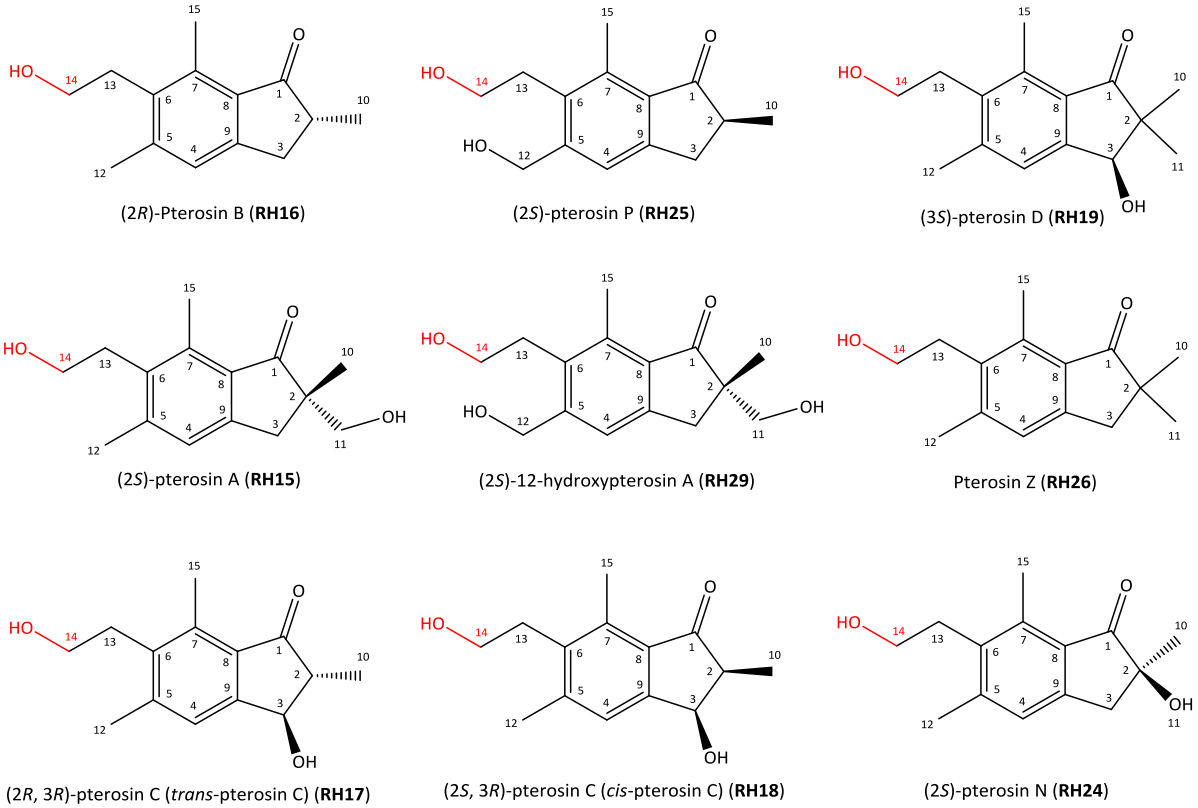

Figure 103: Pterosin compounds having OH substitution on position C-14 hypothesised to have arisen from ptaquiloside degradation.

In addition to hydroxyl group, other nucleophiles such as chloride (Cl^-), sulfate (SO_4^{2-}) and formate ($HCOO^-$) are present *in planta* and position C-14 was found to show chloride (Cl^-), hydrogen sulfate (HSO_4^-) and formate ($HCOO^-$) substitution (Figure 104). As argued above, **RH9**, **RH20** and **RH21** are hypothesised to be direct ptaquiloside degradation products. **RH5**, **RH8**, **RH22**, **RH29** show additional hydroxylation at positions C-2, C-3 and C-13. When considering the substitutions on the five-membered ring, again the presence of two methyl substituents on position C-2 for **RH6** or an additional hydroxymethyl substituent on position C-2 for **RH7**, **RH23** and **RH27** was noted for which a biosynthetic origin is thought more likely.

An additional six-membered ring containing an ether functionality formed part of **RH1** while **RH3**, **RH4** and **RH14** contain six-membered cyclic esters (Figure 105). These structural features are hypothesised to have derived from intramolecular cyclisation reactions. For example, **RH1** could be the product of nucleophilic substitution from **RH29**. While no possible precursors for **RH3**, **RH4** and **RH14** have been isolated, they would require both formate and hydroxyl substitution on positions C-14 and C-12.

In addition to alterations due to environmental conditions, enzymatic activity from enzymes present within the plant could have caused hydroxylation and glycosylation (Figure 106) which are well known degradation pathways. In addition, glycosylation is often employed to increase aqueous solubility. Pterosin A was isolated in the highest yield (Table 44) and was the only aglycone for which the corresponding glycoside with linkage at position C-14 (**RH30**) and position C-11 (**RH2**) was isolated (Figure 106). Pterosin B was the second highest yielding isolated pterosin followed by pterosin D. Both corresponding glycosides **RH31** and **RH32** along with **RH33** showed a glycosidic linkage at position C-14. The position C-14 has the least steric hindrance of all the hydroxyl substitutions present in the pterosin aglycones, and **RH33** also. The hydroxymethyl substitution at position C-2 provides the second least sterically hindered hydroxyl for glycosylation that was determined for **RH2**, **RH34** and **RH35**. Equal distance from the bicyclic pterosin core is present at position C-12 and **RH11** and **RH12** were glycosylated there. Only two pterosides showed glycosylation to hydroxy groups directly attached to the bicyclic system at position C-2 for **RH10** and position C-3 for **RH13**.

Overall, the structural diversity observed suggests that the majority of the pterosins isolated are a product of ptaquiloside degradation. The presence of two methyl groups on position C-2 require further investigation in view of whether there is ptaquiloside homologues present in bracken.

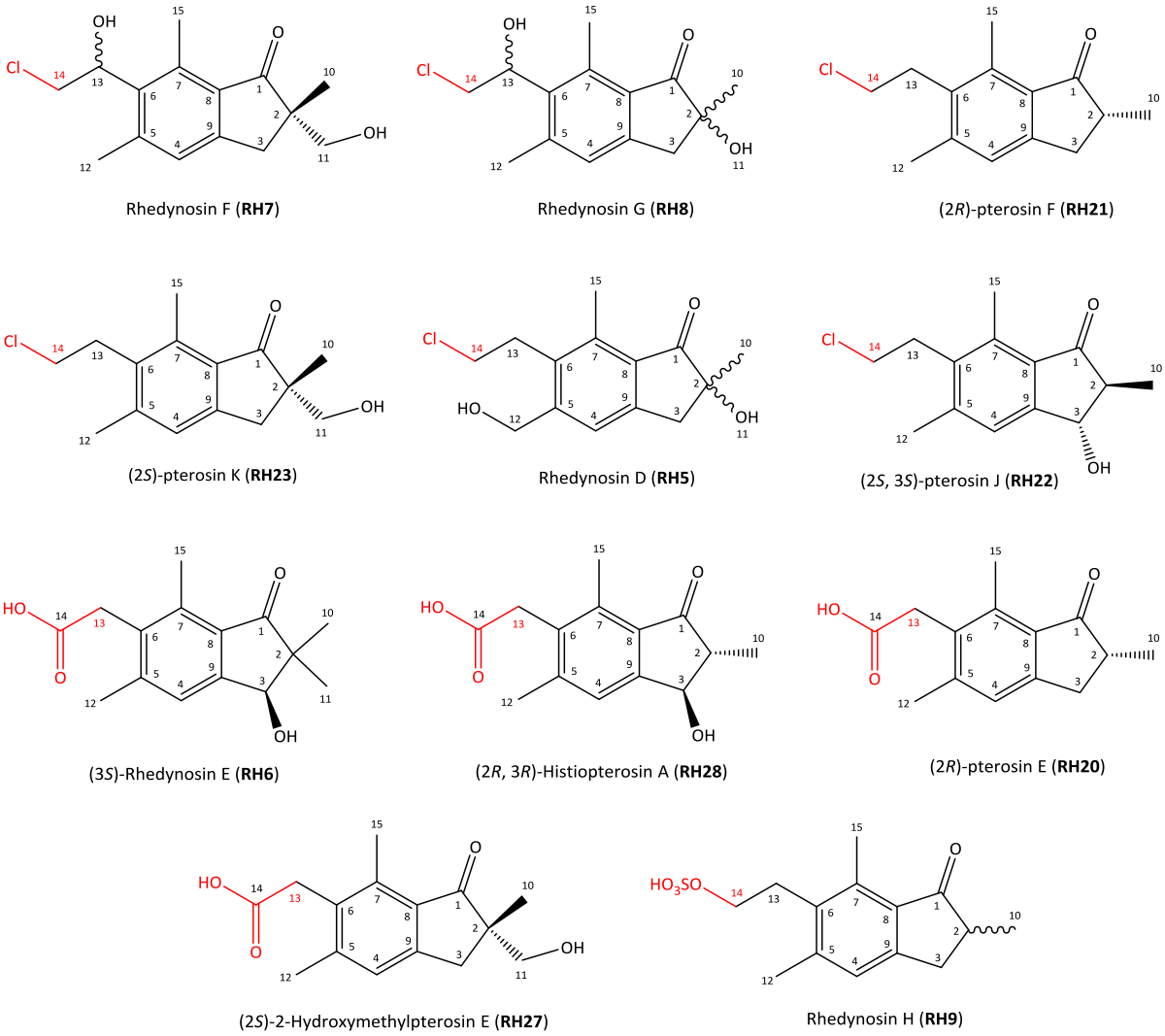

Figure 104: Pterosin compounds having Cl and HSO_4 substitutions on position C-14 or COOH group on position C-13 hypothesised to have arisen from ptaquiloside degradation.

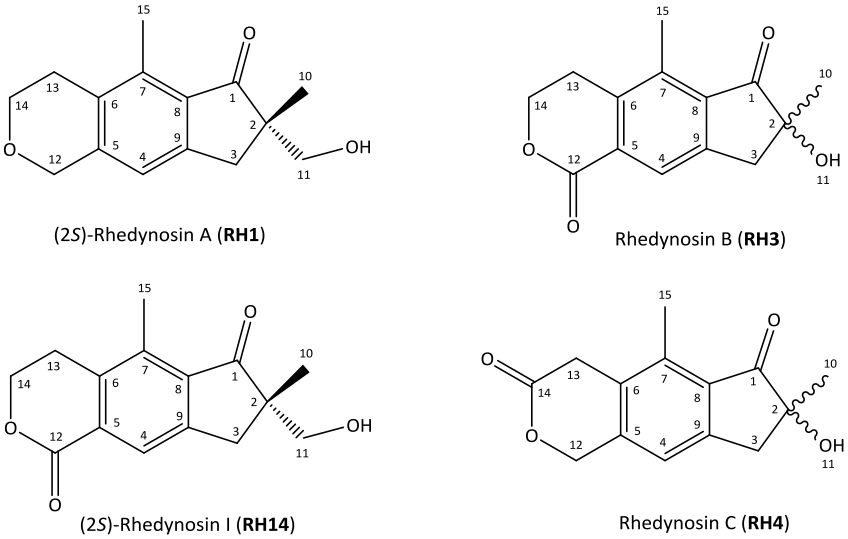

Figure 105: Examples for six-membered cyclic pterosins in bracken.

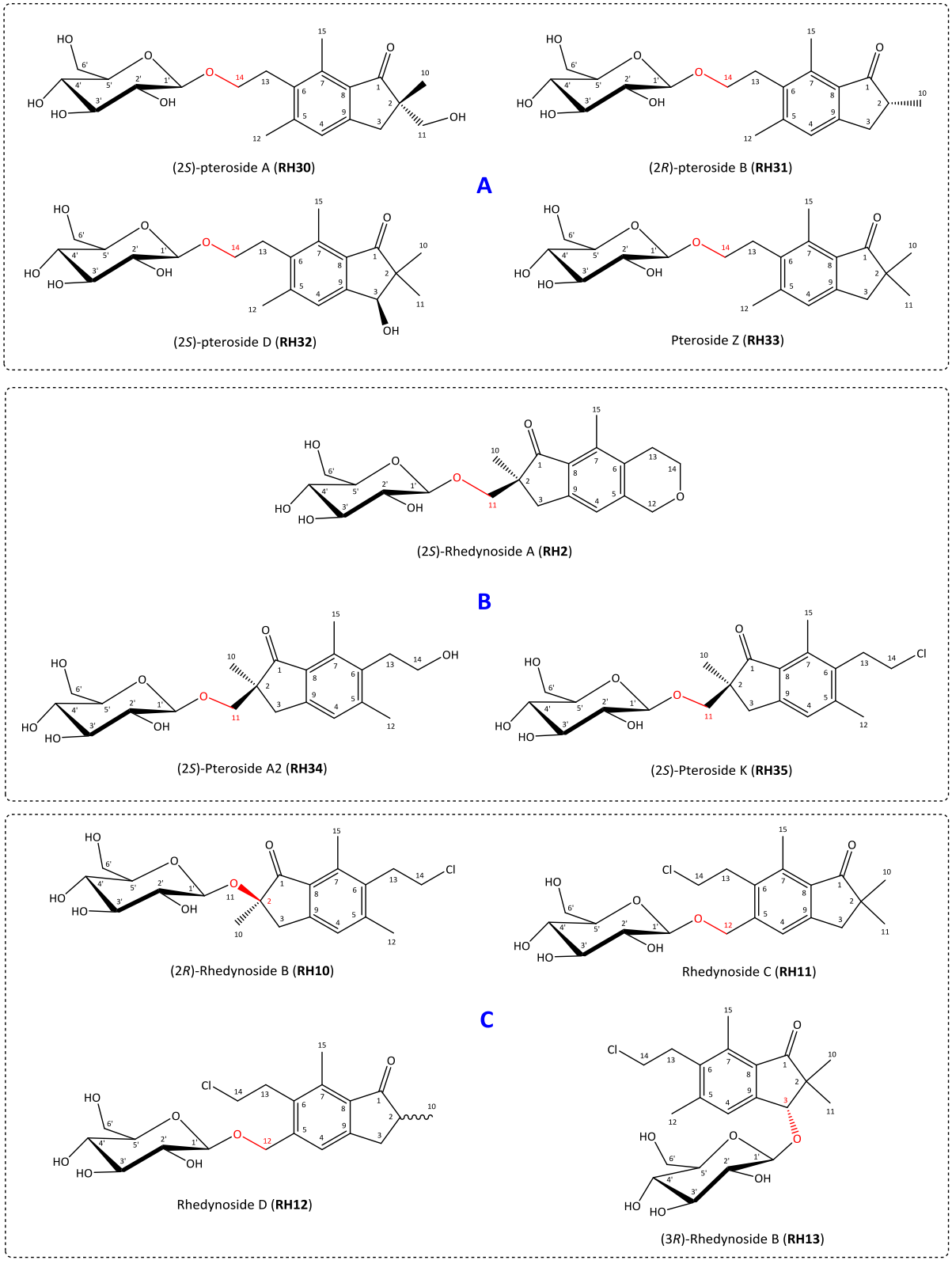

Figure 106: Pterosin glycoside compounds with glucose-*O*-linkage to the aglycones at positions **a**) C-14, **b**) C-11 and **c**) C-2, C-3 and C-12.

6.2. BIOLOGICAL ACTIVITIES OF THE ISOLATED COMPOUNDS

Bracken has been known for a long time to be a successful colonising plant whose consumption is detrimental to livestock. There are many examples of bracken extracts that have shown distinct biological effects on model systems. Ptaquiloside has been identified as the main compound in bracken with adverse effects on different biological processes, particularly showing DNA adduct formation and hence being carcinogenic. This study continued to search for biologically active compounds from bracken and the 35 isolated pterosins and pterosides were used in different assays. Historically bracken was used as an antihelminthic (Marrs and Watt, 2006), hence 20 compounds were used in a motility assay for the intestinal flatworm *Schistosoma mansoni*, however, none of the compounds showed any significant activity. Because of the tendency of bracken to take over whole areas of countryside, it was suspected to contain potential agrochemicals. A screen undertaken by Syngenta to assess the anti-fungal, anti-insecticidal and herbicidal activity, did not yield any positive responses when compared to the best commercially available product. However, because mild, moderate and low antifungal activity was detected for 7 out of the 20 submitted compounds on at least one occasion, this was considered worth following up. A different anti-fungal screen targeting the medically-relevant *Candida albicans* species was utilised for 21 compounds, however, no susceptibility to any compound was returned. Pterosins have been patented as anti-diabetics thus 6 compounds, consisting of matched aglycones and glycosides, were used in a glucose transport assay. It was concluded that they exhibited negligible inhibitory effect on the main glucose transporters found in the intestine. Finally, a subset of 21 compounds was used to investigate their antitrypanosomal activity and rhedynosin G (**RH8**) was found to give 79% inhibition against *Trypanosoma brucei brucei* at a rate of 20 µM. All other compounds were found to be almost inactive. When testing for the anti-bacterial activity, only moderate inhibition at 100 µM was found for **RH35** again *Mycobacterium marinum*. Compounds **RH2**, **RH8**, **RH20**, **RH30** and **RH34** showed moderate activity against *Klebsiella pneumonia* at 100 µM.

The absence of biological activity, even for conditions where traditional use of bracken has been known or pterosins have been patented for, was unexpected. However, this suggest a surprising efficiency on behalf of bracken in its biosynthesis of ptaquiloside as it is thought that the main biological active compound in bracken is ptaquiloside. As pterosins and pterosides are more stable when compared to ptaquiloside, they may be a second line of chemical defence that requires a higher concentration to exert a biological effect.

6.3. QUANTIFICATION AND SEASONAL VARIATIONS OF PTEROSIN B AND PTEROSIDE B

The environmental fate of pterosin B and pteroside B was assessed by quantifying its presence in all bracken tissues (rhizomes, stems and fronds), associated soil and water. This was undertaken for two growth periods of bracken (2014 and 2015). Quantitation of the two compounds (pterosin B and pteroside B) was performed by using an accurate and precise developed RP-HPLC-UV method. A SPE method (using 500 mg SPE cartridges) has also been developed and used for preconcentration, clean-up and sample preparation.

The recovery and % RSD for both analytes were calculated. Acceptable and satisfactory recoveries ranging from $90.29 - 96.23$ % (pterosin B) and $93.64 - 101.03$ % (pteroside B) were obtained with the developed SPE-HPLC-UV method (Table 56). This supports that the developed method is accurate. The method can be used for quantification of pterosin B and pteroside B in plant tissues, water and soil samples. Also, the method is recommended to be used for indirect detection and quantification of ptaquiloside in water and soil samples after degradation of ptaquiloside resulting in formation of a stable natural pterosin B.

As it was expected, the amounts of both pterosin B and pteroside B decreased from the crosiers to the mature fronds. In general, the highest concentration of pterosin B was found in all parts of bracken and soil samples when shoots emerged and crosiers started to grow, i.e. in mid-May to July (Figure 97-Figure **100**). It was found that the rhizome is the main storage organ for pteroside B as its concentration was reached about 3000 mg/kg (Figure 97) which is much higher than that found in the stems and fronds (Figure 99). Pterosin B, on the other hand, had a similar concentration range in fronds and stems (Figure 98), while its concentration declined to half in rhizomes especially at the beginning of bracken growth in May to June (Figure 97). The excess of pteroside B was thought to derive for two main reasons. Firstly, it is the glycoside of the main ptaquiloside degradation product pterosins B. By being glycosylated, pteroside B is easier to translocate within the plant, and is also thought to derive as a consequence of the starch richness of bracken. It seems that pteroside B is not catabolised on senescence, rather it accumulates in the storage organ, the rhizome. Secondly, it presents a means of chemical defence for bracken by being available for transport to tissue in need of most defence, particularly the crosiers. The increased concentration in the crosiers and the young stems and fronds support this (Figure 99).

The soil samples equally picked up the increased pterosin B concentration during the critical young tissue formation between May to June (Figure 100), which supports the overall relocation of pterosin B, most probably in the form of the glycoside pteroside B. Young tissues,

such as shoots and crosiers, are characterised by abundant growth and little differentiation, meaning that the cell wall is probably not fully formed, making it leaky. To our knowledge, no pteroside B is detected in the soil which contradicts the quantification of pteroside B in the water samples, and this absence may be attributed to the abundance of glycosidases in soil.

Considering the overall secondary metabolism of bracken as investigated here, it can be concluded that bracken has evolved with ptaquiloside as its main agent for chemical defence. In an environment that induces hydrolysis, the structure of ptaquiloside lends itself to latch onto the nearest susceptible target. This study showed clearly that the structural variety of pterosins and pterosides are conceivably ptaquiloside degradation products. Following the environmental fate of the main aglycone pterosin B and glycoside pteroside B, it was shown that the glycoside is used for storage in the carbohydrate-rich bracken. From the plant, pterosins are sufficiently stable to translocate into the soil and to be leached out into the groundwater. The reduction in concentration is roughly a factor 1000 less in the soil and another factor 10000 less in the water.

List of References

Ader, K.G., 1988. Factors controlling the distribution and spread of bracken (*Pteridium aquilinum*) in Scotland. PhD thesis, University of Glasgow, Glasgow, UK, October 1988.

Agnew, M.P., Lauren, D.R., 1991. Determination of ptaquiloside in bracken fern (*Pteridium esculentum*). J. Chromatogr. A 538, 462–468.

Almeida Santos, M. de F.M., Dórea, J.G., Luna, H., 2006. Bracken-fern extracts can be clastogenic or aneugenic depending on the tissue cell assay. Food Chem. Toxicol. 44, 1845–1848.

Alonso-Amelot, M., Avendano, M., 2002. Human carcinogenesis and bracken fern: A review of the evidence. Curr. Med. Chem. 9, 675–686.

Alonso-Amelot, M.E., Avendaño, M., 2001. Possible association between gastric cancer and bracken fern in Venezuela: An epidemiologic study. Int. J. Cancer 91, 252–259.

Alonso-Amelot, M.E., Castillo, U., Smith, B.L., Lauren, D.R., 1998. Excretion, through milk, of ptaquiloside in bracken-fed cows. A quantitative assessment. Lait 78, 413–423.

Alonso-Amelot, M.E., Pérez-Mena, M., Calcagno, M.P., Jaimes-Espinoza, R., 1992a. Quantitation of pterosins A and B, and ptaquiloside, the main carcinogen of pteridium aquilinum (L. Kuhn), by high pressure liquid chromatography. Phytochem. Anal. 3, 160–164.

Alonso-Amelot, M.E., Pérez-Mena, M., Calcagno, M.P., Jaimes-Espinoza, R., Castillo, U., 1992b. Ontogenic variation of biologically active metabolites of *Pteridium aquilinum* (L. Kuhn) pterosins A and B, and ptaquiloside in a bracken population of the tropical Andes. J. Chem. Ecol. 18, 1405–1420.

Aoyama, K., Tanaka, N., Suzuki, N., Murakami, T., Yasuhisa, S., 1977. Neue pterosin-derivate aus *Pteris wallichiana* Agardh. und *P. semipinnata L.*. Chem. Pharm. Bull. (Tokyo). 25, 2461–2464.

Aranha, P.C.R., Hansen, H.C.B., Rasmussen, L.H., Strobel, B.W., Friis, C., 2014. Determination of ptaquiloside and pterosin B derived from bracken (*Pteridium aquilinum*) in cattle plasma, urine and milk. J. Chromatogr. B. Analyt. Technol. Biomed. Life Sci. 951-952, 44–51.

Attya, M., Nardi, M., Tagarelli, A., Sindona, G., 2012. A new facile synthesis of D4-pterosin B and D4-bromopterosin, deuterated analogues of ptaquiloside. Molecules 17, 5795–5802.

Averis, A., Averis, B., Birks, J., Horsfield, D., Thompson, D., Yeo, M., 2004. An illustrated guide to British upland vegetation. Joint Nature Conservation Committee, Peterborough.

Ayala-Luis, K.B., Hansen, P.B., Rasmussen, L.H., Hansen, H.C.B., 2006. Kinetics of ptaquiloside hydrolysis in aqueous solution. Environ. Toxicol. Chem. 25, 2623–2629.

Ayer, W.A., McCaskill, R.H., 1981. The cybrodins, a new class of sesquiterpenes. Can. J. Chem. 59, 2150–2158.

Bardouille, V., Mootoo, B.S., Hirotsu, K., Clardy, J., 1978. Sesquiterpenes from Pityrogramma calomelanos. Phytochemistry 17, 275–277.

Blagodatskaya, E., Kuzyakov, Y., 2008. Mechanisms of real and apparent priming effects and their dependence on soil microbial biomass and community structure: critical review. Biol. Fertil. Soils 45, 115–131.

Bonadies, F., Borzacchiello, G., Dezzi, S., Nicoletti, R., Roperto, S., 2004. Mass spectrometric analysis of ptaquiloside, the toxic sesquiterpene from bracken fern. Rapid Commun. Mass Spectrom. 18, 825–828.

Burkhalter, P.W., Groux, P.M.J., Candrian, U., Hubner, P., Luthy, J., 1996. Isolation, determination and degradation of ptaquiloside-a bracken fern carcinogen. J. Nat. Toxins 5, 141–159.

Campos-da-Paz, M., Pereira, L.O., Bicalho, L.S., Dórea, J.G., Poças-Fonseca, M.J., Santos, M. de F.M.A., 2008. Interaction of bracken-fern extract with vitamin C in human submandibular gland and oral epithelium cell lines. Mutat. Res. 652, 158–163.

Castillo, U.F., Ojika, M., Alonso-Amelot, M., Sakagami, Y., 1998. Ptaquiloside Z, a new toxic unstable sesquiterpene glucoside from the neotropical bracken fern *pteridium aquilinum* var. *caudatum*. Bioorg. Med. Chem. 6, 2229–2233.

Castillo, U.F., Wilkins, A.L., Lauren, D.R., Smith, B.L., Alonso-Amelot, M., 2003. Pteroside A2-a new illudane-type sesquiterpene glucoside from *Pteridium caudatum* L. Maxon, and the spectrometric characterization of caudatodienone. J. Agric. Food Chem. 51, 2559–2564.

Castillo, U.F., Wilkins, A.L., Lauren, D.R., Smith, B.L., Towers, N.R., Alonso-Amelot,

M.E., Jaimes-Espinoza, R., 1997. Isoptaquiloside and caudatoside, illudane-type sesquiterpene glucosides from *Pteridium aquilinum* var. *caudatum*. Phytochemistry 44, 901–906.

Chen, C.-Y., Chiu, F.-Y., Lin, Y., Huang, W.-J., Hsieh, P.-S., Hsu, F.-L., 2015. Chemical constituents analysis and antidiabetic activity validation of four fern species from Taiwan. Int. J. Mol. Sci. 16, 2497–2516.

Chen, J.-J., Wang, T.-C., Yang, C.-K., Liao, H.-R., Sung, P.-J., Chen, I.-S., Cheng, M.-J., Peng, C.-F., Chen, J.-F., 2013. New pterosin sesquiterpenes and antitubercular constituents from *Pteris ensiformis*. Chem. Biodivers. 10, 1903–1908.

Chen, Y.-H., Chang, F.-R., Lu, M.-C., Hsieh, P.-W., Wu, M.-J., Du, Y.-C., Wu, Y.-C., 2008. New benzoyl glucosides and cytotoxic pterosin sesquiterpenes from *Pteris ensiformis* Burm. Molecules 13, 255–266.

Clauson-Kaas, F., Jensen, P.H., Jacobsen, O.S., Juhler, R.K., Hansen, H.C.B., 2014. The naturally occurring carcinogen ptaquiloside is present in groundwater below bracken vegetation. Environ. Toxicol. Chem. 33, 1030–1034.

Cooper-Driver, G., 1976. Chemotaxonomy and phytochemical ecology of bracken. Bot. J. Linn. Soc. 73, 35–46.

Cooper-Driver, G., Finch, S., Swain, T., Bernays, E., 1977. Seasonal variation in secondary plant compounds in relation to the palatability of *Pteridium aquilinum*. Biochem. Syst. Ecol. 5, 177–183.

Cooper-Driver, G.A., 1990. Defense strategies in bracken, *pteridium aquilinum* (L.) Kuhn. Ann. Missouri Bot. Gard. 77, 281–286.

D'Mello, J.P.F., 1997. Handbook of plant and fungal toxicants. CRC Press, New York.

Felipe, D., Brambilla, L., Porto, C., Pilau, E., Cortez, D., 2014. Phytochemical analysis of *Pfaffia glomerata* inflorescences by LC-ESI-MS/MS. Molecules 19, 15720–15734.

Fenwick, G.R., 1988. Bracken (*Pteridium aquilinum*)—toxic effects and toxic constituents. J. Sci. Food Agric. 46, 147–173.

Ferguson, L.R., Philpott, M., 2008. Nutrition and mutagenesis. Annu. Rev. Nutr. 28, 313–329.

Fletcher, M.T., Hayes, P.Y., Somerville, M.J., De Voss, J.J., 2010. Ptesculentoside, a novel

norsesquiterpene glucoside from the Australian bracken fern *Pteridium esculentum*. Tetrahedron Lett. 51, 1997–1999.

Fletcher, M.T., Reichmann, K.G., Brock, I.J., McKenzie, R. a, Blaney, B.J., 2011. Residue potential of norsesquiterpene glycosides in tissues of cattle fed Austral bracken (*Pteridium esculentum*). J. Agric. Food Chem. 59, 8518–8523.

Francesco, B., Giorgio, B., Rosario, N., Saverio, R.F., Francesco, D.G., Romano, M., Adriano, S., Cinzia, R., Antonio, T., Franco, R., Valeria, R., Sante, R., 2011. A new, very sensitive method of assessment of ptaquiloside, the major bracken carcinogen in the milk of farm animals. Food Chem. 124, 660–665.

Freitas, R.N., O'Connor, P.J., Prakash, A.S., Shahin, M., Povey, A.C., 2001. Bracken (*Pteridium aquilinum*)-induced DNA adducts in mouse tissues are different from the adduct induced by the activated form of the Bracken carcinogen ptaquiloside. Biochem. Biophys. Res. Commun. 281, 589–594.

Fukuoka, M., Kuroyanagi, M., Toyama, M., Yoshihira, K., Natori, S., 1972. Pterosins J, K, and L and six acylated pterosins from bracken, *Pteridium aquilinum* var. *latiusculum*. Chem. Pharm. Bull. (Tokyo). 20, 2282–2285.

Fukuoka, M., Kuroyanagi, M., Yoshihira, K., Natori, S., 1978. Chemical and toxicological studies on bracken fern, *Pteridium aquilinum* var. *latiusculum*. II. Structures of pterosins, sesquiterpenes having 1-indanone skeleton. Chem. Pharm. Bull. (Tokyo). 26, 2365–2385.

Fukuoka, M., Yoshihira, K., Natori, S., Mihashi, K., Nishi, M., 1983. Carbon-13 nuclear magnetic resonance spectra of pterosin-sesquiterpenes and related indan-1-one derivatives. Chem. Pharm. Bull. (Tokyo). 31, 3113–3128.

Galpin, O.P., Whitaker, C.J., Whitaker, R., Kassab, J.Y., 1990. Gastric cancer in Gwynedd. Possible links with bracken. Br. J. Cancer 61, 737–740.

Ge, X., Ye, G., Li, P., Tang, W.-J., Gao, J.-L., Zhao, W.-M., 2008. Cytotoxic diterpenoids and sesquiterpenoids from *Pteris multifida*. J. Nat. Prod. 71, 227–231.

German, D.P., Weintraub, M.N., Grandy, A.S., Lauber, C.L., Rinkes, Z.L., Allison, S.D., 2011. Optimization of hydrolytic and oxidative enzyme methods for ecosystem studies. Soil Biol. Biochem. 43, 1387–1397.

Gil da Costa, R.M., Bastos, M.M.S.M., Oliveira, P. a, Lopes, C., 2012. Bracken-associated

human and animal health hazards: chemical, biological and pathological evidence. J. Hazard. Mater. 203-204, 1–12.

Guarrera, P.M., Salerno, G., Caneva, G., 2005. Folk phytotherapeutical plants from Maratea area (Basilicata, Italy). J. Ethnopharmacol. 99, 367–378.

Hayashi, Y., Nishizawa, M., Harita, S., Sakan, T., 1972. Structures and syntheses of hypolepin A, B and C, sesquiterpenes from *Hypolepis Punctata* Mett. Chem. Lett. 375–378.

Hikino, H., Miyase, T., Takemoto, T., 1976. Biosynthesis of pteroside B in *Pteridium aquilinum* var. *Latiusculum*, proof of the sesquiterpenoid origin of the pterosides. Phytochemistry (Elsevier) 15, 121–123.

Hikino, H., Takahashi, T., Arihara, S., Takemoto, T., 1970. Structure of pteroside B, glycoside of *pteridium aquilinum* var. *latiusculum*. Chem. Pharm. Bull. (Tokyo). 18, 1488–1489.

Hikino, H., Takahashi, T., Takemoto, T., 1972. Structure of pteroside A and C, glycosides of Pteridium aquilinum var. latiusculum. Chem. Pharm. Bull. (Tokyo). 20, 210–212.

Hikino, H., Takahashi, T., Takemoto, T., 1971. Structure of pteroside Z and D, glycosides of *Pteridium aquilinum* var. *latiusculum*. Chem. Pharm. Bull. (Tokyo). 19, 2424–2425.

Hirono, I., 1986. Carcinogenic principles isolated from bracken fern. Crit. Rev. Toxicol. 17, 1–22.

Hirono, I., Aiso, S., Hosaka, S., Yamaji, T., Haga, M., 1983. Induction of mammary cancer in CD rats fed bracken diet. Carcinogenesis 4, 885–887.

Hirono, I., Aiso, S., Yamaji, T., Mori, H., Yamada, K., Niwa, H., Ojika, M., Wakamatsu, K., Kigoshi, H., Niiyama, K., 1984a. Carcinogenicity in rats of ptaquiloside isolated from bracken. Gan 75, 833–836.

Hirono, I., Shibuya, C., Shimizu, M., Fushimi, K., 1972. Carcinogenic activity of processed bracken used as human food. J Natl Cancer Inst 48, 1245–1250.

Hirono, I., Yamada, K., Niwa, H., Shizuri, Y., Ojika, M., Hosaka, S., Yamaji, T., Wakamatsu, K., Kigoshi, H., Niiyama, K., Uosaki, Y., 1984b. Separation of carcinogenic fraction of bracken fern. Cancer Lett. 21, 239–246.

Hopkins, A., 1990. Bracken (*Pteridium aquilinum*): Its distribution and animal health

implications. Br. Vet. J. 146, 316–326.

Hsu, F.-L., Huang, C.-F., Chen, Y.-W., Yen, Y.-P., Wu, C.-T., Uang, B.-J., Yang, R.-S., Liu, S.-H., 2013. Antidiabetic Effects of Pterosin A, a Small-Molecular-Weight Natural Product, on Diabetic Mouse Models. Diabetes 62, 628–638.

Hsu, F.-L., Liu, S.-H., Uang, B.-J., 2014. Use of pterosin compounds for treating diabetes and obesity. U.S. Patent 8633252 B2.

Jensen, P.H., Jacobsen, O.S., Hansen, H.C.B., Juhler, R.K., 2008. Quantification of ptaquiloside and pterosin B in soil and groundwater using liquid chromatography-tandem mass spectrometry (LC-MS/MS). J. Agric. Food Chem. 56, 9848–9854.

Jermy, A., Arnold, H., Farrell, L., Perring, F., 1978. Atlas of ferns of the British Isles. Botanical Society of the British Isles and British Pteridological Society, London.

Jones, C.G., Firn, R.D., 1978. The role of phytoecdysteroids in bracken fern, *Pteridium aquilinum* (L.) Kuhn as a defense against phytophagous insect attack. J. Chem. Ecol. 4, 117–138.

Kaplanis, J.N., Thompson, M.J., Robbins, W.E., Bryce, B.M., 1967. Insect hormones: Alpha ecdysone and 20-hydroxyecdysone in bracken fern. Science (80-.). 157, 1436–1438.

Kellett, G.L., Brot-Laroche, E., 2005. Apical GLUT2: A Major Pathway of Intestinal Sugar Absorption. Diabetes 54, 3056–3062.

Kigoshi, H., Sawada, A., Imamura, Y., Niwa, H., Yamada, K., 1989. Ptaquilosin, the aglycone of a bracken carcinogen ptaquiloside: Chemical derivation from ptaquiloside and the reactivity. Tetrahedron 45, 2551–2556.

Kobayashi, A., Egawa, H., Koshimizu, K., Mitsui, T., 1975. Antimicrobial constituents in *Pteris inaequalis* bak. Agric. Biol. Chem. 39, 1851–1856.

Kobayashi, A., Koshimizu, K., 1980. Cytotoxic effects of bracken fern constituents, pterosins, on sea urchin embryos and a ciliate. Agric. Biol. Chem. 44, 393–398.

Konečný, K., Streibl, M., Vašíčková, S., Buděšínský, M., Šaman, D., Ubik, K., Herout, V., 1985. Constituents of the liverwort *Bazzania trilobata* of Czech origin. Collect. Czechoslov. Chem. Commun. 50, 80–93.

Kovganko, N. V., Kashkan, Z.N., Krivenok, S.N., 2004. Bioactive compounds of the flora of Belarus. 4. Pterosins A and B from *Pteridium aquilinum*. Chem. Nat. Compd. 40, 227–

229.

Kuraishi, T., Murakami, T., Taniguchi, T., Kobuki, Y., Maehashi, H., Tanaka, N., Saiki, Y., Chen, C., 1985. Chemical and chemotaxonomical studies of ferns. LIV. Pterosin derivatives of the genus *Microlepia* (Pteridaceae). Chem. Pharm. Bull. (Tokyo). 33, 2305–2312.

Kuroyanagi, M., Fukuoka, M., Yoshihira, K., Natori, S., 1979a. Chemical and toxicological studies on bracken fern, *Pteridium aquilinum* var. *latiusculum.* III. Further characterization of pterosins and pterosides, sesquiterpenes and the glucosides having 1-indanone skeleton, from the rhizomes. Chem. Pharm. Bull. (Tokyo). 27, 592–601.

Kuroyanagi, M., Fukuoka, M., Yoshihira, K., Natori, S., 1979b. Circular dichroism and conformations of pterosins, 1-indanone derivatives from bracken. Chem. Pharm. Bull. (Tokyo). 27, 731–741.

Kuroyanagi, M., Fukuoka, M., Yoshihira, K., Natori, S., 1974a. Pterosin N and O, phenylacetylpterosin C,and pteroside P from bracken, *Pteridium aquilinum* var. *latiusculum.* Chem. Pharm. Bull. (Tokyo). 22, 2762–2764.

Kuroyanagi, M., Fukuoka, M., Yoshihira, K., Natori, S., 1974b. The Absolute Configurations of Pterosins, 1-Indanone Derivatives from Bracken, *Pteridium aquilinum var. latiusculum*. Chem. Pharm. Bull. (Tokyo). 22, 723–726.

Lee, Y.-P., Hsu, F.-L., Kang, J.-J., Chen, C.-K., Lee, S.-S., 2012. Metabolism of (2*S*)-pterosin A: identification of the phase I and phase II metabolites in rat urine. Drug Metab. Dispos. 40, 1566–1574.

Levandi, T., Püssa, T., Vaher, M., Ingver, A., Koppel, R., Kaljurand, M., 2014. Principal component analysis of HPLC–MS/MS patterns of wheat (*Triticum aestivum*) varieties. Proc. Est. Acad. Sci. 63, 86–92.

Liu, J., Shu, J., Zhang, R., Zhang, W., 2011. Two new pterosin dimers from *Pteris mutifida* Poir. Fitoterapia 82, 1181–1184.

Madeja, J., Harmata, K., Kolaczek, P., Karpinska-Kolaczek, M., Piatek, K., Naks, P., 2009. Bracken (*Pteridium aquilinum* (L.) Kuhn), Mistletoe (*Viscum album* (L.)) and Bladder-nut (*Staphylea pinnata* (L.))-Mysterious Plants with Unusual Applications. Cultural and Ethnobotanical Studies, in: Morel, J.-P., Mercuri, A.M. (Eds.), Plants and Cultural: Seeds of the Cultural Heritage of Europe. Edipuglia, pp. 207–215.

Marrs, R.H., Watt, a. S., 2006. Biological flora of the British Isles: *Pteridium aquilinum* (L.) Kuhn. J. Ecol. 94, 1272–1321.

McGlone, M.S., Wilmshurst, J.M., Leach, H.M., 2005. An ecological and historical review of bracken (*Pteridium esculentum*) in New Zealand, and its cultural significance. N. Z. J. Ecol. 29, 165–184.

McKee, T.C., II, J.H.C., Riccio, R., D'Auria, M.V., Iorizzi, M., Minale, L., Moran, R.A., Gulakowski, R.J., McMahon, J.B., 1994. HIV-inhibitory natural products. 11. Comparative studies of sulfated sterols from marine invertebrates. J. Med. Chem. 37, 793–797.

Miao, J., Charalambous, P., Kirz, J., Sayre, D., 1999. Extending the methodology of X-ray crystallography to allow imaging of micrometre-sized non-crystalline specimens. Nature 400, 342–344.

Murakami, T., Haruka, M., Nobutoshi, T., Satake, T., Kuraishi, T., Komazawa, Y., Saiki, Y., Chen, C., 1985. Chemical and chemotaxonomical studies on filices. LV. Studies on the constituents of several species of *Pteris*. Yakugaku Zasshi 640–648.

Murakami, T., Satake, T., Ninomiya, K., Iida, H., Yamauchi, K., Tanaka, N., Saiki, Y., Chen, C.-M., 1980. Pterosin-derivate aus der familie pteridaceae. Phytochemistry (Elsevier) 19, 1743–1746.

Murakami, T., Taguchi, S., Chen, C., 1976. Chemische untersuchungen der inhaltsstoffe von *Hypolepis punctata* (THUNB.) METT. Chem. Pharm. Bull. 24, 2241–2243.

Murakami, T., Tanaka, N., Tanaka, K., Chen, C.M., 1974. Pterosin Q und Pterosid Q aus *Pteris oshimensis* Hieron, und *Histiopteris incisa* (Thunb.) J. smith. Chem. Pharm. Bull. (Tokyo). 22, 2758–2761.

Nambudiry, M.E.N., Rao, G.S.K., 1974. Studies in terpenoids. Part XXX. Synthesis of pterosin E, a sesquiter-penoid from bracken. J. Chem. Soc. Perkin Trans. 1 317–319.

Neeson, S.J., Stevenson, P.J., 1988. Rhodium catalysed [2+2+2] cycloadditions- An efficient regiospecific route to calomelanolactone. Tetrahedron Lett. 29, 813–814.

Ng, K.-M.E., McMorris, T.C., 1984. An efficient synthesis of pterosin C and other pterosins. Can. J. Chem. 62, 1945–1953.

Niwa, H., Ojika, M., Wakamatsu, K., Yamada, K., Hirono, I., Matsushita, K., 1983. Ptaquiloside, a novel norsesquiterpene glucoside from bracken, var. Tetrahedron Lett.

24, 4117–4120.

Nugroho, A.E., Morita, H., 2014. Circular dichroism calculation for natural products. J. Nat. Med. 68, 1–10.

O'Driscoll, C., Ramwell, C., Harhen, B., Morrison, L., Clauson-Kaas, F., Hansen, H.C.B., Campbell, G., Sheahan, J., Misstear, B., Xiao, L., 2016. Ptaquiloside in Irish bracken ferns and receiving waters, with implications for land managers. Molecules 21, 543 (1–16).

Oelrichs, P.B., Ng, J.C., Bartley, J., 1995. Purification of ptaquiloside, a carcinogen from *Pteridium aquilinum*. Phytochemistry 40, 53–56.

Ojika, M., Kigoshi, H., Kuyama, H., Niua, H., Yamada, K., 1985. Studies on *Pteridium aquilinum* var. *latiusculum*, IV. Isolation of Three p-Hydroxystyrene Glycosides and an Efficient Method for the Isolation of Ptaquiloside, an Unstable Bracken Carcinogen. J. Nat. Prod. 48, 634–637.

Ojika, M., Wakamatsu, K., Niwa, H., Yamada, K., 1987. Ptaquilpside, a potent carcinogen isolated from *pteridium aquilinum* var. *latiusculum*: structure elucidation based on chemical and spectral evidence, and reactions with amino acids, nucleosides, and nucleotides. Tetrahedron 43, 5261–5274.

Oliveira, R.M.G.D.C., 2012. Studies on the biopathological actions of *pteridium aquilinum*. University of Porto, Instituto de Ciências Biomédicas Abel Salazar, 1-184.

Ouyang, D.-W., Ni, X., Xu, H.-Y., Chen, J., Yang, P.-M., Kong, D.-Y., 2010. Pterosins from *Pteris multifida*. Planta Med. 76, 1896–1900.

Ovesen, R.G., Rasmussen, L.H., Hansen, H.C.B., 2008. Degradation kinetics of ptaquiloside in soil and soil solution. Environ. Toxicol. Chem. 27, 252–259.

Padwa, A., Curtis, E.A., Sandanayaka, V.P., 1996. Generation and cycloaddition behavior of spirocyclic carbonyl ylides. Application to the synthesis of the pterosin family of sesquiterpenes †. J. Org. Chem. 61, 73–81.

Page, C.N., 1976. The taxonomy and phytogeography of bracken-a review. Bot. J. Linn. Soc. 73, 1–34.

Page, C.N., Mill, R.R., 1995. The taxa of Scottish bracken in a European perspective. Bot. J. Scotl. 47, 229–247.

Pakeman, R., Marrs, R., Howard, D., Barr, C., Fuller, R., 1996. The bracken problem in Great Britain: Its present extent and future changes. Appl. Geogr. 16, 65–86.

Palatinus, L., Chapuis, G., 2007. *SUPERFLIP* – a computer program for the solution of crystal structures by charge flipping in arbitrary dimensions. J. Appl. Crystallogr. 40, 786–790.

Pamukcu, A.M., ErtUrk, E., Yalciner, S., Milli, U., Bryan, G.T., 1978. Carcinogenic and mutagenic activities of milk from cows fed bracken fern (*Pteridium aquilinum*). Cancer Res. 38, 1556–1560.

Pearman, D., Corner, R.W.M., 2004. Altitudinal limits of British and Irish vascular plants, 2nd ed. Summerfield Books / BSBI, London, UK.

Pieroni, A., 2005. Gathering food form wild, in: Prance, G.T., Nesbitt, M. (Eds.), The Cultural History of Plants. Routledge, New York, London, pp. 29–44.

Pitman, R.M., Webber, J., 2013. The character of composted bracken (*Pteridium aquilinum* L. Kuhn) and its potential as a peat replacement medium. Eur. J. Hortic. Sci. 78, 145–152.

Potter, D.M., Baird, M.S., 2000. Carcinogenic effects of ptaquiloside in bracken fern and related compounds. Br. J. Cancer 83, 914–920.

Potter, D.M., R.M. Pitman, 1994. Contributions to an international conference Bracken 94, University of Wales, Aberystwyth, in: Smith, R.T., Taylor, J.A. (Eds.), Bracken : An Environmental Issue. pp. 110–115.

Prakash, A.S., Pereira, T.N., Smith, B.L., Shaw, G., Seawright, A.A., 1996. Mechanism of bracken fern carcinogenesis: Evidence for H-ras activation via initial adenine alkylation by ptaquiloside. Nat. Toxins 4, 221–227.

Qu, J., Liang, Q., Liang, Q., Luo, G., Wang, Y., 2004. Screening and identification of glycosides in biological samples using energy-gradient neutral loss scan and liquid chromatography tandem mass spectrometry. Anal. Chem. 76, 2239–2247.

Rasmussen, L.H., 2003. Ptaquiloside - an environmental hazard? Occurrence and fate of a bracken (*Pteridium sp.*) toxin in terrestrial environments. PhD thesis, The Royal Veterinary and Agricultural University, Frederiksberg, Denmark, October 2003.

Rasmussen, L.H., Donnelly, E., Strobel, B.W., Holm, P.E., Hansen, H.C.B., 2015. Land management of bracken needs to account for bracken carcinogens-A case study from

Britain. J. Environ. Manage. 151, 258–266.

Rasmussen, L.H., Hansen, H.C.B., Lauren, D., 2005. Sorption, degradation and mobility of ptaquiloside, a carcinogenic Bracken (*Pteridium sp.*) constituent, in the soil environment. Chemosphere 58, 823–835.

Rasmussen, L.H., Jensen, L.S., Hansen, H.C.B., 2003a. Distribution of the carcinogenic terpene ptaquiloside in bracken fronds, rhizomes (*Pteridium aquilinum*), and litter in Denmark. J. Chem. Ecol. 29, 771–778.

Rasmussen, L.H., Kroghsbo, S., Frisvad, J.C., Hansen, H.C.B., 2003b. Occurrence of the carcinogenic bracken constituent ptaquiloside in fronds, topsoils and organic soil layers in Denmark. Chemosphere 51, 117–127.

Rasmussen, L.H., Schmidt, B., Sheffield, E., 2013. Ptaquiloside in bracken spores from Britain. Chemosphere 90, 2539–2541.

Robinson, R.C., 2009. Invasive and problem ferns: A european perspective. Int. Urban Ecol. Rev. 4, 83–91.

Rymer, L., 1976. The history and ethnobotany of bracken. Bot. J. Linn. Soc. 73, 151–176.

Saito, K., Nagao, T., Matoba, M., Koyama, K., 1989. Chemical assay of ptaquiloside, the carcinogen of *pteridium aquilinum*, and the distribution of related compounds in the pteridaceae. Phytochemistry 28, 1605–1611.

Saito, K., Nagao, T., Takatsuki, S., Koyama, K., Natori, S., 1990. The sesquiterpenoid carcinogen of bracken fern, and some analogues, from the pteridaceae. Phytochemistry 29, 1475–1479.

Saito, M., Umeda, M., Enomoto, M., Hatanaka, Y., Natori, S., Yoshihira, K., Fukuoka, M., Kuroyanagi, M., 1976. The role of pterosins and pterosides in bracken toxicity. Food Cosmet. Toxicol. 14, 514.

Saito, M., Umeda, M., Enomoto, M., Hatanaka, Y., Natori, S., Yoshihira, K., Fukuoka, M., Kuroyanagi, M., 1975. Cytotoxicity and carcinogenicity of pterosins and pterosides, 1-indanone derivatives from bracken (*Pteridium aquilinum*). Experientia 31, 829–831.

Sanderson, H., Prendergast, H.D.V., 2002. Commercial uses of wild and traditionally managed plants in England and Scotland, Centre for Economic Botany, Royal Botanic Gardens. Kew, pp. 53-56.

Satake, T., Murakami, T., Saiki, Y., Chen, C., Gomez P., L.D., 1984. Chemical and chemotaxonomical studies on filices. LI. Chemical studies on the constituents of Costa Rican ferns. Chem. Pharm. Bull. (Tokyo). 32, 4620–4624.

Scholz, K., Dekant, W., Völkel, W., Pähler, A., 2005. Rapid detection and identification of *N*-acetyl-*L*-cysteine thioethers using constant neutral loss and theoretical multiple reaction monitoring combined with enhanced product-ion scans on a linear ion trap mass spectrometer. J. Am. Soc. Mass Spectrom. 16, 1976–1984.

Sengupta, P., Sen, M., Kumar Niyogi, S., Chandra Pakrashi, S., Ali, E., 1976. Isolation and structure of wallichoside, a novel pteroside from *Pteris wallichiana*. Phytochemistry (Elsevier) 15, 995–998.

Shahin, M., Smith, B.L., Prakash, A.S., 1999. Bracken carcinogens in the human diet. Mutat. Res. Toxicol. Environ. Mutagen. 443, 69–79.

Sheldrick, G.M., 2008. A short history of *SHELX*. Acta Crystallogr. A. 64, 112–122.

Sheridan, H., Frankish, N., Farrell, R., 1999. Smooth muscle relaxant activity of pterosin Z and related compounds. Planta Med. 65, 271–272.

Sheridan, H., Lemon, S., Frankish, N., McArdle, P., Higgins, T., James, J., Bhandari, P., 1990. Synthesis and antispasmodic activity of nature identical substituted indanes and analogues. Eur. J. Med. Chem. 25, 603–608.

Sheridan, H., Walsh, J.J., Jordan, M., Cogan, C., Frankish, N., 2009. A series of 1, 2-coupled indane dimers with mast cell stabilisation and smooth muscle relaxation properties. Eur. J. Med. Chem. 44, 5018–5022.

Skujiņš, J., Burns, R.G., 1976. Extracellular enzymes in soil. CRC Crit. Rev. Microbiol. 4, 383–421.

Smith, B.L., Seawright, A.A., 1995. Bracken fern (*Pteridium spp.*) carcinogenicity and human health—a brief review. Nat. Toxins 3, 1–5.

Smith, B.L., Seawright, A.A., Ng, J.C., Hertle, A.T., Thomson, J.A., Bostock, P.D., 1994. Concentration of ptaquiloside, a major carcinogen in bracken fern (*Pteridium spp.*), from eastern australia and from a cultivated worldwide collection held in Sydney, Australia. Nat. Toxins 2, 347–353.

Somvanshi, R., Lauren, D.R., Smith, B.L., Dawra, R.K., Sharma, O.P., Sharm, V.K., Singh, A.K., Gangwar, N.K., 2006. Estimation of the fern toxin, ptaquiloside, in certain Indian

ferns other than bracken. Curr. Sci. 91, 1547–1552.

Suzuki, S., Murayama, T., Shiono, Y., 2006. Echinolactones C and D: Two illudalane sesquiterpenoids isolated from the cultured mycelia of the fungus Echinodontium japonicum. Zeitschrift für Naturforsch. B 61, 1295–1298.

Tanaka, J., Adachi, K., 1990. Studies on aromatic sesquiterpenes. XII. Synthesis of (±)-*cis*-5-hydroxycalamenene. Bull. Chem. Soc. Jpn. 63, 272–274.

Tanaka, J., Adachi, K., 1989. Studies on aromatic sesquiterpenes. X. Synthesis of 5-hydroxyisocalamenene and its naphthalene derivatives. Nippon Kagaku Kaishi 268–274.

Tanaka, N., Satake, T., Takahashi, A., Mochizuki, M., Murakami, T., Saiki, Y., Yang, J., Chen, C., 1982. Chemical and chemotaxonomical studies of ferns. XXXIX. Chemical studies on the constituents of *Pteris bella* Tagawa and *Pteridium aquilinum* subsp. *wightianum* (Wall) Shich. Chem. Pharm. Bull. (Tokyo). 30, 3640–3646.

Thomson, J.A., 2008. Morphotype and conflicting taxonomies in *Pteridium* (Dennstaedtiaceae : Pteridophyta). Fern Gaz. 18, 101–109.

Thomson, J.A., Alonso-Amelot, M.E., 2002. Clarification of the taxonomic status and relationships of *Pteridium caudatum* (Dennstaedtiaceae) in Central and South America. Bot. J. Linn. Soc. 140, 237–248.

Thoss, V., Murphy, P.J., Marriott, R., Wilson, T., 2012. Triacylglycerol composition of British bluebell (*Hyacinthoides non-scripta*) seed oil. RSC Adv. 2, 5314–5322.

Tourchi-Roudsari, M., 2014. Multiple Effects of Bracken Fern under *in vivo* and *in vitro* Conditions. Asian Pacific J. Cancer Prev. 15, 7505–7513.

Tryon, R.M.J., 1941. Revision of the genus pteridium. J. New Engl. Bot. Club 43, 1–30.

Tsumaki, N., Takemori, H., Fuchino, H., Nobuo, K., 2015. Pterosin derivative-containing therapeutic preparation for disease associated with cartilage loss, cartilage degeneration and/or cartilage thinning. U.S. Patent 20150051293 A1.

Uddin, S.J., Jason, T.L.H., Beattie, K.D., Grice, I.D., Tiralongo, E., 2011. (2*S*,3*S*)-sulfated pterosin C, a cytotoxic sesquiterpene from the Bangladeshi Mangrove fern *Acrostichum aureum*. J. Nat. Prod. 74, 2010–2013.

van der Hoeven, J.C.M., Lagerweij, W.J., Posthumus, M.A., van Veldhuizen, A., Holterman, H.A.J., 1983. Aquilide A, a new mutagenic compound isolated from bracken fern

(*Pteridium aquilinum* (L.) Kuhn). Carcinogenesis 4, 1587–1590.

Vetter, J., 2009. A biological hazard of our age: Bracken fern [*Pteridium aquilinum* (L.) Kuhn] - A review. Acta Vet. Hung. 57, 183–196.

Warnke, I., Furche, F., 2012. Circular dichroism: electronic. Wiley Interdisciplinary Reviews: Comput. Mol. Sci. 2, 150–166.

Wells, A.J. and McNally, R., 1989. Appraisal of the spatial association of bracken and cancer in England and Wales. *Bracken: An Environmental Issue*. University of Wales, Aberystwyth.

Wilson, D., Donaldson, L.J., Sepai, O., 1998. Should we be frightened of bracken? A review of the evidence. J. Epidemiol. Community Health 52, 812–817.

Wink, M., 2003. Evolution of secondary metabolites from an ecological and molecular phylogenetic perspective. Phytochemistry 64, 3–19.

Wright, J.E., Chamberlain, W.F., Barrett, C.C., 1971. Ovarian maturation in stable flies: Inhibition by 20-hydroxyecdysone. Science (80-.). 172, 1247–1248.

Wu, H.-H., Hsu, S.-C., Hsu, F.-L., Uang, B.-J., 2014. Asymmetric synthesis of (-)-pterosin N from a chiral 1,3-dioxolanone. European J. Org. Chem. 2014, 4351–4355.

Wynn, J.M., Small, J.L., Pakeman, R.J., Sheffield, E., 2000. An assessment of genetic and environmental effects on sporangial development in bracken [*Pteridium aquilinum*, (L.) Kuhn] using a novel quantitative method. Ann. Bot. 85, 113–115.

Yahara, Y., Takemori, H., Okada, M., Kosai, A., Yamashita, A., Kobayashi, T., Fujita, K., Itoh, Y., Nakamura, M., Fuchino, H., Kawahara, N., Fukui, N., Watanabe, A., Kimura, T., Tsumaki, N., 2016. Pterosin B prevents chondrocyte hypertrophy and osteoarthritis in mice by inhibiting Sik3. Nat. Commun. 7, 1–12.

Yamada, K., Ojika, M., Kigoshi, H., 2007. Ptaquiloside, the major toxin of bracken, and related terpene glycosides: chemistry, biology and ecology. Nat. Prod. Rep. 24, 798–813.

Yoshihira, K., Fukuoka, M., Kuroyanagi, M., Natori, S., 1971. 1-Indanone derivatives from bracken, *Pteridium aquilinum* var. *latiusculum*. Chem. Pharm. Bull. (Tokyo). 19, 1491–1495.

Yoshihira, K., Fukuoka, M., Kuroyanagi, M., Natori, S., Umeda, M., Morohoshi, T.,

Enomoto, M., Saito, M., 1978. Chemical and toxicological studies on bracken fern, *Pteridium aquilinum* var. *latiusculum.* I. Introduction, extraction and fractionation of constituents, and toxicological studies including carcinogenicity tests. Chem. Pharm. Bull. (Tokyo). 26, 2346–2364.

Zhan, Z.-J., Ying, Y.-M., Zhang, F.-Y., Li, C.-P., Shan, W.-G., 2010. Three New Illudalane Sequiterpenoids from *Pteris semipinnata*. Helv. Chim. Acta 93, 550–554.

Appendices

Appendix I: NMR spectra of compounds **RH3 - RH38**.

1) NMR spectra of compound **RH3** in $CDCl_3$.

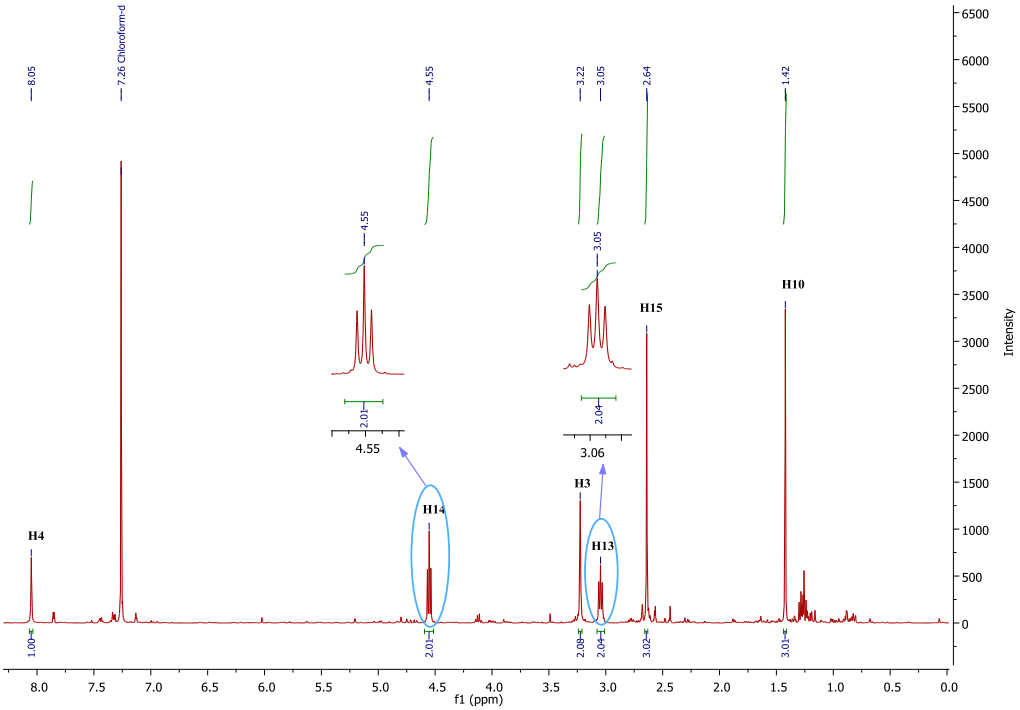

Figure A-1: ^1H NMR ($CDCl_3$, 400 MHz) spectrum of compound **RH3**.

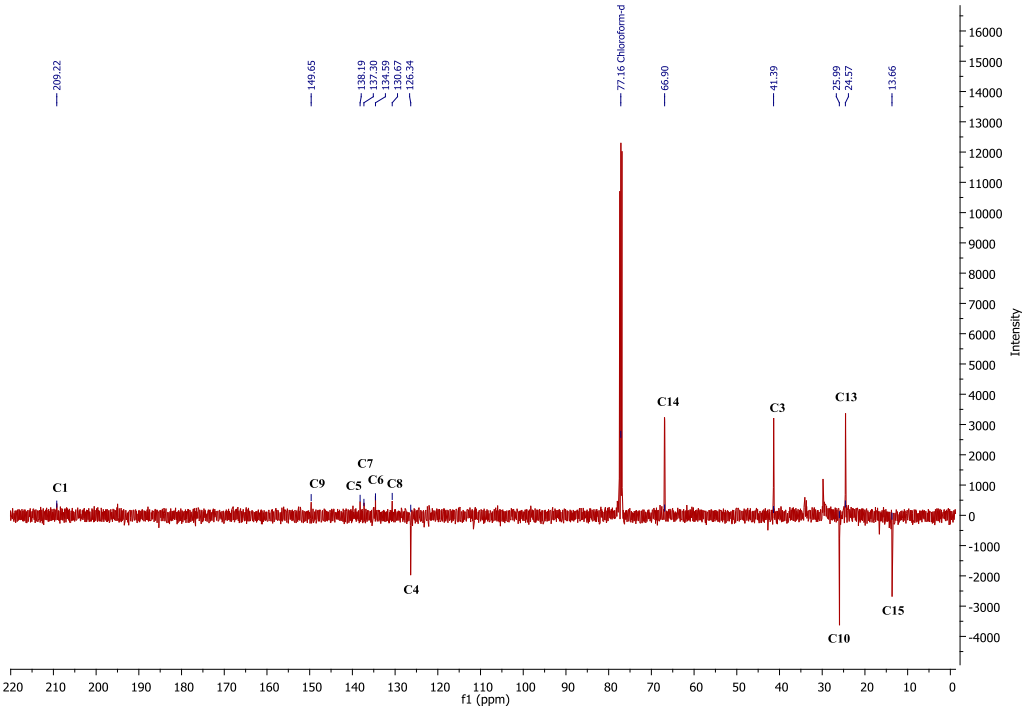

Figure A-2: DEPTQ NMR ($CDCl_3$, 100 MHz) spectrum of compound **RH3.**

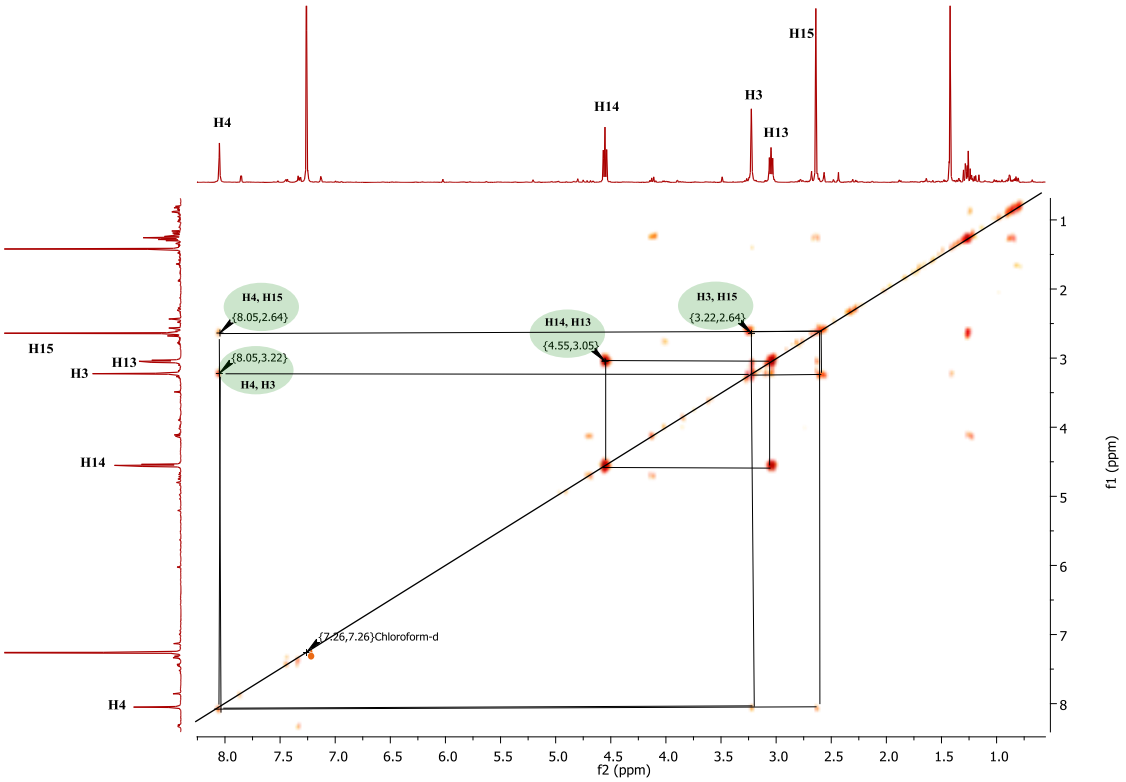

Figure A-3: ^{1}H-^{1}H COSY NMR ($CDCl_3$, 400 MHz) spectrum of compound **RH3**.

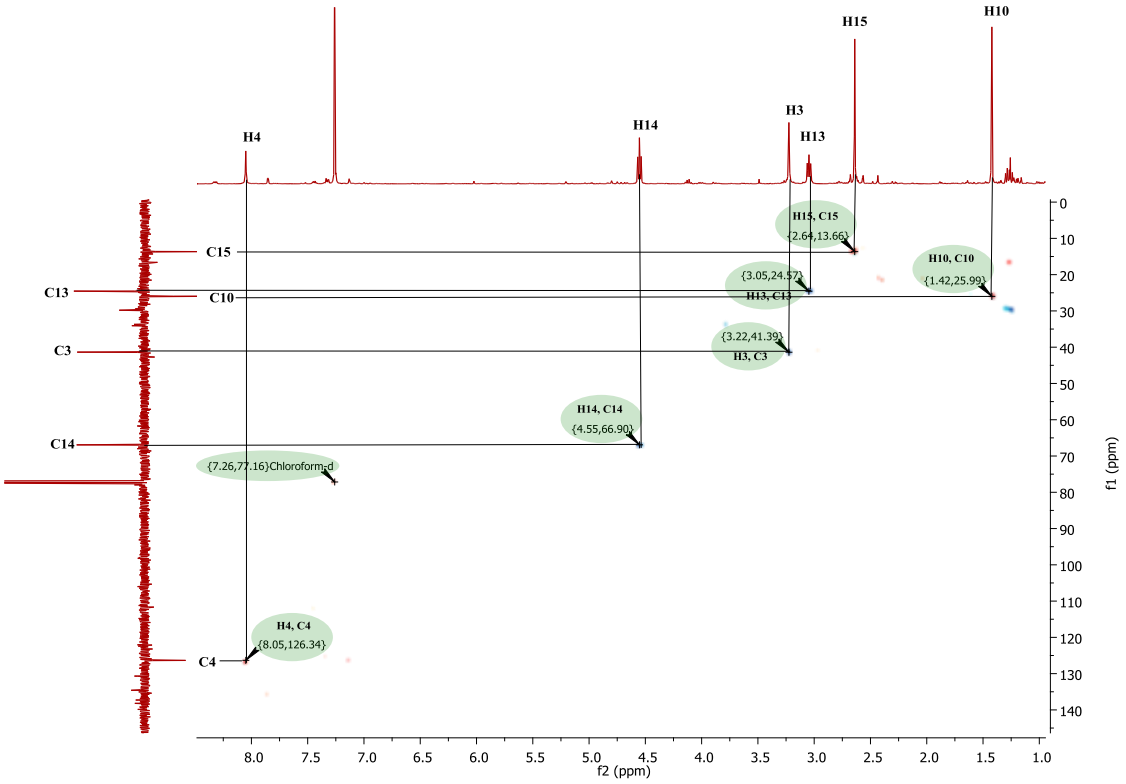

Figure A-4: ^{1}H-^{13}C HSQC NMR spectrum of compound **RH3** in $CDCl_3$.

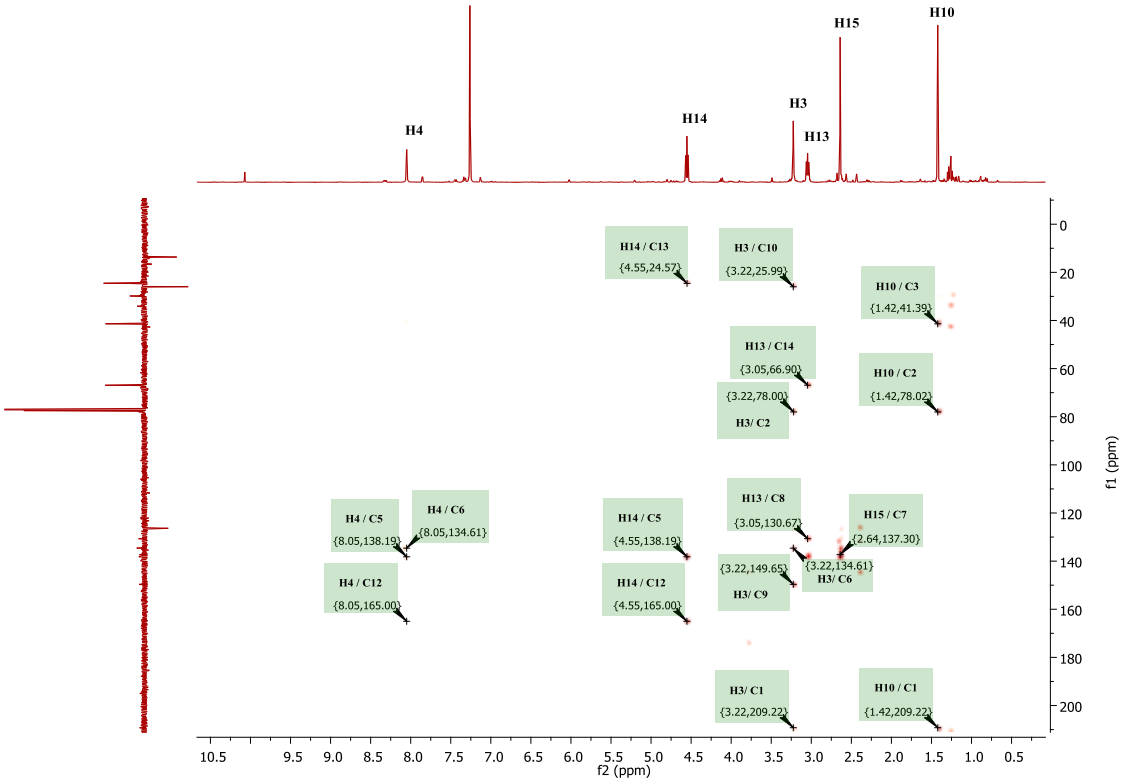

Figure A-5: ^{1}H-^{13}C HMBC NMR spectrum of compound **RH3** in $CDCl_3$.

2) NMR spectra of compound **RH4** in CD_3OD.

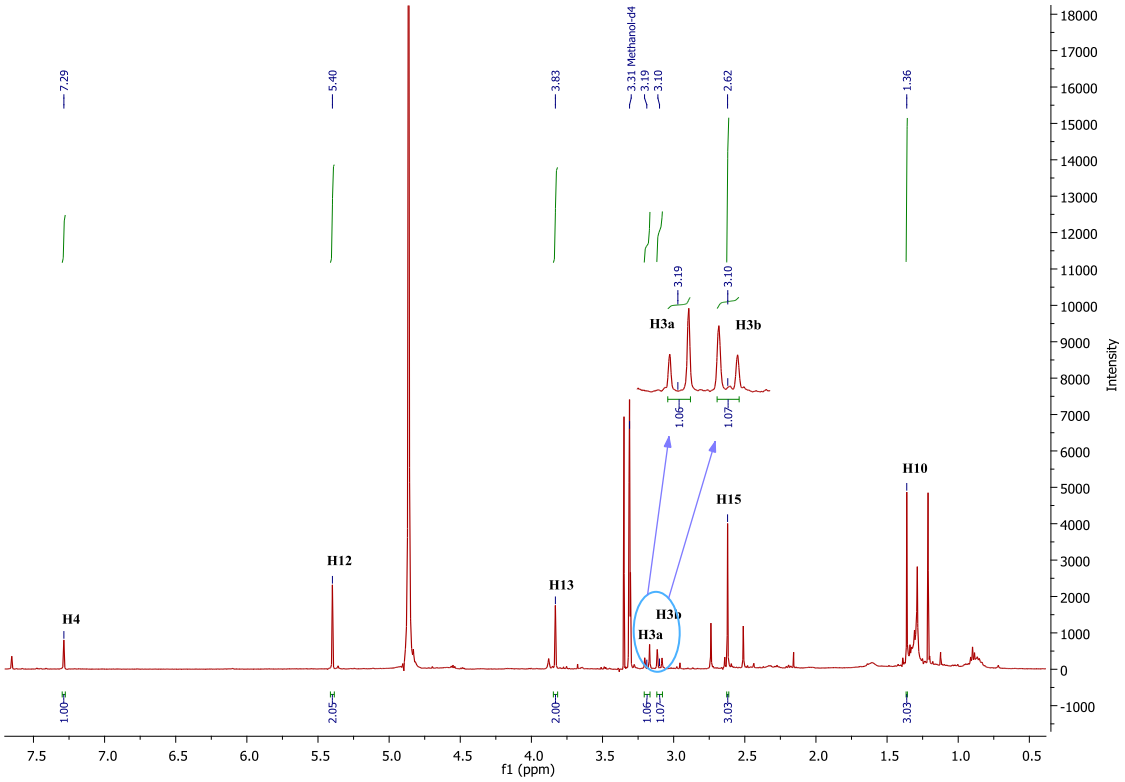

Figure A-6: ^{1}H NMR (CD_3OD, 400 MHz) spectrum of compound **RH4**.

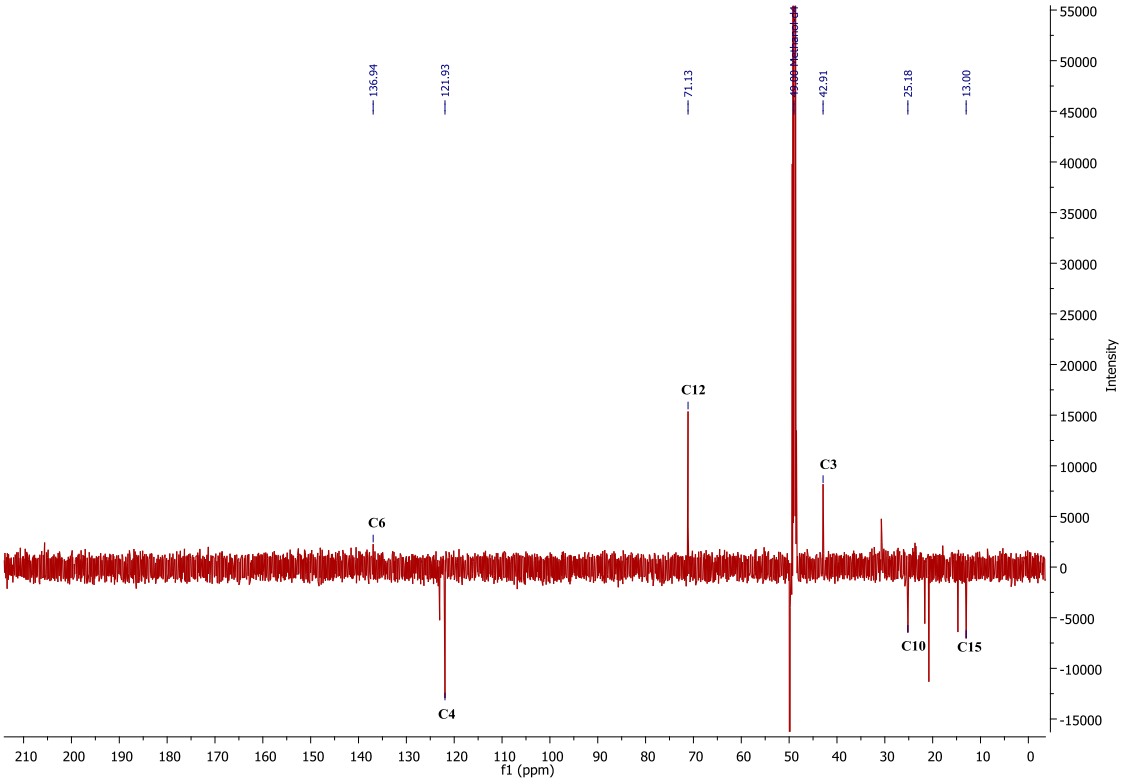

Figure A-7: DEPTQ NMR (CD_3OD, 100 MHz) spectrum of compound **RH4**.

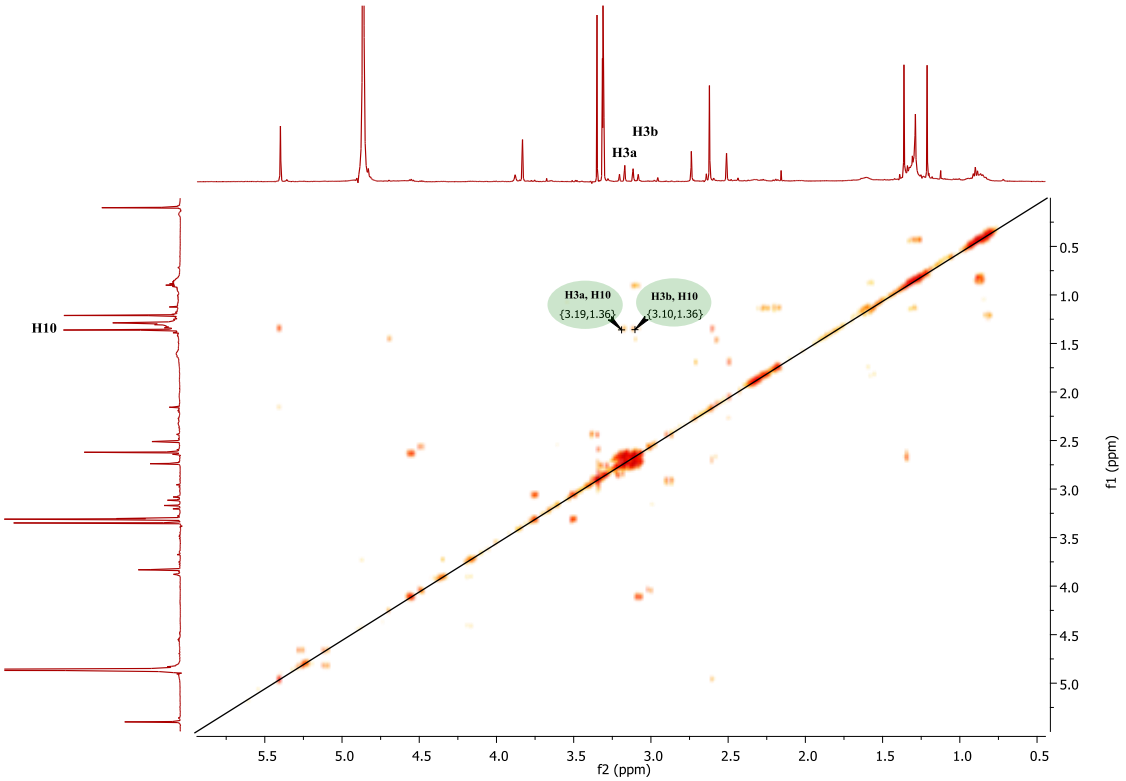

Figure A-8: ^1H-^1H COSY NMR (CD_3OD, 400 MHz) spectrum of compound **RH4**.

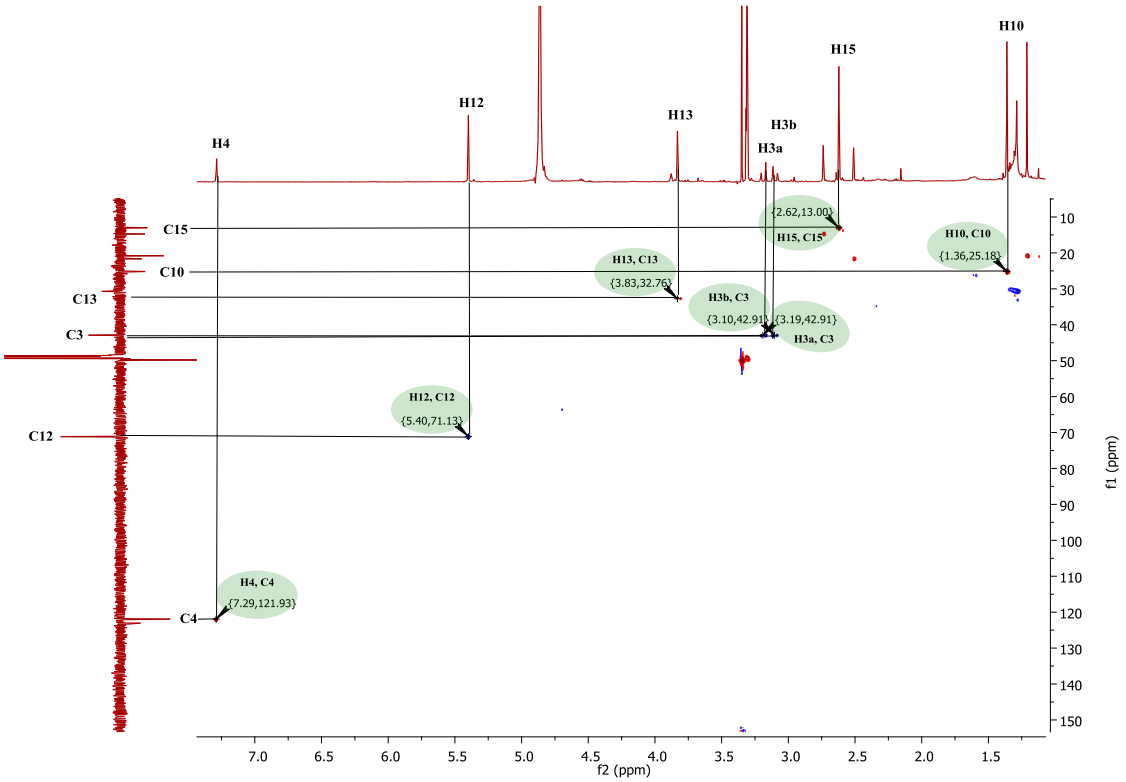

Figure A-9: ^{1}H-^{13}C HSQC NMR spectrum of compound **RH4** in CD_3OD.

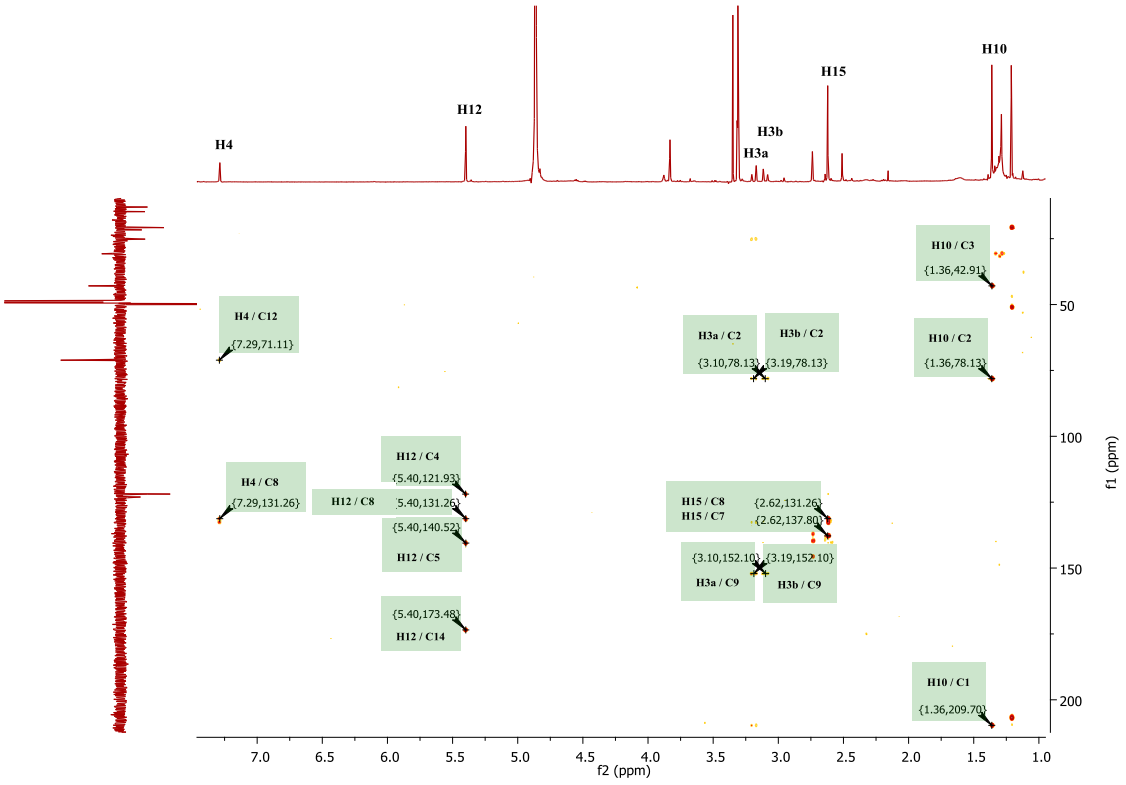

Figure A-10: ^{1}H-^{13}C HMBC NMR spectrum of compound **RH4** in CD_3OD.

3) NMR spectra of compound **RH5** in $CDCl_3$.

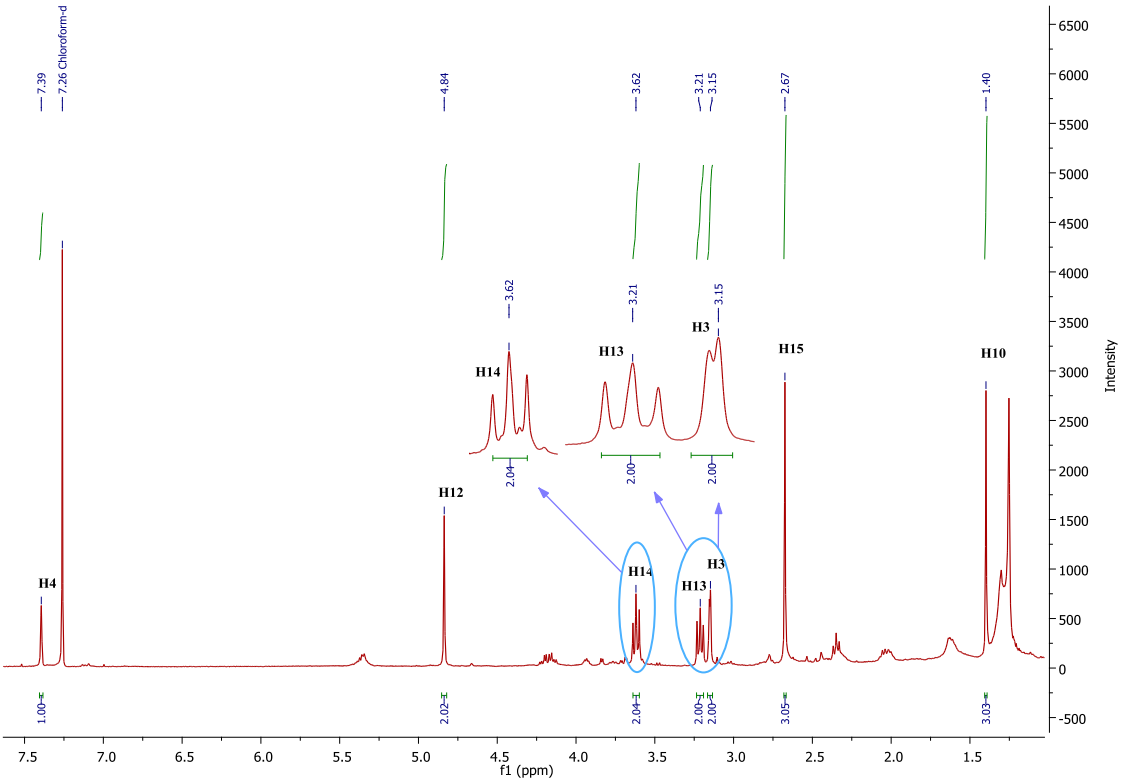

Figure A-11: ^{1}H NMR ($CDCl_3$, 400 MHz) spectrum of compound **RH5**.

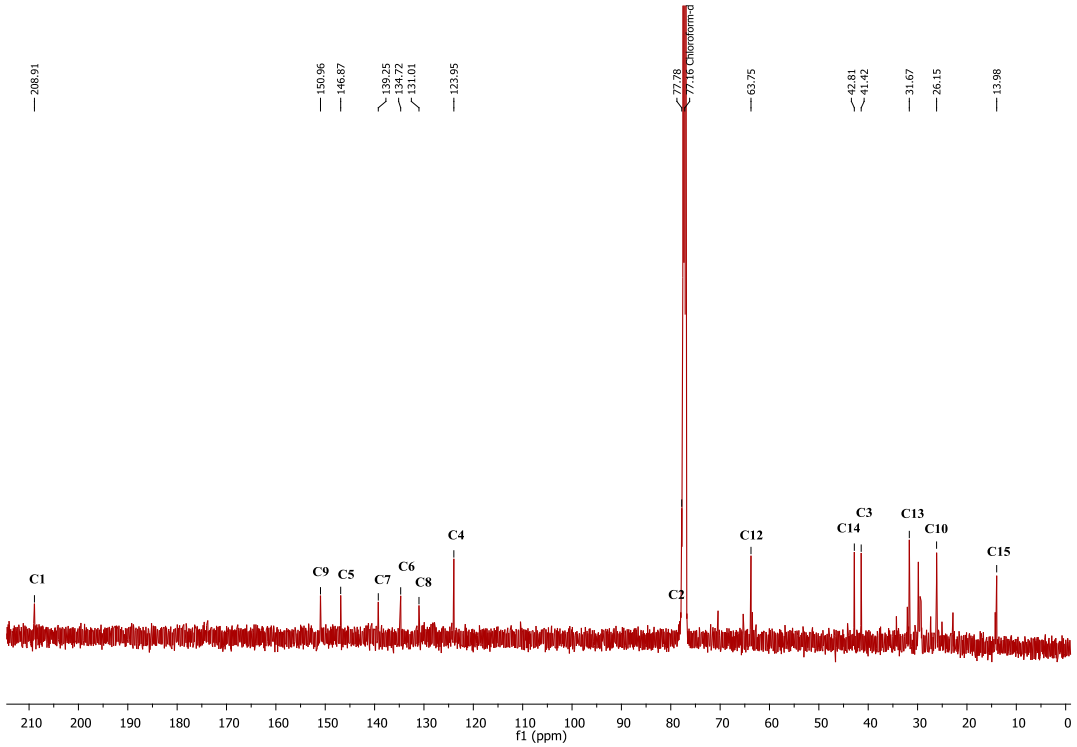

Figure A-12: ^{13}C NMR ($CDCl_3$, 100 MHz) spectrum of compound **RH5**.

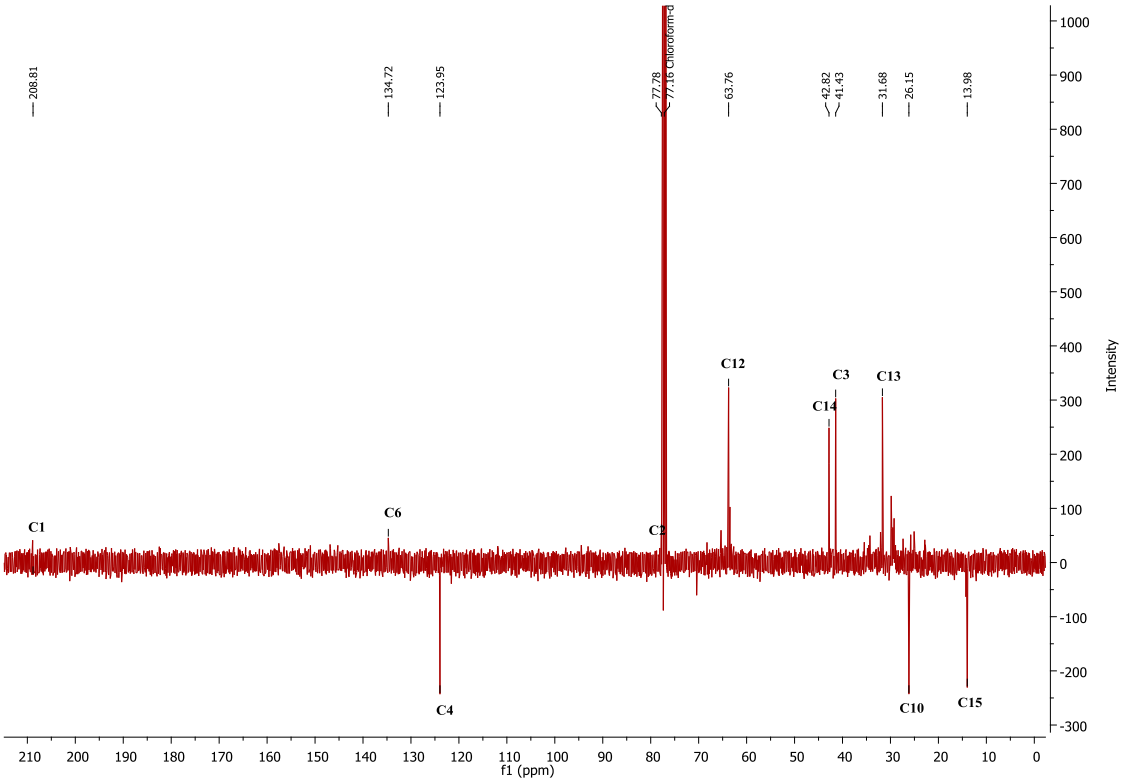

Figure A-13: DEPTQ NMR ($CDCl_3$, 100 MHz) spectrum of compound **RH5**.

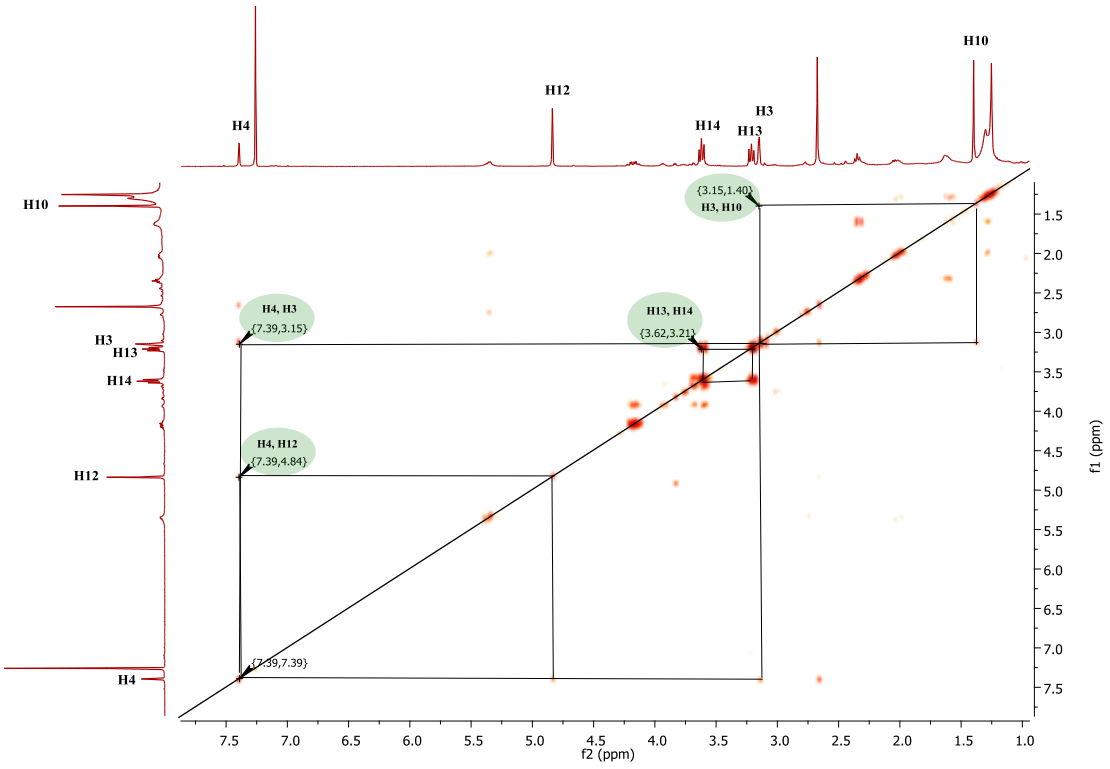

Figure A-14: ^{1}H-^{1}H COSY NMR ($CDCl_3$, 400 MHz) spectrum of compound **RH5**.

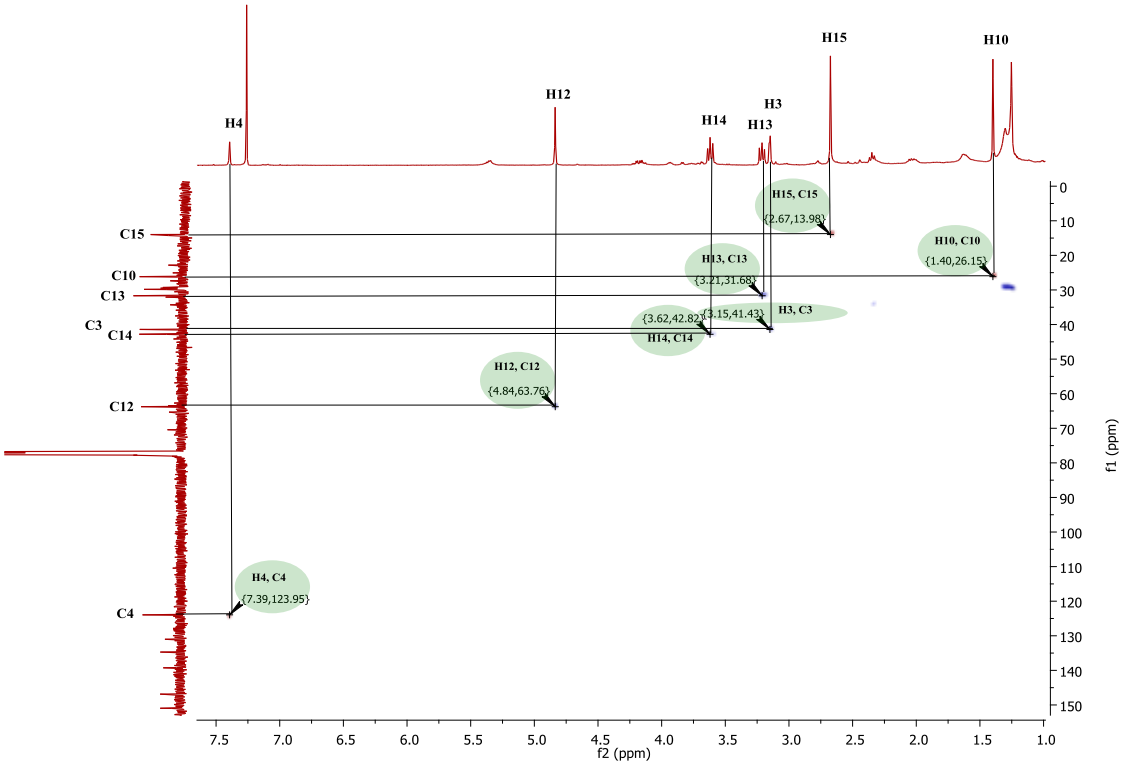

Figure A-15: ^{1}H-^{13}C HSQC NMR spectrum of compound **RH5** in $CDCl_3$.

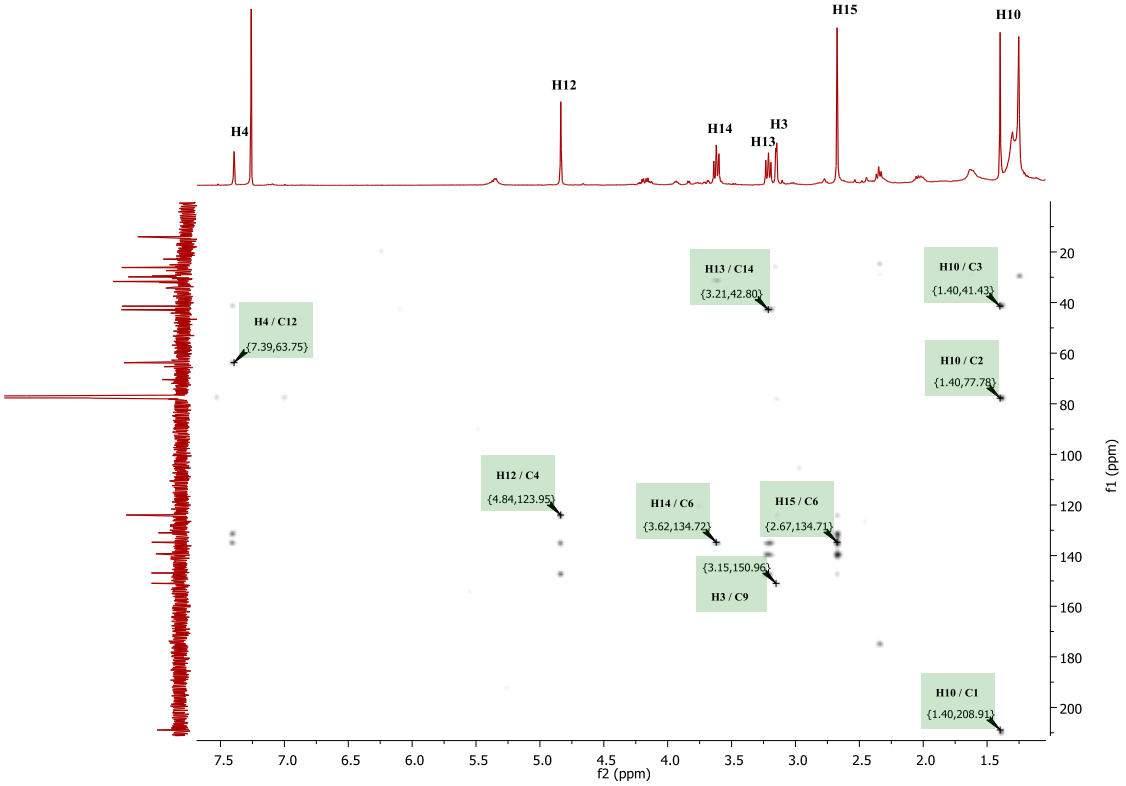

Figure A-16: ^{1}H-^{13}C HMBC NMR spectrum of compound **RH5** in $CDCl_3$.

4) NMR spectra of compound **RH6** in CD_3OD.

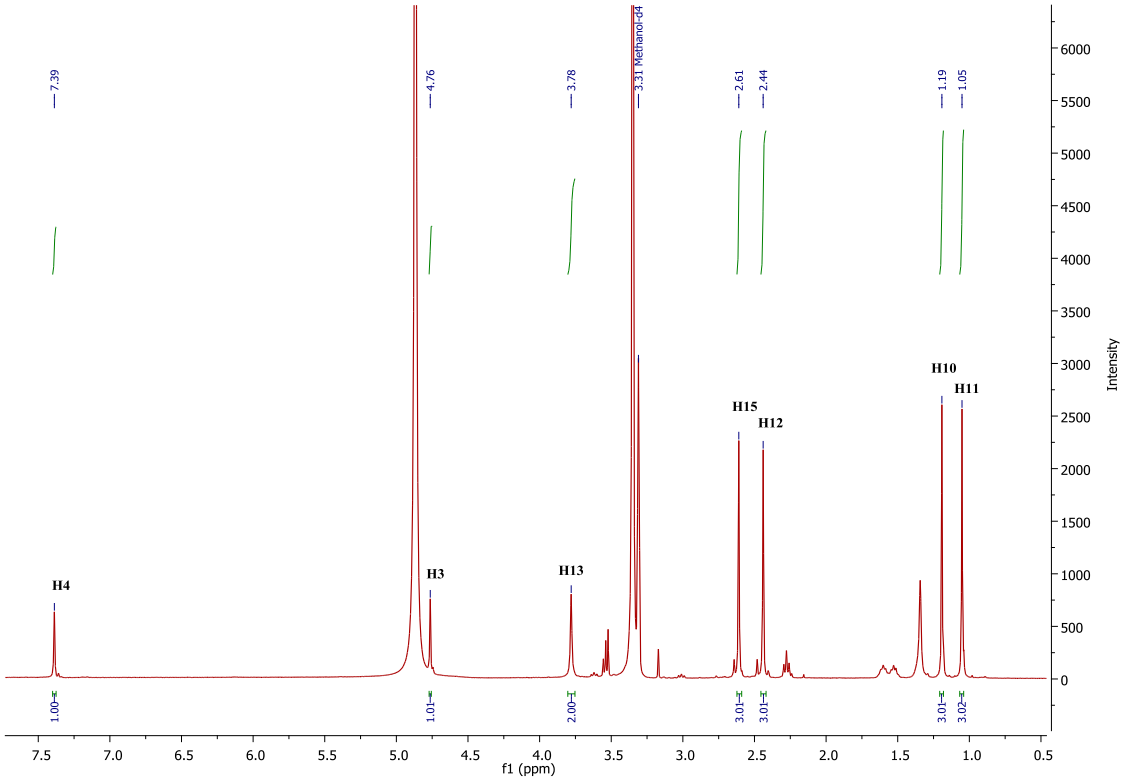

Figure A-17: ^1H NMR (CD_3OD, 400 MHz) spectrum of compound **RH6**.

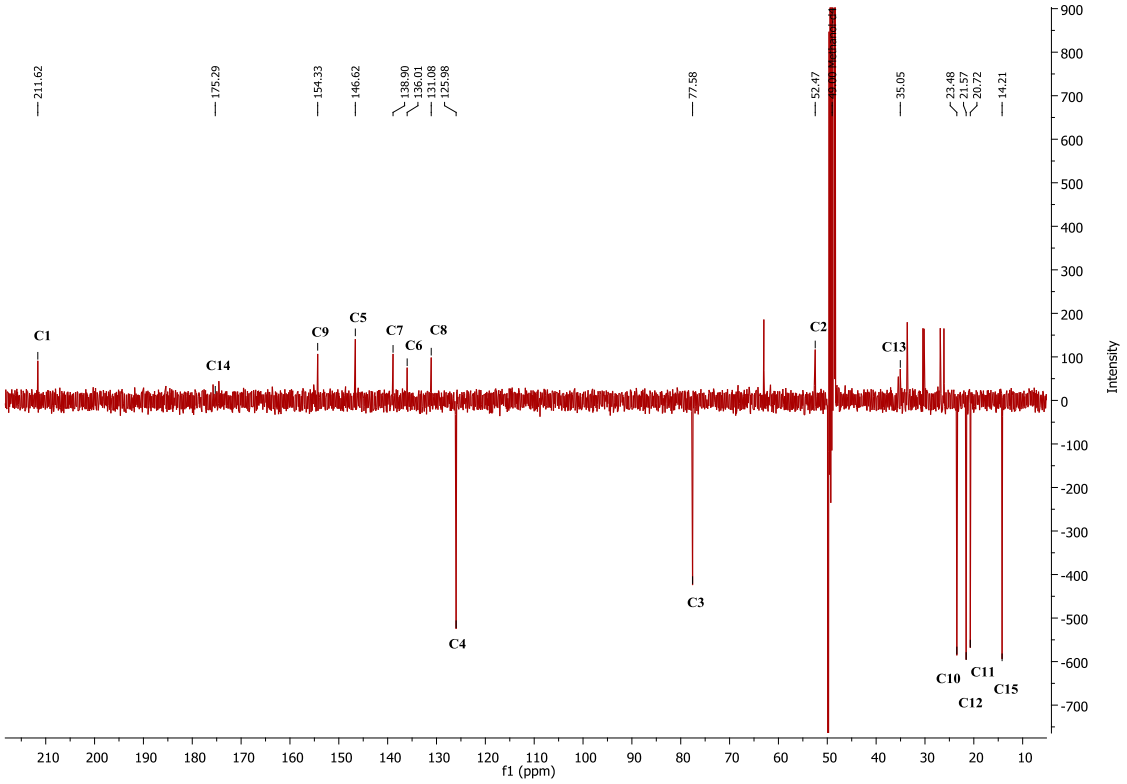

Figure A-18: DEPTQ NMR (CD_3OD, 100 MHz) spectrum of compound **RH6**.

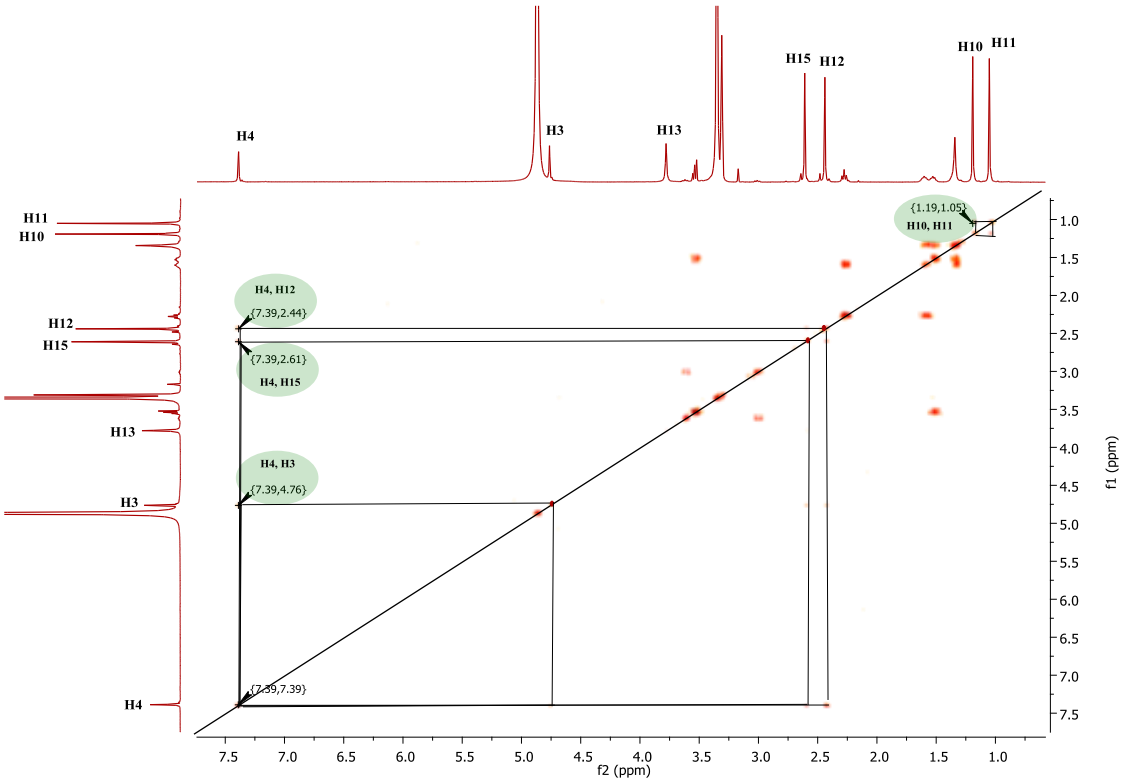

Figure A-19: ^{1}H-^{1}H COSY NMR (CD_3OD, 400 MHz) spectrum of compound **RH6**.

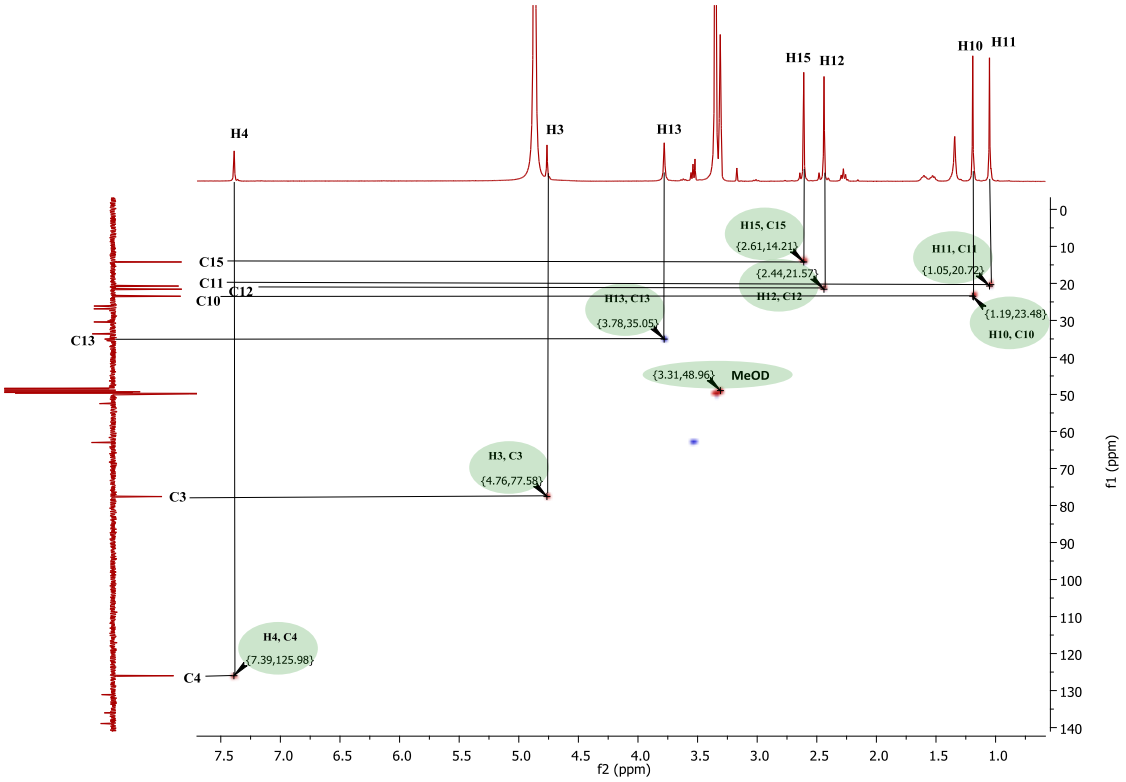

Figure A-20: ^{1}H-^{13}C HSQC NMR spectrum of compound **RH6** in CD_3OD.

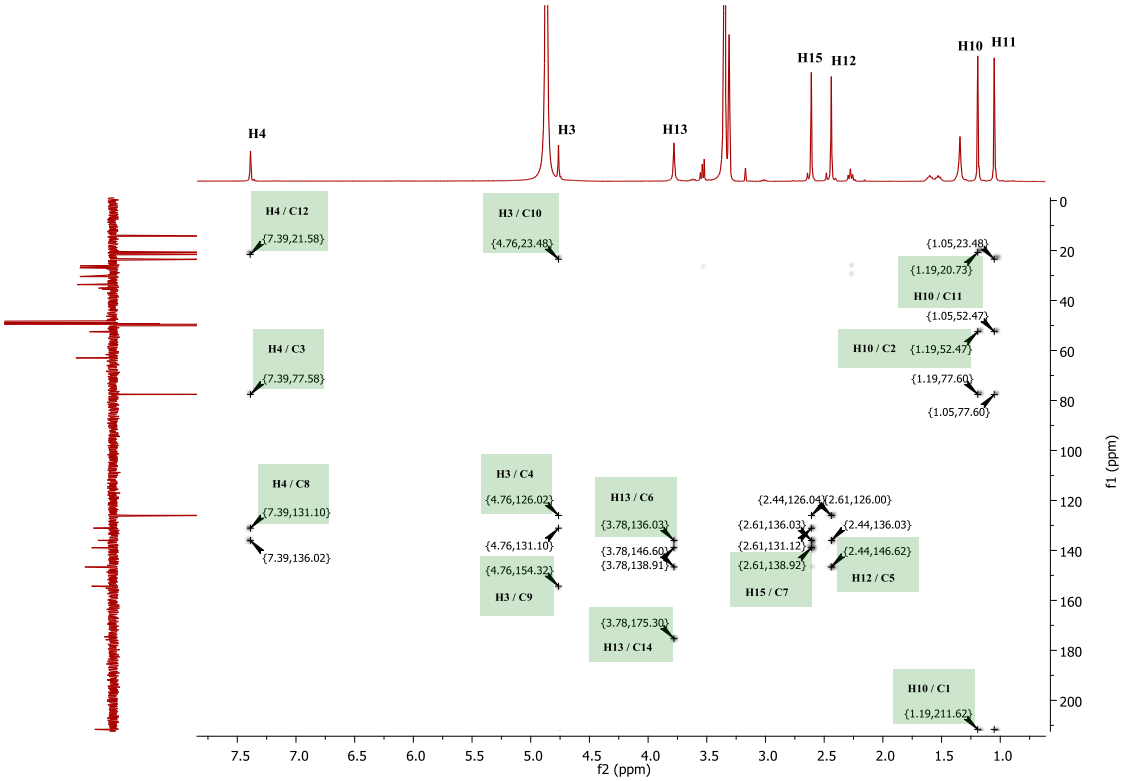

Figure A-21: ^{1}H-^{13}C HMBC NMR spectrum of compound **RH6** in CD_3OD.

5) NMR spectra of compound **RH7** in $CDCl_3$.

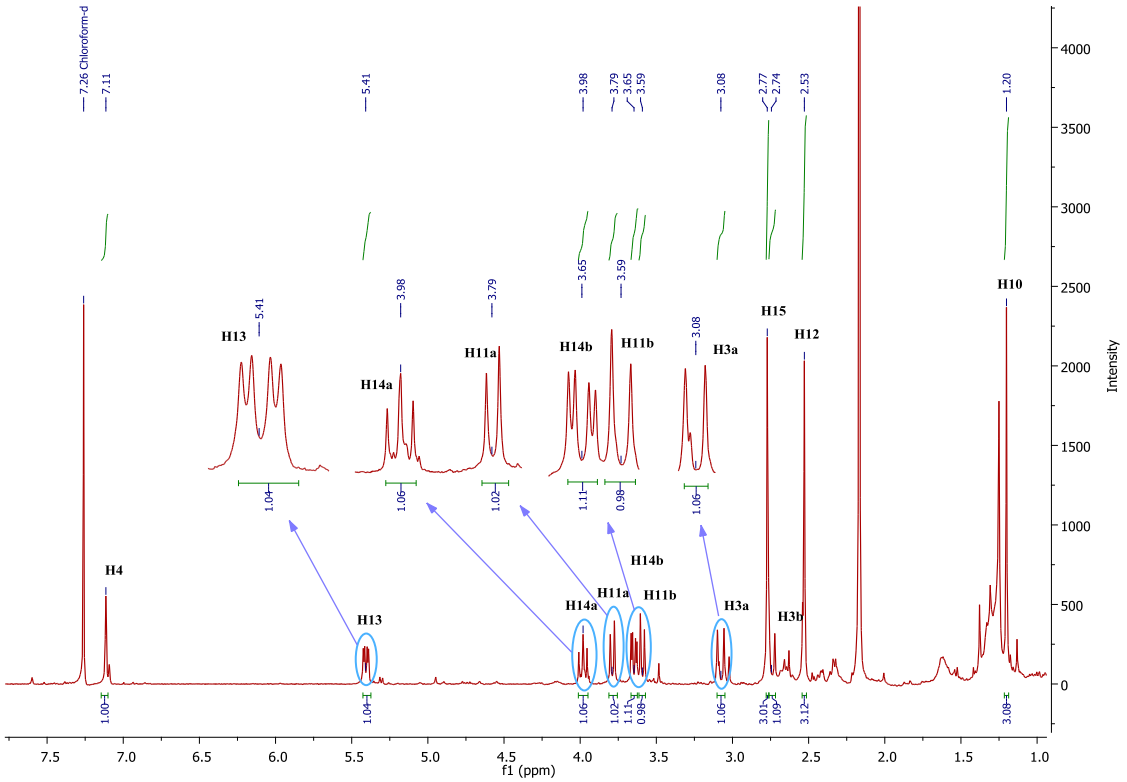

Figure A-22: ^{1}H NMR ($CDCl_3$, 400 MHz) spectrum of compound **RH7**.

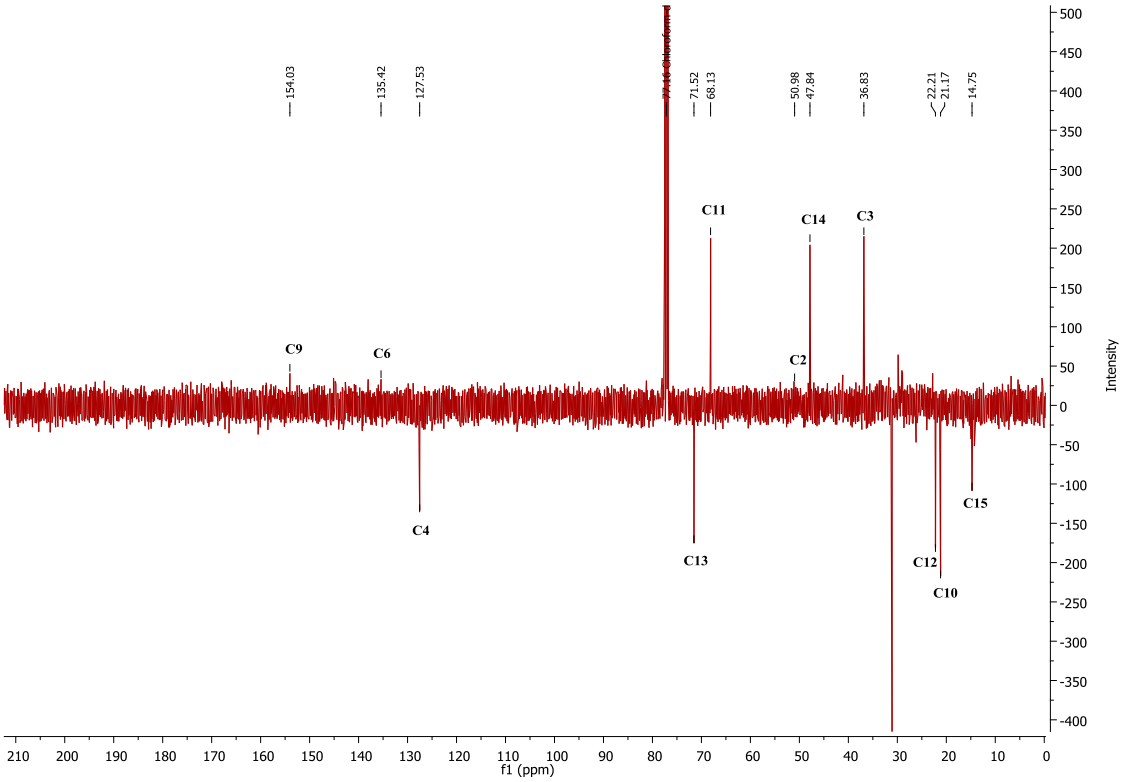

Figure A-23: DEPTQ NMR ($CDCl_3$, 100 MHz) spectrum of compound **RH7**.

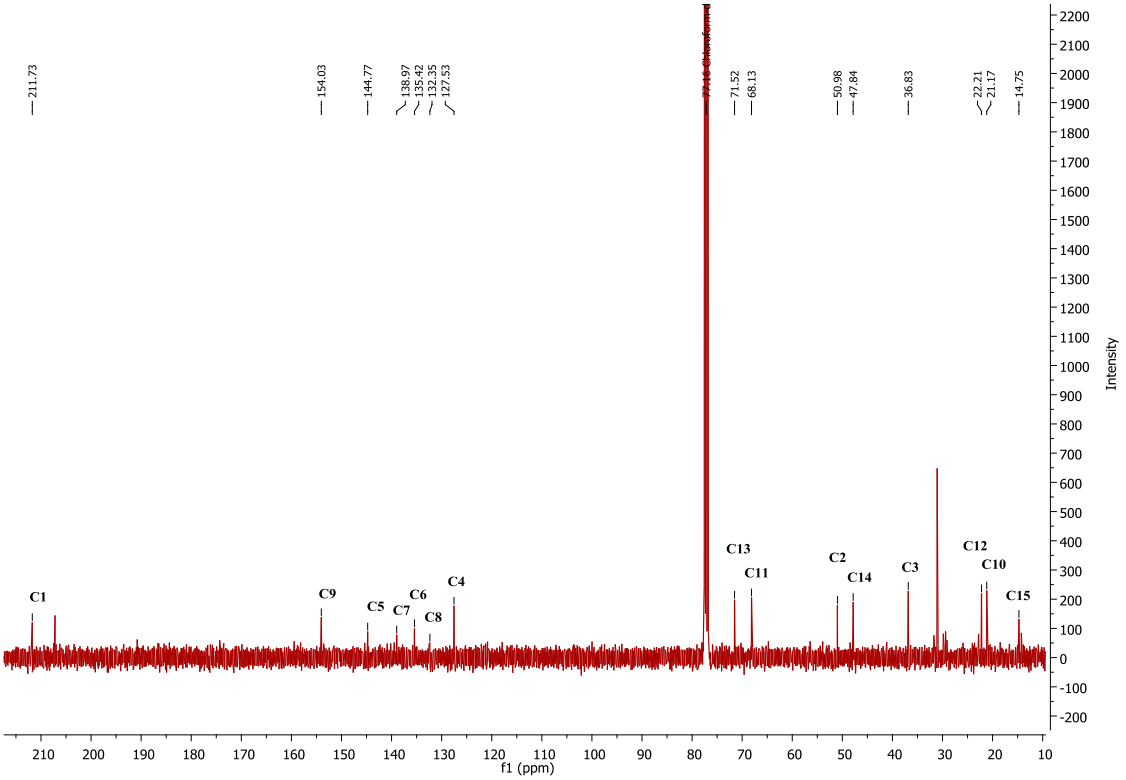

Figure A-24: ^{13}C NMR ($CDCl_3$, 100 MHz) spectrum of compound **RH7**.

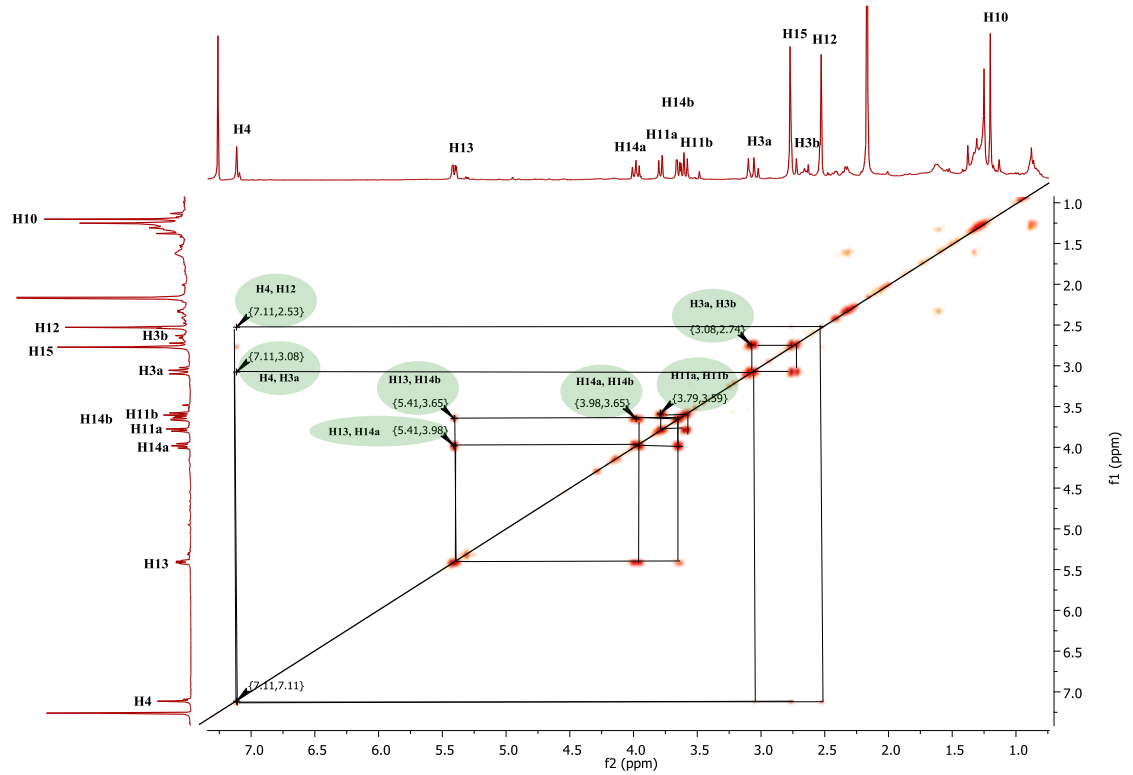

Figure A-25: ^{1}H-^{1}H COSY NMR ($CDCl_3$, 400 MHz) spectrum of compound **RH7**.

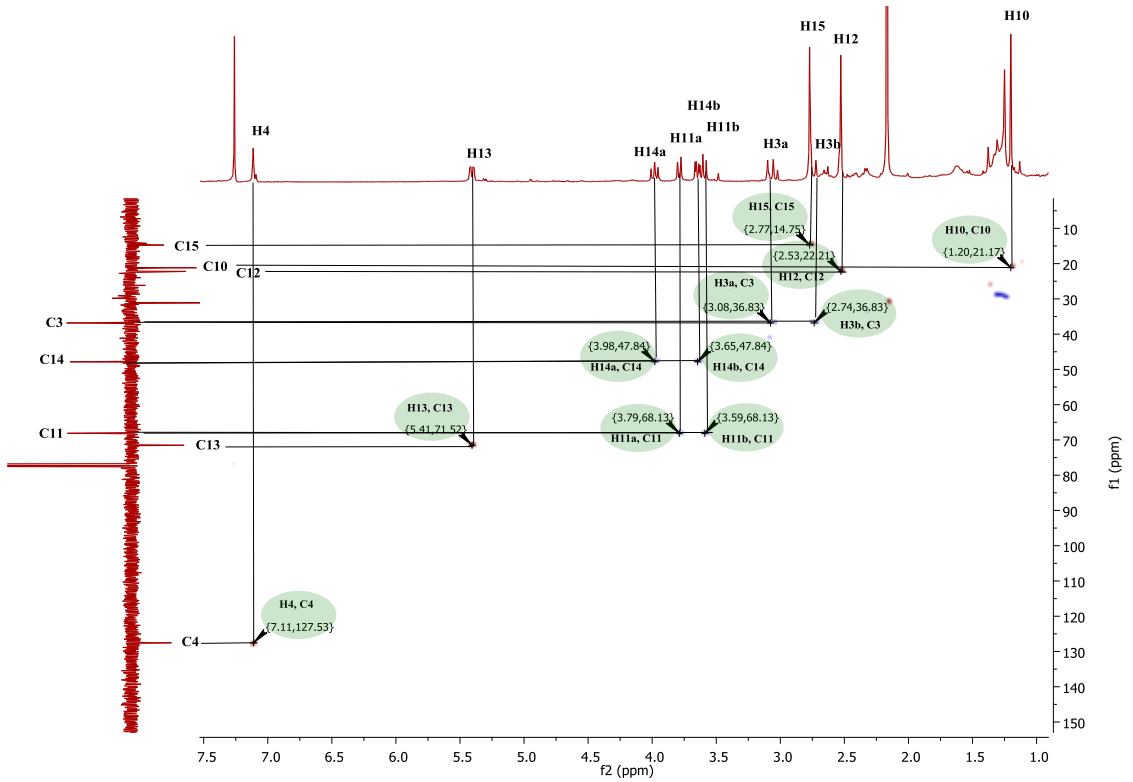

Figure A-26: ^{1}H-^{13}C HSQC NMR spectrum of compound **RH7** in $CDCl_3$.

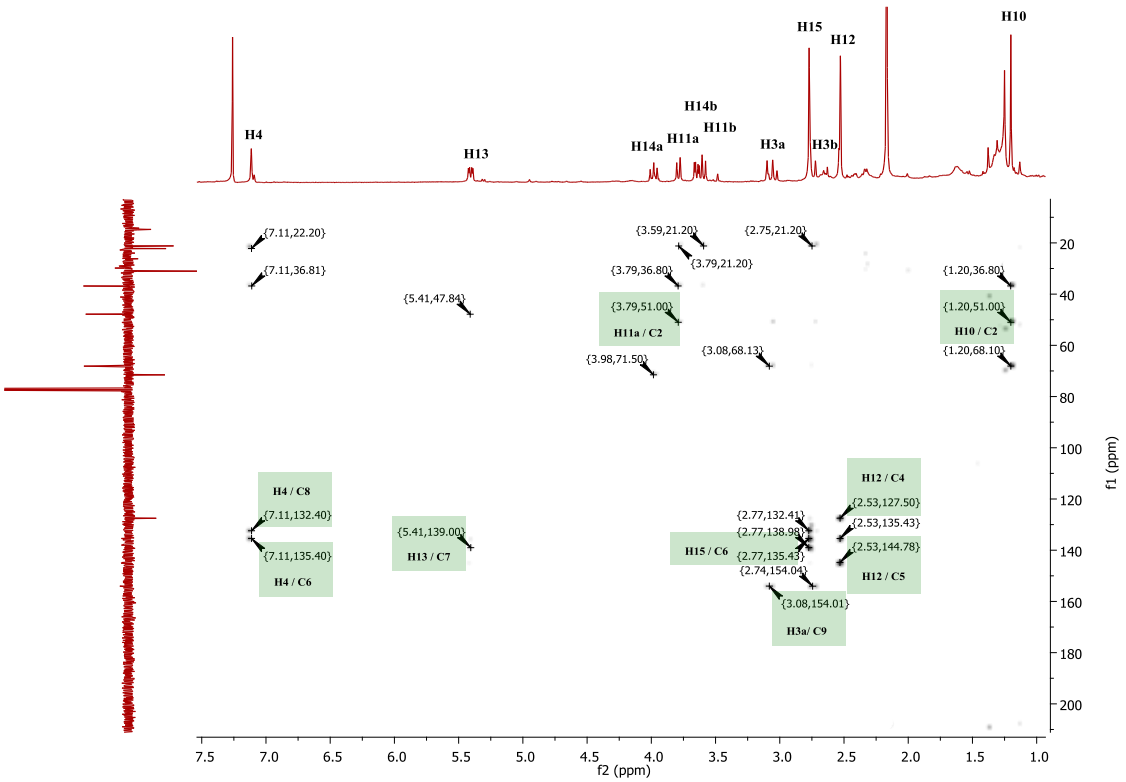

Figure A-27: ^{1}H-^{13}C HMBC NMR spectrum of compound **RH7** in $CDCl_3$.

6) NMR spectra of compound **RH8** in $(CD_3)_2CO$.

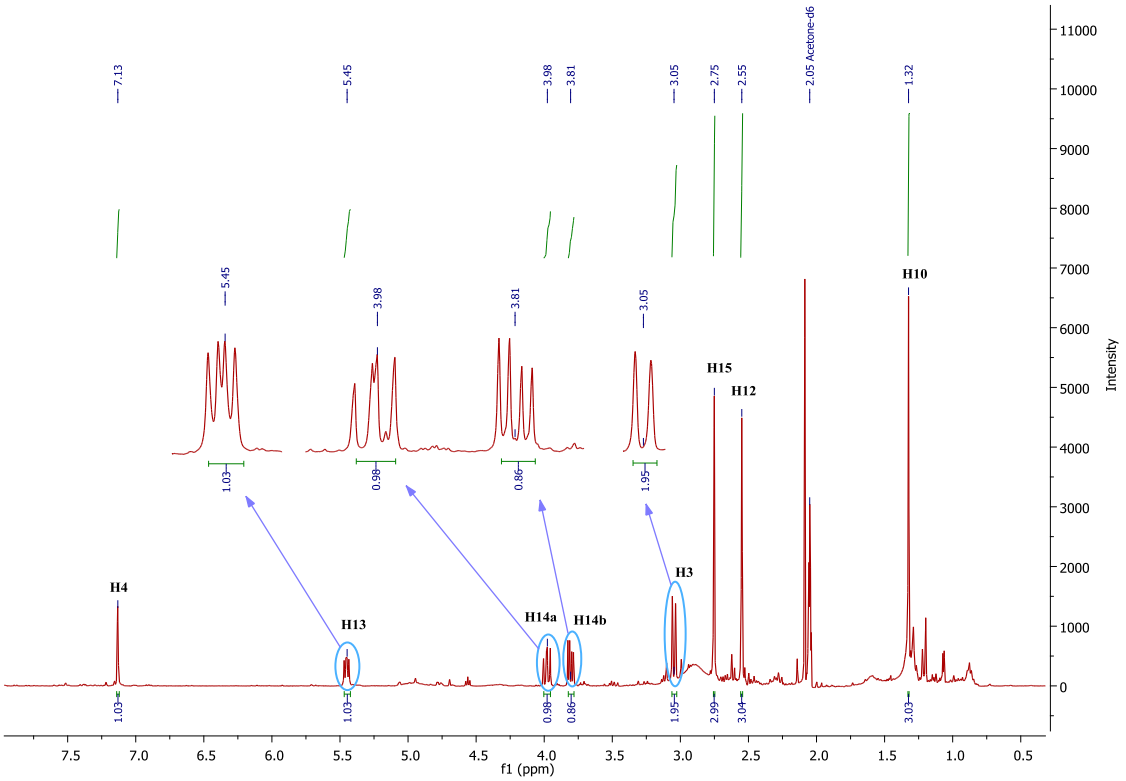

Figure A-28: ^{1}H NMR ($(CD_3)_2CO$, 400 MHz) spectrum of compound **RH8**.

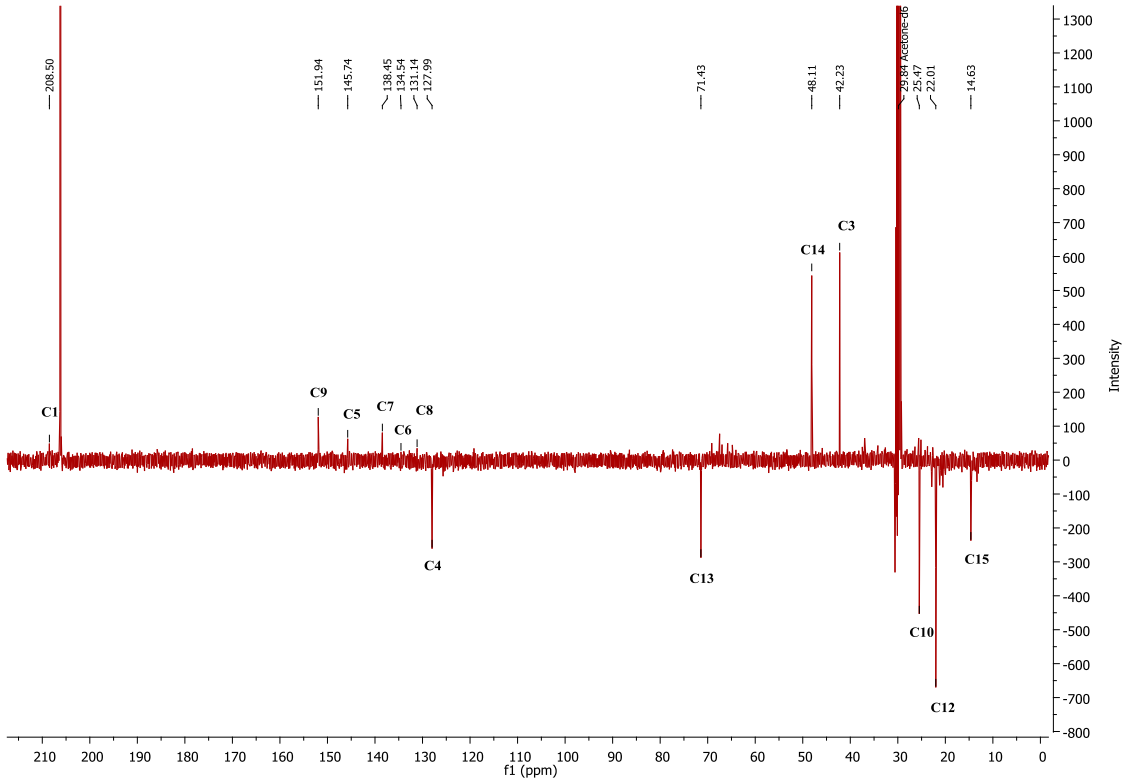

Figure A-29: DEPTQ NMR ($(CD_3)_2CO$, 100 MHz) spectrum of compound **RH8**.

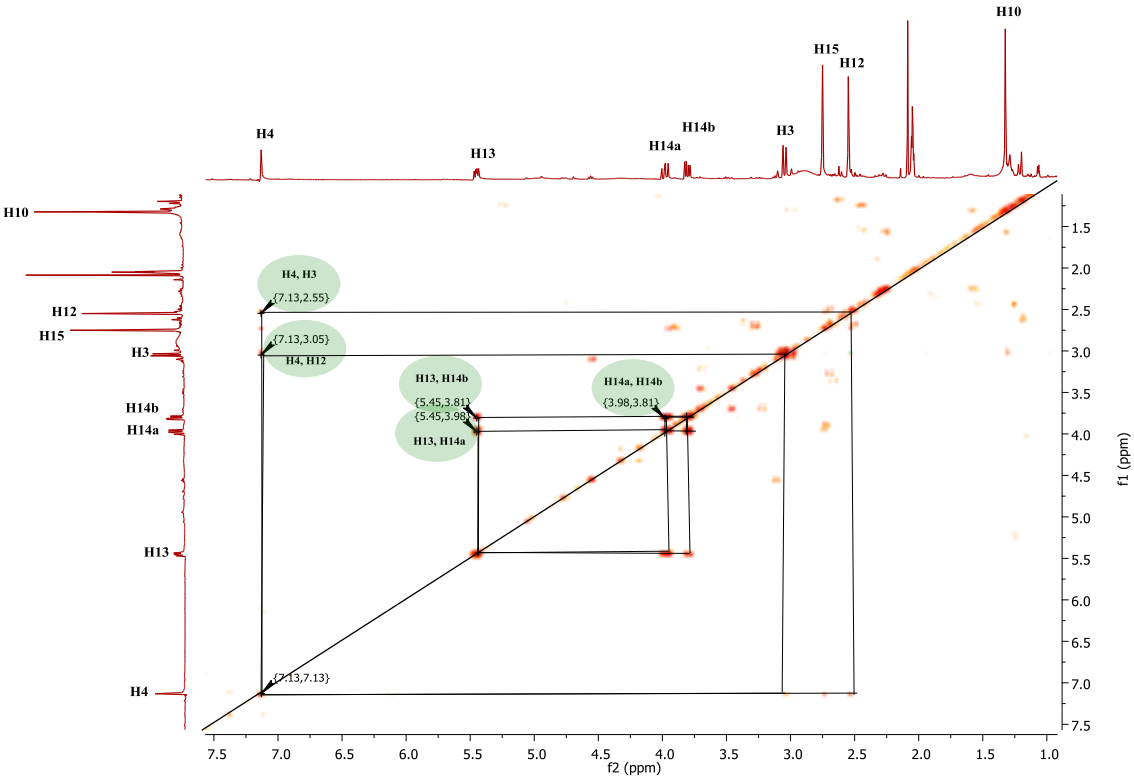

Figure A-30: ^{1}H-^{1}H COSY NMR ($(CD_3)_2CO$, 400 MHz) spectrum of compound **RH8**.

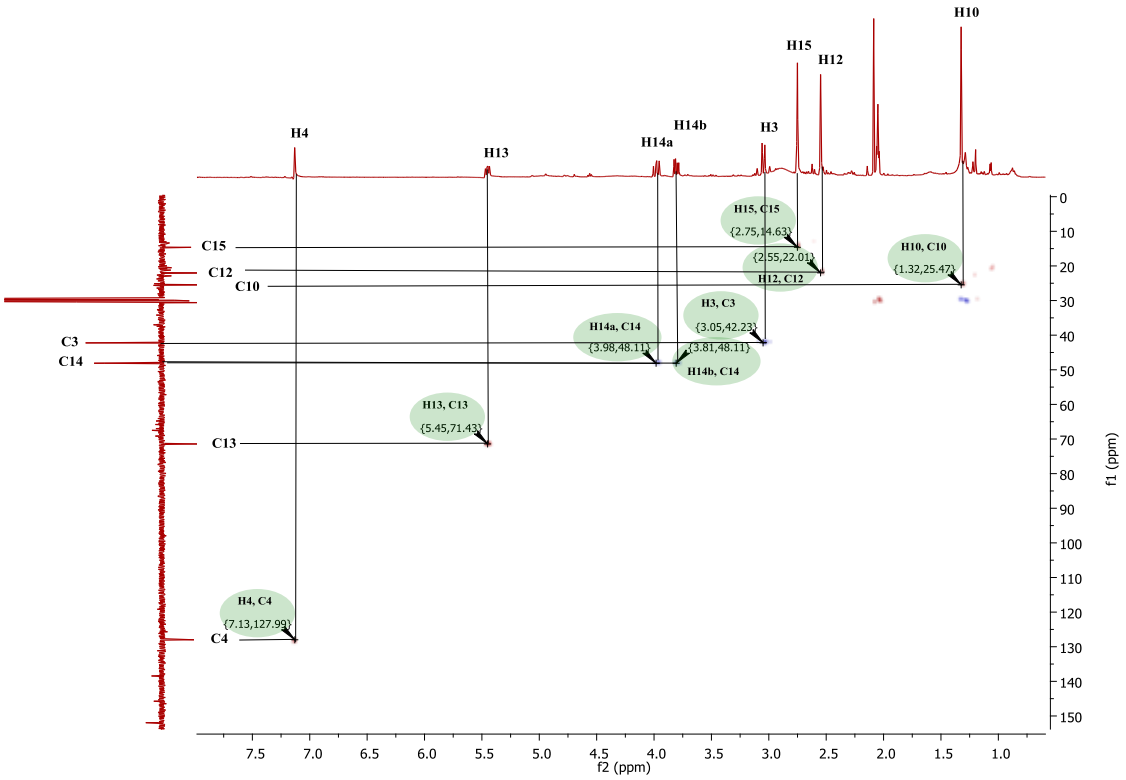

Figure A-31: ^{1}H-^{13}C HSQC NMR spectrum of compound **RH8** in $(CD_3)_2CO$.

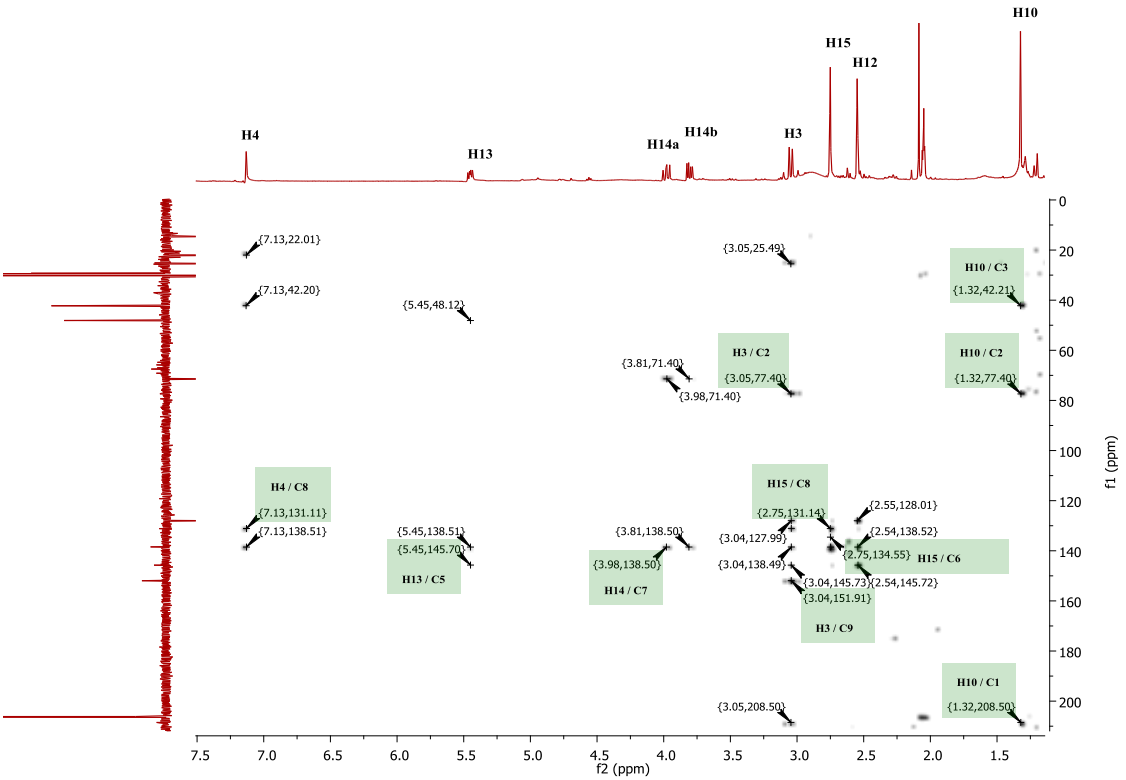

Figure A-32: ^{1}H-^{13}C HMBC NMR spectrum of compound **RH8** in $(CD_3)_2CO$.

7) NMR spectra of compound **RH9** in CD_3OD.

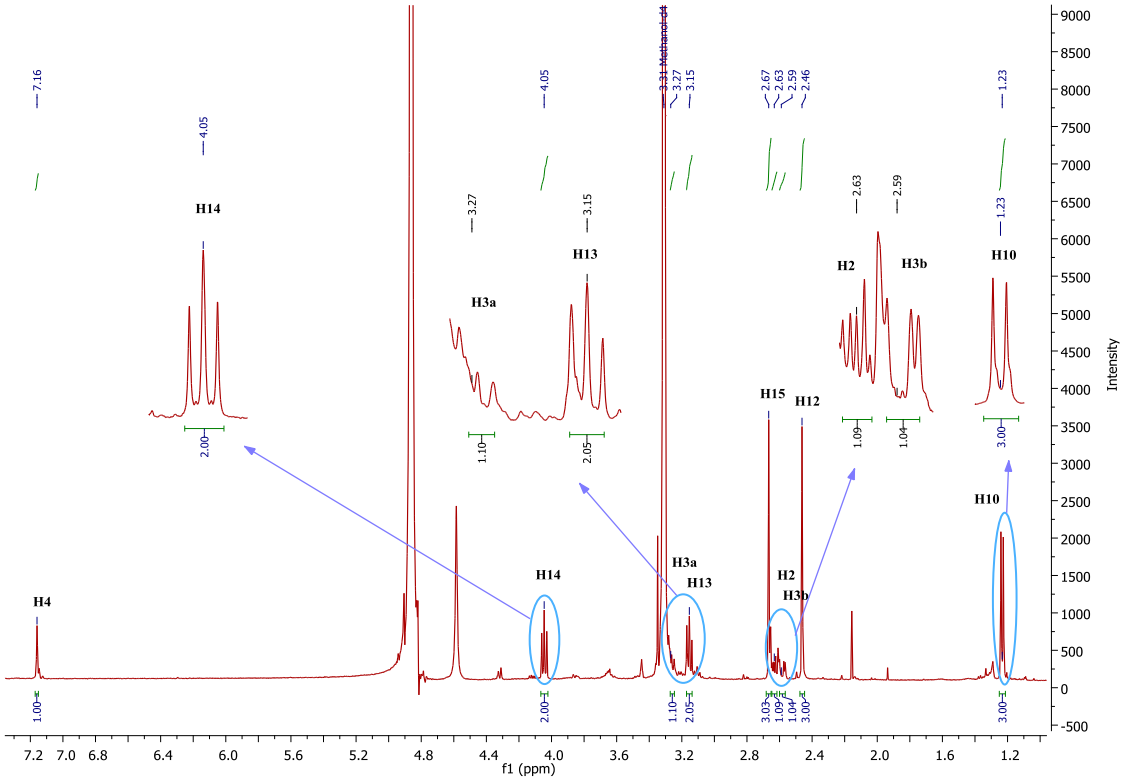

Figure A-33: ^1H NMR (CD_3OD, 500 MHz) spectrum of compound **RH9**.

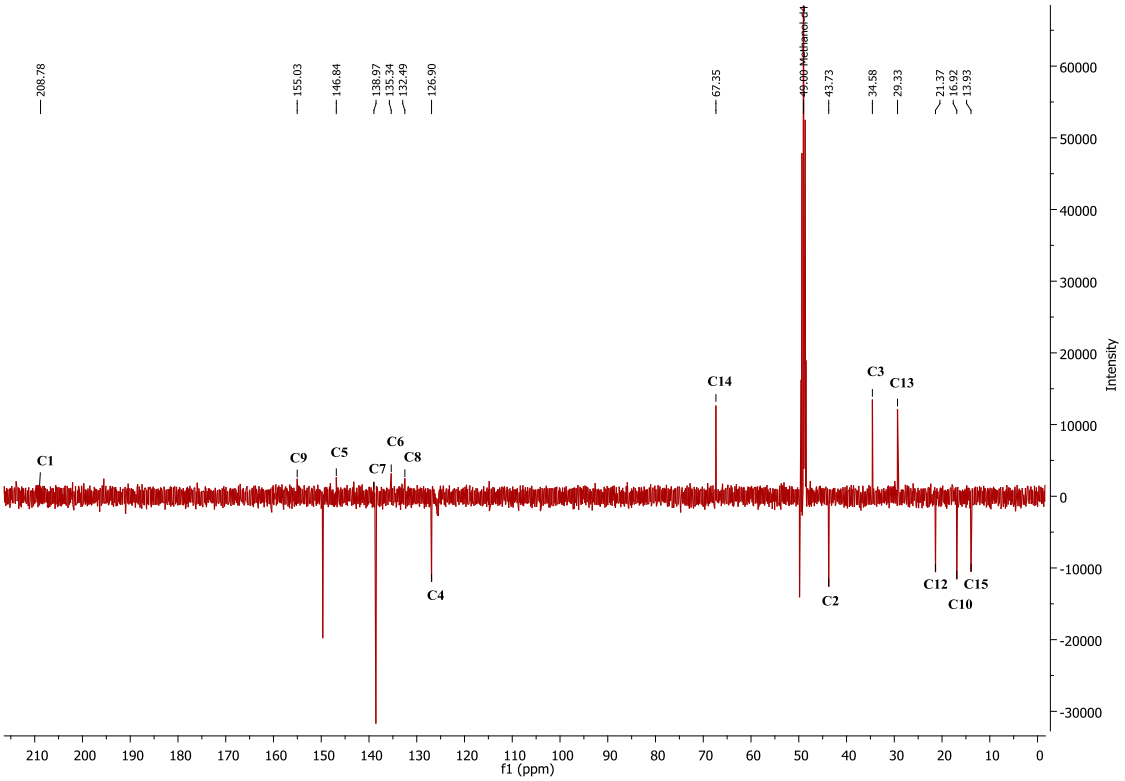

Figure A-34: DEPTQ NMR (CD_3OD, 125 MHz) spectrum of compound **RH9**.

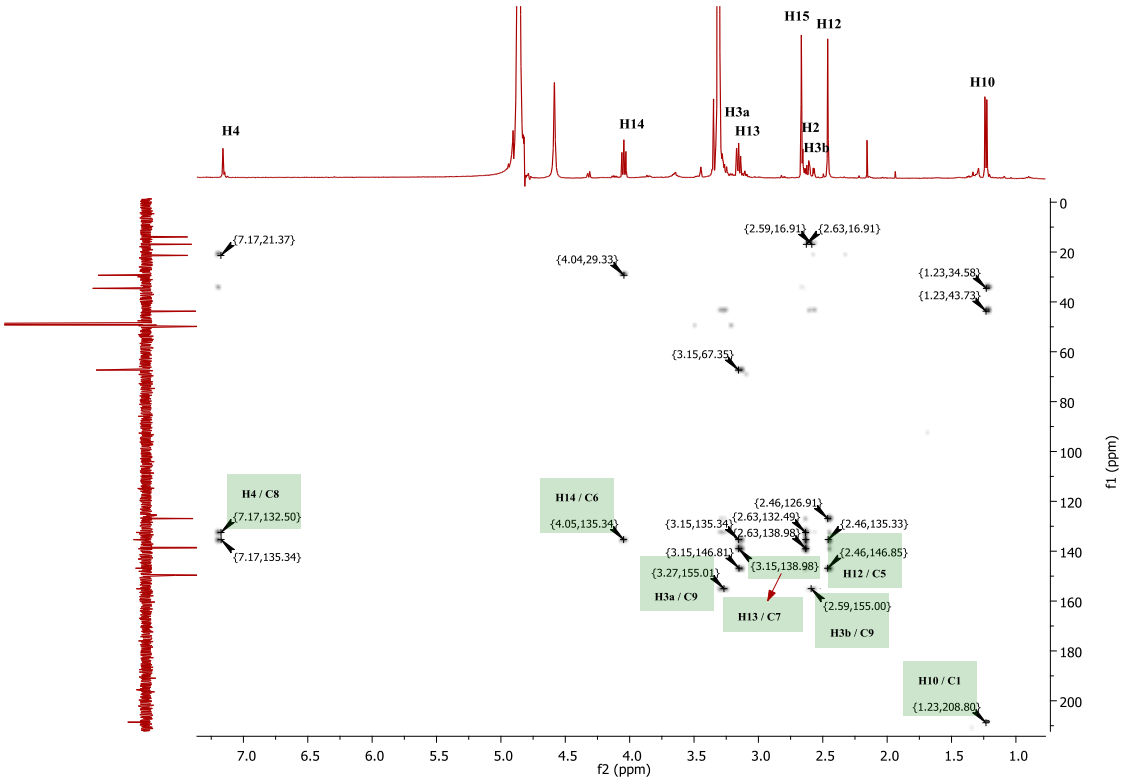

Figure A-35: ^{1}H-^{13}C HMBC NMR spectrum of compound **RH9** in CD_3OD.

8) NMR spectra of compound **RH10** in CD_3OD.

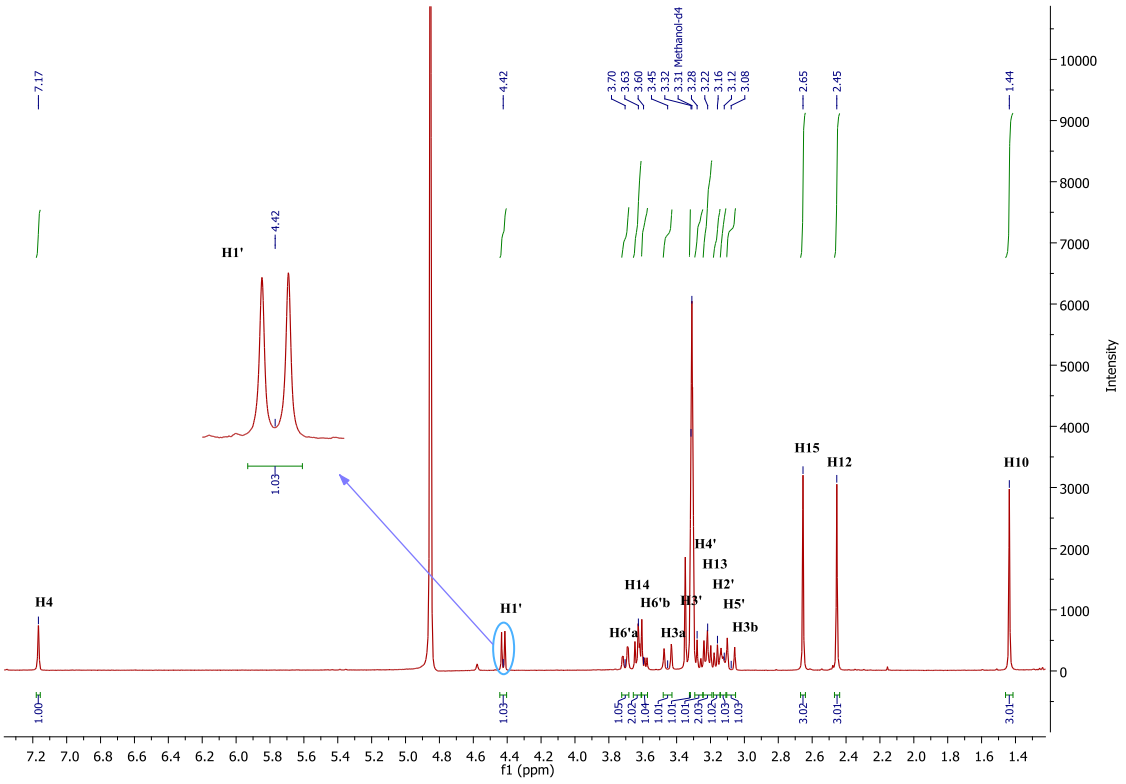

Figure A-36: ^{1}H NMR (CD_3OD, 400 MHz) spectrum of compound **RH10**.

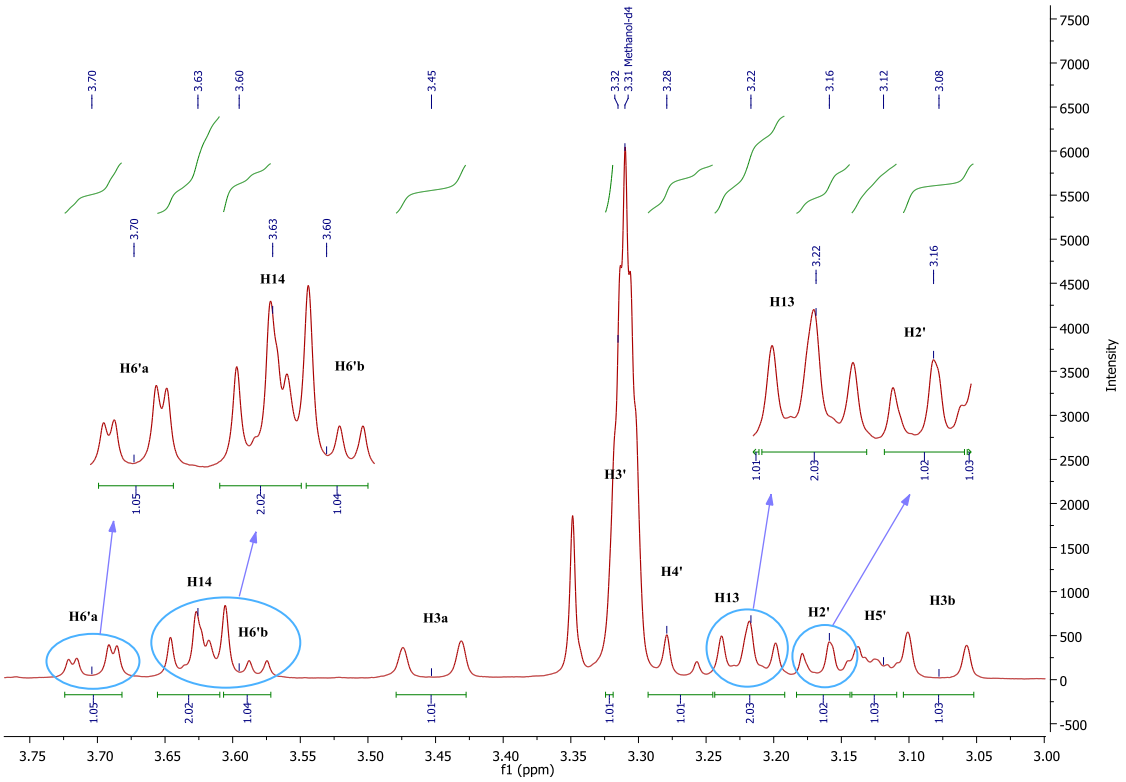

Figure A-37: Expanded ^{1}H NMR (CD_3OD, 400 MHz) spectrum of **RH10** (3.0 – 3.75 ppm).

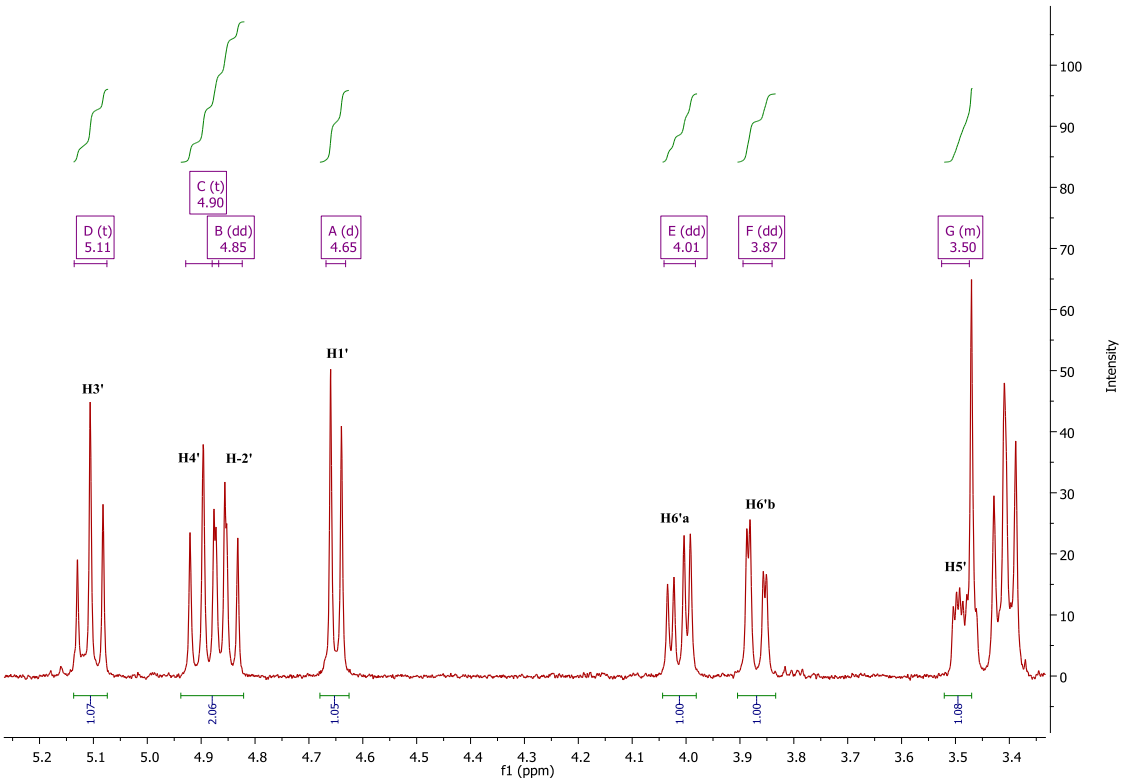

Figure A-38: ^{1}H NMR ($CDCl_3$, 400 MHz) spectrum of compound **RH10** after acetylation.

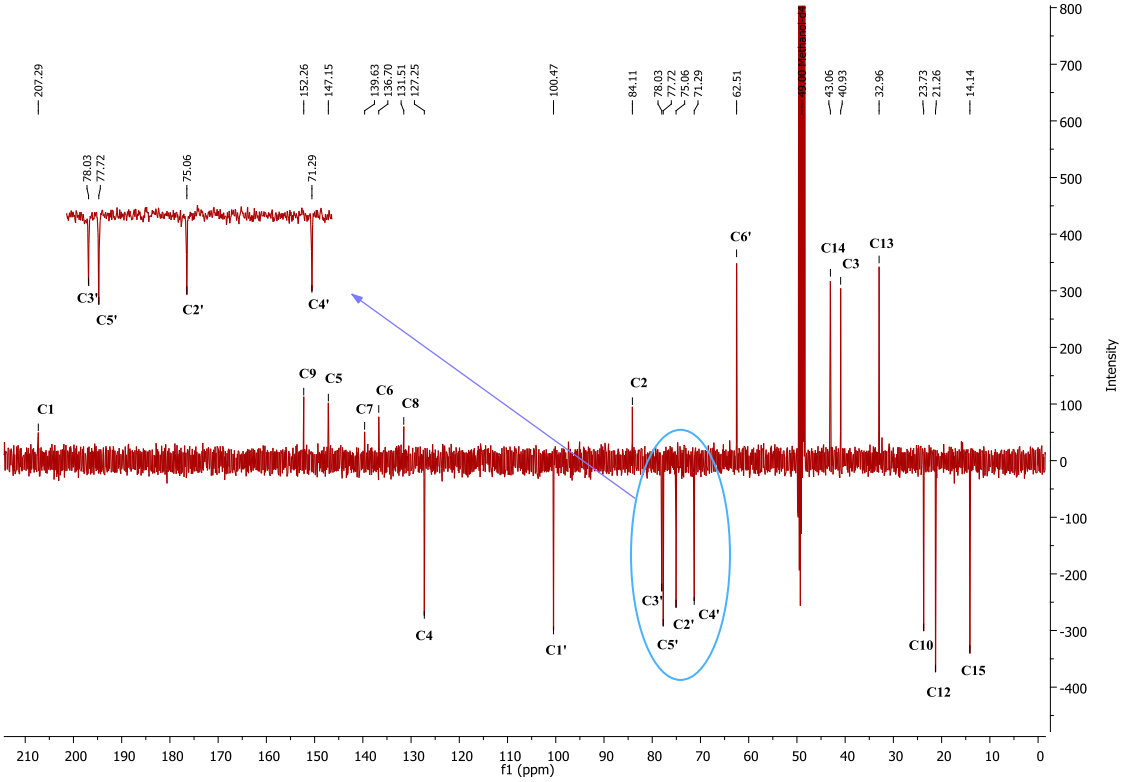

Figure A-39: DEPTQ NMR (CD_3OD, 100 MHz) spectrum of compound **RH10**.

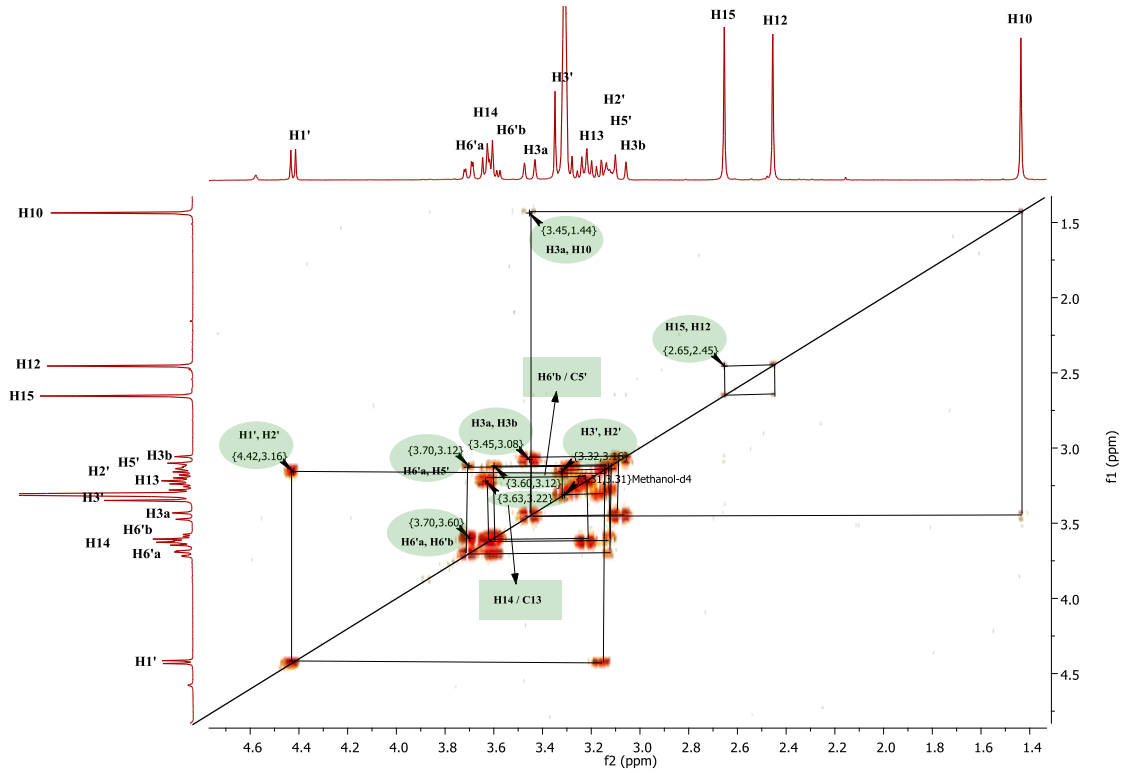

Figure A-40: ^1H-^1H COSY NMR (CD_3OD, 400 MHz) spectrum of compound **RH10**.

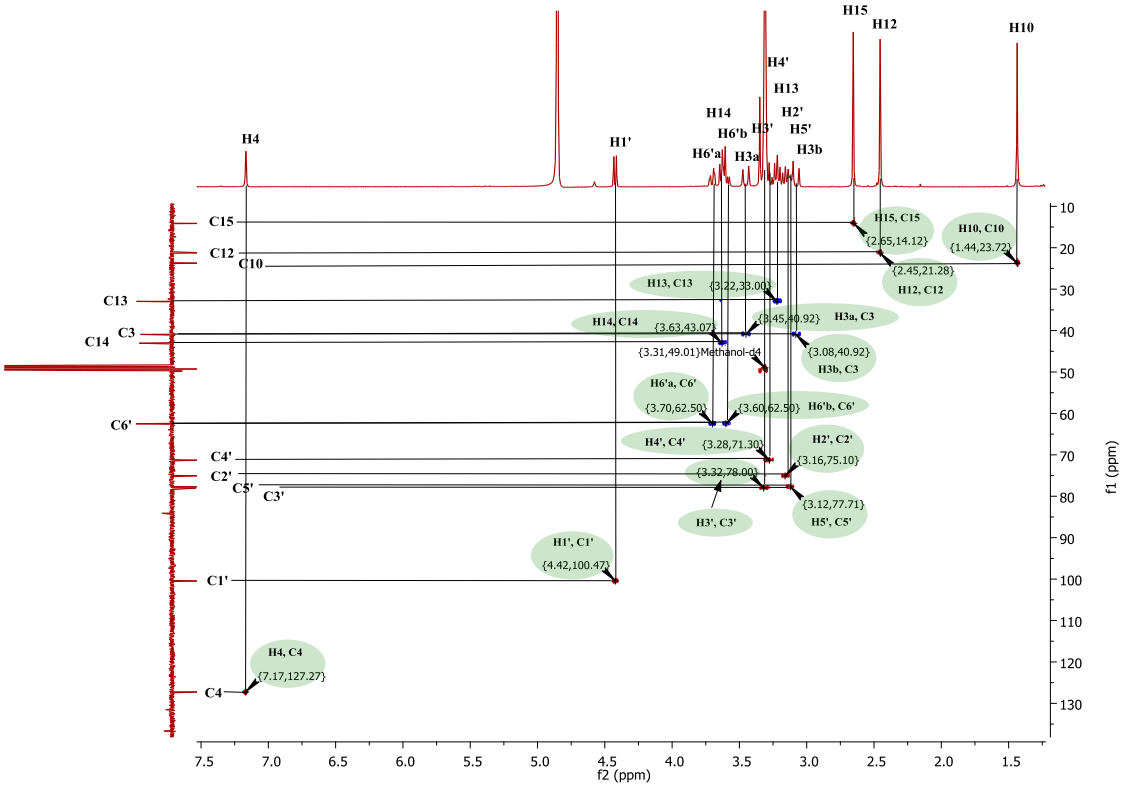

Figure A-41: ^{1}H-^{13}C HSQC NMR spectrum of compound **RH10** in CD_3OD.

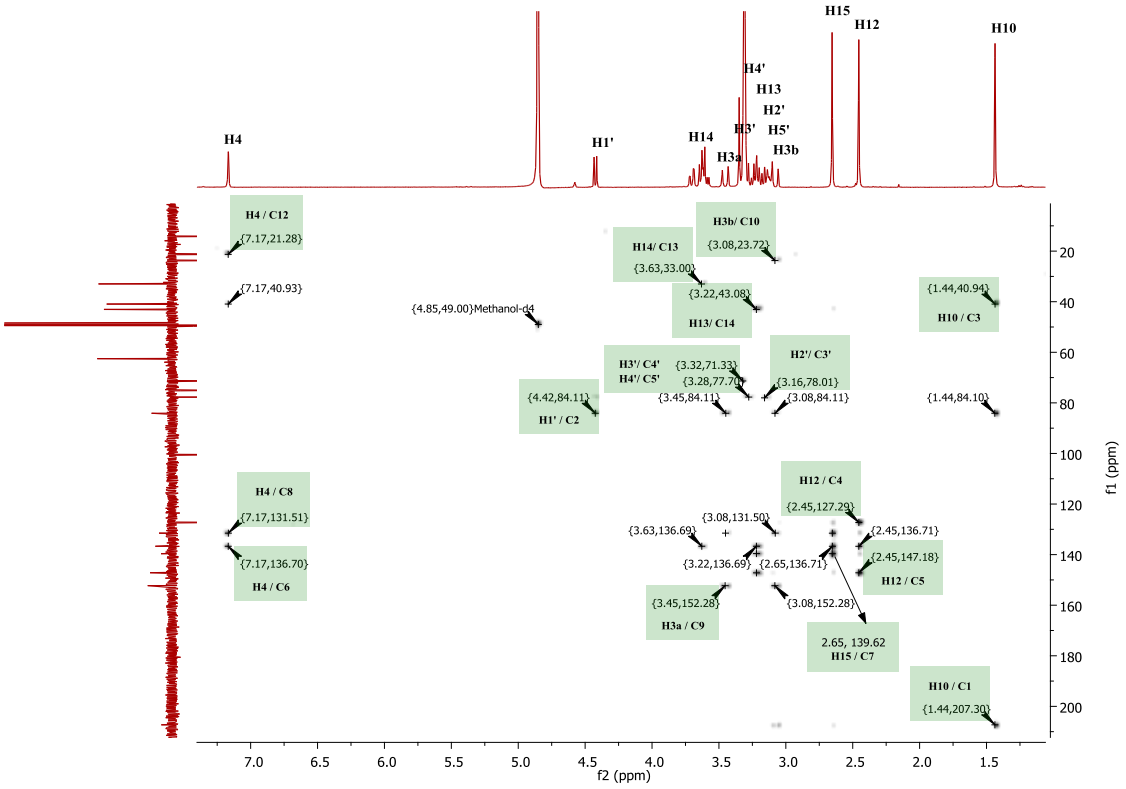

Figure A-42: ^{1}H-^{13}C HMBC NMR spectrum of compound **RH10** in CD_3OD.

9) NMR spectra of compound **RH11** in CD_3OD.

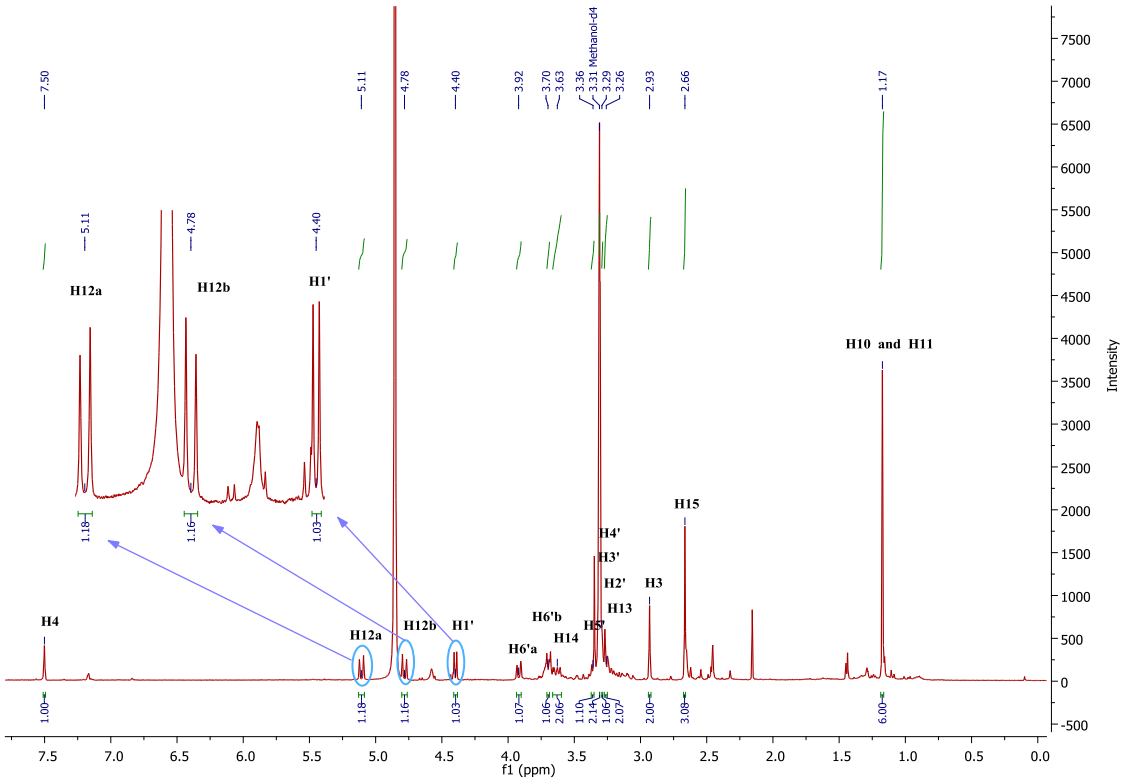

Figure A-43: ^1H NMR (CD_3OD, 400 MHz) spectrum of compound **RH11**.

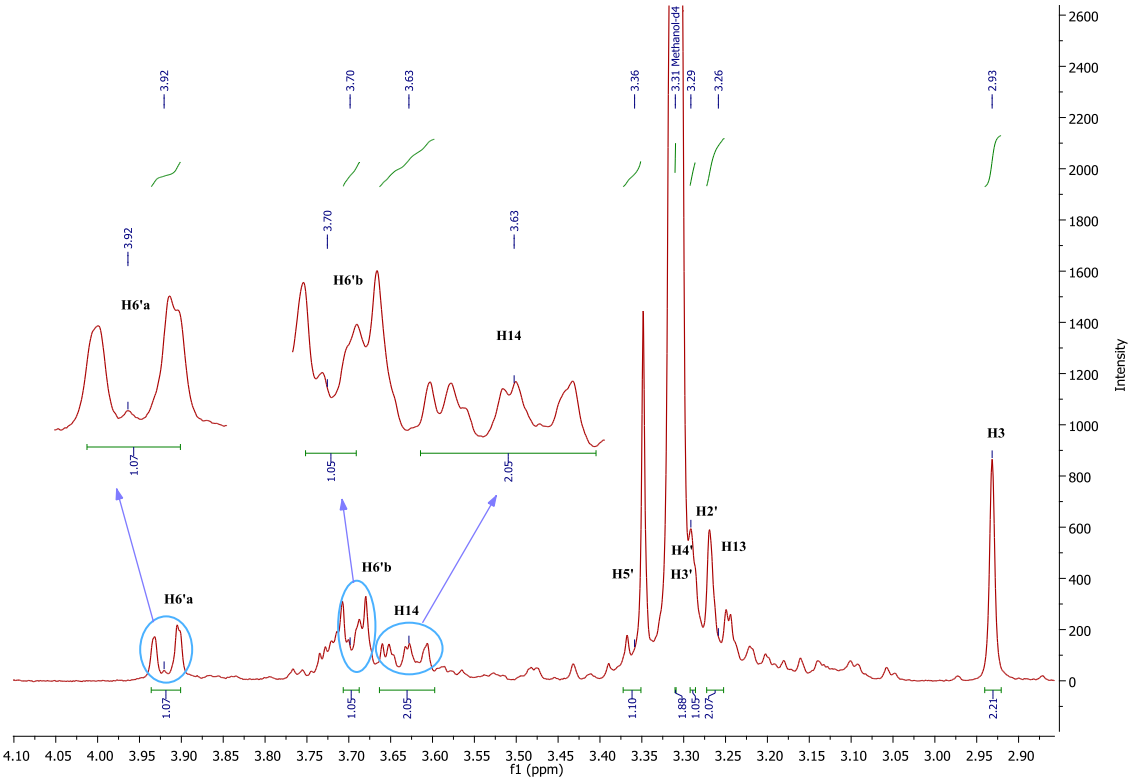

Figure A-44: Expanded ^1H NMR (CD_3OD, 400 MHz) spectrum of **RH11** (2.9 – 4.1 ppm).

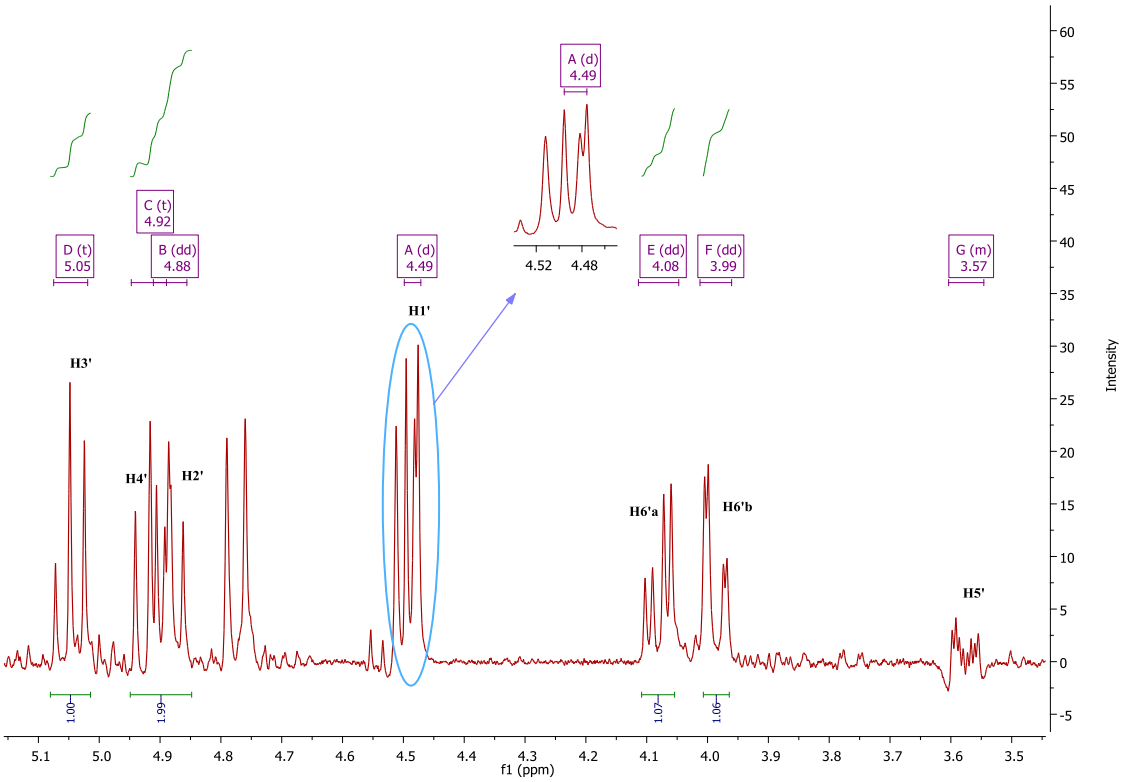

Figure A-45: ^{1}H NMR ($CDCl_3$, 400 MHz) spectrum of compound **RH11** after acetylation.

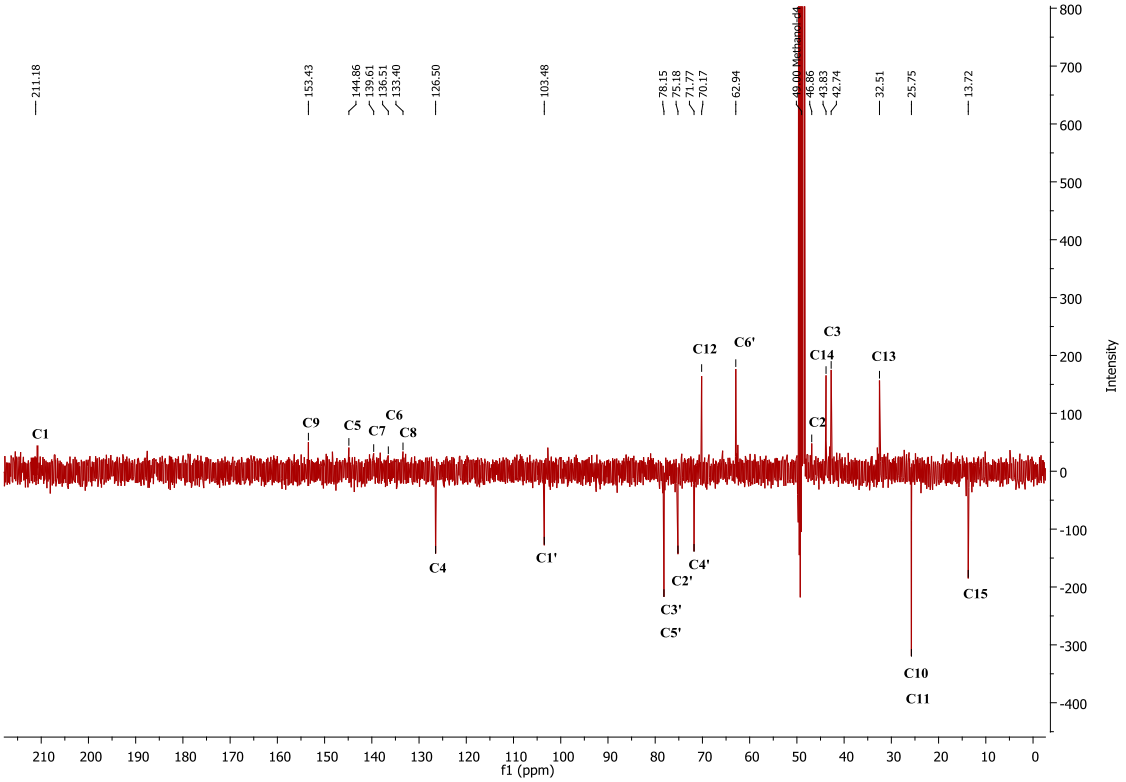

Figure A-46: DEPTQ NMR (CD_3OD, 100 MHz) spectrum of compound **RH11**.

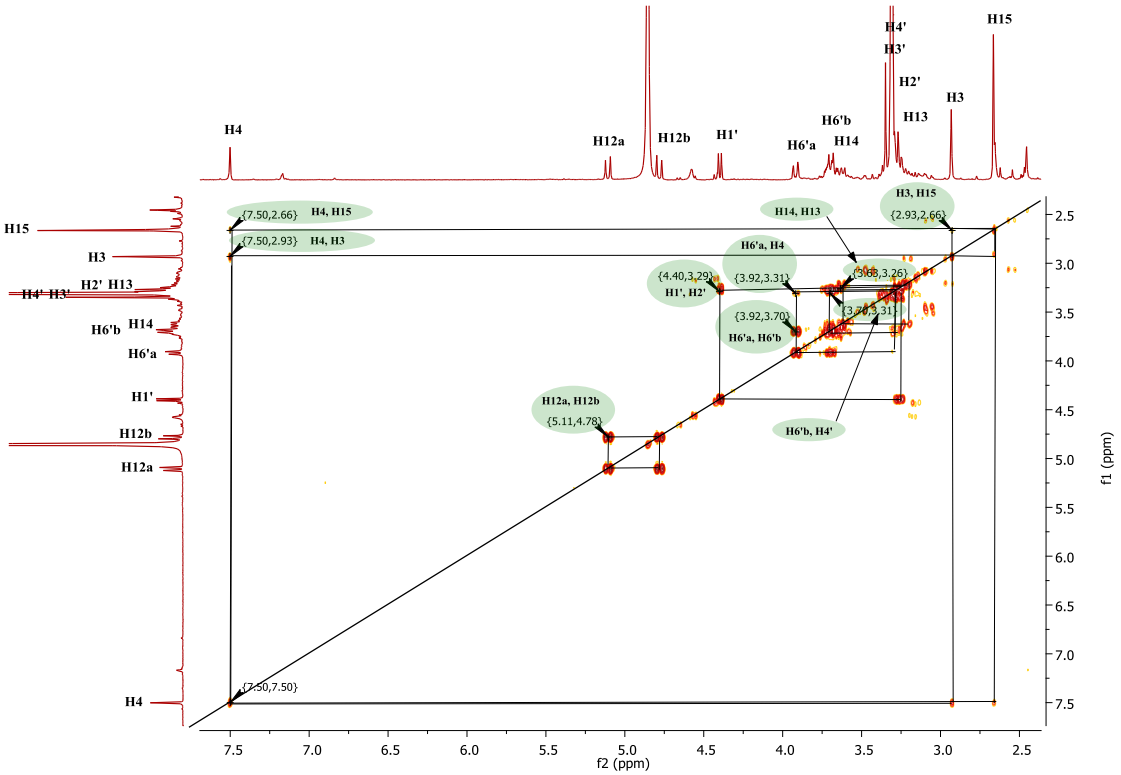

Figure A-47: ^{1}H-^{1}H COSY NMR (CD_3OD, 400 MHz) spectrum of compound **RH11**.

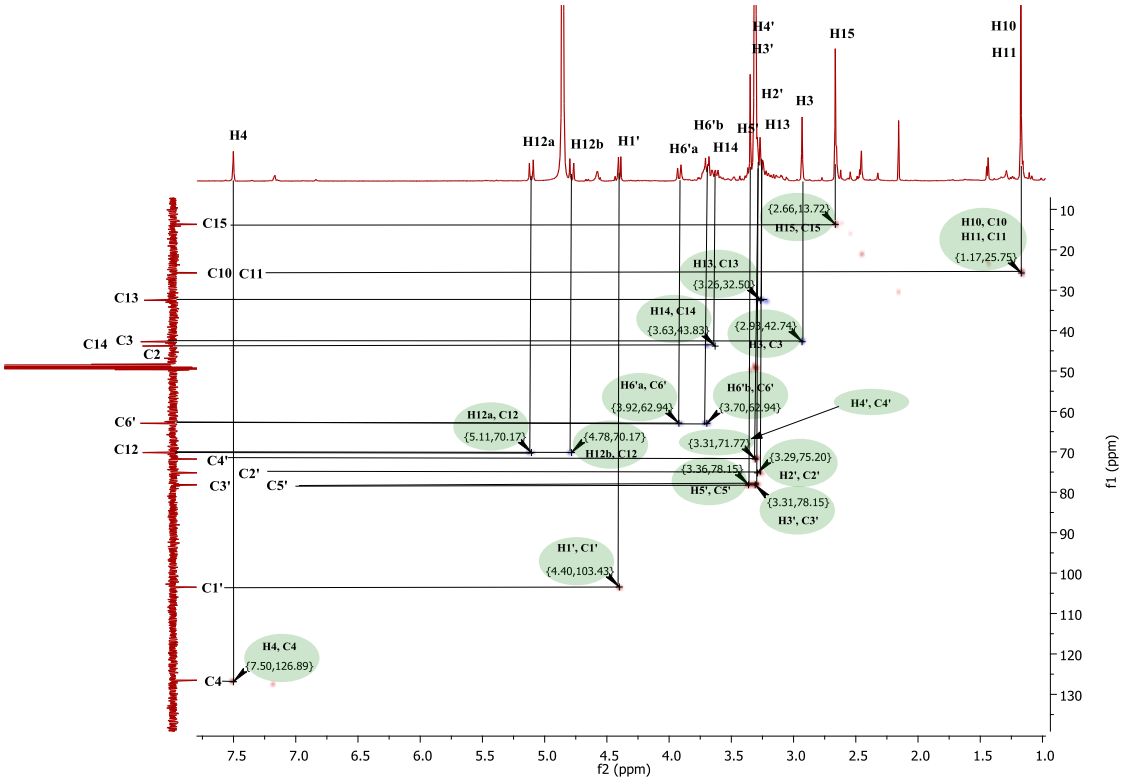

Figure A-48: ^{1}H-^{13}C HSQC NMR spectrum of compound **RH11** in CD_3OD.

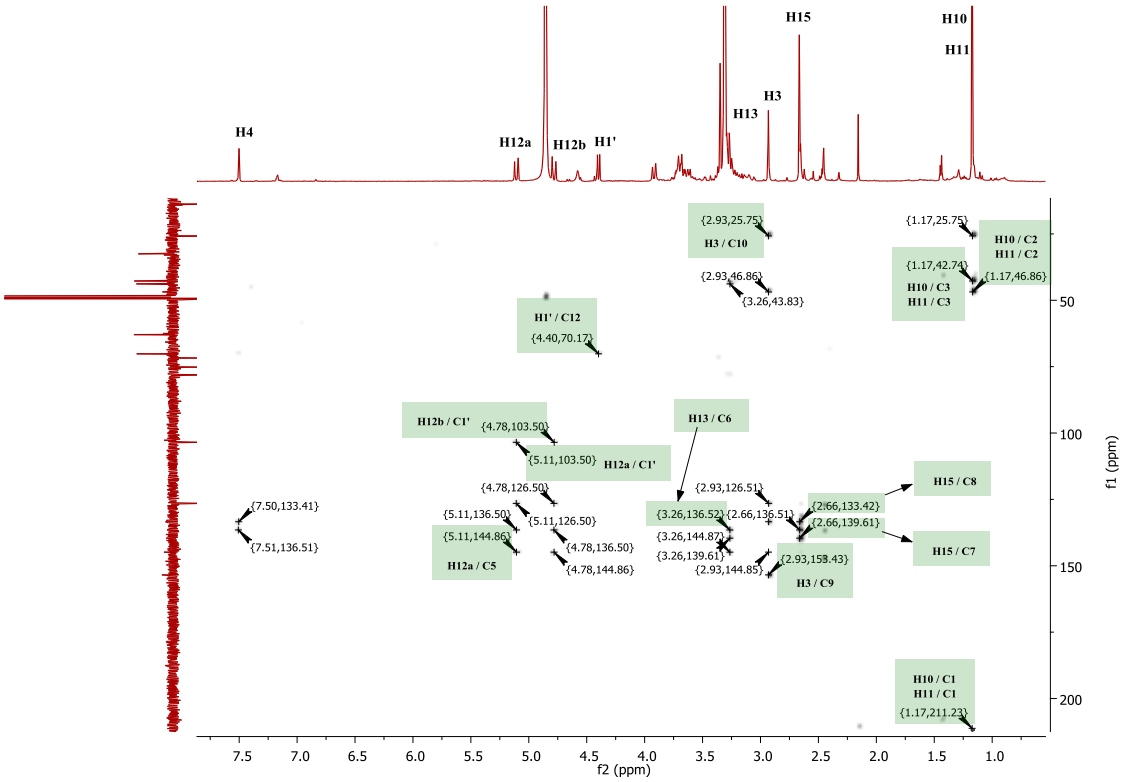

Figure A-49: ^{1}H-^{13}C HMBC NMR spectrum of compound **RH11** in CD_3OD.

10) NMR spectra of compound **RH12** in CD_3OD.

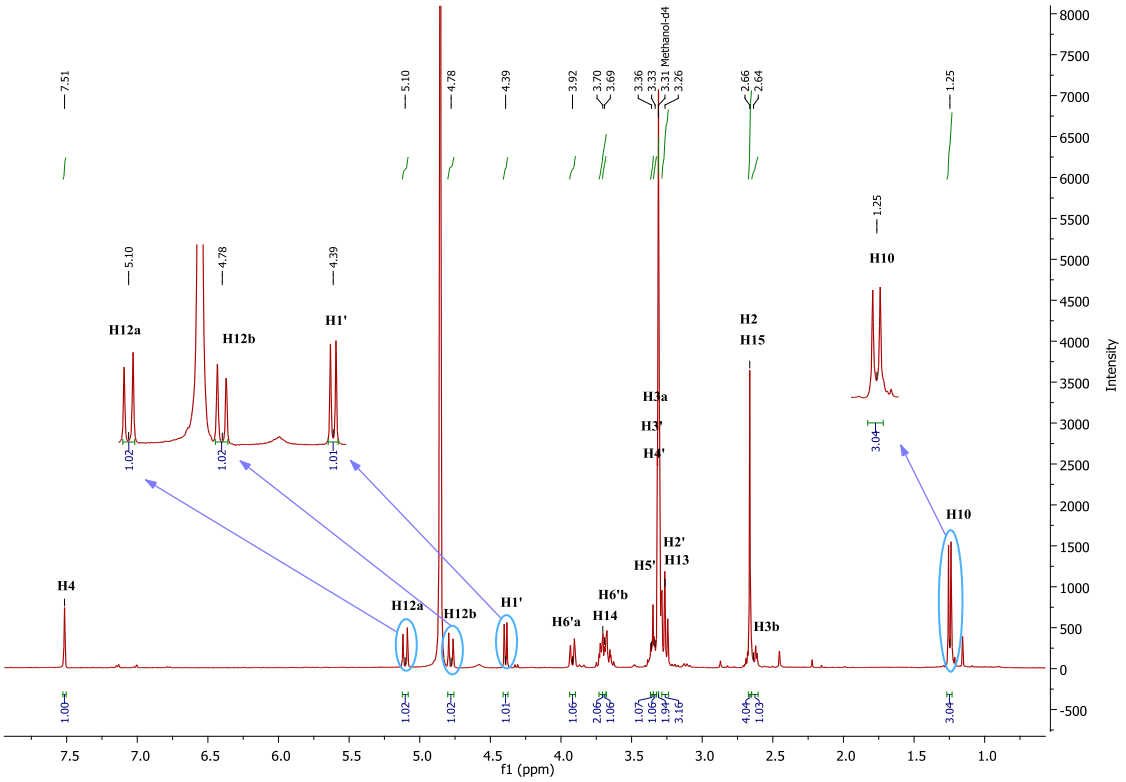

Figure A-50: ^{1}H NMR (CD_3OD, 400 MHz) spectrum of compound **RH12**.

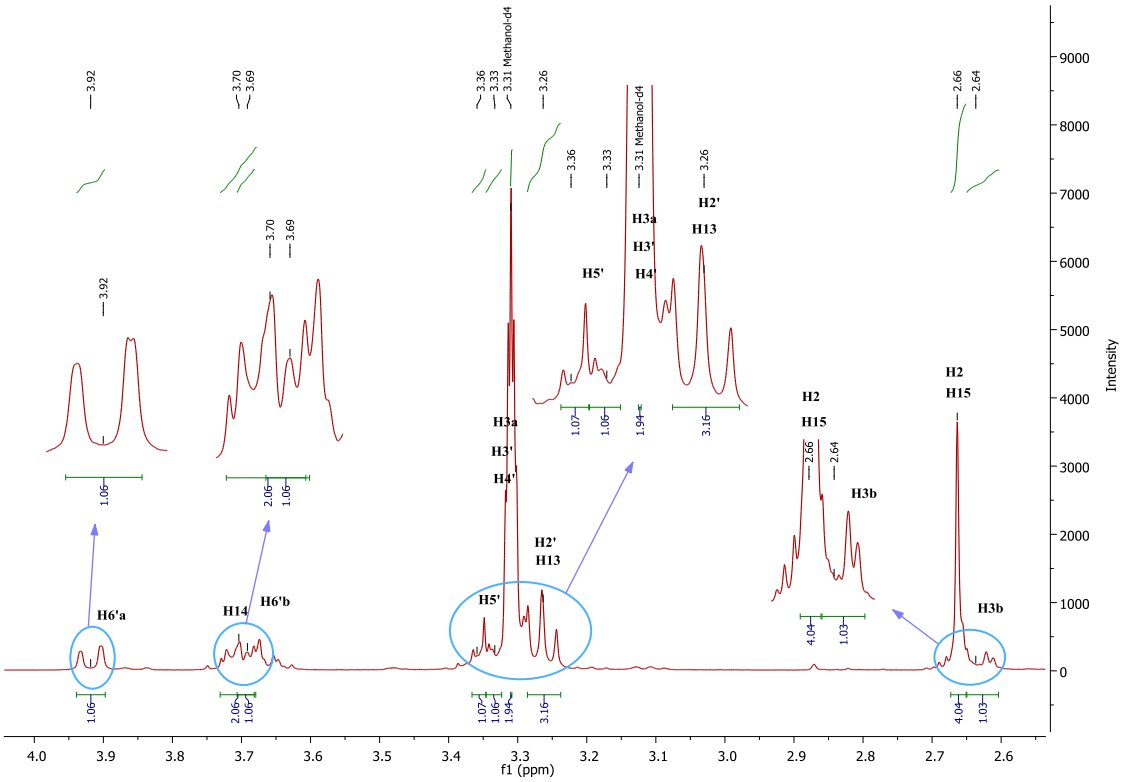

Figure A-51: Expanded ^{1}H NMR (CD_3OD, 400 MHz) spectrum of **RH12** (2.6 – 4.0 ppm).

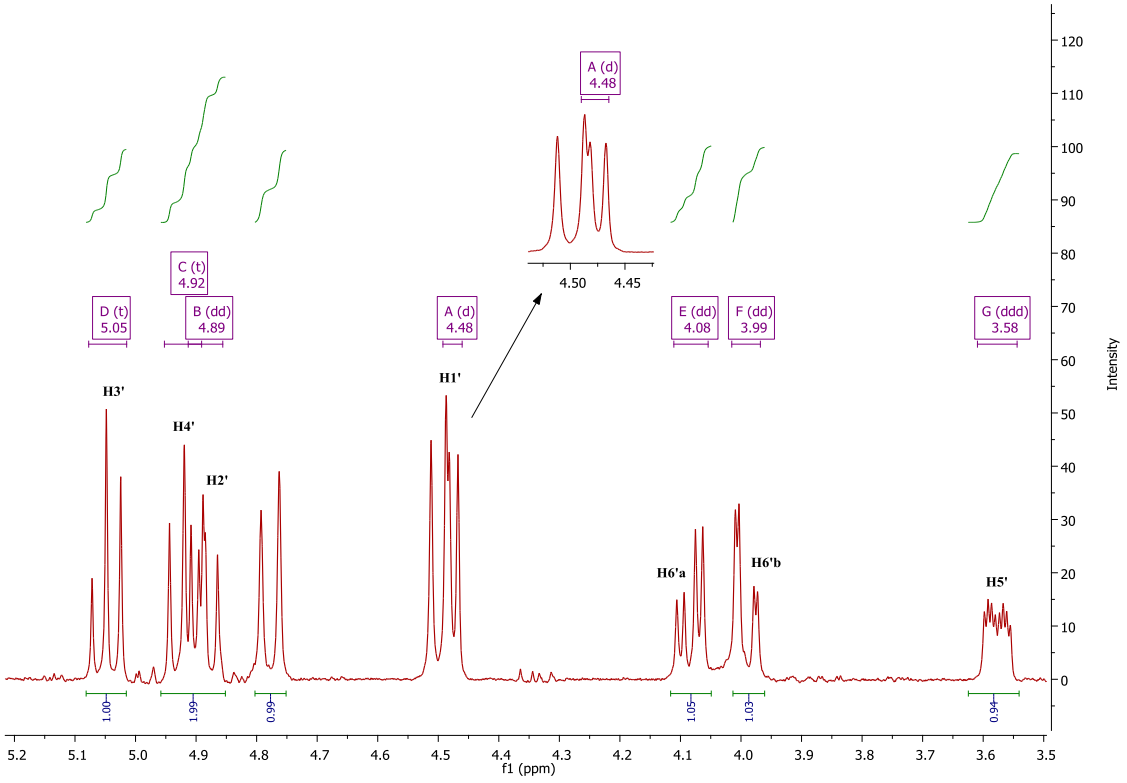

Figure A-52: ^{1}H NMR ($CDCl_3$, 400 MHz) spectrum of compound **RH12** after acetylation.

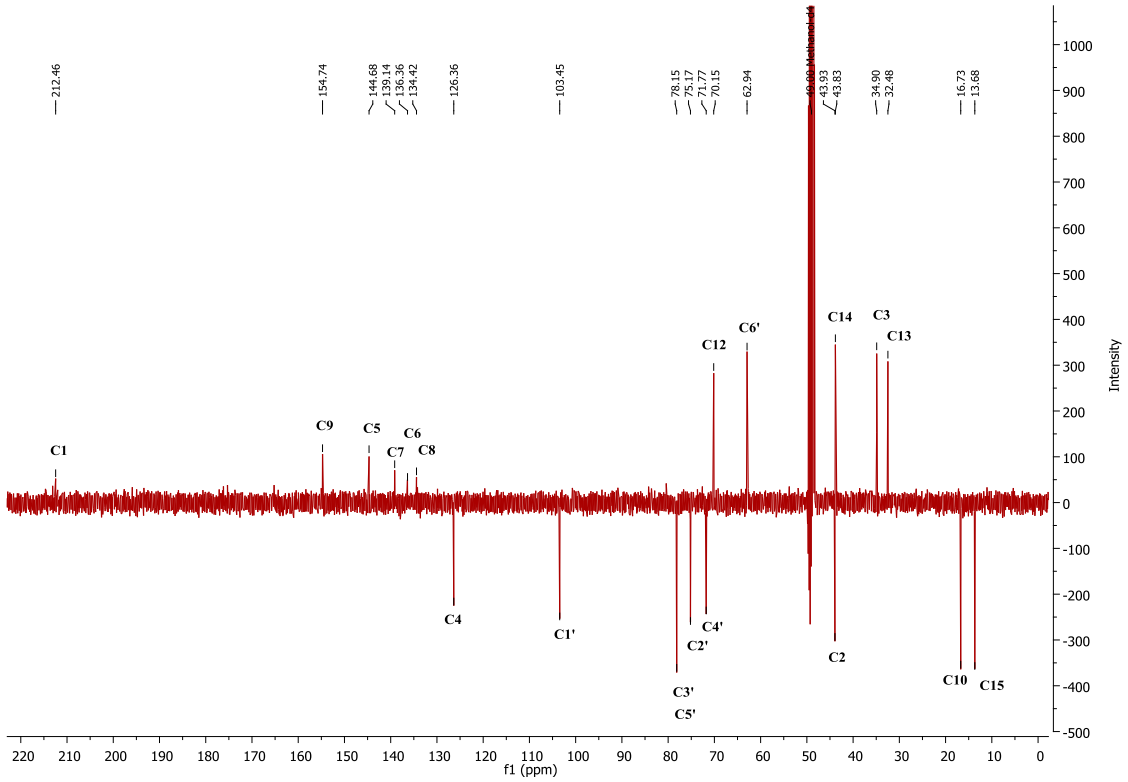

Figure A-53: DEPTQ NMR (CD_3OD, 100 MHz) spectrum of compound **RH12**.

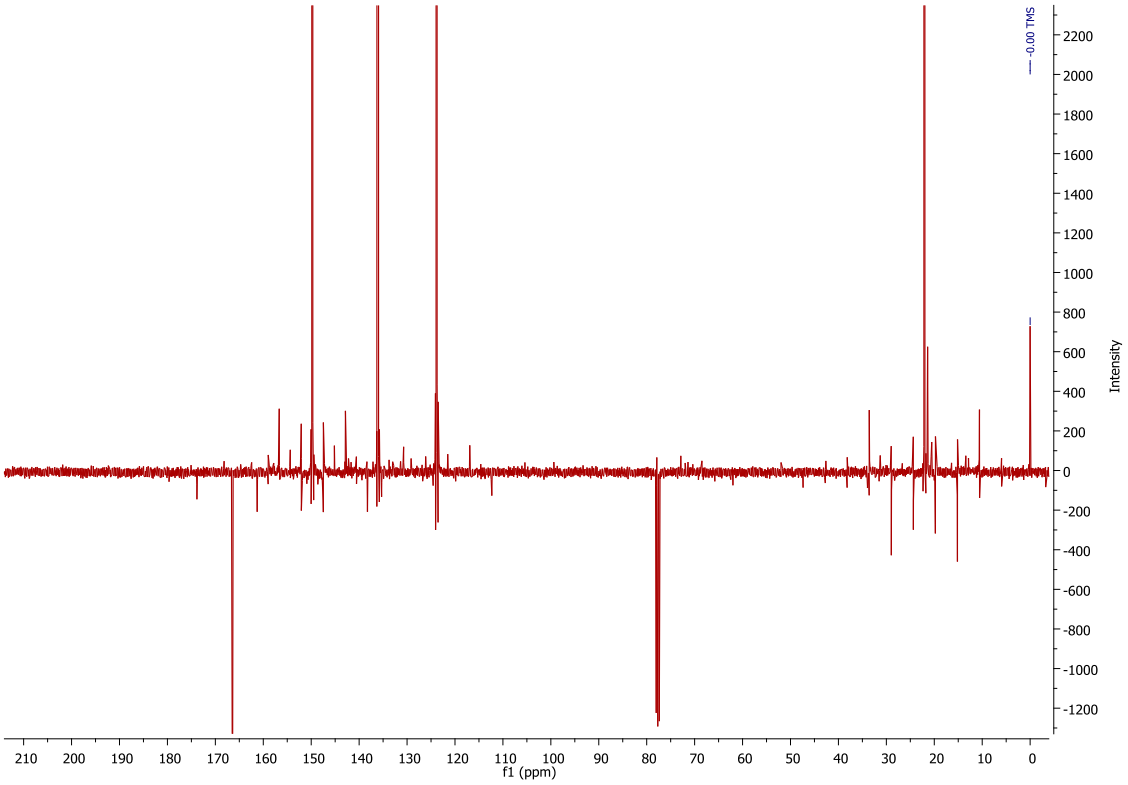

Figure A-54: DEPTQ NMR ($CDCl_3$, 100 MHz) spectrum of compound **RH12** after acetylation.

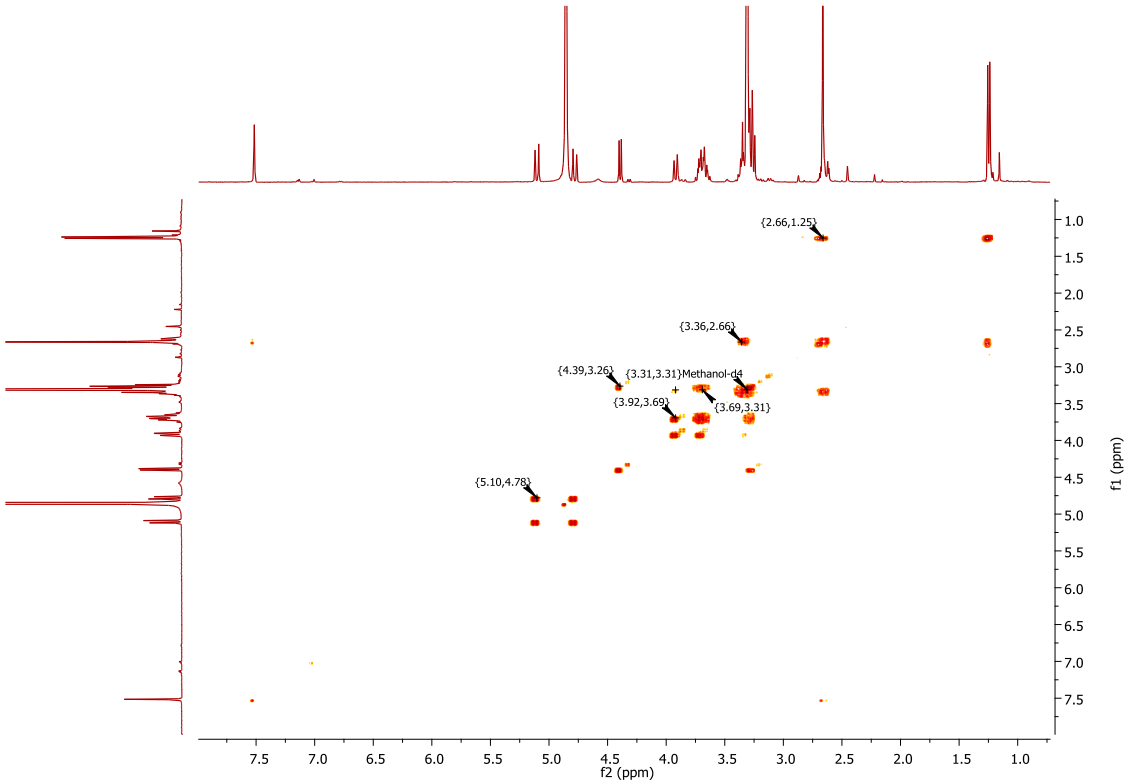

Figure A-55: ^{1}H-^{1}H COSY NMR (CD_3OD, 400 MHz) spectrum of compound **RH12**.

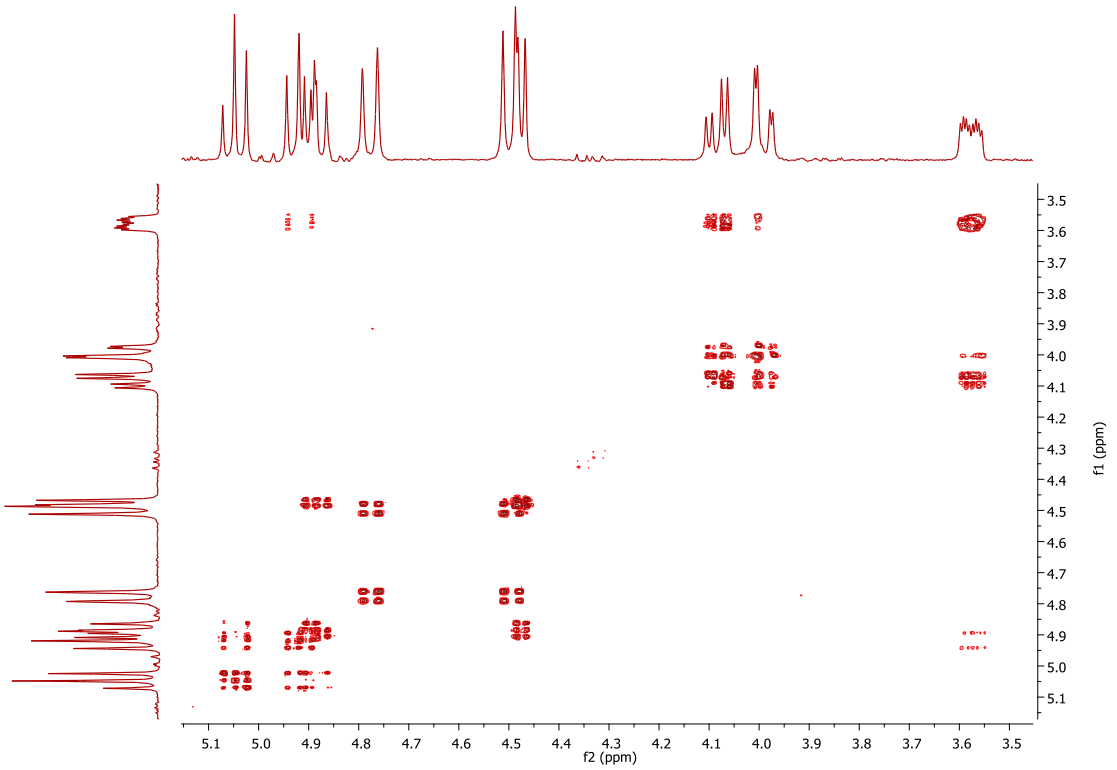

Figure A-56: ^{1}H-^{1}H COSY NMR ($CDCl_3$, 400 MHz) spectrum of compound **RH12** after acetylation.

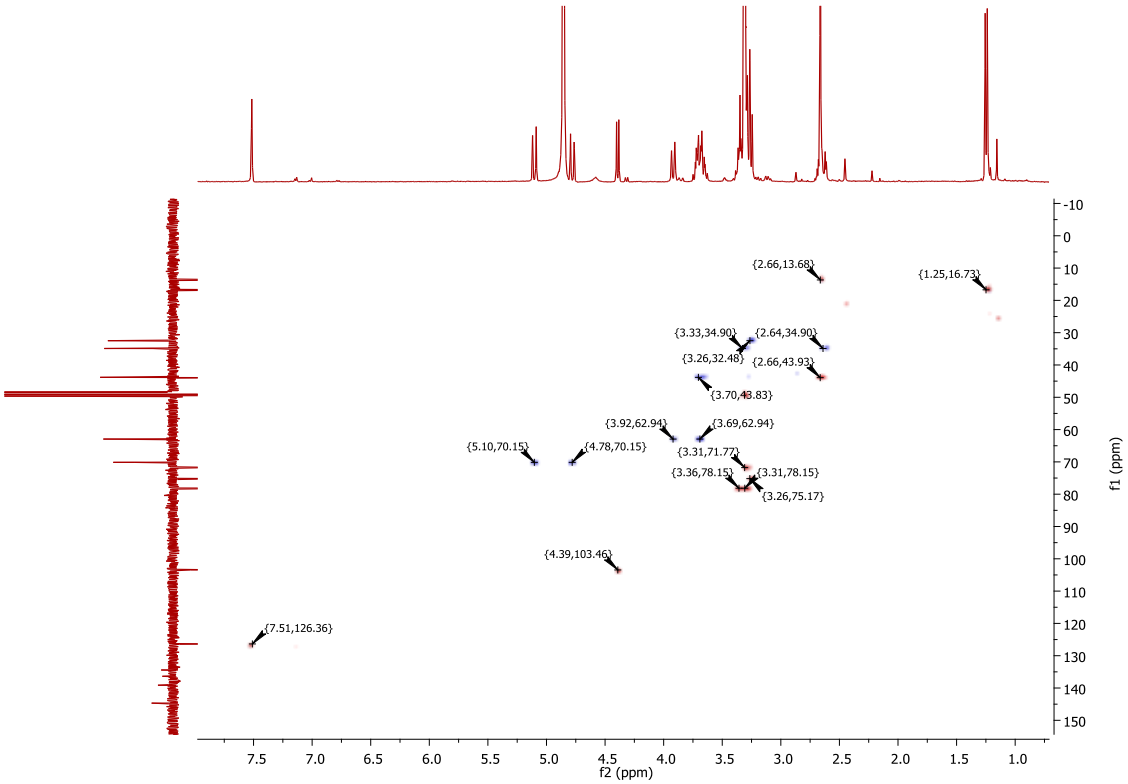

Figure A-57: ^{1}H-^{13}C HSQC NMR spectrum of compound **RH12** in CD_3OD.

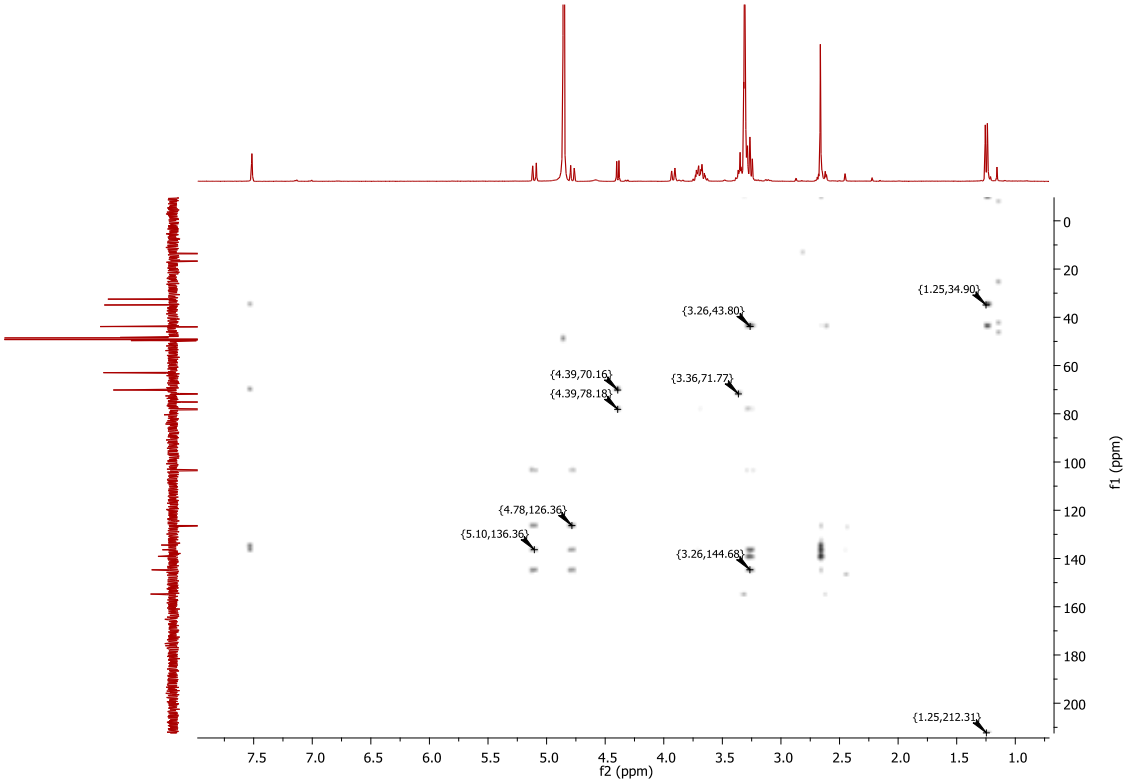

Figure A-58: ^{1}H-^{13}C HMBC NMR spectrum of compound **RH12** in CD_3OD.

11) NMR spectra of compound **RH13** in CD_3OD.

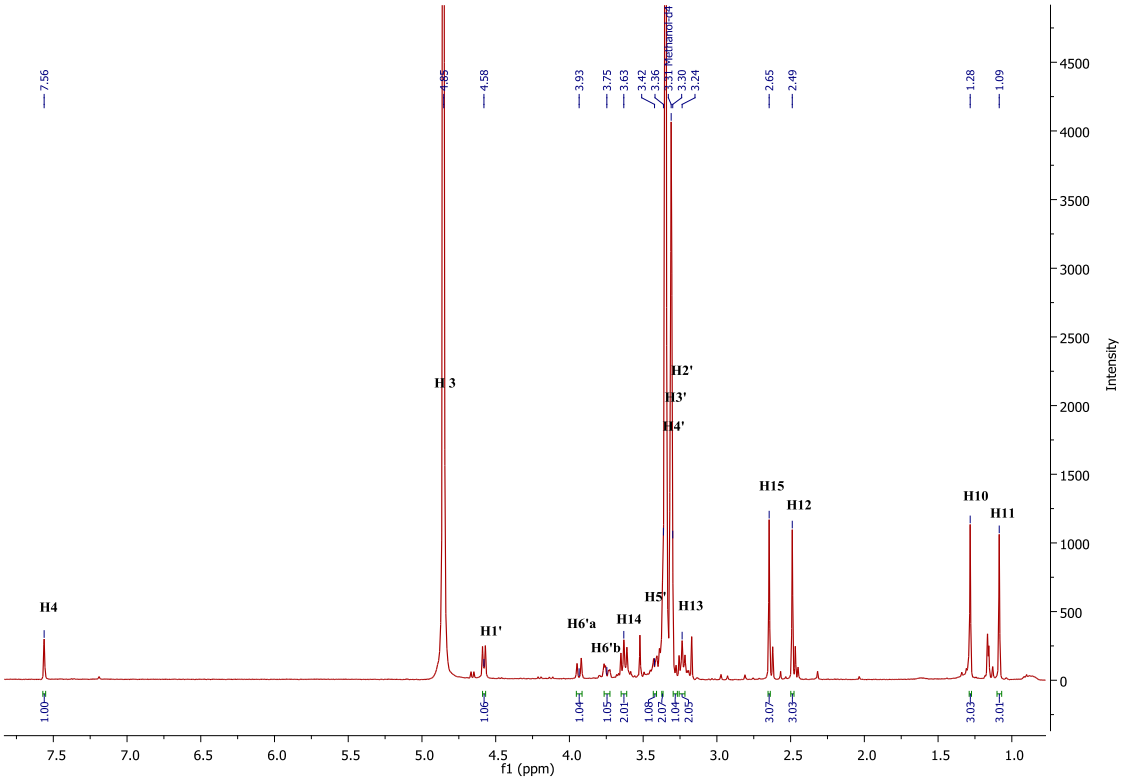

Figure A-59: ^{1}H NMR (CD_3OD, 400 MHz) spectrum of compound **RH13**.

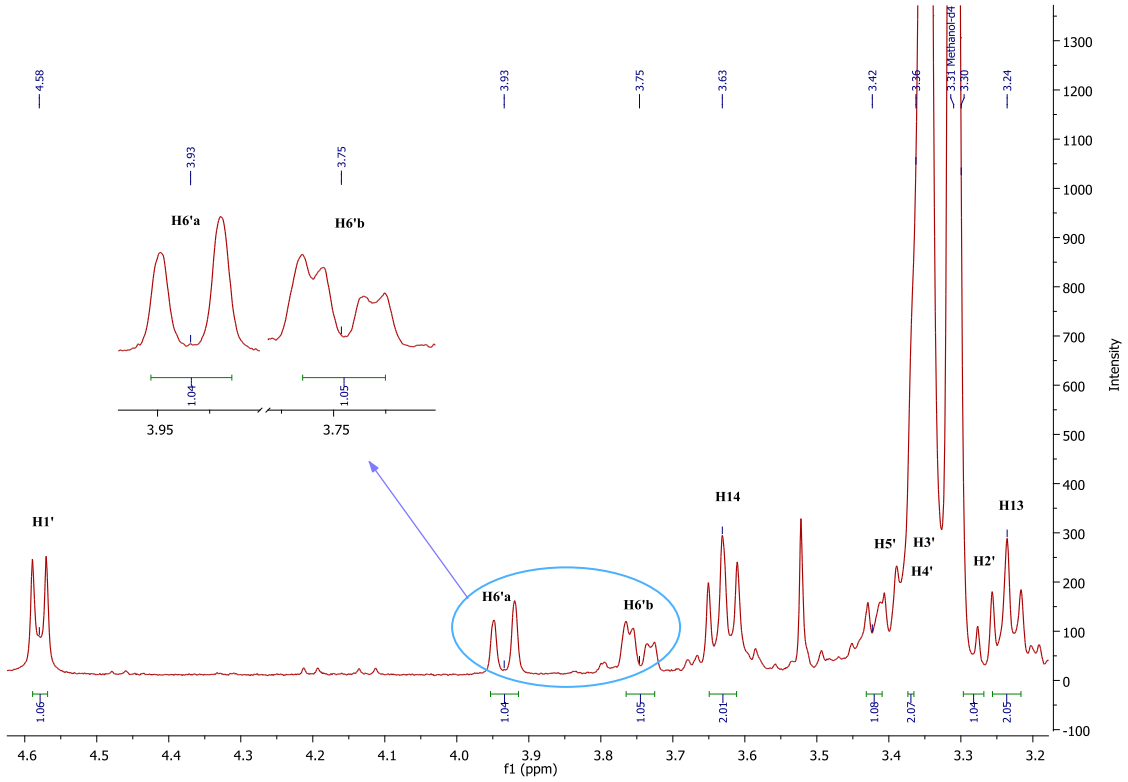

Figure A-60: Expanded ^{1}H NMR (CD_3OD, 400 MHz) spectrum of **RH13** (3.2 – 4.6 ppm).

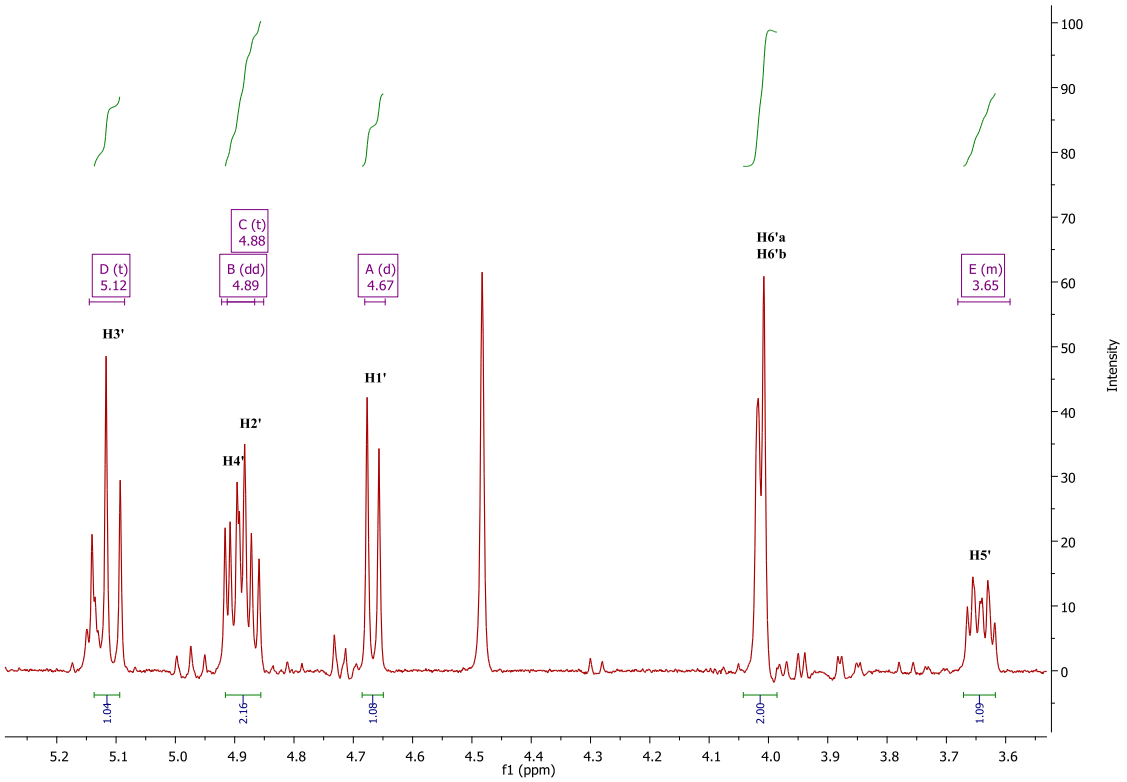

Figure A-61: ^{1}H NMR ($CDCl_3$, 400 MHz) spectrum of compound **RH13** after acetylation.

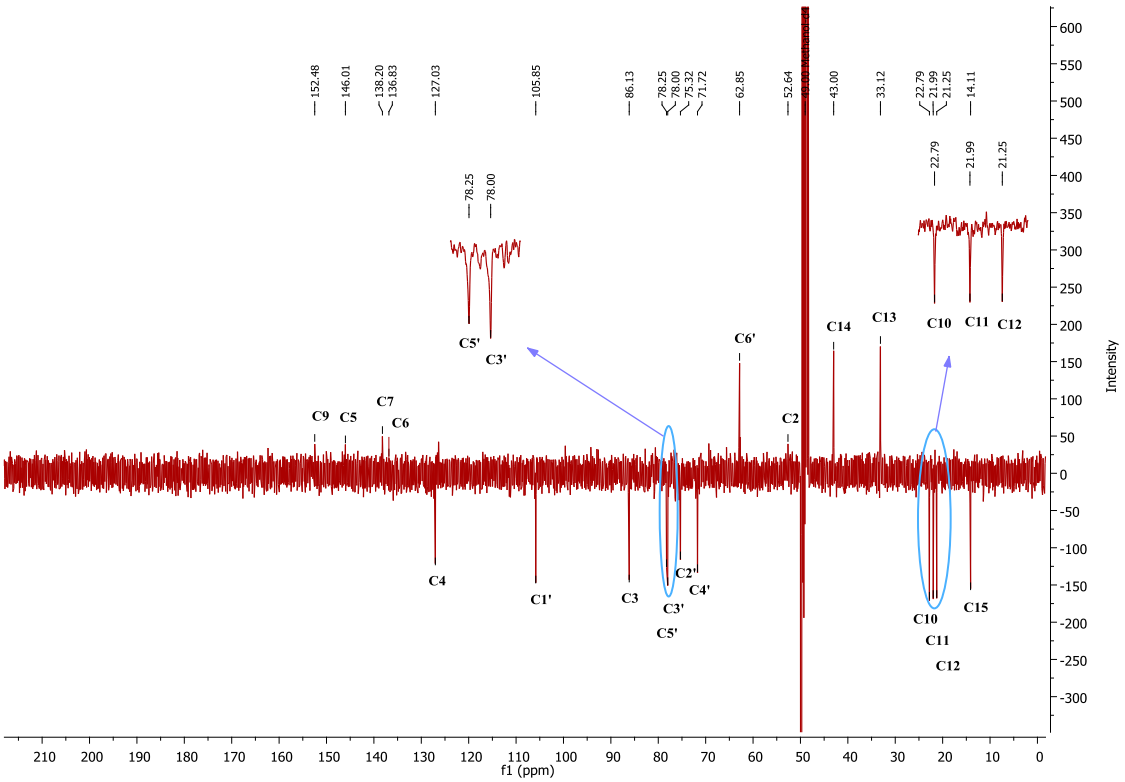

Figure A-62: DEPTQ NMR (CD_3OD, 100 MHz) spectrum of compound **RH13**.

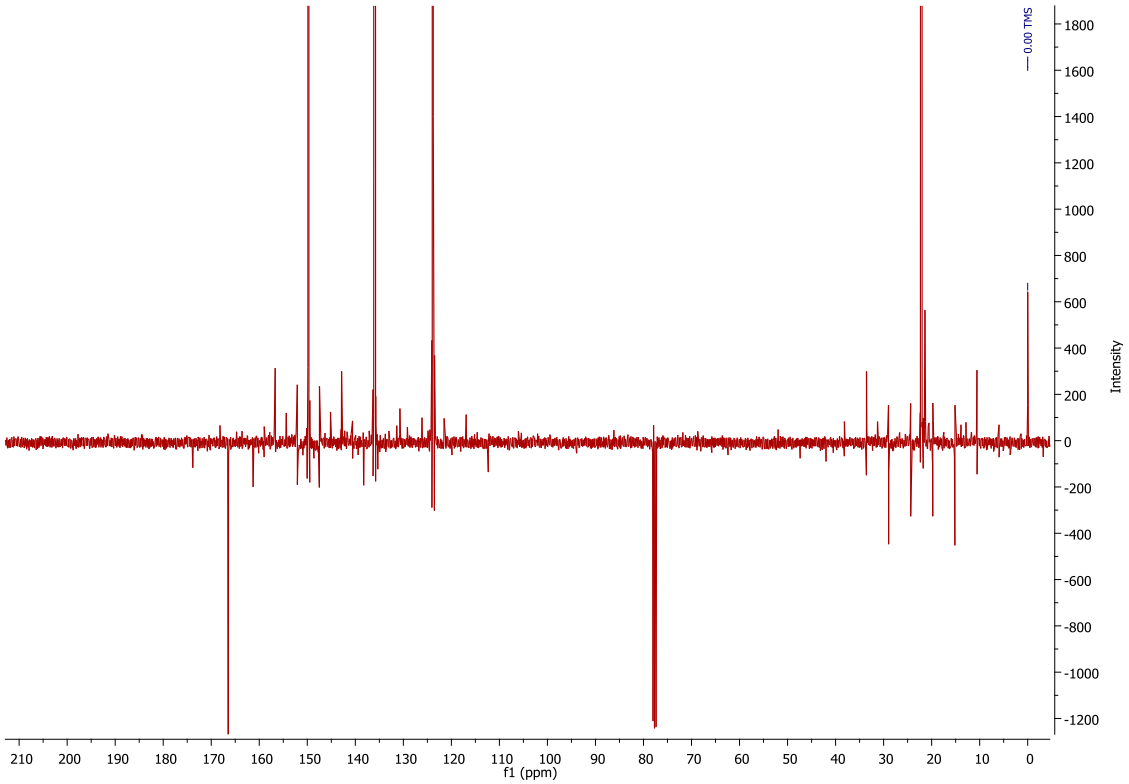

Figure A-63: DEPTQ NMR ($CDCl_3$, 100 MHz) spectrum of compound **RH13** after acetylation.

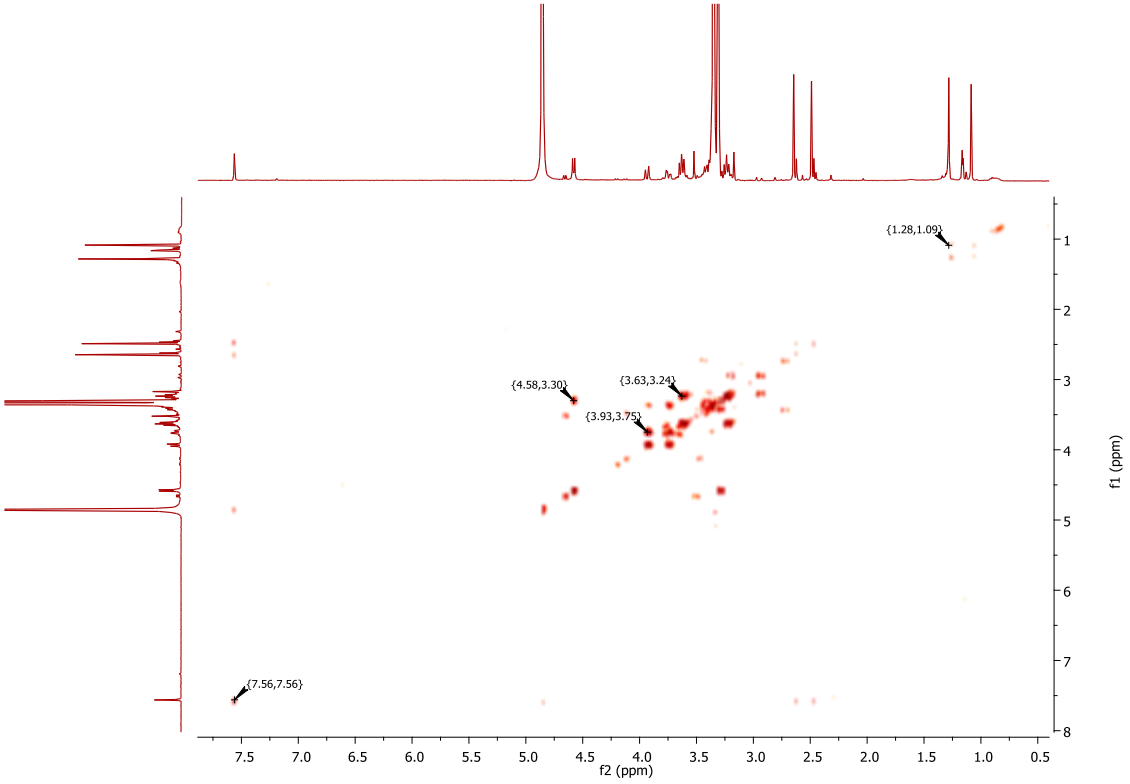

Figure A-64: ^1H-^1H COSY NMR (CD_3OD, 400 MHz) spectrum of compound **RH13**.

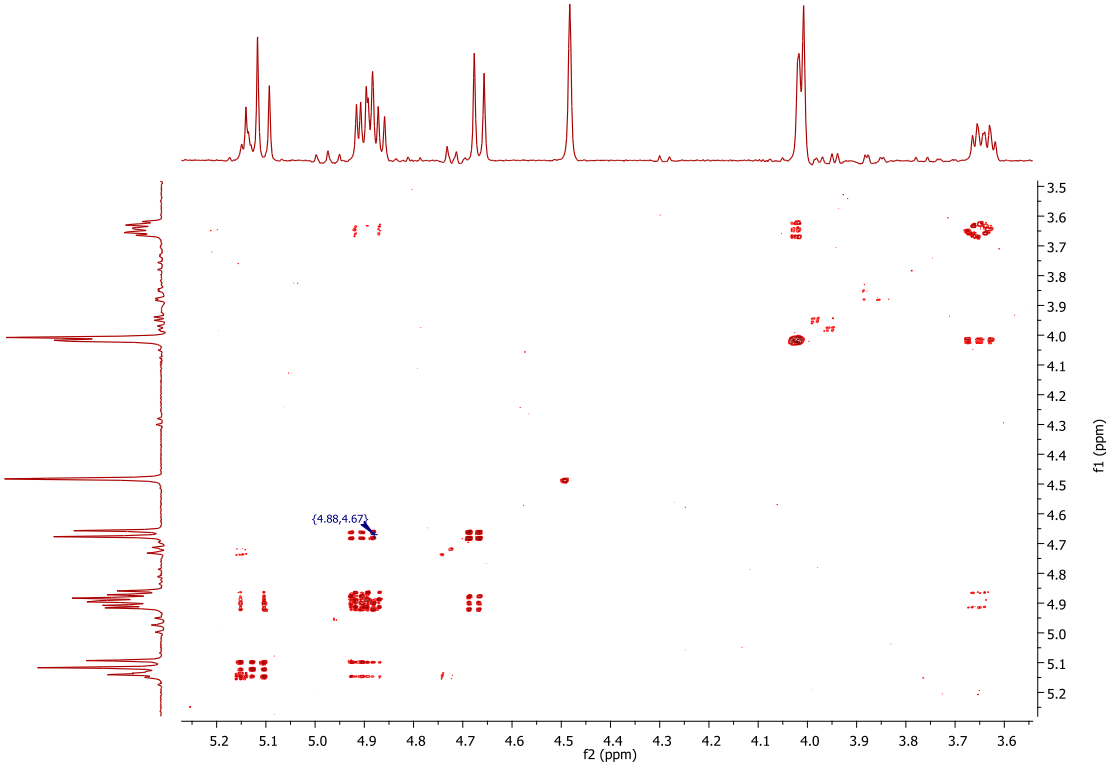

Figure A-65: ^{1}H-^{1}H COSY NMR ($CDCl_3$, 400 MHz) spectrum of compound **RH13** after acetylation.

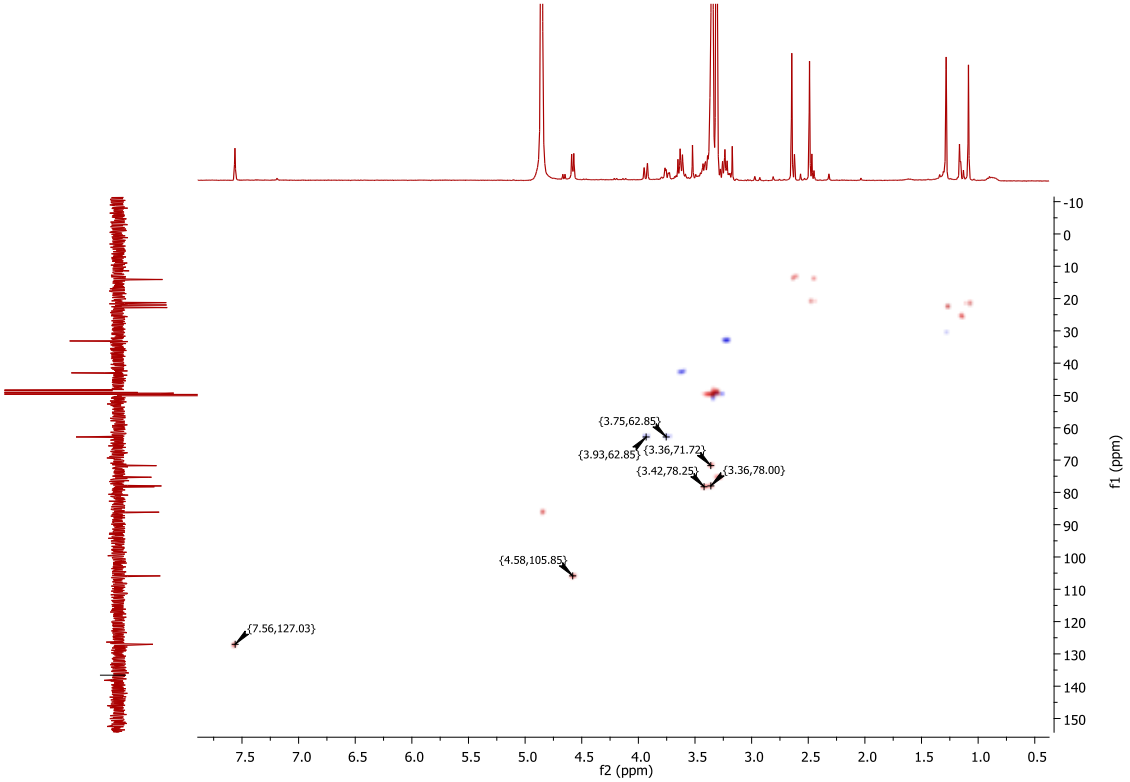

Figure A-66: ^{1}H-^{13}C HSQC NMR spectrum of compound **RH13** in CD_3OD.

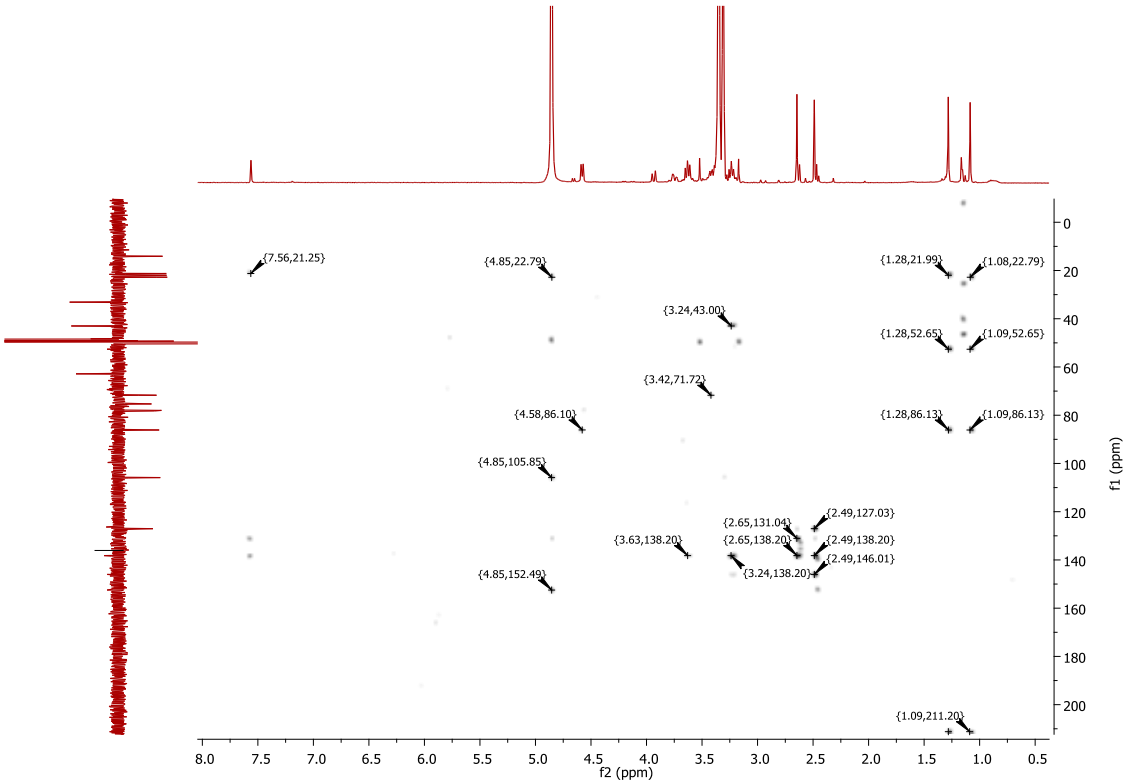

Figure A-67: ^{1}H-^{13}C HMBC NMR spectrum of compound **RH13** in CD_3OD.

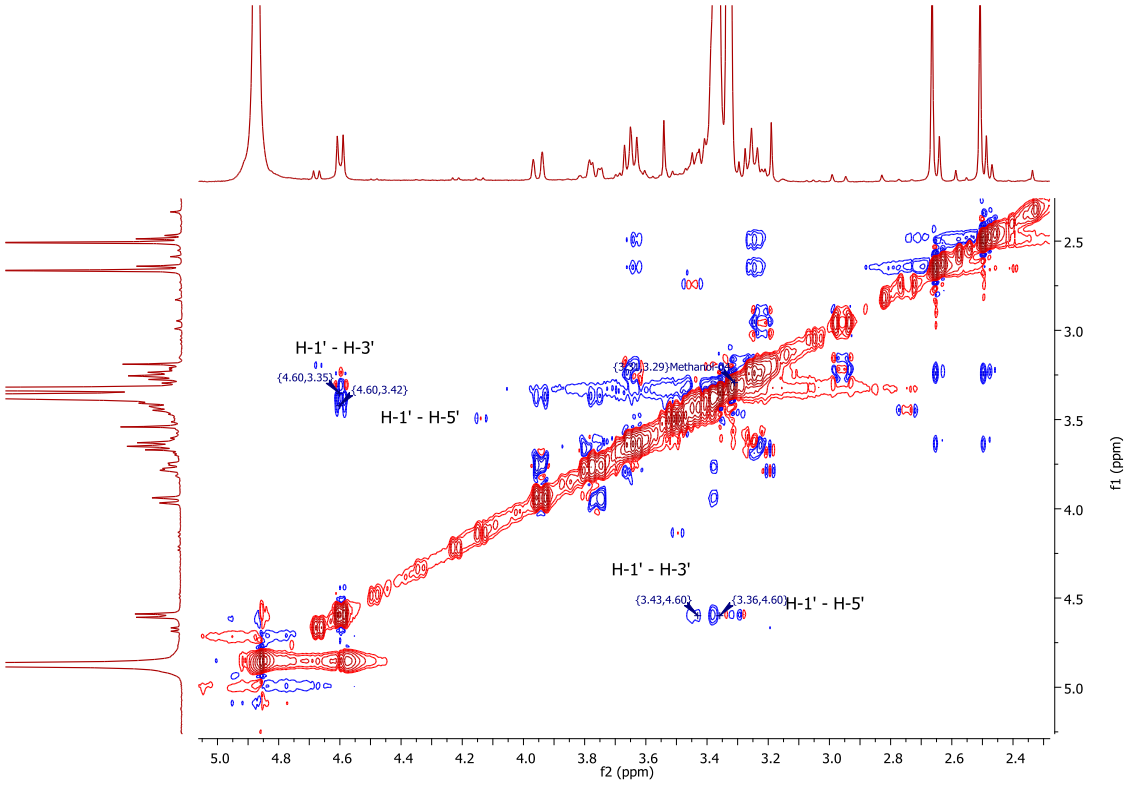

Figure A-68: ^{1}H-^{1}H NOESY NMR (CD_3OD, 400 MHz) spectrum of compound **RH13**.

12) NMR spectra of compound **RH14** in CD_3OD.

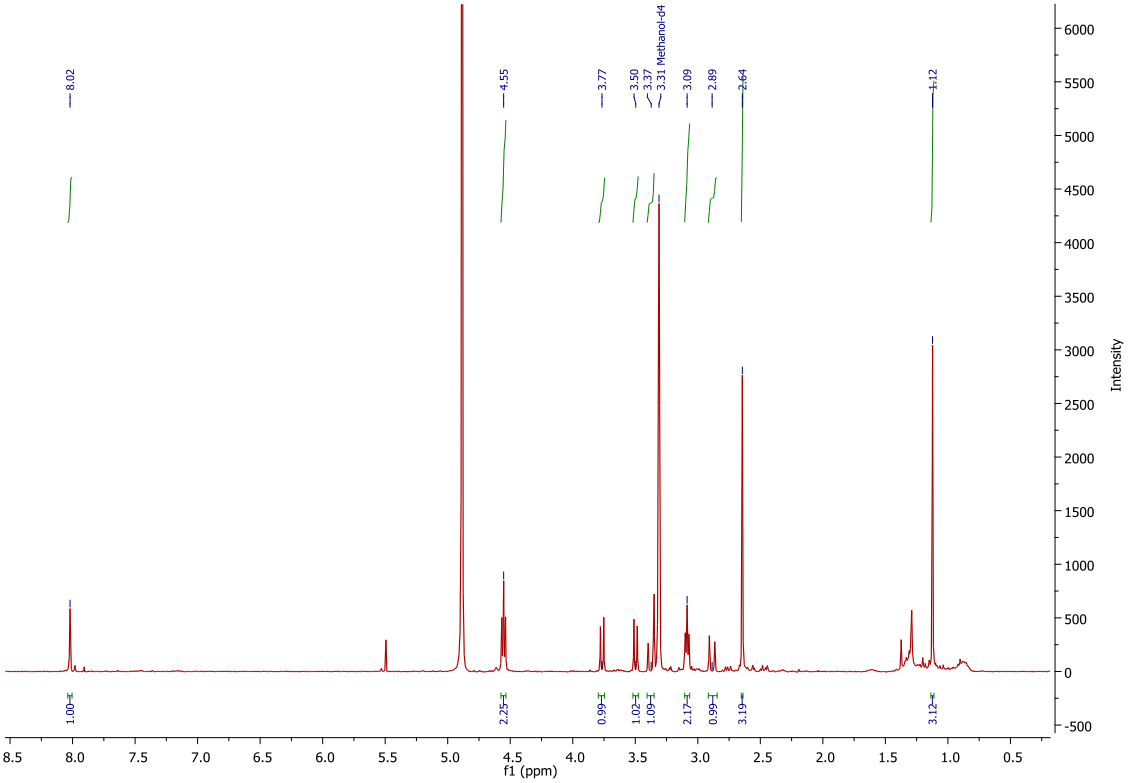

Figure A-69: ^1H NMR (CD_3OD, 400 MHz) spectrum of compound **RH14**.

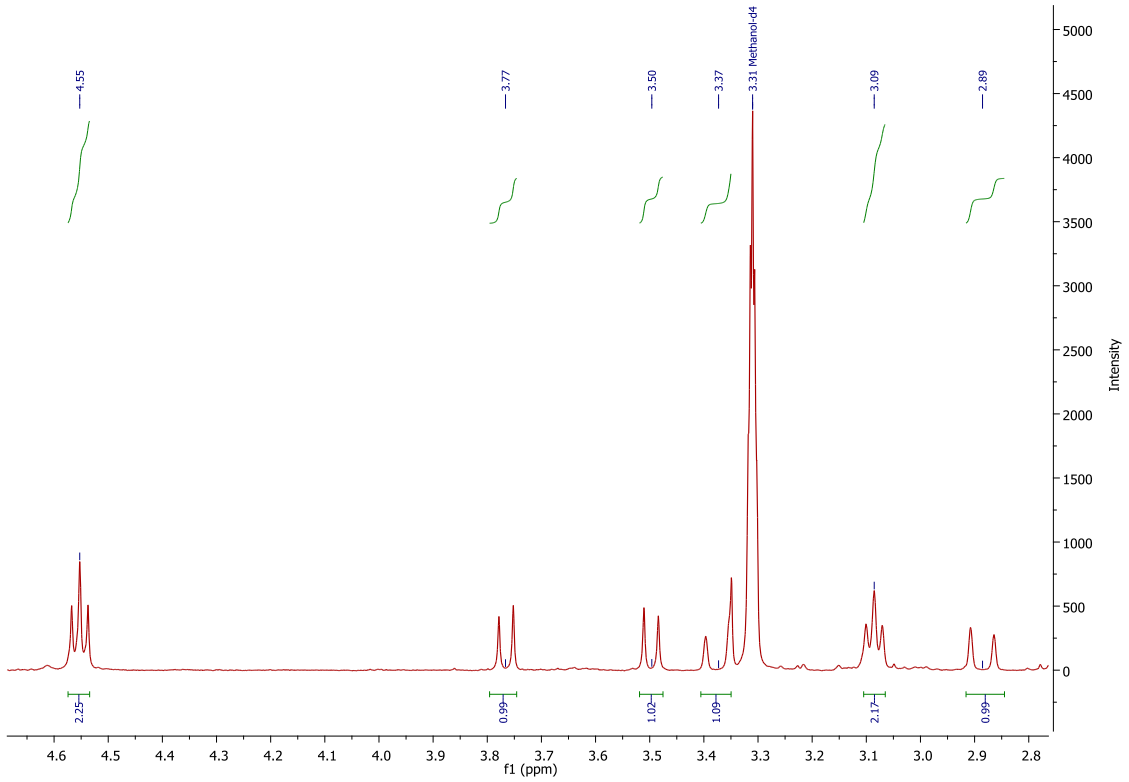

Figure A-70: Expanded ^1H NMR (CD_3OD, 400 MHz) spectrum of **RH14** (2.8 – 4.6 ppm).

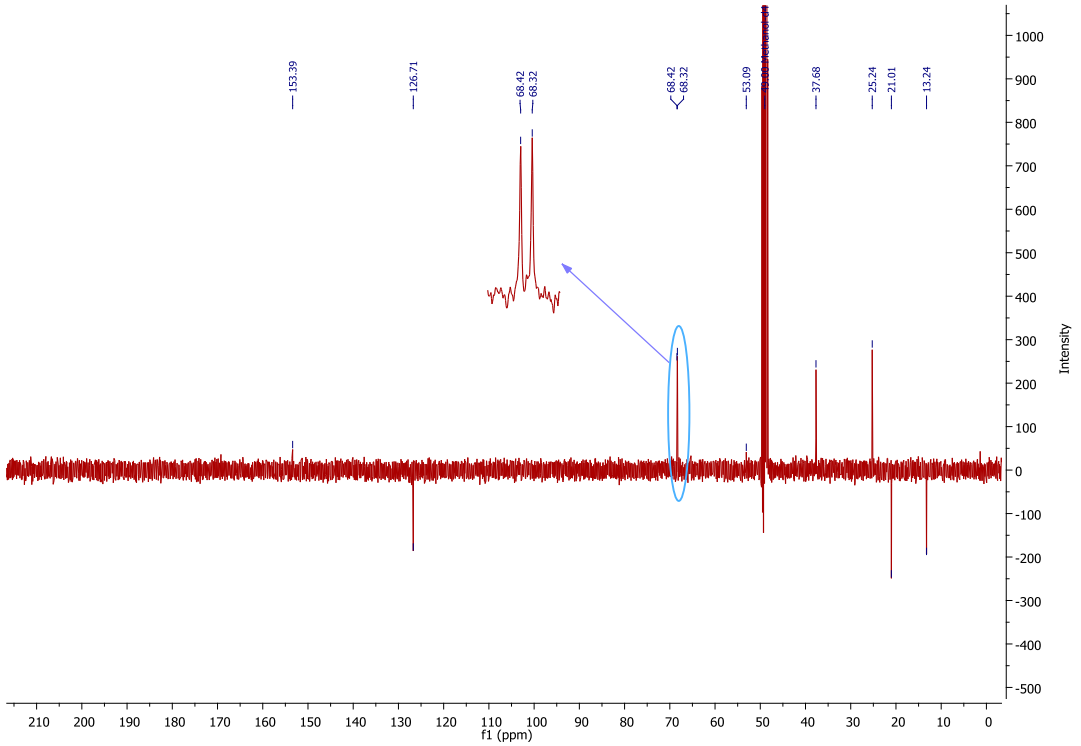

Figure A-71: DEPTQ NMR (CD_3OD, 100 MHz) spectrum of compound **RH14**.

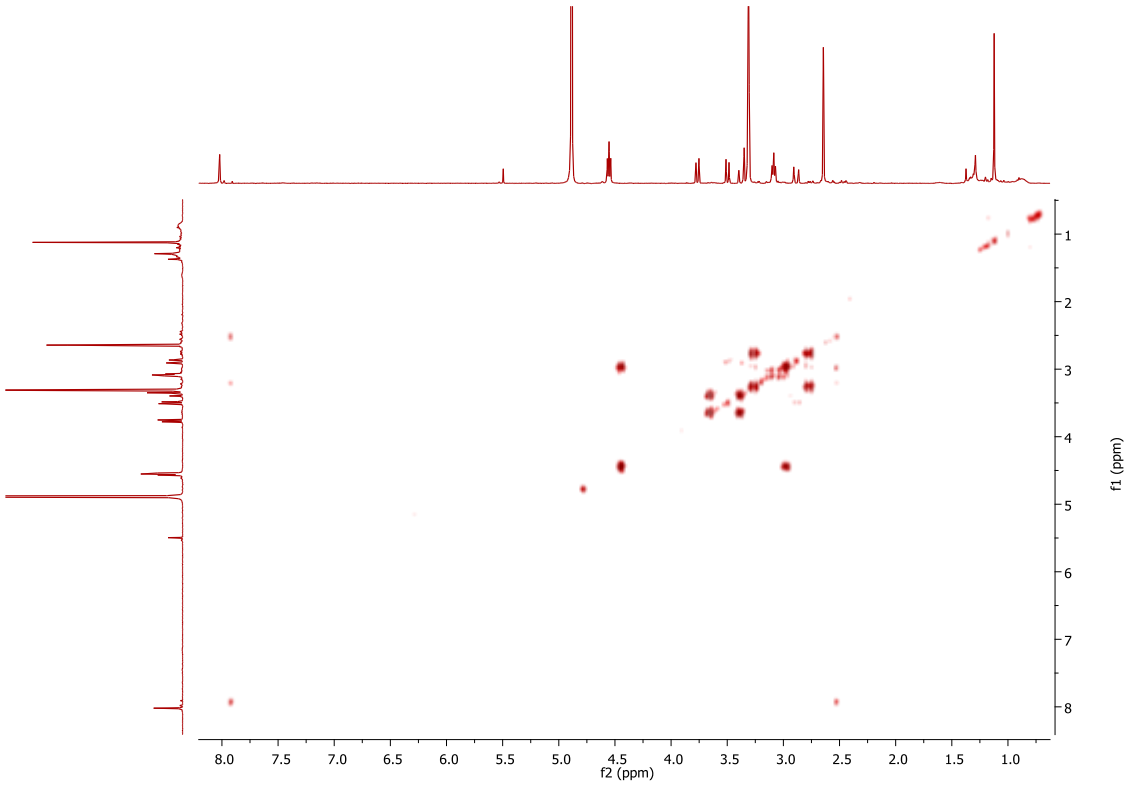

Figure A-72: ^{1}H-^{1}H COSY NMR (CD_3OD, 400 MHz) spectrum of compound **RH14**.

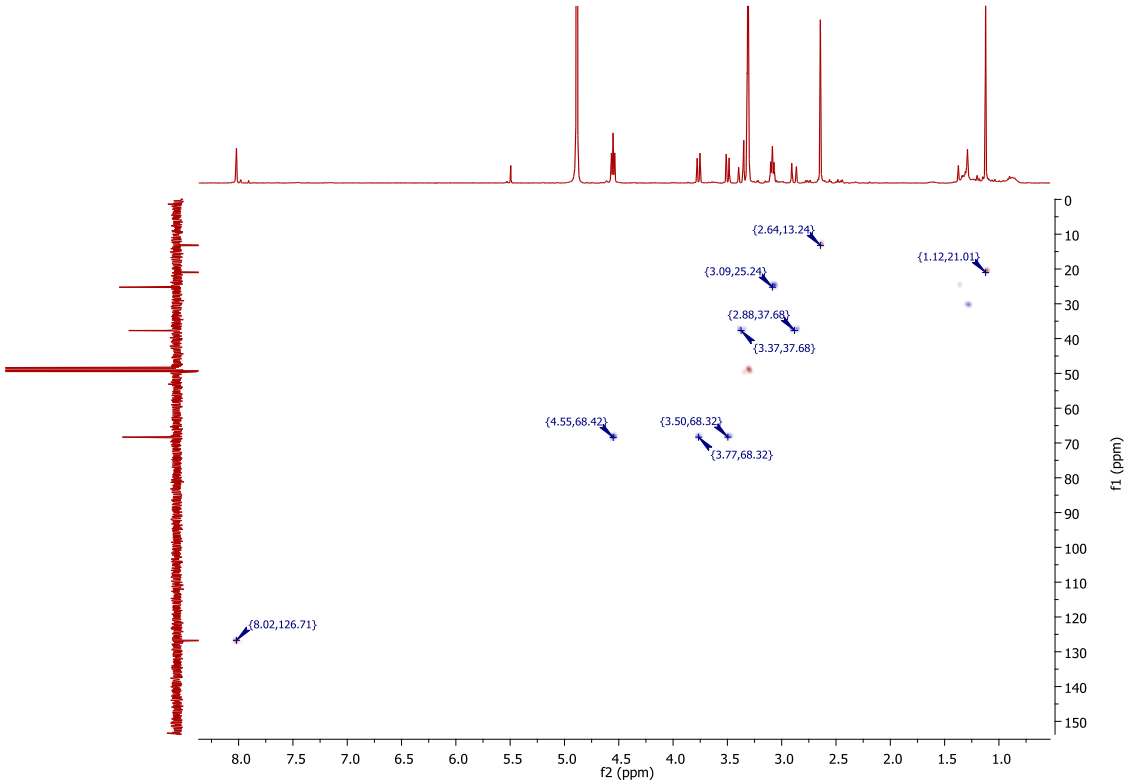

Figure A 73: ^{1}H-^{13}C HSQC NMR spectrum of compound **RH14** in CD_3OD.

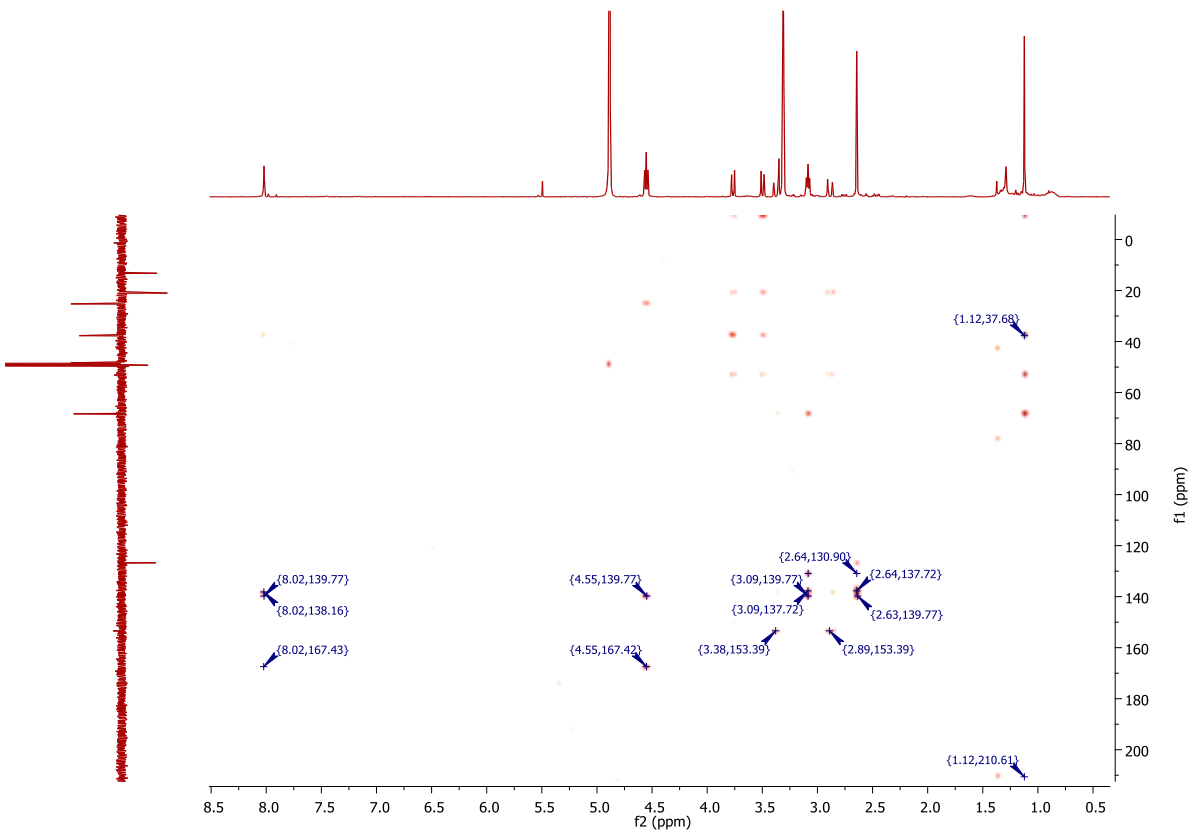

Figure A-74: ^{1}H-^{13}C HMBC NMR spectrum of compound **RH14** in CD_3OD.

13) NMR spectra of compound **RH15** in CD_3OD.

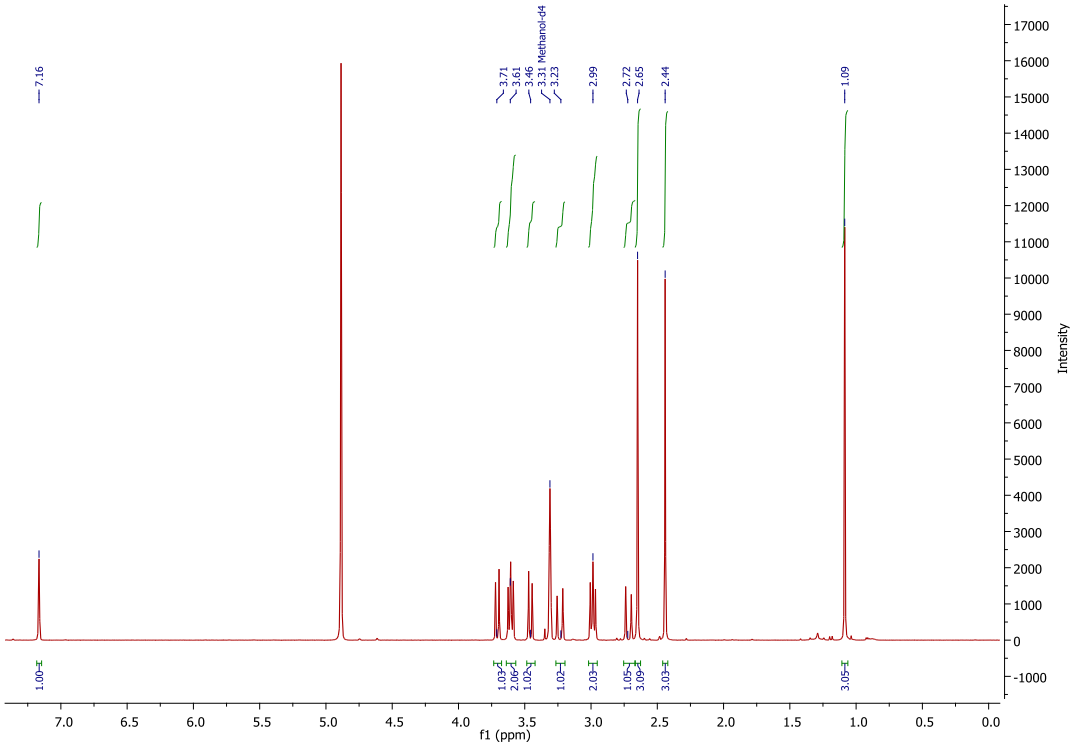

Figure A-75: ^1H NMR (CD_3OD, 400 MHz) spectrum of compound **RH15**.

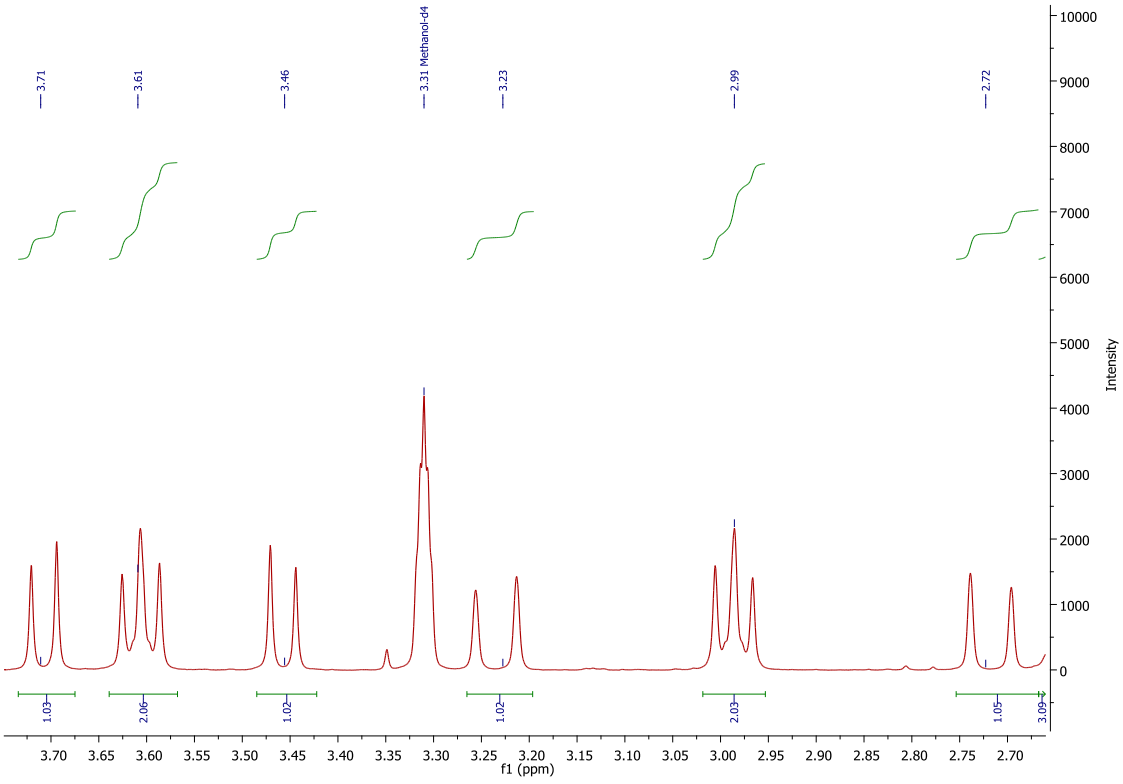

Figure A-76: Expanded ^1H NMR (CD_3OD, 400 MHz) spectrum of **RH15** (2.7 – 3.7 ppm).

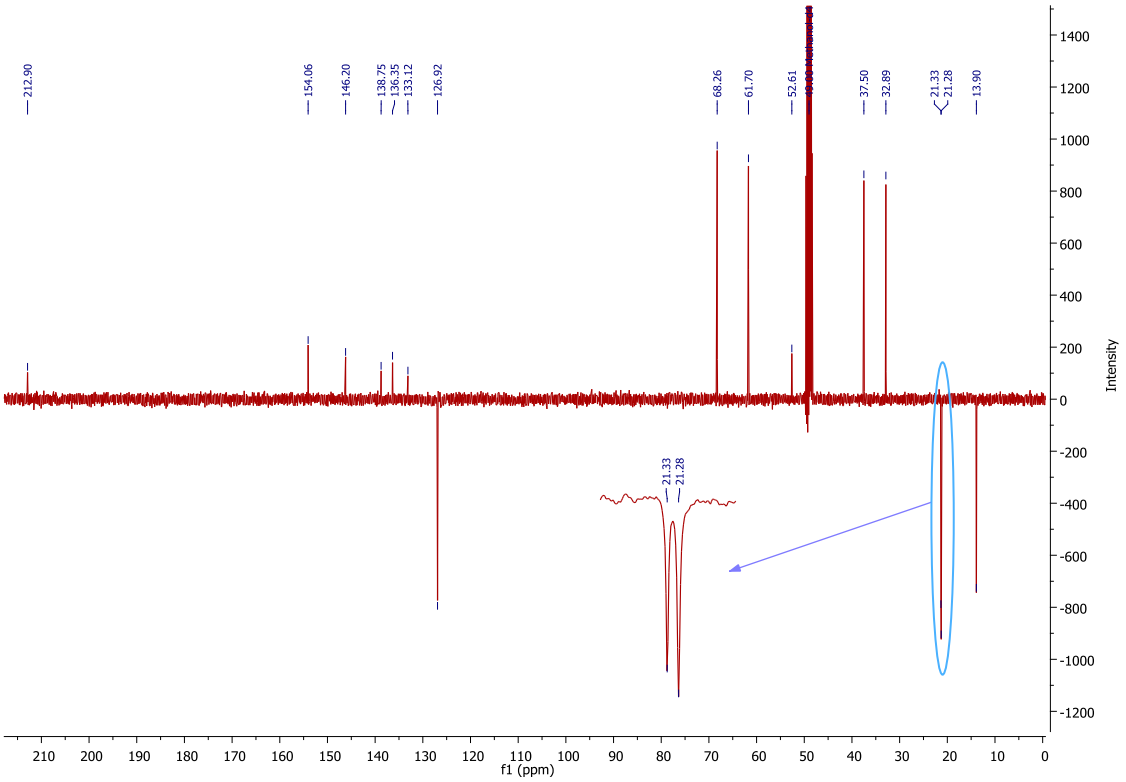

Figure A-77: DEPTQ NMR (CD_3OD, 100 MHz) spectrum of compound **RH15**.

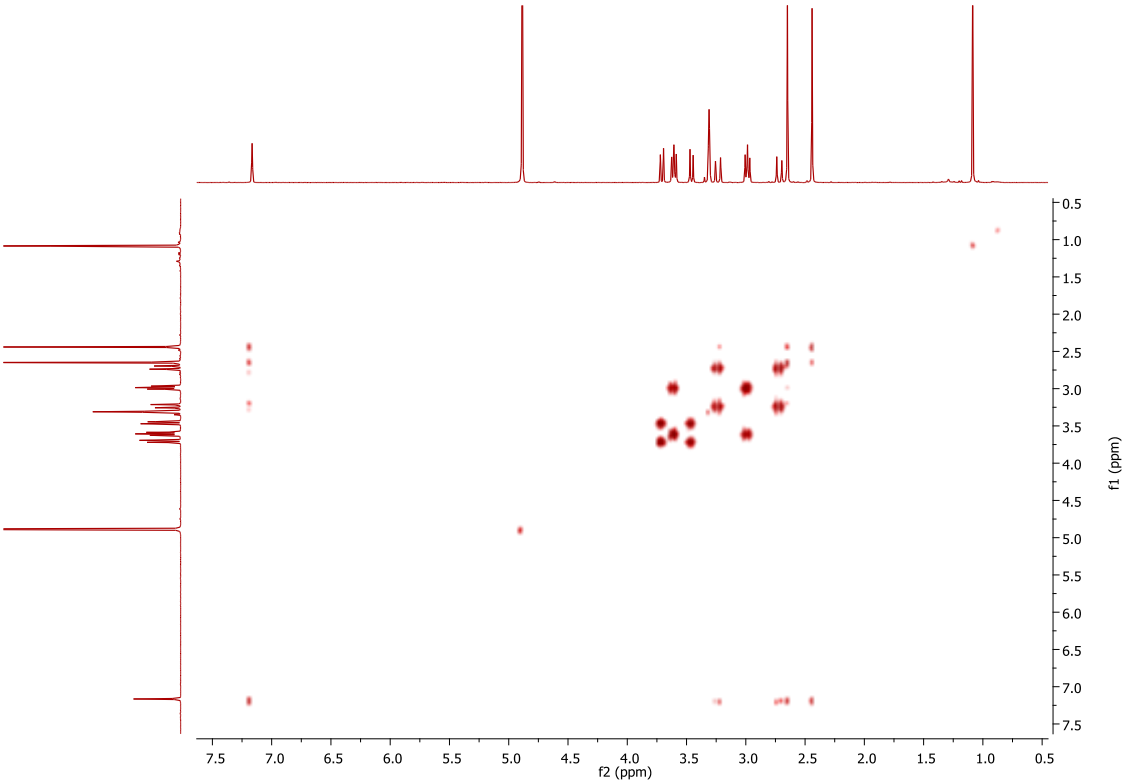

Figure A-78: ^{1}H-^{1}H COSY NMR (CD_3OD, 400 MHz) spectrum of compound **RH15**.

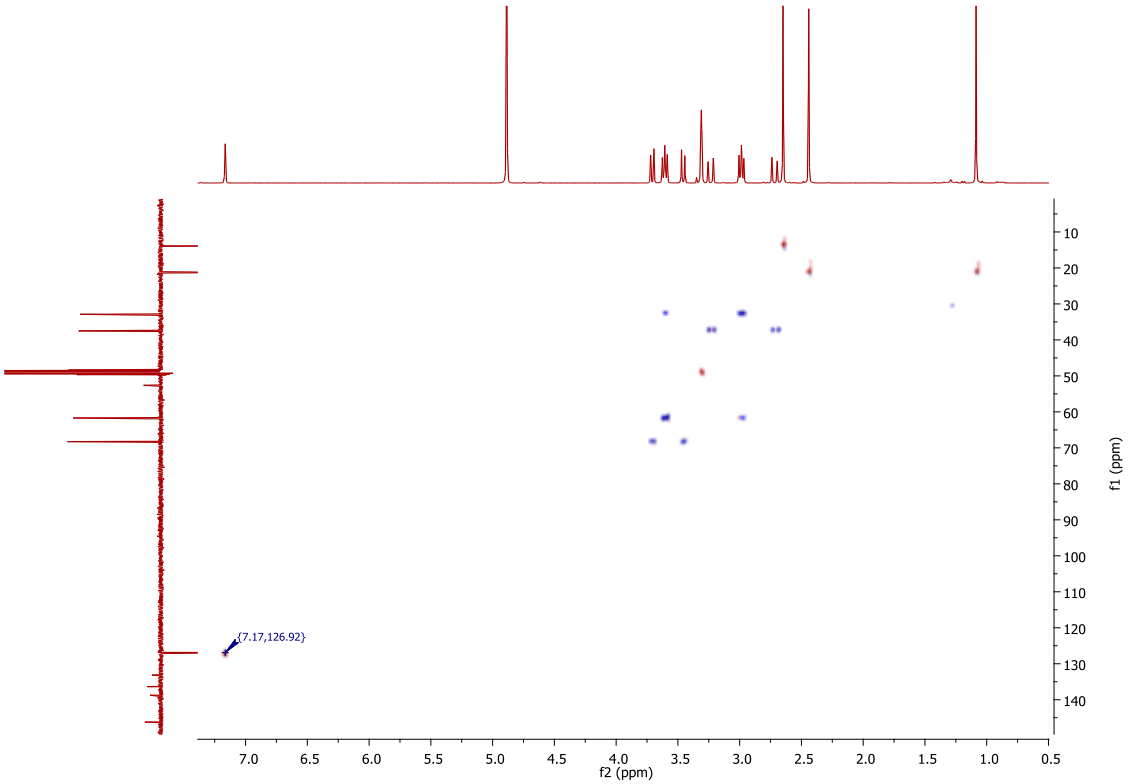

Figure A-79: ^{1}H-^{13}C HSQC NMR spectrum of compound **RH15** in CD_3OD.

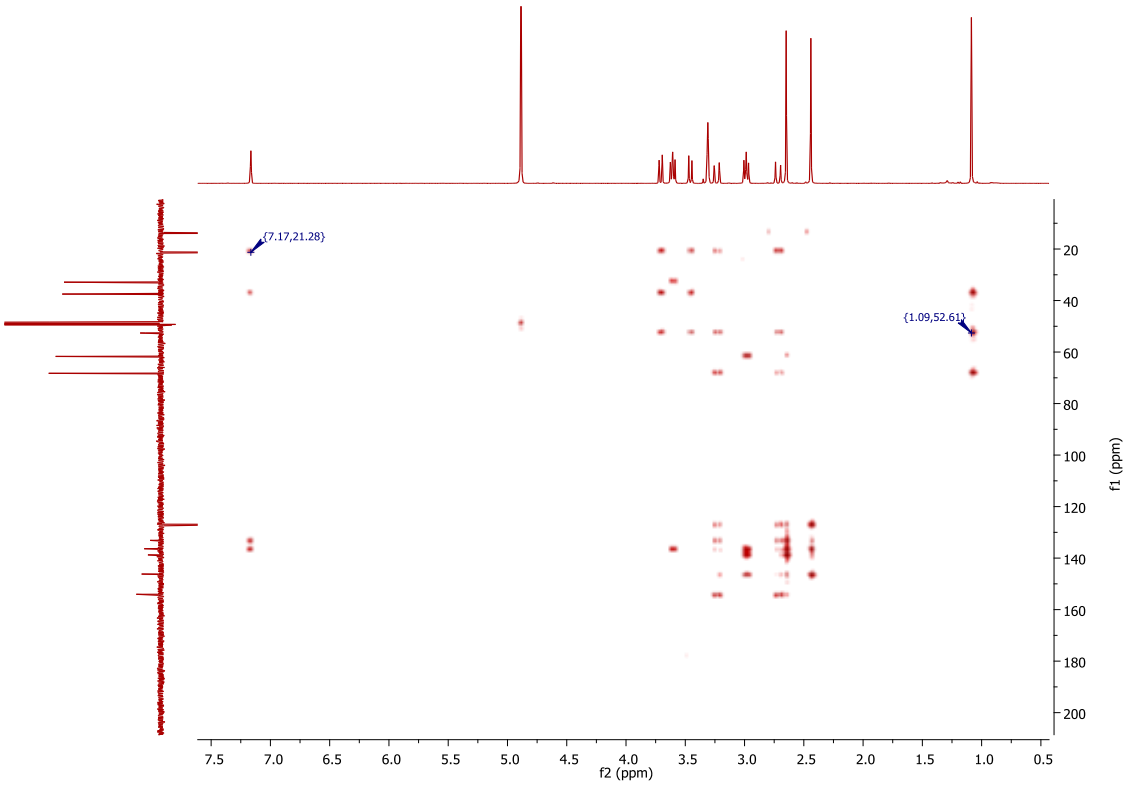

Figure A-80: ^{1}H-^{13}C HMBC NMR spectrum of compound **RH15** in CD_3OD.

14) NMR spectra of compound **RH16** in $CDCl_3$.

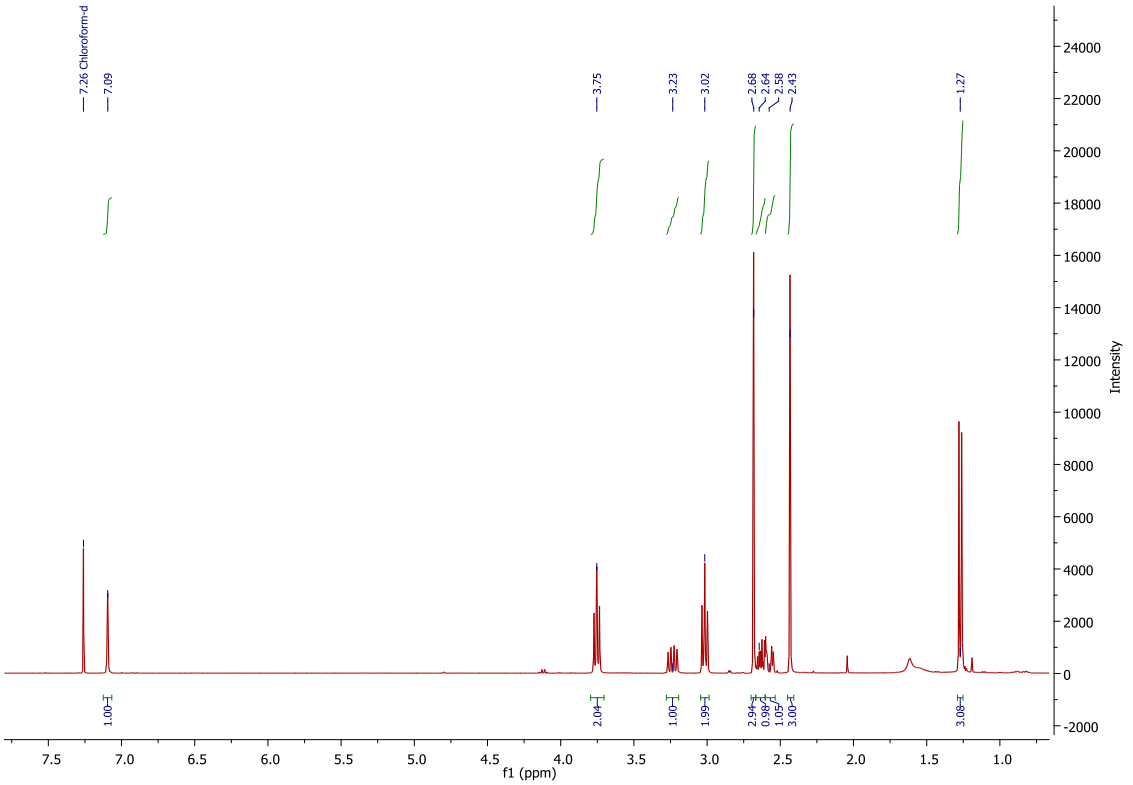

Figure A-81: ^{1}H NMR ($CDCl_3$, 400 MHz) spectrum of compound **RH16**.

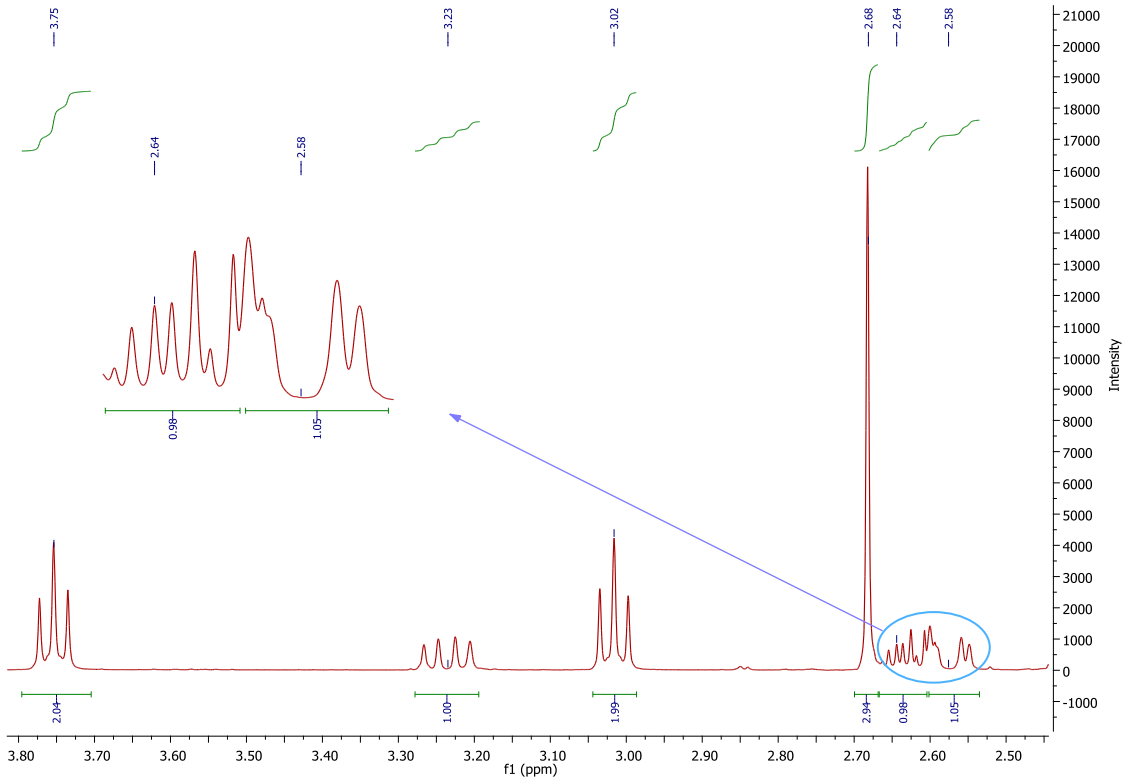

Figure A-82: Expanded ^{1}H NMR ($CDCl_3$, 400 MHz) spectrum of **RH16** (2.5 – 3.8 ppm).

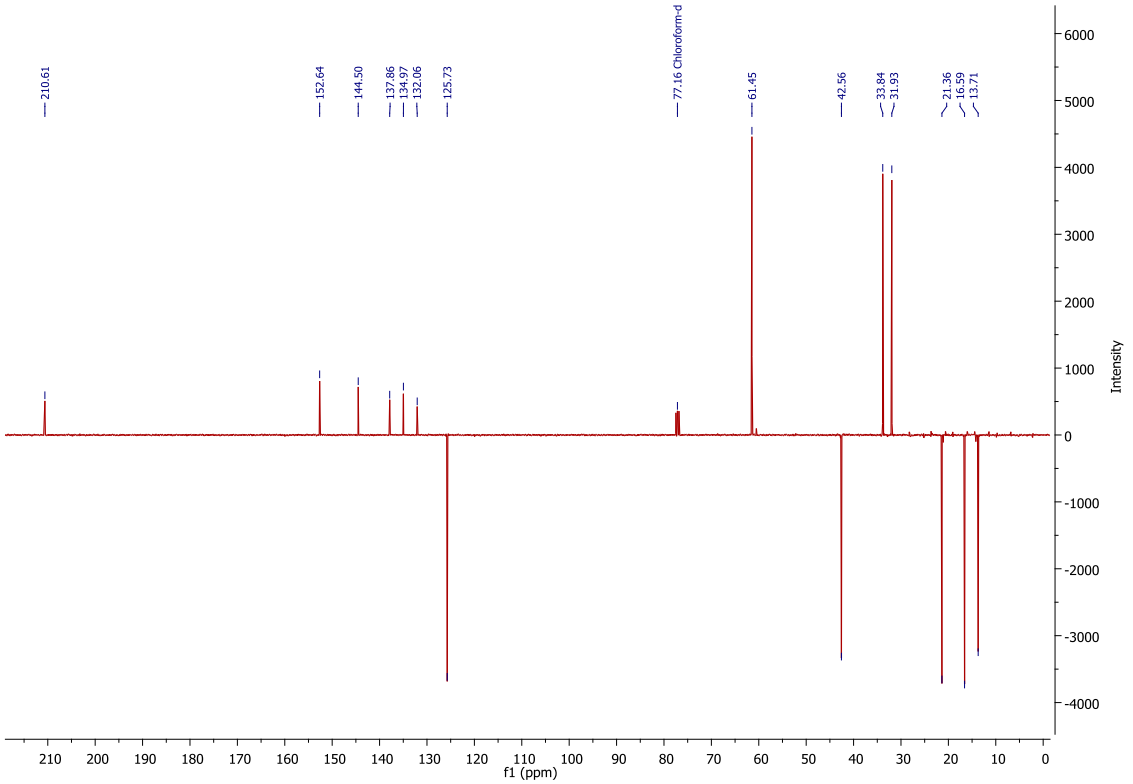

Figure A-83: DEPTQ NMR ($CDCl_3$, 100 MHz) spectrum of compound **RH16**.

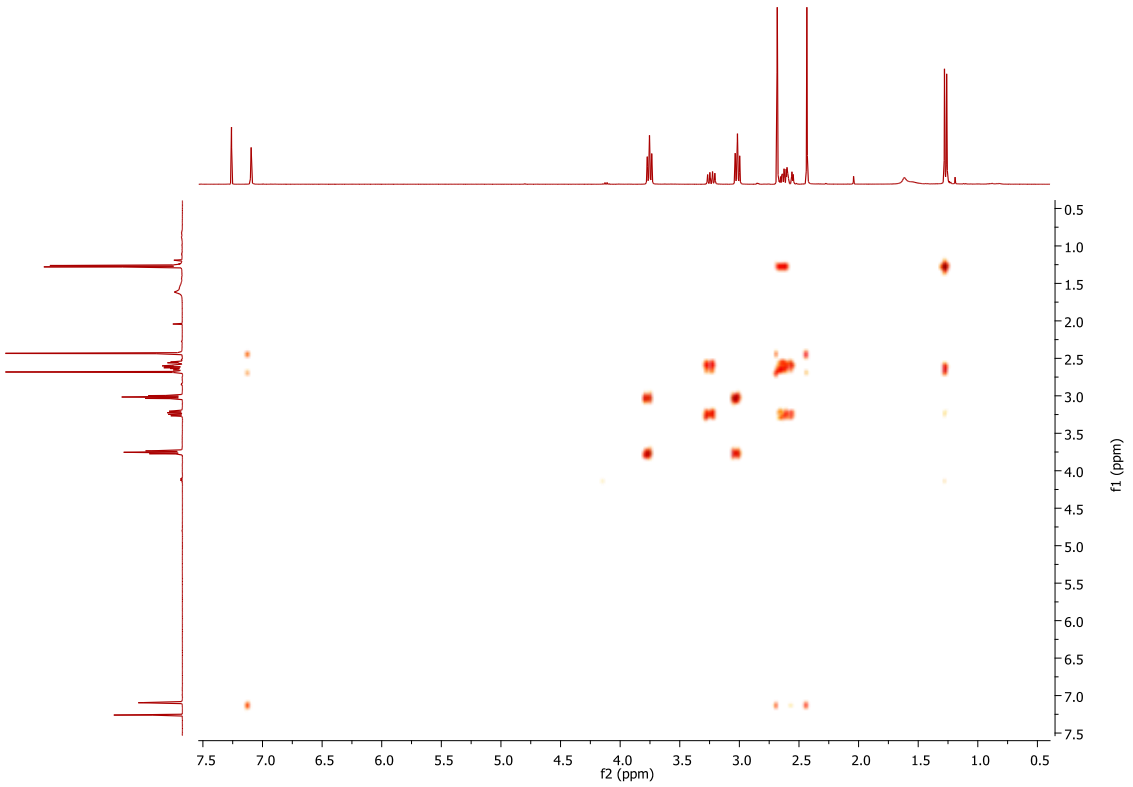

Figure A-84: ^{1}H-^{1}H COSY NMR ($CDCl_3$, 400 MHz) spectrum of compound **RH16**.

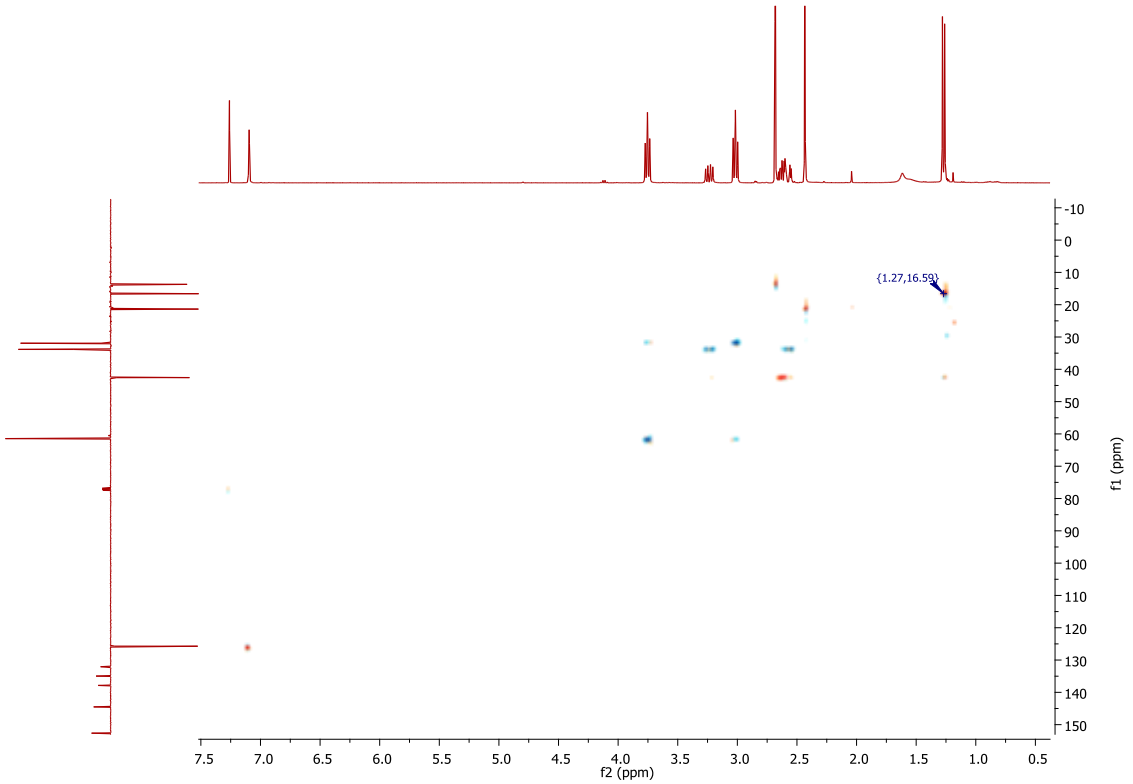

Figure A-85: ^{1}H-^{13}C HSQC NMR spectrum of compound **RH16** in $CDCl_3$.

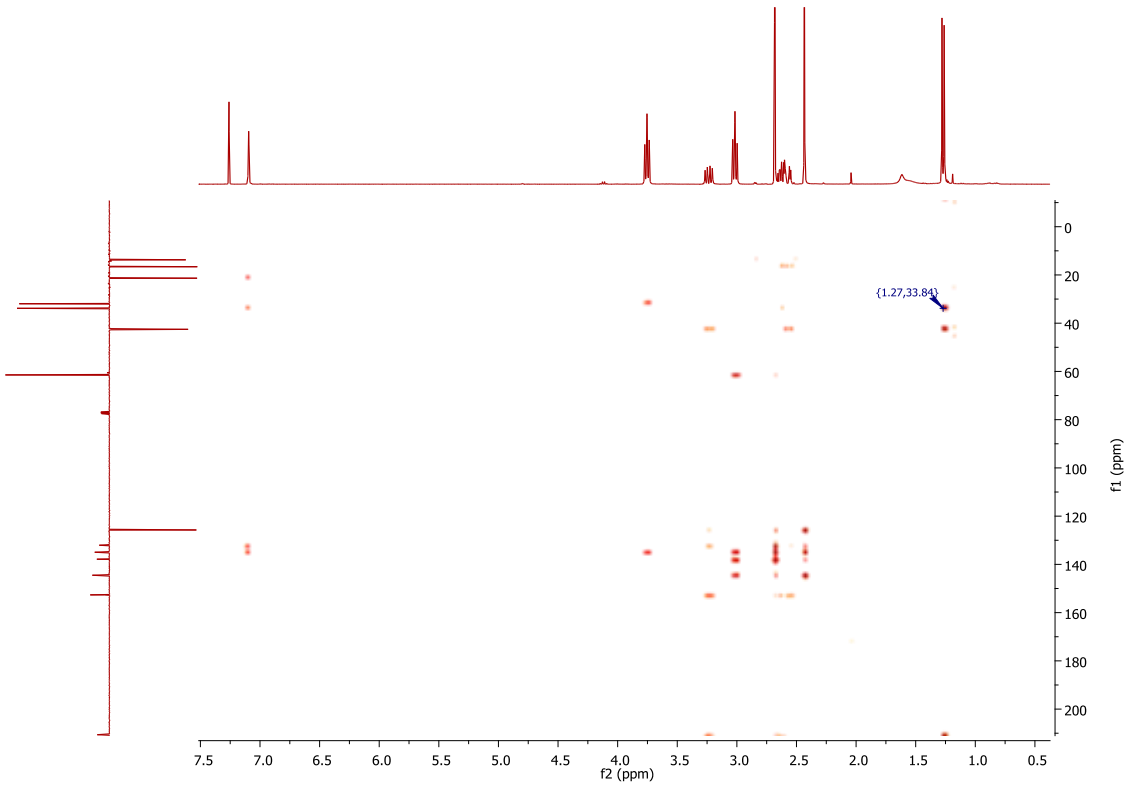

Figure A-86: ^{1}H-^{13}C HMBC NMR spectrum of compound **RH16** in $CDCl_3$.

15) NMR spectra of compound **RH17** in CD_3OD.

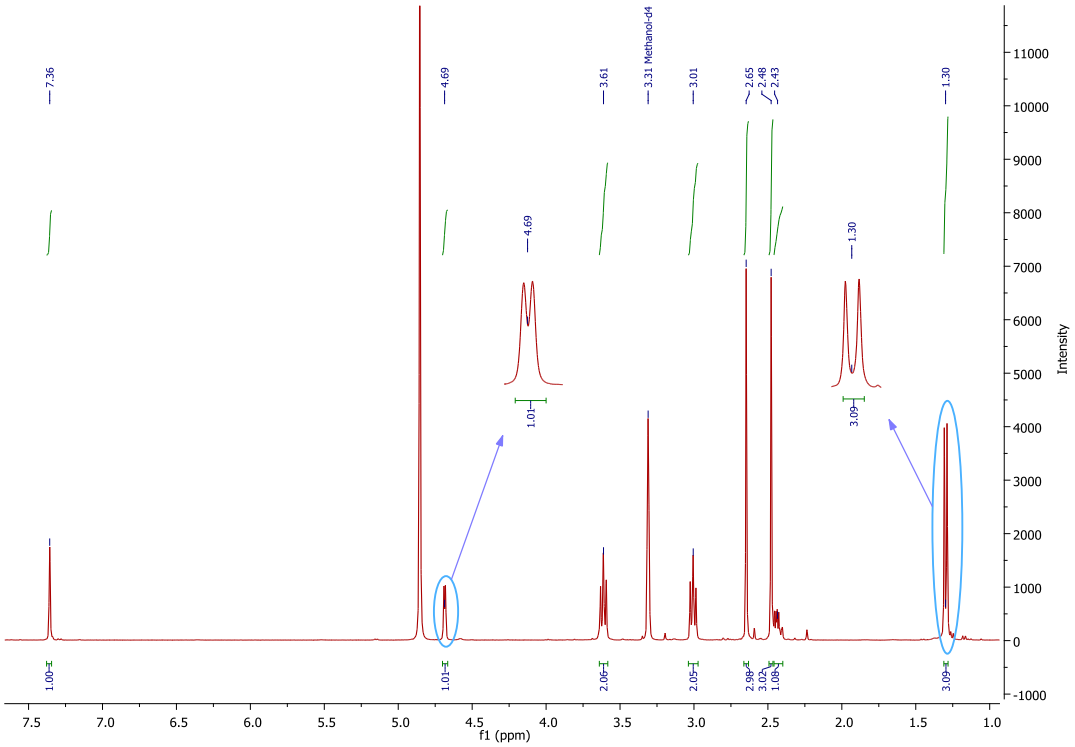

Figure A-87: ^1H NMR (CD_3OD, 400 MHz) spectrum of compound **RH17**.

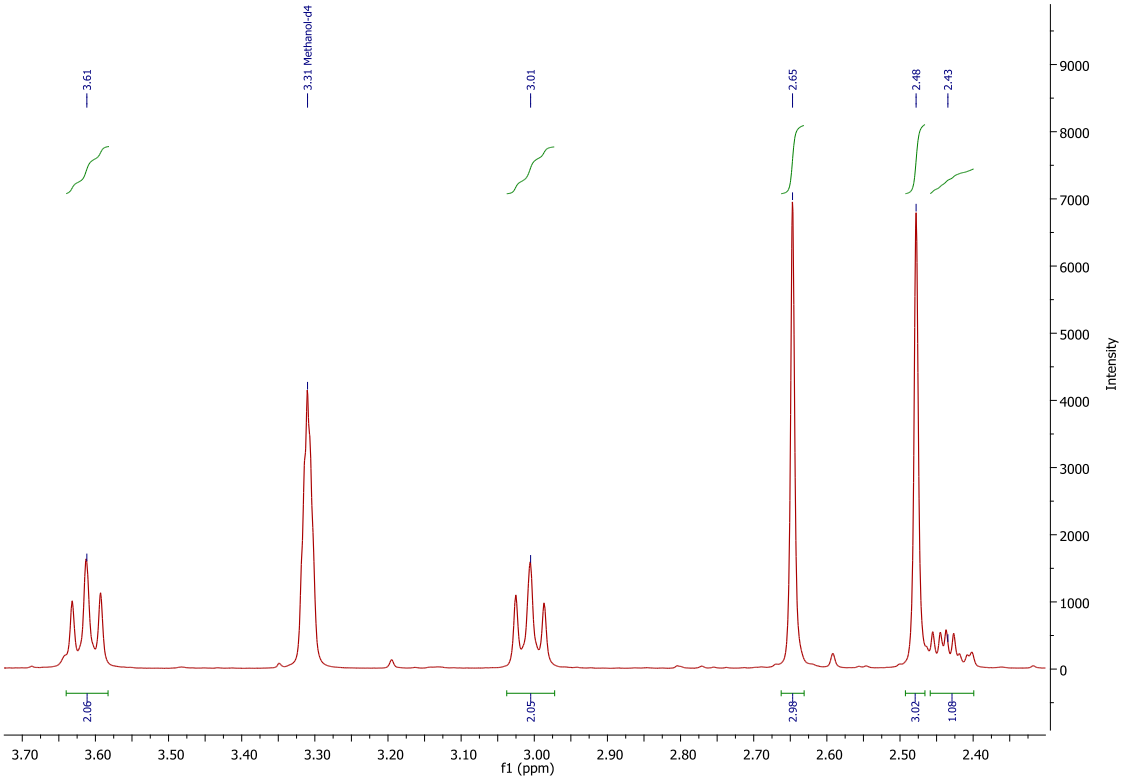

Figure A-88: Expanded ^1H NMR (CD_3OD, 400 MHz) spectrum of **RH17** (2.4 – 3.7 ppm).

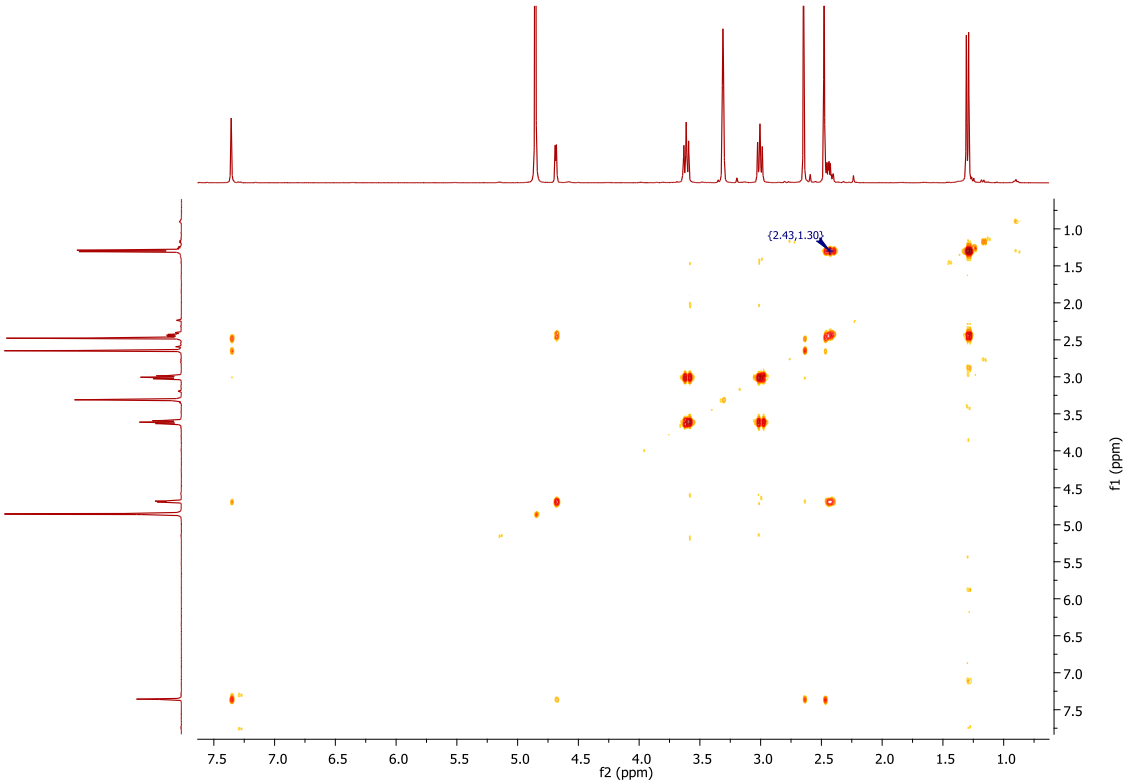

Figure A-89: ^{1}H-^{1}H COSY NMR (CD_3OD, 400 MHz) spectrum of compound **RH17**.

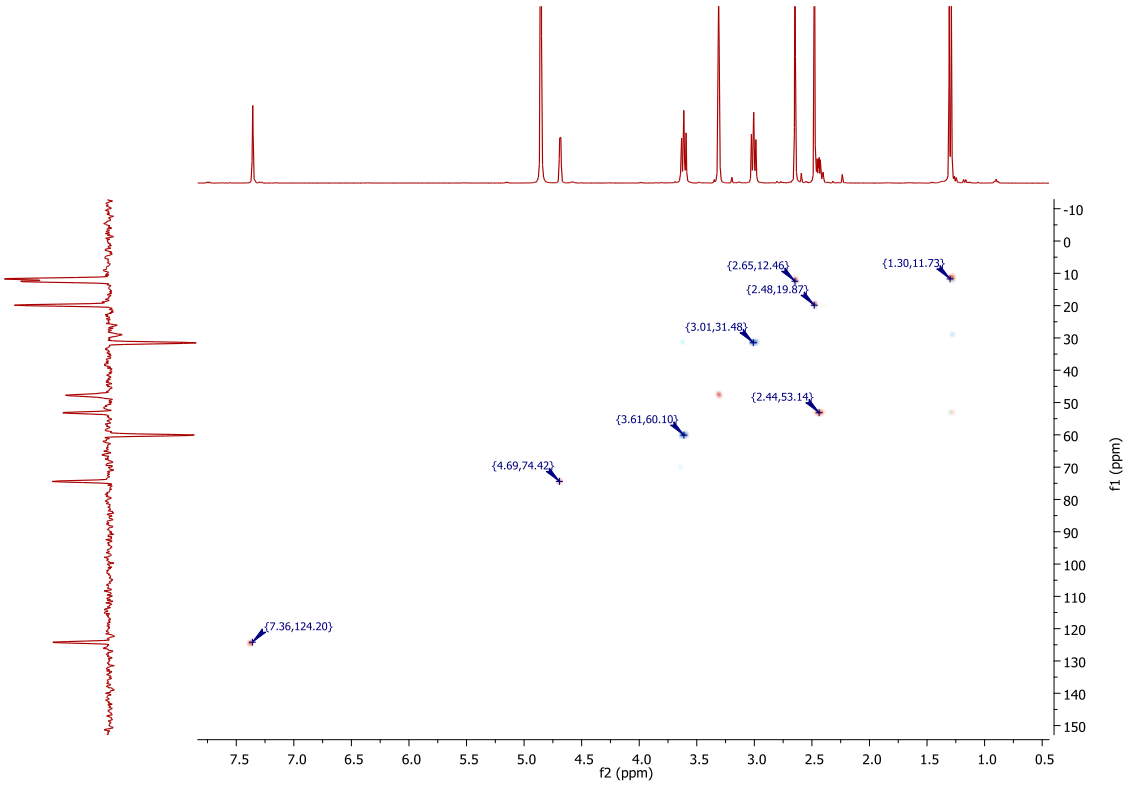

Figure A-90: ^{1}H-^{13}C HSQC NMR spectrum of compound **RH17** in CD_3OD.

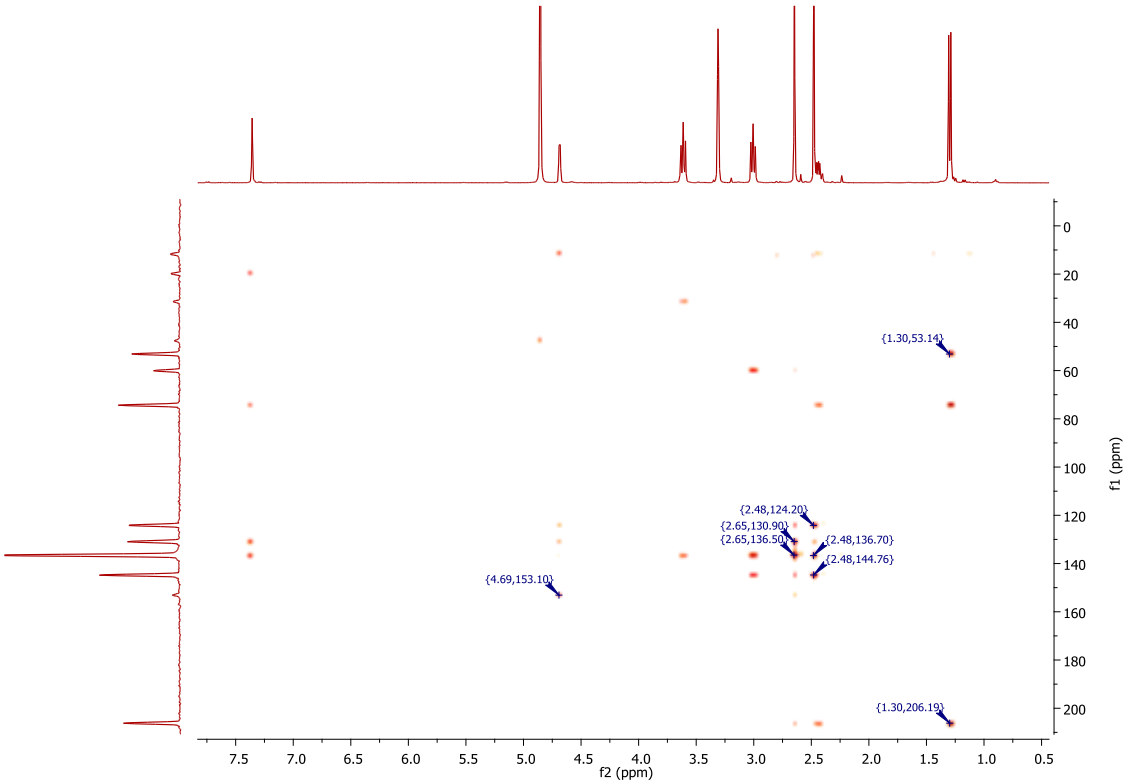

Figure A-91: ^{1}H-^{13}C HMBC NMR spectrum of compound **RH17** in CD_3OD.

16) NMR spectra of compound **RH18** in CD_3OD.

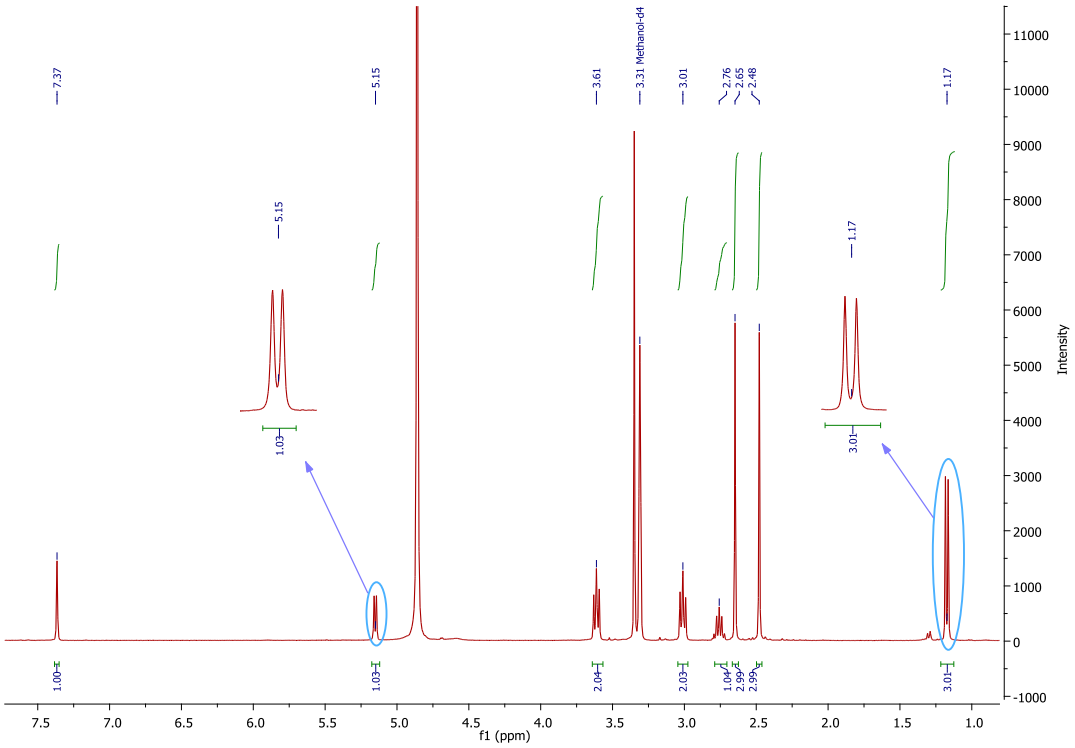

Figure A-92: ^{1}H NMR (CD_3OD, 400 MHz) spectrum of compound **RH18**.

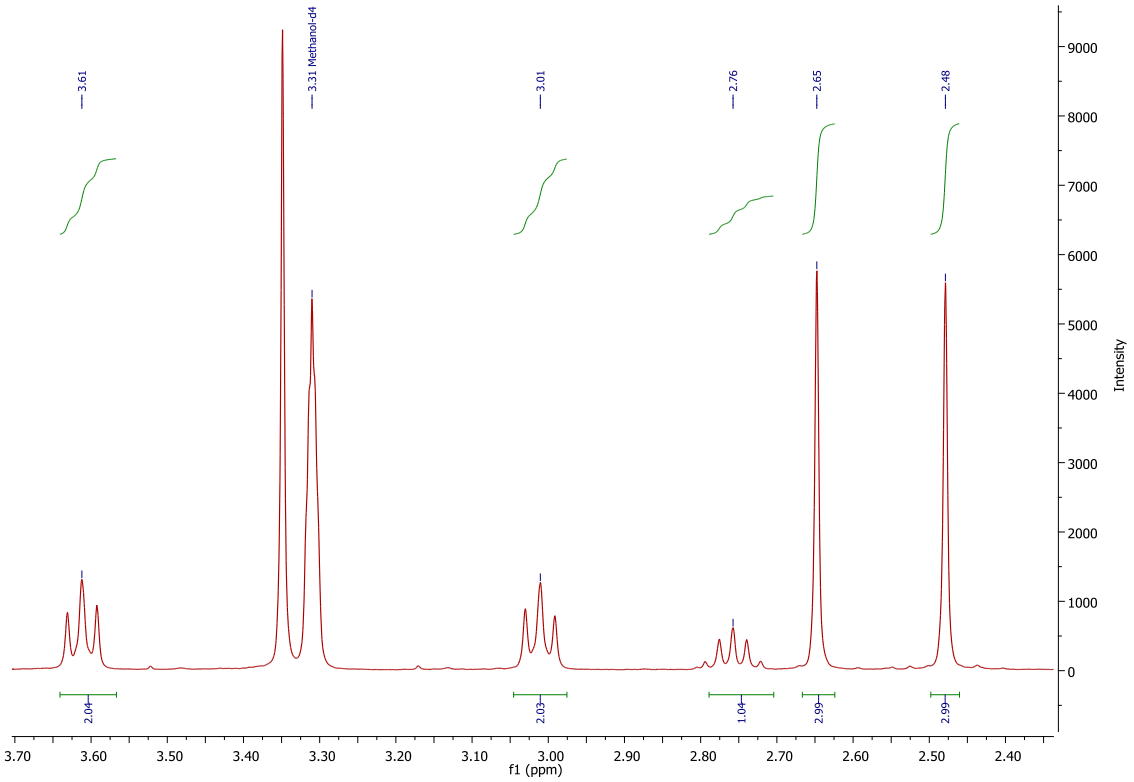

Figure A-93: Expanded ^{1}H NMR (CD_3OD, 400 MHz) spectrum of **RH18** (2.4 – 3.7 ppm).

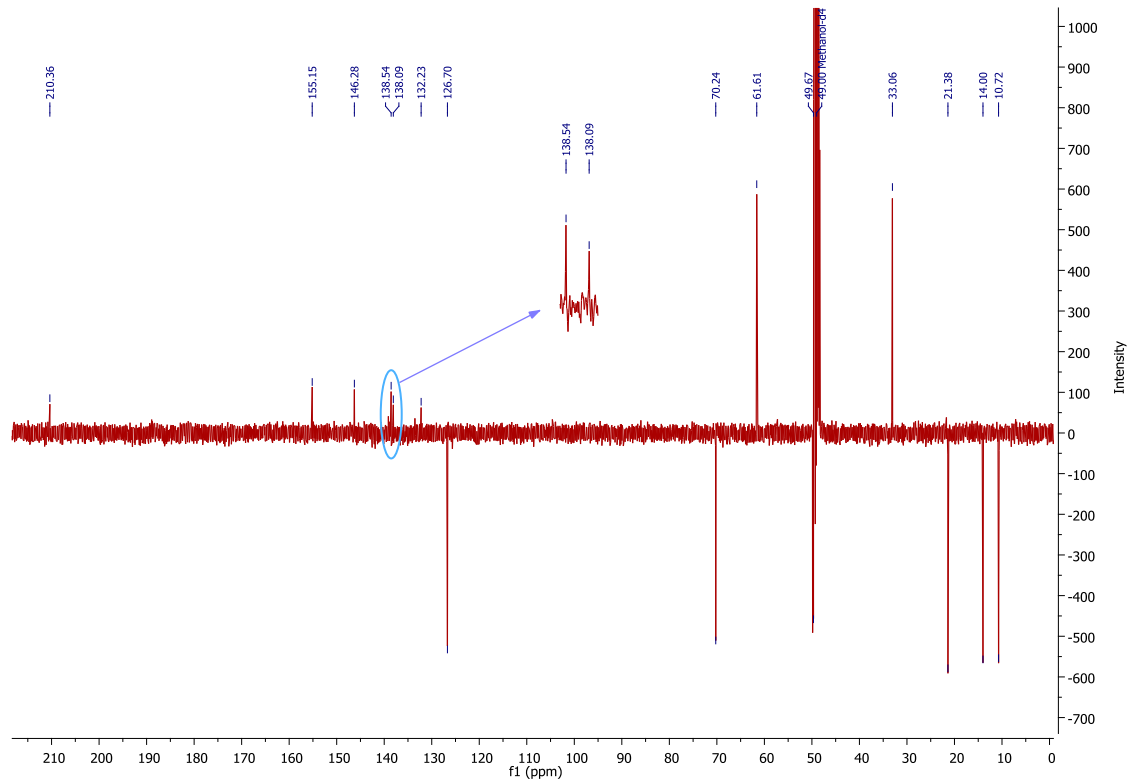

Figure A-94: DEPTQ NMR (CD_3OD, 100 MHz) spectrum of compound **RH18**.

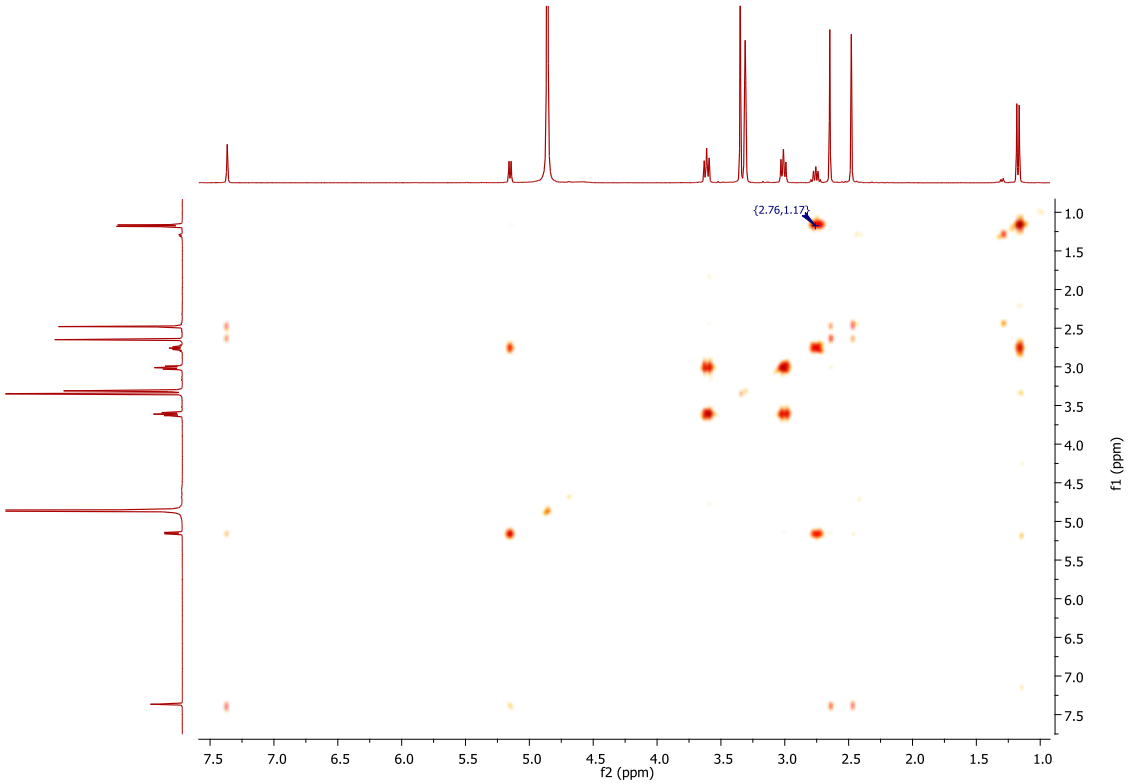

Figure A-95: ^{1}H-^{1}H COSY NMR (CD_3OD, 400 MHz) spectrum of compound **RH18**.

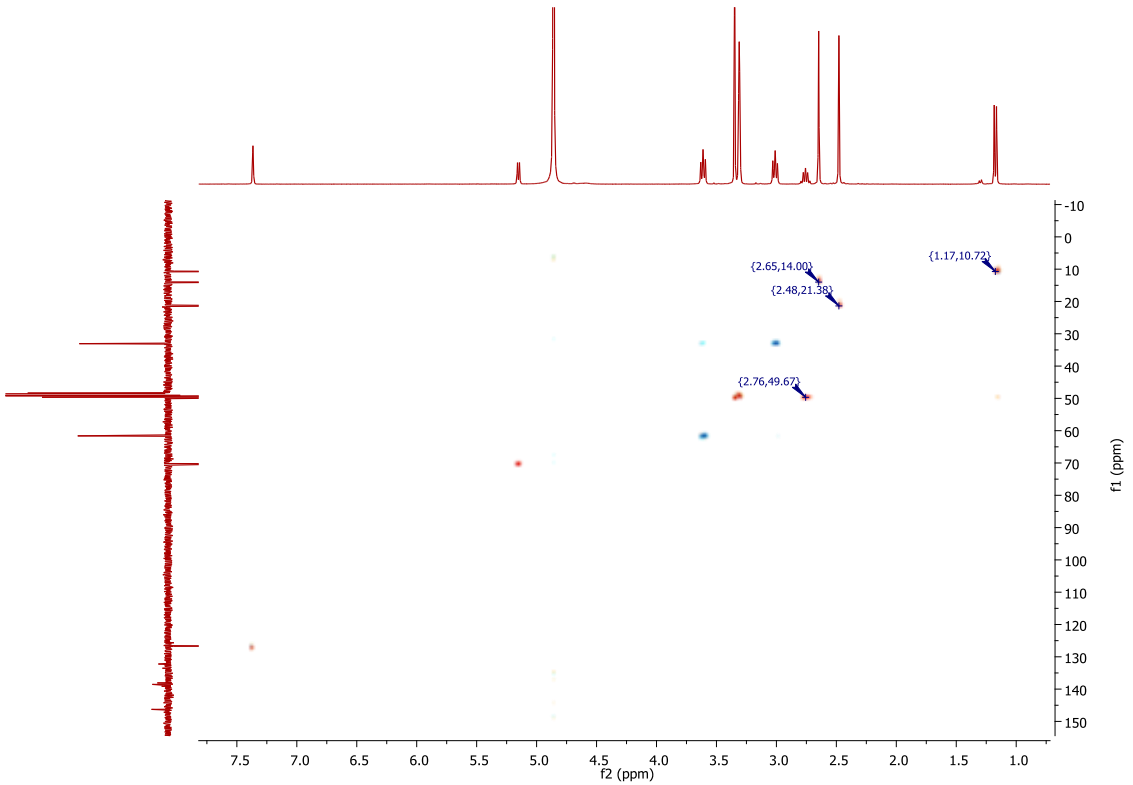

Figure A-96: ^{1}H-^{13}C HSQC NMR spectrum of compound **RH18** in CD_3OD.

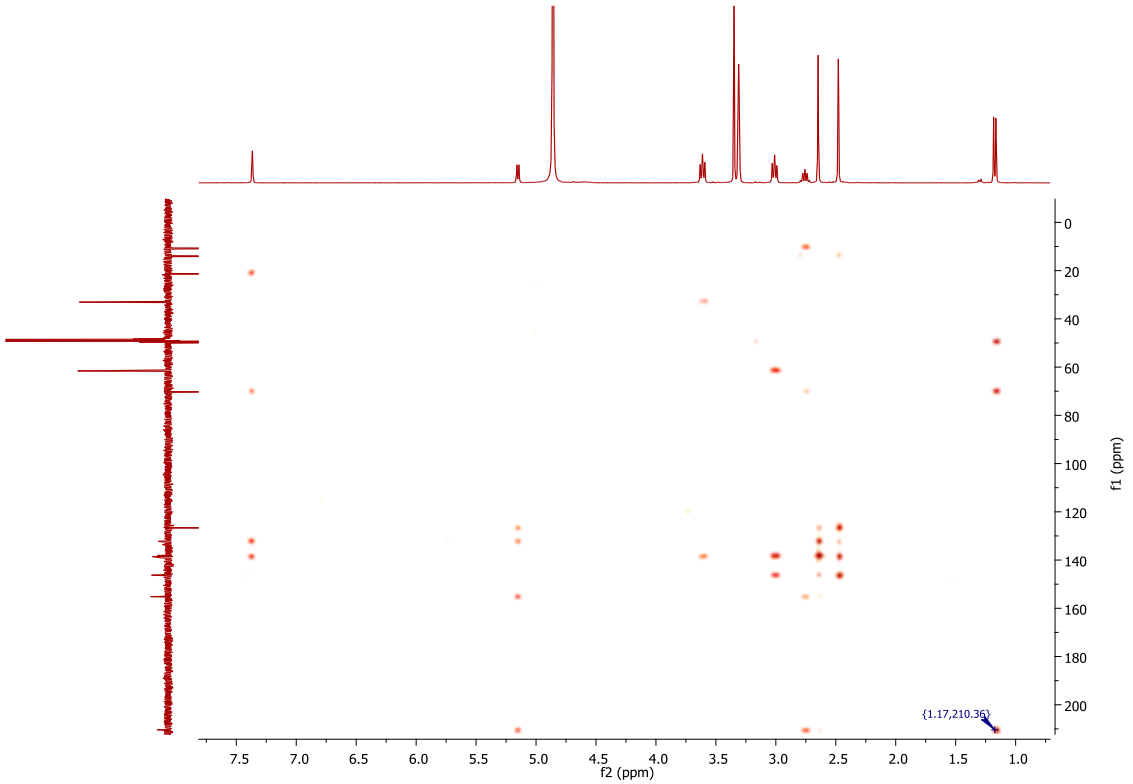

Figure A-97: ^{1}H-^{13}C HMBC NMR spectrum of compound **RH18** in CD_3OD.

17) NMR spectra of compound **RH19** in CD_3OD.

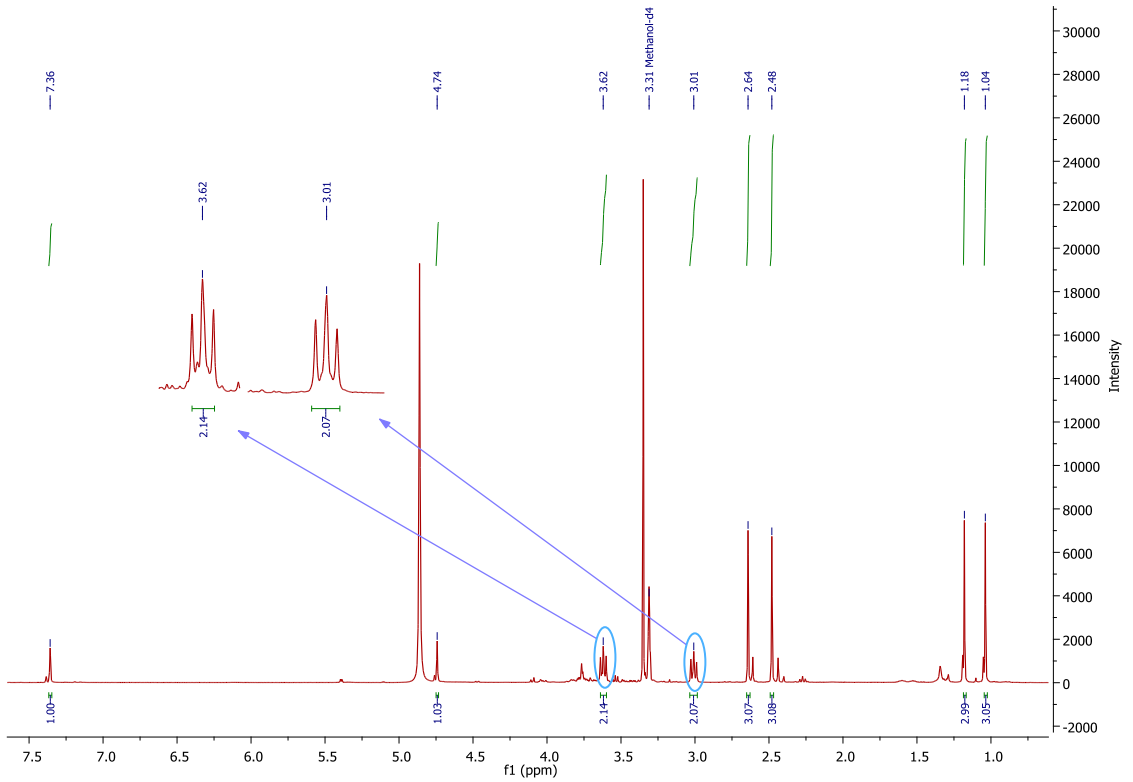

Figure A-98: ^{1}H NMR (CD_3OD, 400 MHz) spectrum of compound **RH19**.

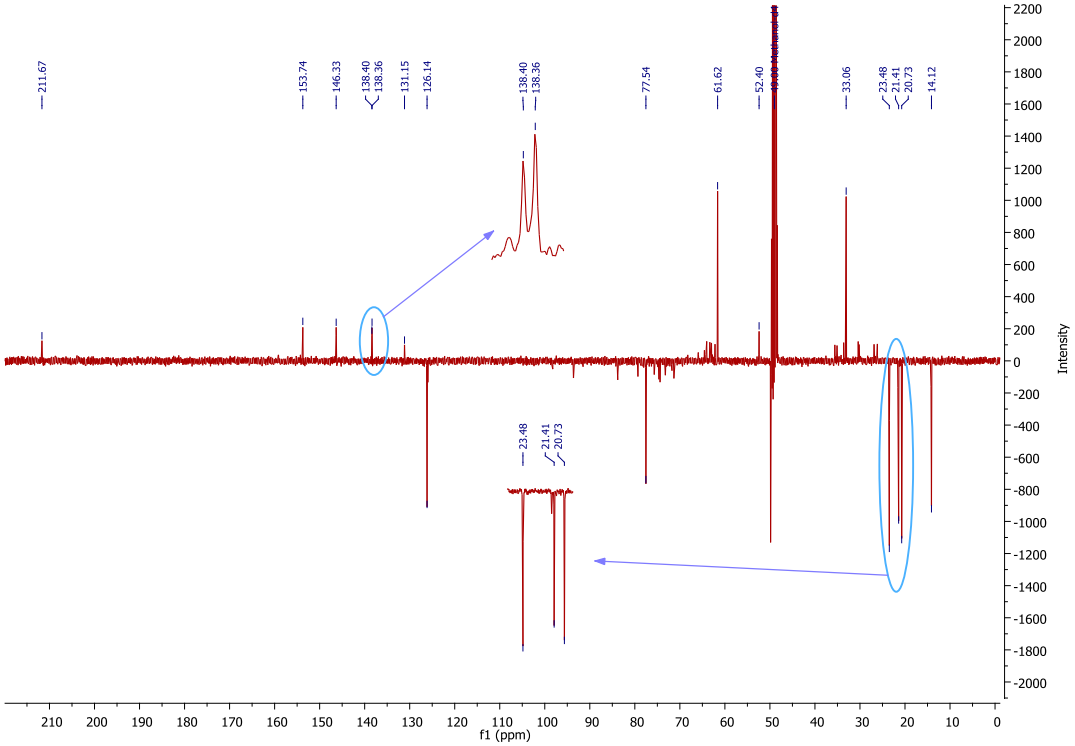

Figure A-99: DEPTQ NMR (CD_3OD, 100 MHz) spectrum of compound **RH19**.

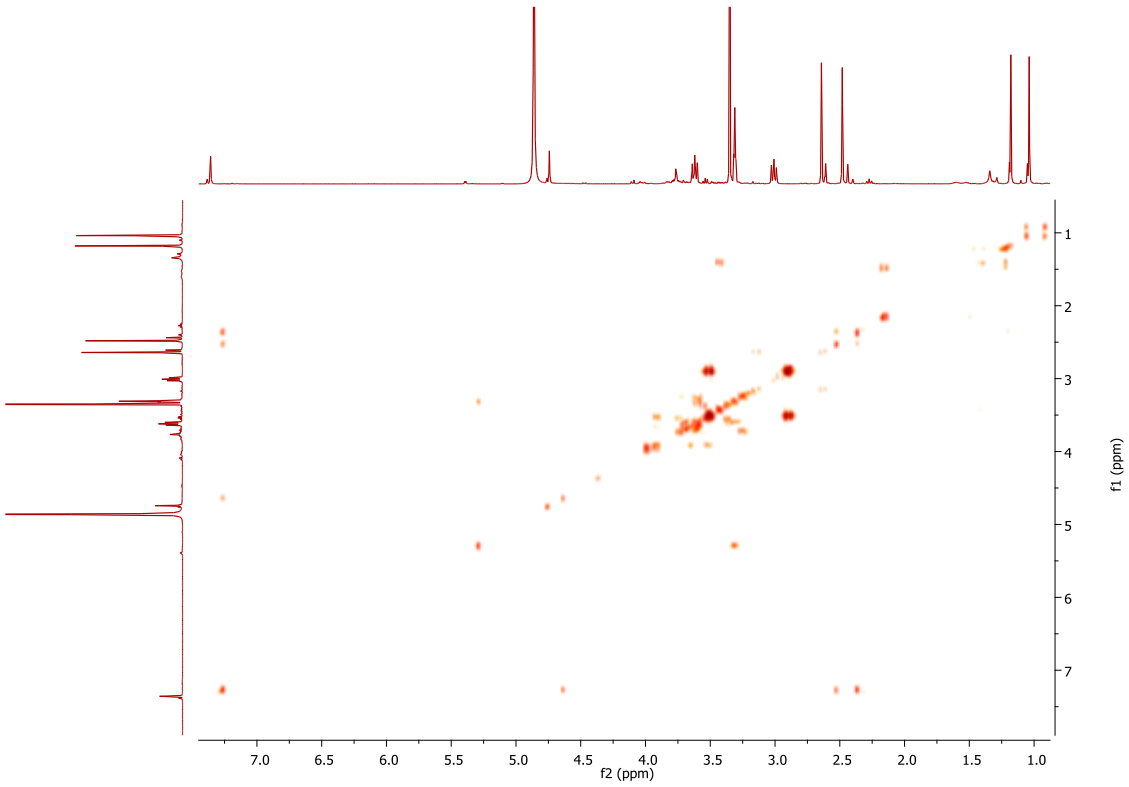

Figure A-100: ^{1}H-^{1}H COSY NMR (CD_3OD, 400 MHz) spectrum of compound **RH19**.

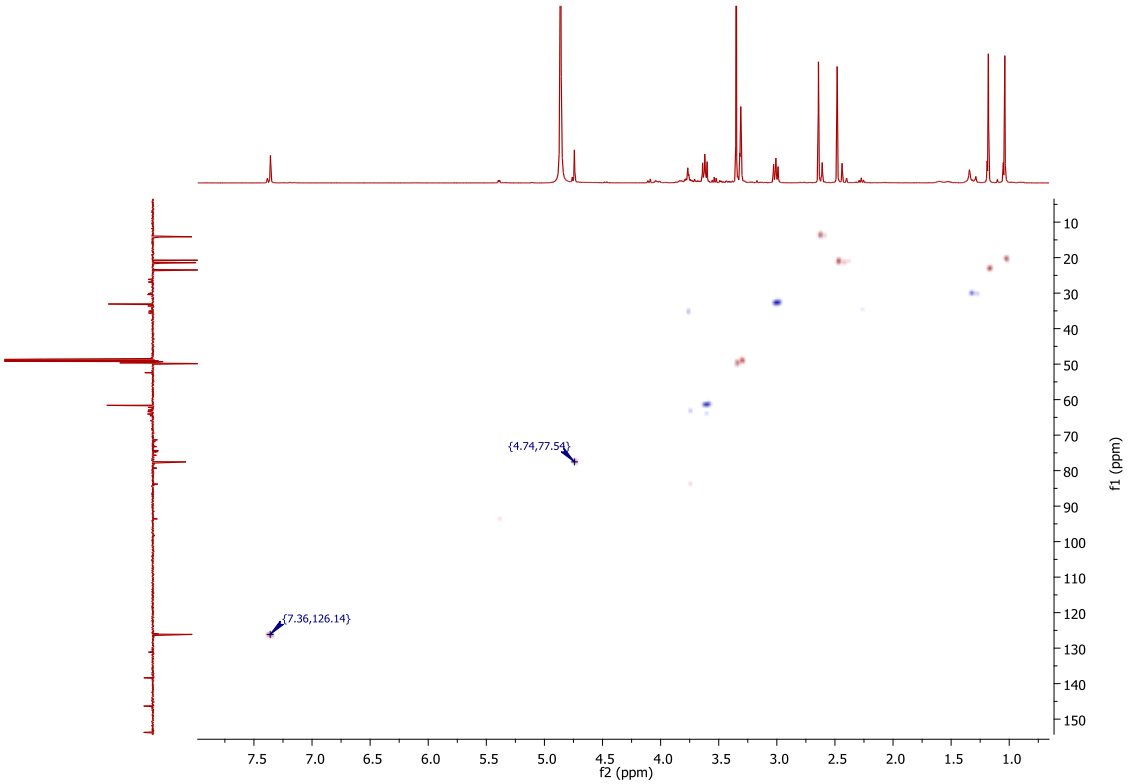

Figure A-101: ^{1}H-^{13}C HSQC NMR spectrum of compound **RH19** in CD_3OD.

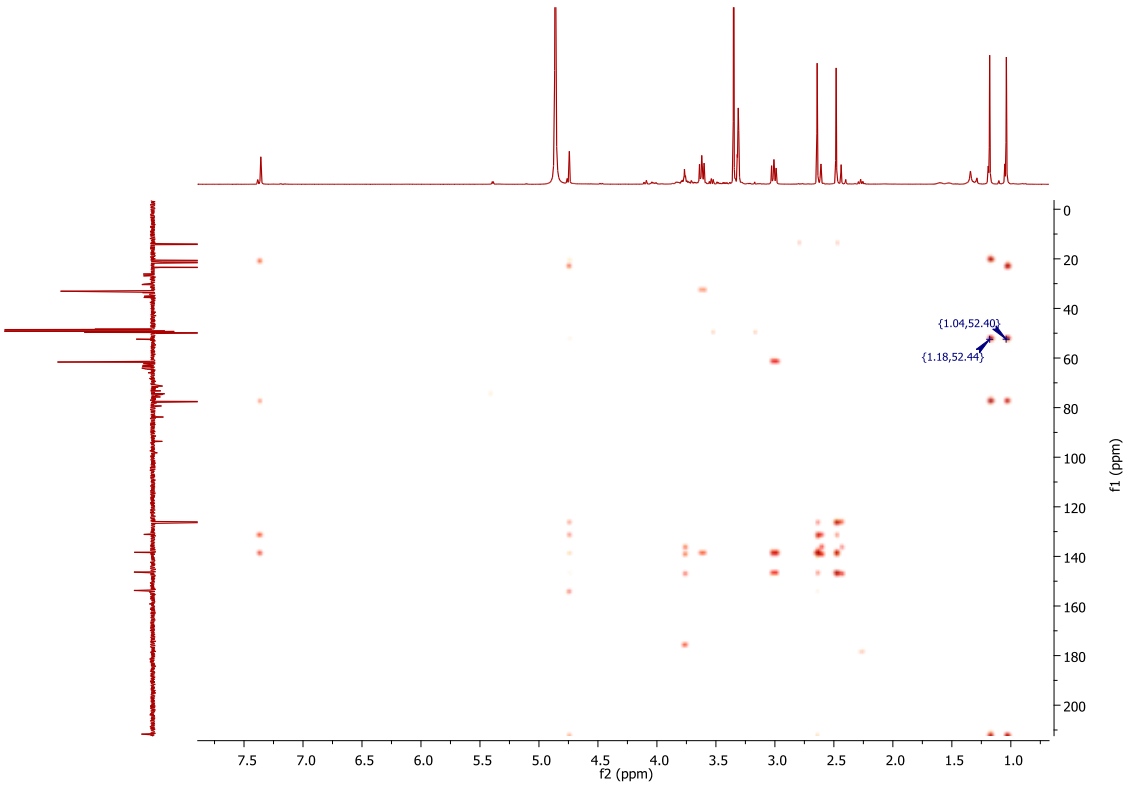

Figure A-102: ^{1}H-^{13}C HMBC NMR spectrum of compound **RH19** in CD_3OD.

18) NMR spectra of compound **RH20** in $CDCl_3$.

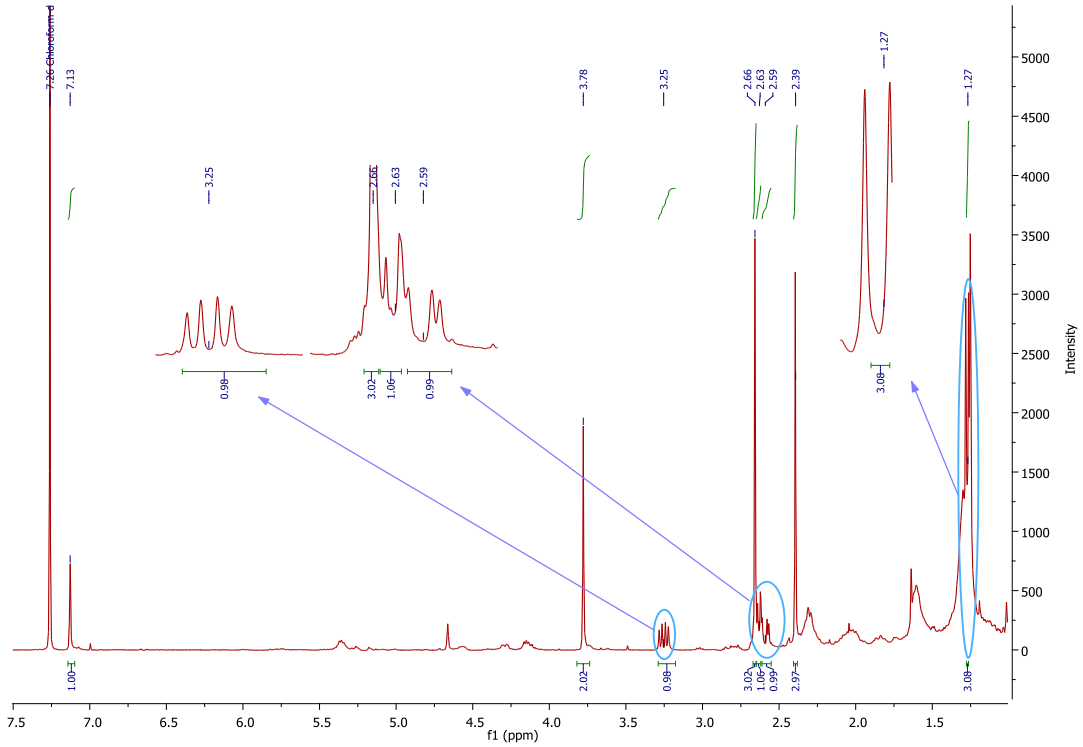

Figure A-103: ^{1}H NMR ($CDCl_3$, 400 MHz) spectrum of compound **RH20**.

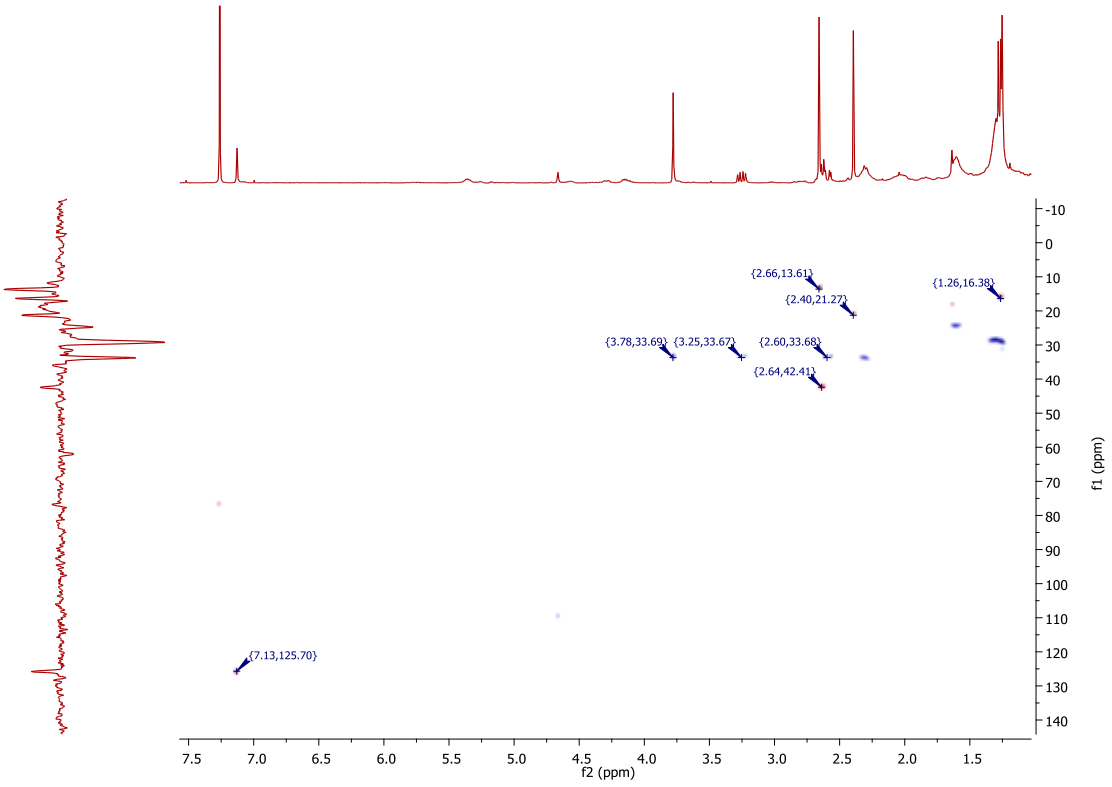

Figure A-104: ^{1}H-^{13}C HSQC NMR spectrum of compound **RH20** in $CDCl_3$.

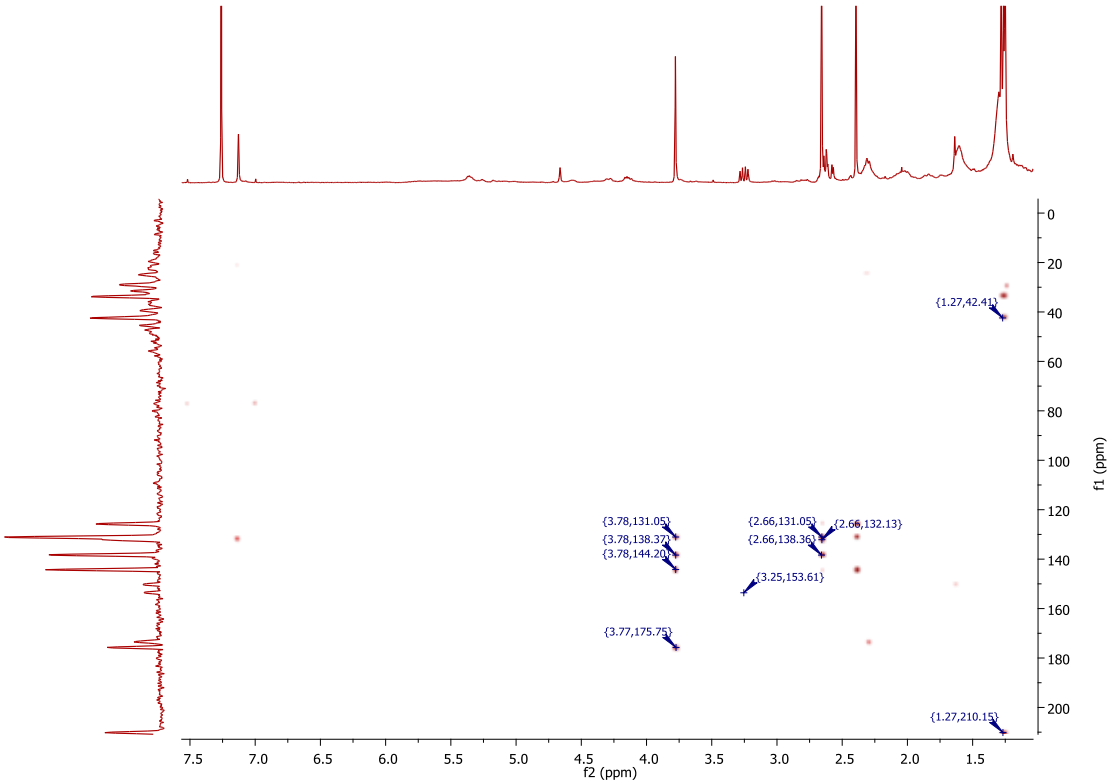

Figure A-105: ^{1}H-^{13}C HMBC NMR spectrum of compound **RH20** in $CDCl_3$.

19) NMR spectra of compound **RH21** in $CDCl_3$.

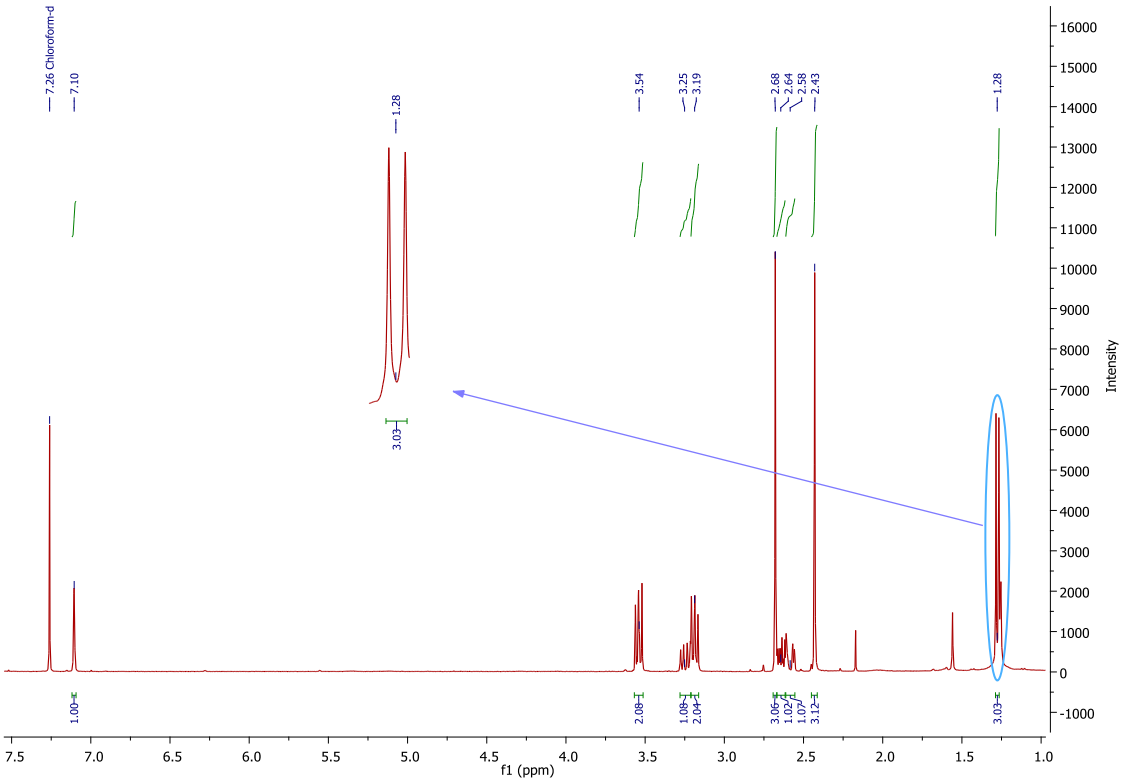

Figure A-106: ^{1}H NMR ($CDCl_3$, 400 MHz) spectrum of compound **RH21**.

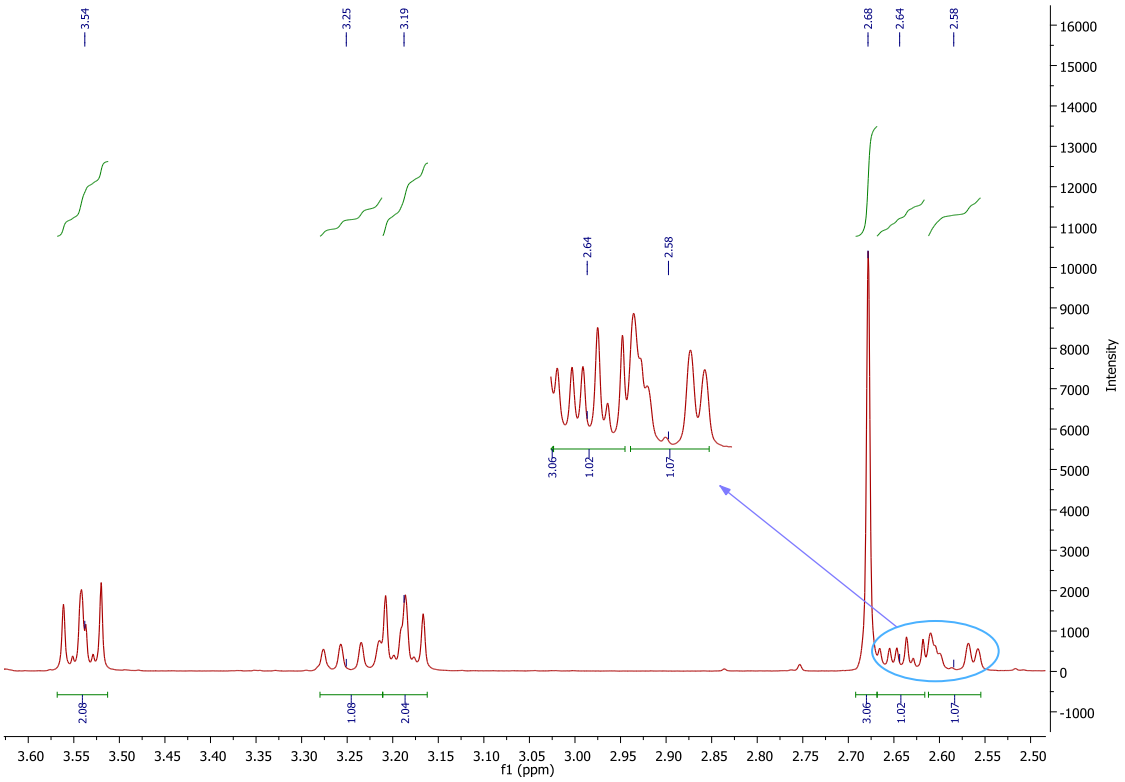

Figure A-107: Expanded ^{1}H NMR ($CDCl_3$, 400 MHz) spectrum of **RH21** (2.5 – 3.6 ppm).

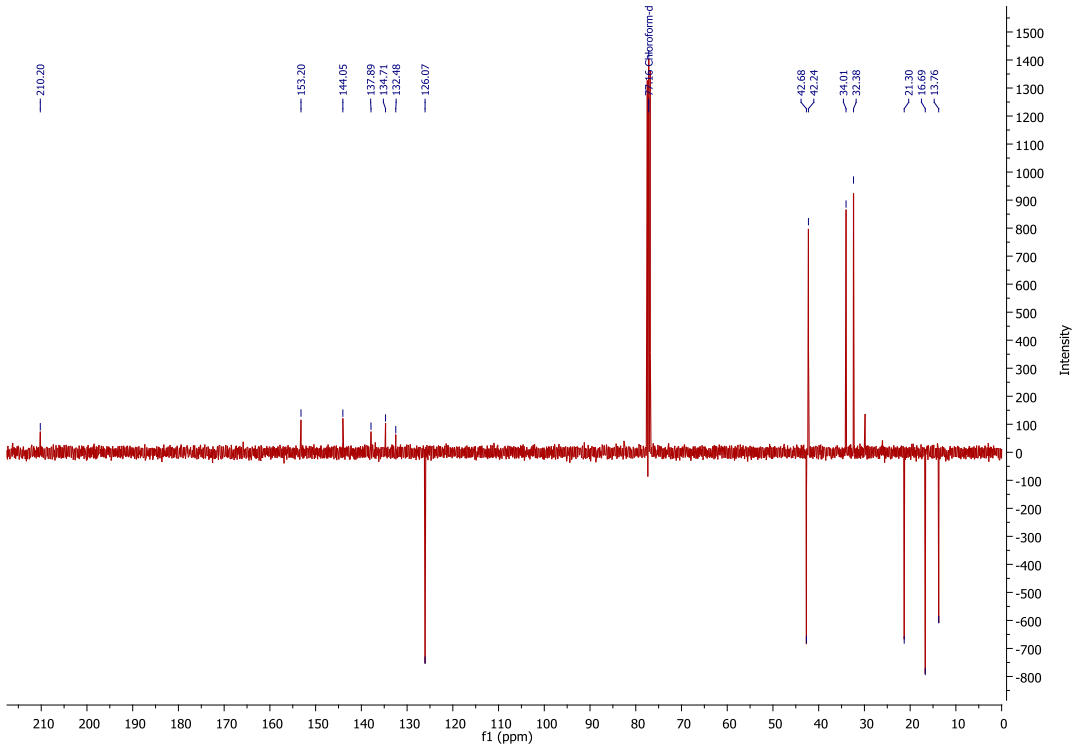

Figure A-108: DEPTQ NMR ($CDCl_3$, 100 MHz) spectrum of compound **RH21**.

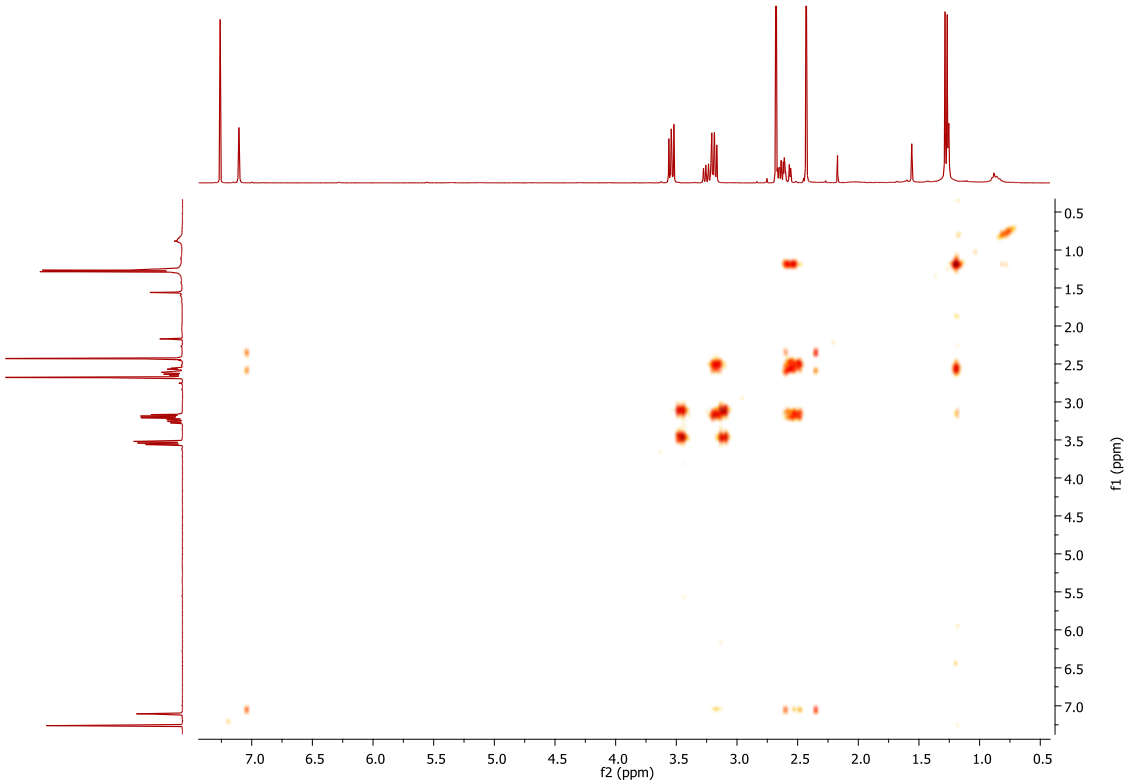

Figure A-109: ^{1}H-^{1}H COSY NMR ($CDCl_3$, 400 MHz) spectrum of compound **RH21**.

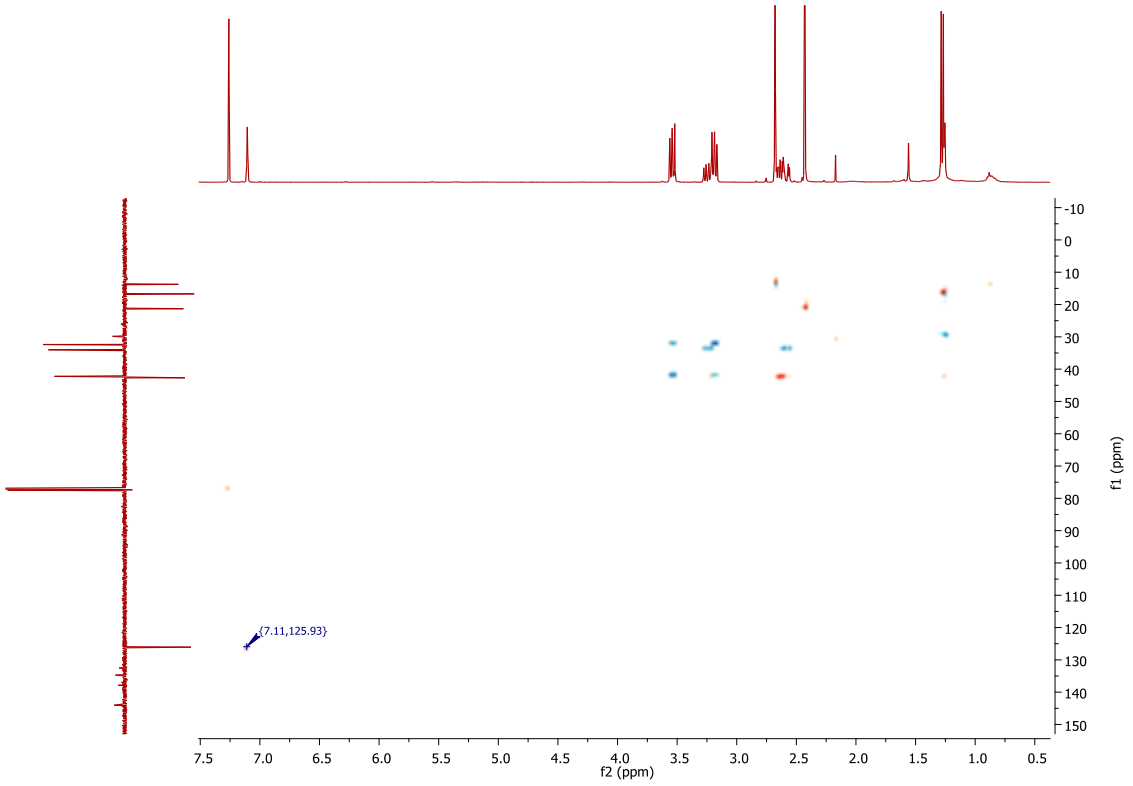

Figure A-110: ^{1}H-^{13}C HSQC NMR spectrum of compound **RH21** in $CDCl_3$.

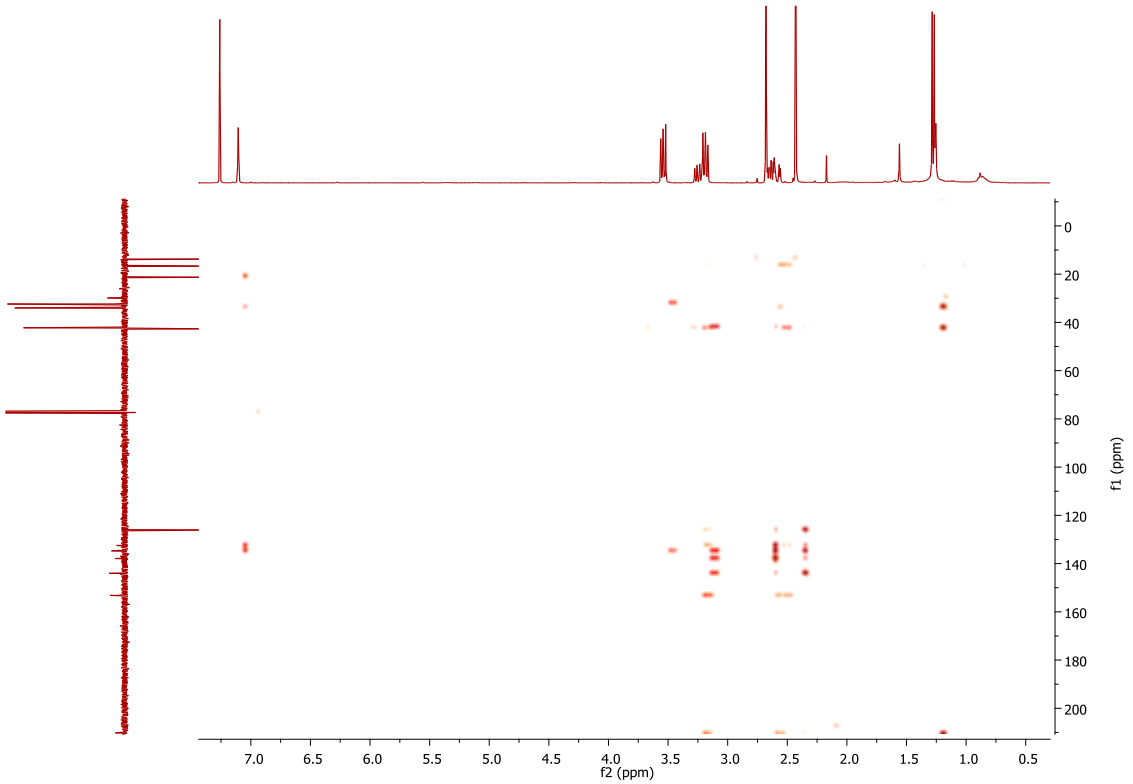

Figure A-111: ^{1}H-^{13}C HMBC NMR spectrum of compound **RH21** in $CDCl_3$.

20) NMR spectra of compound **RH22** in $CDCl_3$.

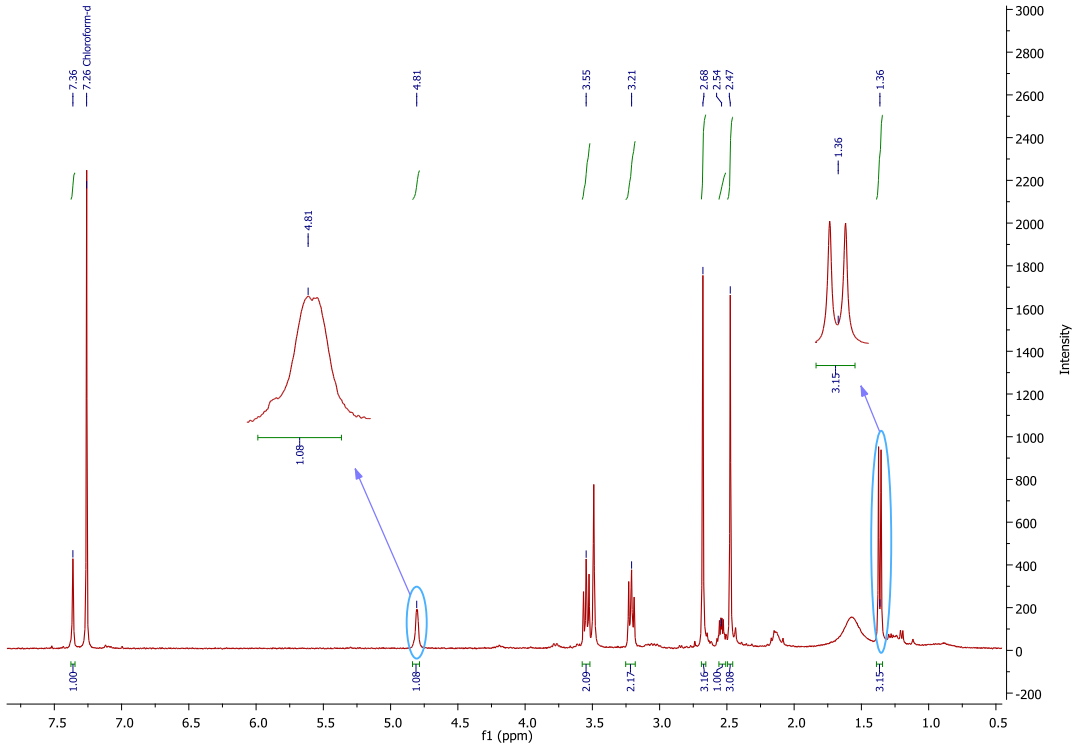

Figure A-112: ^{1}H NMR ($CDCl_3$, 400 MHz) spectrum of compound **RH22**.

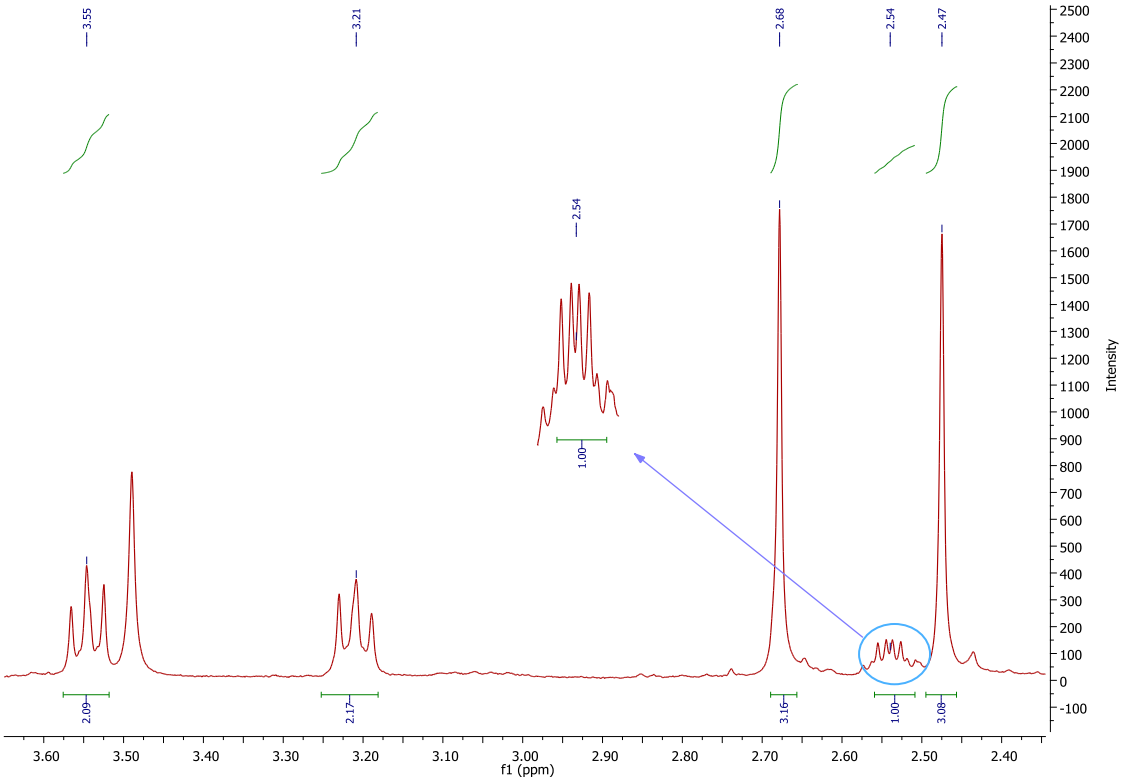

Figure A-113: Expanded ^{1}H NMR ($CDCl_3$, 400 MHz) spectrum of **RH22** (2.4 – 3.6 ppm).

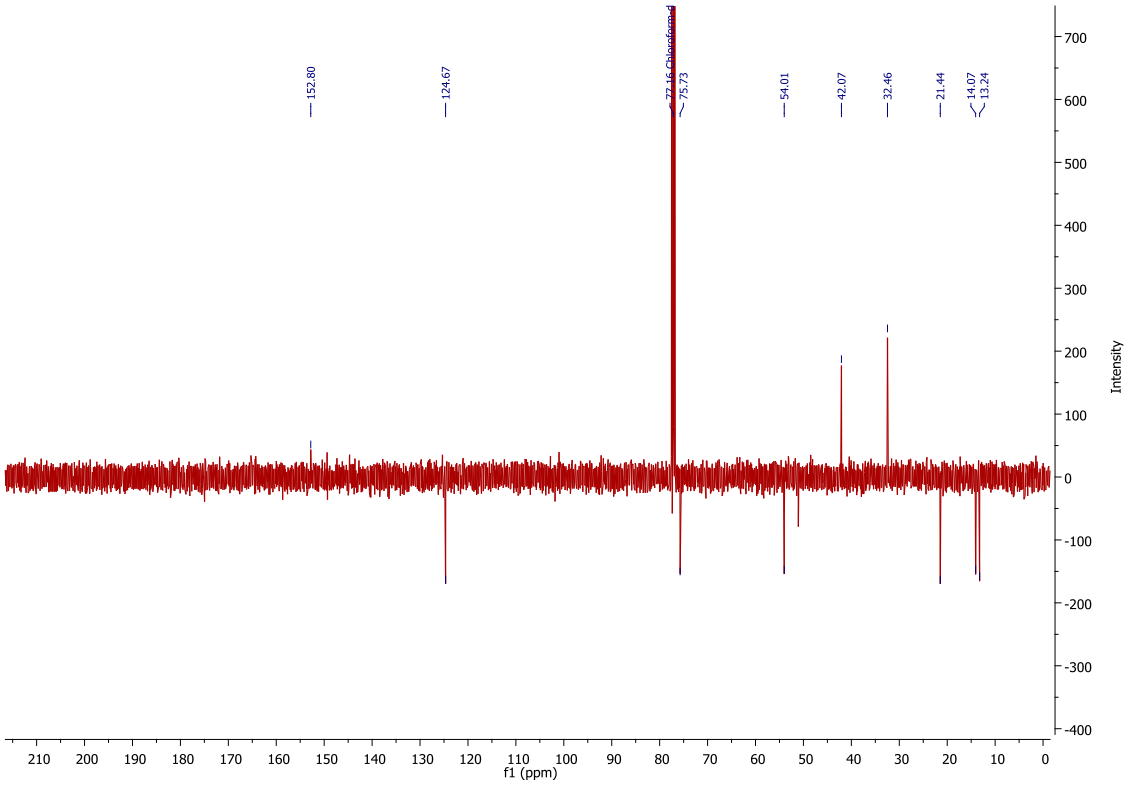

Figure A-114: DEPTQ NMR ($CDCl_3$, 100 MHz) spectrum of compound **RH22**.

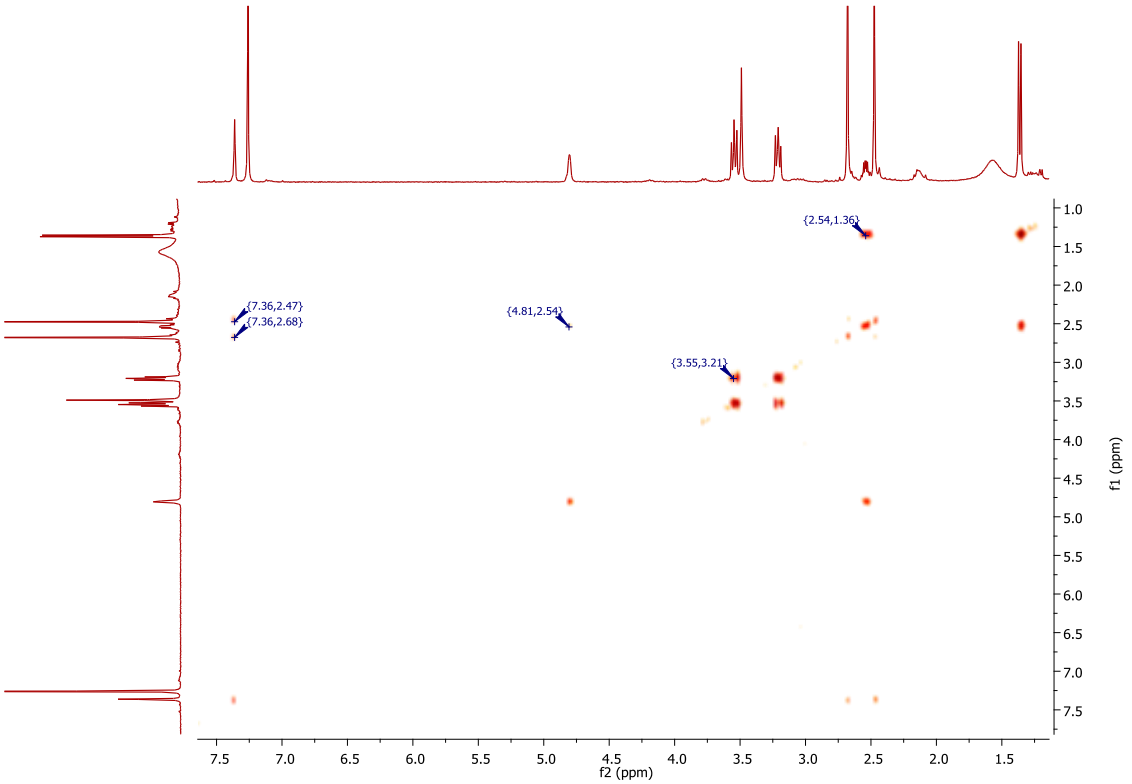

Figure A-115: ^{1}H-^{1}H COSY NMR ($CDCl_3$, 400 MHz) spectrum of compound **RH22**.

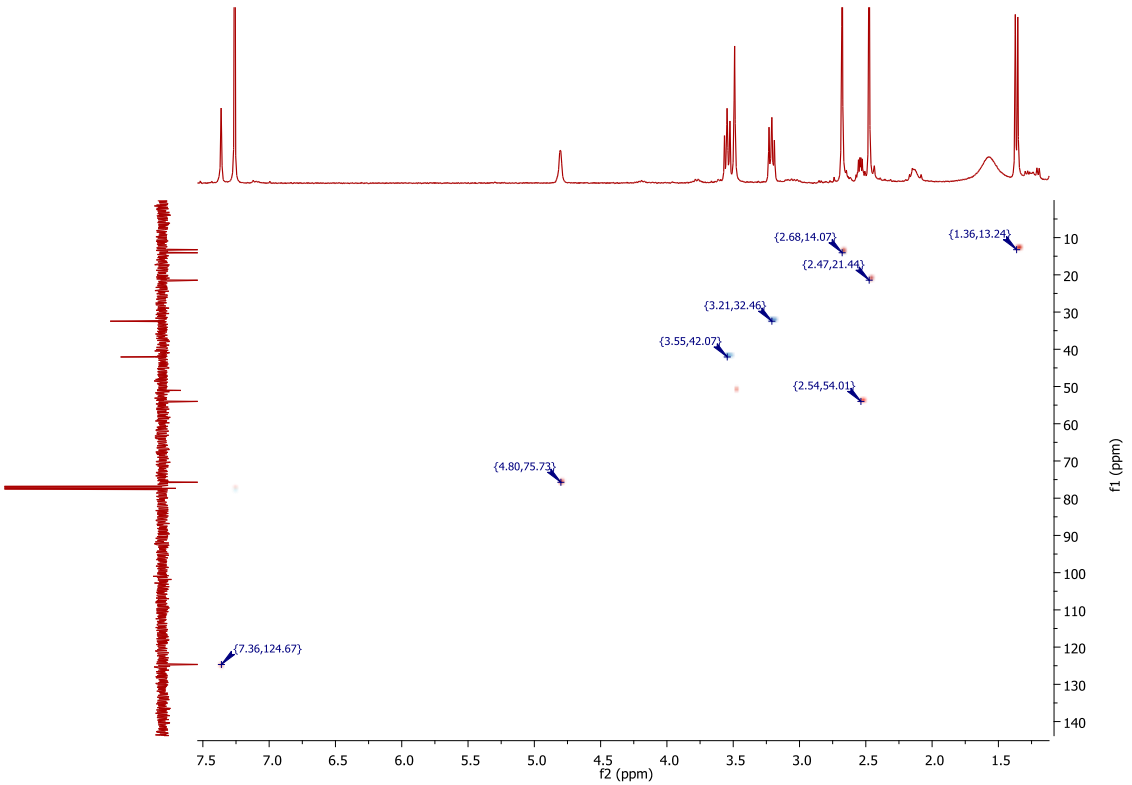

Figure A-116: ^{1}H-^{13}C HSQC NMR spectrum of compound **RH22** in $CDCl_3$.

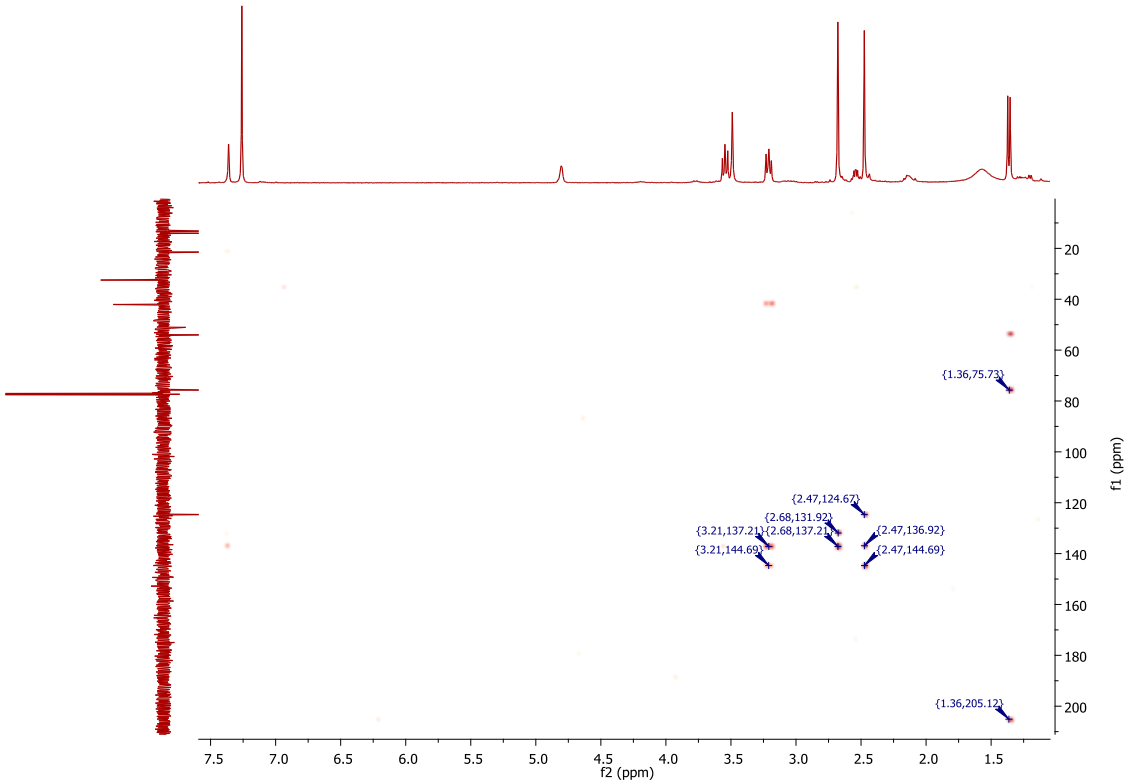

Figure A-117: ^{1}H-^{13}C HMBC NMR spectrum of compound **RH22** in $CDCl_3$.

21) NMR spectra of compound **RH23** in $CDCl_3$.

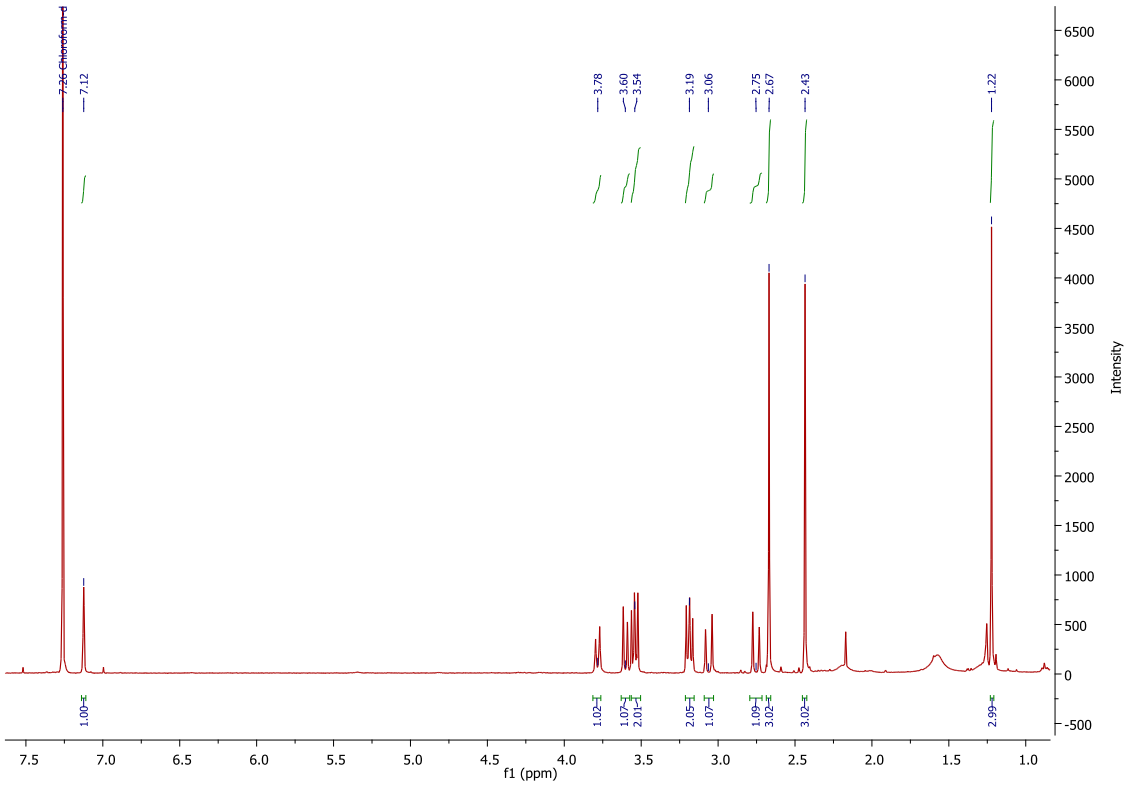

Figure A-118: ^{1}H NMR ($CDCl_3$, 400 MHz) spectrum of compound **RH23**.

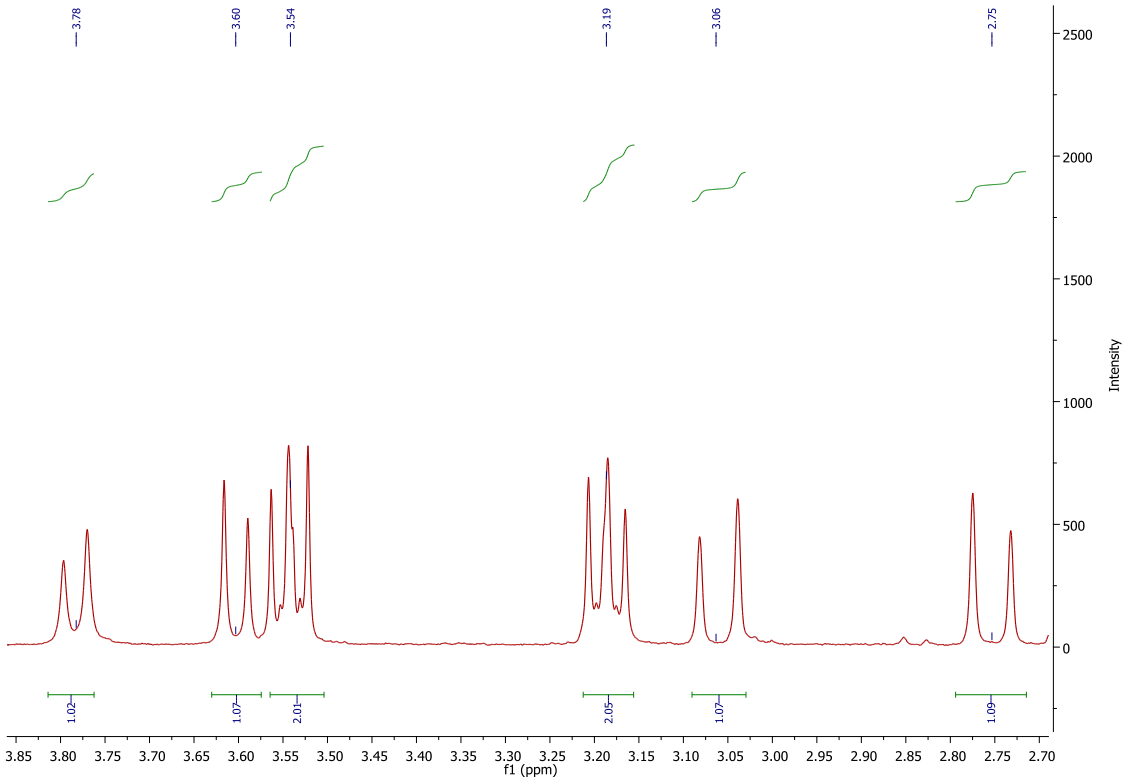

Figure A-119: Expanded ^{1}H NMR ($CDCl_3$, 400 MHz) spectrum of **RH23** (2.70-3.85 ppm).

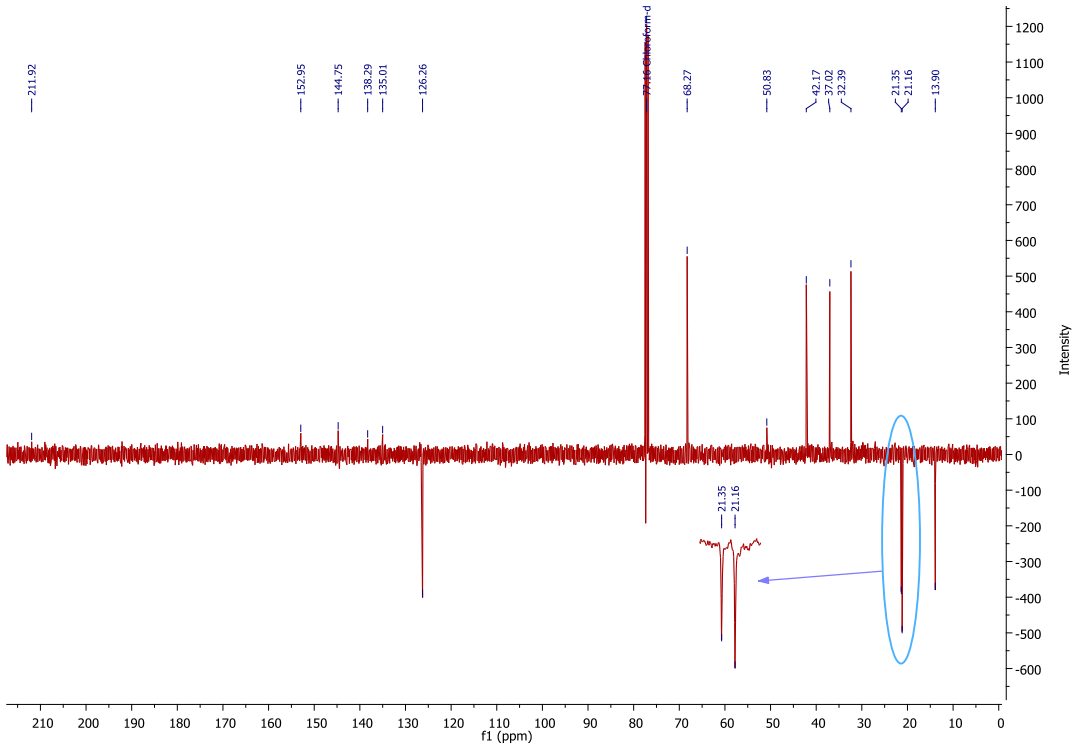

Figure A-120: DEPTQ NMR ($CDCl_3$, 100 MHz) spectrum of compound **RH23**.

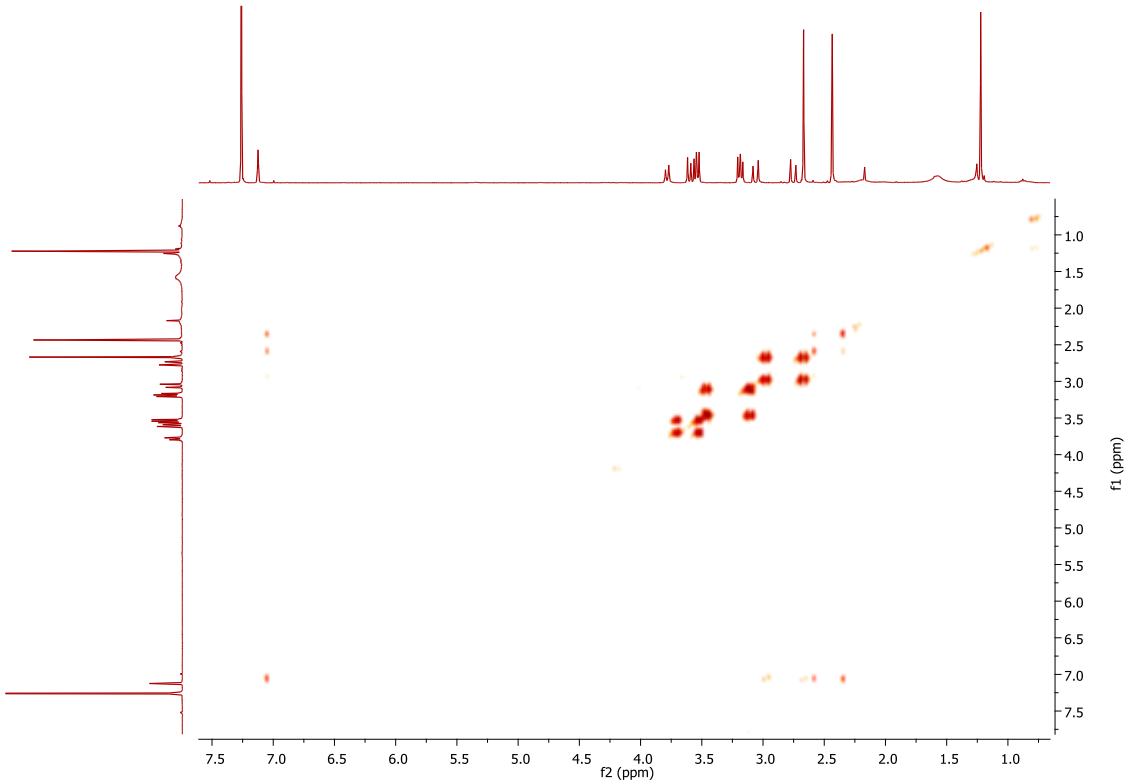

Figure A-121: ^{1}H-^{1}H COSY NMR ($CDCl_3$, 400 MHz) spectrum of compound **RH23**.

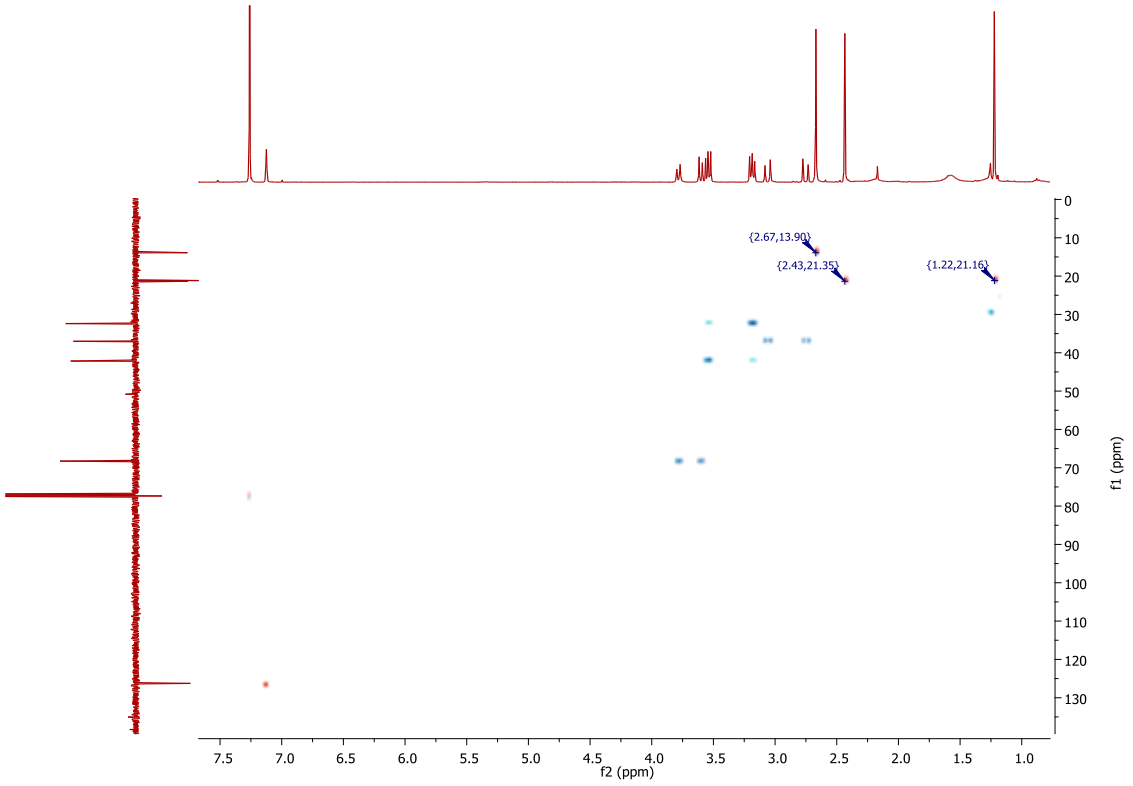

Figure A-122: ^{1}H-^{13}C HSQC NMR spectrum of compound **RH23** in $CDCl_3$.

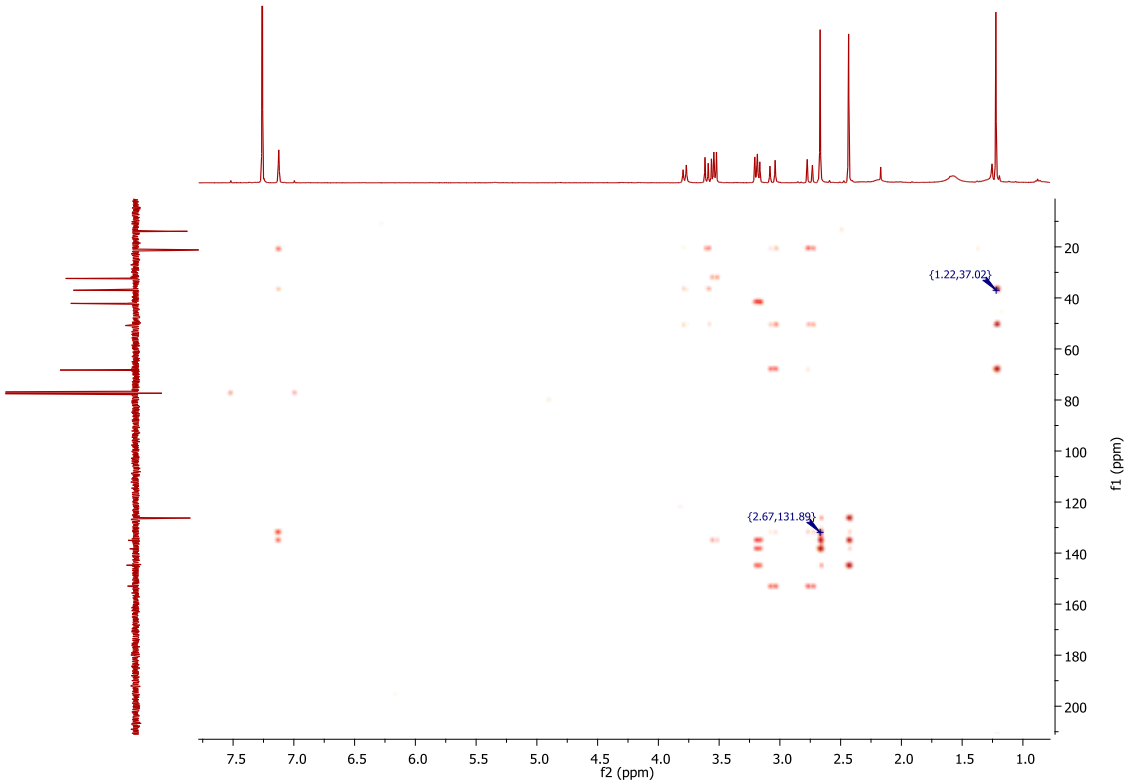

Figure A-123: ^{1}H-^{13}C HMBC NMR spectrum of compound **RH23** in $CDCl_3$.

22) NMR spectra of compound **RH24** in CD_3OD.

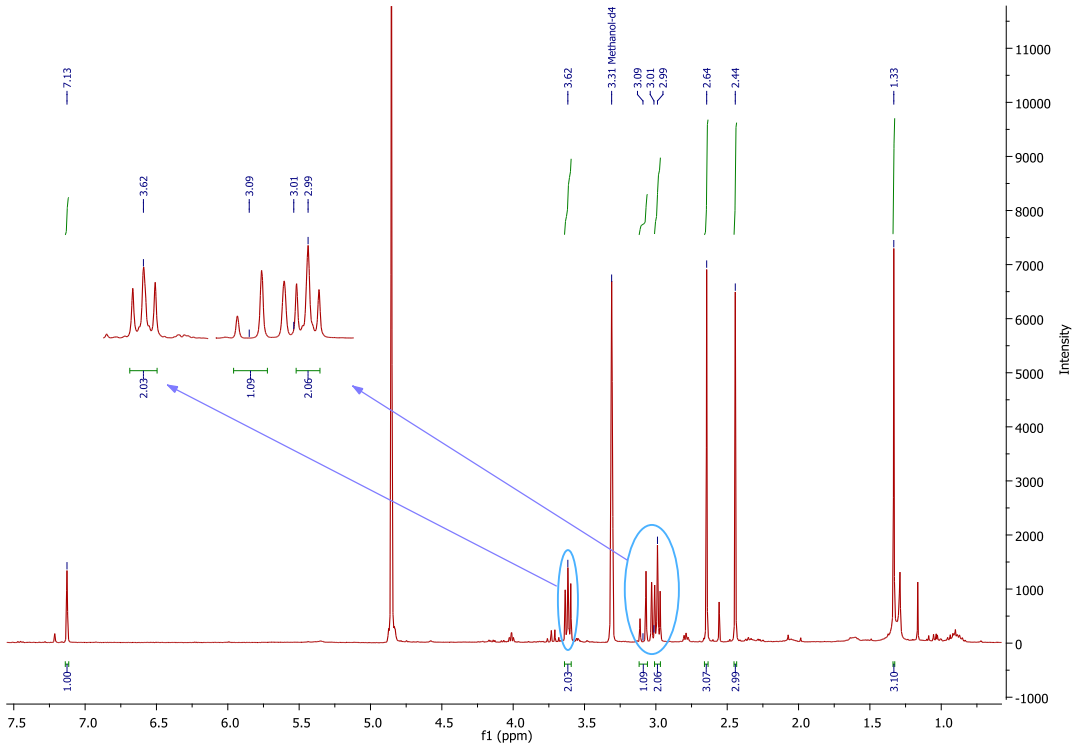

Figure A-124: ^{1}H NMR (CD_3OD, 400 MHz) spectrum of compound **RH24**.

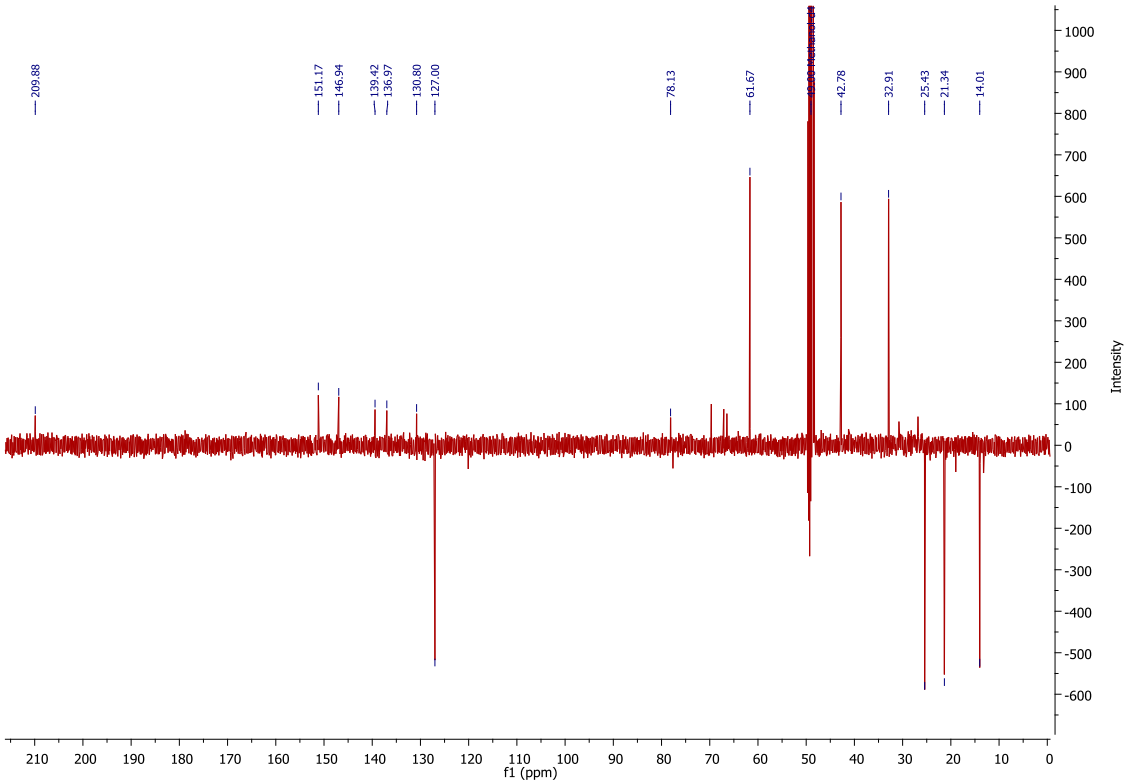

Figure A-125: DEPTQ NMR (CD_3OD, 100 MHz) spectrum of compound **RH24**.

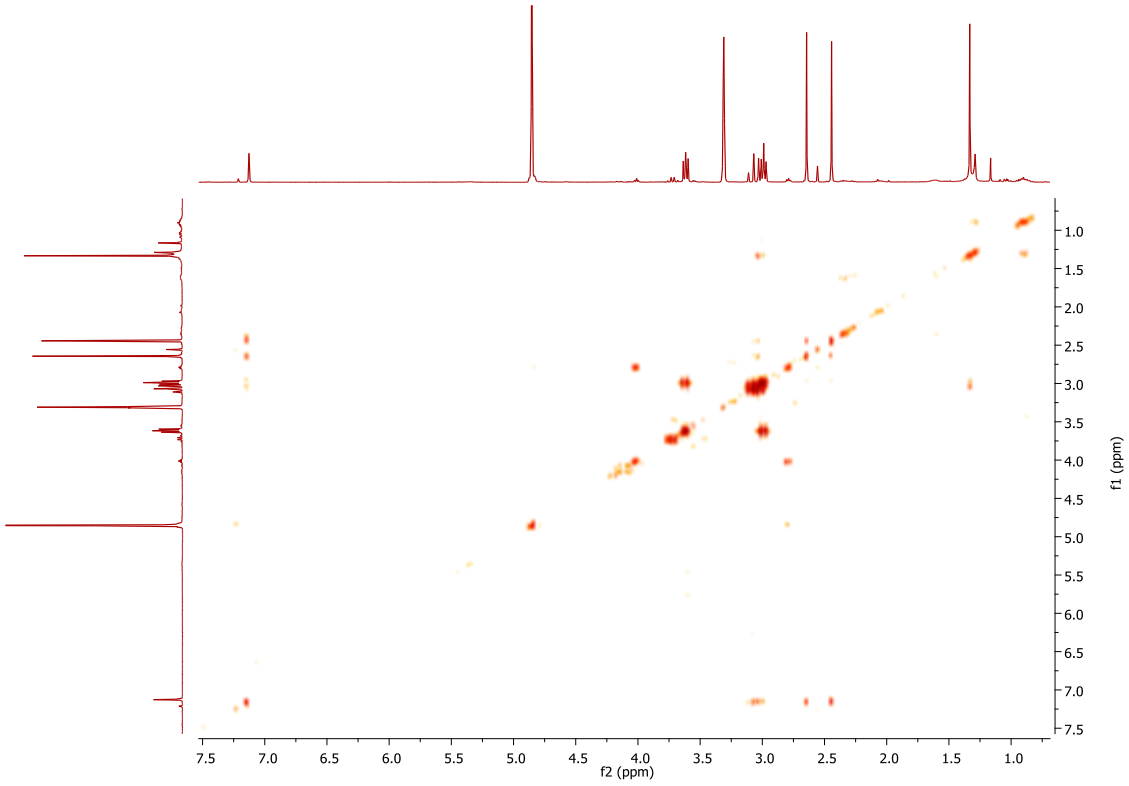

Figure A-126: ^{1}H-^{1}H COSY NMR (CD_3OD, 400 MHz) spectrum of compound **RH24**.

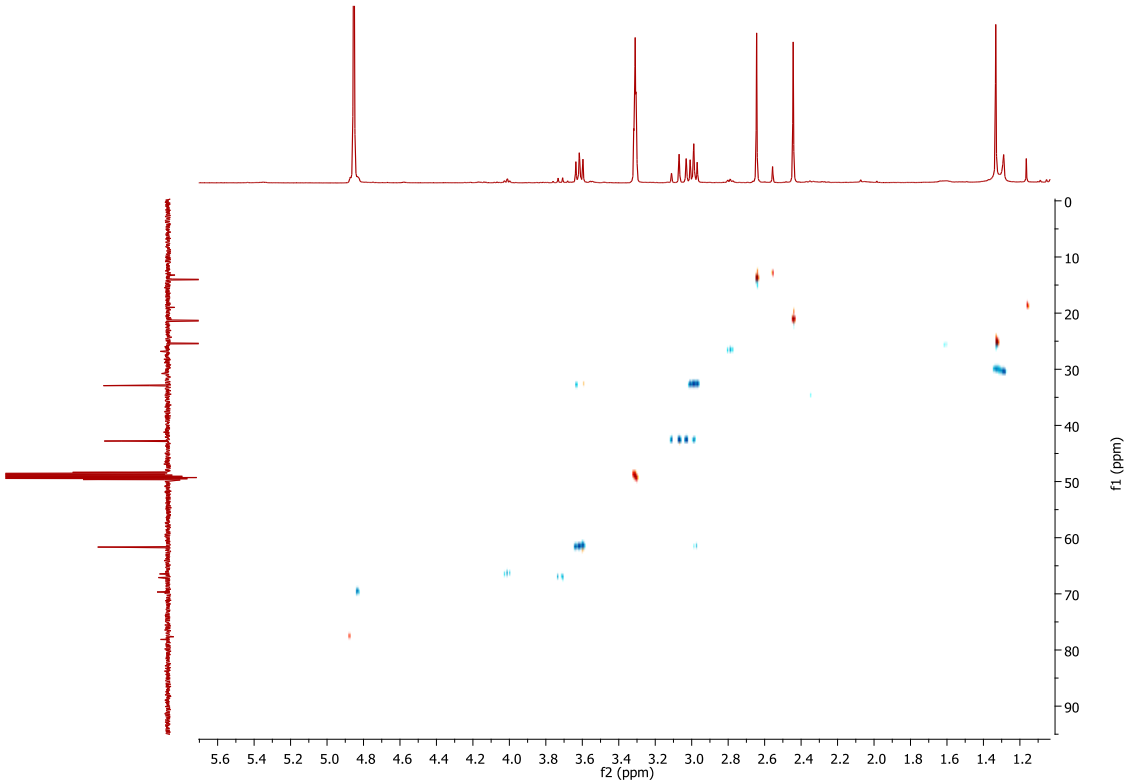

Figure A-127: ^{1}H-^{13}C HSQC NMR spectrum of compound **RH24** in CD_3OD.

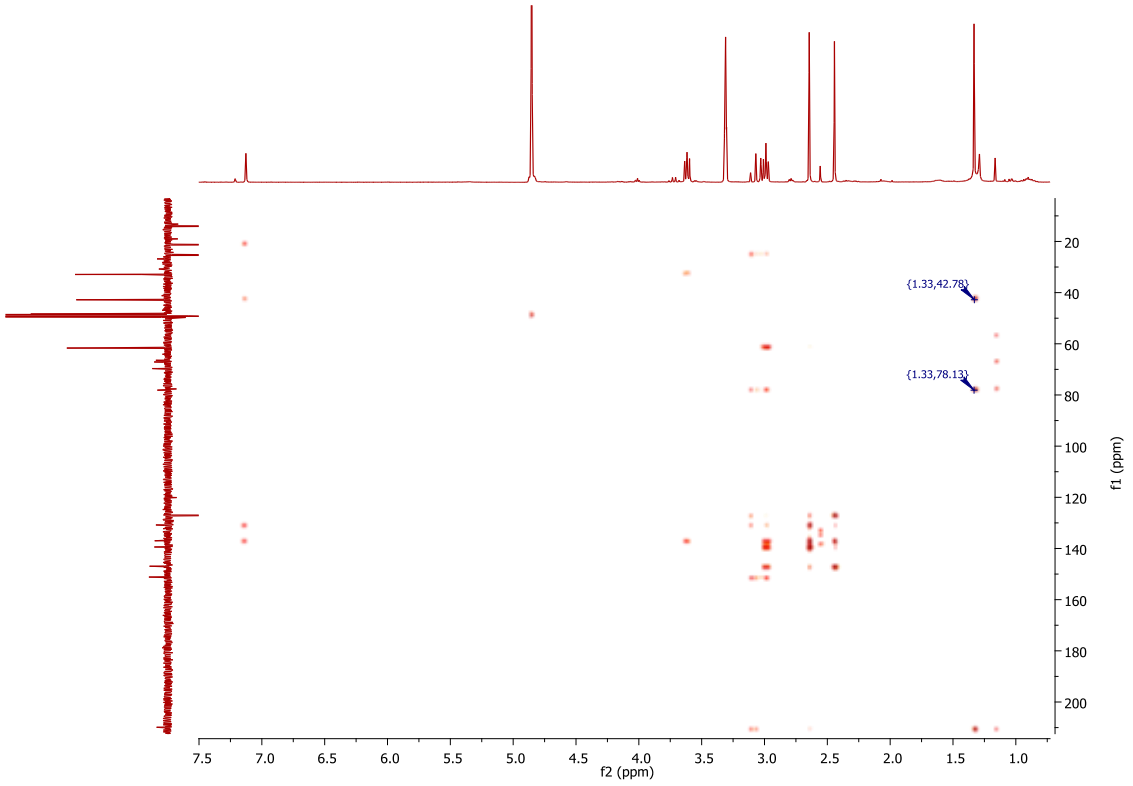

Figure A-128: ^{1}H-^{13}C HMBC NMR spectrum of compound **RH24** in CD_3OD.

23) NMR spectra of compound **RH25** in $CDCl_3$.

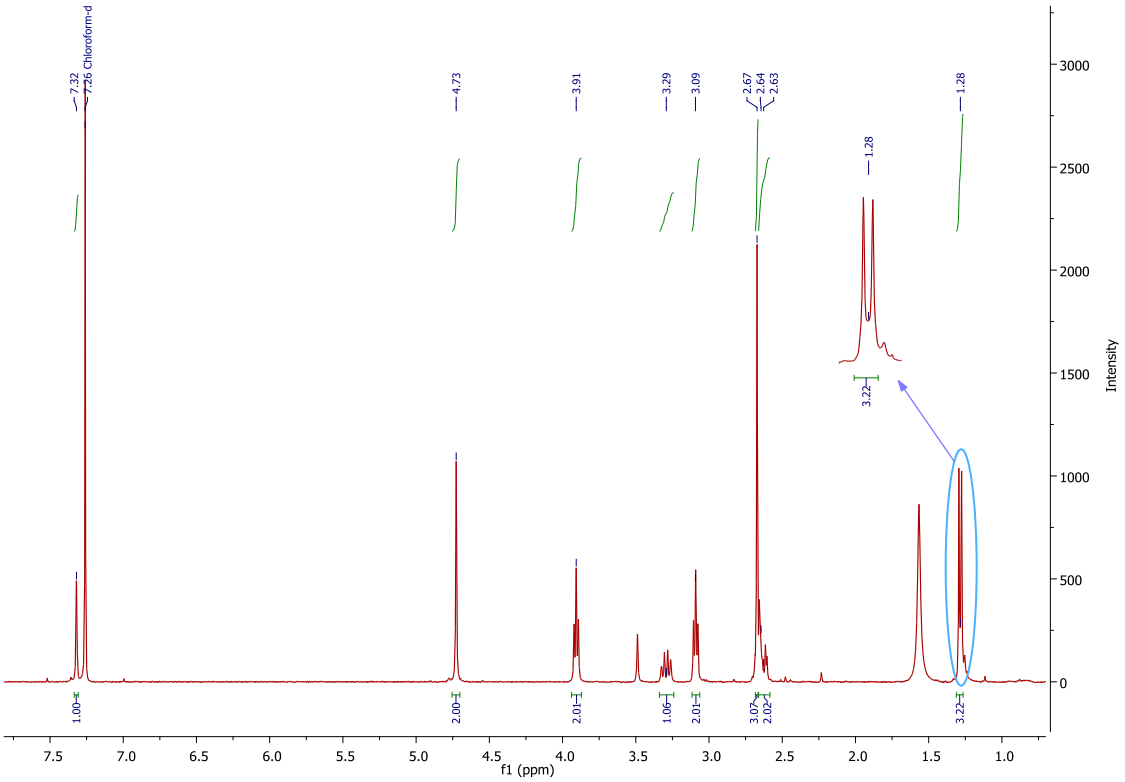

Figure A-129: ^{1}H NMR ($CDCl_3$, 400 MHz) spectrum of compound **RH25**.

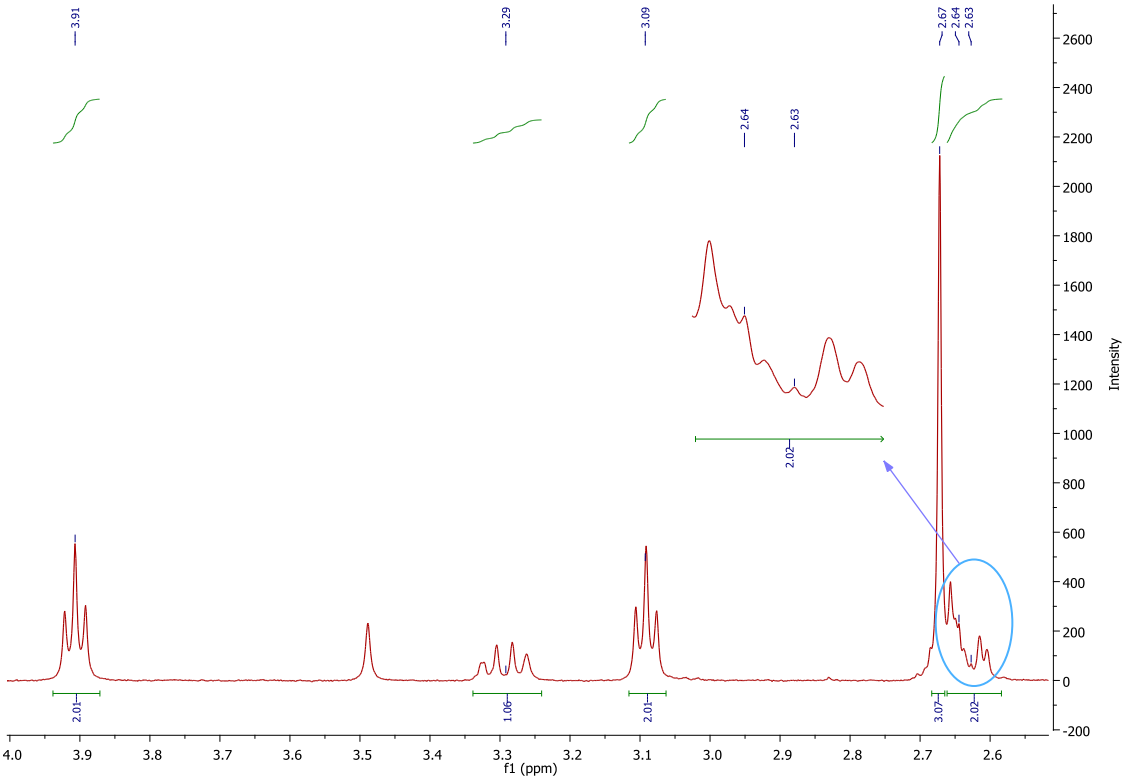

Figure A-130: Expanded ^{1}H NMR ($CDCl_3$, 400 MHz) spectrum of **RH25** (2.6 – 4.0 ppm).

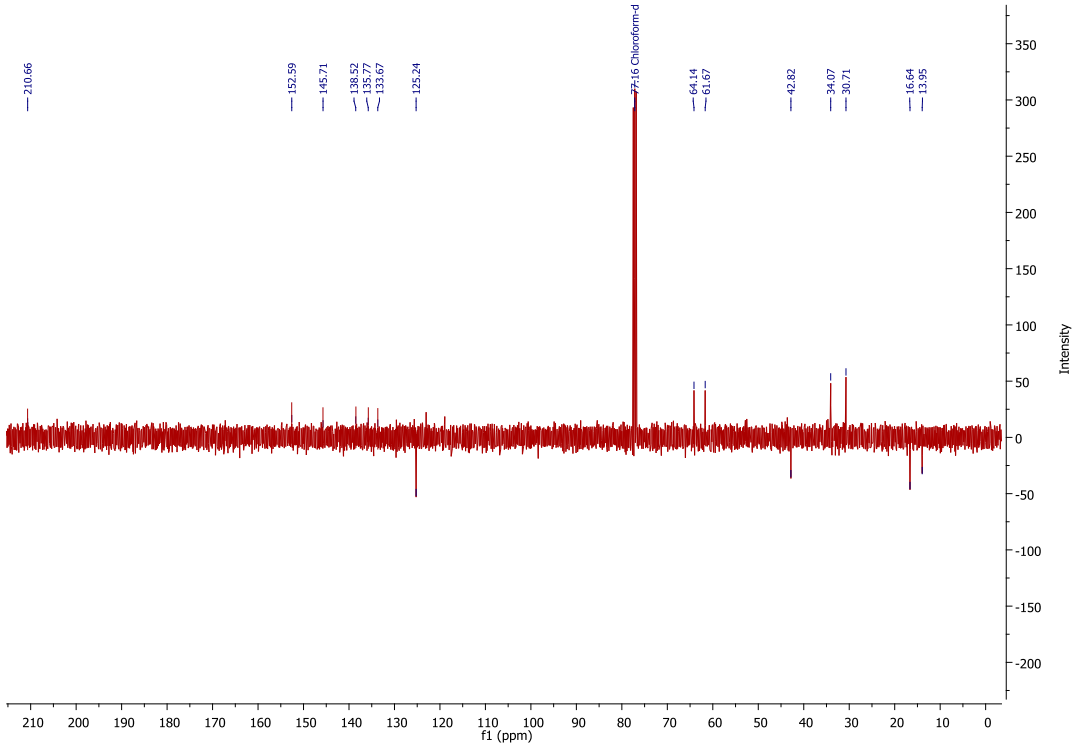

Figure A-131: DEPTQ NMR ($CDCl_3$, 100 MHz) spectrum of compound **RH25**.

24) NMR spectra of compound **RH26** in $CDCl_3$.

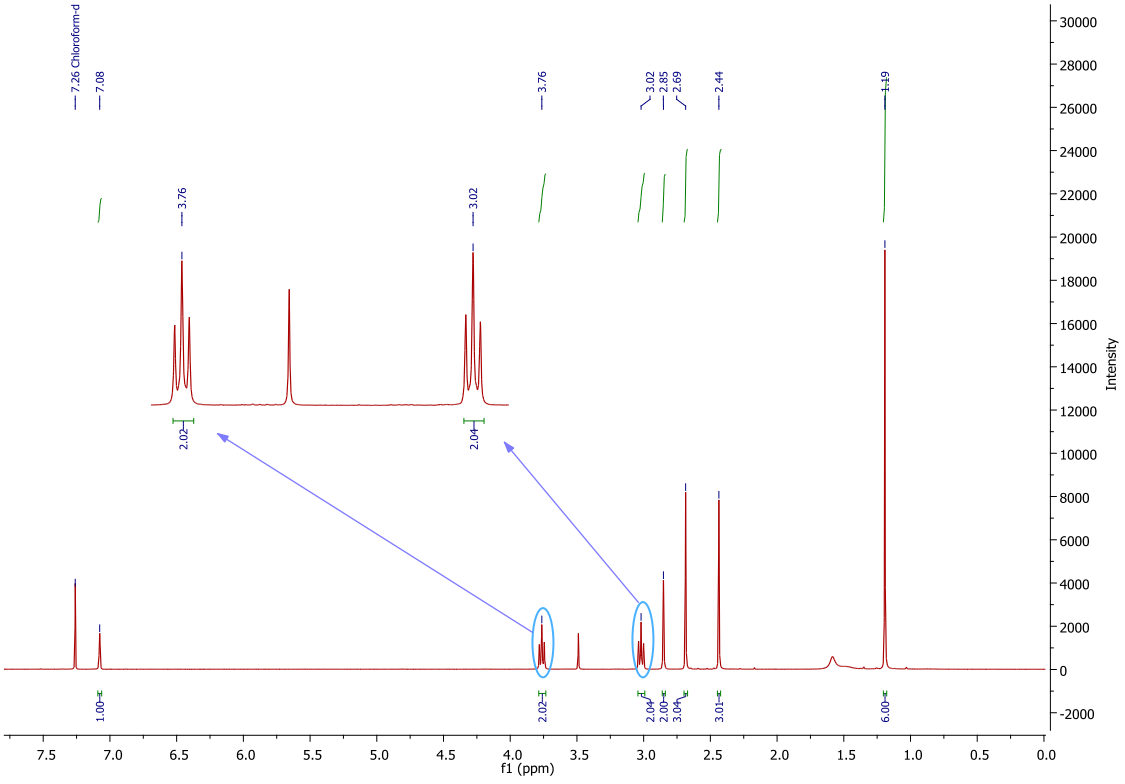

Figure A-132: ^1H NMR ($CDCl_3$, 400 MHz) spectrum of compound **RH26**.

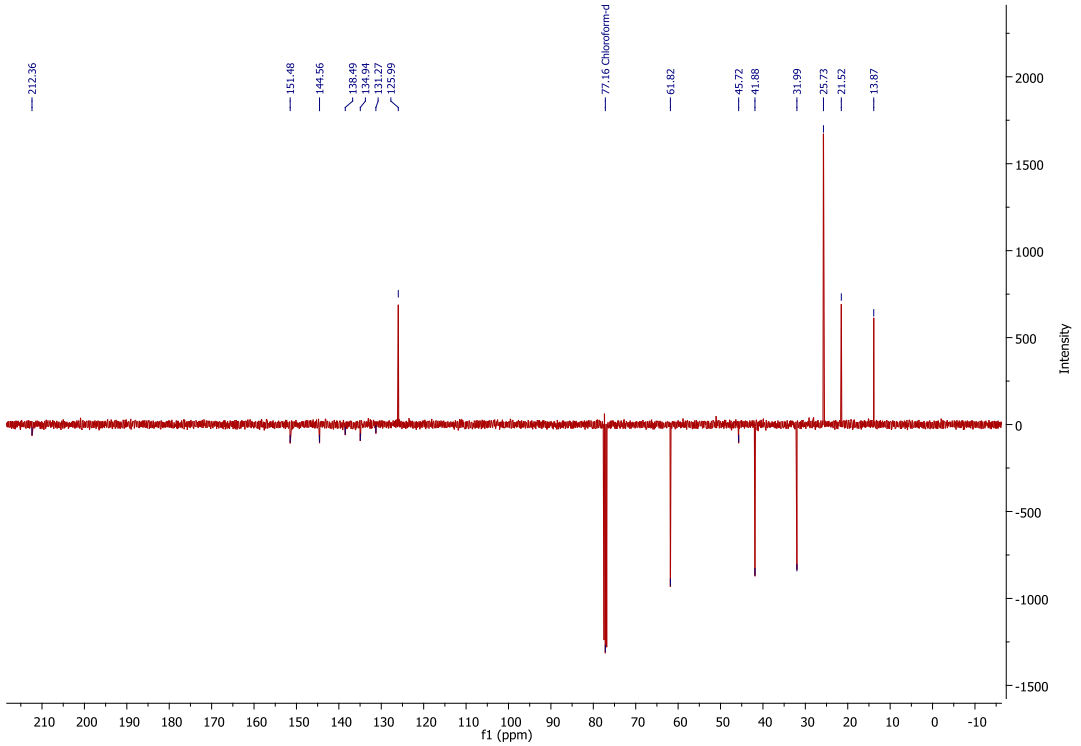

Figure A-133: DEPTQ NMR ($CDCl_3$, 100 MHz) spectrum of compound **RH26**.

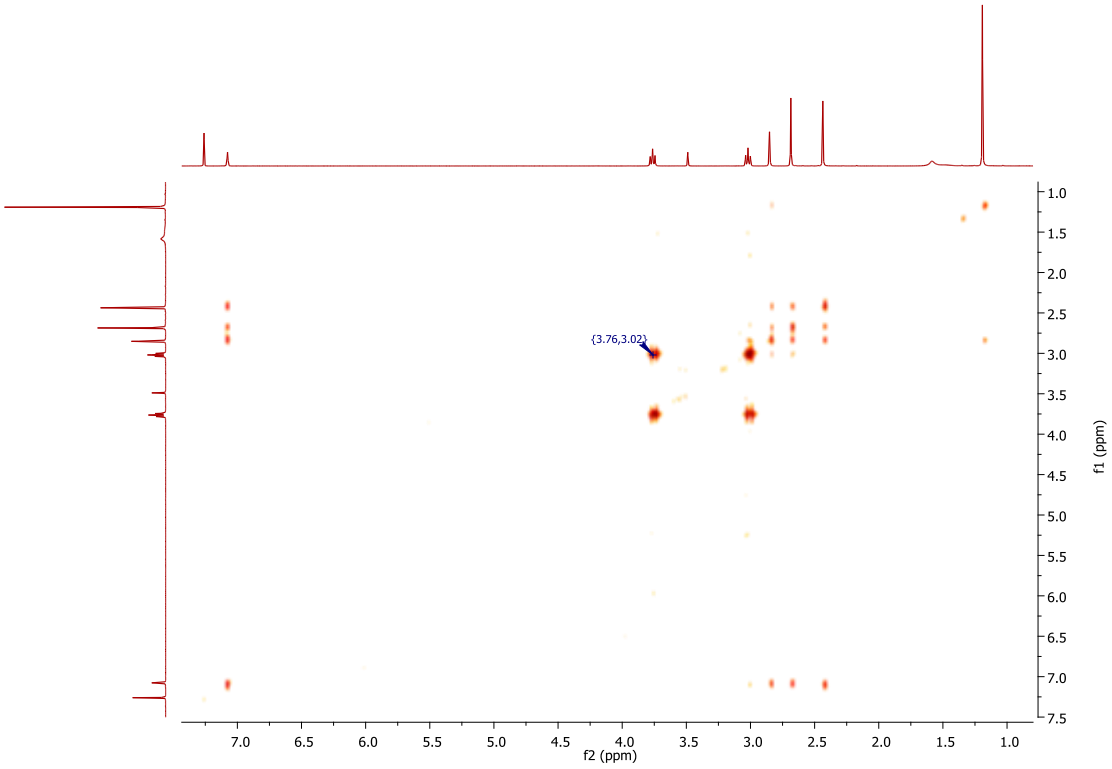

Figure A-134: ^{1}H-^{1}H COSY NMR ($CDCl_3$, 400 MHz) spectrum of compound **RH26**.

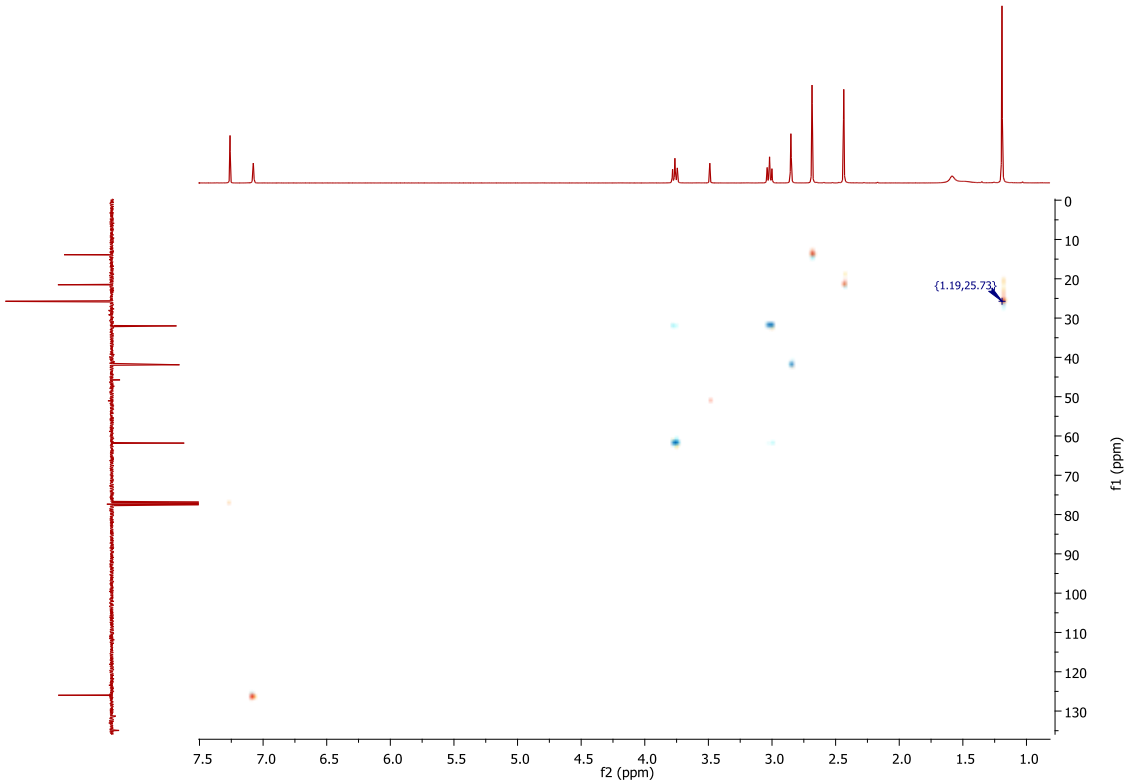

Figure A-135: ^{1}H-^{13}C HSQC NMR spectrum of compound **RH26** in $CDCl_3$.

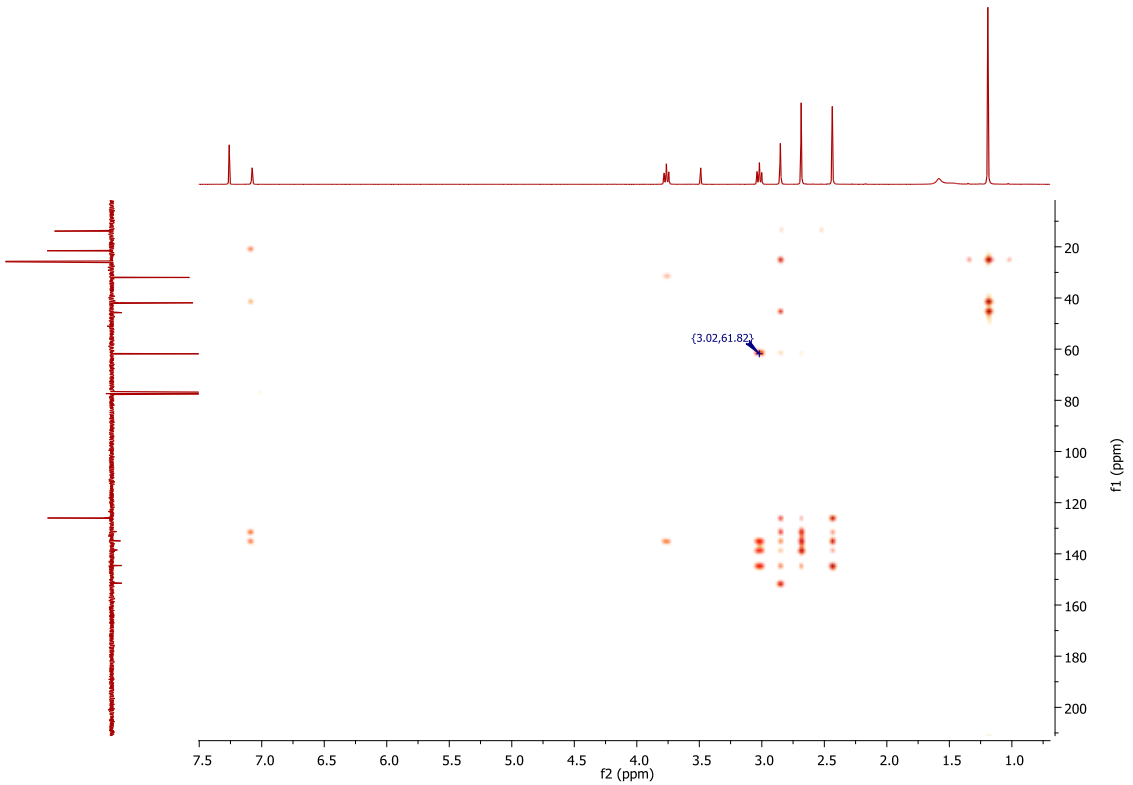

Figure A-136: ^{1}H-^{13}C HMBC NMR spectrum of compound **RH26** in $CDCl_3$.

25) NMR spectra of compound **RH27** in CD_3OD.

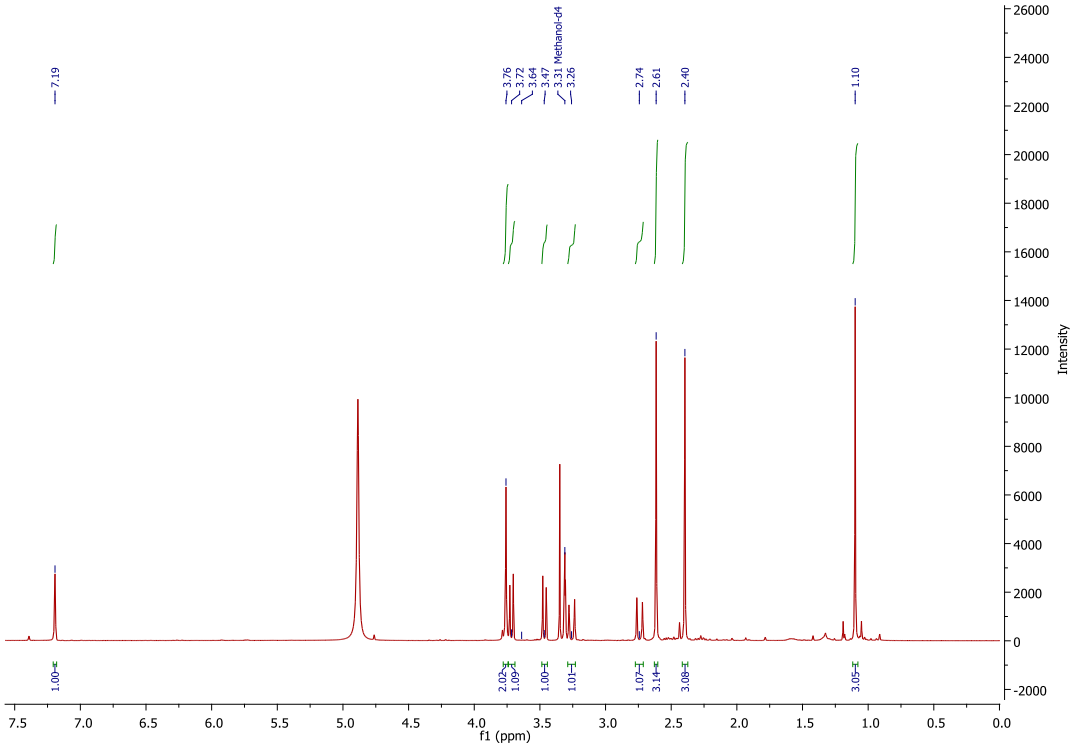

Figure A-137: ^1H NMR (CD_3OD, 400 MHz) spectrum of compound **RH27**.

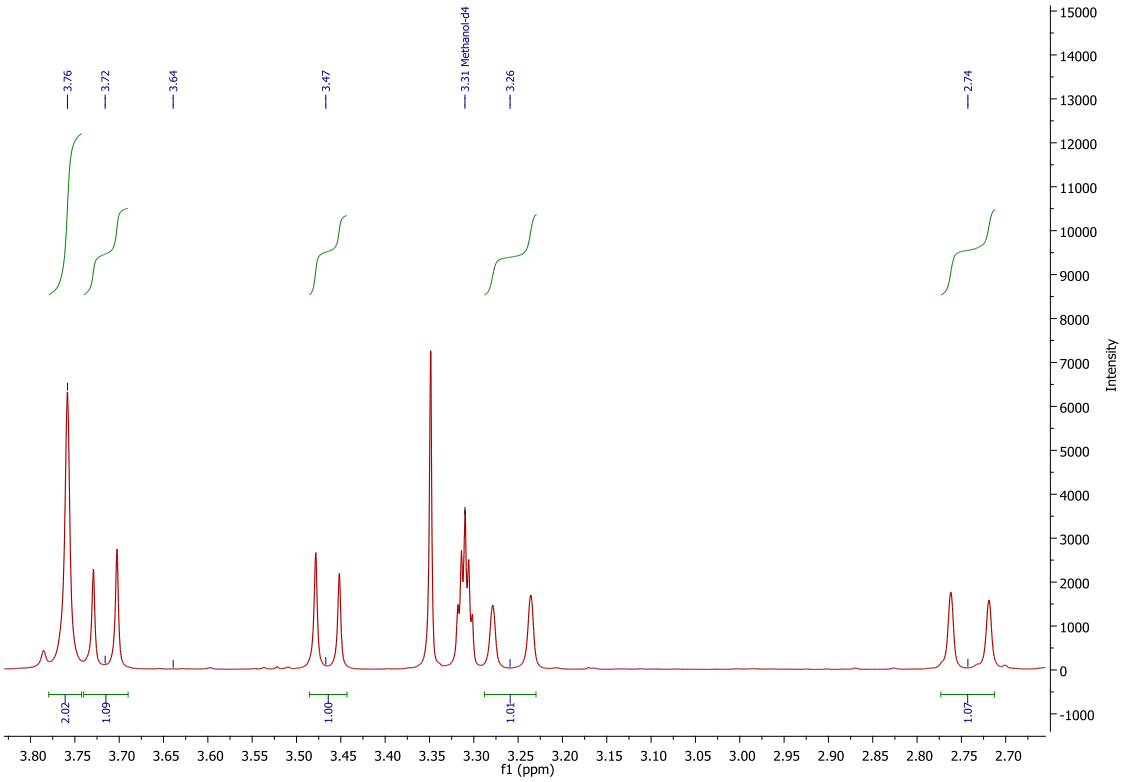

Figure A-138: Expanded ^1H NMR (CD_3OD, 400 MHz) spectrum of **RH27** (2.7 – 3.8 ppm).

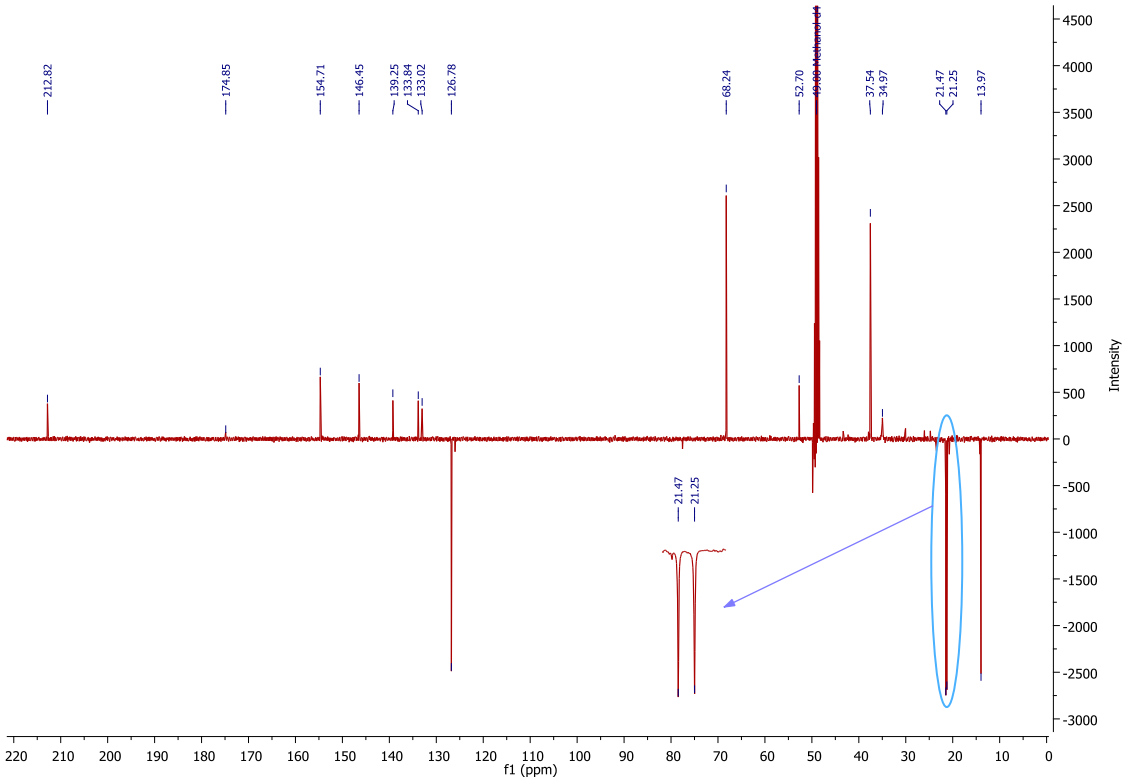

Figure A-139: DEPTQ NMR (CD_3OD, 100 MHz) spectrum of compound **RH27**.

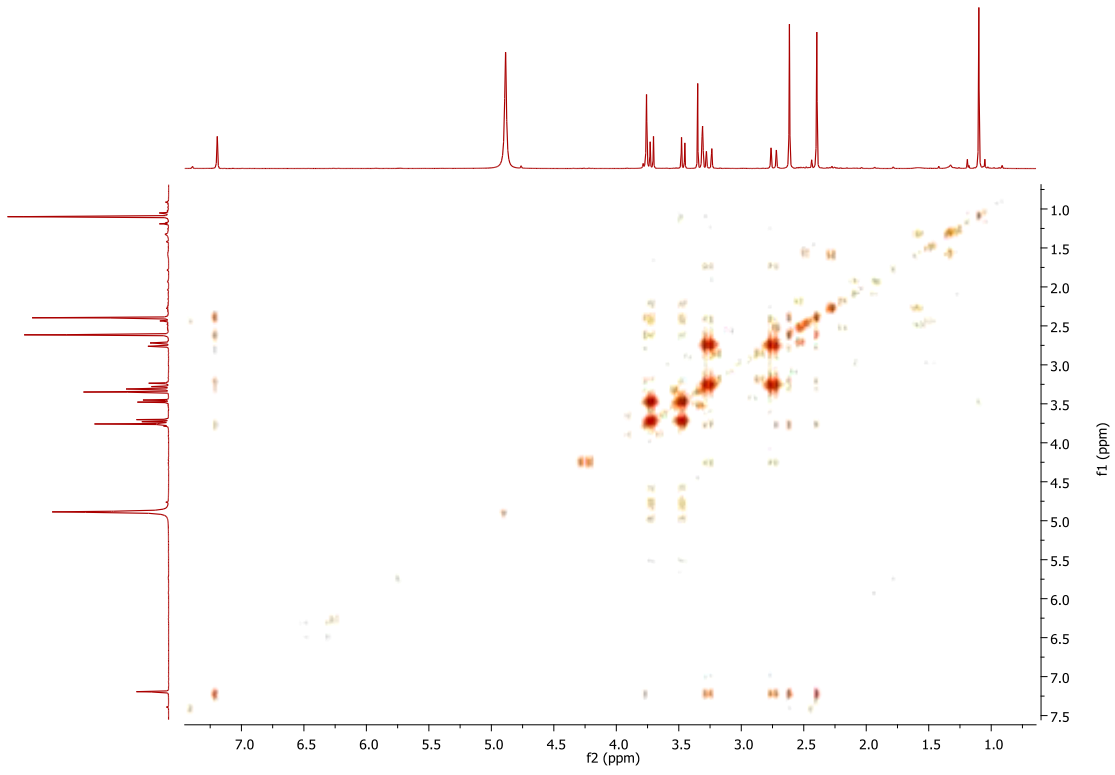

Figure A-140: ^{1}H-^{1}H COSY NMR (CD_3OD, 400 MHz) spectrum of compound **RH27**.

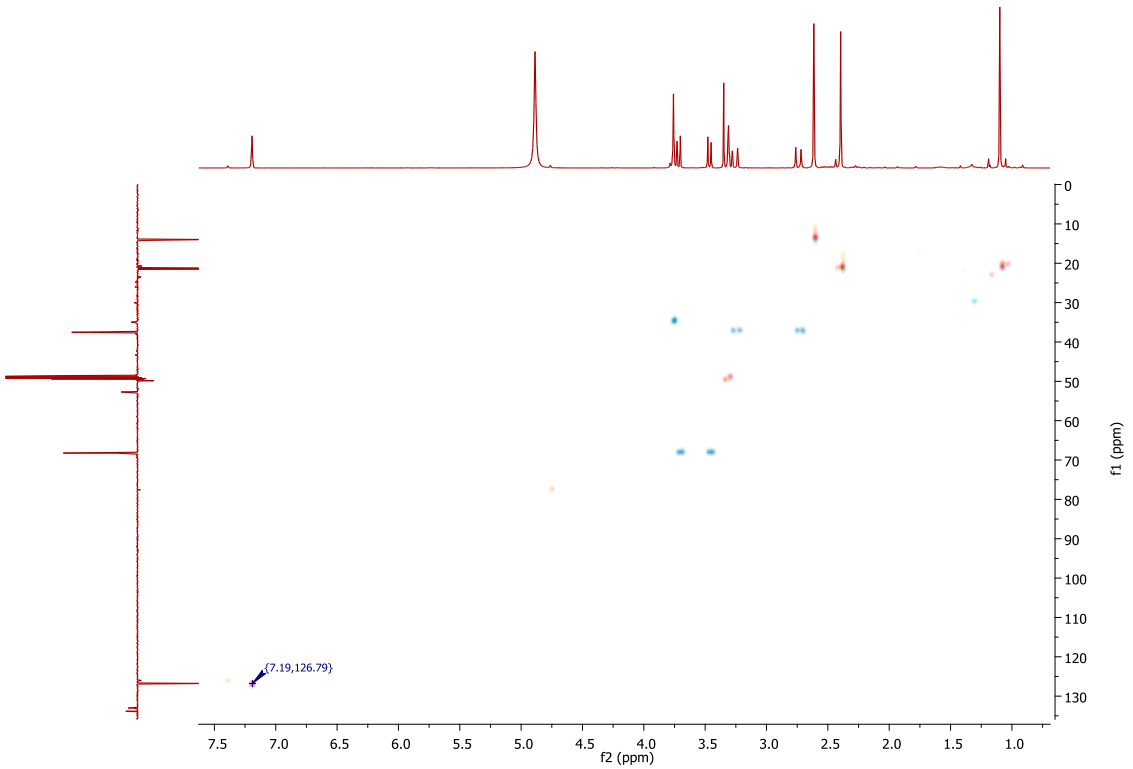

Figure A-141: ^{1}H-^{13}C HSQC NMR spectrum of compound **RH27** in CD_3OD.

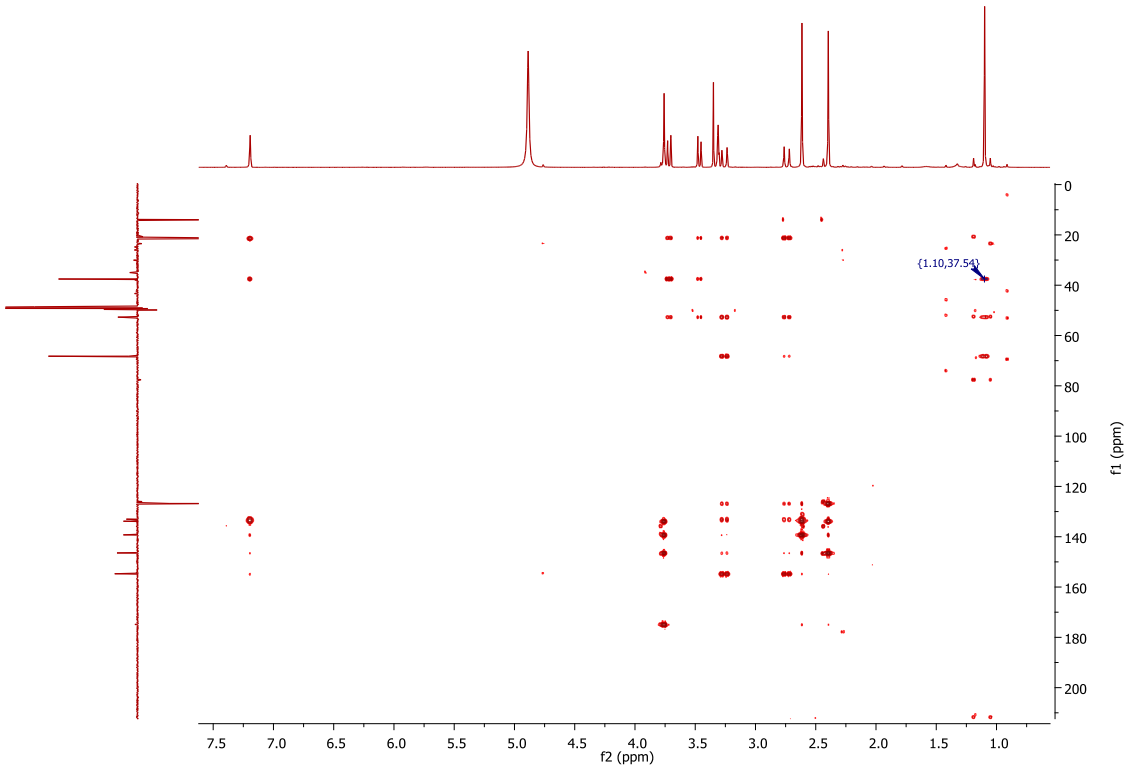

Figure A-142: ^{1}H-^{13}C HMBC NMR spectrum of compound **RH27** in CD_3OD.

26) NMR spectra of compound **RH28** in CD_3OD.

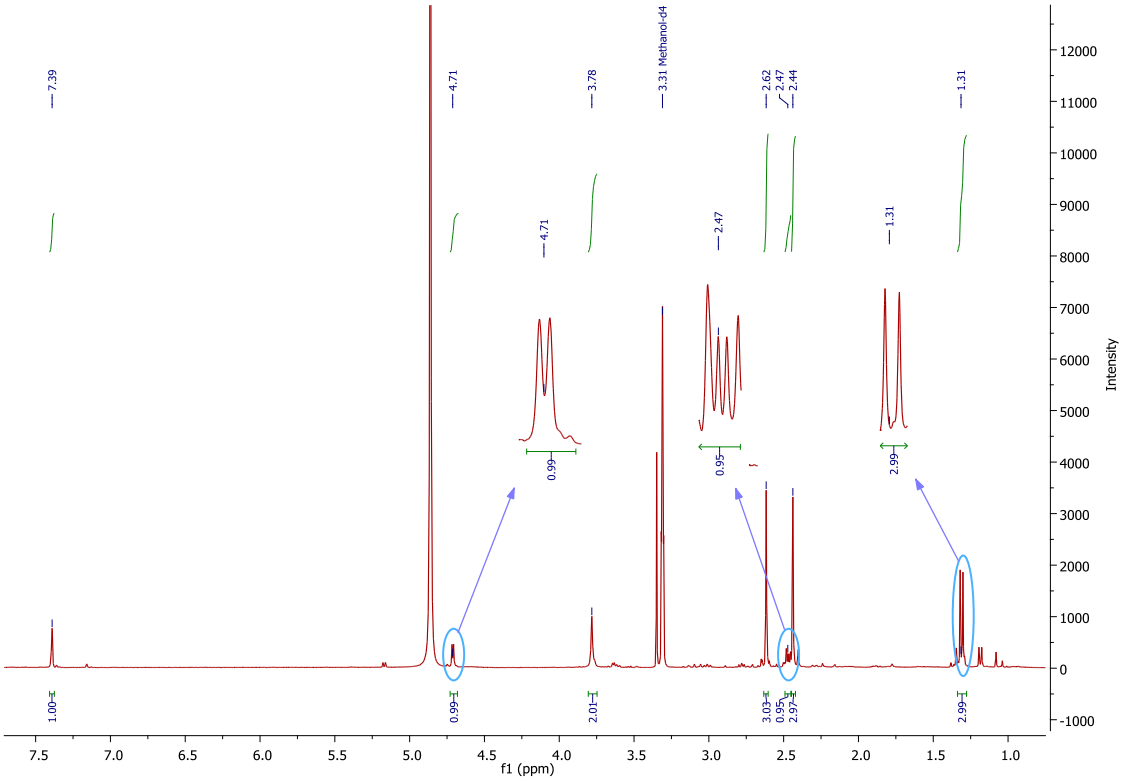

Figure A-143: ^1H NMR (CD_3OD, 400 MHz) spectrum of compound **RH28**.

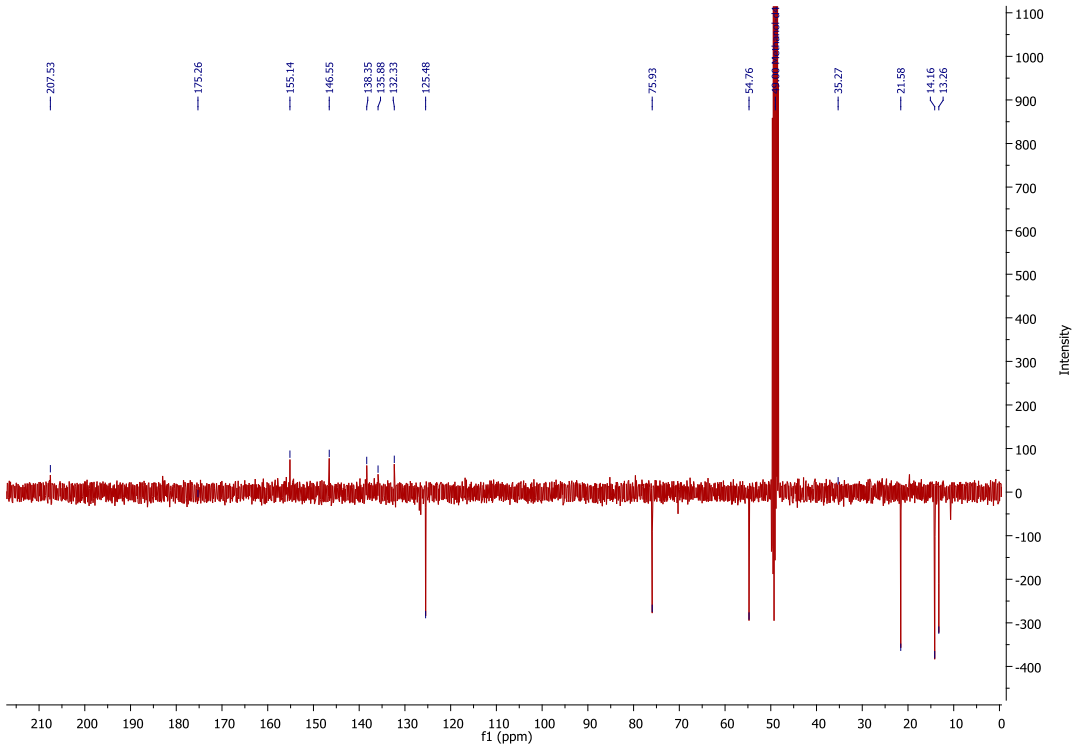

Figure A-144: DEPTQ NMR (CD_3OD, 100 MHz) spectrum of compound **RH28**.

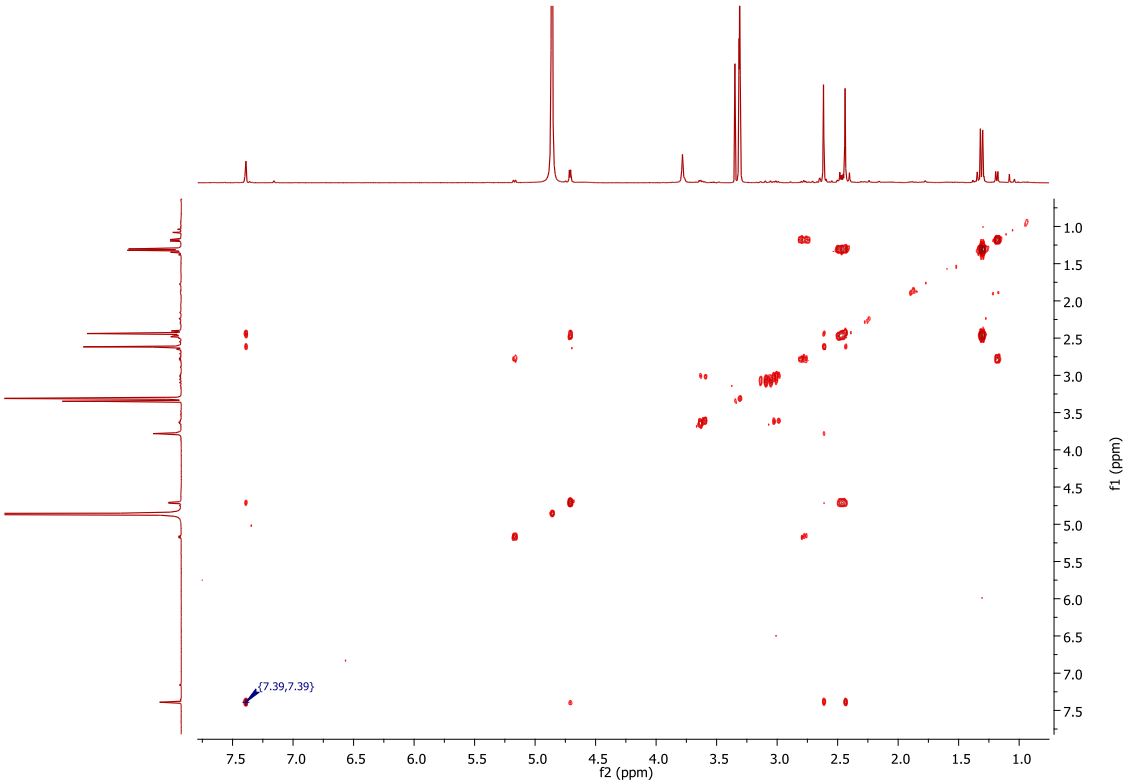

Figure A-145: ^{1}H-^{1}H COSY NMR (CD_3OD, 400 MHz) spectrum of compound **RH28**.

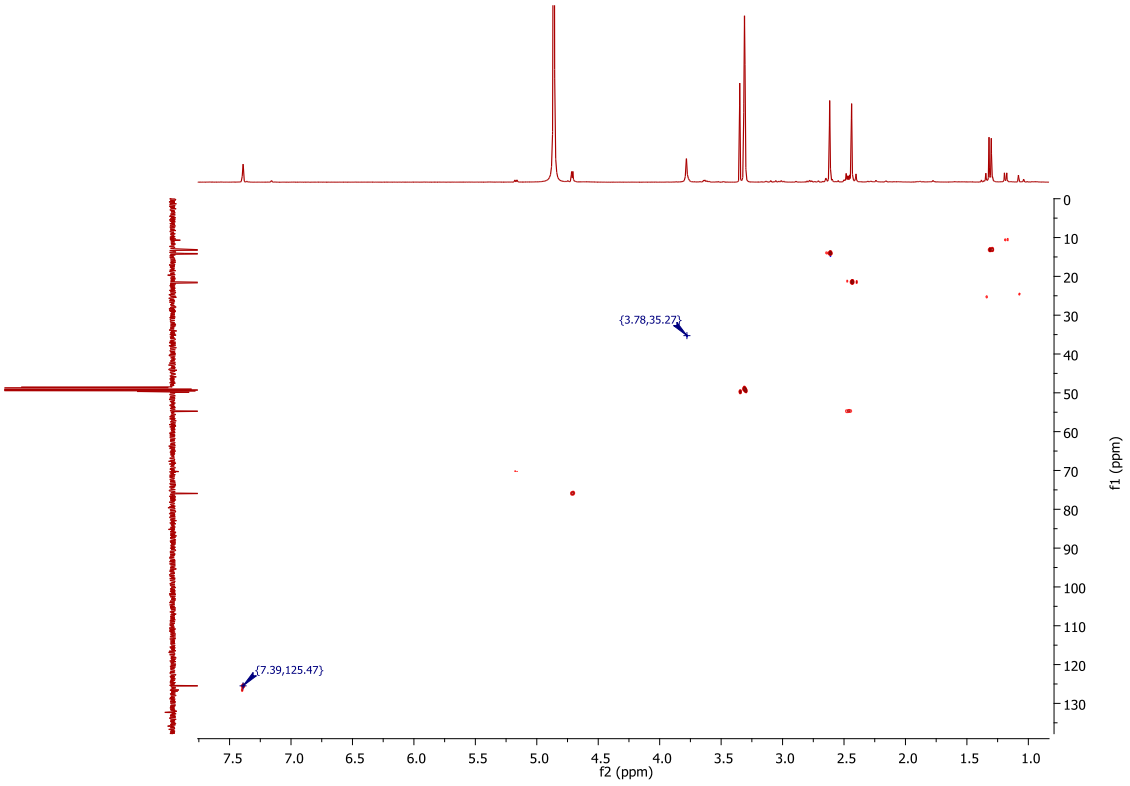

Figure A-146: ^{1}H-^{13}C HSQC NMR spectrum of compound **RH28** in CD_3OD.

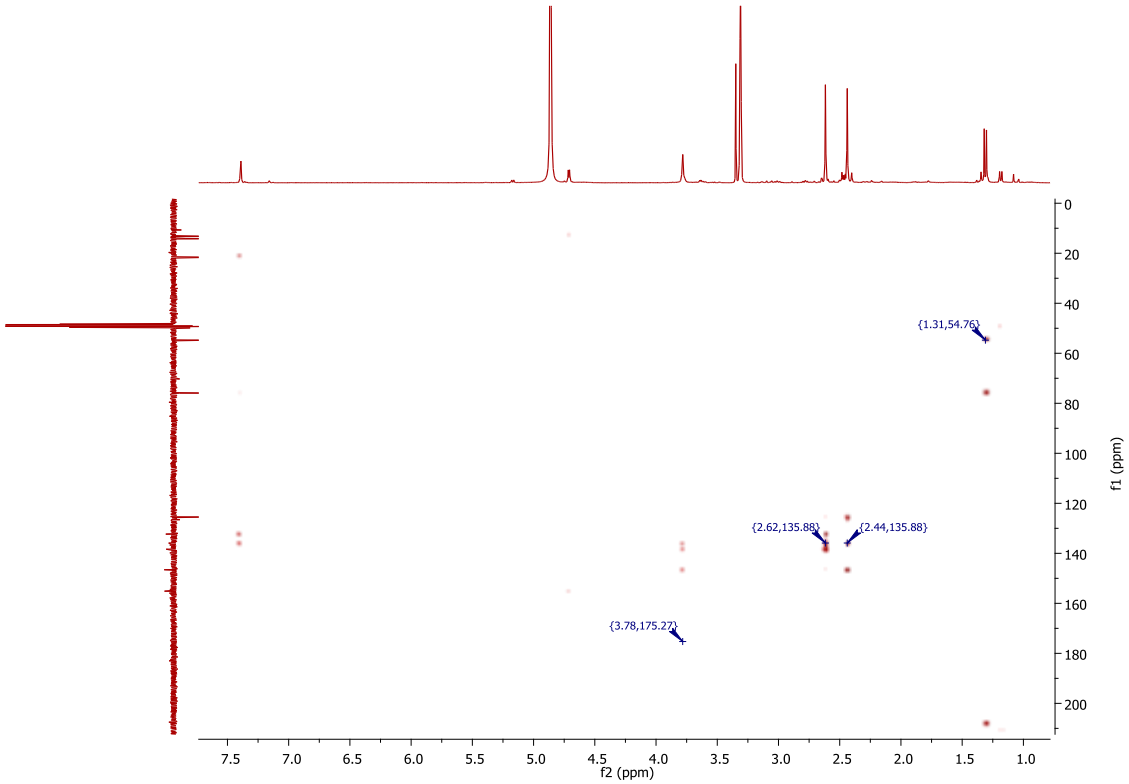

Figure A-147: ^{1}H-^{13}C HMBC NMR spectrum of compound **RH28** in CD_3OD.

27) NMR spectra of compound **RH29** in CD_3OD.

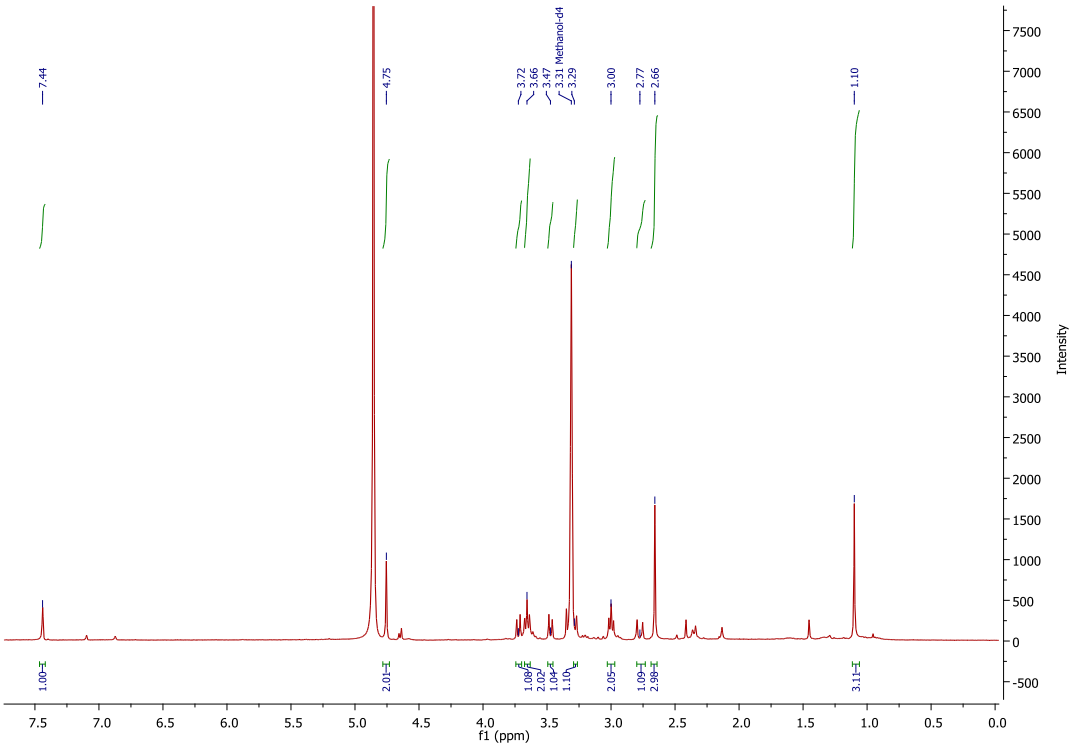

Figure A-148: ^{1}H NMR (CD_3OD, 400 MHz) spectrum of compound **RH29**.

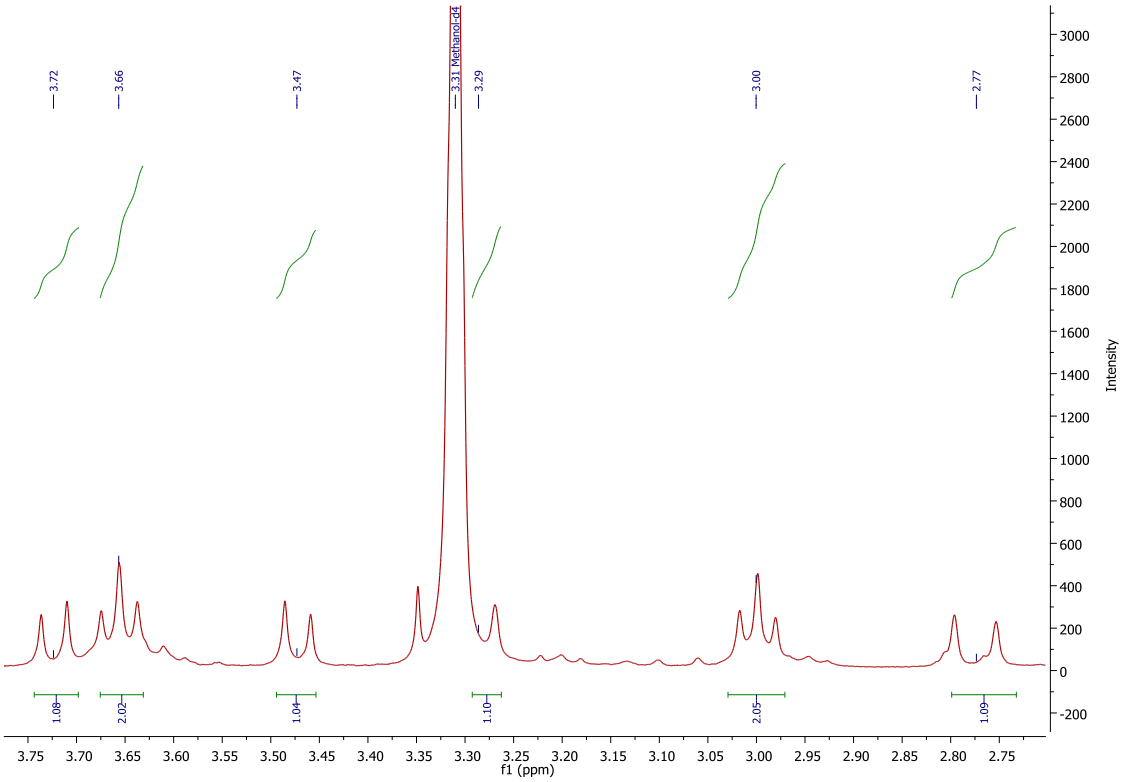

Figure A-149: Expanded ^{1}H NMR (CD_3OD, 400 MHz) spectrum of **RH29** (2.7 – 3.7 ppm).

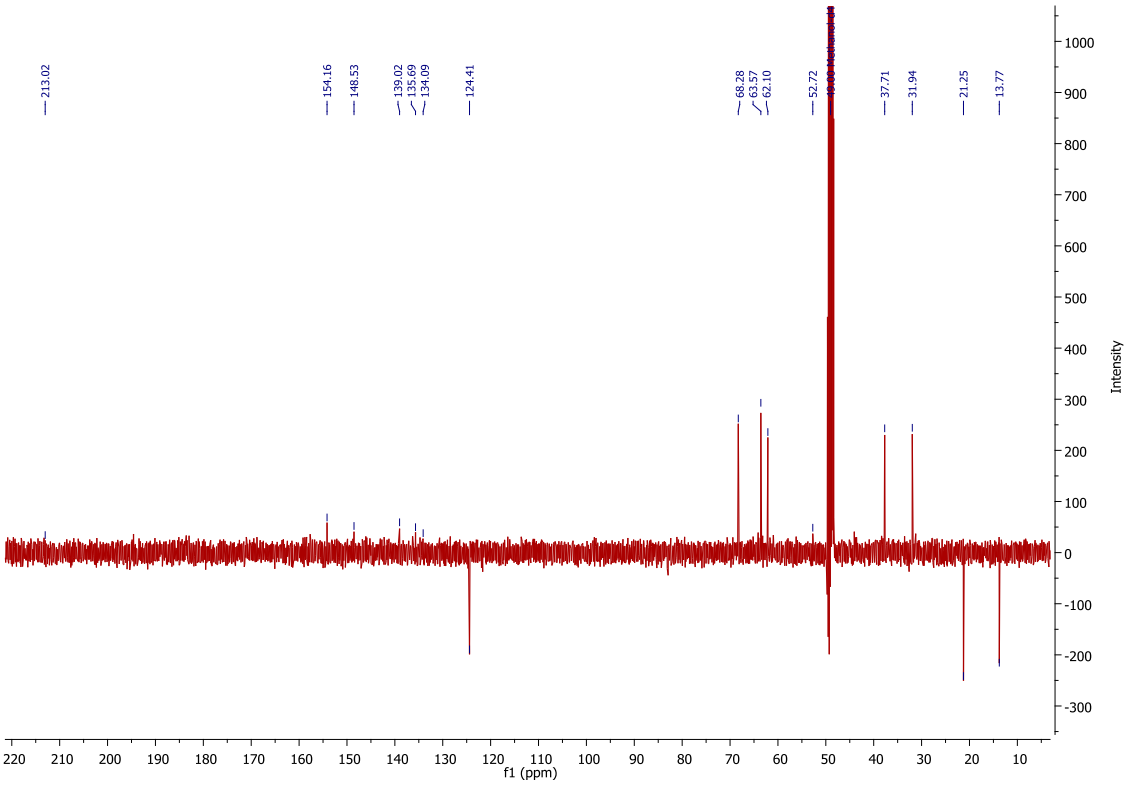

Figure A-150: DEPTQ NMR (CD_3OD, 100 MHz) spectrum of compound **RH29**.

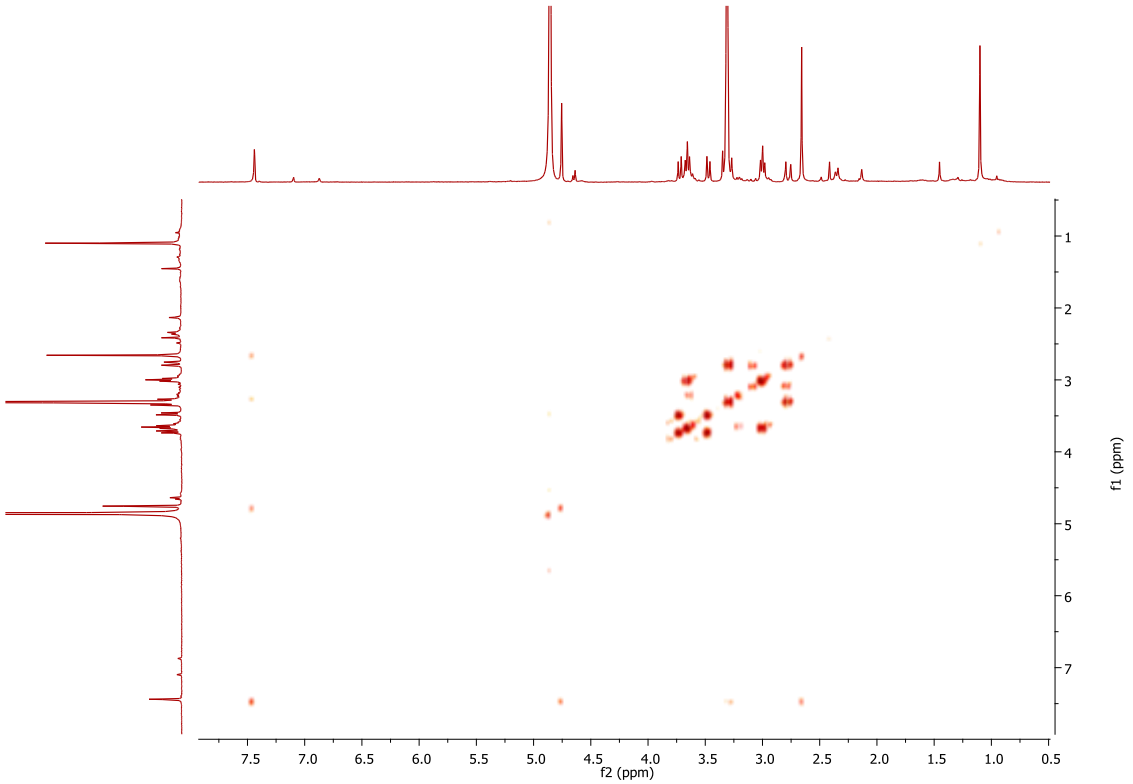

Figure A-151: ^{1}H-^{1}H COSY NMR (CD_3OD, 400 MHz) spectrum of compound **RH29**.

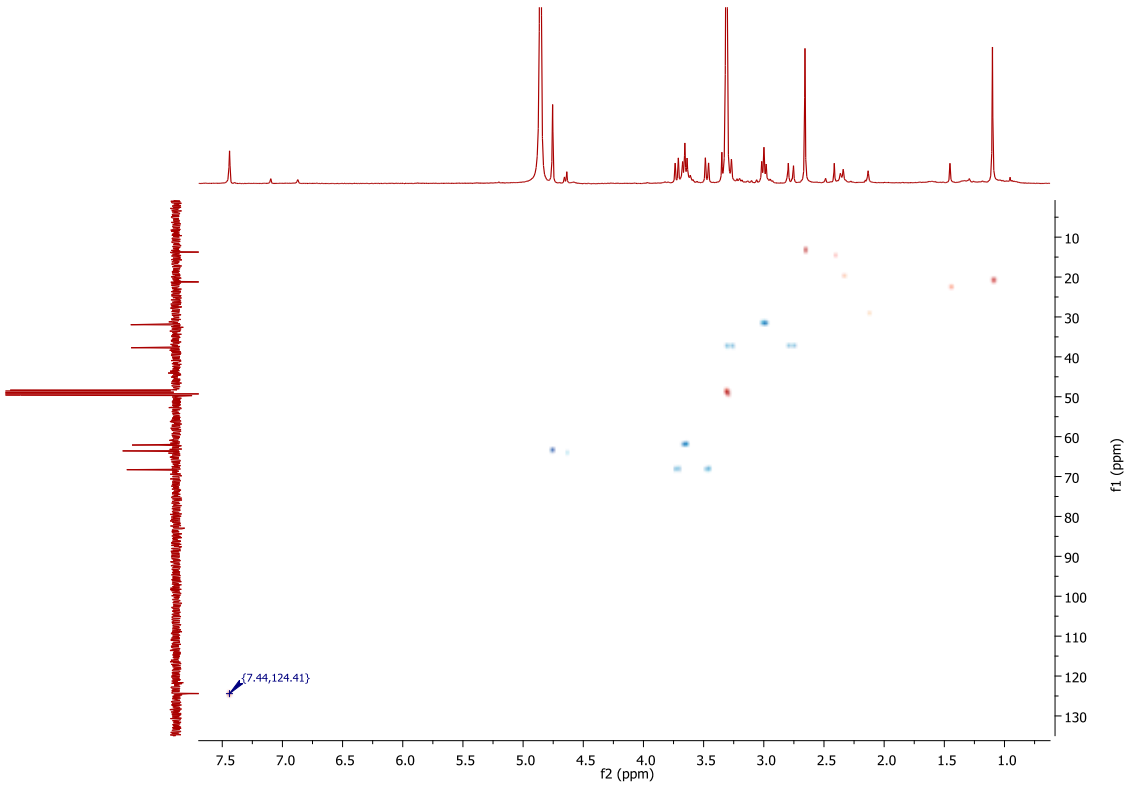

Figure A-152: ^{1}H-^{13}C HSQC NMR spectrum of compound **RH29** in CD_3OD.

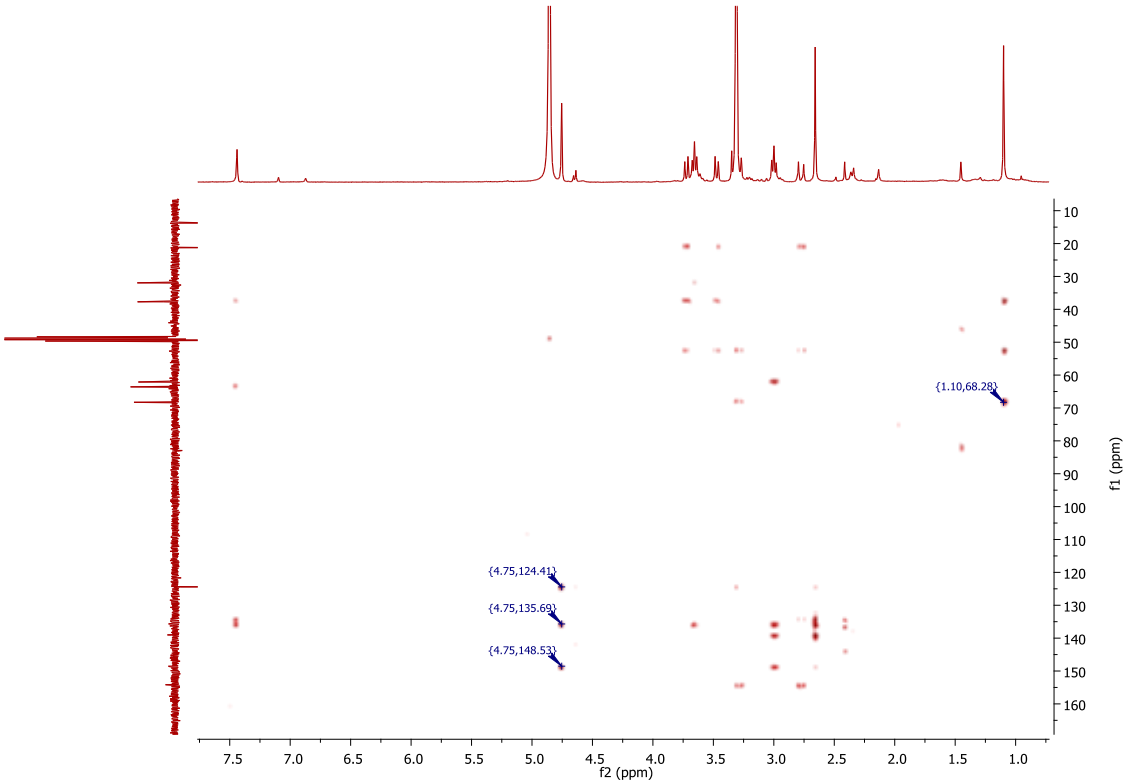

Figure A-153: ^{1}H-^{13}C HMBC NMR spectrum of compound **RH29** in CD_3OD.

28) NMR spectra of compound **RH30** in CD_3OD.

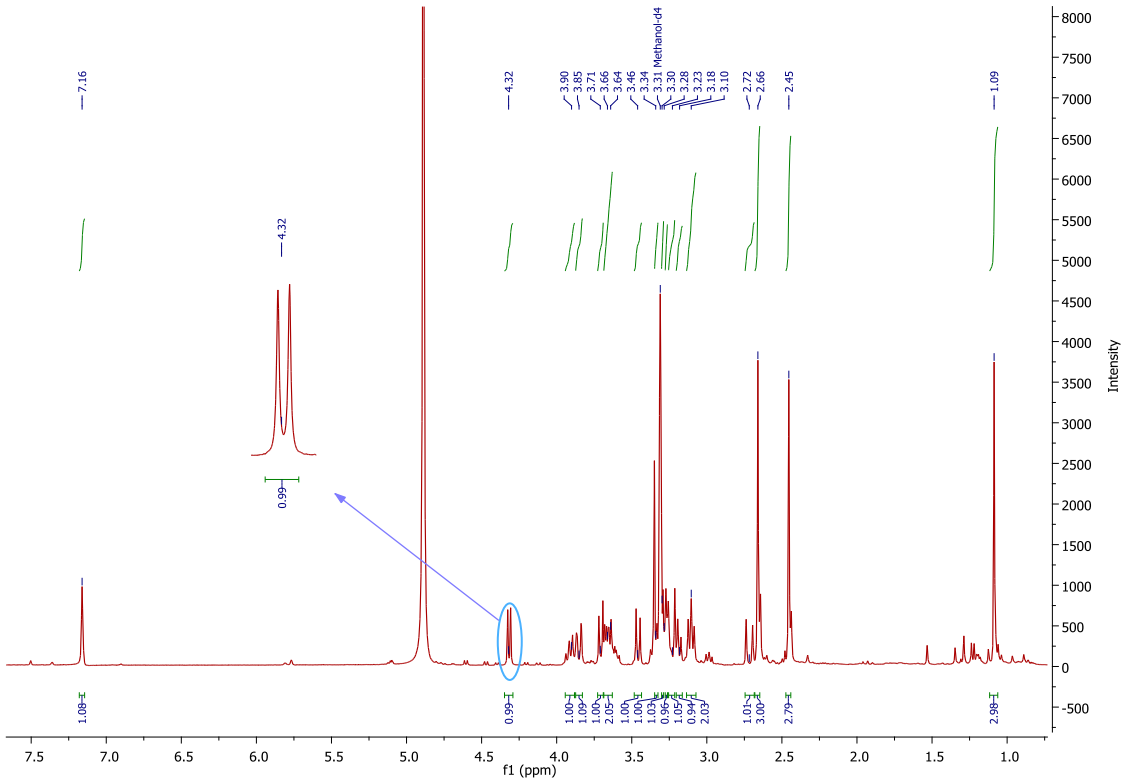

Figure A-154: ^{1}H NMR (CD_3OD, 400 MHz) spectrum of compound **RH30**.

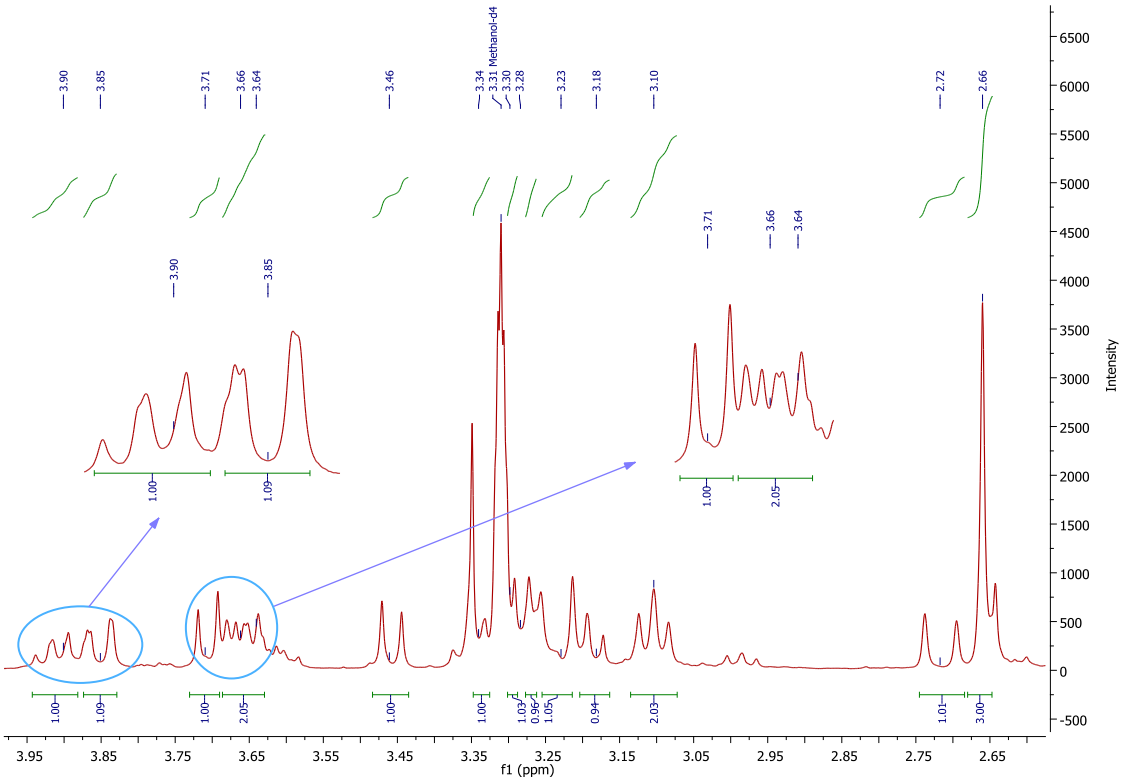

Figure A-155: Expanded ^{1}H NMR (CD_3OD, 400 MHz) spectrum of **RH30** (2.6 – 3.9 ppm).

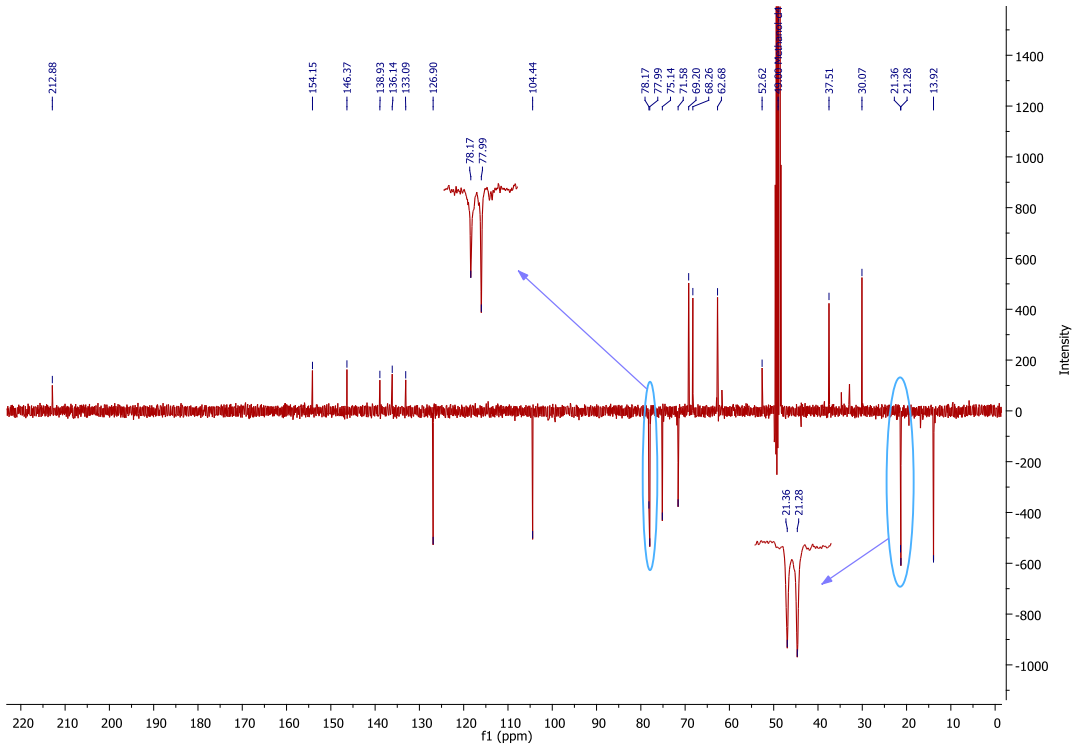

Figure A-156: DEPTQ NMR (CD_3OD, 100 MHz) spectrum of compound **RH30**.

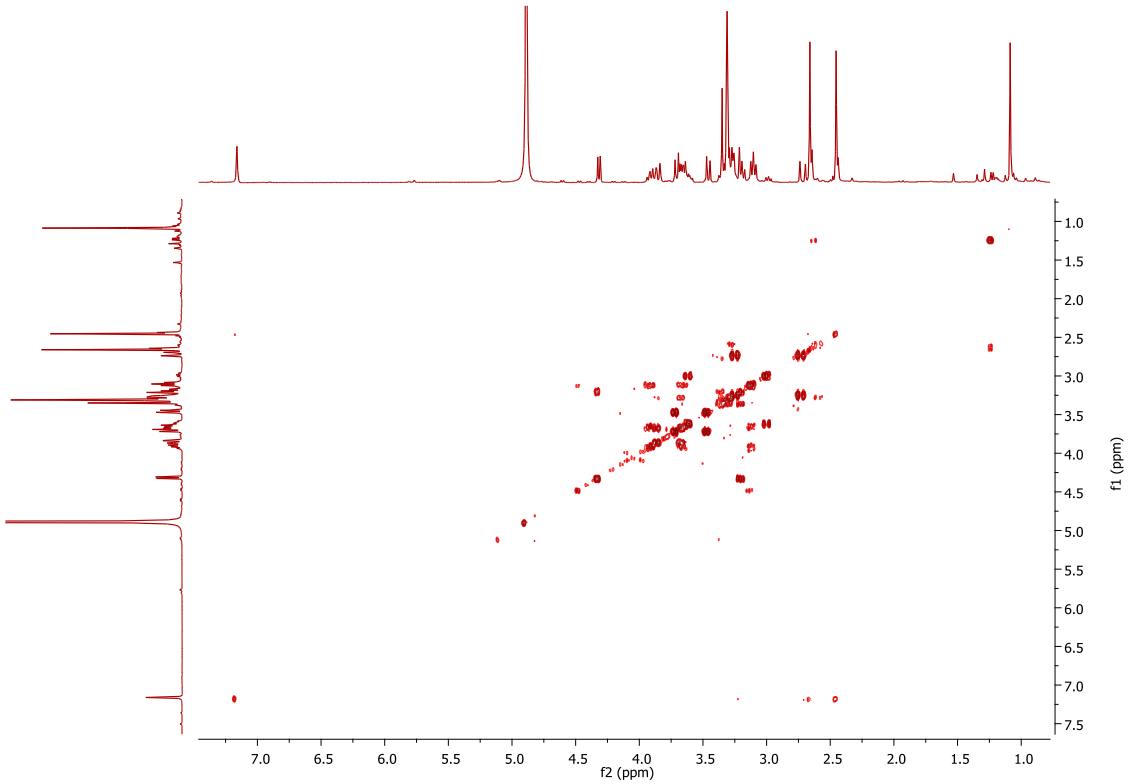

Figure A-157: ^{1}H-^{1}H COSY NMR (CD_3OD, 400 MHz) spectrum of compound **RH30**.

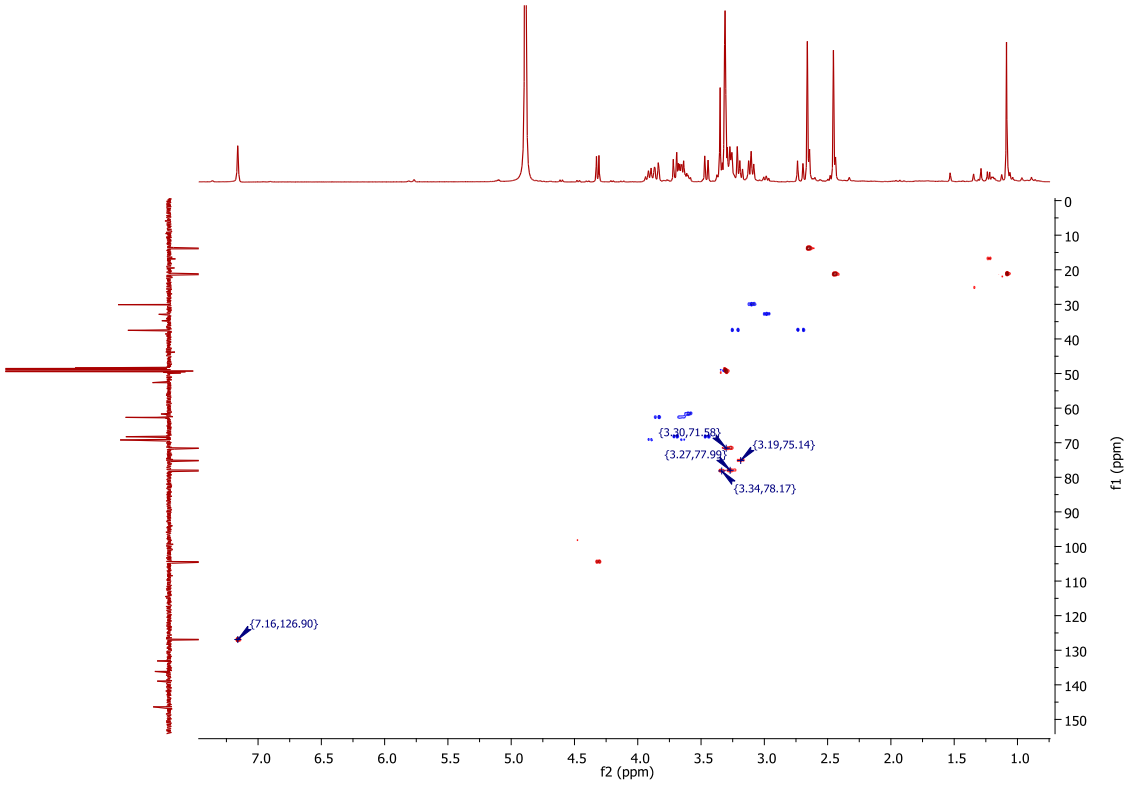

Figure A-158: ^{1}H-^{13}C HSQC NMR spectrum of compound **RH30** in CD_3OD.

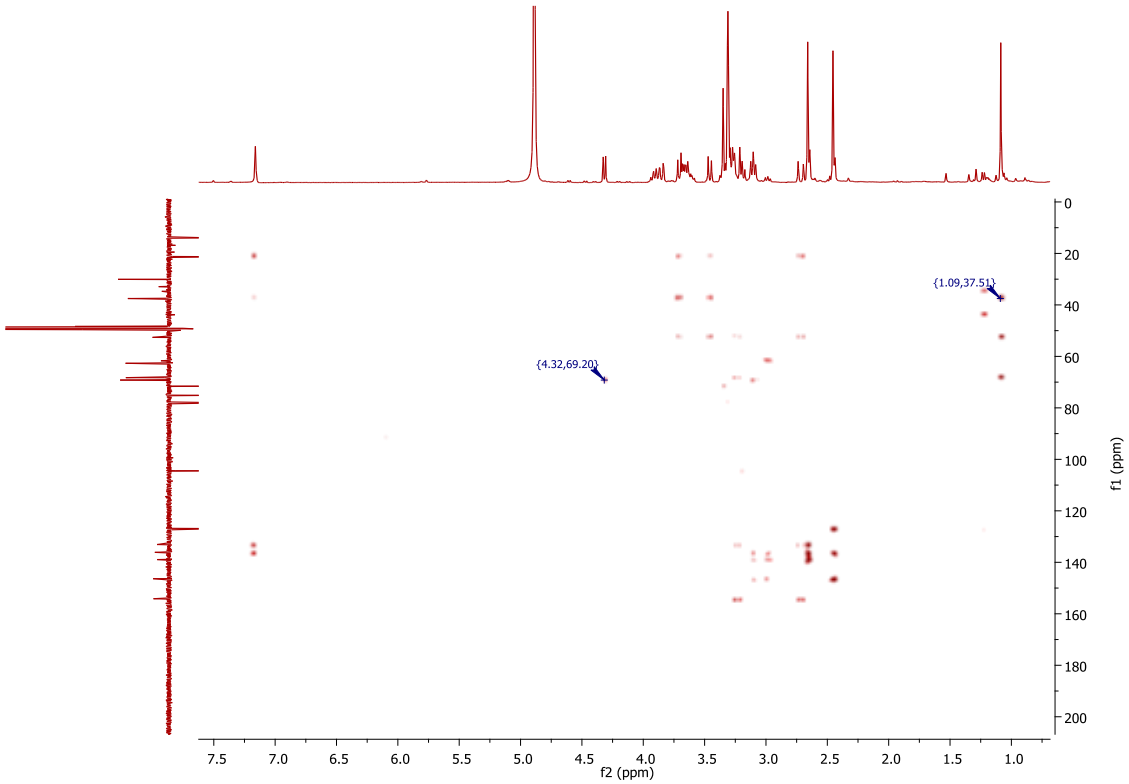

Figure A-159: ^{1}H-^{13}C HMBC NMR spectrum of compound **RH30** in CD_3OD.

29) NMR spectra of compound **RH31** in CD_3OD.

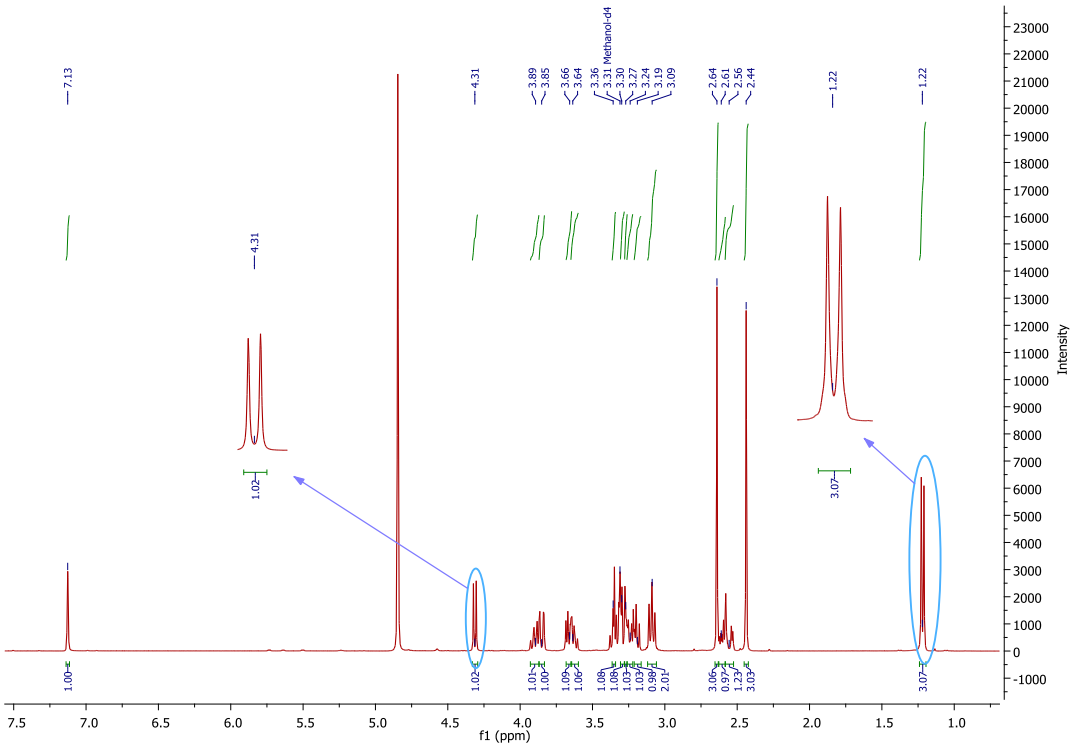

Figure A-160: ^{1}H NMR (CD_3OD, 400 MHz) spectrum of compound **RH31**.

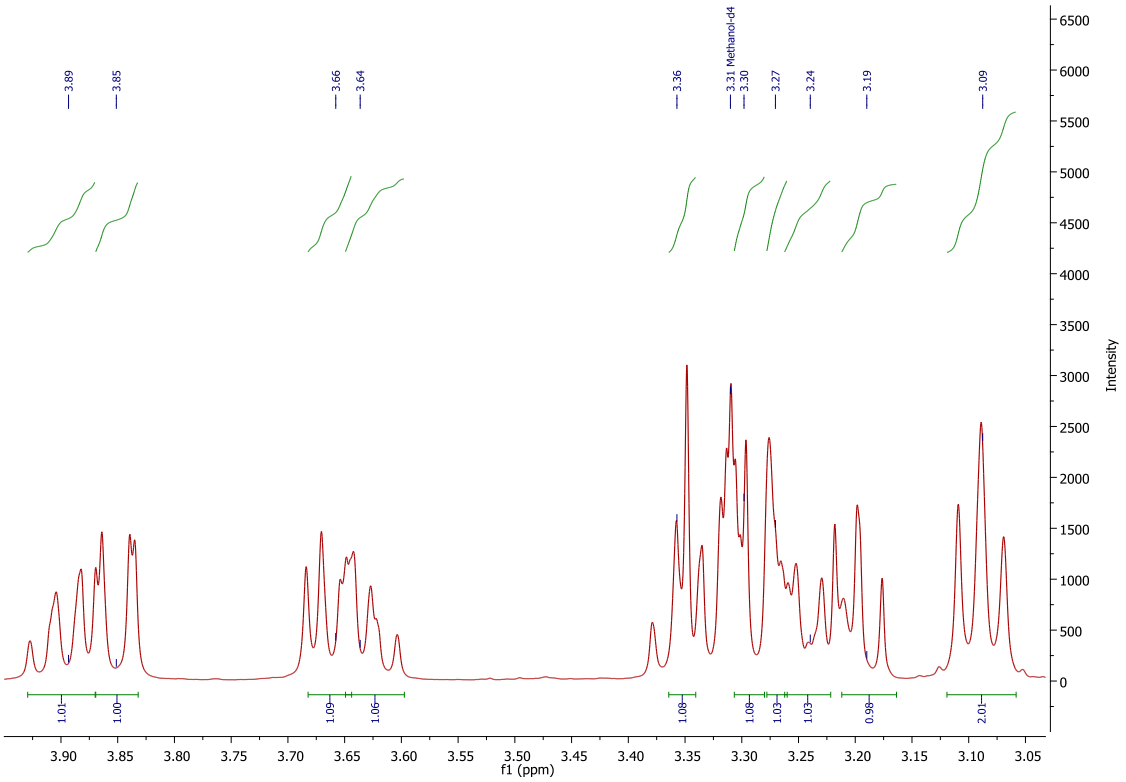

Figure A-161: Expanded ^{1}H NMR (CD_3OD, 400 MHz) spectrum of **RH31** (3.1 – 3.9 ppm).

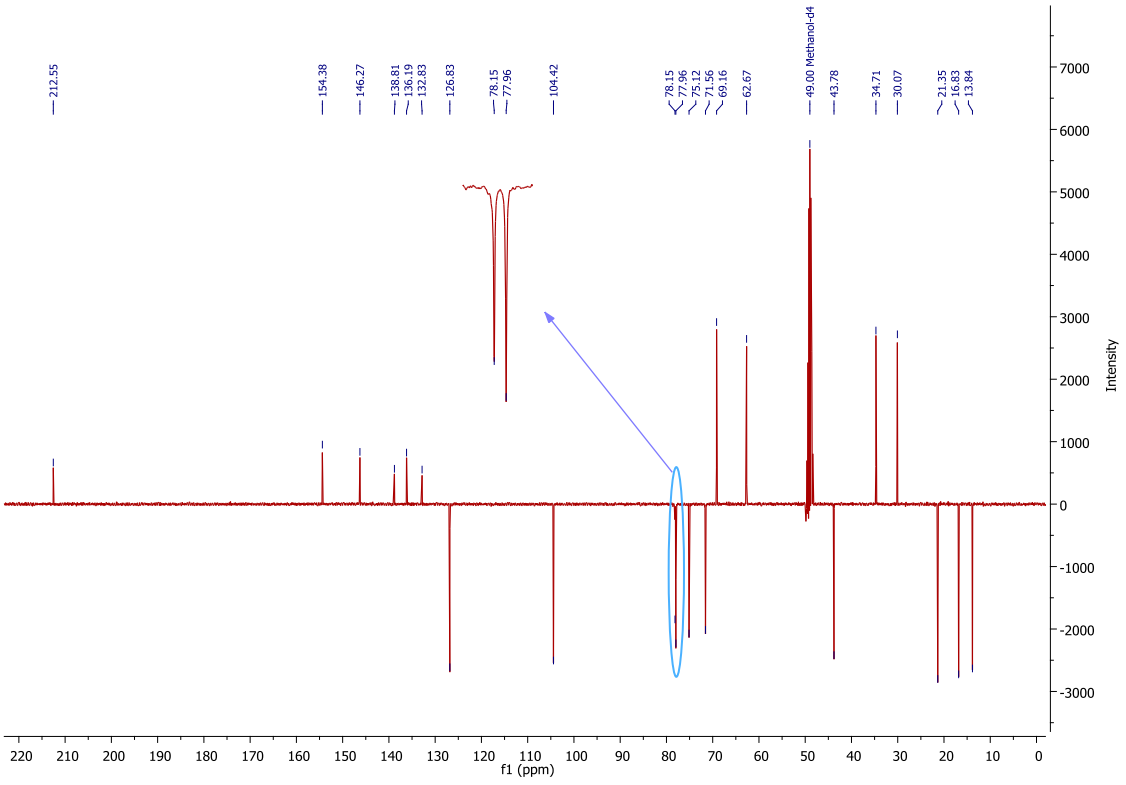

Figure A-162: DEPTQ NMR (CD_3OD, 100 MHz) spectrum of compound **RH31**.

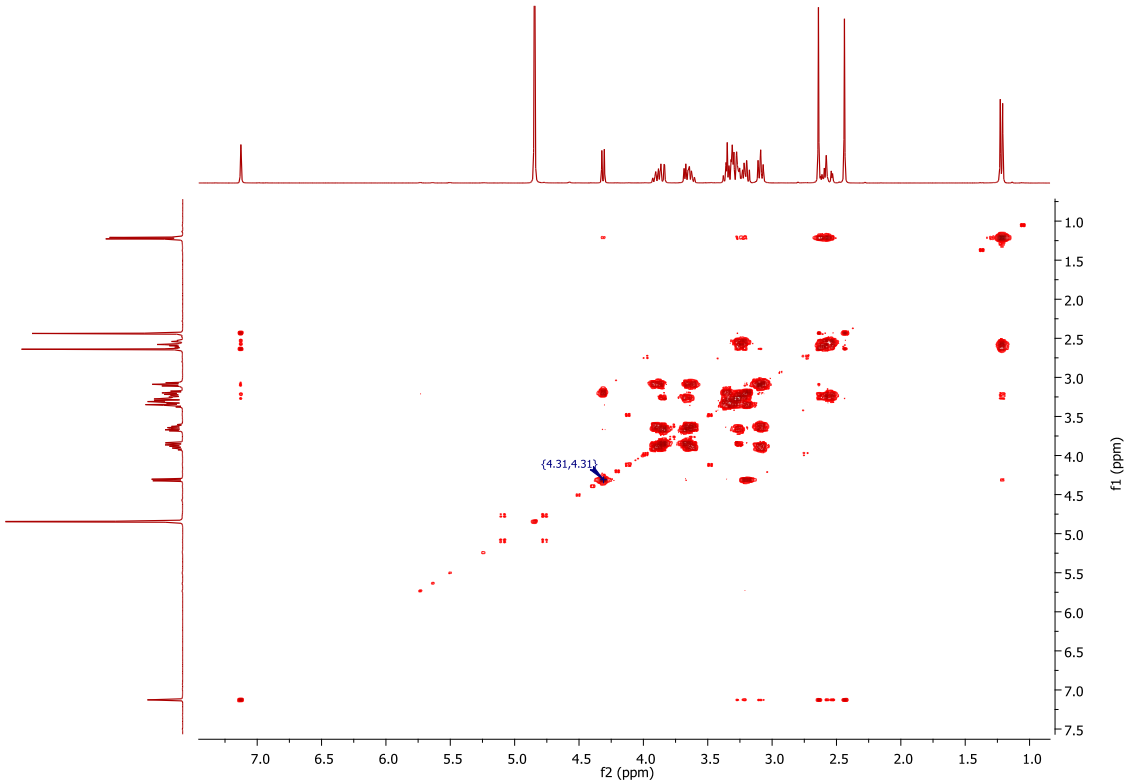

Figure A-163: ^{1}H-^{1}H COSY NMR (CD_3OD, 400 MHz) spectrum of compound **RH31**.

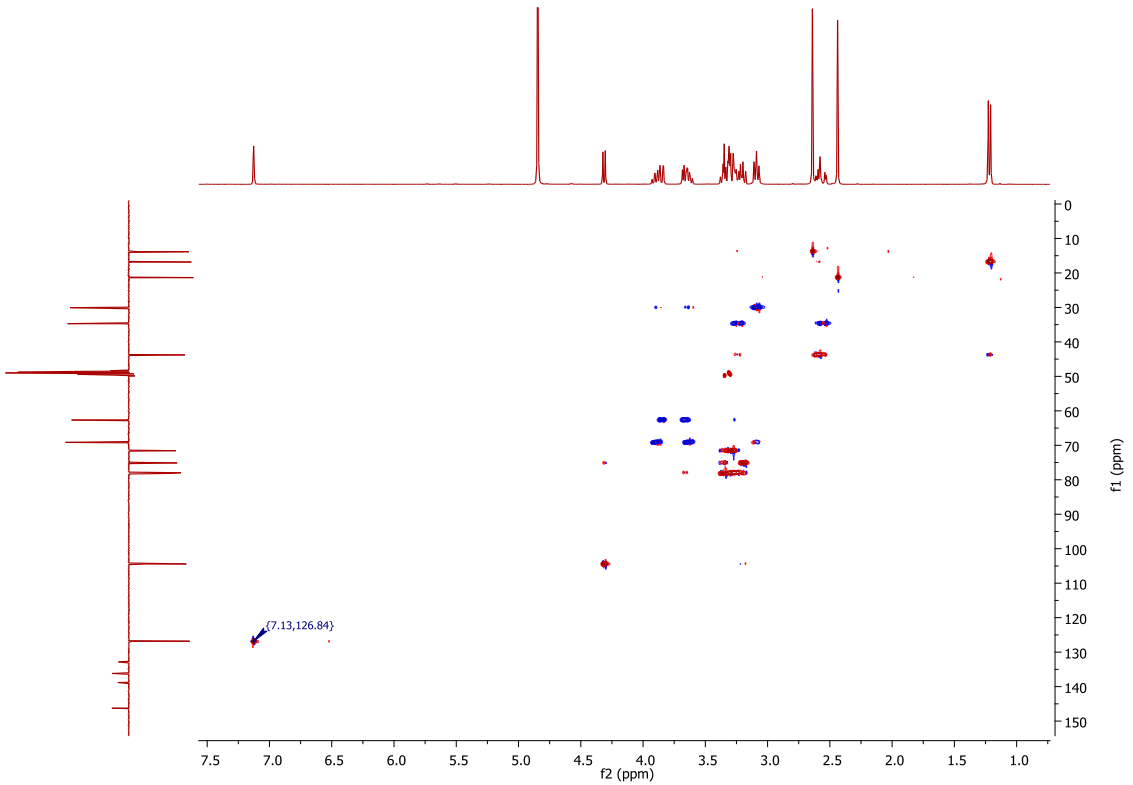

Figure A-164: ^{1}H-^{13}C HSQC NMR spectrum of compound **RH31** in CD_3OD.

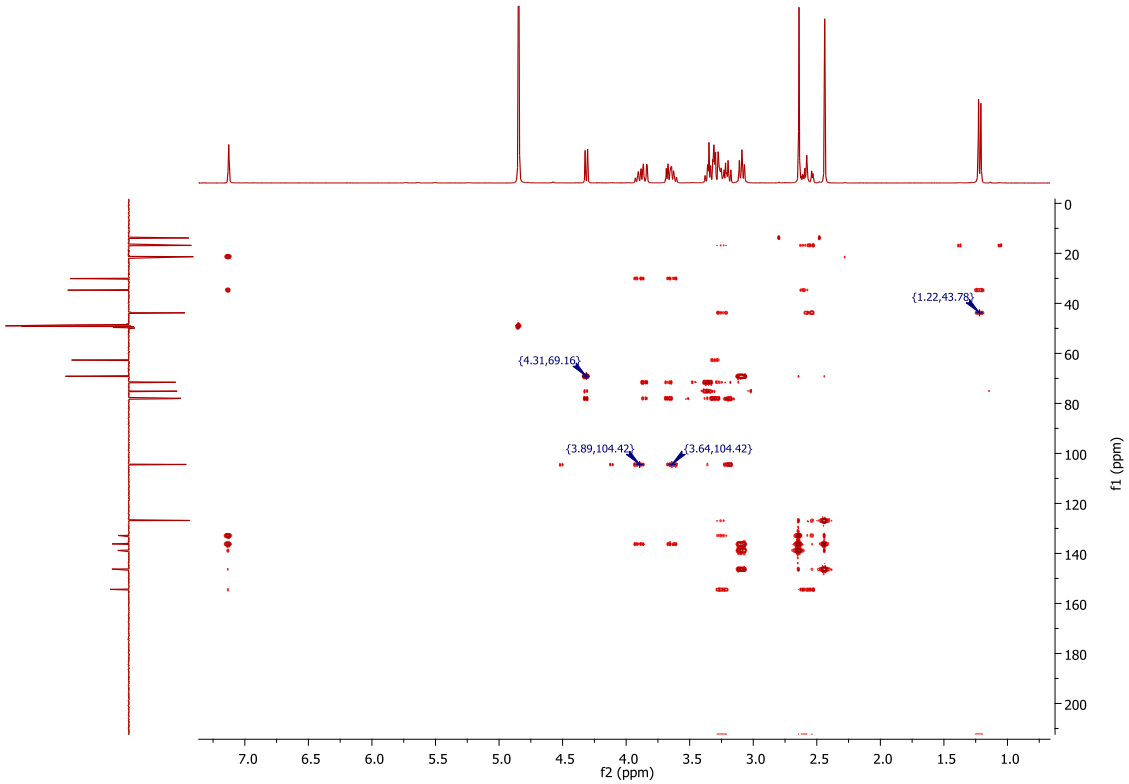

Figure A-165: ^{1}H-^{13}C HMBC NMR spectrum of compound **RH31** in CD_3OD.

30) NMR spectra of compound **RH32** in CD_3OD.

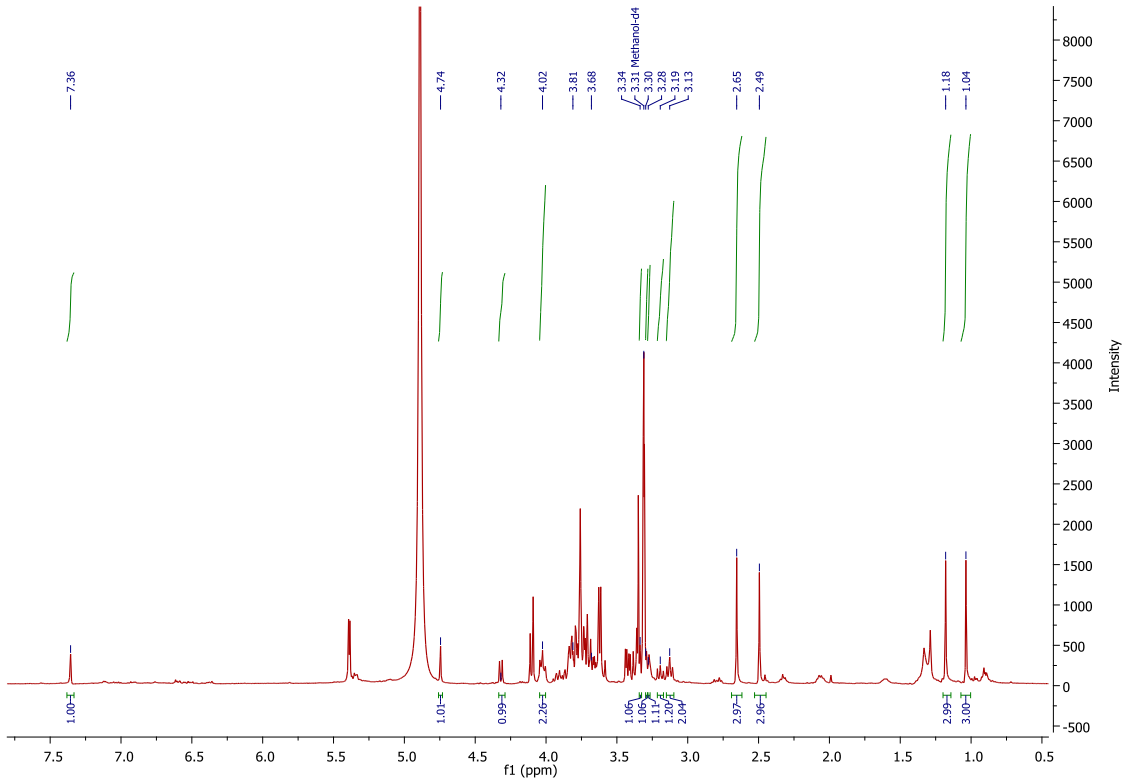

Figure A-166: ^{1}H NMR (CD_3OD, 400 MHz) spectrum of compound **RH32**.

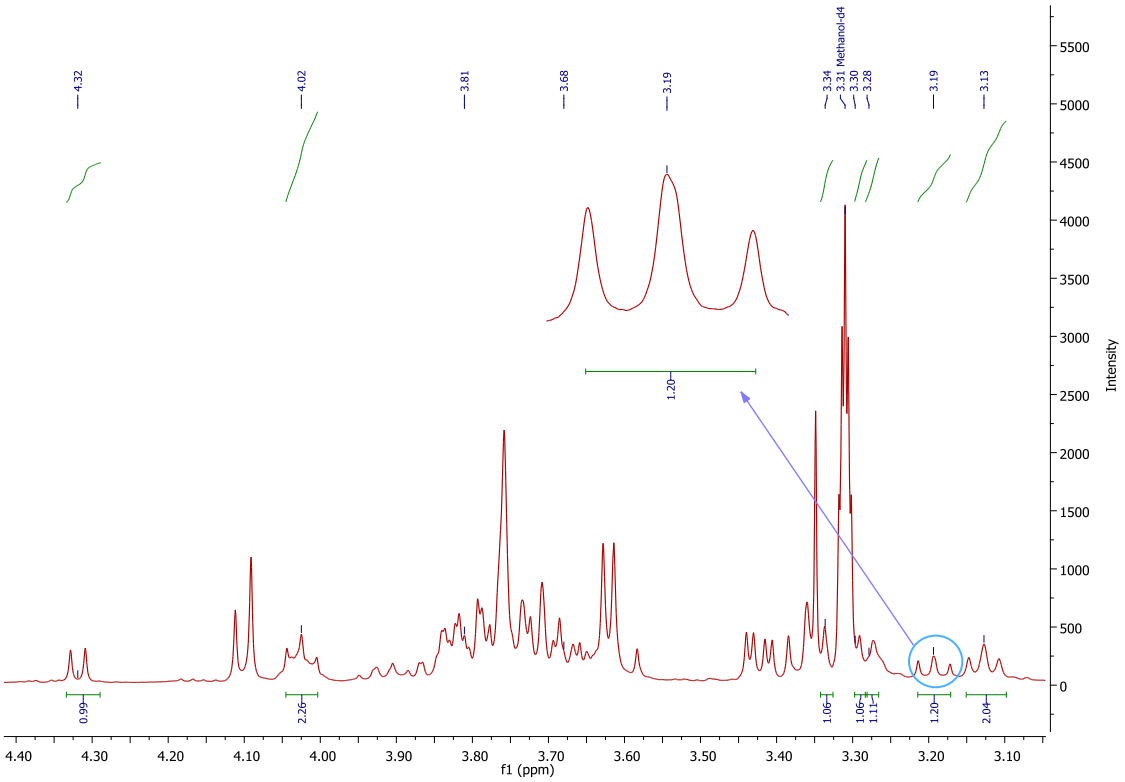

Figure A-167: Expanded ^{1}H NMR (CD_3OD, 400 MHz) spectrum of RH32 (3.1 – 4.4 ppm).

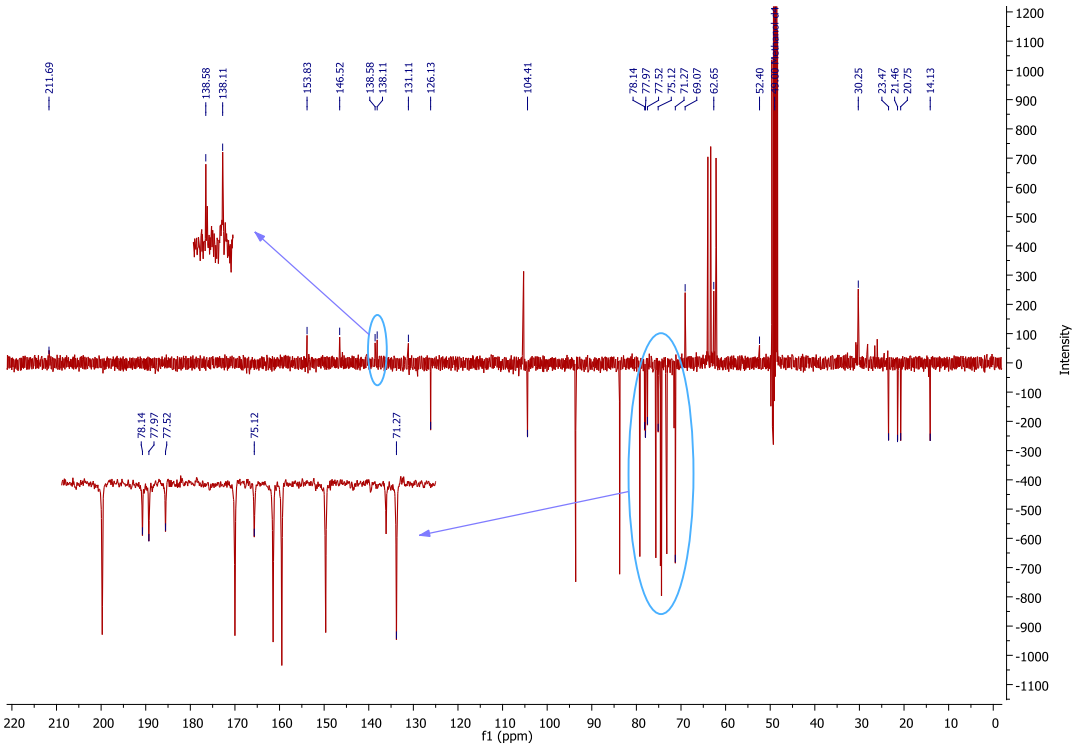

Figure A-168: DEPTQ NMR (CD_3OD, 100 MHz) spectrum of compound **RH32**.

31) NMR spectra of compound **RH33** in CD_3OD.

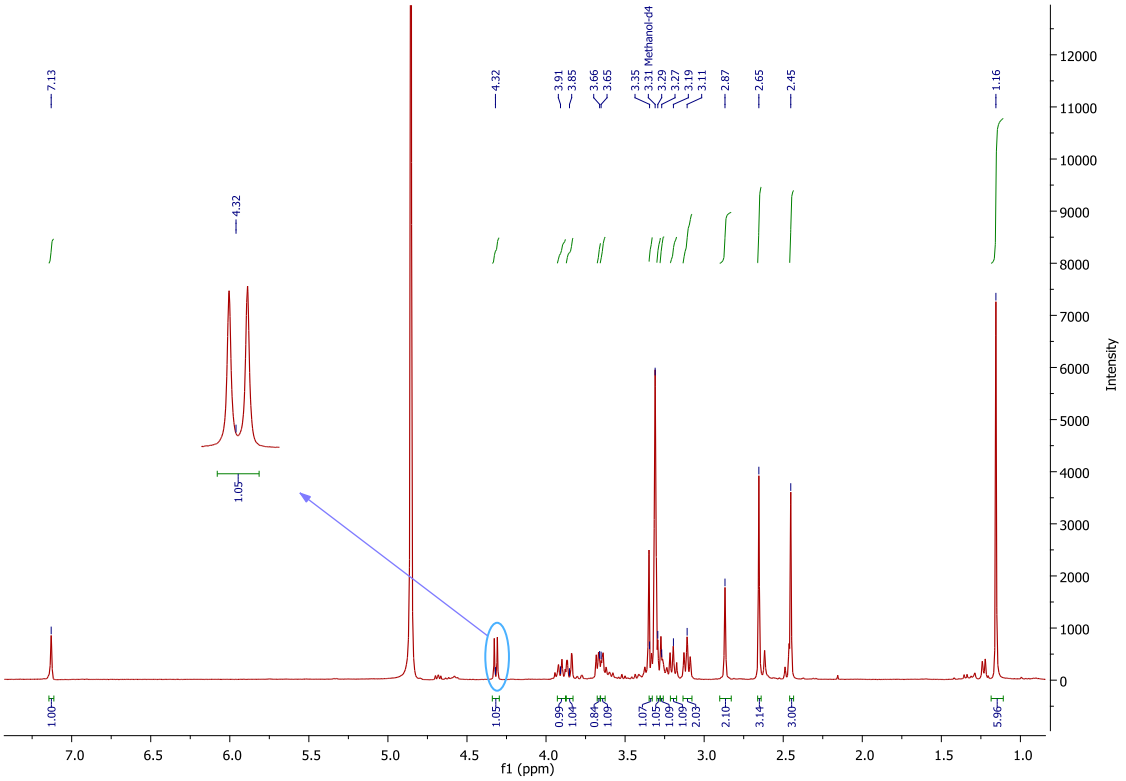

Figure A-169: ^1H NMR (CD_3OD, 400 MHz) spectrum of compound **RH33**.

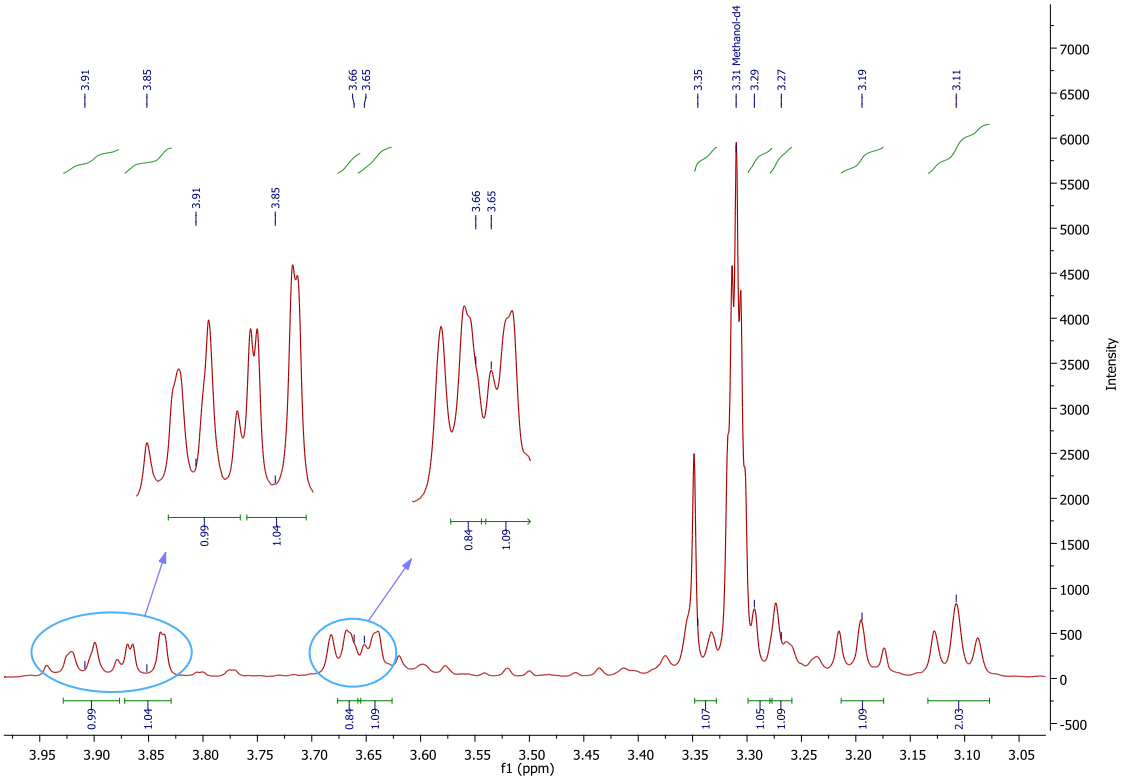

Figure A-170: Expanded ^1H NMR (CD_3OD, 400 MHz) spectrum of **RH33** (3.1 – 3.9 ppm).

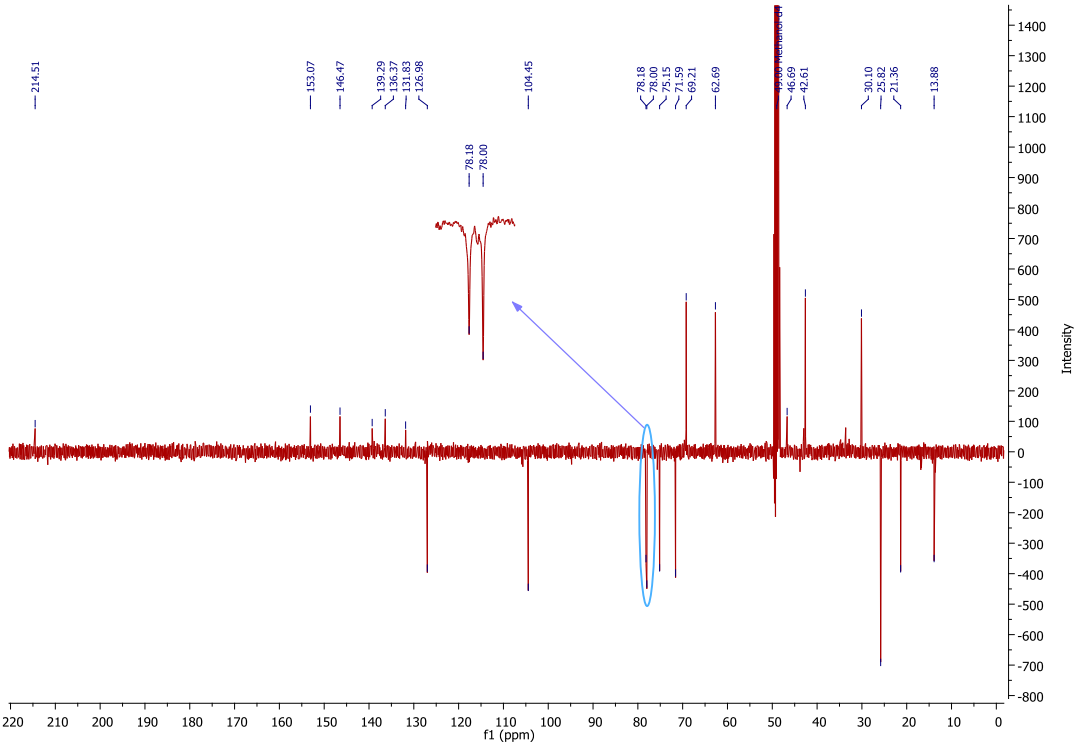

Figure A-171: DEPTQ NMR (CD_3OD, 100 MHz) spectrum of compound **RH33**.

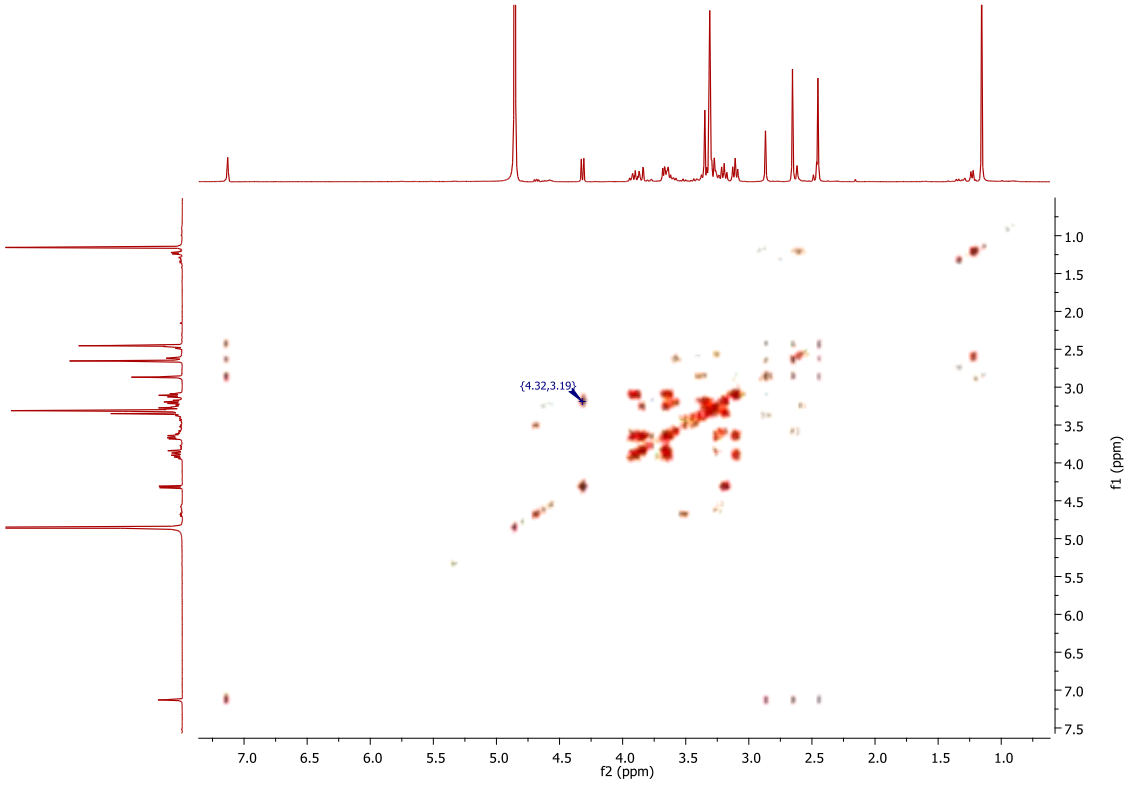

Figure A-172: ^{1}H-^{1}H COSY NMR (CD_3OD, 400 MHz) spectrum of compound **RH33**.

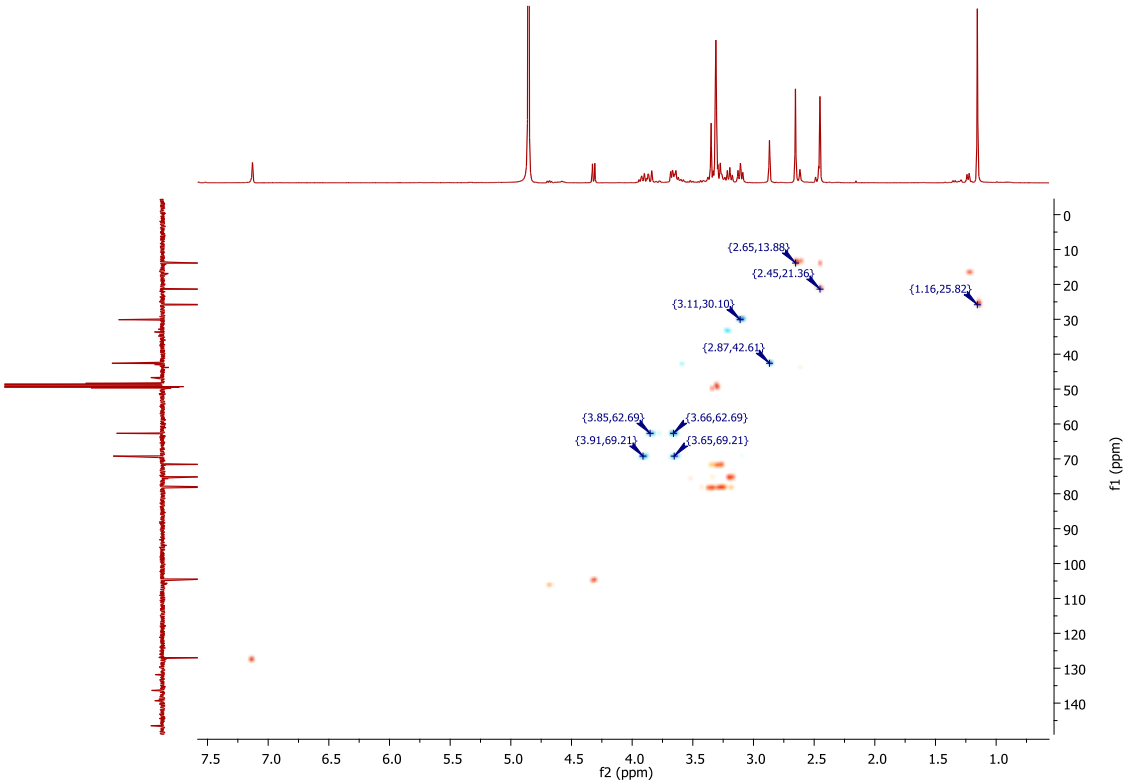

Figure A-173: ^{1}H-^{13}C HSQC NMR spectrum of compound **RH33** in CD_3OD.

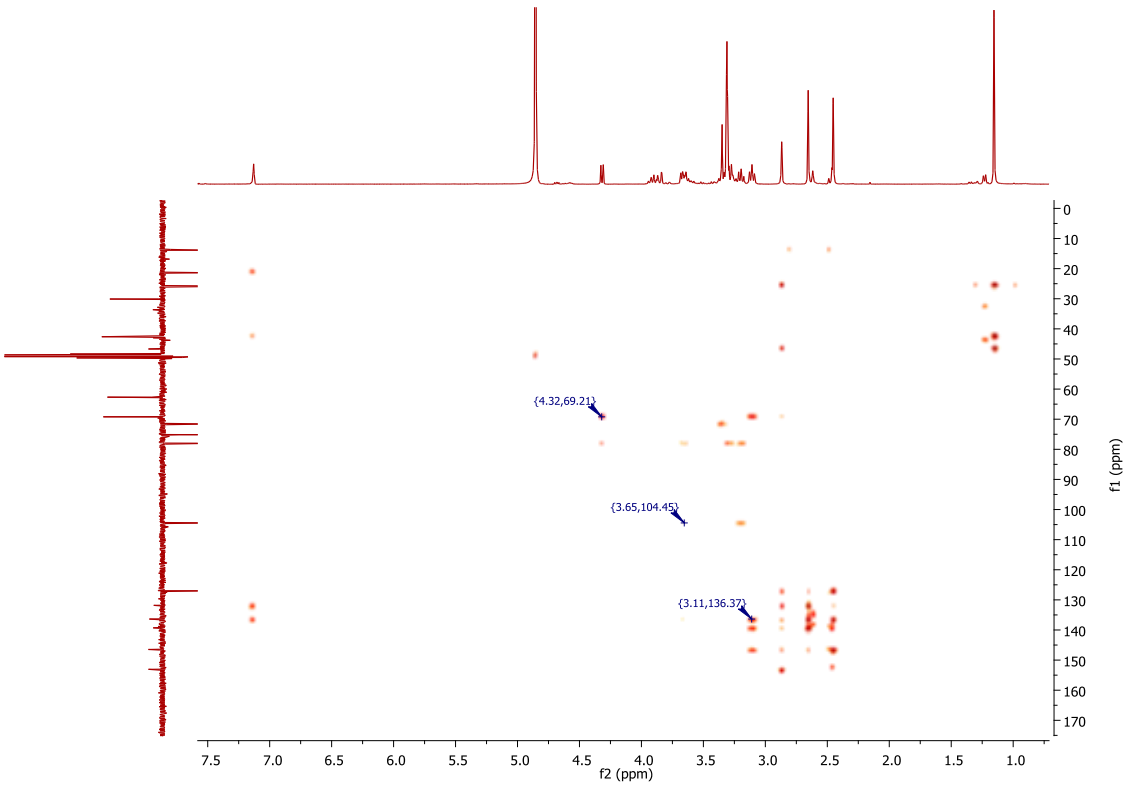

Figure A-174: ^{1}H-^{13}C HMBC NMR spectrum of compound **RH33** in CD_3OD.

32) NMR spectra of compound **RH34** in CD_3OD.

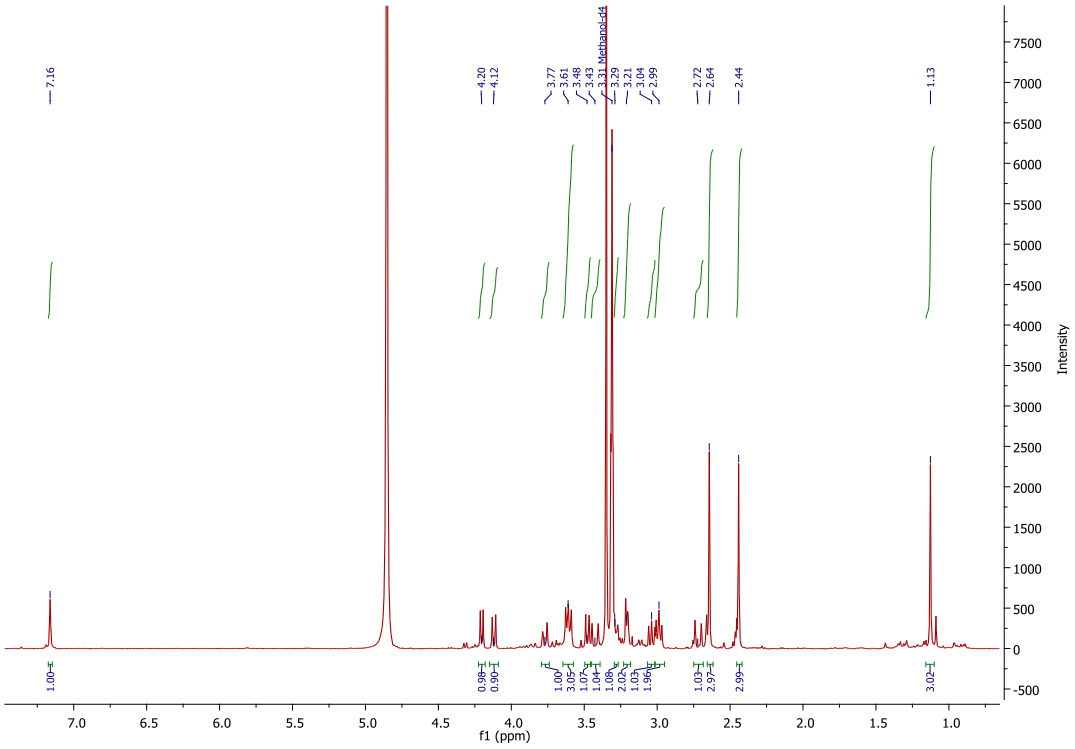

Figure A-175: ^1H NMR (CD_3OD, 400 MHz) spectrum of compound **RH34**.

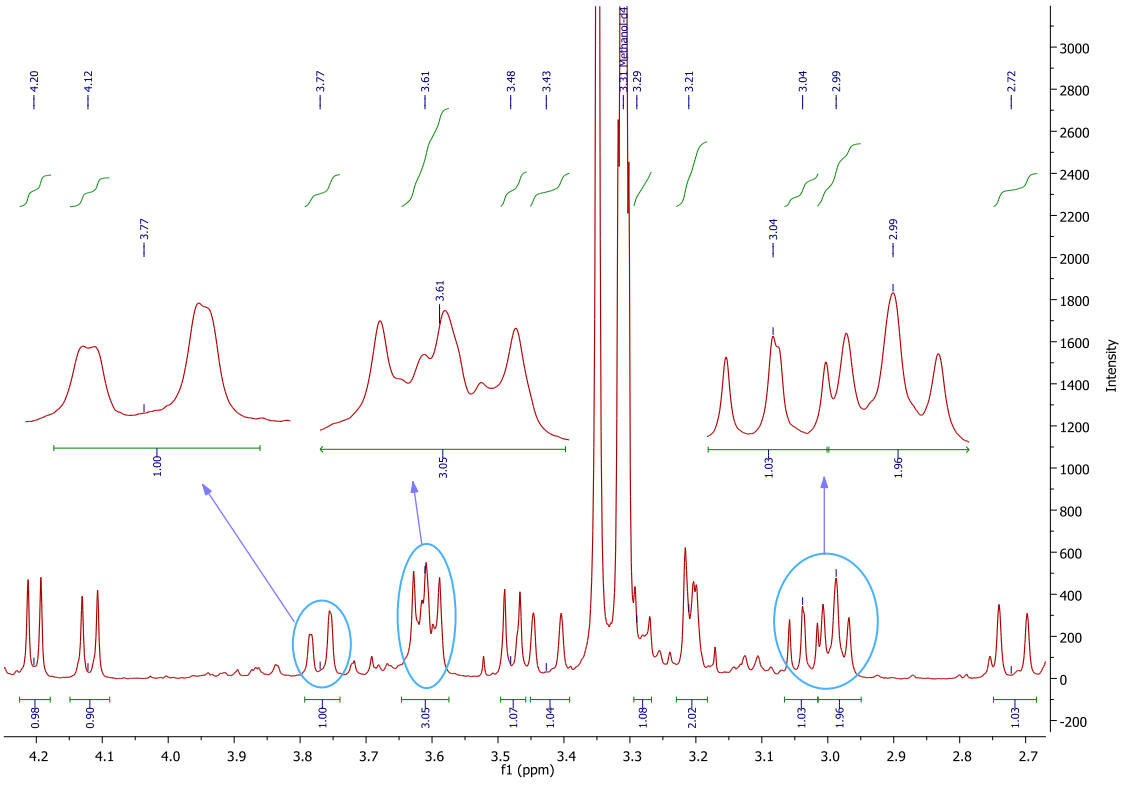

Figure A-176: Expanded ^1H NMR (CD_3OD, 400 MHz) spectrum of **RH34** (2.7 – 4.2 ppm).

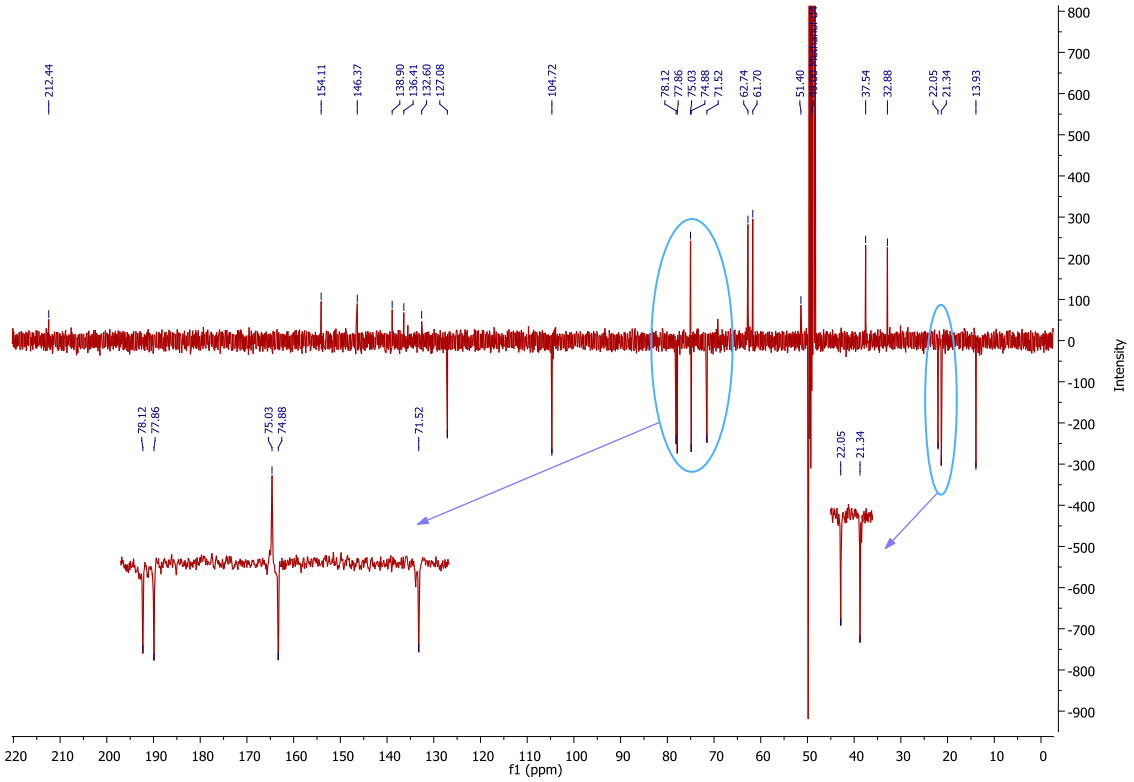

Figure A-177: DEPTQ NMR (CD_3OD, 100 MHz) spectrum of compound **RH34**.

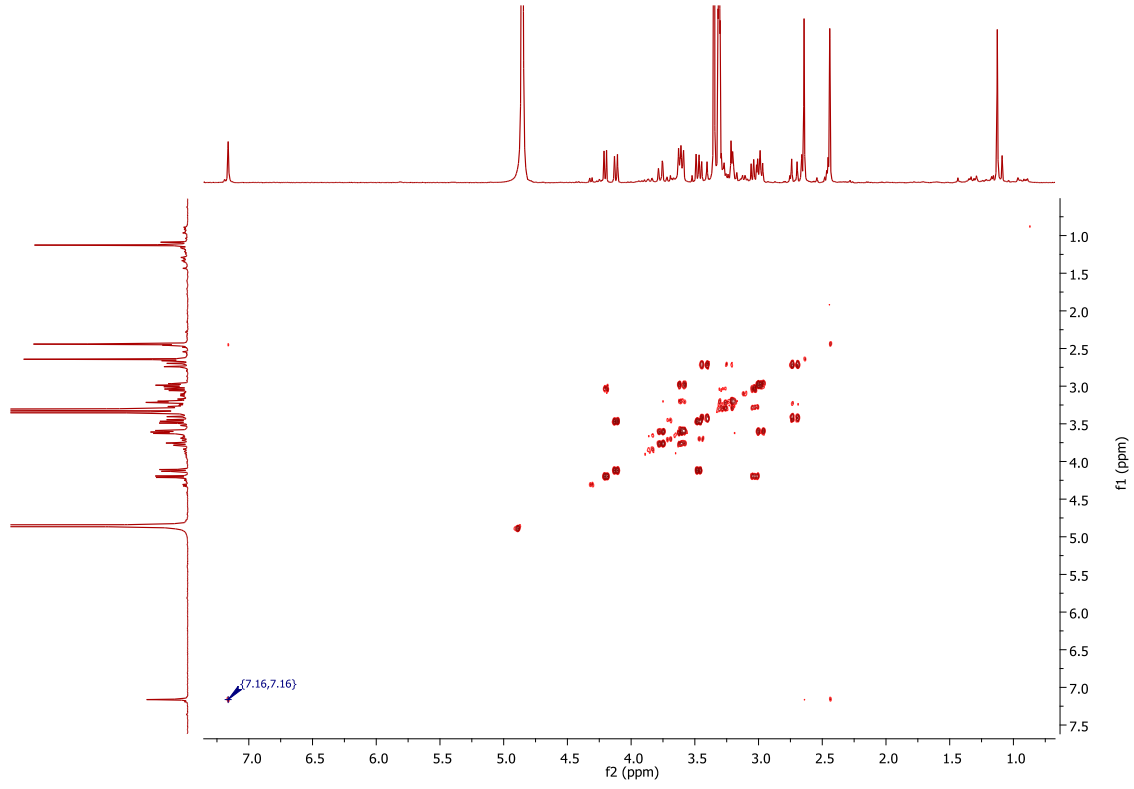

Figure A-178: ^{1}H-^{1}H COSY NMR (CD_3OD, 400 MHz) spectrum of compound **RH34**.

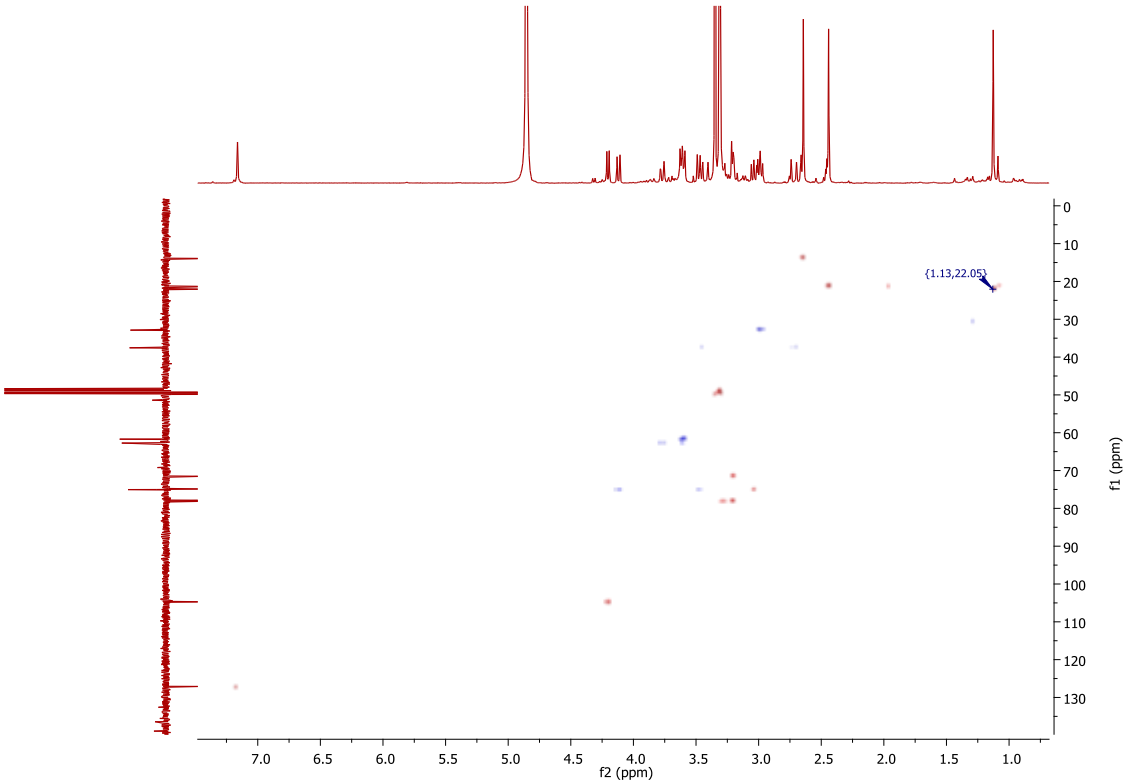

Figure A-179: ^{1}H-^{13}C HSQC NMR spectrum of compound **RH34** in CD_3OD.

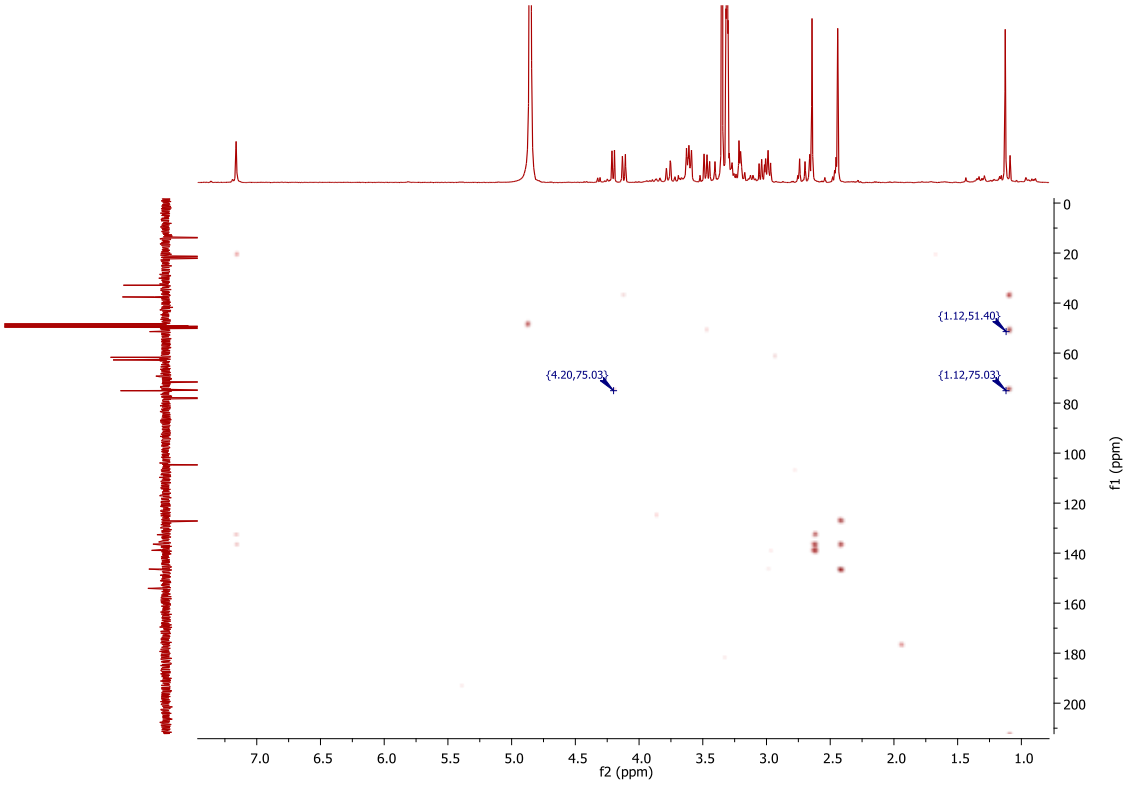

Figure A-180: ^{1}H-^{13}C HMBC NMR spectrum of compound **RH34** in CD_3OD.

33) NMR spectra of compound **RH35** in CD_3OD.

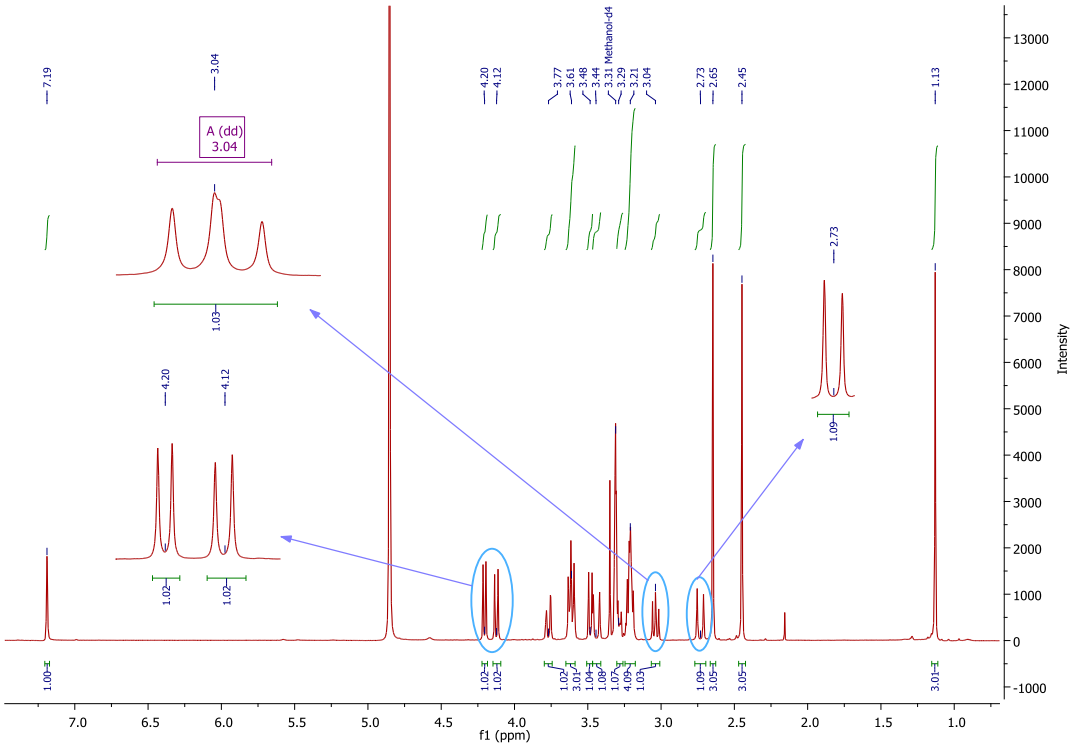

Figure A-181: ^1H NMR (CD_3OD, 400 MHz) spectrum of compound **RH35**.

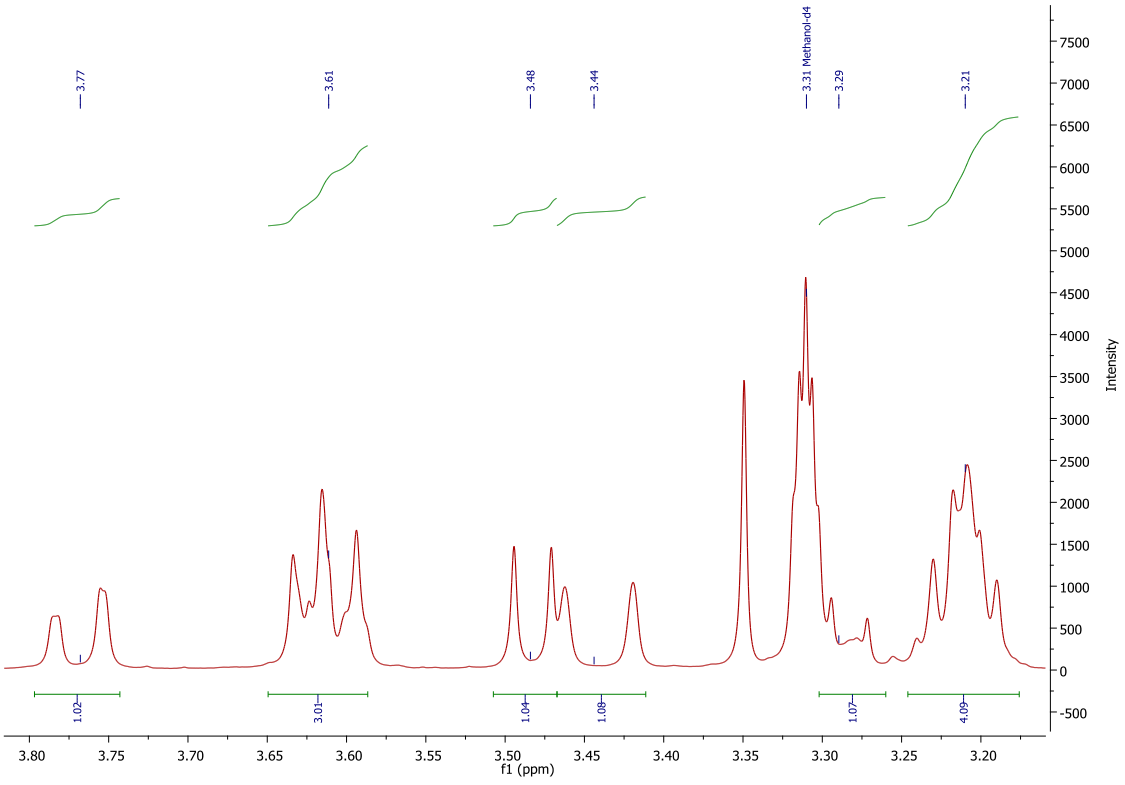

Figure A-182: Expanded ^1H NMR (CD_3OD, 400 MHz) spectrum of **RH35** (3.2 – 3.8 ppm).

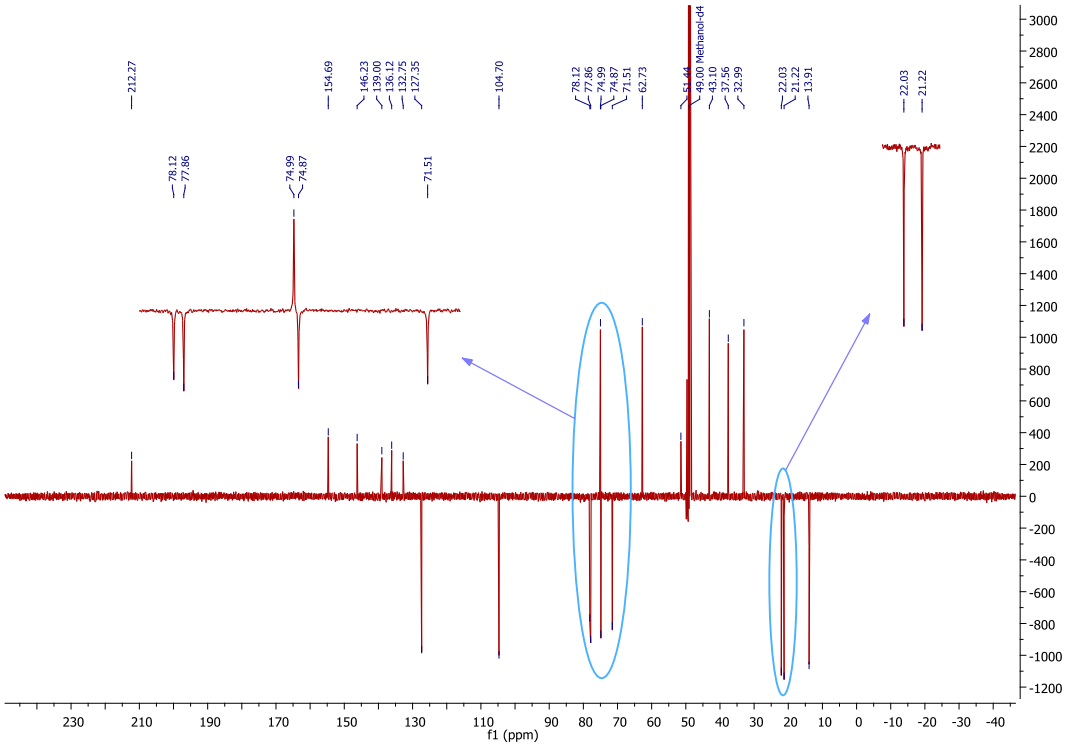

Figure A-183: DEPTQ NMR (CD_3OD, 100 MHz) spectrum of compound **RH35**.

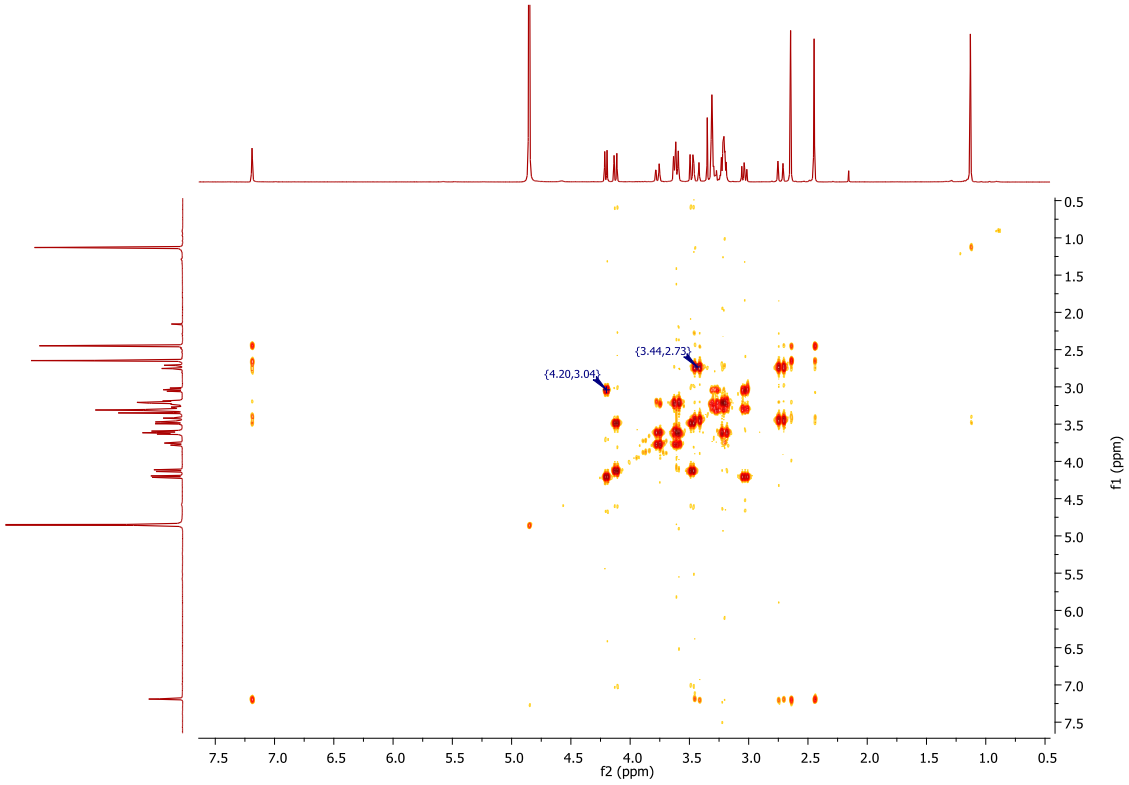

Figure A-184: ^{1}H-^{1}H COSY NMR (CD_3OD, 400 MHz) spectrum of compound **RH35**.

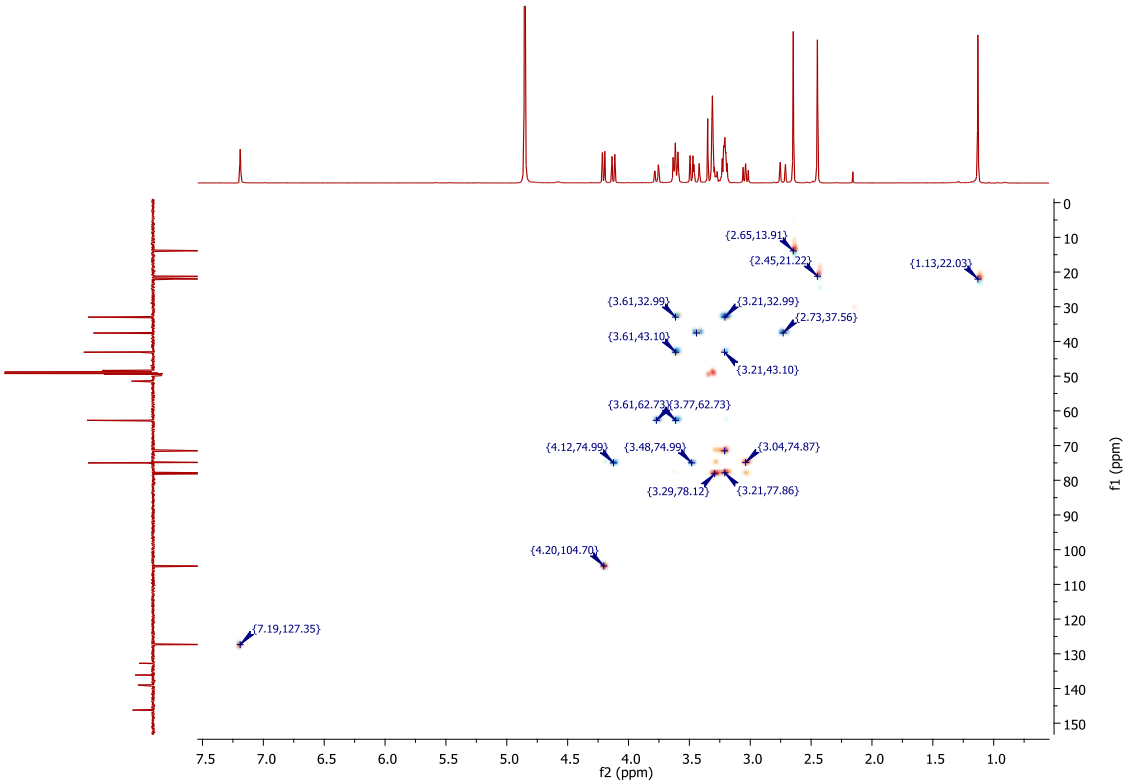

Figure A-185: ^{1}H-^{13}C HSQC NMR spectrum of compound **RH35** in CD_3OD.

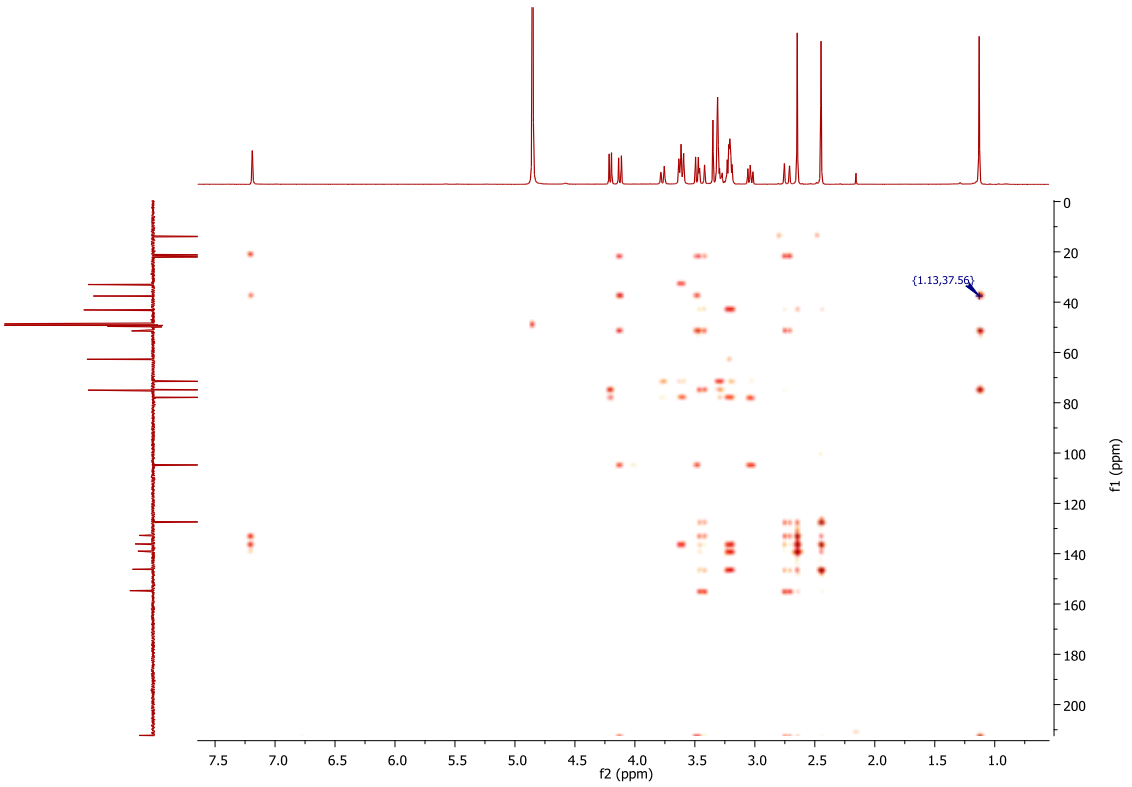

Figure A-186: ^{1}H-^{13}C HMBC NMR spectrum of compound **RH35** in CD_3OD.

34) NMR spectra of compound **RH36** in CD_3OD.

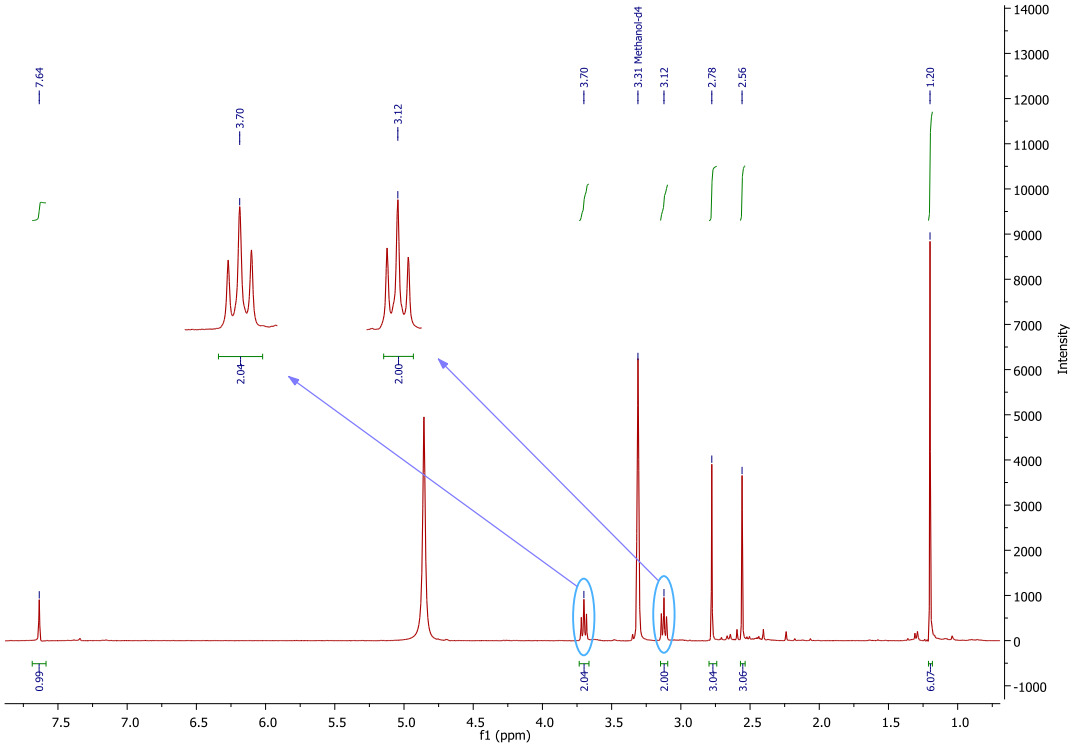

Figure A-187: ^1H NMR (CD_3OD, 400 MHz) spectrum of compound **RH36**.

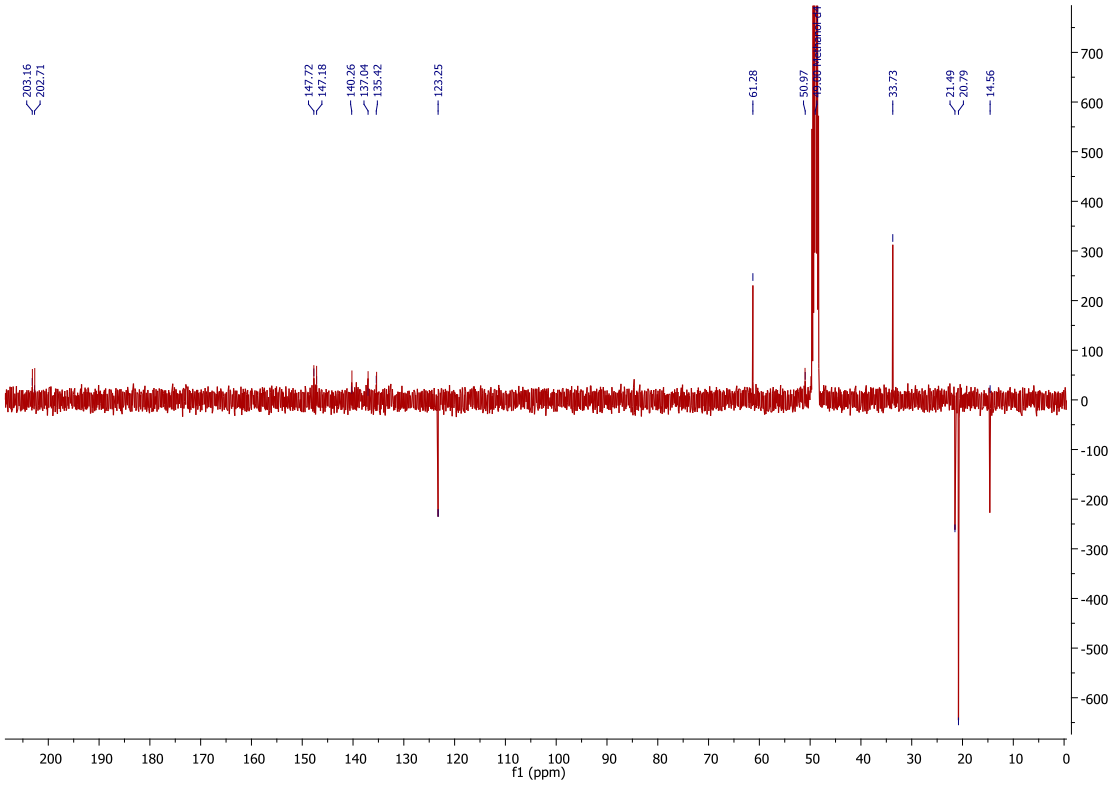

Figure A-188: DEPTQ NMR (CD_3OD, 100 MHz) spectrum of compound **RH36**.

35) NMR spectra of compound **RH37** in CD_3OD.

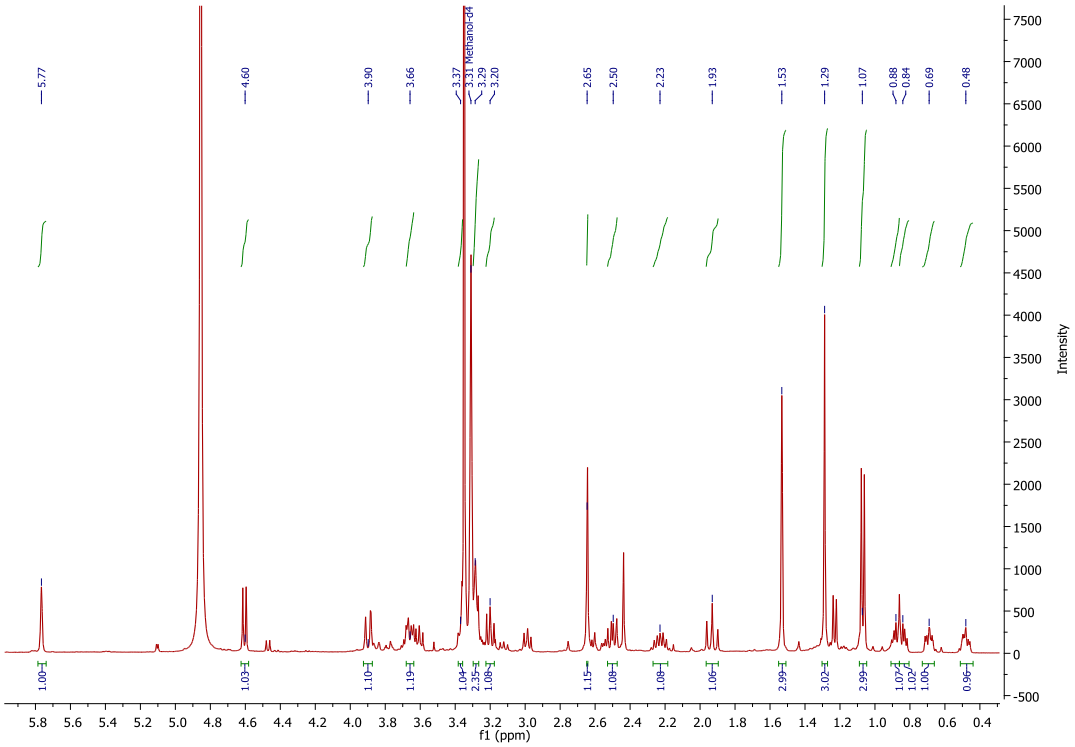

Figure A-189: ^{1}H NMR (CD_3OD, 400 MHz) spectrum of compound **RH37**.

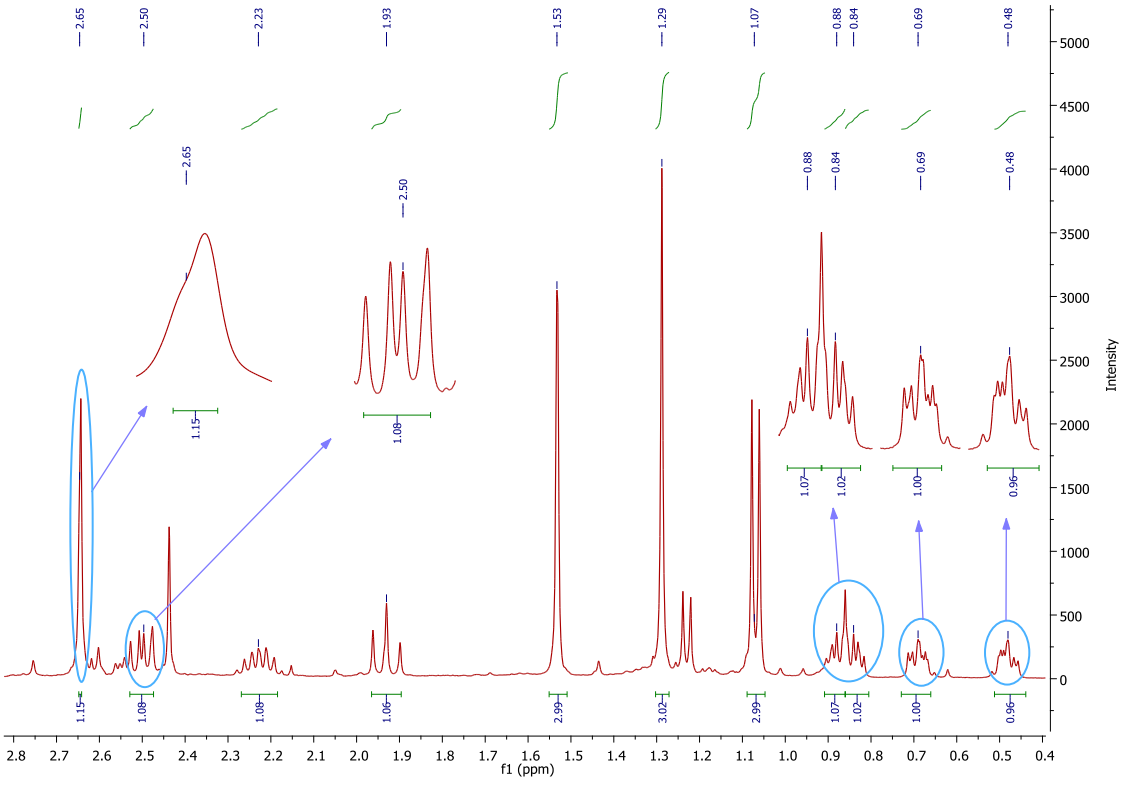

Figure A-190: Expanded ^{1}H NMR (CD_3OD, 400 MHz) spectrum of **RH37** (0.4 – 2.8 ppm).

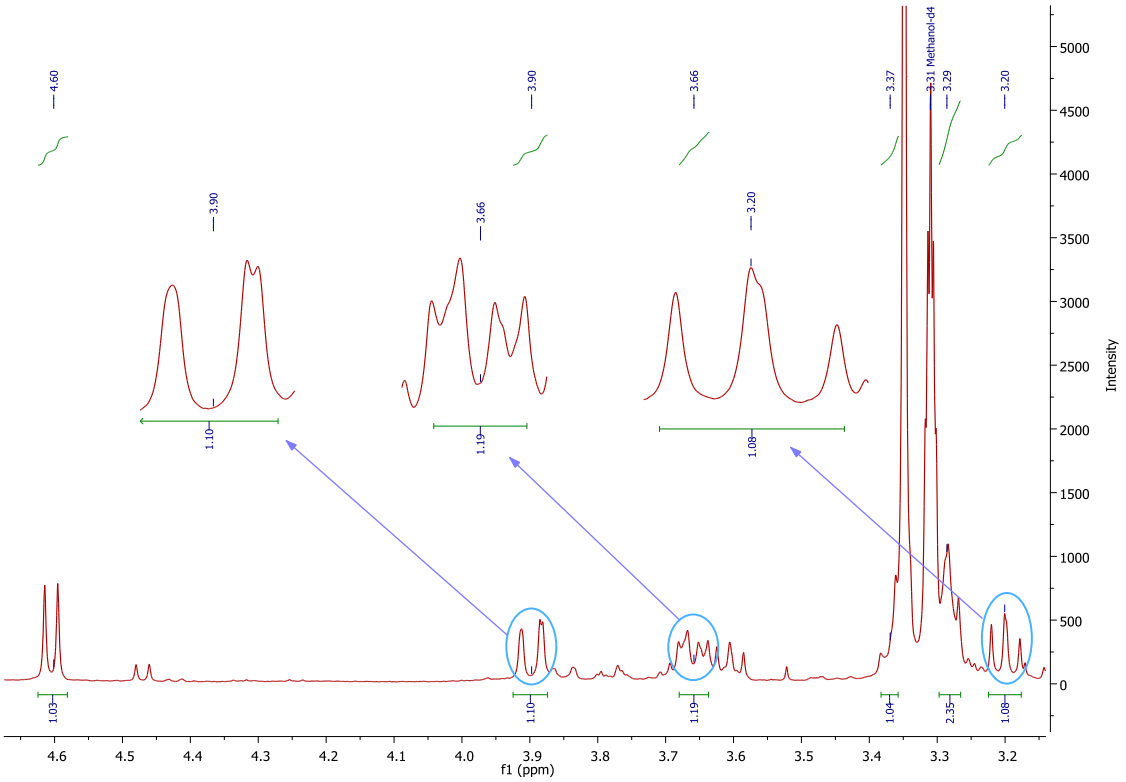

Figure A-191: Expanded ^{1}H NMR (CD_3OD, 400 MHz) spectrum of **RH37** (3.2 – 4.6 ppm).

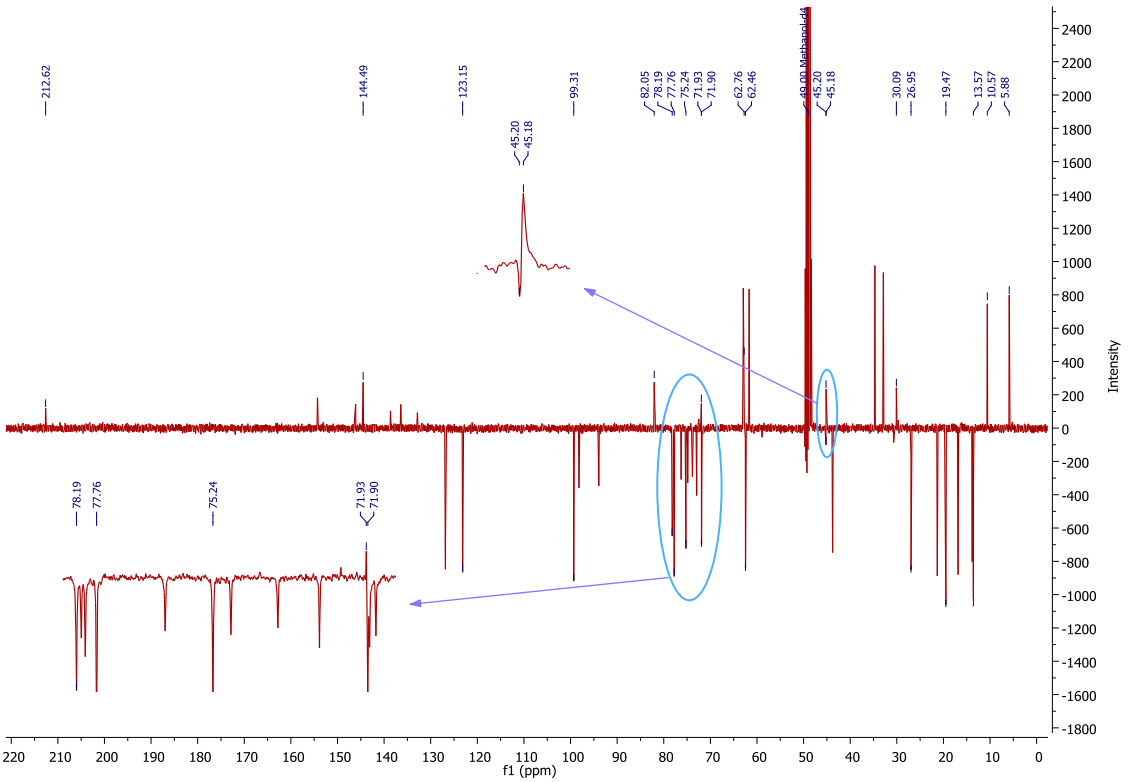

Figure A-192: DEPTQ NMR (CD_3OD, 100 MHz) spectrum of compound **RH37**.

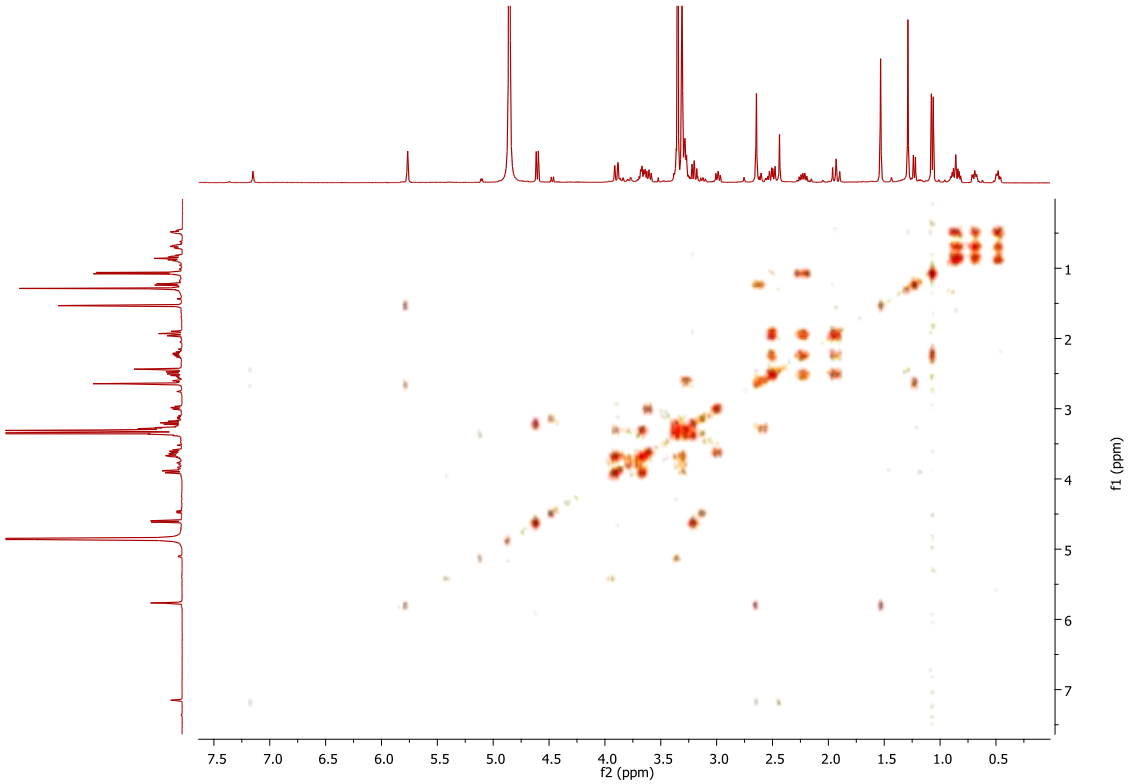

Figure A-193: ^{1}H-^{1}H COSY NMR (CD_3OD, 400 MHz) spectrum of compound **RH37**.

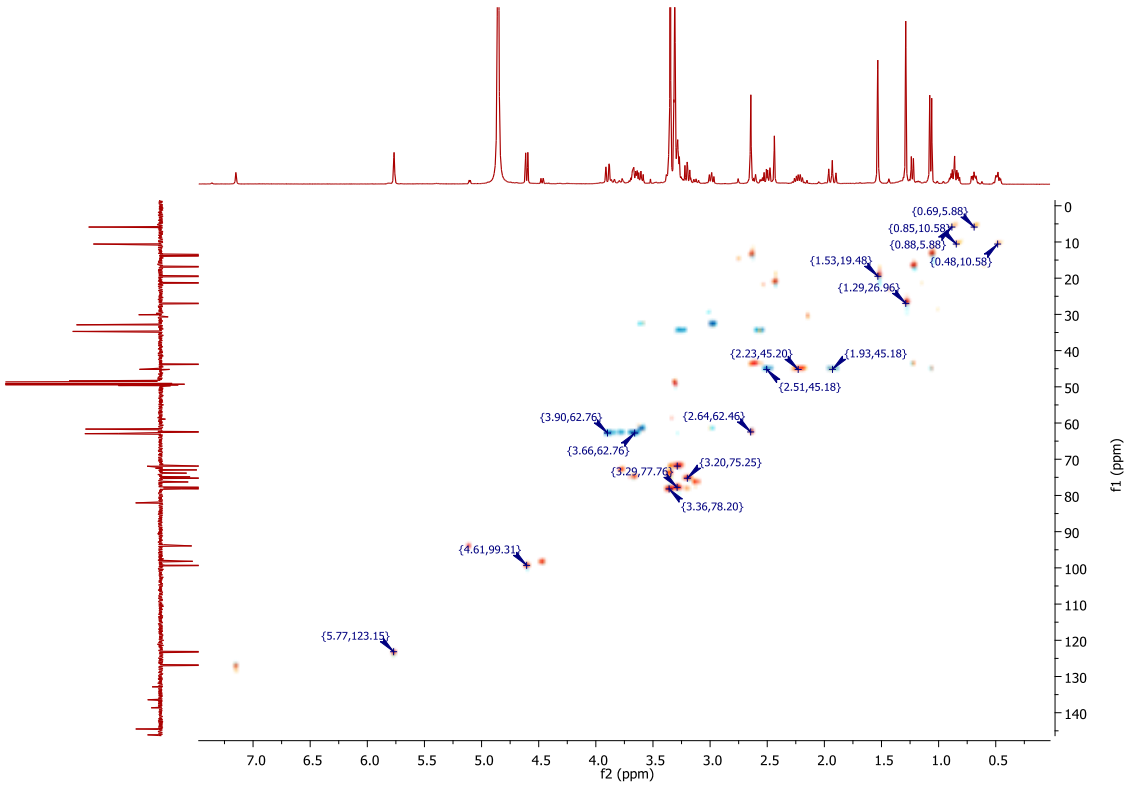

Figure A-194: ^{1}H-^{13}C HSQC NMR spectrum of compound **RH37** in CD_3OD.

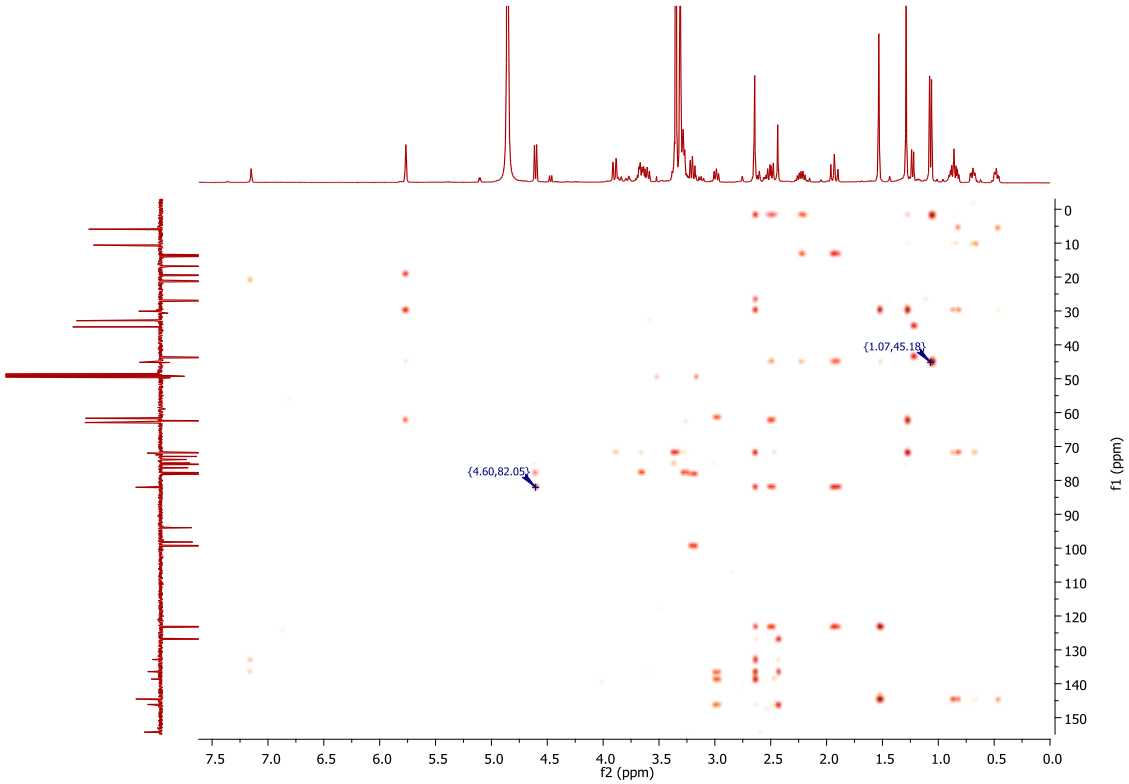

Figure A-195: ^{1}H-^{13}C HMBC NMR spectrum of compound **RH37** in CD_3OD.

36) NMR spectra of compound **RH38** in $CDCl_3$.

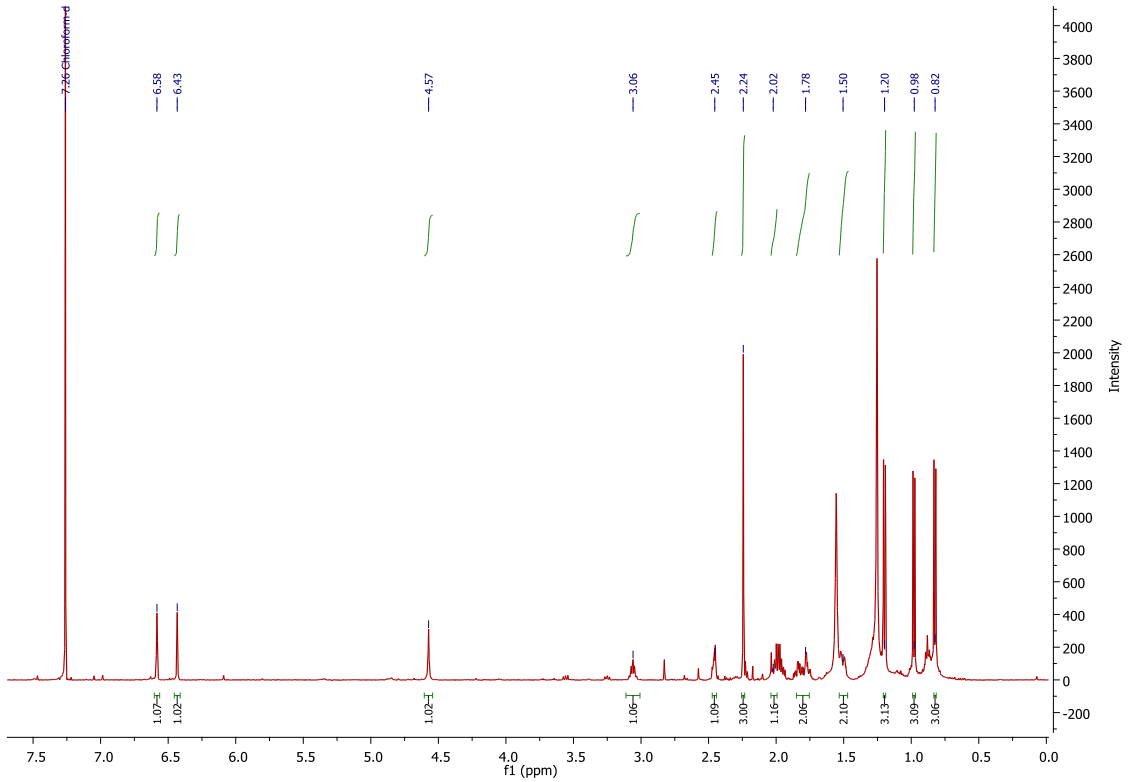

Figure A-196: ^{1}H NMR ($CDCl_3$, 400 MHz) spectrum of compound **RH38**.

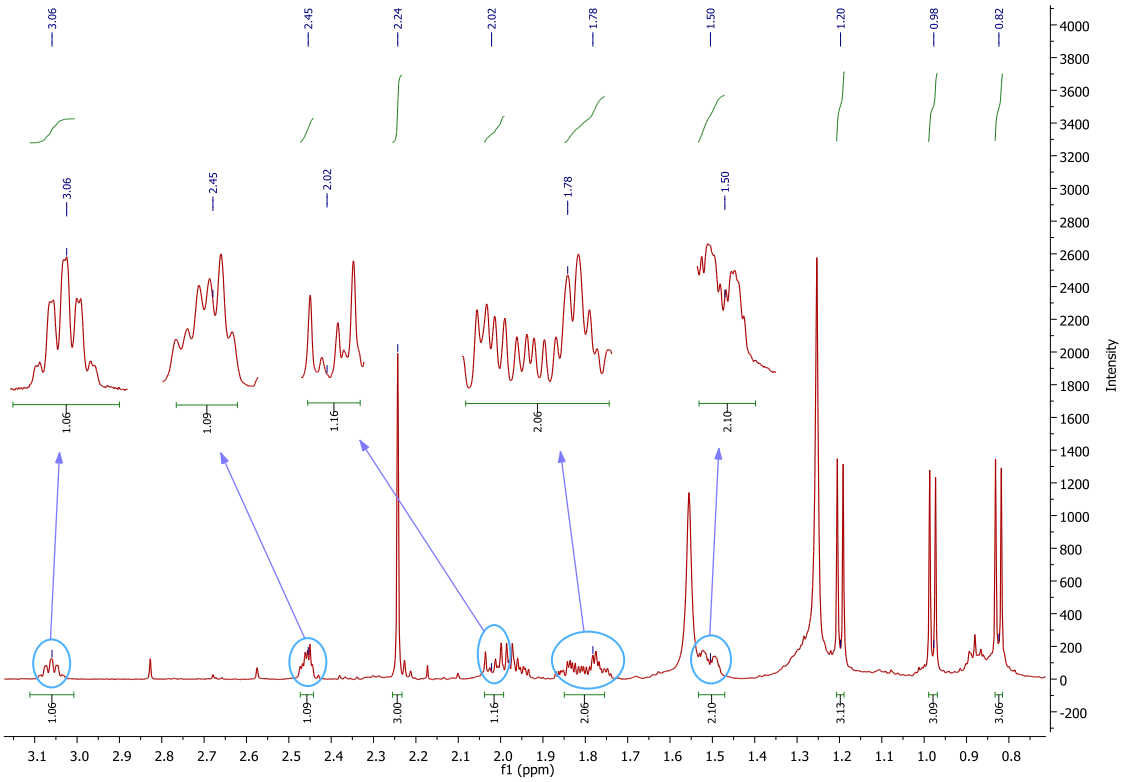

Figure A-197: Expanded ^{1}H NMR ($CDCl_3$, 400 MHz) spectrum of **RH38** (0.8 – 3.1 ppm).

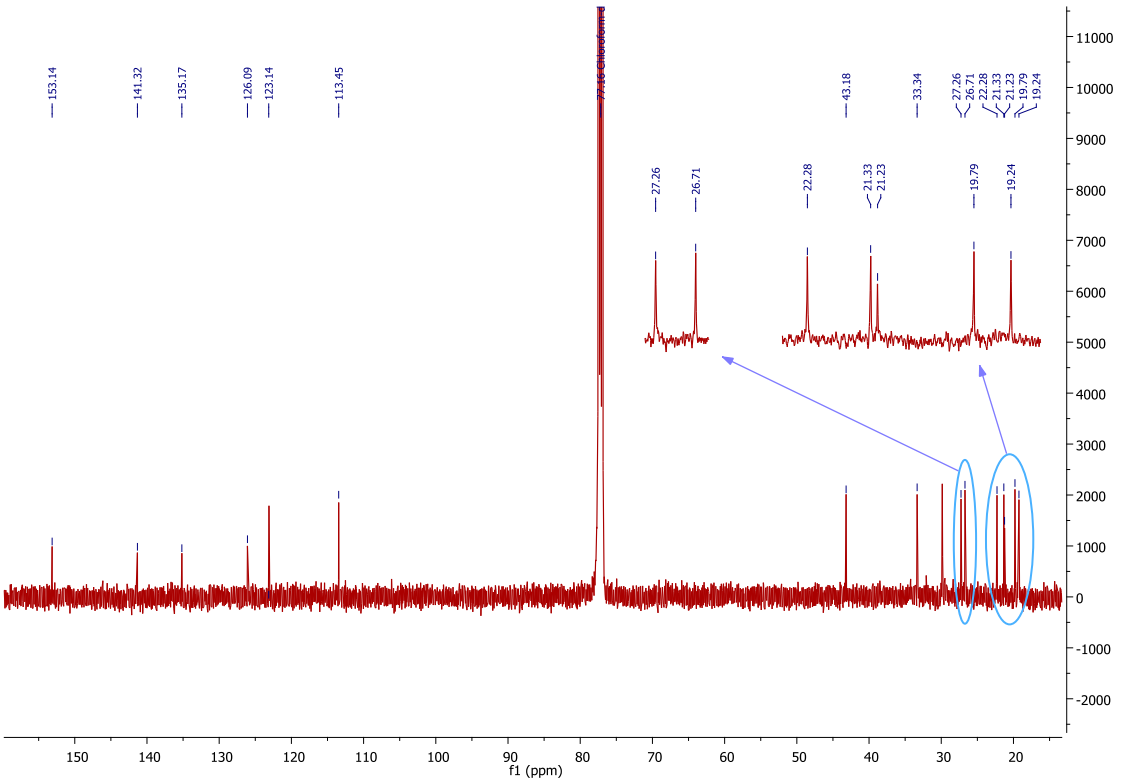

Figure A-198: ^{13}C NMR ($CDCl_3$, 100 MHz) spectrum of compound **RH38**.

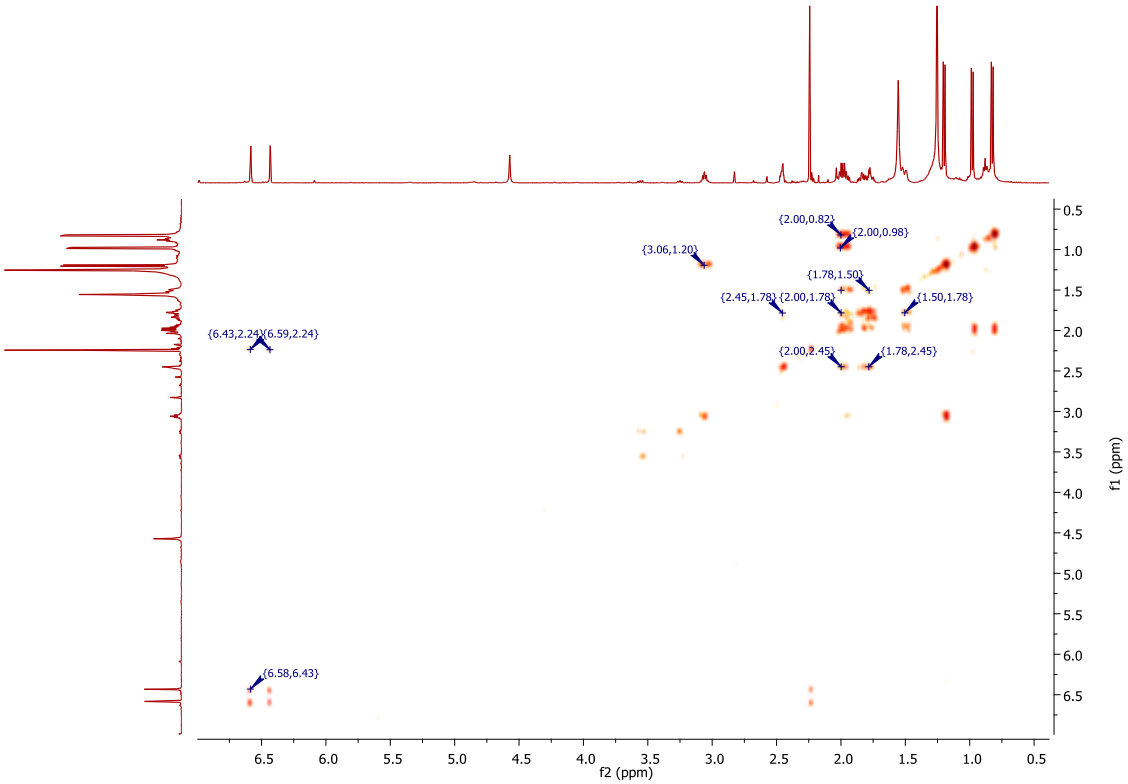

Figure A-199: ^{1}H-^{1}H COSY NMR ($CDCl_3$, 400 MHz) spectrum of compound **RH38**.

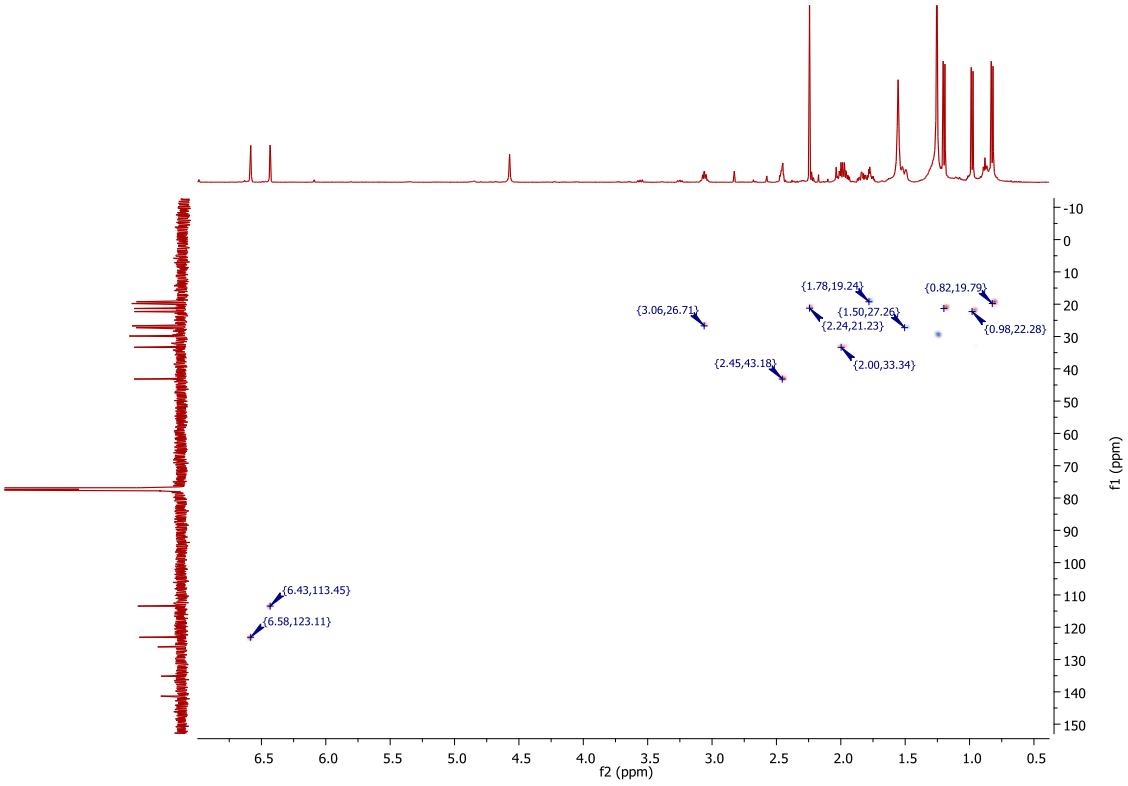

Figure A-200: ^{1}H-^{13}C HSQC NMR spectrum of compound **RH38** in $CDCl_3$.

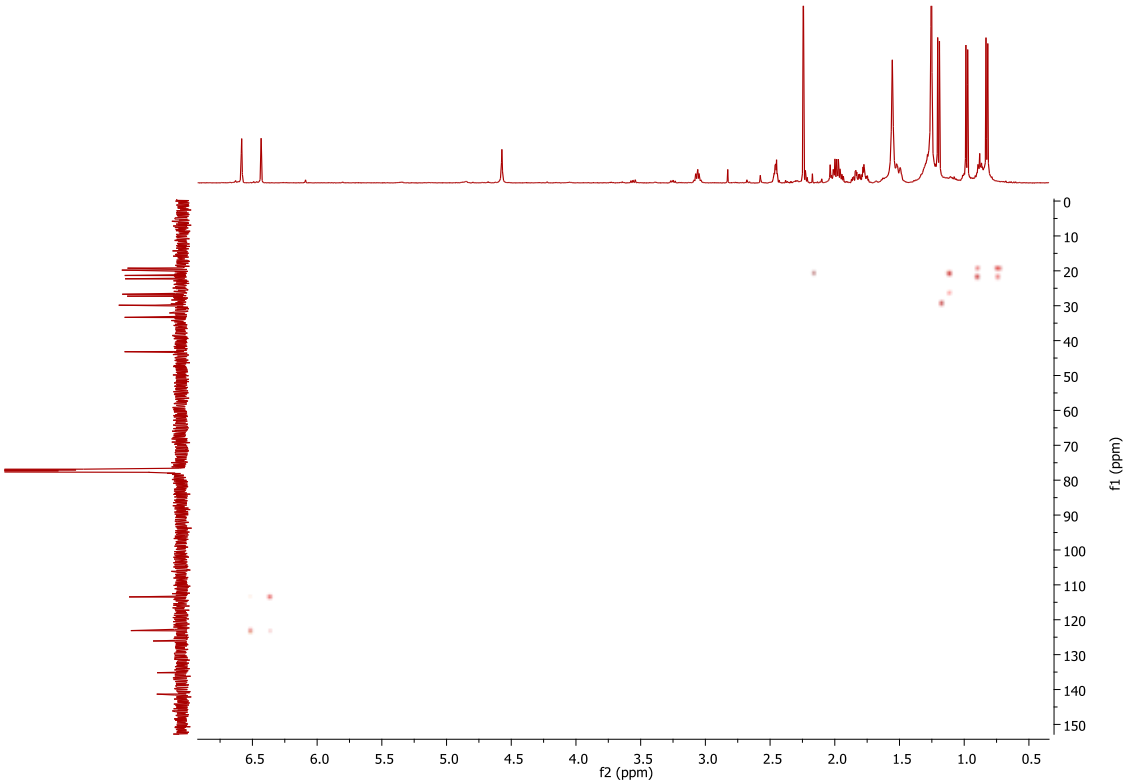

Figure A-201: ^{1}H-^{13}C HSQC-TOCSY NMR spectrum of compound **RH38** in $CDCl_3$.

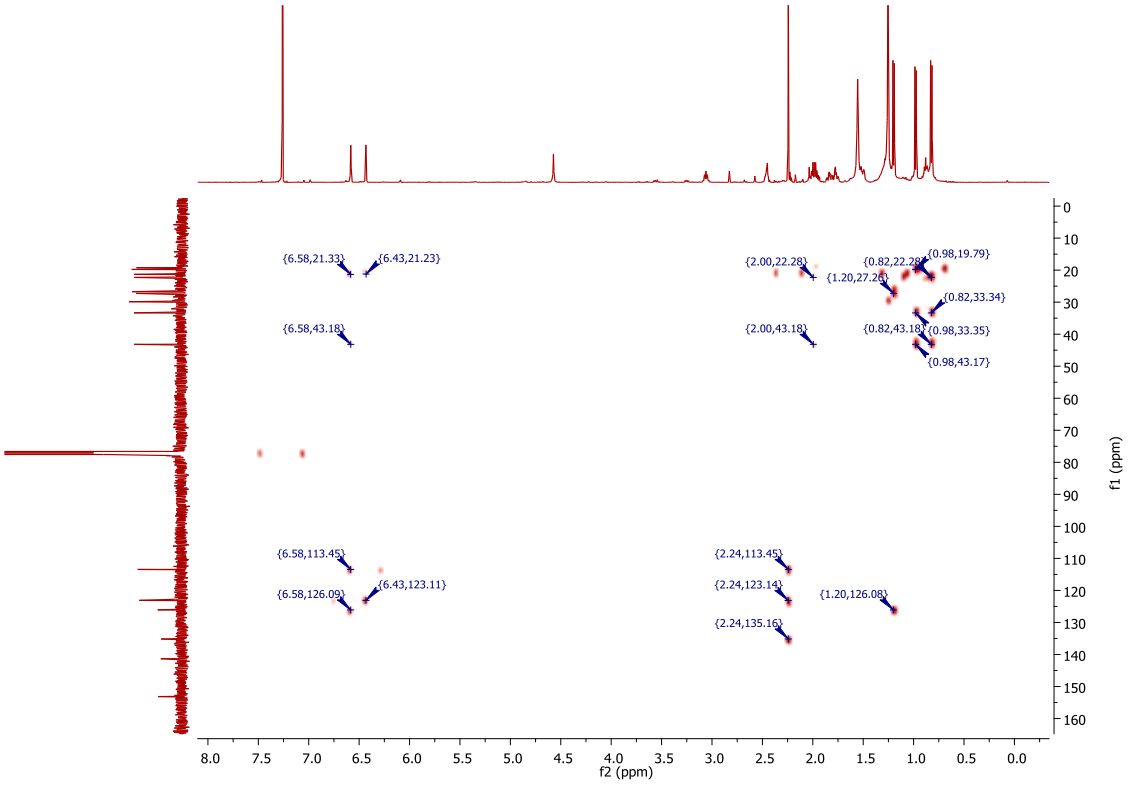

Figure A-202: ^{1}H-^{13}C HMBC NMR spectrum of compound **RH38** in $CDCl_3$.

Appendix II: Accurate MS spectra of compounds **RH3 - RH38**.

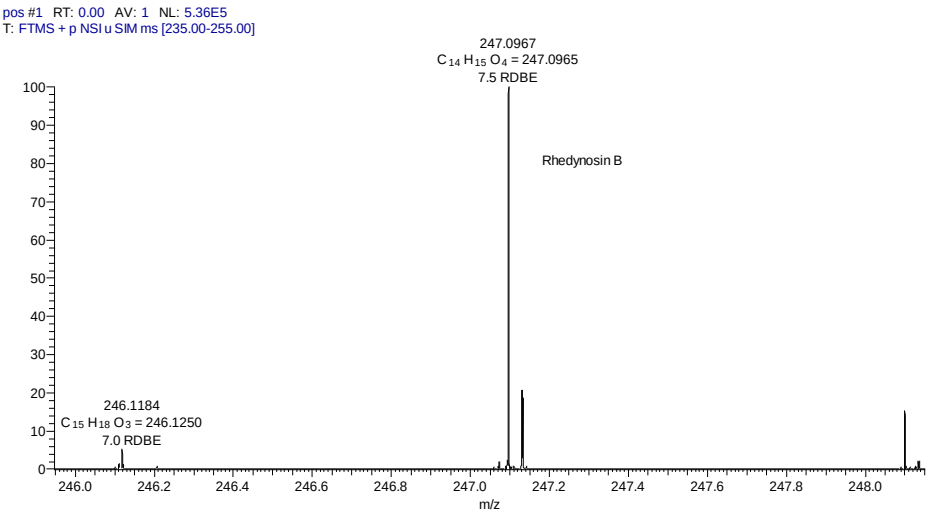

Figure A-203: FT-ICR-MS spectrum of compound **RH3** in $[M+H]^+$ positive ion mode

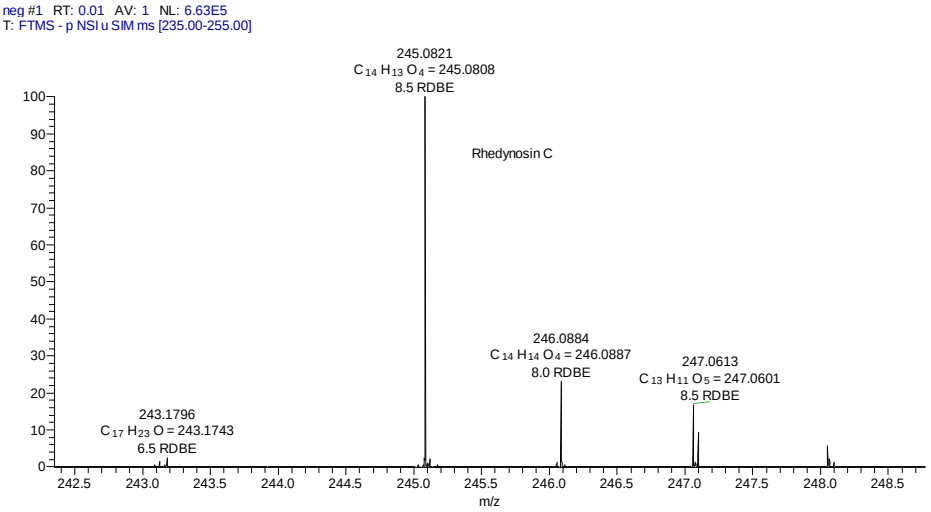

Figure A-204: FT-ICR-MS spectrum of compound **RH4** in $[M-H]^-$ negative ion mode.

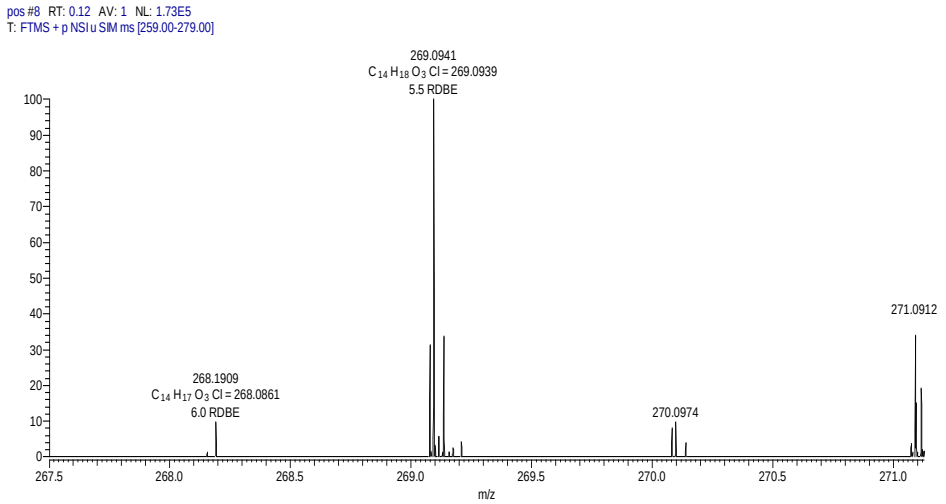

Figure A-205: FT-ICR-MS spectrum of compound **RH5** in $[M+H]^+$ positive ion mode.

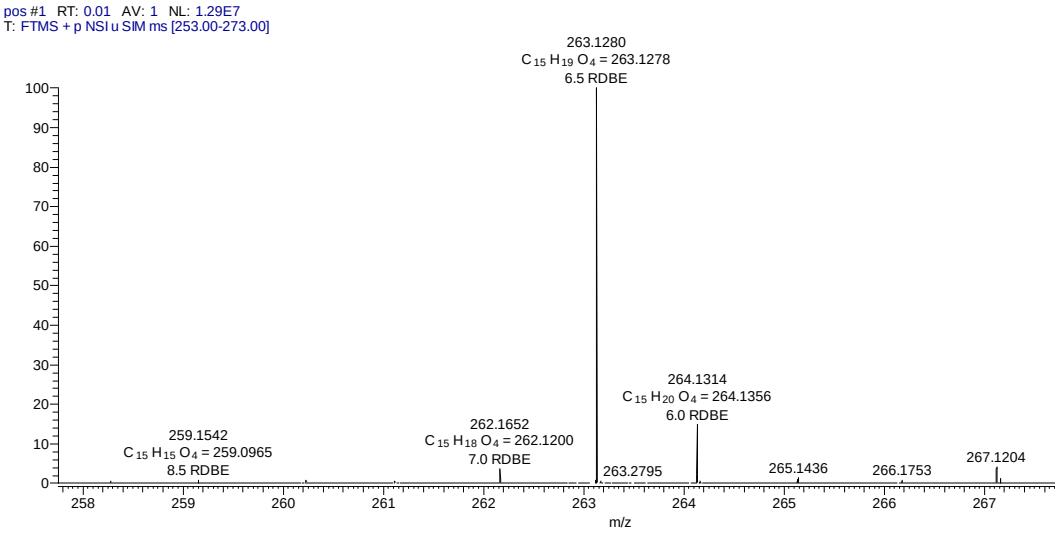

Figure A-206: FT-ICR-MS spectrum of compound **RH6** in $[M+H]^+$ positive ion mode.

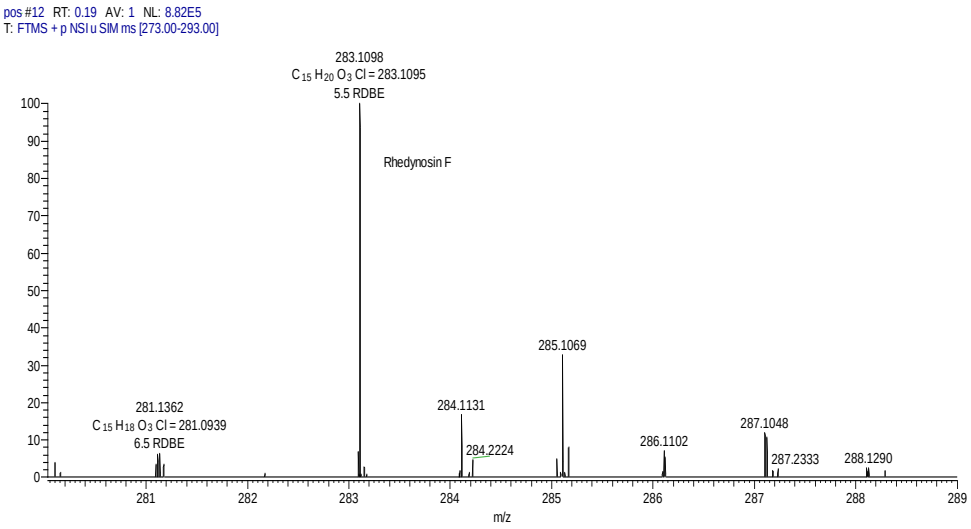

Figure A-207: FT-ICR-MS spectrum of compound **RH7** in $[M+H]^+$ positive ion mode.

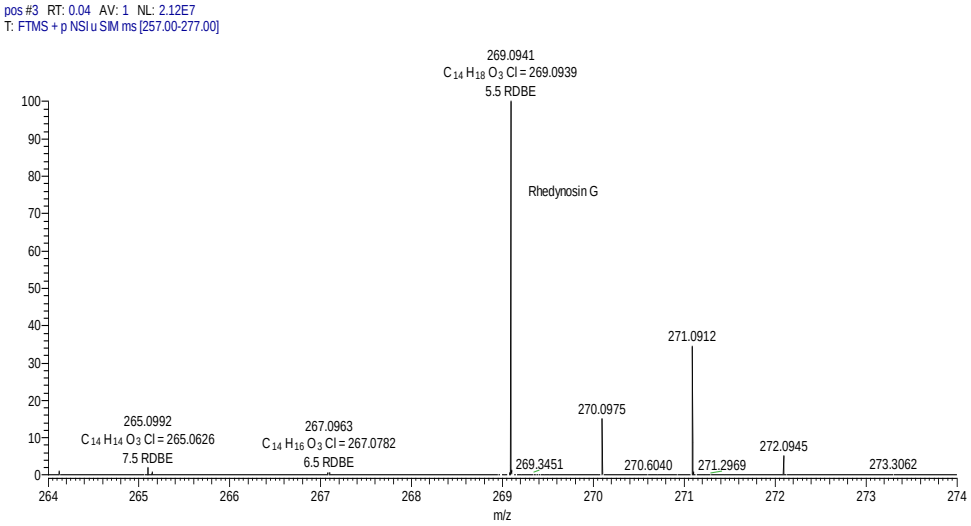

Figure A-208: FT-ICR-MS spectrum of compound **RH8** in $[M+H]^+$ positive ion mode.

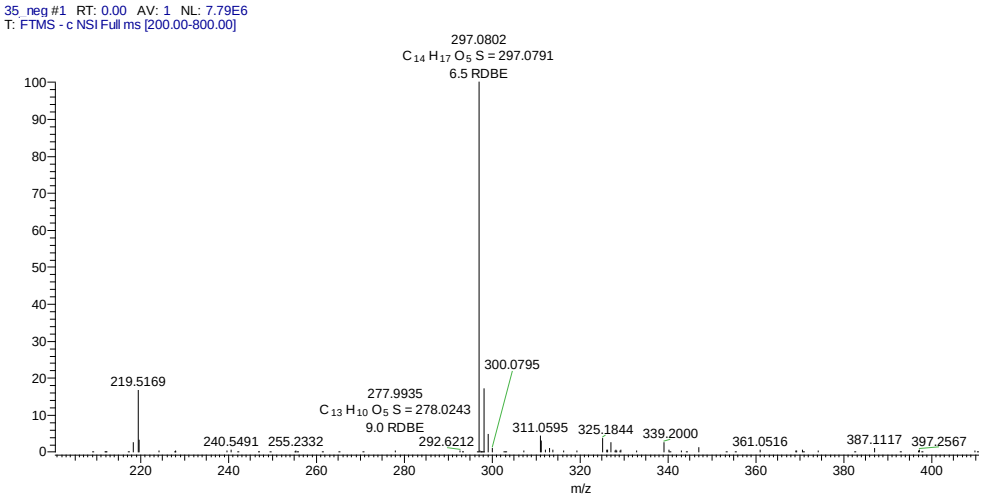

Figure A-209: FT-ICR-MS spectrum of compound **RH9** in $[M-H]^-$ negative ion mode.

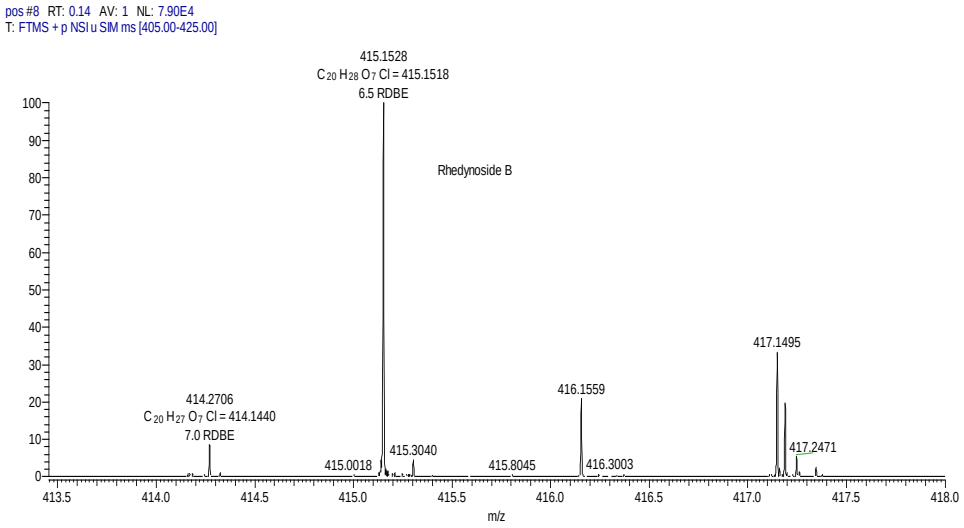

Figure A-210: FT-ICR-MS spectrum of compound **RH10** in $[M+H]^+$ positive ion mode.

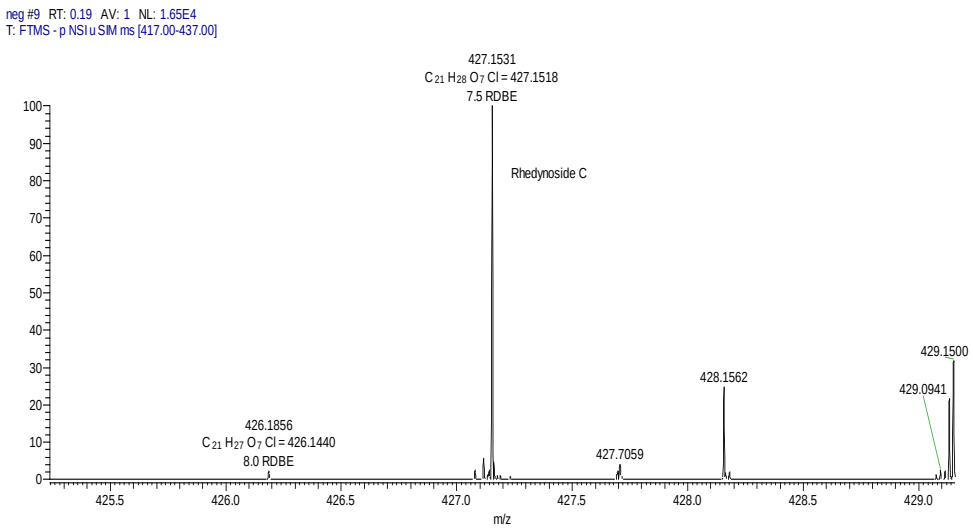

Figure A-211: FT-ICR-MS spectrum of compound **RH11** in $[M+H]^+$ positive ion mode.

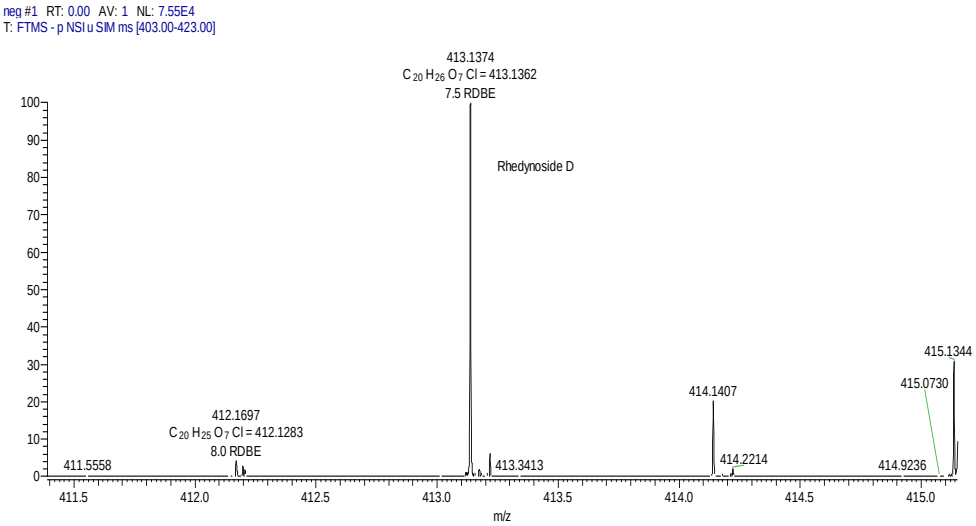

Figure A-212: FT-ICR-MS spectrum of compound **RH12** in $[M-H]^-$ negative ion mode.

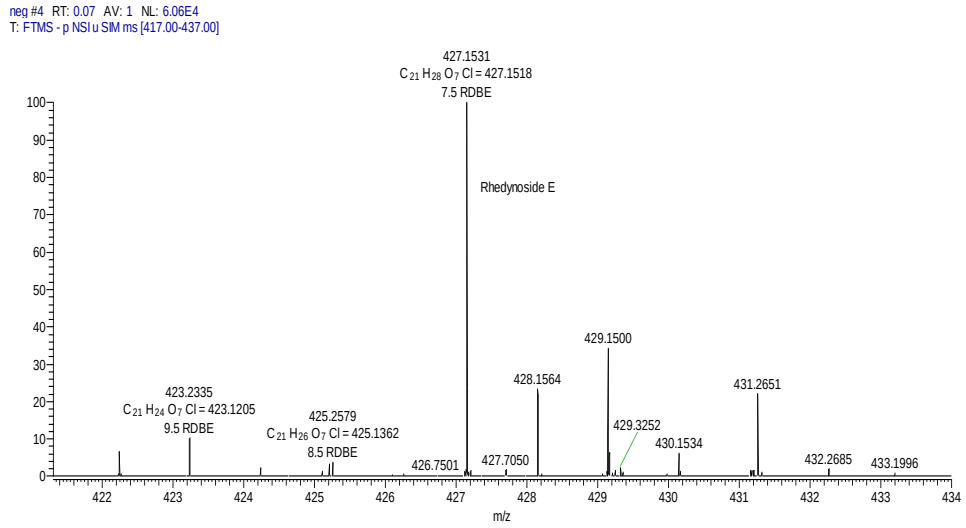

Figure A-213: FT-ICR-MS spectrum of compound **RH13** in $[M-H]^-$ negative ion mode.

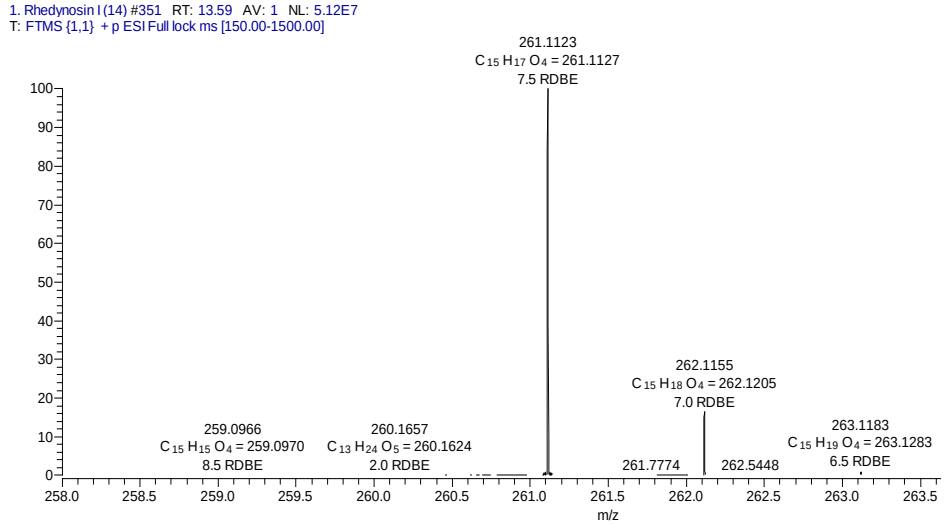

Figure A-214: HR-ESI-MS spectrum of compound **RH14** in $[M+H]^+$ positive ion mode.

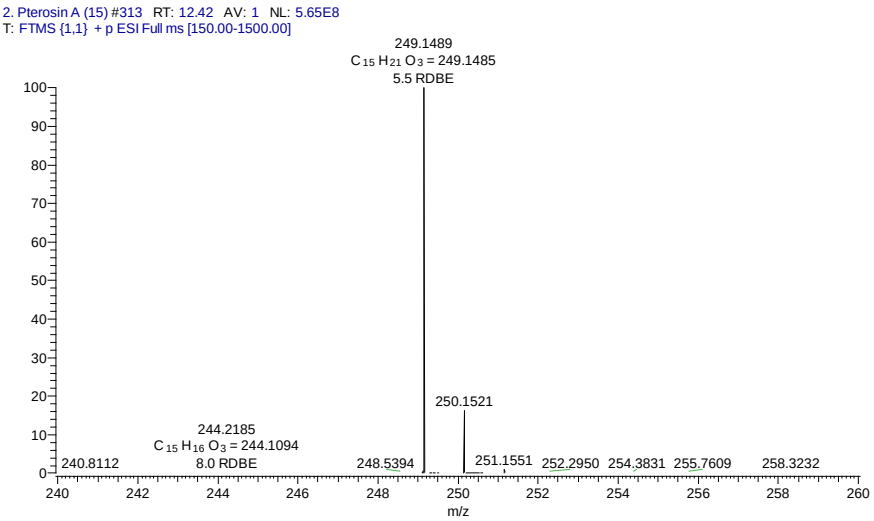

Figure A-215: HR-ESI-MS spectrum of compound **RH15** in $[M+H]^+$ positive ion mode.

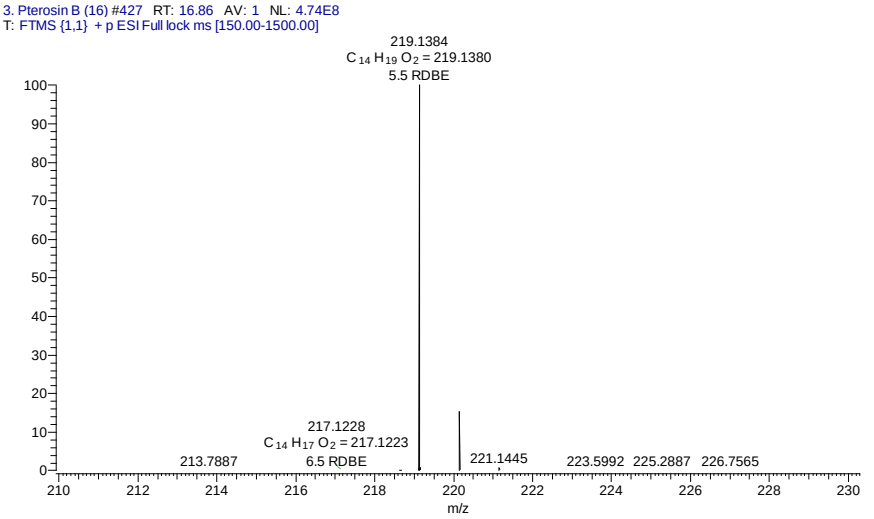

Figure A-216: HR-ESI-MS spectrum of compound **RH16** in $[M+H]^+$ positive ion mode.

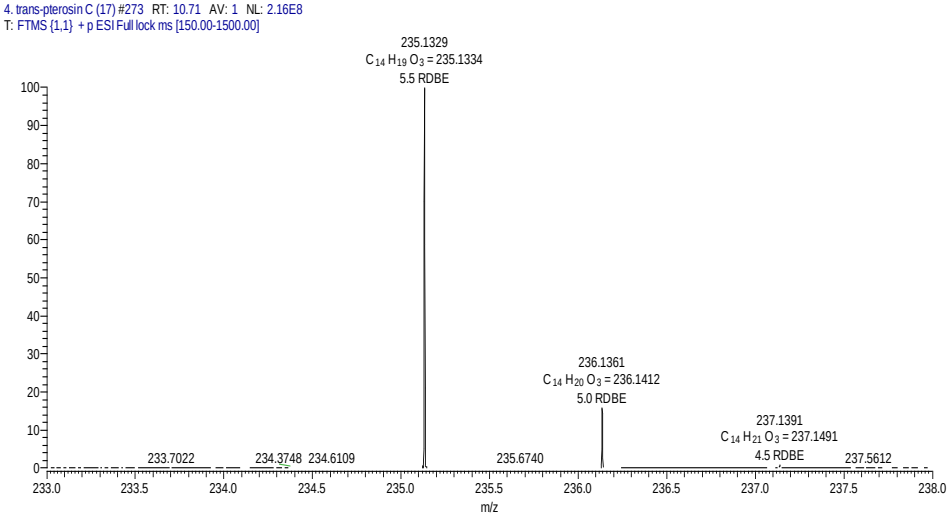

Figure A-217: HR-ESI-MS spectrum of compound **RH17** in $[M+H]^+$ positive ion mode.

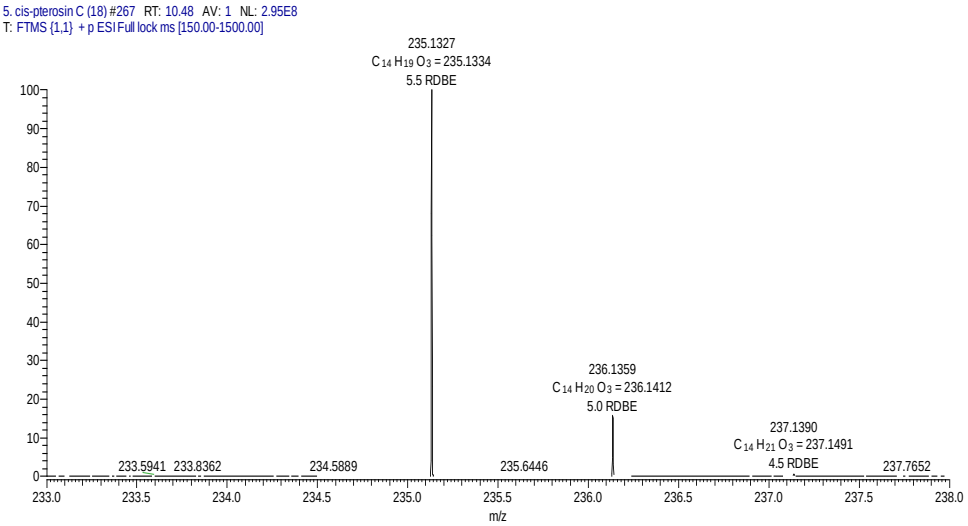

Figure A-218: HR-ESI-MS spectrum of compound **RH18** in $[M+H]^+$ positive ion mode.

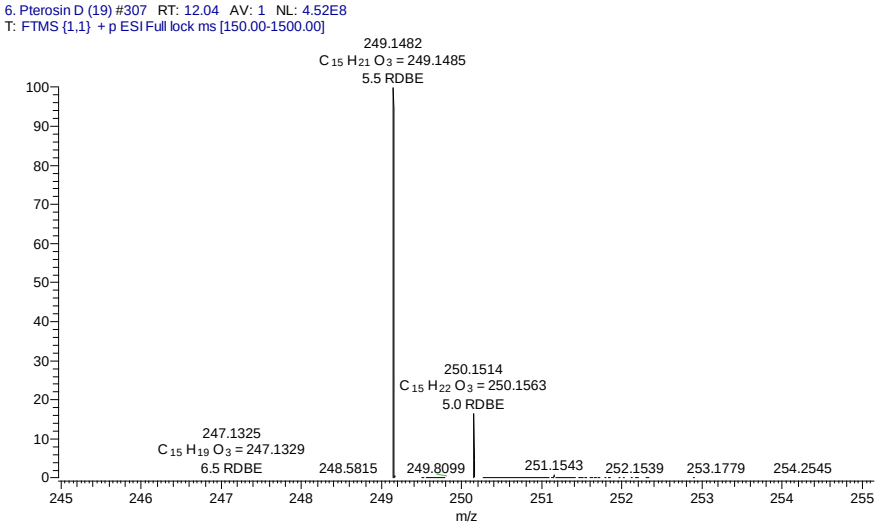

Figure A-219: HR-ESI-MS spectrum of compound **RH19** in $[M+H]^+$ positive ion mode.

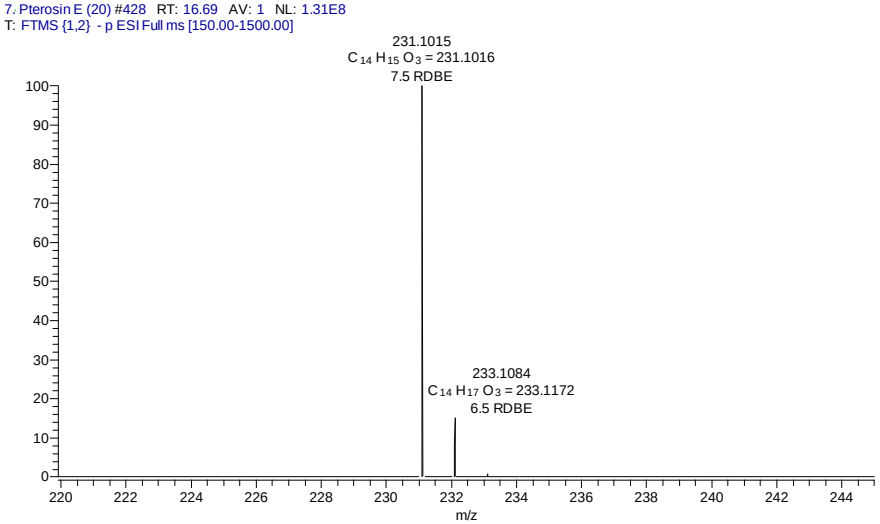

Figure A-220: HR-ESI-MS spectrum of compound **RH20** in $[M-H]^-$ negative ion mode.

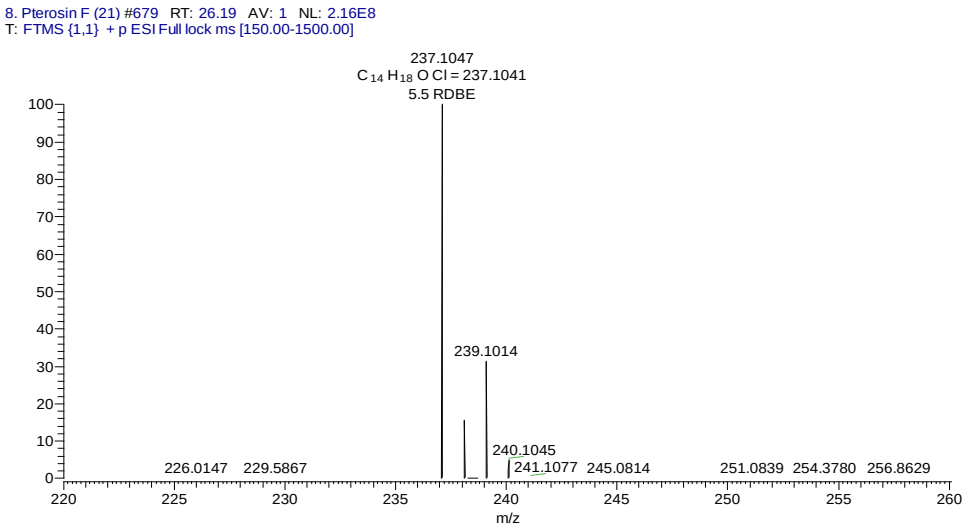

Figure A-221: HR-ESI-MS spectrum of compound **RH21** in $[M+H]^+$ positive ion mode.

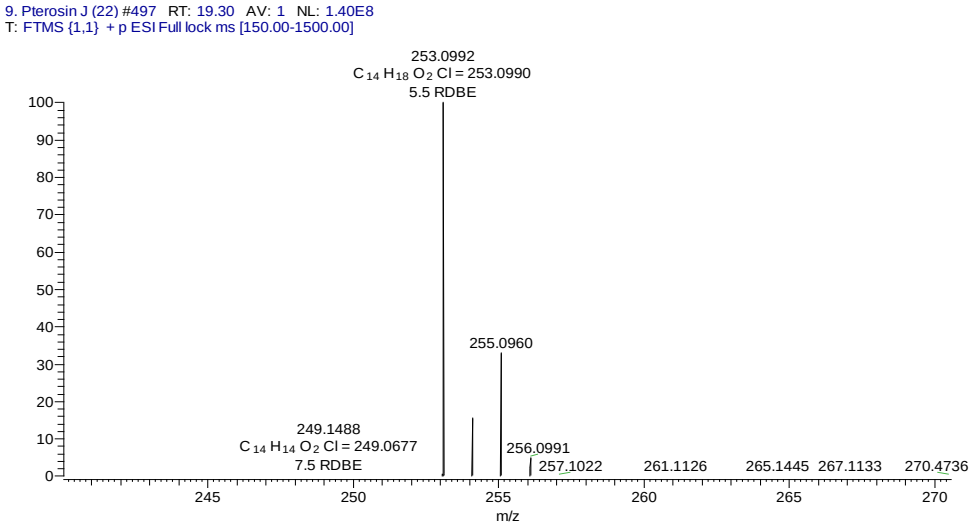

Figure A-222: HR-ESI-MS spectrum of compound **RH22** in $[M+H]^+$ positive ion mode.

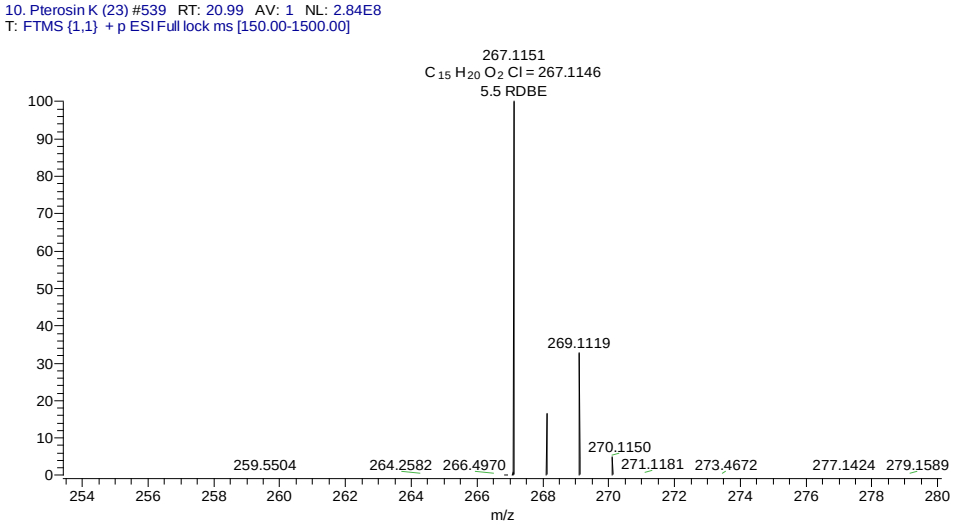

Figure A-223: HR-ESI-MS spectrum of compound **RH23** in $[M+H]^+$ positive ion mode.

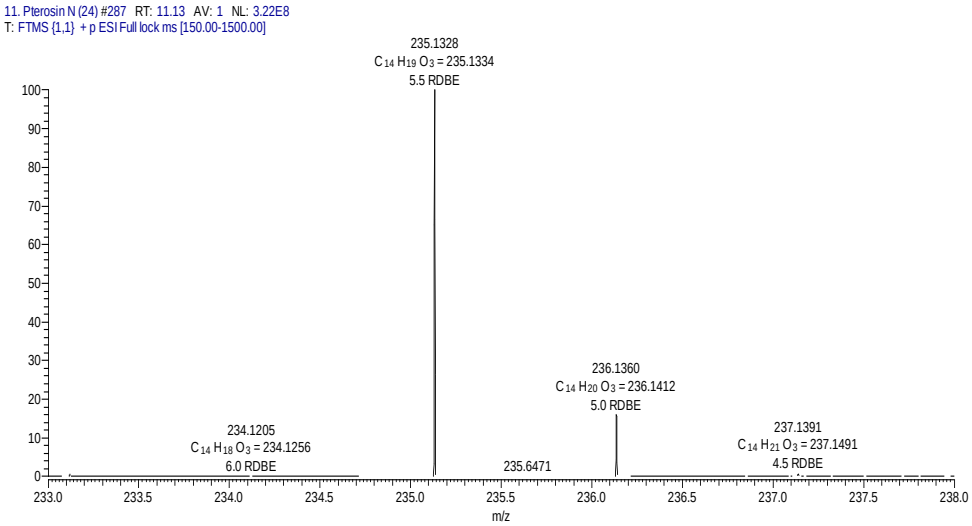

Figure A-224: HR-ESI-MS spectrum of compound **RH24** in $[M+H]^+$ positive ion mode.

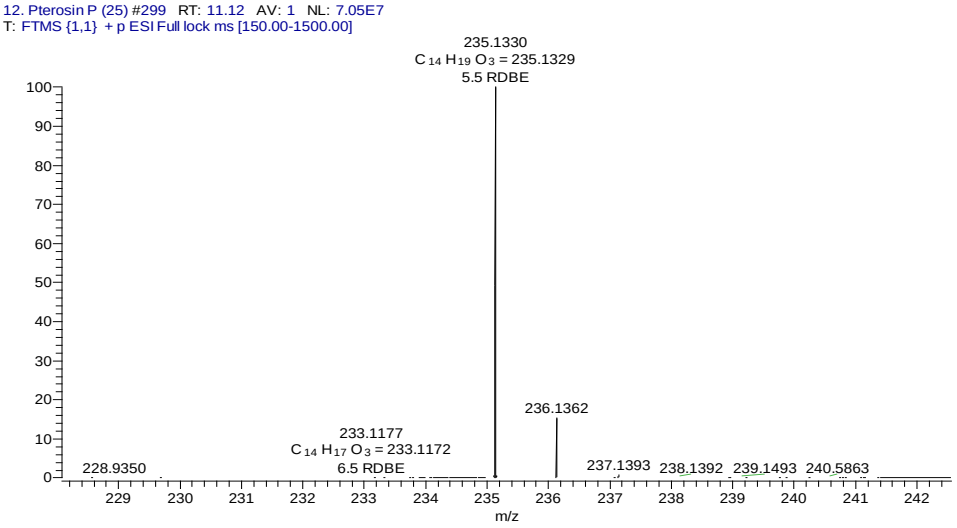

Figure A-225: HR-ESI-MS spectrum of compound **RH25** in $[M+H]^+$ positive ion mode.

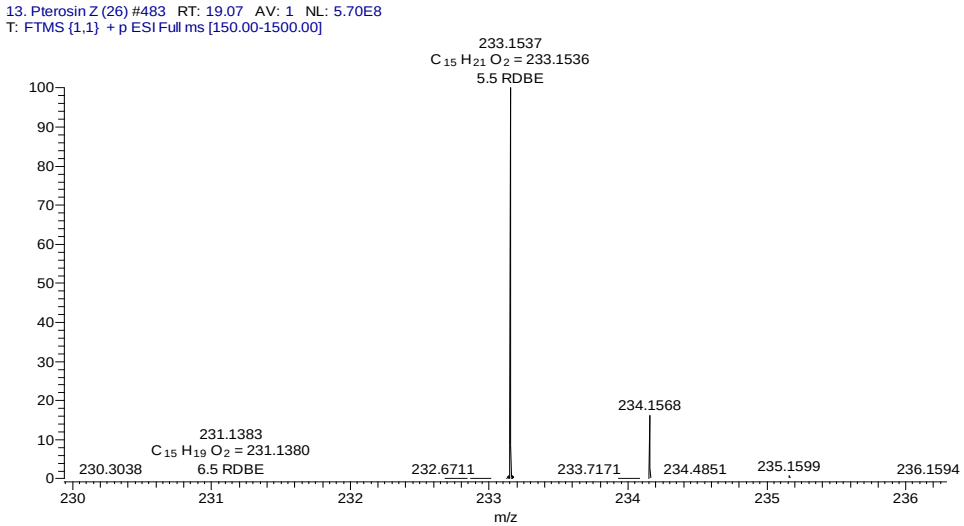

Figure A-226: HR-ESI-MS spectrum of compound **RH26** in $[M+H]^+$ positive ion mode.

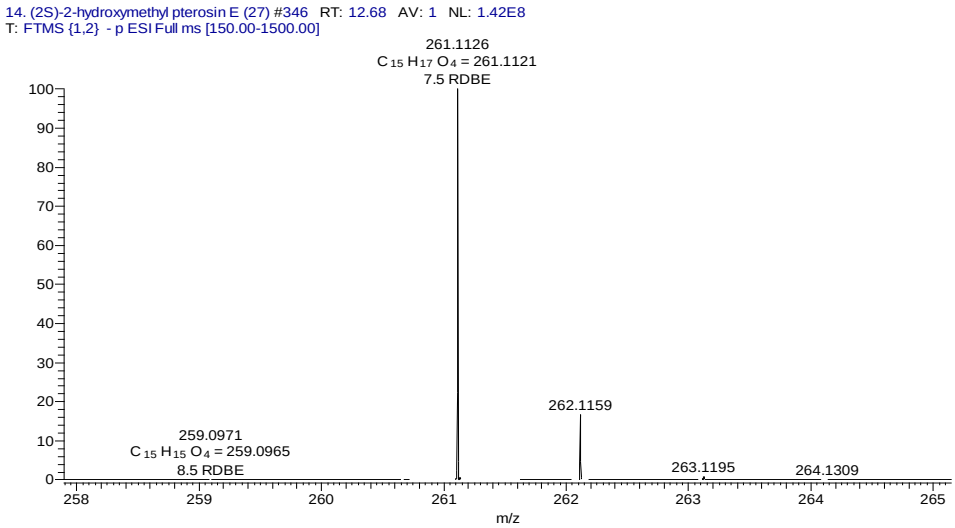

Figure A-227: HR-ESI-MS spectrum of compound **RH27** in $[M-H]^-$ negative ion mode.

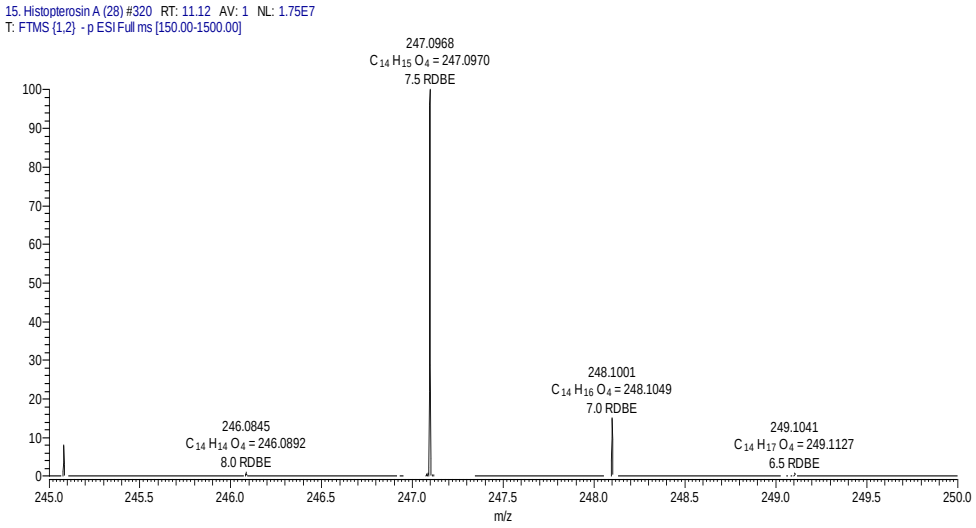

Figure A-228: HR-ESI-MS spectrum of compound **RH28** in $[M-H]^-$ negative ion mode.

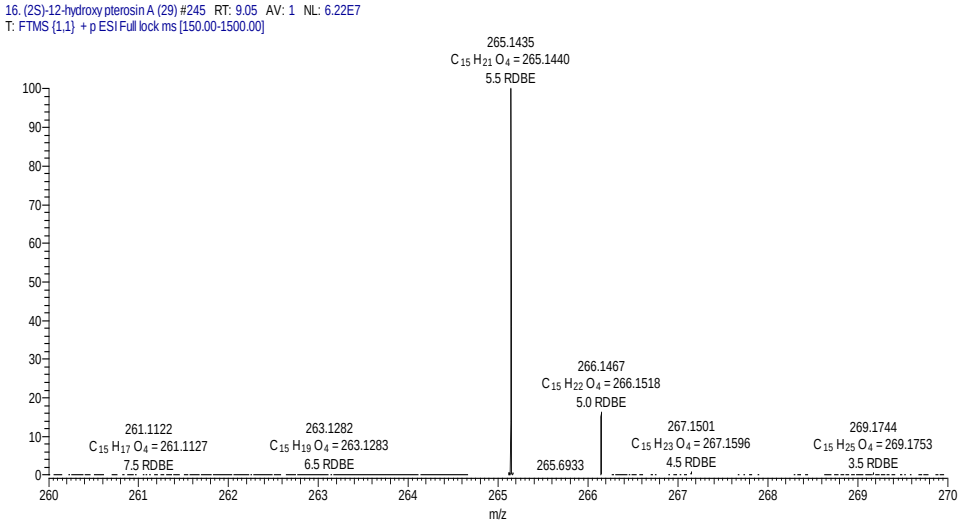

Figure A-229: HR-ESI-MS spectrum of compound **RH29** in $[M+H]^+$ positive ion mode.

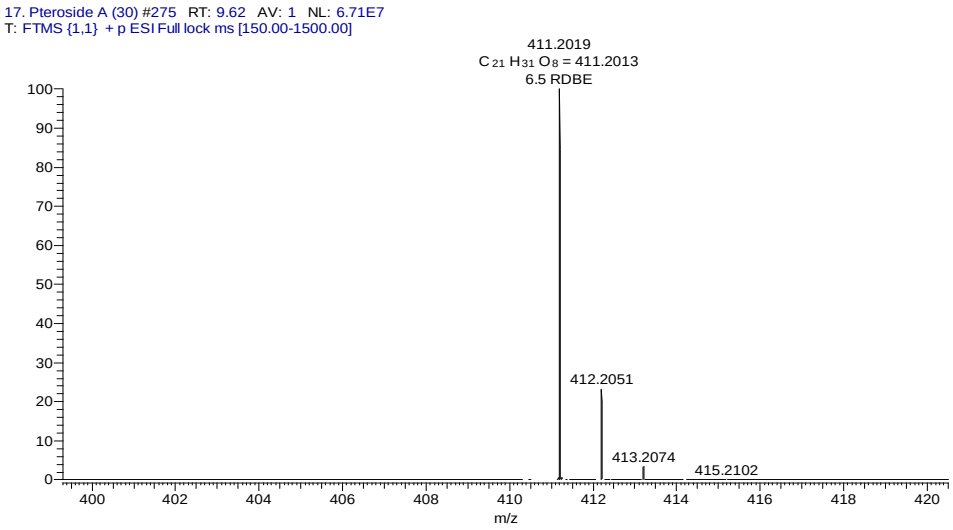

Figure A-230: HR-ESI-MS spectrum of compound **RH30** in $[M+H]^+$ positive ion mode.

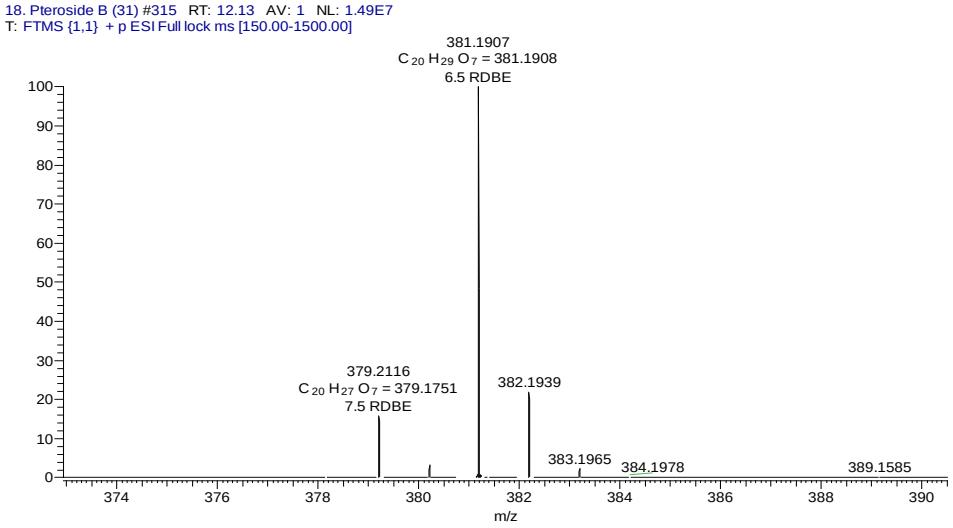

Figure A-231: HR-ESI-MS spectrum of compound **RH31** in $[M+H]^+$ positive ion mode.

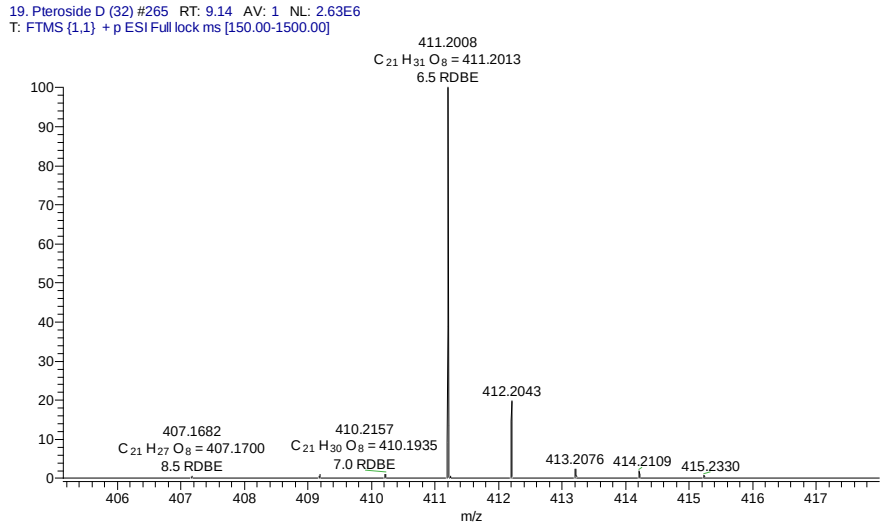

Figure A-232: HR-ESI-MS spectrum of compound **RH32** in $[M+H]^+$ positive ion mode.

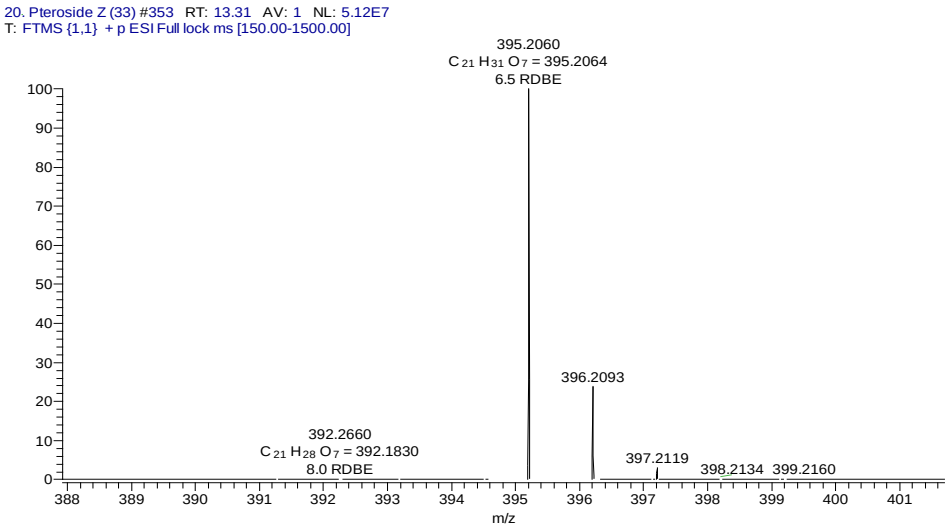

Figure A-233: HR-ESI-MS spectrum of compound **RH33** in $[M+H]^+$ positive ion mode.

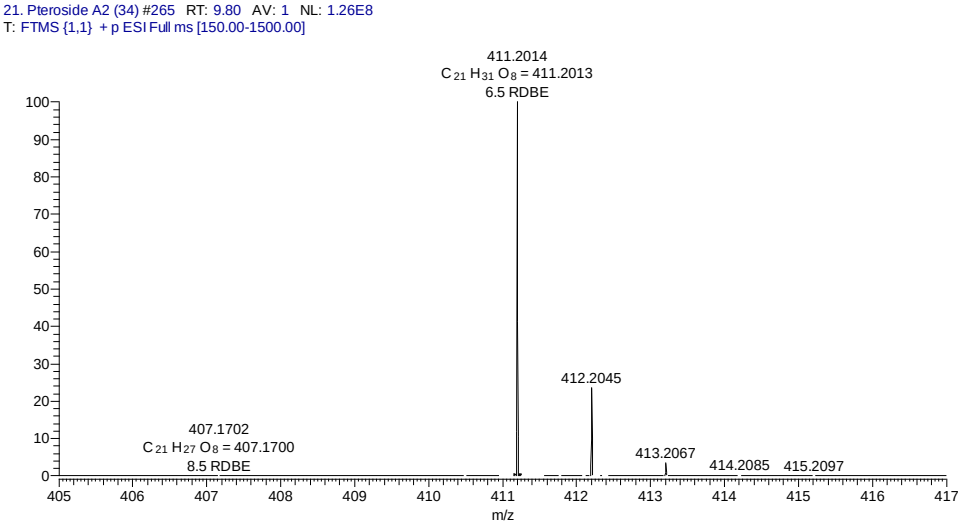

Figure A-234: HR-ESI-MS spectrum of compound **RH34** in $[M+H]^+$ positive ion mode.

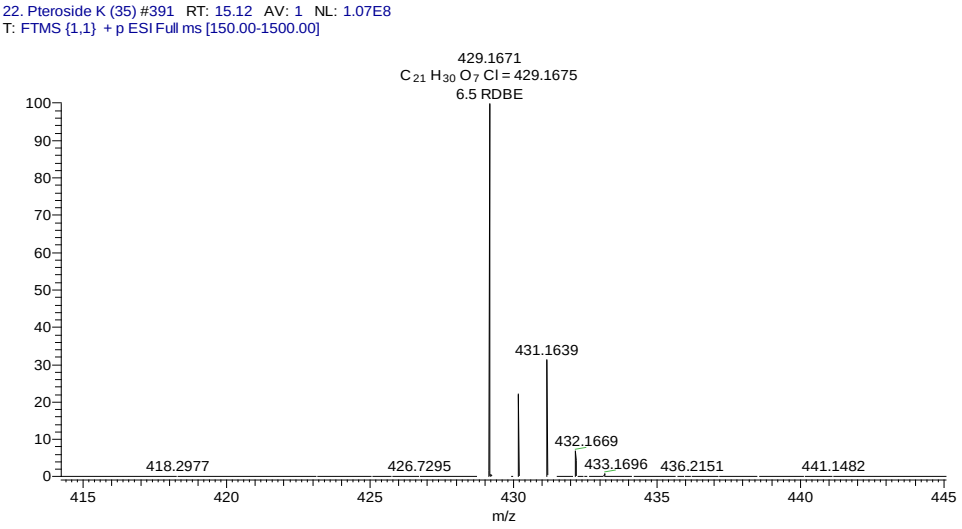

Figure A-235: HR-ESI-MS spectrum of compound **RH35** in $[M+H]^+$ positive ion mode.

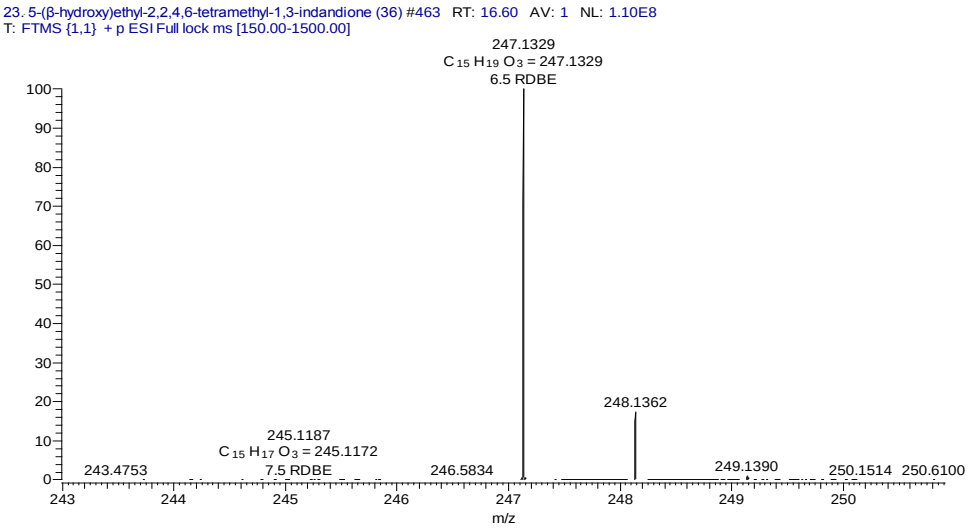

Figure A-236: HR-ESI-MS spectrum of compound **RH36** in $[M+H]^+$ positive ion mode.

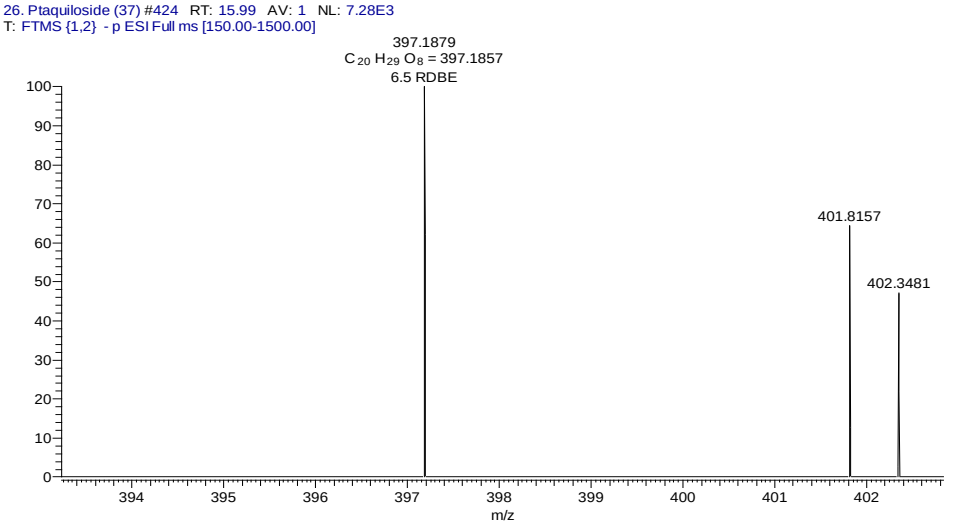

Figure A-237: HR-ESI-MS spectrum of compound **RH37** in $[M-H]^-$ negative ion mode.

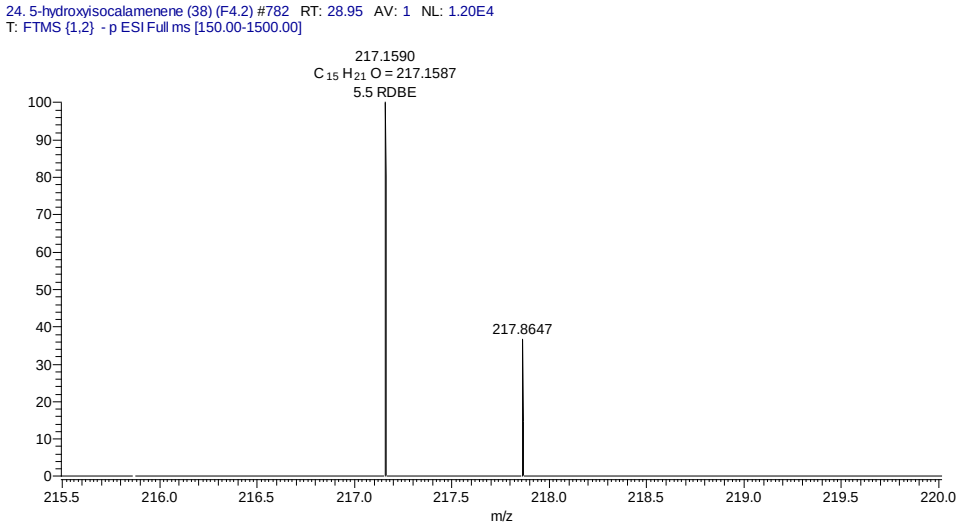

Figure A-238: HR-ESI-MS spectrum of compound **RH38** in $[M-H]^-$ negative ion mode.

Appendix III: IR spectra of compounds **RH2 - RH13**.

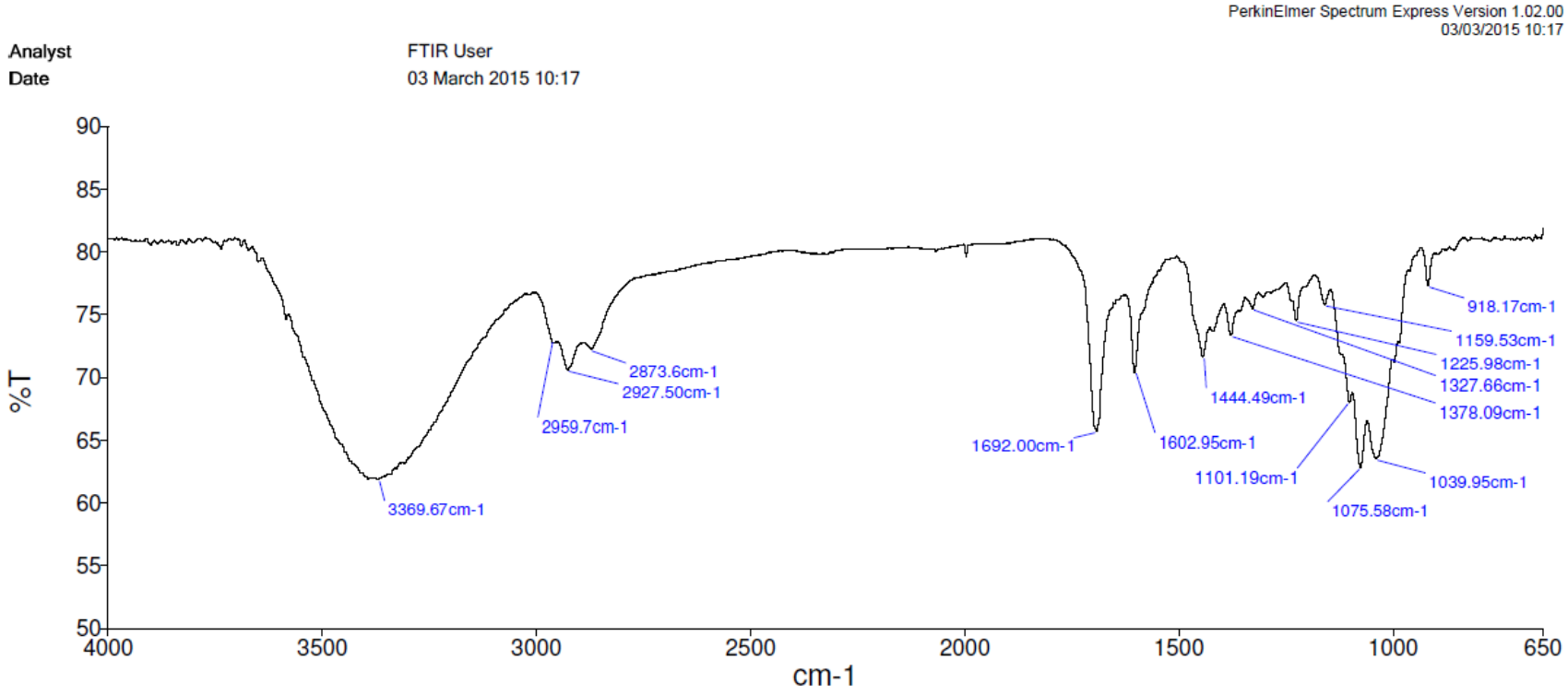

Sample Name	Description	Quality Checks
2. FTIR Rhedynoside A (2)	Sample 007 By FTIR date Thursday, February 26 2015	The Quality Checks give rise to multiple warnings for the sample.

Figure A-239: FT-IR spectrum of compound **RH2** in CH_3OH.

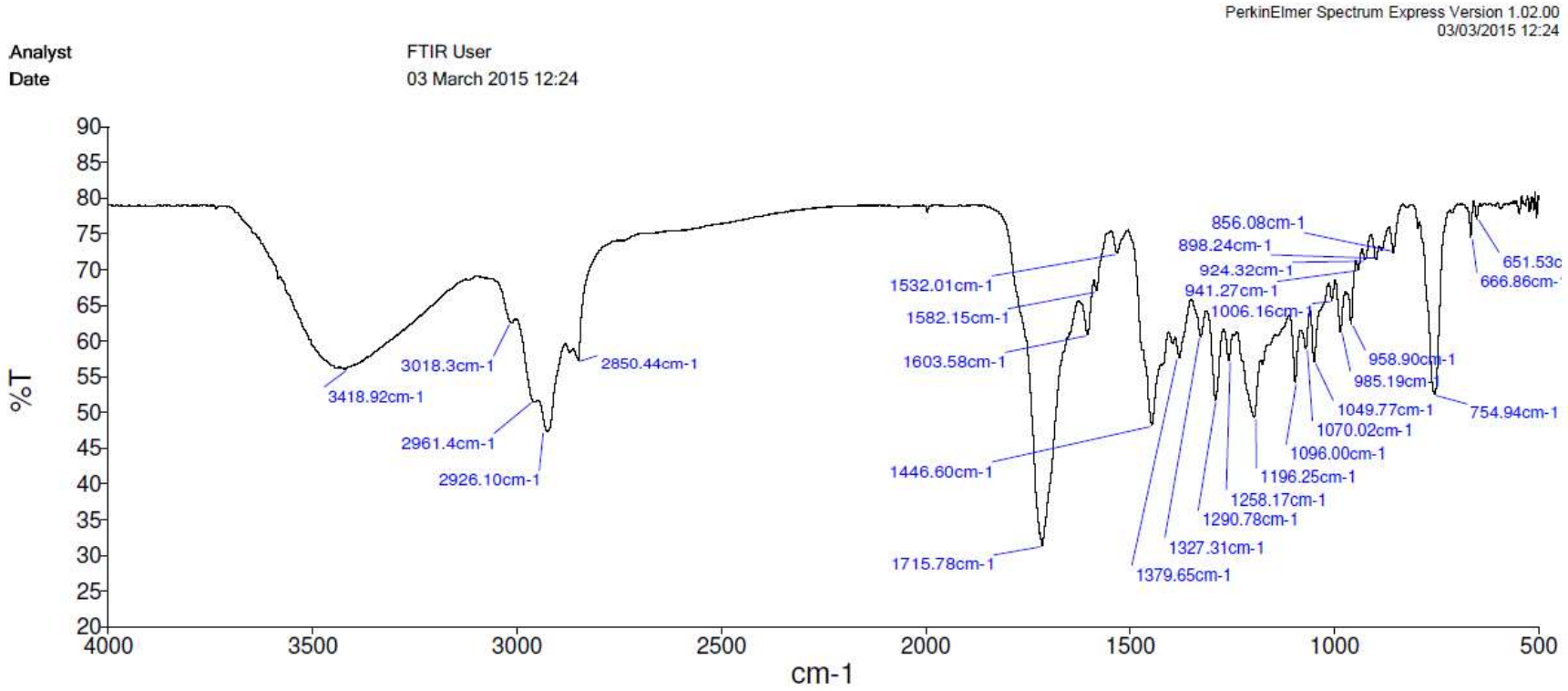

Sample Name	Description	Quality Checks
3. FTIR Rhedynosin B (3)	Sample 010 By FTIR date Thursday, February 26 2015	The Quality Checks give rise to multiple warnings for the sample.

Figure A-240: FT-IR spectrum of compound **RH3** in $CHCl_3$.

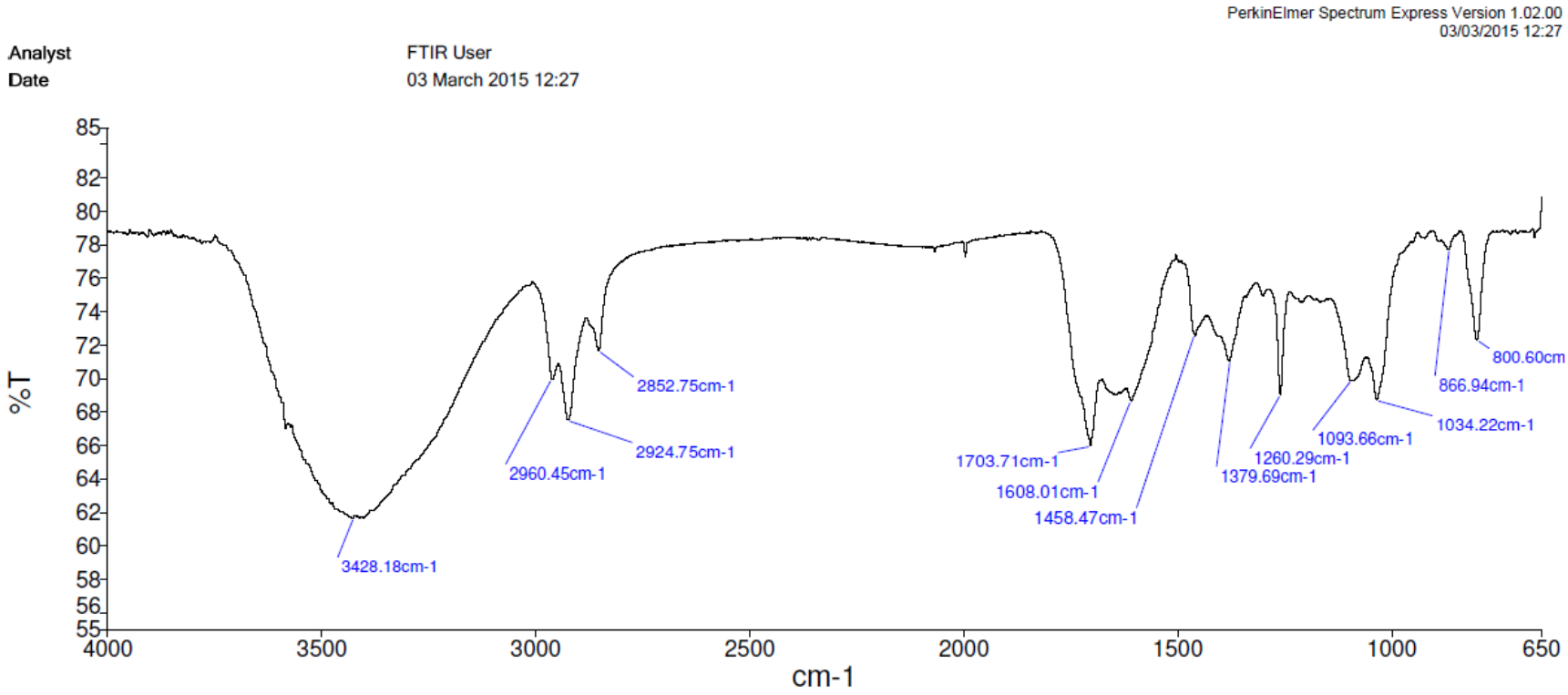

Sample Name	Description	Quality Checks
4. FTIR Rhedynosin C (4)	Sample 013 By FTIR date Friday, February 27 2015	The Quality Checks give rise to multiple warnings for the sample.

Figure A-241: FT-IR spectrum of compound **RH4** in CH_3OH.

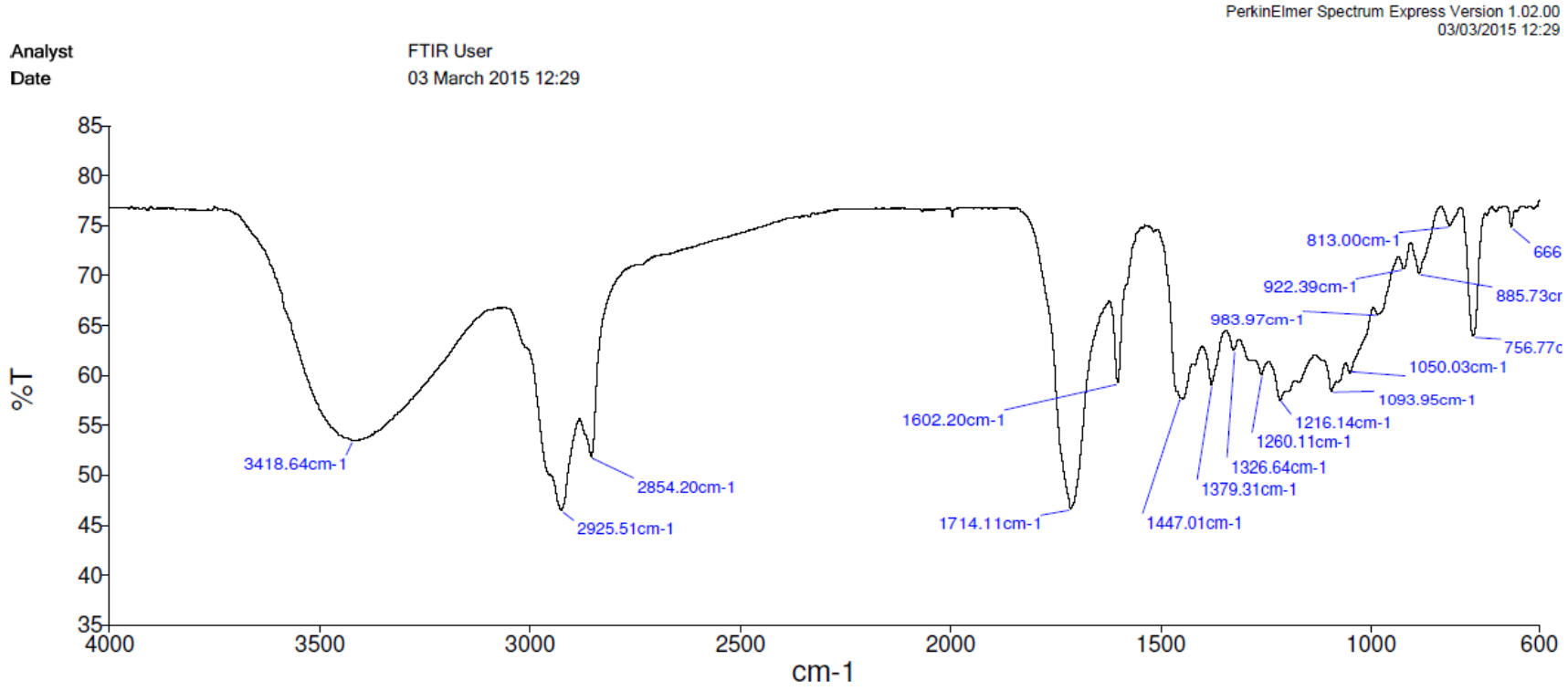

Sample Name	Description	Quality Checks
5. FTIR Rhedynosin D (5)	Sample 015 By FTIR date Friday, February 27 2015	The Quality Checks give rise to multiple warnings for the sample.

Figure A-242: FT-IR spectrum of compound **RH5** in $CHCl_3$.

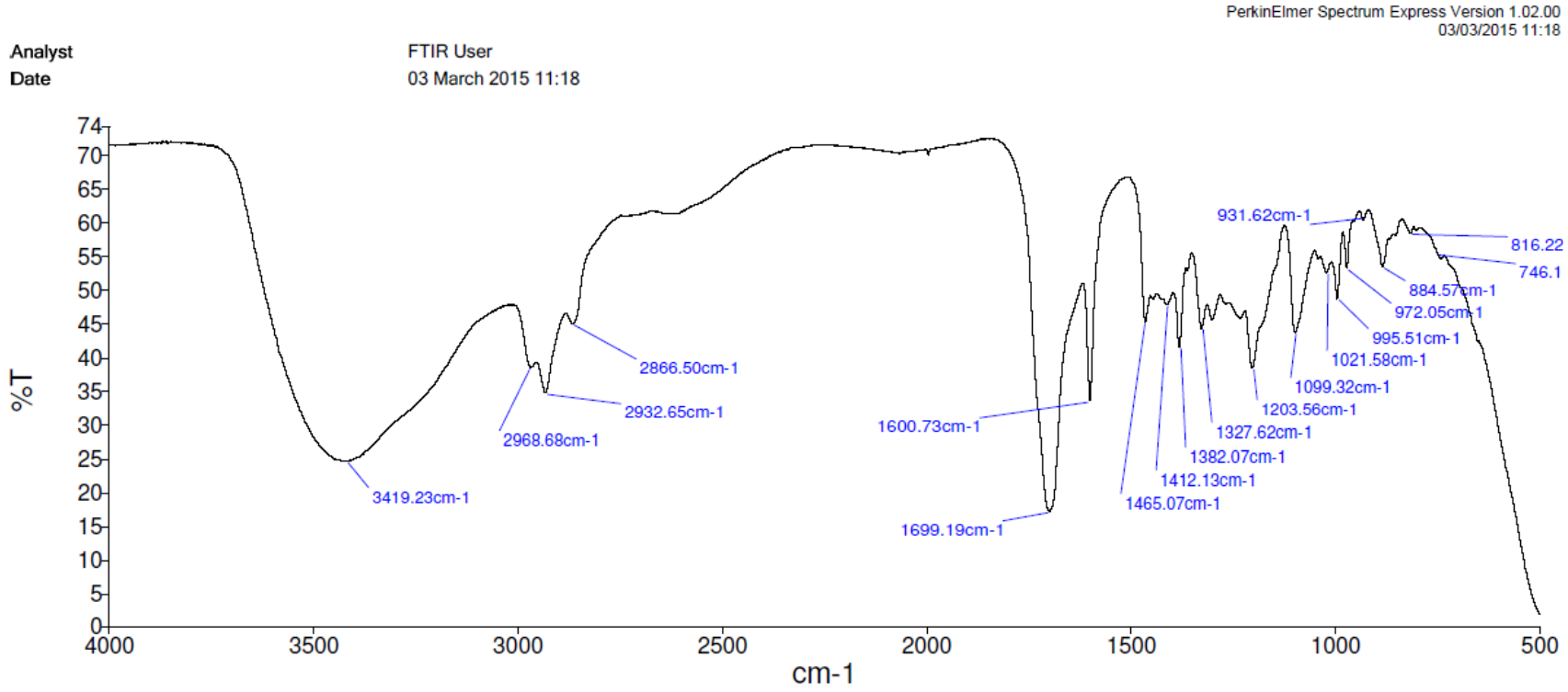

Sample Name	Description	Quality Checks
6. FTIR Rhedynosin E (6)	Sample 016 By FTIR date Friday, February 27 2015	The Quality Checks give rise to multiple warnings for the sample.

Figure A-243: FT-IR spectrum of compound **RH6** in CH_3OH.

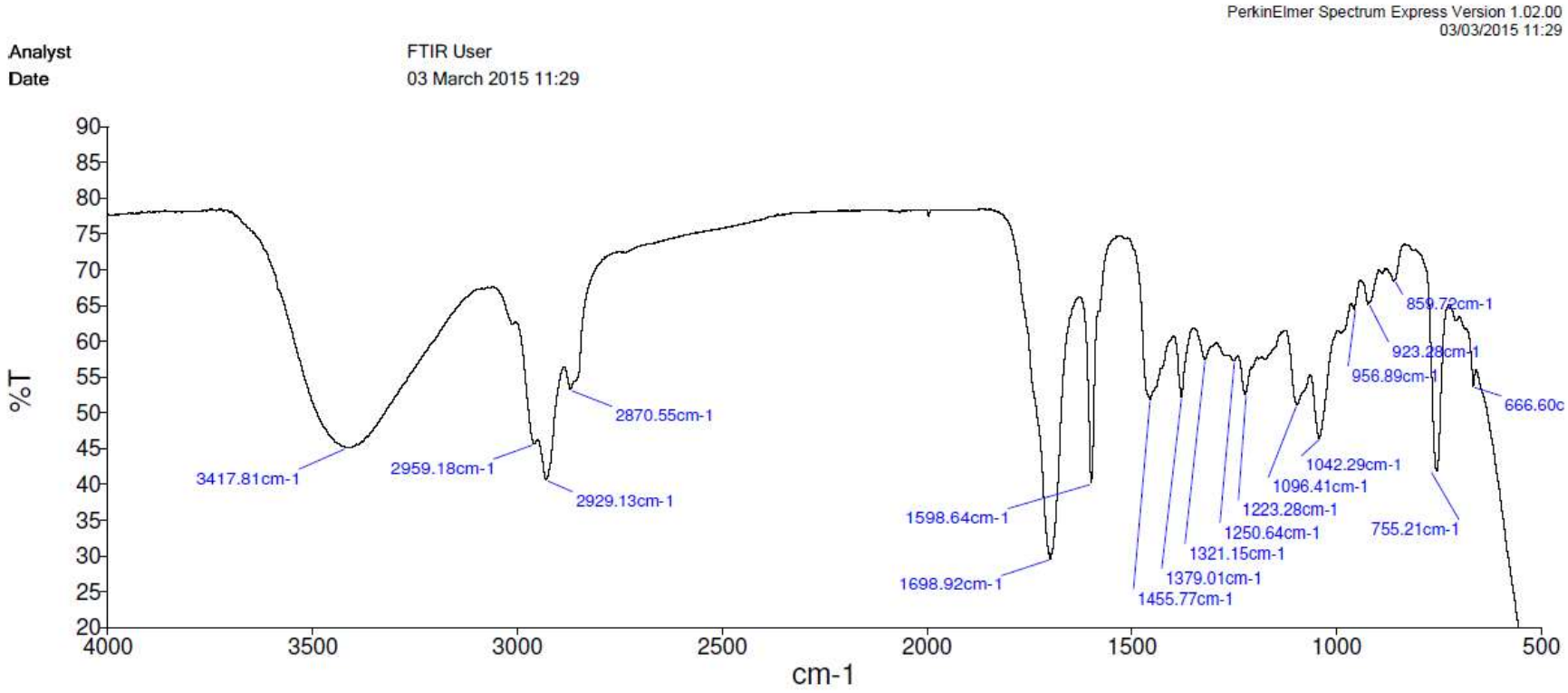

Sample Name	Description	Quality Checks
7. FTIR Rhedynosin F (7)	Sample 017 By FTIR date Friday, February 27 2015	The Quality Checks give rise to multiple warnings for the sample.

Figure A-244: FT-IR spectrum of compound **RH7** in $CHCl_3$.

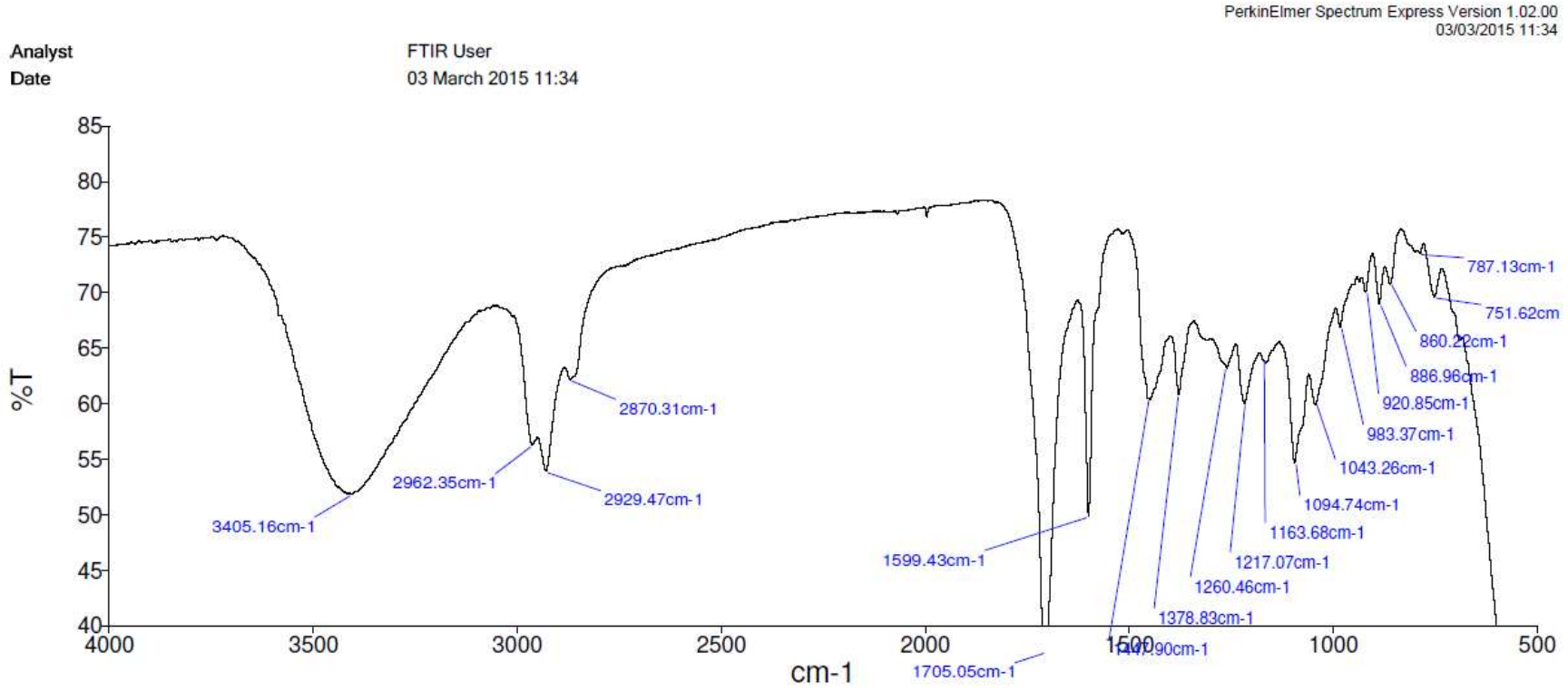

Sample Name	Description	Quality Checks
8. FTIR Rhedynosin G (8)	Sample 002 By FTIR date Thursday, February 26 2015	The Quality Checks give rise to multiple warnings for the sample.

Figure A-245: FT-IR spectrum of compound **RH8** in CH_3OH.

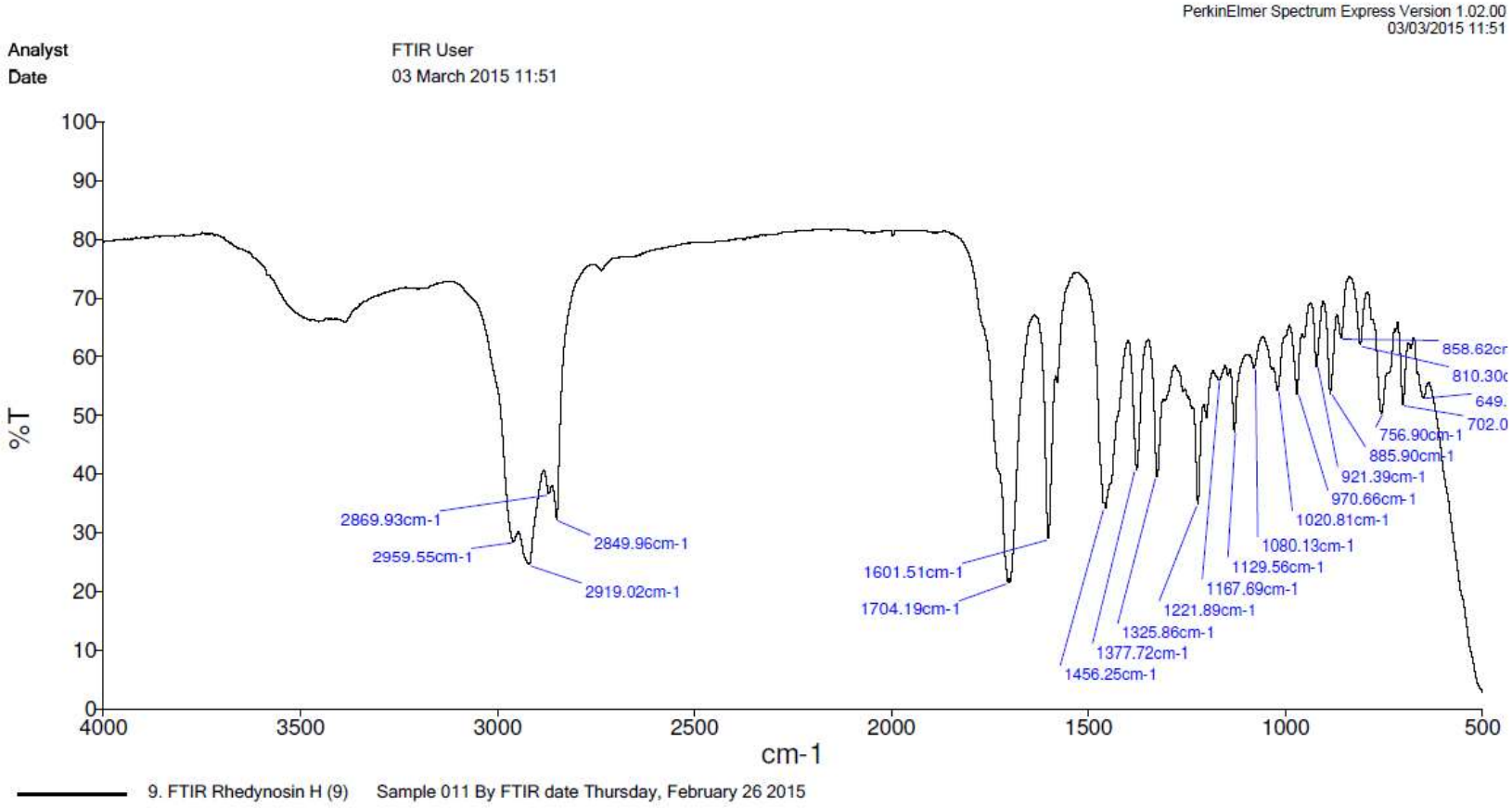

Figure A-246: FT-IR spectrum of compound **RH9** in CH_3OH.

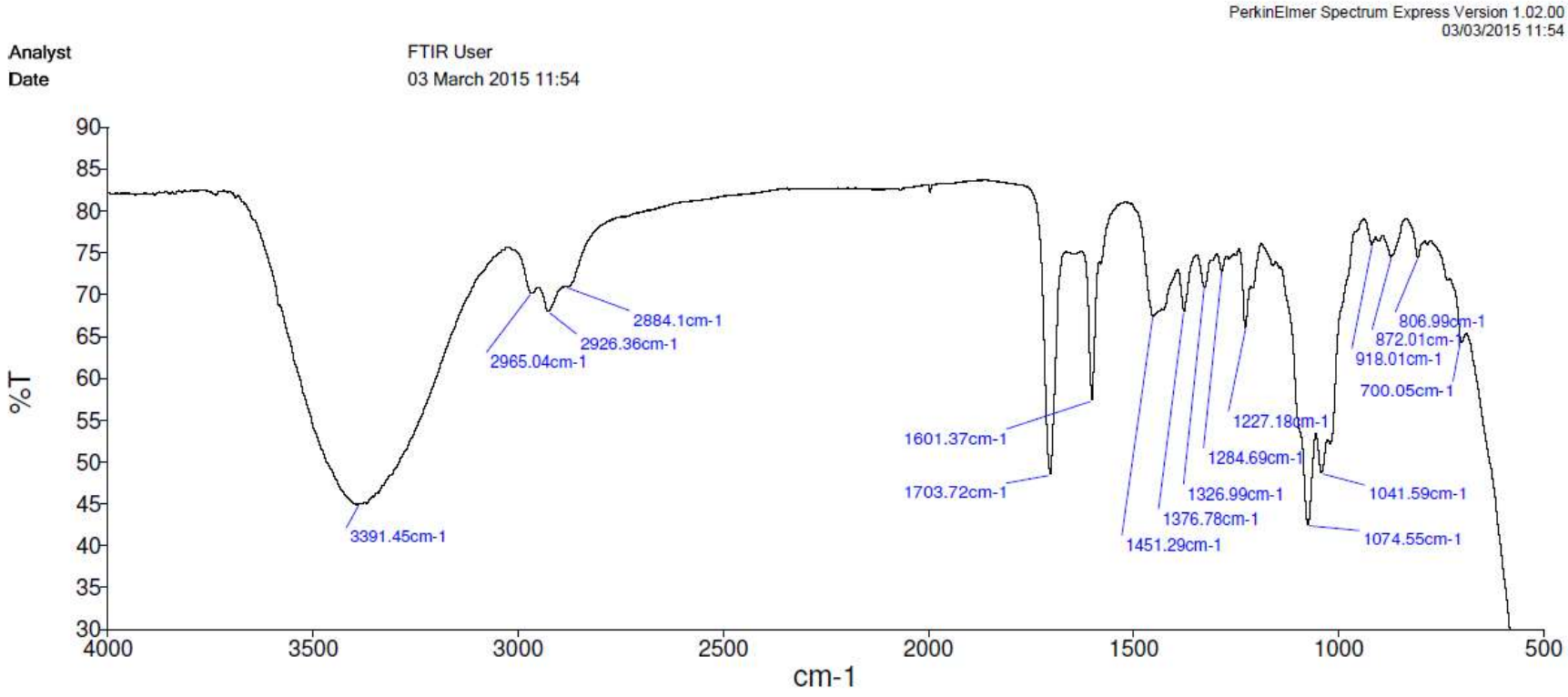

Sample Name	Description	Quality Checks
10. FTIR Rhedynoside B (10)	Sample 004 By FTIR date Thursday, February 26 2015	The Quality Checks give rise to multiple warnings for the sample.

Figure A-247: FT-IR spectrum of compound **RH10** in CH_3OH.

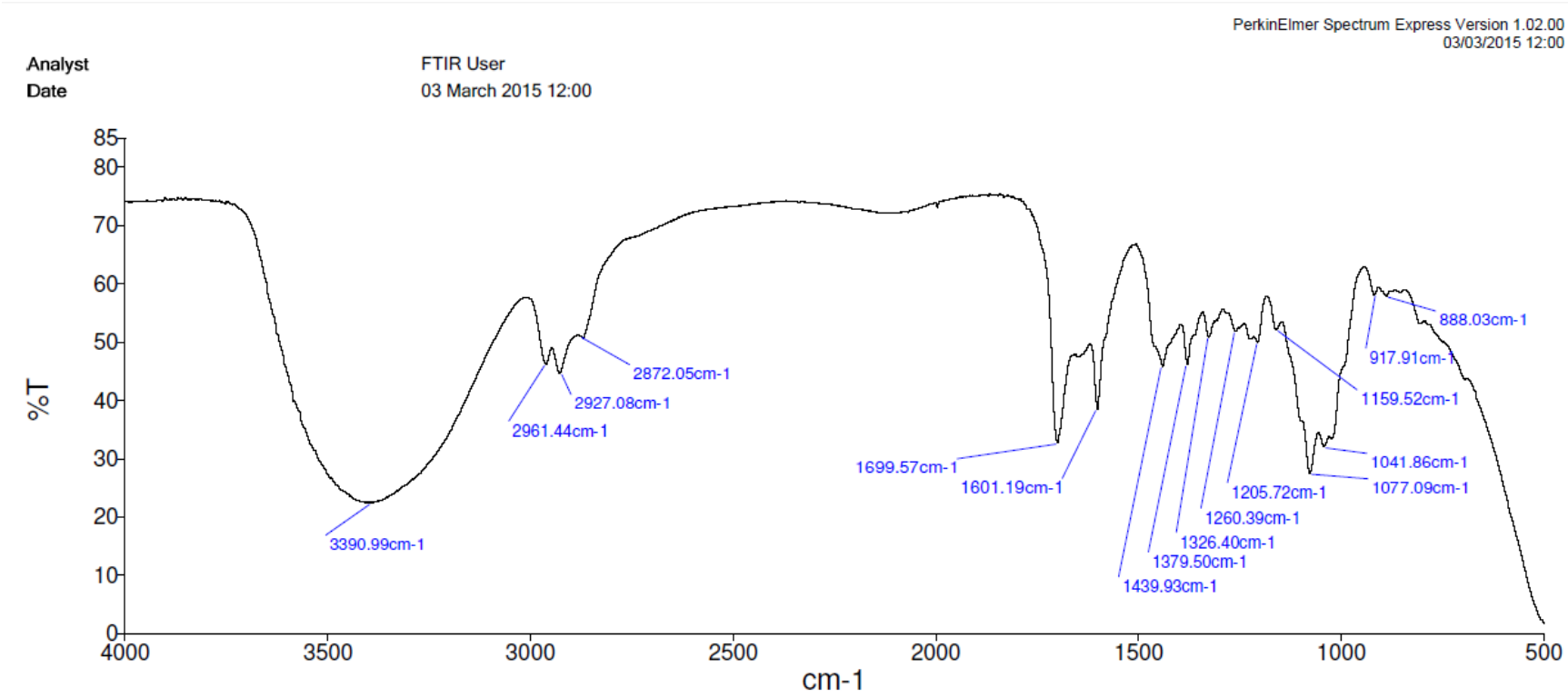

Sample Name	Description	Quality Checks
11. FTIR Rhedynoside C (11)	Sample 018 By FTIR date Friday, February 27 2015	The Quality Checks give rise to multiple warnings for the sample.

Figure A-248: FT-IR spectrum of compound **RH11** in CH_3OH.

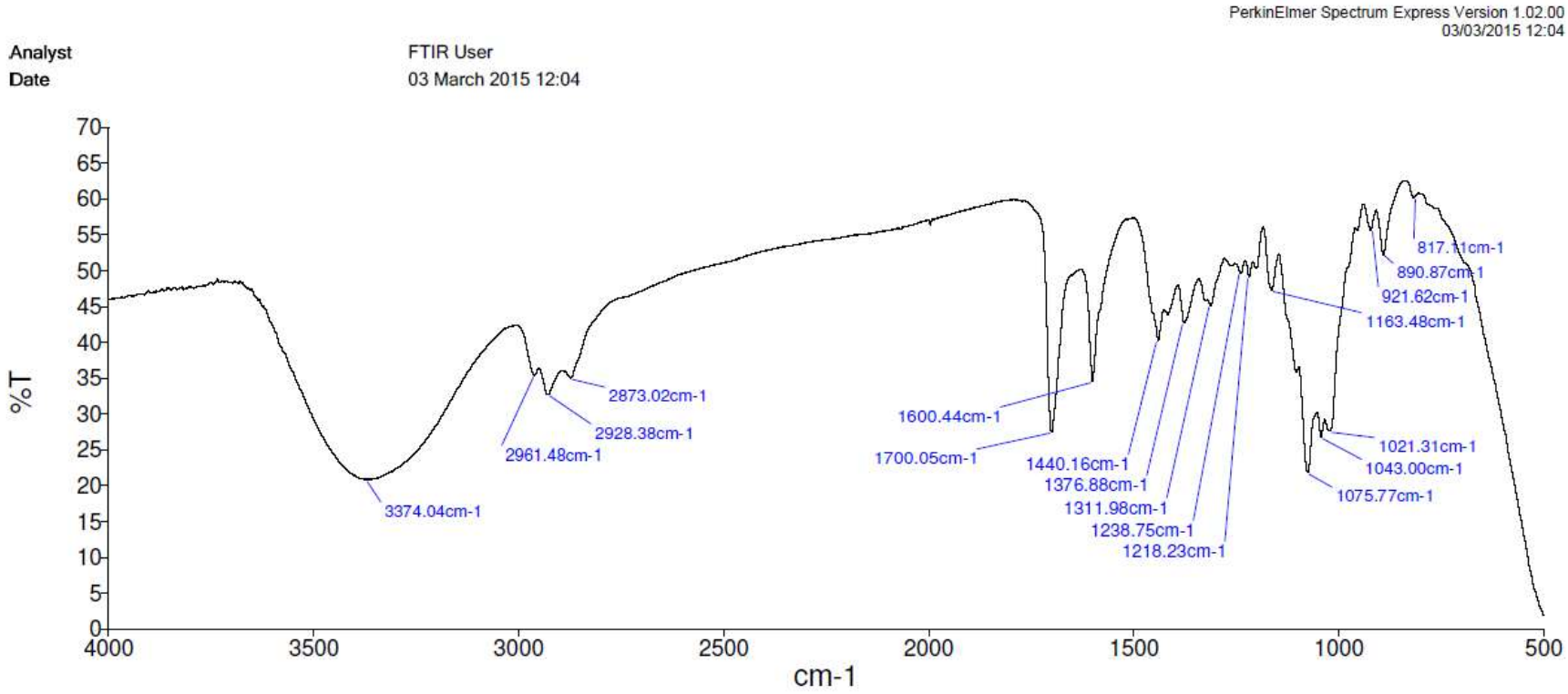

Sample Name	Description	Quality Checks
12. FTIR Rhedynoside D (12)	Sample 005 By FTIR date Thursday, February 26 2015	The Quality Checks give rise to multiple warnings for the sample.

Figure A-249: FT-IR spectrum of compound **RH12** in CH_3OH.

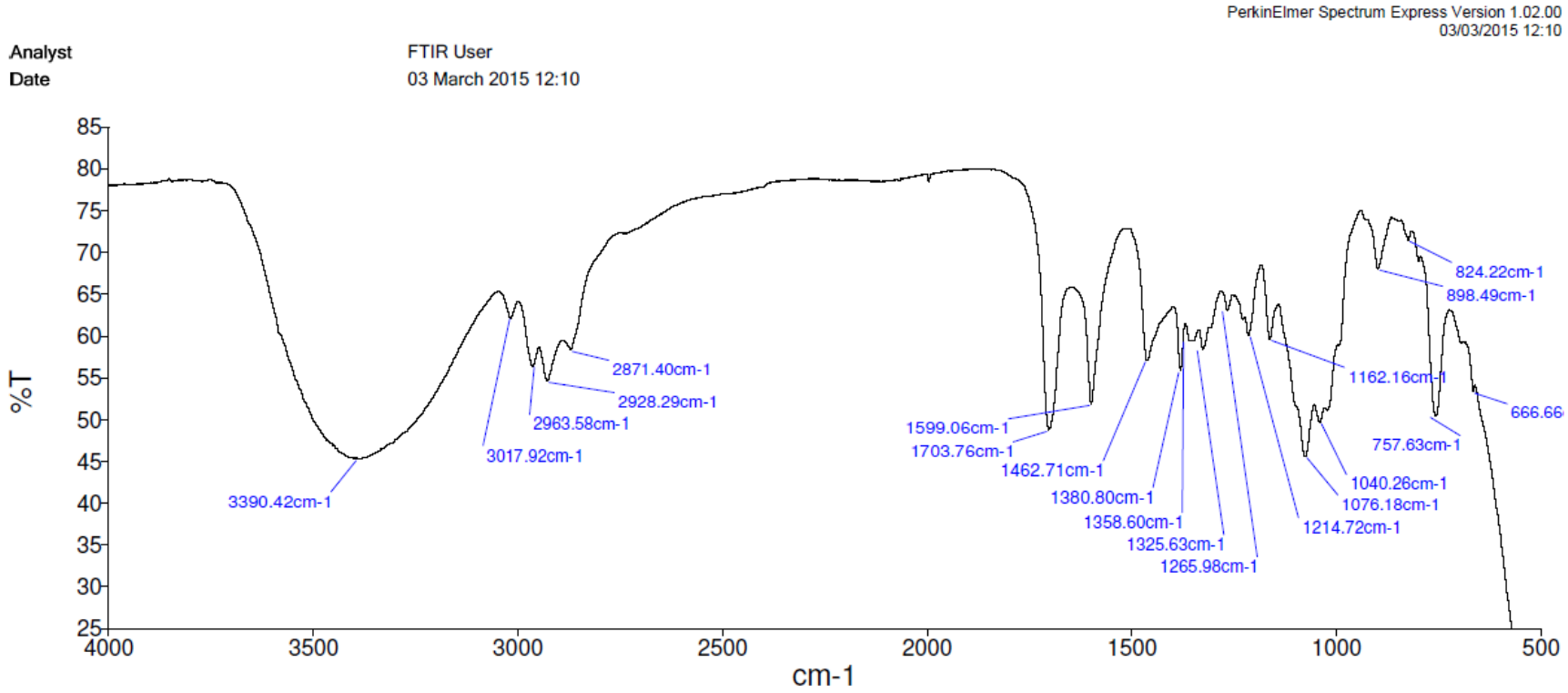

Sample Name	Description	Quality Checks
13. FTIR Rhedynoside E (13)	Sample 068 By FTIR date Monday, March 02 2015	The Quality Checks give rise to multiple warnings for the sample.

Figure A-250: FT-IR spectrum of compound **RH13** in CH_3OH.

Appendix IV: UV spectra of compounds **RH2 - RH13**.

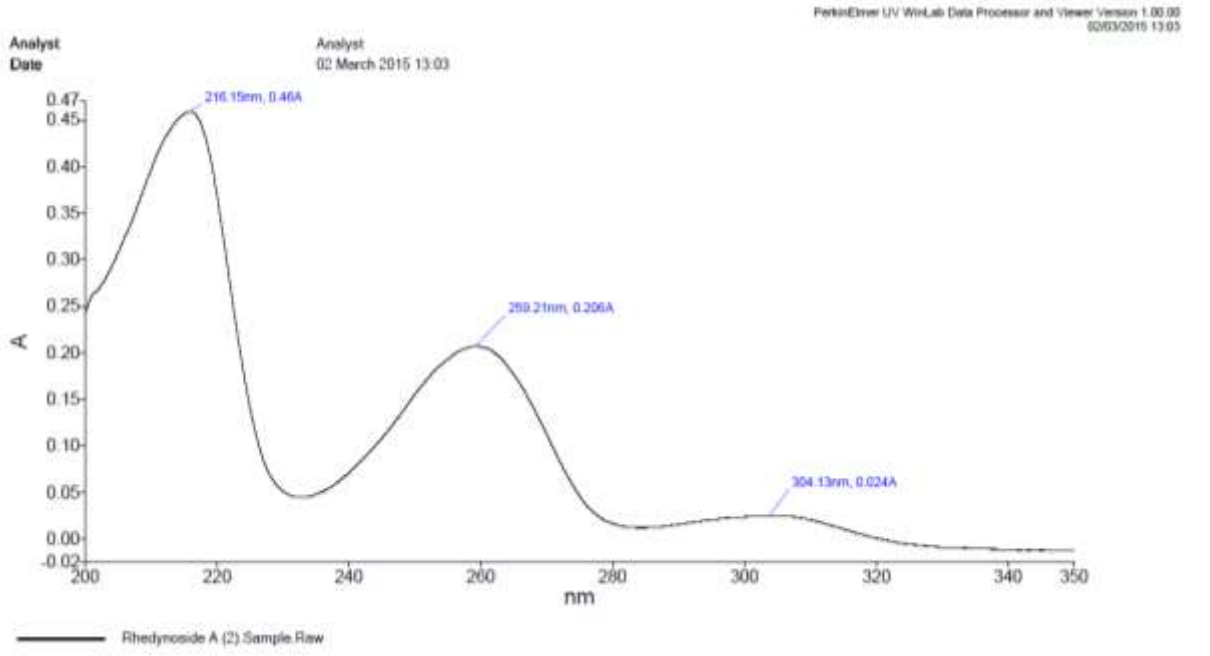

Figure A-251: UV spectrum of compound **RH2** in CH_3OH.

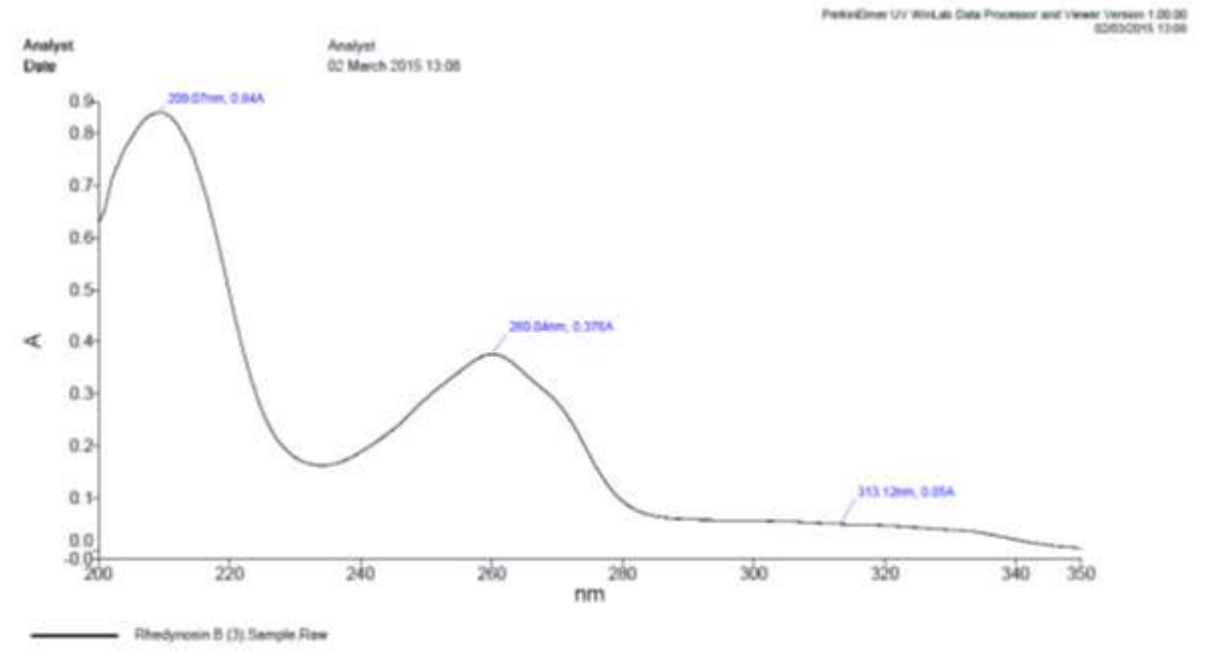

Figure A-252: UV spectrum of compound **RH3** in CH_3OH.

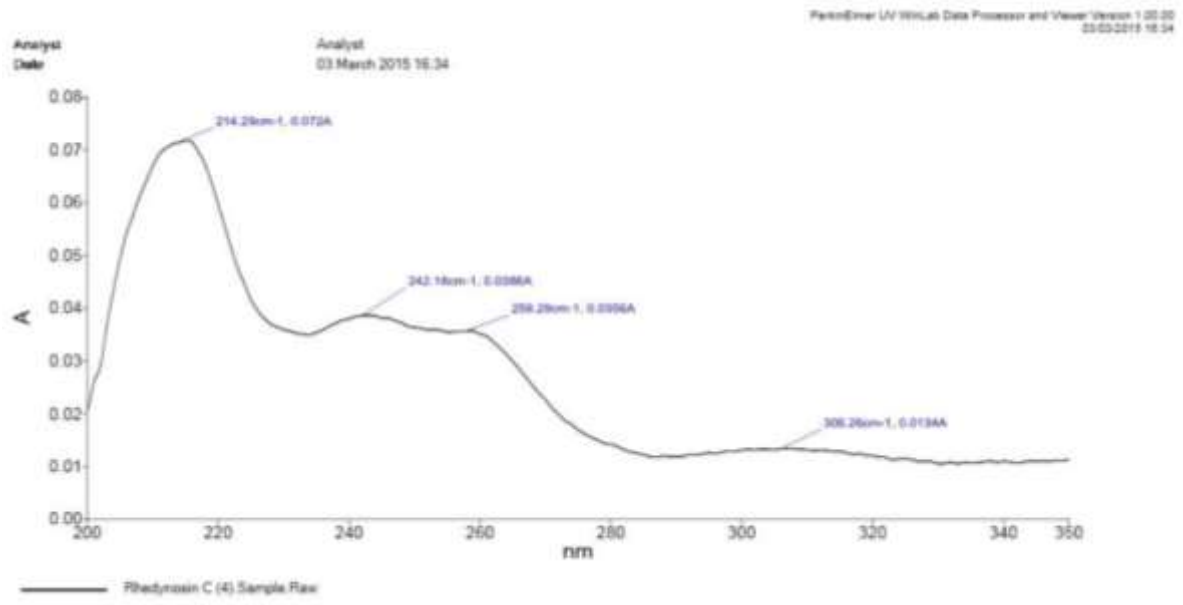

Figure A-253: UV spectrum of compound **RH4** in CH_3OH.

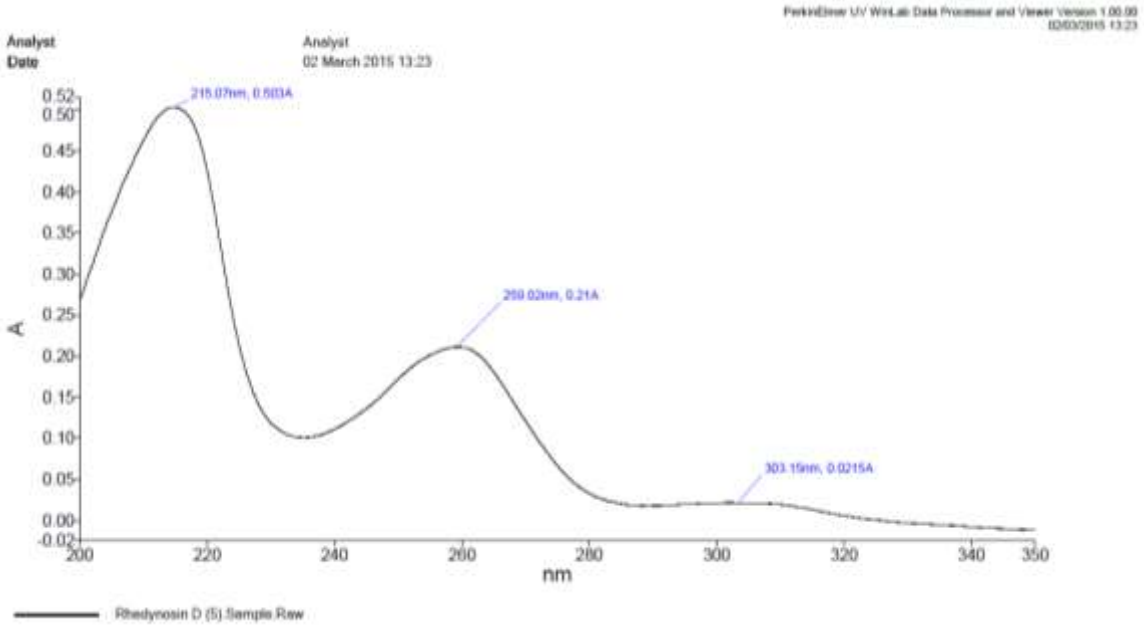

Figure A-254: UV spectrum of compound **RH5** in CH_3OH.

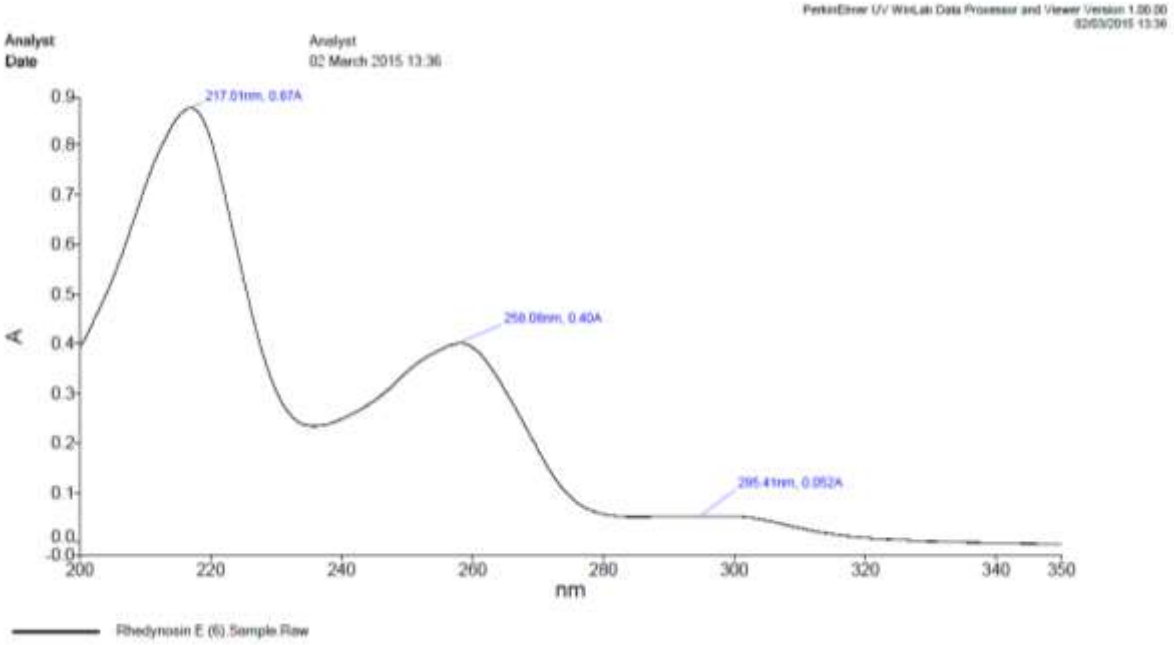

Figure A-255: UV spectrum of compound **RH6** in CH_3OH.

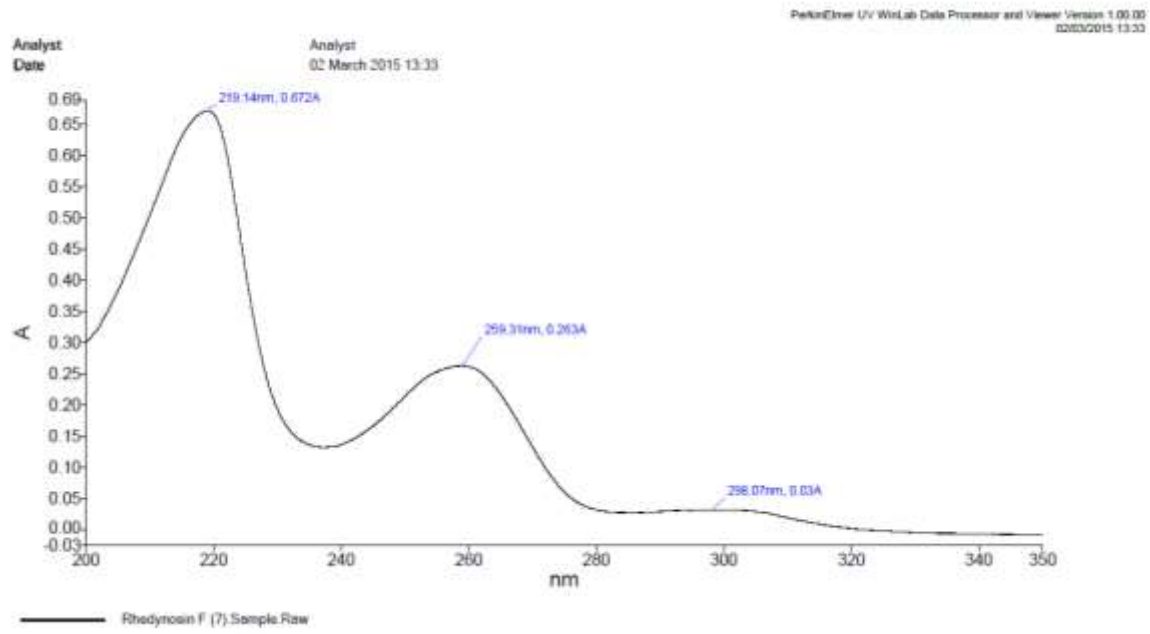

Figure A-256: UV spectrum of compound **RH7** in CH_3OH.

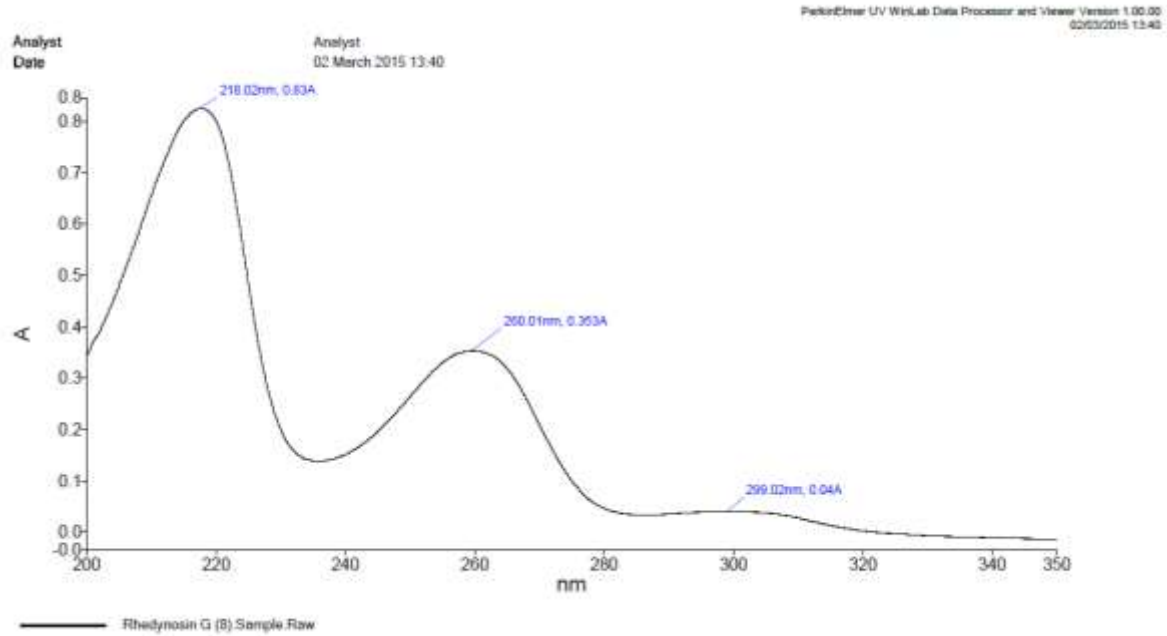

Figure A-257: UV spectrum of compound **RH8** in CH_3OH.

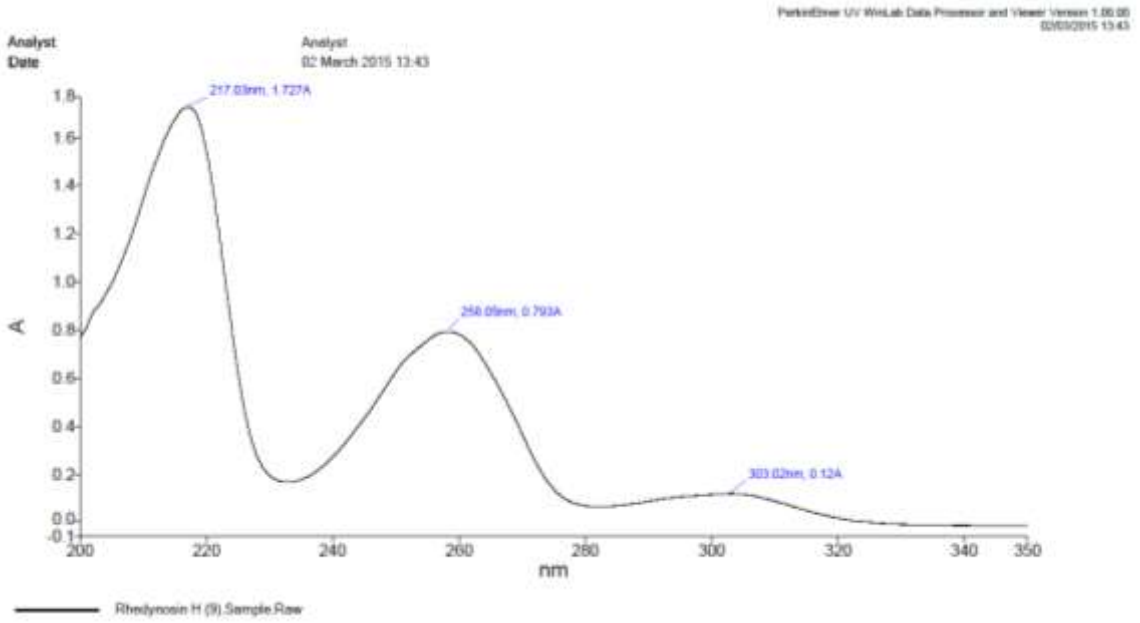

Figure A-258: UV spectrum of compound **RH9** in CH_3OH.

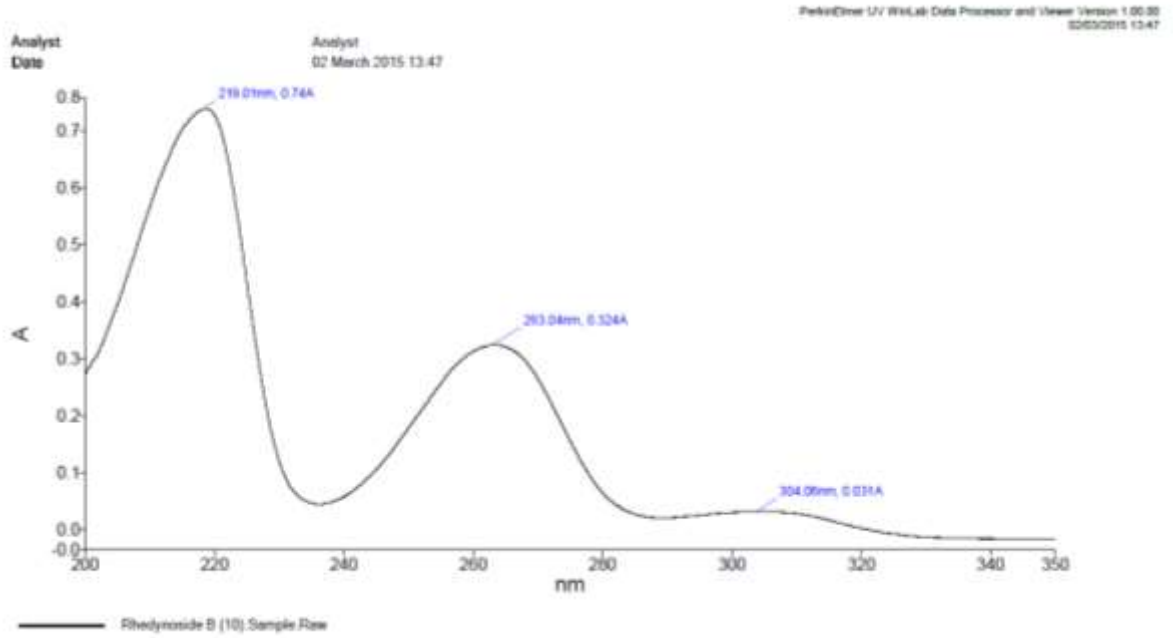

Figure A-259: UV spectrum of compound **RH10** in CH_3OH.

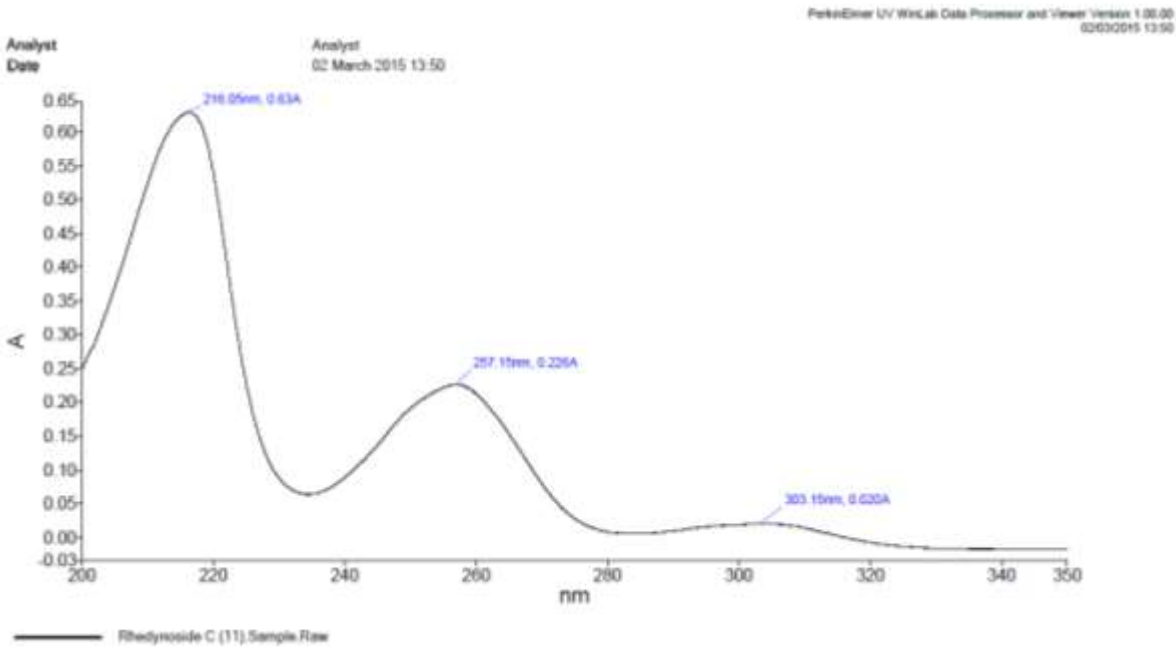

Figure A-260: UV spectrum of compound **RH11** in CH_3OH.

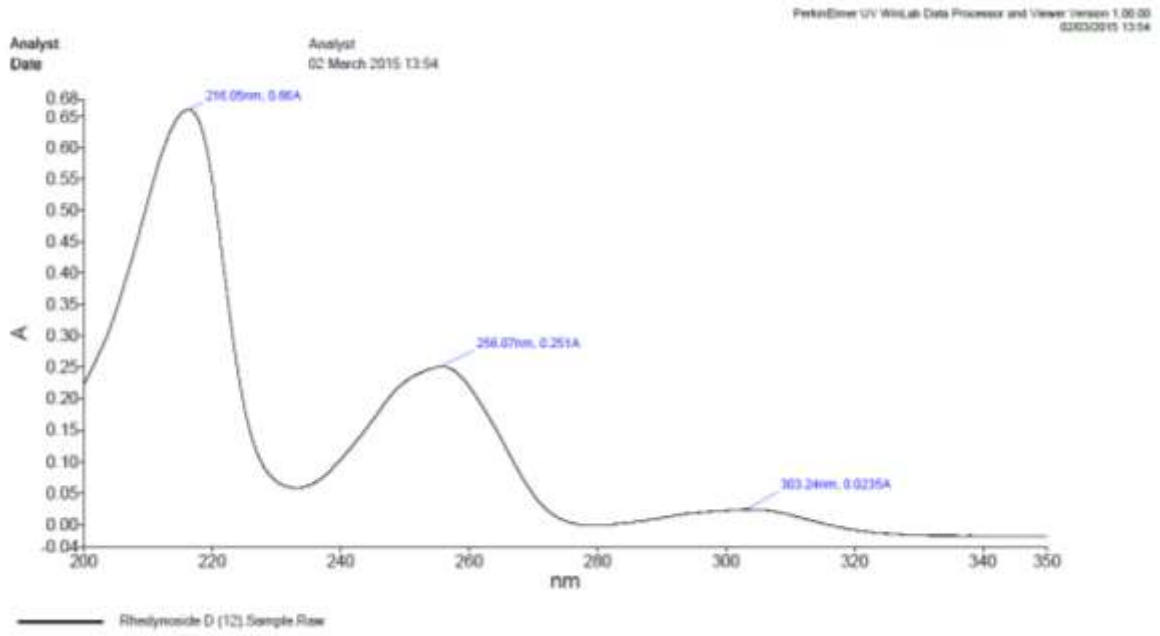

Figure A-261: UV spectrum of compound **RH12** in CH_3OH.

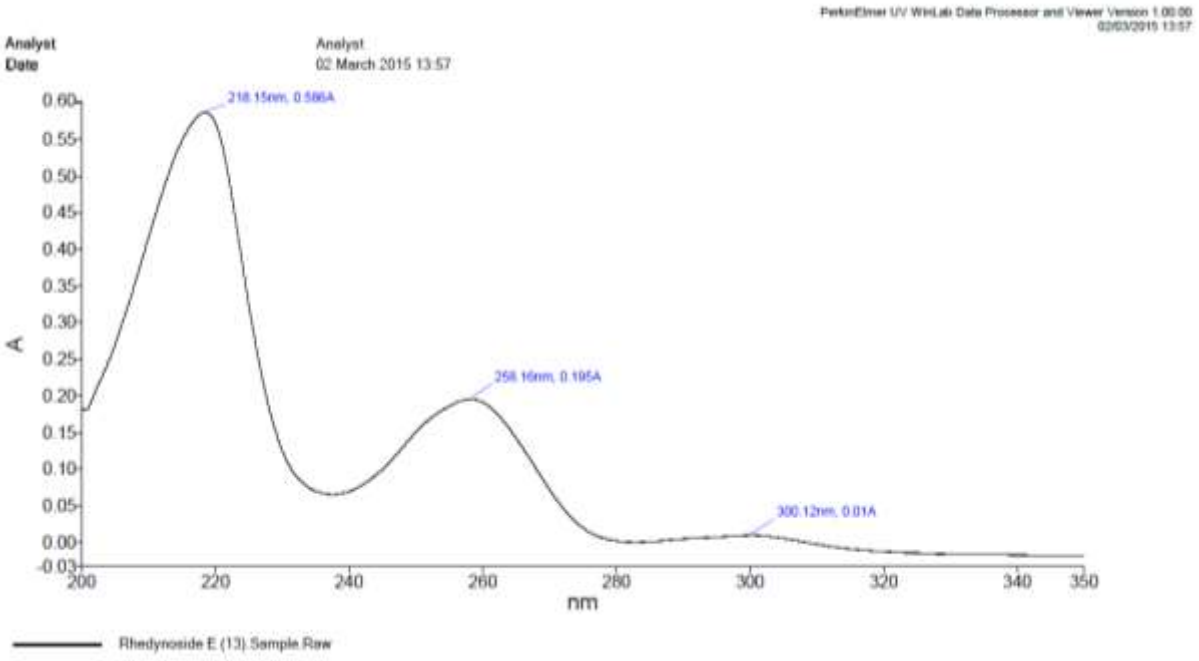

Figure A-262: UV spectrum of compound **RH13** in CH_3OH.

Appendix V: Glucose transport assays.

1) Routine cell culture

Human epithelial colorectal adenocarcinoma (Caco-2) cells were obtained from the American Type Culture Collection (ATCC) and cultured in Growth Medium consisting of Dulbecco's modified Eagle's medium (containing Glutamax-1, 4.5 g/L D-Glucose & 25 mM Hepes (Invitrogen)), 10% Fetal Bovine Serum (Sigma), 1% Non-Essential Amino Acids (Invitrogen) & 1 mM Sodium pyruvate (Sigma). The cells were routinely passaged at approximately 80% confluence using TrypLE™ Express Stable Trypsin-Like Enzyme (Invitrogen) to detach the cells, and seeded at approximately 114 cells per mm^2 in fresh tissue culture flasks. Only cells between the passage numbers 45 and 49 were used for experiments.

2) Preparation of differentiated Caco-2 cell monolayers

Corning® HTS Transwell® 96 well permeable insert supports (Sigma) were collagen coated with 40 µl of 50 µg/ml Rat Tail Collagen Type I (BD Biosciences) in 0.02 M acetic acid for one hour at room temperature under sterile conditions. The inserts were washed twice in Phosphate Buffered Saline (PBS (Invitrogen)) and the Caco-2 cells seeded into the inserts at 9.6 x 105 cell/ml (75 µl per insert) in Growth Medium and 30 ml of Growth medium added to the feeder plate below. The cells were left to attach to the collagen matrix and form monolayers over 48 hrs at 37 ºC, 5% CO_2. Both inserts and feeder plate were washed in PBS and the cells incubated with BD Entero-STIM™ Enterocyte Differentiation Medium containing MITO+™ Serum Extender solution (both BD Biosciences),75 µl per insert & 30 ml in feeder plate, for a further 48 hrs at 37 ºC, 5% CO_2.